CHROMIUM(III) PHOTOCATALYSIS: CATALYST DESIGN AND REACTION DEVELOPMENT

by

BRADLEY KARL GALL

(Under the Direction of Eric M. Ferreira)

ABSTRACT

Over the past decade, photoredox catalysis has emerged as a powerful technique in synthetic organic chemistry for its ability to perform difficult transformations under mild reaction conditions. Complexes of ruthenium or iridium, under activation of visible light, have garnered significant attention for their ability to execute single-electron processes. Using complexes of light-activated earth-abundant metals, such as chromium, our group has developed a sustainable approach to the field of photocatalysis. To find new chromium complexes as potential photocatalysts, a series of novel ligands and chromium photocatalysts were synthesized. The photophysical properties of the unique Cr complexes were investigated, as well as the use of these complexes as the photocatalysts in different reactions. Remarkably, we found a Cr photocatalyst that increases reactivity in cycloaddition reactions. Recent research has uncovered a dearomative Cr-photocatalyzed radical-cation [3+2] cycloaddition reaction using indoles and vinyl diazo species. Nucleophilic interception of indole radical-cation species, generated by Cr photocatalysis, by vinyl diazo compounds yields new indoline structural motifs. This is the first example of a photocatalyzed [3+2] cycloaddition reaction using indoles. Furthermore, progress toward the synthesis of the Cripowellin alkaloids using Cr photocatalysis

has developed an intramolecular Baeyer-Villiger transformation to synthesize a key intermediate along the synthetic pathway. Overall, new Cr photocatalysts has made tremendous strides to overtake traditional Ru/Ir catalysts.

INDEX WORDS: Photoredox catalysis, visible light photoredox catalysis, radical cation cycloaddition, sustainable chemistry, Baeyer-Villiger reaction

CHROMIUM(III) PHOTOCATALYSIS: CATALYST DESIGN AND REACTION DEVELOPMENT

by

BRADLEY KARL GALL

B.S., Pennsylvania State University, 2016

A Dissertation Submitted to the Graduate Faculty of The University of Georgia in Partial Fulfillment of the Requirements for the Degree

DOCTOR OF PHILOSOPHY

ATHENS, GEORGIA

2021

CHROMIUM(III) PHOTOCATALYSIS: CATALYST DESIGN AND REACTION DEVELOPMENT

by

BRADLEY KARL GALL

Major Professor: Eric M. Ferreira

Committee: Robert Phillips
StevenWheeler

Electronic Version Approved:

Ron Walcott
Vice Provost for Graduate Education and Dean of the Graduate School
The University of Georgia
August 2021

DEDICATION

For B, Riley, Ethan

ACKNOWLEDGMENTS

First and foremost, I would like to thank my mother, father, and brother, who have been so supportive on this journey through graduate school. I cannot even put into words what your encouragement and love has meant to me. I know that Gram, Pap, and UE are still helping me in ways they probably never thought. I could not have done this without you all, including the people that could not be here. I love you guys. To my Florida family that essentially taken me in as their own, I am forever thankful. Over the past 5 years, to see the growth my two favorite humans, E and Princess Riley, and for providing comedic relief, I love you guys.

I owe a tremendous deal of thanks to Eric. Taking a chance on a kid from a university where there was not much of an organic program, and by providing guidance and encouragement, you have helped mold me into the scientist I am today, and I am forever grateful. I am glad that we are also friends. You have been a tremendous mentor and leader to the lab and myself. I wish you and the lab nothing but future success. I hope that we can remain in contact and be friends throughout the years.

I would also like to acknowledge the Ferreira Lab as a whole. There have been so many memories that I will never forget. Francisco, you were a fantastic mentor and extremely patient with me. I hope that my accomplishments and progress has made you proud. Phil, we went from being like enemies to being great friends. I could always count on you to keep me in line, go get a beer with, or even talk about football. I really wish you tremendous success in your career. Sheneika, you have been my friend since day one in the lab and I am truly going to miss our conversations about pop culture and department drama. Avery, I could not be happier to

leave my project in your hands; you are going to do big things with it. To Haofan, Andrew, and Tim, it has been a pleasure to see you all succeed in your own ways and grow independent. Best of luck in your futures.

Lastly, I must acknowledge my friends. Cole, Thomas, Craig, Cory, Chris, John, you all have been so supportive of me during this journey. Some of us have been friends since we've been 5 years old or thereabouts. I could not have imagined you guys not being a part of this process. From talking about sports or catching me up on life events that I have missed, I am grateful for our friendship. To Flan, Liz, Em, Brit, and Tay, I am thankful for the love you have shown me throughout this process. Being down here has made me realize how much I love and miss you all.

Ian and Mel, I love you guys and could not have done this without you. You are like my second family and always will be. I miss Luna and Zeus-y so much, especially Luna. To Rob, Chelsea, Marilyn, Sam, Fred, you all are my Athens family, and I am so happy to have gotten to know you all. I wish you all luck in your careers. Lastly, Liv, I am so grateful that I had a friend that understood the pain and struggle of the graduate research process. I am sorry you had to hear me complain for the last 5 years, but we made it. I am just so thankful for our friendship.

TABLE OF CONTENTS

Page

LIST OF TABLES

Page

LIST OF FIGURES

Page

LIST OF SCHEMES

CHAPTER 1

FIRST-ROW TRANSITION METAL COMPLEXES: AN OVERVIEW OF THEIR PHOTOPHYSICAL PROPERTIES TOWARD PHOTOCATALYSIS

1.1 Introduction: Photoredox Catalysis

Photoredox catalysis entails a catalytic system between a photocatalyst and an organic substrate where electron transfer can occur in the presence of light. Common photocatalysts are organometallic complexes or organic molecules, whereas semiconductors are far less frequent. The liberal use of d-block metals in complexes as photocatalysts insinuates that their excitation relies on the nature of the metal itself and the ligand systems on the complex upon visible light irradiation. With that said, tuning the photoredox and photophysical properties of these transition metal complexes is highly flexible and solely relies on metal and ligand choice.

Since the early 2000s, the number of reports on visible light photoredox-catalyzed processes has dramatically increased.[1] The two most popular transition metals for photoredox catalysis are ruthenium(II) and iridium(III) due to their photophysical properties (Figure 1.1). Despite their capability to catalyze a wide variety of challenging and unique transformations, the cost of these noble metals and their toxicity serve as barriers for universal adoption. Therefore, the design of alternative photocatalysts, either based on earth-abundant elements or organic-based dyes, has become an exciting area of research.

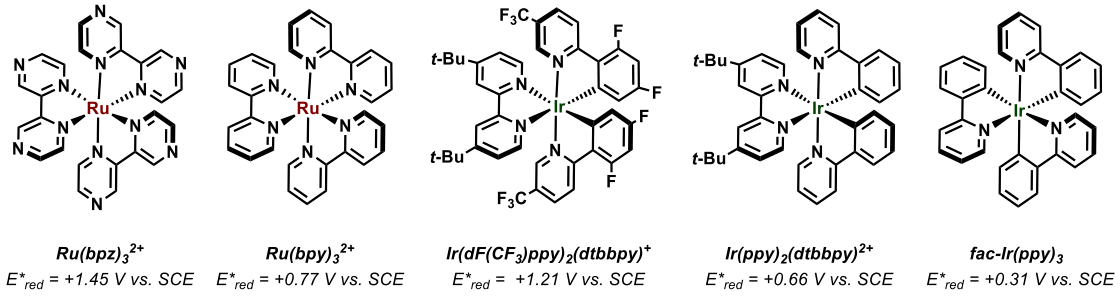

Figure 1.1. Commonly used Ru(II)- and Ir(III)-based photocatalysts.

Favored photocatalysts, such as $[Ru(bpy)_3]^{2+}$ or *fac*-$Ir(ppy)_3$, have an extensive list of attractive qualities for photocatalytic transformations. First, both photocatalysts absorb in the visible region, whereas most organic substrates do not. These photocatalysts are beneficial due to the cost of the light source, where commonly employed compact fluorescent bulbs are inexpensive and often recyclable. Second, these photocatalysts exhibit long-lived excited-state lifetimes. These lifetimes are long enough for these photocatalysts to interact and sufficiently react with organic substrates. Both ruthenium(II) and iridium(III) photocatalysts exhibit excited-state lifetimes in the microsecond range, which is enough time to react with organic substrates. Third, ruthenium(II) and iridium(III) complexes display a wide range of ground-state or excited-state redox potentials. This allows for a broad range of diverse organic molecules to undergo these oxidative or reductive electron transfers. Lastly, due to their reversible electrochemical nature and photostability, there is no degradation of the ruthenium(II) or iridium(III) photocatalysts in the excited-state, oxidized, or reduced forms. No breakdown of the ruthenium(II) or iridium(III) photocatalysts in solution lead to more reliable reactivity across various organic substrates.

Photoredox catalyzed reactions can be classified accordingly into three different reaction mechanisms (Figure 1.2).[2] The most common is a photoinduced electron transfer (PeT) mechanism. This occurs when an electron is transferred between the substrates and the

photocatalyst. Second, an atom can be transferred from the substrate to the excited-state of the photocatalyst, forming a new substrate radical. These atom transfer radical addition (ATRA) reactions can generate highly reactive radical intermediates. Lastly, an inner sphere reaction can occur at the photoexcited metal center. A substrate can interact directly with the photoexcited metal center, in which an oxidative addition, migratory insertion, reductive elimination process can occur. PeT mechanisms also allow for the tunability of the photocatalyst to provide increased reactivity.

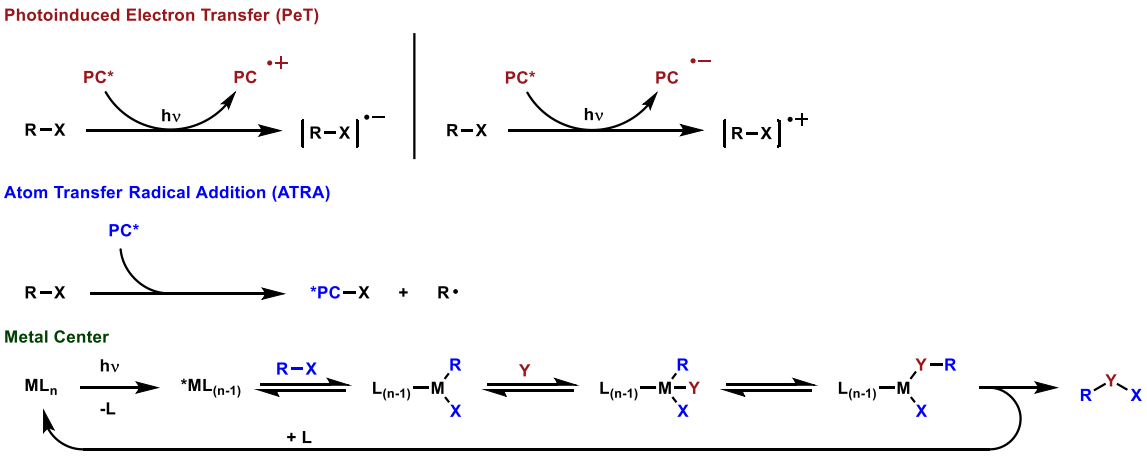

Figure 1.2. Possible photocatalytic mechanisms.

Photoinduced redox chemistry of $[Ru(bpy)_3]^{2+}$ can proceed in two different mechanisms. Photoinduced energy transfer (PET) processes with ruthenium(II) photocatalysts are known;[3] however, the photoinduced electron transfer (PeT) reaction is commonly deployed. As a case study, in a PeT mechanism, $[Ru(bpy)_3]^{2+}$ can be utilized in a reductive or oxidative quenching cycle (Figure 1.3). Upon irradiation of the ground state $[Ru(bpy)_3]^{2+}$ with visible light, the excited $[*Ru(bpy)_3]^{2+}$ can diverge to either cycle. In the reductive quenching cycle, the excited $[*Ru(bpy)_3]^{2+}$ is reduced to $[Ru(bpy)_3]^{+}$ by a single electron transfer (SET) from a donor, generating a donor radical-cation in the process. $[Ru(bpy)_3]^{+}$ can then be oxidized back to $[Ru(bpy)_3]^{2+}$ from the SET from an acceptor, forming an acceptor radical-anion in the process.

The oxidative quenching cycle is similar to the reductive cycle by involving electron donors and acceptors. In the oxidative quenching cycle, an electron is abstracted from the excited $[*Ru(bpy)_3]^{2+}$ by an acceptor, generating $[Ru(bpy)_3]^{3+}$ and an acceptor radical-anion in the process. $[Ru(bpy)_3]^{3+}$ can then be reduced back to $[Ru(bpy)_3]^{2+}$ by the donation of an electron from a donor, creating a donor radical-cation in the process.

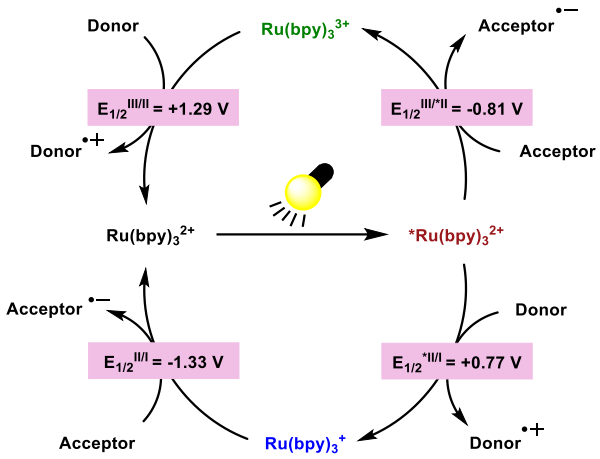

Figure 1.3. Oxidative and reductive quenching cycle of $[Ru(bpy)_3]^{2+}$ (reproduced from MacMillan and coworkers[1a]).

To further understand this photoinduced excited-state, $[Ru(bpy)_3]^{2+}$ is used as a model, and an oversimplified orbital diagram can be seen in Figure 1.4. When the ground state catalyst is irradiated with light, one of the electrons from the metal t_{2g} orbital is excited to the higher energy π^* ligand orbital. This process is known as metal-to-ligand-charge-transfer (MLCT). MLCT helps promote an electron in the singlet state to the triplet excited state. The triplet state is the long-lived photoexcited species that can participate in electron transfer. Since decay back to the ground-state is spin-forbidden, prolonged excited-state lifetimes in complexes can be seen. Once in this triplet excited-state configuration, a single electron transfer event can transpire. $[*Ru(bpy)_3]^{2+}$ can then act as a photooxidant or photoreductant by donating or accepting electrons from an organic substrate.

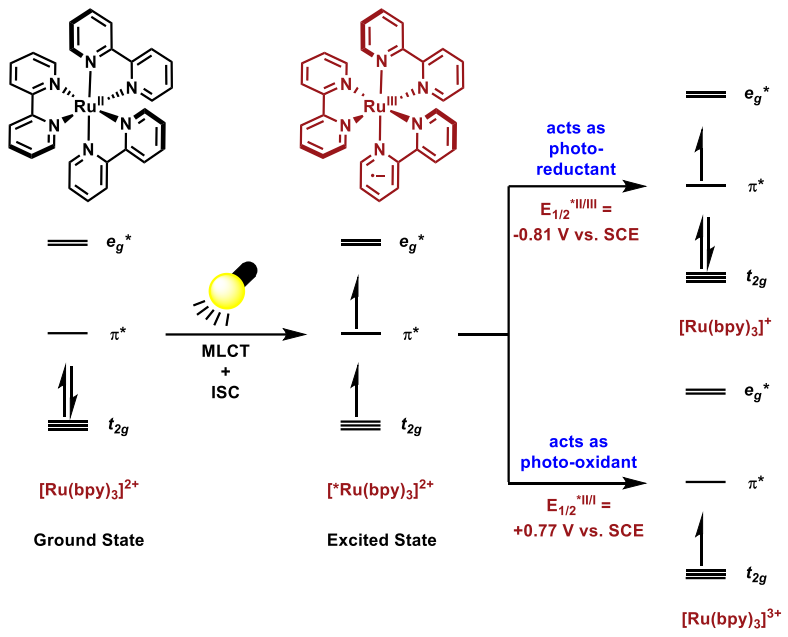

Figure 1.4. Simplified molecular orbital diagram of $[Ru(bpy)_3]^{2+}$ (reproduced from MacMillan and coworkers[1a]).

When analyzing a complex as a potential photocatalyst, four key features are desirable to have. First, the complex must be able to absorb light to be promotable to the excited-state. This absorbance can fall within the near-IR region (> 700 nm), visible region (390 – 700 nm), or near-UV region (250 – 390 nm). Light sources used can vary depending on the maximum absorbance (λ_{max}) of the complexes. Secondly, the excited-state redox potentials can help identify whether a complex is suited for use as a photocatalyst. The excited-state redox potentials can be tuned based upon the ligands of the complex. The addition of electron donating groups decreases the photooxidation capabilities of the complex while the addition of electron withdrawing groups increases it. Similarly, the addition of electron donating groups increases (less negative) photoreductant capabilities, while electron withdrawing groups decrease (more negative) it. The larger the window of the excited-state redox potentials of the complex, the diversity of organic substrates that can participate in electron transfer increases. Emissions data also help determine the excited-state oxidation and reduction potentials of the complex. Next, the lifetimes of the triplet state complex (excited-state lifetimes) can provide crucial information toward use of a

complex in photocatalysis. These lifetimes can be manipulated by the ligand systems on the metal center. Excited-state lifetimes can vary depending on the metal complex. The last important factor into designing new transition metal photocatalysts is the complex's stability in solution. Degradation of metal-ligand bonds can have an overarching effect on the reactivity of the complex. Analysis of transition metal complex in a variety of different solutions to affirm stability is a must before the complex can be potentially utilized as a photocatalyst.

In recent years, there has been a significant increase in reports of first-row transition metal photocatalysts.[4] These photocatalysts include complexes of scandium(III), titanium(IV), vanadium(V), chromium(III), manganese(IV), iron(II), cobalt(III), nickel(II), nickel (0), copper(I), and zinc(II). This work serves as a starting point for the potential use of first-row transition metal photocatalysts. In this review, the excited-state oxidation and reduction potentials of first-row transition metal photocatalysts (reported against a saturated calomel electrode, SCE), the λ_{max} in absorbance and emission (λ_{em}), and their applications will be described.

1.2 Photocatalysts of Scandium(III), Titanium(IV), Vanadium(V), Chromium(III), and Manganese(IV)

1.2.1 Introduction

A compilation of scandium(III), titanium(II), vanadium(V), and chromium(III) complexes with unique photophysical properties can be seen in Table 1.1. The excited-state oxidation (E^*_{ox}) and reduction potentials (E^*_{red}) of these metal complexes, their λ_{max} in absorbance and emission, and excited state lifetimes (τ) are also described. As it is well appreciated, heterogeneous photocatalysis with transition metal-doped composites or materials is

outside the scope of this review; therefore, only complexes directly employing a first-row transition metal will be discussed.[5]

Complex	λ_{max} (nm)	λ_{em} (nm)	E^*_{red} (V vs. SCE)	E^*_{ox} (V vs. SCE)	Excited-state lifetime (μs)
RFT-2Sc(OTf)$_3$	390	486	+2.45	--	--
[Sc(Cp*)$_2$]Cl	390	521	--	--	2.0
[Sc(Cp*)$_2$]I	393	555	--	--	--
[Sc(Cp*)$_2$](NHPh)	391	600	--	--	2.0
TiOPc	704	--	+1.23	-0.72	--
[Ti(Me-PDP)$_2$]	777	--	+0.850	-2.24	--
V(OXO)	396	507	+0.393	--	--
V(F2OXO)	397	507	+0.408	--	--
V(*t*-BuFOXO)	398	507	+0.290	--	--
V(*p*-FOXO)	389	507	+0.520	--	--
V(NO$_2$-*p*-FOXO)	373	507	+0.720	--	--
V(DiNO$_2$-*p*-FOXO)	355	507	+0.820	--	--
VOL-F	425	--	--	--	--
[Cr(phen)$_3$](OTf)$_3$	454	730	+1.45	--	304
[Cr(bpy)$_3$](OTf)$_3$	458	729	+1.48	--	69
[Cr(Ph$_2$phen)$_3$](OTf)$_3$	484	744	+1.40	--	425
[Cr(Me-bpy)$_3$](OTf)$_3$	418	732	+1.31	--	196
[Cr(4-dmcbpy)$_3$](BF$_4$)$_3$	448	733	+1.84	--	7.7
[Cr(4,4'-Ph$_2$bpy)$_3$](ClO$_4$)$_3$	445	--	--	--	140
[Cr(5-Cl-phen)$_3$](ClO$_4$)$_3$	466	--	+1.53	--	130
[Cr(Me$_2$phen)$_3$](ClO$_4$)$_3$	450	--	+1.24	--	340
[Cr(Me$_4$phen)$_3$](ClO$_4$)$_3$	456	--	+1.15	--	470
[Cr(phen)$_2$(4-dmcbpy)](OTf)$_3$	450	732	+1.68	--	87
[Cr(Ph$_2$phen)$_2$(4-dmcbpy)](OTf)$_3$	491	742	+1.63	--	108
[Cr(Me-bpy)$_2$(4-dmcbpy)](OTf)$_3$	398	734	+1.63	--	47
[Cr(PMP$_2$phen)$_3$](BF$_4$)$_3$	--	748	+1.32	--	--
[Cr(Naph$_2$phen)$_3$](BF$_4$)$_3$	--	739	+1.40	--	--
[Cr([4-CO$_2$Me]C$_6$H$_4$)$_2$phen)$_3$](BF$_4$)$_3$	--	743	+1.45	--	--
[Cr([4-NMe$_2$]C$_6$H$_4$)$_2$phen)$_3$](BF$_4$)$_3$	--	--	--	--	--
Cr(CNt-BuArCN)$_3$	474	620	--	-2.03	0.0022
[Cr(Im-Py)$_3$](BF$_4$)$_3$	320	--	--	--	--
[Cr(4-CO$_2$Me-Im-Py)$_3$](BF$_4$)$_3$	325	--	--	--	--
[Cr(tri-Im-Py)](BF$_4$)$_3$	315	--	--	--	--
[Cr(4-CO$_2$Me-tri-Im-Py)](BF$_4$)$_3$	390	740	--	--	--
[Cr(ddpd)$_2$](PF$_6$)$_3$	425	774	+0.89	--	443
[Cr(ddpd)(terpy)](PF$_6$)$_3$	470	771	--	--	100
[Cr(ddpd)(terpy-CO$_2$Et)](PF$_6$)$_3$	486	774	--	--	98
[Cr(terpy)$_2$](PF$_6$)$_3$	473	771	+1.44	--	< 0.03
[Cr(sep)](ClO$_4$)$_3$	460	666	--	--	10
[Cr(en)](ClO$_4$)$_3$	456	666	--	--	6.2
[Cr(diasmar)](ClO$_4$)$_3$	446	698	+1.35	--	--
[(Bn-TPEN)Mn(O)](Sc(OTf)$_3$)$_2$	520	--	+2.11	--	6.4

Table 1.1. Compilation of Sc(III), Ti(IV), V(V), Cr(III), and Mn(IV) complexes for photocatalysis.

1.2.2 Scandium(III) Photocatalysts

There are unique scandium(III) complexes with interesting photophysical properties that have been or could be utilized in a photocatalyzed reaction. A scandium(III)-flavin complex has been utilized by Mühldorf and Wolf (Figure 1.5A).[6] The excited-state reduction potential of a Sc(III)-flavin complex, RFT-2Sc^{3+}, is +2.45 V vs. saturated calomel electrode (SCE), making it a strong photooxidant. This complex can abstract an electron from phenyl-based compounds and help facilitate benzylic C-H bond oxidation to form ketones and aldehydes. Pfenning and

coworkers discovered a series of Sc(III) complexes that absorb and emit in the visible region (Figure 1.5B).[7] These complexes have never been utilized as photocatalysts, and their excited-state redox values are unknown; however, they exhibit long excited-state lifetimes, up to 2 microseconds.

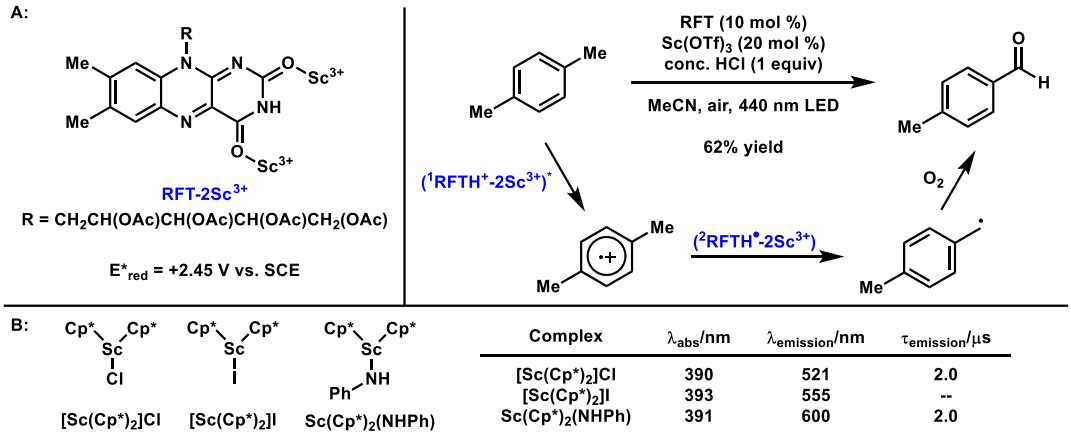

Figure 1.5. A) Scandium(III)-flavin photocatalyst for oxidation of benzylic C-H bonds. B) Scandium(III) complexes and their photophysical properties.

1.2.3 Titanium(IV) Photocatalysts

Transition metal doped titanium oxide (TiO_2) is widely utilized with various metals to generate new heterogeneous catalysts.[8] While this is well appreciated, it has also been well documented over the years. In terms of titanium(IV) photocatalysis, there are only two cited examples in the literature (Figure 1.6). These titanium(IV) complexes absorb in the near-infrared (NIR) region with no reported emission data.

Akçay and coworkers reported the TiOPc complex in Figure 1.6.[9] Interestingly, the electrochemical results saw reductions and oxidations of the metal center in addition to the phthalocyanine ring-based electron transfer. The reduction of titanium(IV) to titanium(II) and the ligand-based electron transfer have been widely debated;[10] however, both have been seen to be operable redox processes. Akçay and coworkers were able to see both the titanium(IV) to

titanium(II) and ligand-based redox couples, which reiterates previous findings. Zhang and coworkers identified another titanium(IV) complex that had unique photophysical properties.[11] With an absorbance in the visible to near-IR (NIR) range, [Ti(Me-PDP)$_2$] has been analyzed as a photooxidant and photoreductant. The excited-state redox potentials of [Ti(Me-PDP)$_2$] are relatively high. It is a very strong photoreductant, given that its excited-state oxidation potential is -2.24 V vs. SCE.

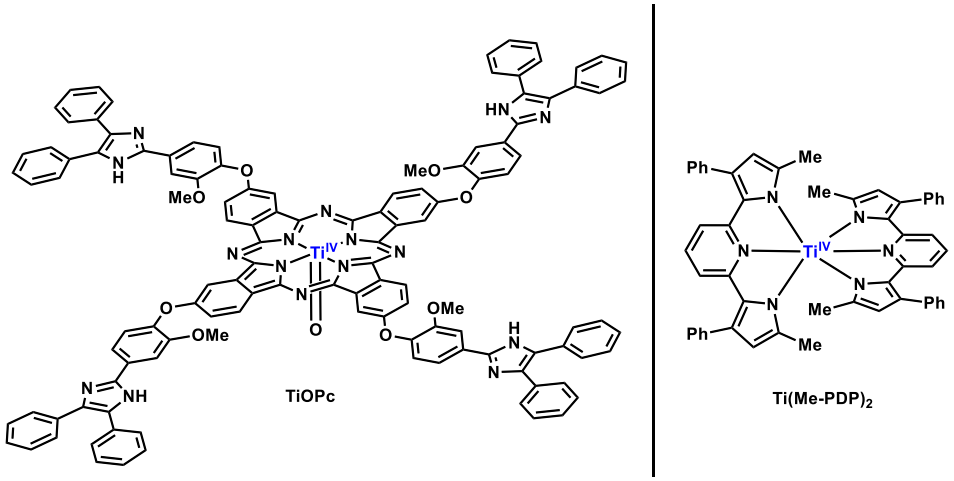

Figure 1.6. Titanium(IV) complexes.

1.2.4 Vanadium(V) Photocatalysts

Vanadium(V) complexes have rarely been seen in photocatalysis. There are only two cited examples of vanadium(V) photocatalysis. Gazi and coworkers studied C–C bond cleavage using new vanadium(V) complexes (Figure 1.7) and visible light.[12] Gazi and coworkers analyzed a series of V(V) complexes as photocatalysts in a C–C bond cleavage reaction. Typical C–C bond cleavage reactions utilize traditional transition metal catalysis with strained substrates, however photocatalytic methods have been developed.[13] Using the OXO-ligand backbone, adjustments to the redox values with electron withdrawing groups see a threshold reached in the rate of C-C bond cleavage, with [V(NO_2-*p*-*F*OXO)(O)(OMe)] being the photocatalyst with the fastest reaction rate. All of these V(V) photocatalysts absorb in the visible region (355-398 nm).

While they are mild photooxidants (E^*_{red} = +0.290 to +0.820 V), they all are still compatible in the C-C bond cleavage reaction. The excited-state lifetimes and stability in solution of these complexes were not interrogated. Choing and coworkers investigated the excited-state dynamics of VOL-F (Figure 1.7).[14] This complex exhibited an absorbance in the visible region (425 nm); however, other photophysical properties leading to this complex being explored as a potential photocatalyst were not investigated.

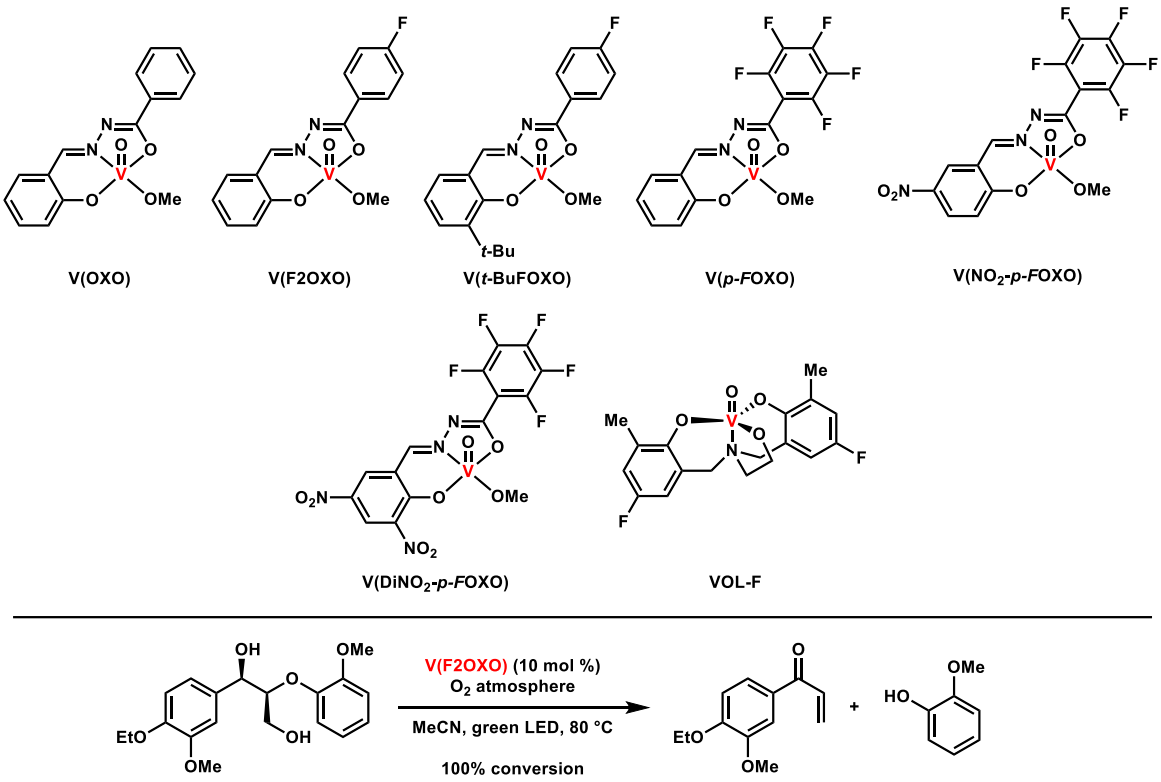

Figure 1.7. Vanadium(V) photocatalysts for C-C bond cleavage.

1.2.5 Chromium(III) and Chromium(0) Photocatalysts

Due to their unique photophysical and electrochemical properties, chromium(III) polypyridine-based complexes offer promise as potential photocatalysts. Chromium(III) complexes lacked photocatalytic application in synthetic organic chemistry up until recently when Ferreira, Shores, and coworkers discovered a Diels-Alder reaction between electron rich

alkenes and dienes using $[Cr(Ph_2phen)_3]^{3+}$ and visible light.[15a] Other applications have since been developed using this photocatalyst.[15b-d]

Detailed in Table 1.1, homoleptic Cr(III) complexes warranted most of the investigation over the past 40 years. The initial report of tris-homoleptic Cr(III) complexes with interesting photophysical properties was presented by Serpone and coworkers (Figure 1.8).[16] Analyzing the excited-states of $[Cr(phen)_3]^{3+}$, $[Cr(bpy)_3]^{3+}$, $[Cr(Me\text{-}bpy)_3]^{3+}$, $[Cr(4,4'\text{-}Ph_2bpy)_3]^{3+}$, $[Cr(5\text{-}Clphen)_3]^{3+}$, $[Cr(Me_2phen)_3]^{3+}$, $[Cr(Ph_2phen)_3]^{3+}$, and $[Cr(Me_4phen)_3]^{3+}$ showed that these catalysts are mild to strong photooxidants (E^*_{red} = +1.15 to +1.53 V) and absorb in the visible region (418 – 484 nm). The excited-state reduction potentials also were strongly dependent on the nature of the ligand, with electron withdrawing groups severely altering the electronics of the ligand. The excited-state lifetimes were also investigated (130 – 340 μs), proving to be 2-3x longer than analogous Ru(II) examples. A bis-homoleptic Cr(III) compound, $[Cr(terpy)_2]^{3+}$, was also interrogated. Due to the ligand's rigidness, $[Cr(terpy)_2]^{3+}$ exhibited very short excited-state lifetimes and was not analyzed any further, which was consistent with previously reported data for the $[Ru(terpy)_2]^{2+}$ complex.[17]

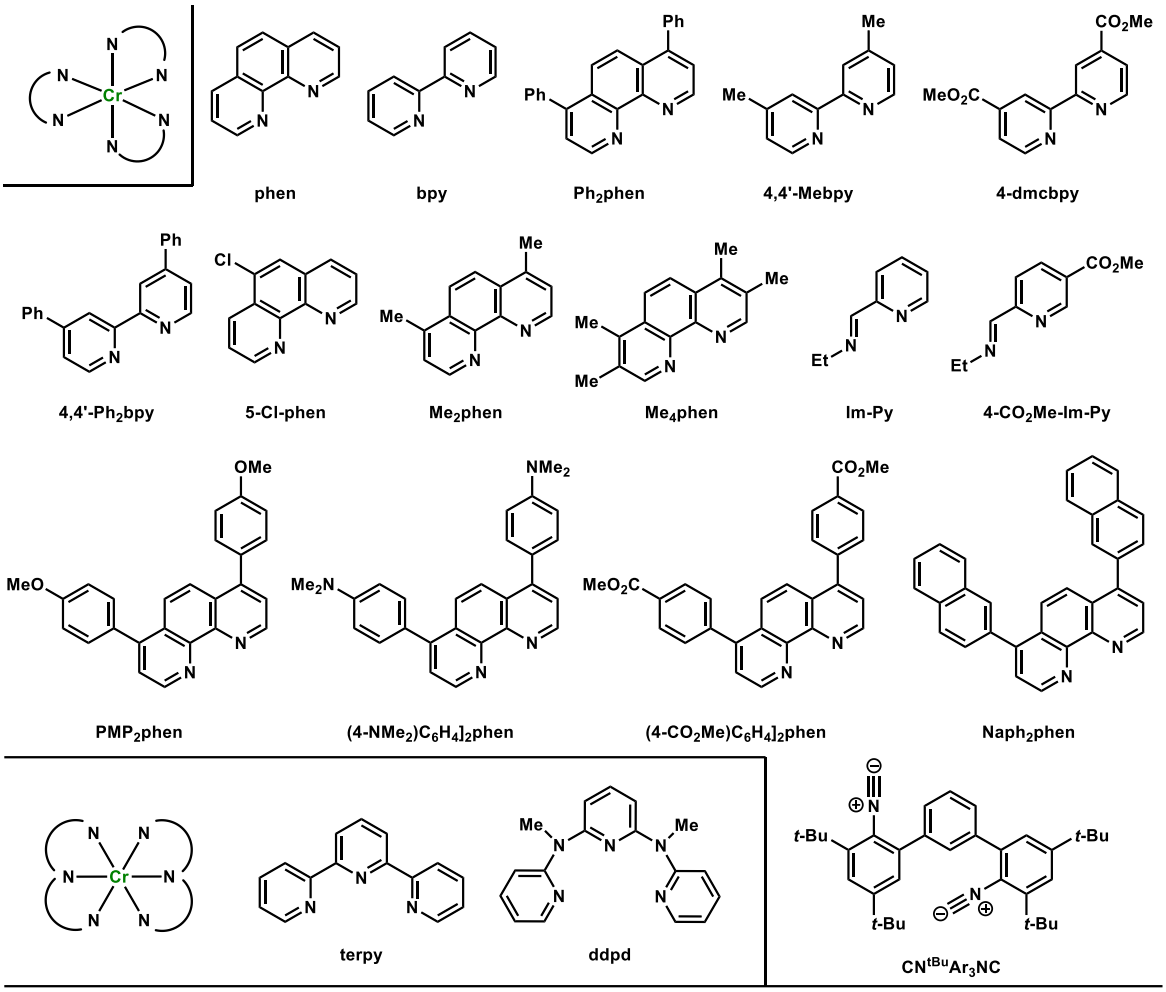

Figure 1.8. Ligands utilized in Cr(III) homo- and heteroleptic complexes.

Shores and coworkers synthesized and characterized a series of homoleptic and heteroleptic chromium(III) complexes (Figure 1.8 – 1.9).[18] The homoleptic Cr(III) complexes exhibited a narrow emission window, from 730-742 nm, absorbed in the visible region (448 – 458 nm), and have relatively high excited-state reduction potentials (E^*_{red} = +1.40 to +1.84 V). Their excited-state lifetimes are long (7.7 – 425 μs) and are stable to acidic solution, making them ideal candidates for photocatalysts. The heteroleptic Cr(III) complexes, $[Cr(phen)_2(4\text{-}dmcbpy)]^{3+}$, $[Cr(Ph_2phen)_2(4\text{-}dmcbpy)]^{3+}$, and $[Cr(Me\text{-}bpy)_2(4\text{-}dmcbpy)]^{3+}$ displayed similar emission (732 - 742 nm) and absorbance data (398 – 491 nm); however, the excited-state

reduction potentials (E^*_{red} = +1.63 to +1.68 V) showed that these catalysts were stronger photooxidants in comparison to their homoleptic counterparts.

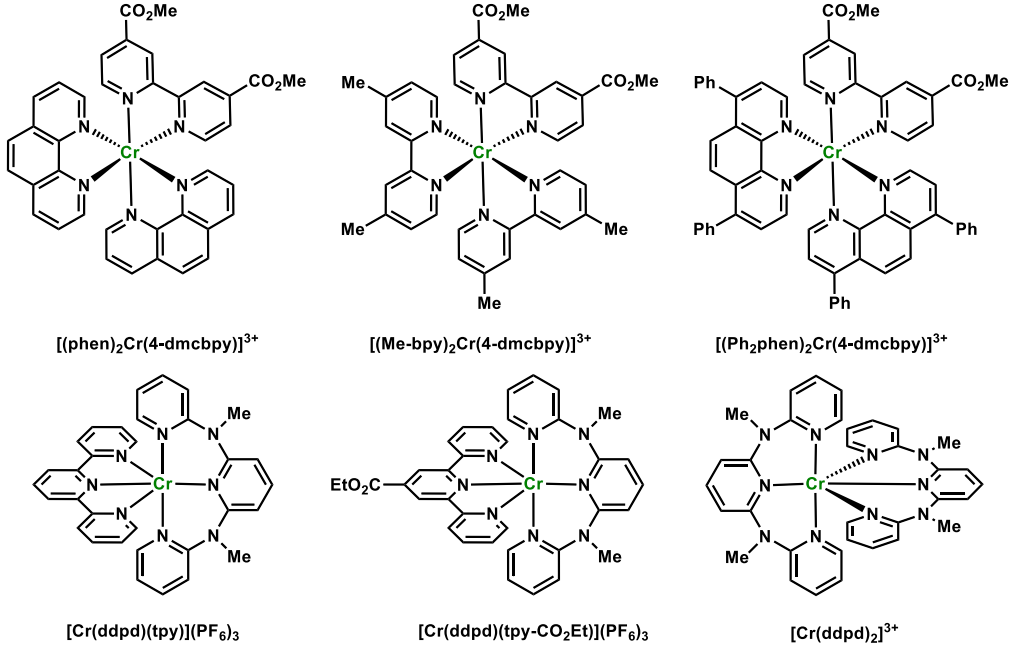

Figure 1.9. Cr(III) complexes for photocatalysis.

Other tris-homoleptic chromium(III) complexes have been synthesized by Heinze and coworkers[19] and Piquet and coworkers[20] (Figure 1.9). Heinze reports that their complex, $[Cr(ddpd)_2]^{3+}$, is strongly absorbing in the visible region (425 nm) with a long excited-state lifetime (443 μs) and low excited-state reduction potential (E^*_{red} = +0.89 V). This comes from a shift in the $^4T_2$ state. The prevention of the back-intersystem crossing from the ^2E to the $^4T_2$ state yields NIR phosphorescence and long excited-state lifetimes for a first-row transition metal complex. Heinze's Cr(III) complex is also water soluble with no degradation reported, making it a potentially greener choice for photocatalysis in aqueous media. Piquet and coworkers make other Cr(III) complexes with ddpd and terpy derivatives as a ligand. These different chromium(III) complexes absorb strongly in the visible region (470 - 486 nm) with emission data in the NIR region (771 – 774 nm). Piquet and coworkers did not measure the excited-state redox

potentials; however, their chromium(III) complexes exhibited long excited-state lifetimes (98 – 100 μs). Having almost all of the desired qualities for a photocatalyst, Heinze's and Piquet's chromium(III) complexes have never been analyzed as such.

To further diversify potential chromium(III) complexes for their use in photoredox catalysis, Gall and coworkers have devised a new strategy to tune reactivity (Figure 1.8).[21] Previously, $[Cr(Ph_2phen)_3]^{3+}$ had been utilized in numerous cycloaddition reactions.[15] New electronically diverse catalysts could be developed by changing the electronics of the bathophenanthroline ligand. Creating new ligands such as PMP_2phen, $[(NMe_2)C_6H_4]_2phen$, $[(4\text{-}CO_2Me)C_6H_4]_2phen$, and $Naph_2phen$ yielded new Cr(III) complexes. The absorbance of $[Cr(PMP_2phen)_3]^{3+}$, $[Cr([(4\text{-}CO_2Me)C_6H_4]_2phen)_3]^{3+}$, $[Cr([(NMe_2)C_6H_4]_2phen)_3]^{3+}$, and $[Cr(Naph_2phen)_3]^{3+}$ is under further investigation for potential ligand loss in solution. Emission data for $[Cr(PMP_2phen)_3]^{3+}$ (748 nm), $[Cr([(4\text{-}CO_2Me)C_6H_4]_2phen)_3]^{3+}$ (743 nm), and $[Cr(Naph_2phen)_3]^{3+}$ (739 nm) were all very consistent with $[Cr(Ph_2phen)_3]^{3+}$ (744 nm). $[Cr([(NMe_2)C_6H_4]_2phen)_3]^{3+}$ did not emit. Compared to $[Cr(Ph_2phen)_3]^{3+}$ (E^*_{red} = +1.40 V), the excited-state reduction potentials of $[Cr(PMP_2phen)_3]^{3+}$ (E^*_{red} = +1.32 V), $[Cr([(4\text{-}CO_2Me)C_6H_4]_2phen)_3]^{3+}$ (E^*_{red} = +1.45 V), $[Cr([(NMe_2)C_6H_4]_2phen)_3]^{3+}$ (did not emit, therefore cannot calculated excited-state redox potentials), and $[Cr(Naph_2phen)_3]^{3+}$ (E^*_{red} = +1.40 V) exhibited changes depending on the electronics on the ligands of the complexes. Their excited-state lifetimes and solution stability have not been analyzed, however, of these complexes, $[Cr(PMP_2phen)_3]^{3+}$ has outperformed ruthenium(II) and iridium(III) counterparts in the development of a new (3+2) photocatalyzed cycloaddition reaction.[22]

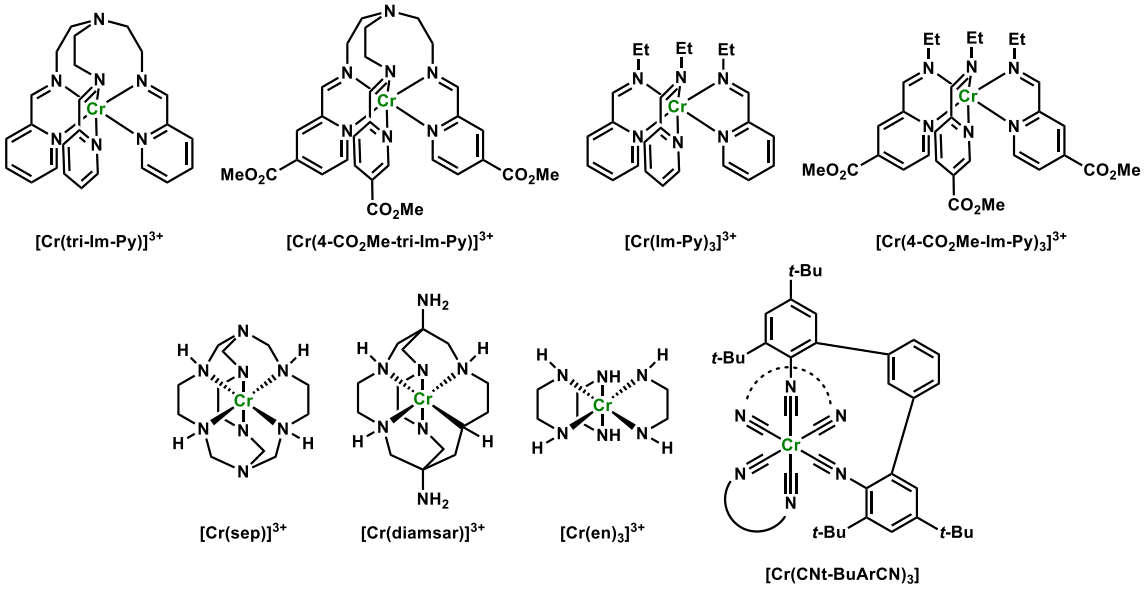

Figure 1.10. Diamine-based Cr(III) complexes.

Shores and coworkers have been very prominent in making chromium(III) complexes. Their most recent endeavor was in 2013 by synthesizing a series of hexadentate imino-pyridine (Im-Py) ligands and the tris(bidentate) analogs, and generating the corresponding chromium(III) complexes (Figure 1.10).[23] The absorbance of these complexes is lower than the usual Cr(III) complexes previously described (315 – 390 nm). The cyclic voltammetry of these complexes exhibits reversible ligand-based reductions, whereas the hexadentate and the tris(bidentate) analogs have almost identical ground-state reduction potentials. The excited-state reduction potentials were not analyzed in this report. Ester-substituted ligands also shifted the absorbance (redshift) and the ground state reduction potentials. In aqueous acidic media, $[Cr(Im\text{-}Py)_3]^{3+}$, $[Cr(4\text{-}CO_2Me\text{-}Im\text{-}Py)_2]^{3+}$, $[Cr(tri\text{-}Im\text{-}Py)]^{3+}$, and $[Cr(4\text{-}CO_2Me\text{-}tri\text{-}Im\text{-}Py)]^{3+}$ all revealed ligand loss and decomposition. Protonation of the bridgehead nitrogen in the $[Cr(tri\text{-}Im\text{-}Py)]^{3+}$ and $[Cr(4\text{-}CO_2Me\text{-}tri\text{-}Im\text{-}Py)]^{3+}$ complexes caused degradation of the complex, which was visualized and characterized by a white precipitate in acidic media. Other photophysical properties of these Cr(III) complexes would need to be probed before being used as photocatalysts.

Macrobicyclic chromium(III) complexes $[Cr(sep)]^{3+}$ and $[Cr(en)]^{3+}$ were first isolated and characterized by Brubaker and coworkers (Figure 1.10).[24] $[Cr(sep)]^{3+}$ and $[Cr(en)]^{3+}$ exhibit relatively long excited-state lifetimes in the microsecond range (6.2 – 10 μs). $[Cr(sep)]^{3+}$ and $[Cr(en)]^{3+}$ absorb in the visible region (456 - 460 nm) and emit in the NIR region (666 nm).[25] Their excited-state reduction potentials have not been determined. A different derivative of the same family, $[Cr(diasmar)]^{3+}$, with pendant $-NH_2$ groups on the bridging methylene, share similar qualities to that of $[Cr(sep)]^{3+}$ and $[Cr(en)]^{3+}$ for absorbance (446 nm) and emission data (698 nm).[26] The excited-state reduction potential of $[Cr(diasmar)]^{3+}$ was calculated to be + 1.35 V vs. SCE, making it a strong photooxidant for organic molecules. Of these macrobicyclic compounds, none have been analyzed in degradation or photodegradation experiments. The lack of degradation experiments limits their synthetic utility regarding being potential photocatalysts.

Most of the work with chromium complexes with photophysical properties has been with a Cr(III) source as the metal center. Wenger and coworkers reported the synthesis, characterization, and analysis of a Cr(0) complex, $Cr(CN\textit{t}\text{-BuArCN})_3$, using isocyanides as the ligands (Figure 1.10).[27] The bidentate chelating ligand stabilizes the Cr(0) oxidation state. $Cr(CN\textit{t}\text{-BuArCN})_3$ luminesces in the visible region (474 nm) at room temperature but a has relatively low excited-state lifetime in the nanosecond range (2.2 ns). This is one of the first examples of a Cr(0) complex that has an excited-state oxidation potential instead of a reduction potential going from Cr(0) to Cr(I). The excited-state oxidation potential is strongly reducing at -2.03 V vs. SCE, and in solution, no degradation or photodegradation occurs. Applications of $Cr(CN\textit{t}\text{-BuArCN})_3$ include studies into solar cells; however, it could be helpful to utilize this in photoredox catalysis, given the overall stability of the chromium(0) complex.

1.2.6 Manganese(IV) Photocatalysts

Photocatalysts with manganese(II) have not yet been reported. However, Fukuzumi and coworkers reported a manganese(IV) complex which interacts with $Sc(OTf)_3$ and becomes photoactive (Scheme 1.1).[28] The isolated intermediate of $[(Bn\text{-}TPEN)Mn(O)]^{2+}$ - $[Sc(OTf)_3]_2$ absorbs at 520 nm. The excited-state reduction potential of $[(Bn\text{-}TPEN)Mn(O)]^{2+}$ - $[Sc(OTf)_3]_2$ for Mn(IV) to Mn(III) is +2.11 V vs. SCE and has been utilized in the photohydroxylation of benzene. Upon irradiation, the excited state intermediate of $[(Bn\text{-}TPEN)Mn(O)]^{2+}$ - $[Sc(OTf)_3]_2$ is a potent photooxidant, even abstracting an electron from benzene. However, since the oxidation potential of benzene is +2.46 V vs. SCE, the mechanism by which this reaction proceeds becomes unclear and not analyzed by the authors. Fukuzumi and coworkers show that the higher the oxidation potential of the substrate, the slower the reaction rate. Due to the natural abundance of manganese and Fukuzumi's breakthrough report, manganese(IV) photocatalysis could be a fascinating area of research soon.

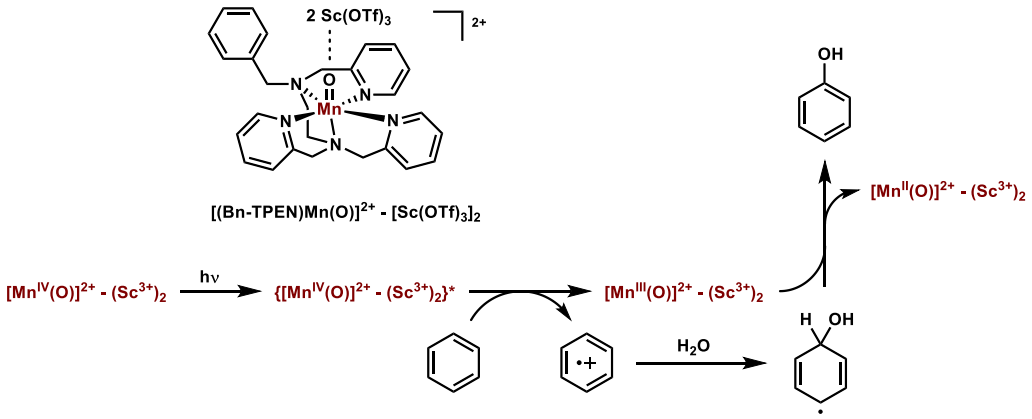

Scheme 1.1. Fukuzumi's Mn(IV) photohydroxylation mechanism.

1.2.7 Conclusions

Factoring in the absorbance, excited-state redox potentials, excited-state lifetimes, and solution stability, only chromium(III) so far shows the most promise to be a long-term alternative solution to commonly used ruthenium(II) or iridium(III) photocatalysts from this series. The

ability to alter the ligands to tune the excited-state reduction potentials for modified reactivity offers a different solution for every problem. The downside of Cr(III) photocatalysis is that it only affords one PeT mechanistic pathway. Substate oxidation and photocatalyst reduction is the only viable photoredox mechanism when using Cr(III) as the photocatalyst. Wenger's design of a Cr(0) complex that participates in catalyst oxidation, from (Cr(0) to Cr(I)), could provide the platform for more exploration into modified Cr(0) complexes. This would open up new mechanistic possibilities with substrate reduction and photocatalyst oxidation pathways becoming operable.

1.3 Photocatalysts of Iron(II), Cobalt(III), and Nickel(II/0)

1.3.1 Introduction

In terms of the relative natural abundance of first-row transition metals, iron is abundant on Earth. Like chromium(III), iron(II) polypyridyl complexes are some of the most extensively studied and sought after due to their potential photophysical properties. Due to their electronic nature, iron(II) and ruthenium(II) could potentially share similar qualities in photoredox catalysis. However, upon further examination of all the potential Fe(II) photocatalysts, the longest-lived excited-state lifetime in an iron(II) complex is 528 picoseconds.[29] This meager excited-state lifetime typically does not translate directly into a potentially valuable photocatalyst. In Table 1.2, a summary of the available Fe(II), Co(III), Ni(II), and Ni(0) complexes with photocatalyst potential is outlined. This table serves as a reference for the potential diversification of iron(II) complexes to utilize first-row transition metals as photocatalysts.

Complex	λ_{max} (nm)	λ_{em} (nm)	E^*_{red} (V vs. SCE)	E^*_{ox} (V vs. SCE)	Excited-state lifetime (ps)
$[Fe(phen)_3](NTf)_2$	520	--	+1.19	-1.17	--
$[Fe(bpy)_3](NTf)_2$	515	--	+1.20	-1.14	--
$[Fe(OMebpy)_3](NTf)_2$	--	--	--	--	--
$[Fe(dtbbpy)_3](NTf)_2$	--	--	--	--	--
$[Fe(btz)_3](PF_6)_3$	730	--	+0.18	-1.67	528
$[Fe(terpy)_2](PF_6)_2$	540	--	+1.30	-1.08	--
$[Fe(4\text{-}NO_2\text{-}Im\text{-}Py)_3](PF_6)_2$	300	--	+1.32	--	--
$[Fe(4\text{-}OH\text{-}Im\text{-}Py)_3](PF_6)_2$	339	--	--	--	--
$[Fe(4\text{-}OMe\text{-}Im\text{-}Py)_3](PF_6)_2$	343	--	+1.08	--	--
$[Fe(3\text{-}NO_2\text{-}Im\text{-}Py)_3](PF_6)_2$	300	--	+0.82	--	--
$[Fe(3\text{-}OMe\text{-}Im\text{-}Py)_3](PF_6)_2$	300	--	--	--	--
$[Fe(4\text{-}CO_2Me\text{-}Im\text{-}Py)_3](PF_6)_2$	300	--	--	--	--
$[Fe(Py\text{-}Im\text{-}Py)_3](PF_6)_2$	380	--	+0.84	--	--
$[Fe\text{-}NHC\text{-}1](PF_6)_2$	430	--	--	--	--
$[Fe\text{-}NHC\text{-}2](PF_6)_2$	457	--	+0.71	-1.95	--
$[Fe\text{-}NHC\text{-}3](PF_6)_2$	478	--	+0.80	--	--
$[Fe\text{-}NHC\text{-}4](PF_6)_2$	520	--	+0.85	-1.35	--
$[Fe(NHC\text{-}5)(terpy)](PF_6)_2$	540	--	+0.96	-1.49	0.100
$[Fe(NHC\text{-}6)_2](PF_6)_2$	460	--	+0.83	--	8.1
$[Fe(NHC\text{-}5)(NHC\text{-}7)](PF_6)_2$	550	--	+0.86	-1.53	3.6
$[Fe(NHC\text{-}7)_2](PF_6)_2$	565	--	+0.88	-1.34	0.100
$[Co(dgpy)_3](BF_4)_2$	311	440	+2.26	--	5,070
$[Co(dgpz)_3](BF_4)_2$	340	412	+2.75	--	5,300
$[(TAML)Co(OH)](OTf)_2$	600	--	+2.11	--	600
[(TAML)Co](OTf)	510	--	--	--	--
[Ni(Maqib)](OTf)	457	--	+1.35	--	10,000
$[Ni(CNR_1NC)_2]$	420	511	+0.10	-0.36	200,000
$[Ni(CNR_2NC)_2]$	425	554	+0.10	-0.36	230,000

Table 1.2. Compilation of potential Fe(II), Co(III), Ni(II), and Ni(0) complexes for photocatalysis.

1.3.2 Iron(II) Photocatalysts

Like the basic chromium(III) polypyridyl complexes, the first subset of iron(II) complexes that have had their photophysical properties analyzed have some of the same ligands as the Cr(III) complexes (Figure 1.11). $[Fe(phen)_3]^{2+}$ and $[Fe(bpy)_3]^{2+}$ share analogous qualities with $[Cr(phen)_3]^{3+}$ and $[Cr(bpy)_3]^{3+}$.[30] Iron(II) complexes strongly absorb in the visible region (515 - 520 nm), akin to chromium(III) complexes. However, where Cr(III) and Fe(II) complexes differ is in redox potentials. Chromium(III) complexes are only photooxidants, whereas iron(II) complexes can display both excited-state reduction and oxidation potentials. $[Fe(phen)_3]^{2+}$ and $[Fe(bpy)_3]^{2+}$ both have relatively high excited-state reduction potentials, at +1.19 and +1.20 V vs. SCE, respectively. $[Fe(phen)_3]^{2+}$ and $[Fe(bpy)_3]^{2+}$ excited-state oxidation potentials are strongly reducing at -1.17 V and -1.14 V vs. SCE, respectively. Derivatives of $[Fe(bpy)_3]^{2+}$ with differently substituted bipyridine ligands were synthesized; however, their photophysical properties were not analyzed. Notably, $[Fe(phen)_3]^{2+}$, $[Fe(bpy)_3]^{2+}$, $[Fe(OMebpy)_3]^{2+}$, and

$[Fe(dtbbpy)_3]^{2+}$ have been utilized as photocatalysts for the synthesis of carbazoles via the oxidation of secondary amines (Scheme 1.2).[31]

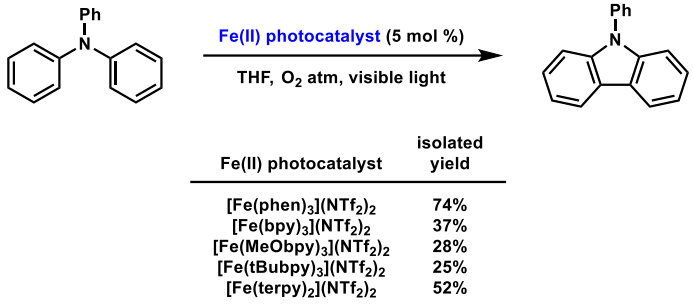

Fe(II) photocatalyst	isolated yield
$[Fe(phen)_3](NTf_2)_2$	74%
$[Fe(bpy)_3](NTf_2)_2$	37%
$[Fe(MeObpy)_3](NTf_2)_2$	28%
$[Fe(tBubpy)_3](NTf_2)_2$	25%
$[Fe(terpy)_2](NTf_2)_2$	52%

Scheme 1.2. Synthesis of carbazoles via Fe(II) photocatalysis.

In the past few years, N-heterocyclic carbenes have received plenty of attention due to their strong ligand fields that display strong σ-donor properties.[32] Iron(III) NHC complexes that are closely related were reported by several different groups (Figure 1.11). Wärnmark and coworkers reported an iron(II) hexa-N-heterocyclic carbene complex, $[Fe(btz)_3]^{2+}$, with unique photophysical properties.[29] $[Fe(btz)_3]^{2+}$ has a λ_{max} at 730 nm and is a weakly photooxidizing photocatalyst (0.18 V vs. SCE). This would not open many different reaction possibilities if $[Fe(btz)_3]^{2+}$ were utilized as a photocatalyst. However, $[Fe(btz)_3]^{2+}$ is a strong photoreductant, with an excited-state oxidation potential of -1.67 V vs. SCE. $[Fe(btz)_3]^{2+}$ is the first example of an iron(II) complex with an excited-state lifetime of longer than 500 picoseconds (528 ps). Solution stability studies have not been performed on this complex. With typical photophysical properties of other photocatalysts, $[Fe(btz)_3]^{2+}$ could be a unique alternative to classical photocatalysts.

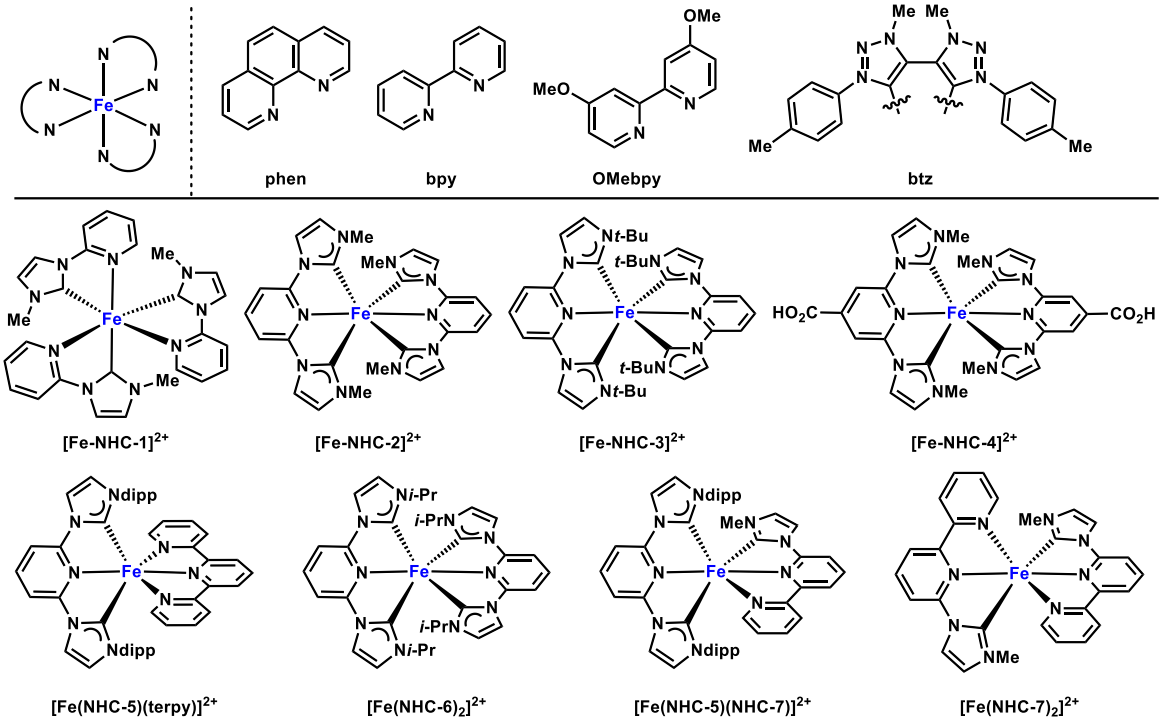

Figure 1.11. Iron(II) complexes with bipyridyl and NHC-based ligands.

Since Wärnmark's discovery, a variety of different Fe-NHC complexes with photophysical properties have been reported. Wärnmark's original report on Fe-NHC complexes shows the synthesis and characterization of $[Fe(NHC\text{-}2)_2]^{2+}$ and $[Fe(NHC\text{-}3)_2]^{2+}$ (Figure 1.11).[33] These Fe(II)-NHC complexes strongly absorb in the visible region (430 – 478 nm) but do not emit. They are both mild photooxidants with excited-state reduction potentials of +0.71 and +0.80 V vs. SCE, respectively. Interestingly, $[Fe(NHC\text{-}2)_2]^{2+}$ is also a potent photoreductant, with an excited-state oxidation potential of -1.95 V vs. SCE. Bauer and coworkers have also developed a series of Fe-NHC complexes that were investigated as potential photosensitizers.[34] $[Fe(NHC\text{-}5)(terpy)]^{2+}$, $[Fe(NHC\text{-}6)_2]^{2+}$, $[Fe(NHC\text{-}5)(NHC\text{-}7)]^{2+}$, $[Fe(NHC\text{-}7)_2]^{2+}$ contain tridentate NHC ligands or other tripyridyl based ligands. These complexes are strong visible light absorbers (460 – 565 nm), and they do not emit, similarly to Wärnmark's reported $[Fe(NHC\text{-}2)_2]^{2+}$ and $[Fe(NHC\text{-}3)_2]^{2+}$. In comparison to Wärnmark's reported $[Fe(NHC\text{-}2)_2]^{2+}$

and $[Fe(NHC\text{-}3)_2]^{2+}$, Bauer's reported $[Fe(NHC\text{-}5)(terpy)]^{2+}$, $[Fe(NHC\text{-}6)_2]^{2+}$, $[Fe(NHC\text{-}5)(NHC\text{-}7)]^{2+}$, $[Fe(NHC\text{-}7)_2]^{2+}$ complexes are analogous in terms of excited-state redox potentials (E^*_{red} = +0.96 to -1.95 V). They are mild photooxidants but strong photoreductants. Unlike Wärnmark's breakthrough report of $[Fe(btz)_3]^{2+}$ with an excited-state lifetime of 528 ps, Bauer's reported Fe(II)-NHC complexes are all less than 8 ps. Bauer's report highlights a correlation between the number of NHC ligands and the excited-state lifetimes. With two or fewer NHC σ-donor ligands, the average excited-state lifetime was well below 100 femtoseconds; however, with three NHC σ-donor ligands, the excited-state lifetimes rose to ~ 4 ps. When four NHC σ-donor ligands are employed, the excited-state lifetime increased to ~ 8 ps.

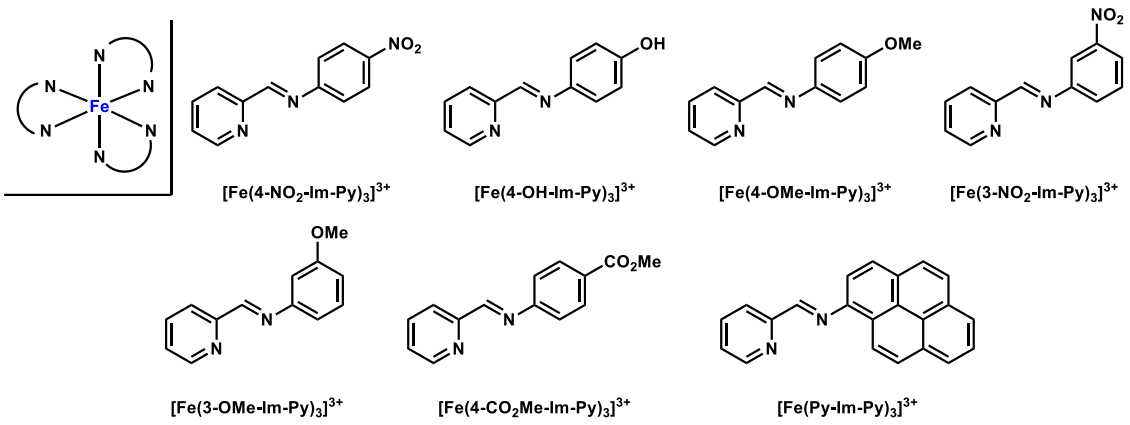

Figure 1.12. Iminyl-pyridine-based ligands for tris-ligated Fe(II) complexes.

The last set of iron(II) complexes that could be utilized as photosensitizers comes from a report by Lalevée and coworkers (Figure 1.12).[35] Interested in understanding whether electronically different ligands exhibit different absorbance and other photophysical properties, a new series of iminyl-pyridine-based ligands were synthesized. Previously, chromium(III) complexes with iminyl-pyridine ligands were discussed. In the chromium(III) iminyl-pyridine examples by Shores, alkyl imines were analyzed; however, Lalevée and coworkers used aniline-based imines as the starting point for diversification. Electron withdrawing and donating groups

were added to the aniline ring system, and different Fe(II) catalysts were then synthesized. $[Fe(4\text{-}NO_2\text{-}Im\text{-}Py)_3]^{2+}$, $[Fe(4\text{-}OH\text{-}Im\text{-}Py)_3]^{2+}$, $[Fe(4\text{-}OMe\text{-}Im\text{-}Py)_3]^{2+}$, $[Fe(3\text{-}NO_2\text{-}Im\text{-}Py)_3]^{2+}$, $[Fe(3\text{-}OMe\text{-}Im\text{-}Py)_3]^{2+}$, $[Fe(4\text{-}CO_2Me\text{-}Im\text{-}Py)_3]^{2+}$, $[Fe(Py\text{-}Im\text{-}Py)_3]^{2+}$ are the complexes of interest. Most of these complexes absorb in the near-UV region (NUV), with only $[Fe(4\text{-}OH\text{-}Im\text{-}Py)_3]^{2+}$, $[Fe(4\text{-}OMe\text{-}Im\text{-}Py)_3]^{2+}$, and $[Fe(Py\text{-}Im\text{-}Py)_3]^{2+}$ absorbing in the visible region. The excited-state redox potential for some of these complexes were not reported. $[Fe(4\text{-}NO_2\text{-}Im\text{-}Py)_3]^{2+}$ and $[Fe(4\text{-}OMe\text{-}Im\text{-}Py)_3]^{2+}$ are mild to strong photooxidants, with excited-state reduction potentials of + 1.32 and + 1.08 V vs. SCE, respectively. The polycyclic aromatic hydrocarbon of pyrene showed a substantial effect in absorbance; however, it was a weaker photooxidant. With all these iminyl-pyridyl complexes, especially the chromium(III) examples, degradation and photodegradation are problems. Lalevée and coworkers do not report any dissociation and degradation experiments with iron(II) iminyl-pyridyl complexes.

1.3.3 Cobalt(III) Photocatalysis

Given that cobalt(III) has the same d-electron count as Fe(II) and there are specific challenges associated with accessing a luminescent Fe(II) complex, exploration of potential cobalt(III) complexes as potential photocatalysts hasn't been investigated. The groups of Hanan and Zysman-Colman developed two new Co(III) complexes as potential photocatalysts (Figure 1.13).[36] $[Co(dgpy)_2]^{3+}$ and $[Co(dgpz)_2]^{3+}$ absorb in the visible region, with λ_{max} of 311 and 340 nm, respectively. Both Co(III) complexes emit in the visible region as well. Interestingly, $[Co(dgpy)_2]^{3+}$ and $[Co(dgpz)_2]^{3+}$ are very potent photooxidants, with excited-state reduction potentials of +2.26 and +2.75 V vs. SCE. $[Co(dgpy)_2]^{3+}$ and $[Co(dgpz)_2]^{3+}$ also have long excited-state lifetimes of 5,070 and 5,300 μs. With these favorable excited-state reduction

potentials and long excited-state lifetimes, as a proof of concept, Hanan and Zysman-Colman utilized both new cobalt(III) complexes in the trifluoromethylation of polycyclic aromatic hydrocarbons.

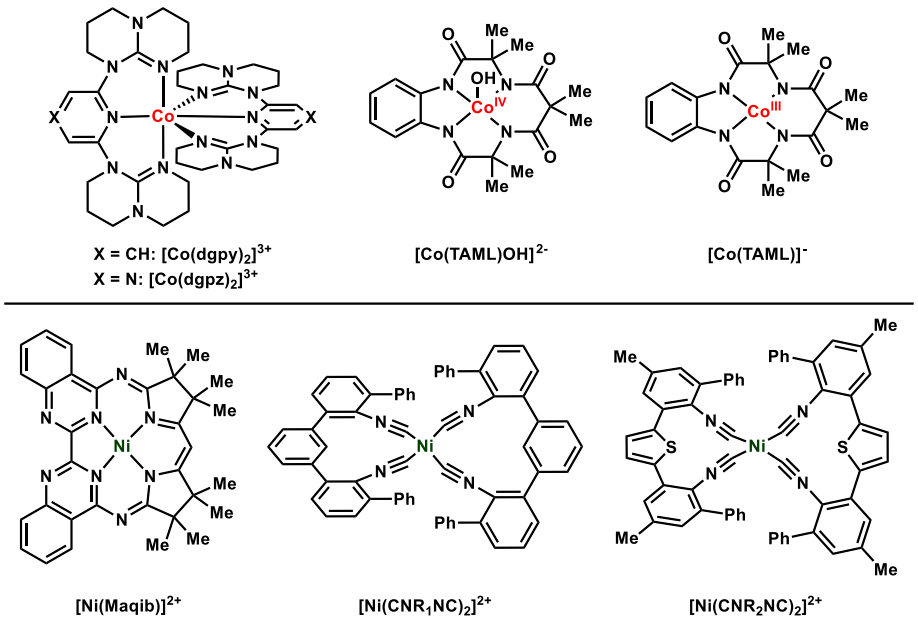

Figure 1.13. Cobalt and nickel complexes for photocatalysis.

More recently, Fukuzumi identified two different cobalt complexes that exhibit some photocatalytic character (Figure 1.13).[37] $[Co^{IV}(OH)(TAML)]^{2+}$ and $[Co^{III}(OH)(TAML)]^{+}$ are strong visible light-absorbing complexes. Oxidation of $[Co^{III}(OH)(TAML)]^{+}$ to generate $[Co^{IV}(OH)(TAML)]^{2+}$ yields the desired Co(IV) photocatalyst. The excited-state reduction potential of $[Co^{IV}(OH)(TAML)]^{2+}$ is +2.11 V vs. SCE, making it a very strong photooxidant. Fukuzumi and coworkers measured single electron oxidations of different arenes with oxidation potentials similar to the $[Co^{IV}(OH)(TAML)]^{2+}$ excited-state reduction potential.

1.3.4 Nickel(II) and Nickel(0) Photocatalysts

After a groundbreaking report by MacMillan[38] in 2017, research into photoactive nickel(II) complexes has significantly increased. Nickel catalysis cycles have been shown to

involve photoexcited nickel intermediates which help facilitate reductive elimination processes. While this area of research is well appreciated, direct nickel complexes that could be used as photocatalysts are scarce. The Bach and Hess groups reported a macrocyclic biquinazoline ligated nickel(II) complex, $[Ni(Maqib)]^{2+}$, with unique photophysical properties (Figure 1.13).[39] $[Ni(Maqib)]^{2+}$ absorbs in the visible region with a λ_{max} of 457 nm, and it does not emit in the visible region. The excited-state reduction potential was calculated to be +1.35 V vs. SCE, similar to most Cr(III) photooxidants. Used as the photocatalyst, $[Ni(Maqib)]^{2+}$ was able to complete the cyclization of bromoalkyl-substituted indole and was superior to previous reports using $[Ru(bpy)_3]^{2+}$ as the photosensitizer. These results show the potential utility of this new Ni(II) photocatalyst.

Analogous to Bach and Hess's findings, Wenger and coworkers theorized using diisocyanide chelating ligands on a Ni metal center, similar to their work on chromium(III) complexes. Wenger and coworkers developed two new Ni(0) isocyanide complexes with different linkers.[40] $[Ni(CNR_1NC)_2]$ and $[Ni(CNR_2NC)_2]$ absorb and have emission in the visible region (420 - 425 nm); however, their excited-state redox potentials (E^*_{red} = +0.10 to -0.36 V) are low (Figure 1.13). Luminescence of these Ni(0) complexes can also only be achieved at low temperatures (77 K), which is a significant drawback for these compounds. However, the excited-state lifetimes of $[Ni(CNR_1NC)_2]$ and $[Ni(CNR_2NC)_2]$ are the relatively long in compared to Fe(II) examples (picosecond range) at 0.20 and 0.23 μs. Wenger proposes that more studies and diversification experiments need to ensue before a complex can participate as the photocatalyst in photoredox catalysis.

1.3.5 Conclusions

In this section, Fe(II), Co(III), Ni(II), and Ni(0) complexes have been outlined as photocatalysts or possible photocatalysts. In the current state of the field, and since iron is the most abundant transition metal on Earth, Fe(II) photocatalysis seems the most promising, given that the nature of the ligand can further increase the excited-state lifetimes. NHC-ligated Fe(II) complexes seem of the most promise and changing the electronic properties of those ligands represents a valuable starting point for potential diversification. Interestingly, the research area of Co(III) photocatalysis represents a blank slate to which researchers can be creative and stamp their mark on the field. So far, Co(III) photocatalysis has revealed potent photooxidants, from Co(III) to Co(II). Photoreduction of the catalyst from Co(II) to Co(III) would represent a revolutionary twist on this underdeveloped field. The search for photoactive nickel(II) complexes is still a very prominent area of research. Most dual catalytic systems that have been developed in recent years have screens for the potential of a photoactive nickel(II) intermediate. In these elements, iron(II) represents the most attractive alternative to common rare-earth metal photocatalysts.

1.4 Copper(I) Photocatalysts

1.4.1 Introduction

Of all the first-row transition metals, the field of luminescent copper(I) complexes is diverse, and only selected examples will be mentioned since there are over 500+ literature reports of copper(I) complexes. In this literature review, basic bis-phosphine ligated and polypyridyl copper(I) complexes will be examined. Cu(I)-NHC complexes will also be discussed against previous metal-NHC complexes. Overarchingly, copper(I) photocatalysts

absorb in the visible region, exhibit long excited-state lifetimes, and are prone to oxidation from molecular oxygen. Copper is the fourth most abundant first-row transition metal, and research in the fields of copper catalysis and photocatalysis is ever-expanding. In Table 1.3, a compilation of some recent copper(I) complexes that have exciting photophysical properties are seen. The absorbance, emission data, and excited-state redox potentials for the corresponding copper(I) photocatalysts are mentioned in this table.

Complex	λ_{max} (nm)	λ_{em} (nm)	E^*_{red} (V vs. SCE)	E^*_{ox} (V vs. SCE)	Excited-state lifetime (μs)
$[Cu(phen)(IPr)](PF_6)$	384	--	+1.39	-1.69	--
$[Cu(bpy)(IPr)](PF_6)$	382	--	+1.38	-1.85	--
$[Cu(dpya)(IPr)](PF_6)$	473	--	+0.62	-0.70	--
$[Cu(mdmdpya)(IPr)](PF_6)$	375	--	+1.36	-1.32	--
$[Cu(dpym)(IPr)](PF_6)$	381	--	+1.33	-1.89	--
$[Cu(bpy)(SIPr)](PF_6)$	370	--	+1.52	-2.02	--
$[Cu(dppp)_2](BF_4)$	347	556	+1.32	-2.44	0.24
$[Cu(dppb)_2](BF_4)$	374	--	+1.06	-2.19	--
$[Cu(dap)_2]Cl$	--	--	--	-1.43	0.27
$[Cu(bpy)(Xant)](BF_4)$	480	--	+1.30	-1.54	--
$[Cu(dmp)(Xant)](BF_4)$	378	545	+0.91	-1.44	--
$[Cu(dBdpp)(Xant)](PF_6)$	387	546	+1.47	-1.80	54.1
$[Cu(4\text{-}Mebpy)(Xant)](BF_4)$	480	--	+1.25	-1.46	--
$[Cu(6\text{-}Mebpy)(Xant)](BF_4)$	470	--	+1.38	-1.45	--
$[Cu(bath)(Xant)](PF_6)$	389	569	+1.52	-1.88	6.4
$[Cu(POP)_2](BF_4)$	332	--	--	-2.34	--
$[Cu(dppp)(POP)](BF_4)$	363	494	+1.13	-1.98	2.44
$[Cu(bpy)(POP)](BF_4)$	480	--	+1.23	-1.48	--
$[Cu(dmp)(POP)](BF_4)$	383	565	--	-1.20	14.3
$[Cu(dppb)(POP)](BF_4)$	--	544	--	-1.27	0.002
$[Cu(dppe)(POP)](BF_4)$	--	546	--	-1.25	0.230
$[Cu(4\text{-}Mebpy)(POP)](BF_4)$	480	--	+1.42	-1.53	--
$[Cu(6\text{-}Mebpy)(POP)](BF_4)$	470	--	+1.09	-1.53	--
$[Cu(bath)(POP)](PF_6)$	--	--	+0.63	-1.02	0.81
$[Cu(bath)(ThioPOP)](PF_6)$	386	545	+1.56	-1.93	16.3
$[Cu(bpy)(PPh_3)_2](BF_4)$	480	--	+1.38	-1.38	--
$[Cu(4\text{-}Mebpy)(PPh_3)_2](BF_4)$	480	--	+1.40	-1.38	--
$[Cu(pytz)(POP)](BF_4)$	--	--	+0.72	-1.71	--
$[Cu(pytz)(dppe)](BF_4)$	--	--	+0.65	-1.42	--
$[Cu(pytz)(dppm)](BF_4)$	--	--	+0.90	-1.27	--
Cu(bath)(dPcarb)	449	602	+1.32	--	1.4
$[Cu_2(Me_2bpy)_2(tdppc)](PF_6)_2$	410	--	+0.61	-2.32	--
$[Cu_2(dmp)_2(tdapc)](PF_6)_2$	420	--	+1.25	-1.77	--
$[Cu(dpp)binc)](BF_4)$	350	--	--	-1.88	17

Table 1.3. Compilation of Cu(I) complexes for photocatalysis.

1.4.2 Copper(I) Photocatalysts

Analogous to Wärnmark's and Bauer's previous Fe-NHC work, Gaillard and coworkers reported six new luminescent Cu(I)-NHC complexes with different bipyridyl ring systems.[41] These complexes can be synthesized in two easy steps with no purifications. Two different NHCs, IPr and SIPr, were analyzed as different derivatives. The six complexes with the most interesting photophysical properties are seen in Figure 1.14. $[Cu(IPr)(phen)]^+$, $[Cu(IPr)(bpy)]^+$,

$[Cu(IPr)(dpym)]^+$, $[Cu(IPr)(dpya)]^+$, $[Cu(IPr)(mdmdpya)]^+$, $[Cu(SIPr)(bpy)]^+$ all absorb in the visible region (370 – 473 nm). These copper(I) complexes exhibit excited-state reduction (E^*_{red} = +0.62 to +1.52 V) and oxidation potentials (E^*_{ox} = -0.70 to -2.02 V), which is typical of most copper(I) complexes. The two most intriguing complexes Gaillard and coworkers synthesized are $[Cu(IPr)(dpym)]^+$ and $[Cu(SIPr)(bpy)]^+$ because they are strong photooxidants and photoreductants. The rigidity between the NHC ligands, IPr and SIPr, profoundly affects the excited-state redox potentials. These complexes have not been utilized or tried as copper(I) photocatalysts.

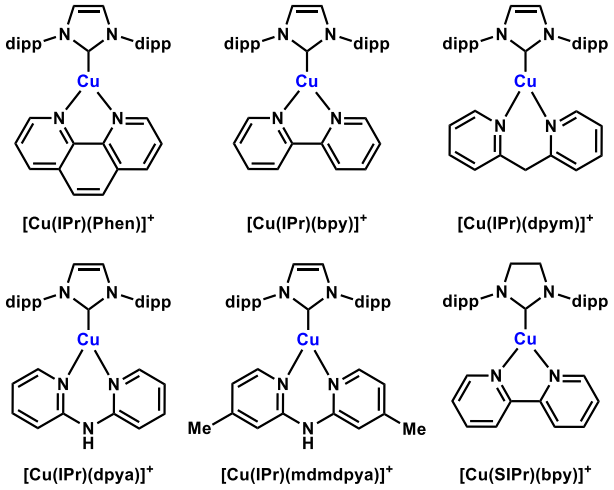

Figure 1.14. Cu(I)-NHC complexes.

Homoleptic copper(I) complexes have been rigorously studied; however, their photophysical properties have been neglected. Ligands that have rarely been considered in metal-centered photocatalysts are bis-phosphine ligands. Due to their dissociation properties, bis-phosphine ligands have never been utilized in photocatalysis; however, this ligand class may offer some advantages. The generation of the metal-ligand photocatalyst in situ could save time and resources over synthesizing, isolating, and purifying the metal-phosphine photocatalyst. Another advantage would be the tunability of the photocatalyst. Screening for reactivity by simply changing the ligand added to the reaction mixture opens more possibilities for potential

photocatalysts that could be used. Lastly, the association/dissociation could open different photoredox mechanistic possibilities. Classical PeT is still operable, but with the dissociation of a phosphine ligand, the prospect of having a substrate directly interacting with the metal center for electron transfer events to occur becomes possible. With this newfound mechanism, chirality in the ligands could lead to chiral-at-the-metal photocatalysts to impart enantioselectivity to the reaction. Nierengarten and coworkers first reported the use of bis-phosphine ligands in potential copper(I) photocatalysts (Figure 1.15).[42,43] Nierengarten and coworkers synthesized $[Cu(dppp)_2]^+$, $[Cu(dppb)_2]^+$, $[Cu(dppp)(DPEphos)]^+$, $[Cu(dppb)(DPEphos)]^+$, and $[Cu(dppe)(DPEphos)]^+$, which all absorb in the visible region (347 – 374 nm). All these complexes are mild photooxidants (E^*_{red} = +1.06 to +1.32 V) and strong photoreductants (E^*_{ox} = -2.19 to -2.44 V) with shorter excited-state lifetimes (0.24 - 2.44 μs) in comparison to chromium(III) complexes. To date, none of the bis-phosphine-derived complexes have been used successfully in a photoredox reaction. Potential problems of dissociation persist with the use of this system.

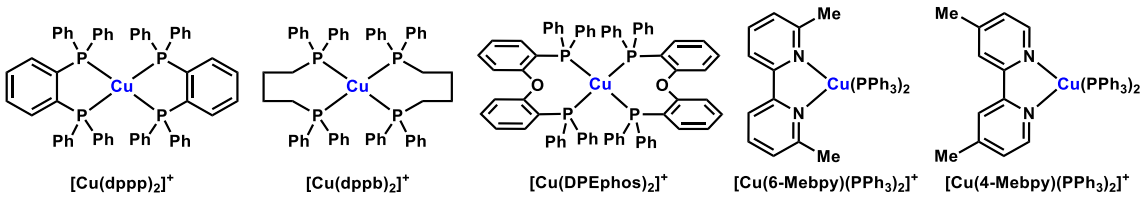

Figure 1.15. Homoleptic bis-phosphine ligated copper(I) complexes and variants.

Liberal use of the DPEphos and Xantphos bis-phosphine ligands, along with differently substituted bipyridyl ligands, has increased the possibility of utilizing a copper(I) species in photocatalysis (Figure 1.16).[42,44] There are many different bipyridyl ligands on copper(I) complexes that offer varying photophysical properties. Most of these bis-phosphine bipyridyl copper(I) complexes absorb (332 – 480 nm) and emit (494 – 565 nm) in the visible region. These DPEphos /Xantphos bipyridyl-derived copper(I) complexes are both excited-state

reductants and oxidants. In the cases of the Xantphos-bipyridyl copper(I) complexes, some trends in the electrochemical data are seen. The more electron rich the bipyridyl ligand is on the copper(I) complex, the greater the excited-state oxidation potential. Compared to the standard bpy ligand, differently substituted bipyridine ligands, 4-Mebpy and 6-Mebpy, do not substantially affect the photophysical properties. However, compared to the dimethylphenanthroline (dmp) ligand, the addition of phenyl rings at the 4- and 7- positions (bath-ligand) greatly affect the overall photophysical properties of these complexes. One of the most interesting DPEphos-ligated copper(I) derivatives is the $[Cu(bpy)(ThioPOP)]^+$ complex. This complex absorbs (386 nm) and emits (545 nm) in the visible region at room temperature. Unlike most copper(I) complexes that are prone to oxidation from molecular oxygen, $[Cu(bpy)(ThioPOP)]^+$ is bench stable and not oxygen sensitive. $[Cu(bpy)(ThioPOP)]^+$ is a potent photooxidant and photoreductants with a long excited-state lifetime (16.3 μs), with excited-state reduction and oxidation potentials of +1.56 V and -1.93 V vs. SCE, respectively. The scope of substrates encompassed within $[Cu(bpy)(ThioPOP)]^+$ excited-state redox potential range is extensive. Further analysis of $[Cu(bpy)(ThioPOP)]^+$ as a photocatalyst was not pursued.

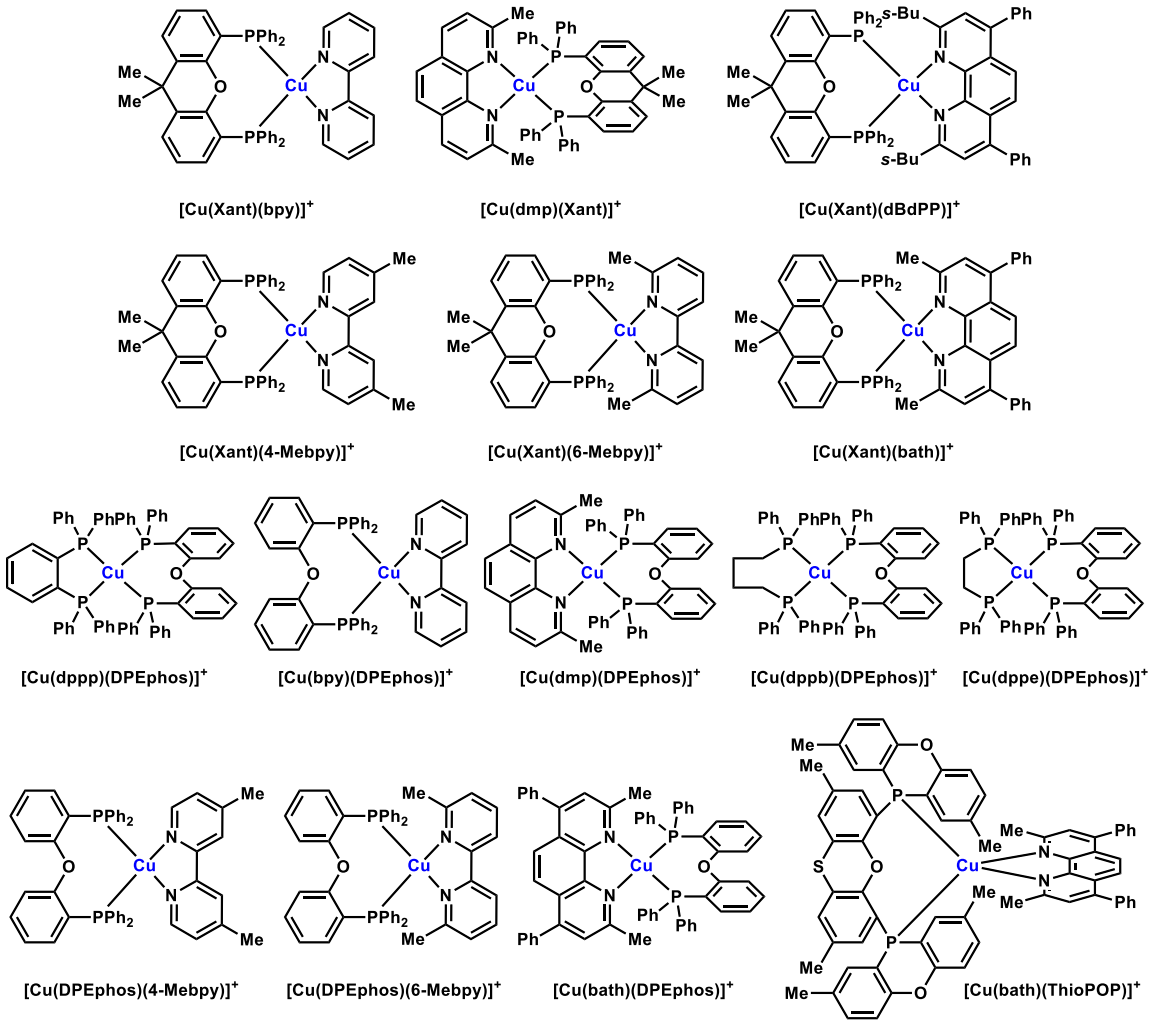

Figure 1.16. DPEphos- and Xantphos- derived copper(I) complexes.

Other bidentate phosphine ligands have been utilized in potential copper(I) photocatalysts, along with bipyridine ligands. The two new bidentate phosphine ligands classes that showed great promise are the nido-carborane-diphosphine ligand (dpcarb)[45] and pyridine-tetrazole ligands (pytz)[46] (Figure 1.17). Complexes synthesized with these ligands include $[Cu(bath)(dpcarb)]^+$, $[Cu(pytz)(DPEphos)]^+$, $[Cu(pytz)(dppm)]^+$, and $[Cu(pytz)(dppe)]^+$. $[Cu(bath)(dpcarb)]^+$ absorbs in the visible region (~ 449 nm); however the absorbances of $[Cu(pytz)(DPEphos)]^+$, $[Cu(pytz)(dppm)]^+$, and $[Cu(pytz)(dppe)]^+$ were not analyzed. Excited-state redox potentials yielded $[Cu(pytz)(DPEphos)]^+$, $[Cu(pytz)(dppm)]^+$, and $[Cu(pytz)(dppe)]^+$

as mild photooxidants (E^*_{red} = +0.65 to +0.92 V) but potent photoreductants (E^*_{ox} = -1.27 to -1.71 V), with the $[Cu(pytz)(DPEphos)]^+$ complex exhibiting strongly reducing excited-state oxidation potential of -1.71 V vs. SCE. $[Cu(bath)(dpcarb)]^+$ also emits in the visible region, with a λ_{max} at 602 nm. This complex is a strong excited-state photooxidant as well (E^*_{red} = +1.32V). $[Cu(bath)(dpcarb)]^+$ was proven capable of being a photocatalyst in an aza-Henry visible-light-induced cross-dehydrogenative coupling reaction with tetraisoquinoline derivatives.

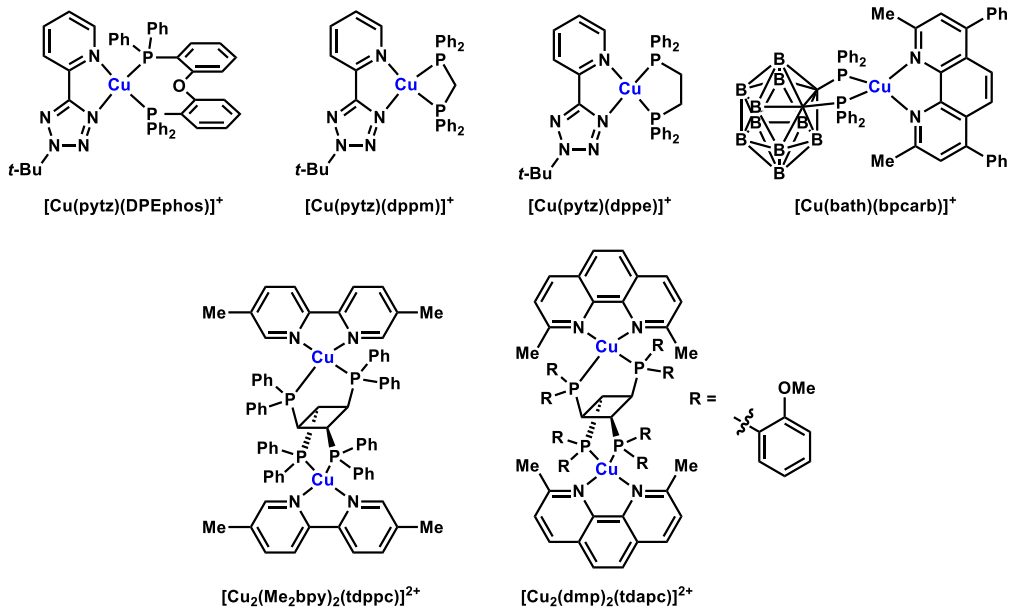

Figure 1.17. Complexes using dbcarb, pytz, and other dinuclear copper(I) complexes.

One of the more unique approaches for the generation of copper(I) photocatalysts was the discovery of dinuclear copper(I) complexes with photophysical properties (Figure 1.17). De Cola and coworkers synthesized and characterized a series of luminescent dinuclear copper(I) complexes with bis(bidentate)phosphine ligands.[47] Dinuclear species $[Cu_2(Me_2bpy)_2(tdppc)]^{2+}$ and $[Cu_2(Me_2bpy)_2(tdppc)]^{2+}$ employ a rigid tetraphosphine linker that can be attributed to the overall absorbance (410 - 420 nm) and excited-state lifetimes (~ 1.4 μs) and redox potentials and (Figure 1.17). The copper(I) complexes are mild photooxidants (E^*_{red} = +0.62 to +1.25 V), however, potent photoreductants (E^*_{ox} = -1.77 to -2.32 V). These complexes also exhibit a

temperature-dependent excited-state lifetime. When the lifetimes were measured at low temperatures (~77 K), the excited-state lifetimes of these complexes increased to ~ 600 microseconds. This phenomenon suggests two emissive excited states and can be classified as delayed fluorescence.

Interestingly, monodentate phosphine ligands such as triphenylphosphine, have been utilized on copper(I) complexes, along with bipyridine ligands (Figure 1.15).[44c] These complexes employ two monodentate phosphine ligands on the copper(I) metal center. $[Cu(bpy)(PPh_3)_2]^+$ and $[Cu(4\text{-}Mebpy)(PPh_3)_2]^+$ absorb in the visible region around 480 nm and do not emit. Curiously, $[Cu(bpy)(PPh_3)_2]^+$ and $[Cu(4\text{-}Mebpy)(PPh_3)_2]^+$ both exhibit an excited-state reduction and oxidation potential. These copper(I) complexes are mild photooxidants (~ +1.40 V vs. SCE) and photoreductants (~ -1.40 V vs. SCE). A major drawback for these copper(I) complexes has been the lack of dissociation or photodegradation experiments. In some phosphine-ligated transition metal complexes, dissociation of a phosphine ligand can initiate reactivity. If this were to happen when using $[Cu(bpy)(PPh_3)_2]^+$ or $[Cu(4\text{-}Mebpy)(PPh_3)_2]^+$ as photocatalysts, different mechanistic possibilities would have to be considered. Therefore, solution stability experiments with the addition of substrates would have to be analyzed before full consideration of using these copper(I) complexes as photocatalysts.

Many reports that are presented have been utilizing phosphine/bipyridine-based ligands on copper(I) metal centers. Recent efforts to shift away from this style of the complex have been vastly limited. Copper(I) complexes that strictly use bipyridine ligands have not been studied extensively for their photophysical properties but more for their catalytic qualities. With that said, $[Cu(dap)_2]^+$ has been extensively studied and utilized as a photocatalyst in many different transformations (Figure 1.18).[48] The photophysical properties of $[Cu(dap)_2]^+$ detail an

absorbance in the visible region (~ 380 nm), along with a long excited-state lifetime of 0.27 microseconds. Reiser and coworkers heavily explored the use of $[Cu(dap)_2]^+$ as a photocatalyst throughout the years.[44,49]

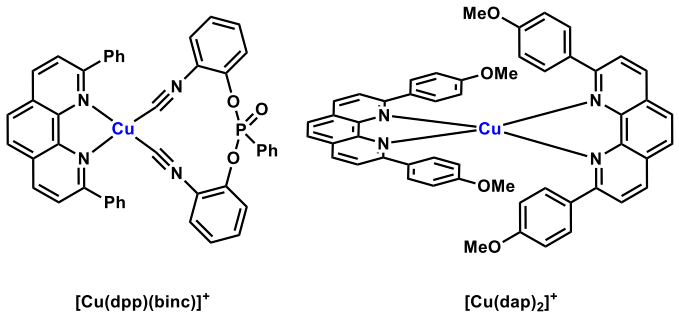

Figure 1.18. $[Cu(dap)_2]^+$ and $[Cu(dpp)(binc)]^+$ potential photocatalysts.

One of the more recent endeavors to not utilize phosphine ligands was presented by Reiser and coworkers. As previously mentioned, isocyanide-ligated chromium(0) and nickel(0) complexes have been reported. Luminescence of these complexes has only been reported at low temperatures, questioning their overall feasibility. With inspiration from Mann and coworkers,[50] Reiser and coworkers synthesized isocyanide ligated copper(I) complexes that absorbed mainly in the NUV region (350 nm).[51] $[Cu(dpp)(binc)]^+$ was isolated as a bench-stable copper(I) complex that was not prone to oxidation by molecular oxygen (Figure 1.18). The excited-state lifetime of the isocyanide copper(I) complex also was temperature-dependent; however, luminescence was seen at ambient temperature, resulting in a 17 μs excited-state lifetime. This differs from Cr(0) and Ni(0) examples, where only low-temperature luminescence occurs. The excited-state oxidation potential of $[Cu(dpp)(binc)]^+$ was calculated to be -1.88 V vs. SCE. $[Cu(dpp)(binc)]^+$ was able to participate as the photocatalyst in ATRA reactions with the addition of α-halomalonates across an alkene using visible light (Scheme 1.3). $[Cu(dpp)(binc)]^+$ was also examined as the photocatalyst in an allylation reaction with allyltrimethylsilane (Scheme 1.3).

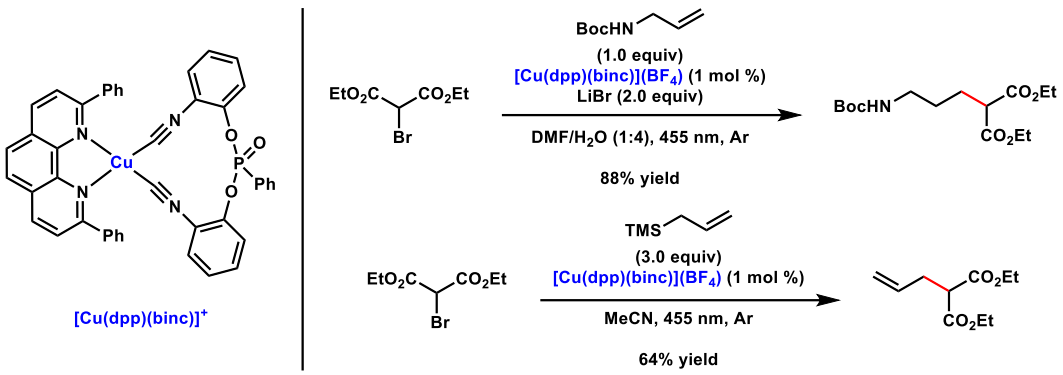

Scheme 1.3. ATRA photoreactions using $[Cu(dpp)(binc)]^+$.

1.4.3 Conclusions

Copper(I) complexes offer different options as potential photocatalysts. With the work described, the main recurring issue with complexes is the stability in a photocatalytic reaction. Most of the work with bidentate phosphine ligands overlooked dissociation, degradation, and photodegradation experiments. These experiments could provide crucial information in picking the correct copper(I) complex in a photocatalytic transformation. Until more is known about the inherent stability of the phosphine-derived copper(I) complexes in solution, they must be excluded from consideration in finding alternatives to ruthenium(II) and iridium(III) catalysts. Of the copper(I) complexes that are remaining, $[Cu(dap)_2]^+$ and $[Cu(dpp)(binc)]^+$ show the most promise as long-term solutions, with the only known issue of strictly being photoreductants. Their excited-state lifetimes and oxidation potentials are two of the key features in using these copper(I) complexes as photocatalysts. Given that $[Cu(dpp)(binc)]^+$ and $[Cu(dap)_2]^+$ have already been utilized in transformations across the literature, more research into understanding their barriers with functional groups and reactivity patterns is needed. Overall, $[Cu(dap)_2]^+$ and $[Cu(dpp)(binc)]^+$ could provide an alternative approach to photocatalysis in the near future.

1.5 Potential Photocatalysts using Zinc(II) Complexes

1.5.1 Introduction

Like copper(I) complexes, the zinc(II) ion has a d^{10} electron configuration which renders the metal-center excited state inaccessible. Most zinc(II) complexes have a high redox potential, which leads to excited-states localized on the ligands. These ligand-centered charge transfers are the driving force for zinc(II) complexes to participate in photocatalysis. Overall, the metal center acts as a Lewis acid and is electronically benign. Applications of zinc(II) complexes typically involve fluorescent materials. The use of zinc(II) complexes as potential photocatalysts are now only garnering attention. Table 1.4 outlines a series of zinc(II) complexes that have similar photophysical properties to ruthenium(II) and iridium(III) cases.

Complex	λ_{max} (nm)	λ_{em} (nm)	E^*_{red} (V vs. SCE)	E^*_{ox} (V vs. SCE)	Excited-state lifetime (μs)
$[Zn(N,O\text{-OPhOxZArH})_2]$	363	428	+1.05	-2.26	--
$[Zn(N,O\text{-OPhOxZArNMe}_2)_2]$	372	482	+0.51	-2.47	--
$[Zn(N,O\text{-OPhOxZArOMe})_2]$	369	440	+0.89	-2.26	--
$[Zn(N,O\text{-OPhOxZArCl})_2]$	362	423	+1.03	-2.18	--
$[Zn(N,O\text{-OPhOxZArCN})_2]$	326	416	+1.11	-2.14	--
$[Zn(N,O\text{-OPhOxZArF})_2]$	357	420	+1.11	-2.23	--
$[Zn(O\text{^}N_1)_2]$	364	445	+1.55	--	--
$[Zn(O\text{^}N_2)_2]$	344	434	+0.56	-0.72	--
$[Zn(O\text{^}N_3)_2]$	346	422	--	-1.62	--
[Zn(TPP)]	588	597,647	+0.96	-1.34	--
ZnPc	--	--	+0.95	-0.99	--
$[Zn_4(HQ)_6(OAc)_2]$	372	503	--	-2.25	--
$[Zn_2(OAc)_2(HQ)_2(MeOH)_2]$	361	534	--	-2.20	--
$[Zn(HQ)_2]Br$	365	497	--	-2.10	--
$[Zn(HQ)_2Br]HBr$	353	543	--	-1.98	--
$[Zn(sal_1)_2]$	422	518	--	-1.56	--
$[Zn(sal_2)_2]$	441	544	--	-1.46	--
$[Zn(sal_3)_2]$	409	496	--	-2.16	--
$[Zn(sal_4)_2]$	430	503	--	-1.81	--
$[Zn(pyr\text{-}1)_2]$	489	508	+0.73	-1.88	2.4
$[Zn(pyr\text{-}2)_2]$	639	655	+0.72	-1.21	5.8
$[Zn(pyr\text{-}3)_2]$	621	639	+0.37	-1.56	4.7
$[Zn(pyr\text{-}4)_2]$	658	673	+0.65	-1.20	--
$[Zn(pyr\text{-}5)_2]$	656	673	+0.38	-1.44	4.4

Table 1.4. Compilation of Zn(II) complexes for photocatalysis.

1.5.2 Zinc(II) Photocatalysts

Imine-derived ligands have been mentioned previously for different first-row transition metals in this discussion. Kang and coworkers developed a new class of oxazolylphenolate ligands with tunable electronics (Figure 1.19).[52] Kang and coworkers synthesized the corresponding tetrahedral zinc(II) complexes and analyzed their photophysical properties.

[Zn(*N*,*O*-OPhOxZArH)$_2$], [Zn(*N*,*O*-OPhOxZArNMe$_2$)$_2$], [Zn(*N*,*O*-OPhOxZArOMe)$_2$], [Zn(*N*,*O*-OPhOxZArCl)$_2$], [Zn(*N*,*O*-OPhOxZArCN)$_2$], [Zn(*N*,*O*-OPhOxZArF)$_2$] all absorb (326 – 372 nm) and emit (416 – 482 nm) in the visible region . A correlation between the photophysical properties and the electronics of the ligand was seen. A blue shift occurred in both the absorption and emission data with the addition of the electron withdrawing groups to the oxazolylphenolate ligands. Since all complexes absorb in the visible region, the tunability of the zinc(II) complexes becomes a real advantage. The excited-state redox potentials of zinc(II) complexes exhibit mild photooxidant (E^*_{red} = +0.51 to +1.11 V) and potent photoreductant (E^*_{ox} = -2.14 to -2.47 V) qualities. Another correlation between the electronics of the ligands and the excited-state redox potentials could also be drawn. Electron donating groups decrease the overall photooxidizing power while increasing the potency of the complex as a photoreductant. Applications of these zinc(II) complexes demonstrated that [Zn(*N*,*O*-OPhOxZArH)$_2$] displayed potential as a blue-emitting material in a multilayered device. These zinc(II) complexes have not been investigated as a photocatalyst yet.

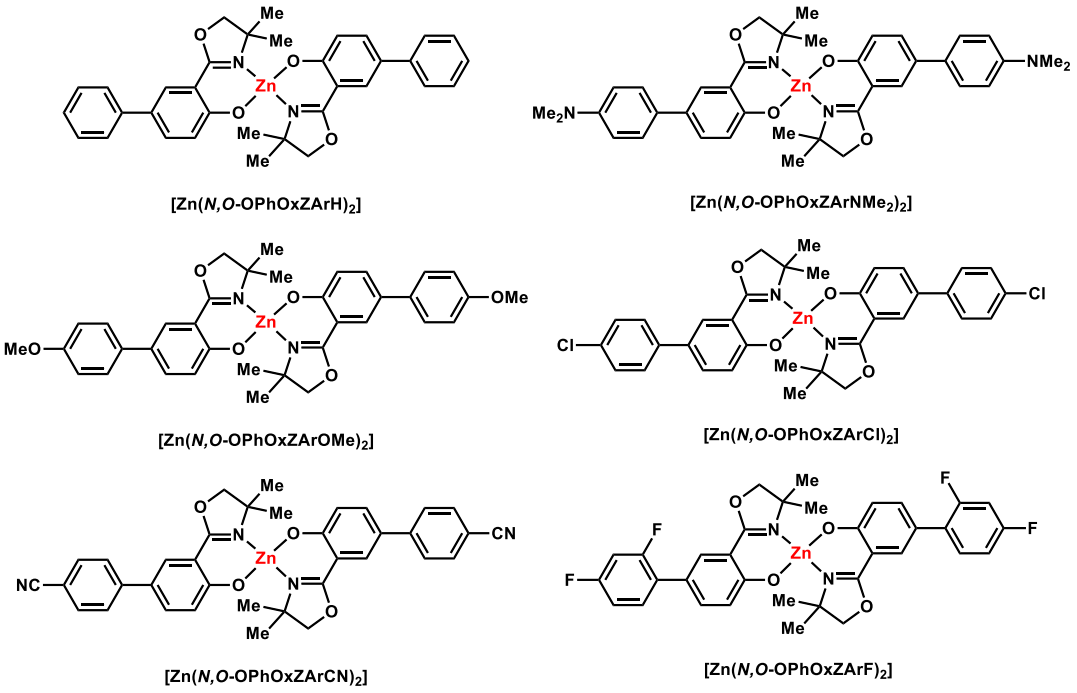

Figure 1.19. Oxazolylphenolate Zn(II) complexes.

Analogous to Kang's report, Zhang and coworkers reported a similar ligand construct. Instead of using the lone pair on the nitrogen of an oxazole to coordinate the zinc(II) metal center, Zhang reported using an imidazole-phenolate ligand system (Figure 1.20). Zhang and coworkers synthesized, isolated, and characterized [Zn(O^N$_1$)$_2$], [Zn(O^N$_2$)$_2$], and [Zn(O^N$_3$)$_2$] complexes. [Zn(O^N$_1$)$_2$], [Zn(O^N$_2$)$_2$], and [Zn(O^N$_3$)$_2$] complexes absorb (344 – 364 nm) and emit (422 – 445 nm) in the visible region.[53] An exciting correlation was noticed between the sizes of the substituent on the adjacent nitrogen atom. The larger the substituent, a blue shift in emission data was noticed, with [Zn(O^N$_3$)$_2$]'s λ_{max} being 422 nm, which is the most NUV emission wavelength for any complex outside of the cobalt(III) examples previously discussed. The excited-state redox potentials (E^*_{red} = +0.56 to +1.55 V and E^*_{ox} = -0.72 to -1.62 V) also displayed a similar trend. The larger the substituent on nitrogen, the excited-state reduction potential decreased, while the excited-state oxidation potential increased. Like Kang's zinc(II) complexes, Zhang's complexes were also subjected to applicational analysis but were not

analyzed as photocatalysts. Of the complexes investigated, [Zn(O^N$_3$)$_2$] showed the most promise as a blue-emitting device; however, all complexes should be analyzed in photoredox catalyzed reactions.

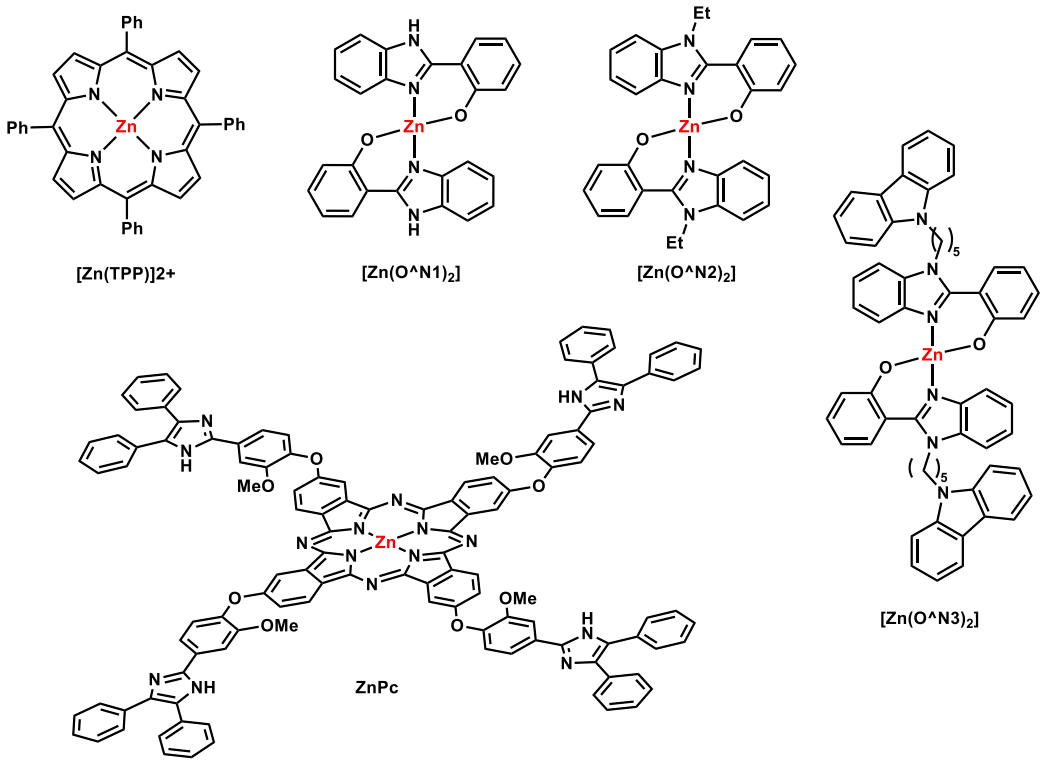

Figure 1.20. Other Zn(II) complexes for photocatalysis.

A ligand class that has not to be mentioned with other first-row transition metals is porphyrins. Many different first-row transition metal porphyrin complexes have been isolated; however, only [Zn(TPP)] has had its photophysical properties analyzed (Figure 1.20).[54] [Zn(TPP)] absorbs in the visible region, with a λ_{max} of 588 nm, and emits in the visible region at 597 and 647 nm wavelengths. The excited-state redox values indicate that [Zn(TPP)] is a mild photooxidant (E^*_{red} = +0.96 V) and photoreductant (E^*_{ox} = -1.34 V). As a photocatalyst, [Zn(TPP)] has been analyzed as the photocatalyst in a photoinduced electron transfer-reversible addition-fragmentation chain transfer radical polymerization reaction of trithiocarbonates with alkene derivatives.

In addition to TiOPc, which was discussed previously as another metalloporphyrin complex, other transition metals were investigated with the Pc-ligand system. Of those isolated, ZnPc showed characteristics of being a potential photocatalyst (Figure 1.20).[55] The absorbance and emission properties of ZnPc have not been measured; however, the excited-state redox potentials were. Both excited-state reduction and oxidation potentials characterize ZnPc as a mild photooxidant (E^*_{red} = +0.95 V) and photoreductant (E^*_{ox} = -0.99 V). That said, absorbance and emission values of ZnPc would be beneficial for gaining a complete profile of this potential photocatalyst.

Of all the zinc complexes that exhibit photocatalyst qualities, none are more unique than the structure and properties of $[Zn_4(HQ)_6(OAc)_2]$, $[Zn_2(OAc)_2(HQ)_2(MeOH)_2]$, $[Zn(HQ)_2]Br$, and $[Zn(HQ)_2Br]HBr$ (Figure 1.21).[56] Besides their different design, they also exhibit potentially interesting photophysical properties. $[Zn_4(HQ)_6(OAc)_2]$, $[Zn_2(OAc)_2(HQ)_2(MeOH)_2]$, $[Zn(HQ)_2]Br$, and $[Zn(HQ)_2Br]HBr$ absorb (353 – 372 nm) and emit (497 – 543 nm) in the visible region. These zinc(II) complexes are potent photoreductants (E^*_{ox} = -1.98 to -2.25 V). Structurally, these complexes have labile ligands. Since most zinc(II) complexes rely on the ligands for electron transfer to occur, the dissociation of the labile ligands could present an issue when screening for reactivity. Dissociation, degradation, and photodegradation experiments would need to be completed before even trying $[Zn_4(HQ)_6(OAc)_2]$, $[Zn_2(OAc)_2(HQ)_2(MeOH)_2]$, $[Zn(HQ)_2]Br$, and $[Zn(HQ)_2Br]HBr$ as photocatalysts.

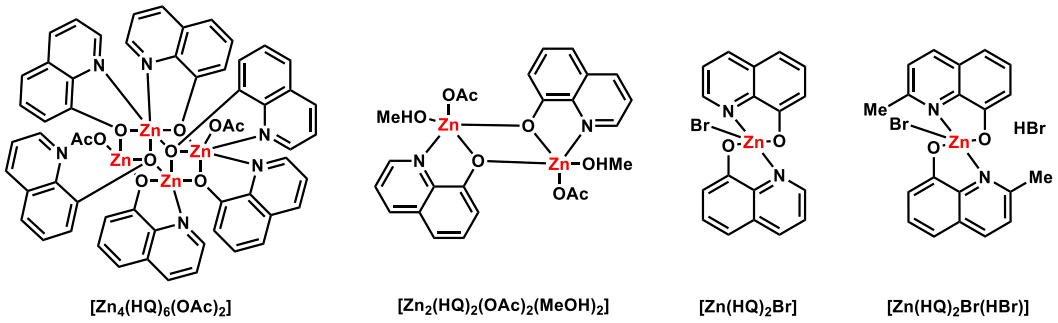

Figure 1.21. Unique potential Zn(II) or Zn(III) photocatalysts.

Metal salen complexes have grown in popularity throughout recent years; however, using a salen-ligated metal complex as a photocatalyst is underappreciated. Gazi and coworkers utilized salen ligand derivatives in 2017 with vanadium(V) metal-centers.[12] These Schiff-base ligated complexes have been shown to participate in C-C bond cleavage reactions. However, before Gazi's reported complexes, Su and coworkers had already reported zinc(II) complexes with similar Schiff-base ligands.[57] Su and coworkers' ligands were salen-derivatives with different π-systems on the imine. These π-systems have been known to have electron transfer capabilities.[58] Since the ligands on the zinc(II) complex are directly involved in the electron-transfer process, the Schiff-base salen derived ligands provide an opportunity for the zinc(II) complex to participate in photocatalysis (Figure 1.22). $[Zn(sal_1)_2]$, $[Zn(sal_2)_2]$, $[Zn(sal_3)_2]$, and $[Zn(sal_4)_2]$ all absorb (409 – 441 nm) and emit (496 – 544 nm) in the visible region. They all exhibit high excited-state oxidation potentials (E^*_{ox} = -1.46 to -2.16 V), making them potent photoreductants. A trend was seen with the addition of the naphthyl-derived salen ligand ($[Zn(sal_2)_2]$ and $[Zn(sal_4)_2]$). These complexes show a decrease in excited-state oxidation potentials in comparison to $[Zn(sal_1)_2]$ and $[Zn(sal_3)_2]$, which do not have the extra phenyl ring.

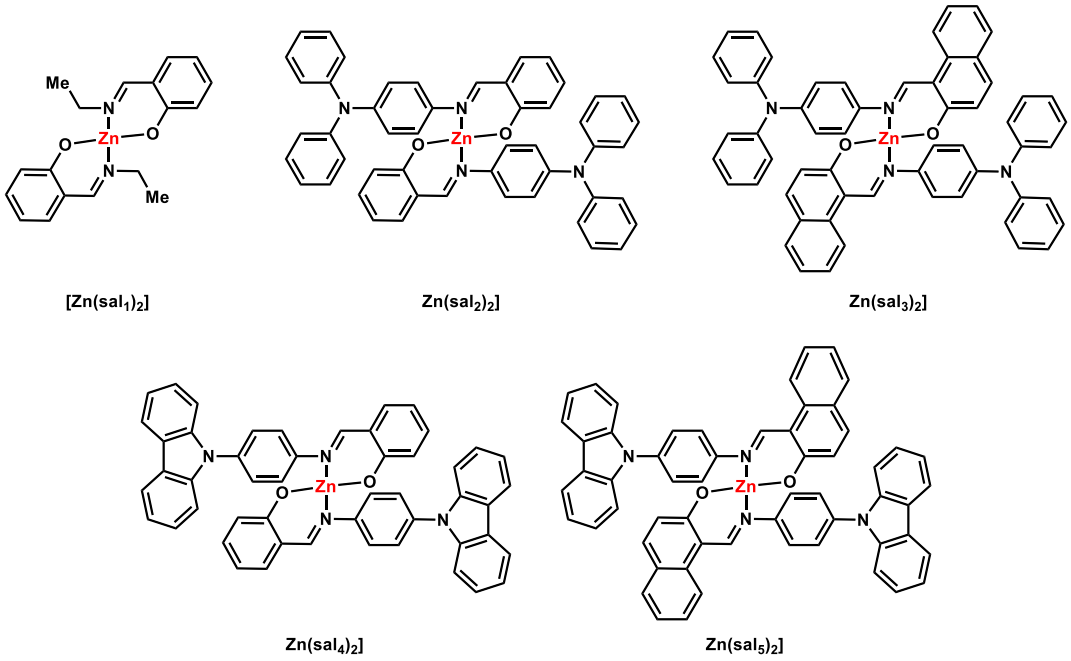

Figure 1.22. Salen-derived Zn(II) complexes.

Analogous to the porphyrin-derived zinc(II) complexes, dipyrrole-based ligands have also warranted investigation. Nishihara and coworkers report on new bis(dipyrrinato)zinc(II) complexes with unique photophysical properties and could make interesting photocatalysts (Figure 1.23).[59] [Zn(pyr-1)$_2$], [Zn(pyr-2)$_2$], [Zn(pyr-3)$_2$], [Zn(pyr-4)$_2$], and [Zn(pyr-5)$_2$] are disymmetric complexes, which have been previously proposed to increase photophysical capabilities.[60] The absorbance of these zinc(II) complexes is in the visible to NIR region (489 – 658 nm) and are very powerful light absorbers. They also emit (508 – 673 nm) in the visible region and are mild photooxidants (E^*_{red} = +0.37 to +0.73 V) and strong photoreductants (E^*_{ox} = -1.20 to -1.88 V). The addition of the methoxy groups in the ligand caused a decrease in the excited-state reduction potential but increased the excited-state oxidation potential. These complexes exhibit ideal characteristics for a photocatalyst and do not display any dissociation in nonpolar solvents.

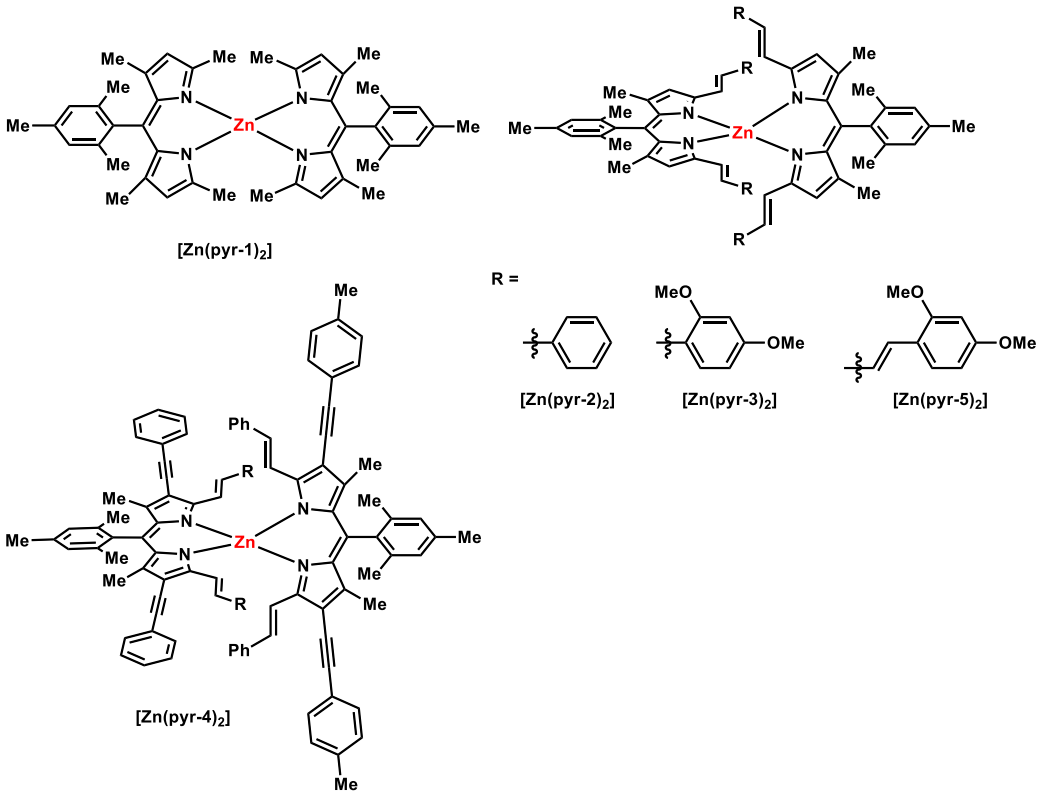

Figure 1.23. Dipyrrole-based Zn(II) complexes.

1.5.3 Conclusions

Zinc(II) photocatalysis is an ever-expanding area of research. The design and synthesis of new zinc(II) complexes with ligand systems that can then participate in electron transfer is becoming increasingly popular within the community. Since the ligands are engaging in the electron-transfer process, the photophysical properties of the ligands themselves should be analyzed. Zinc is one of the most abundant first-row transition metals and would provide a valuable alternative to classical catalysts. Most of the characterization of zinc(II) complexes is complete, and the search for their use as photocatalysts should remain the utmost priority.

1.6 Conclusions

Potential photocatalysts using complexes of first-row transition metals is a vast area of research. Complexes of every first-row transition metal with photophysical properties have been reported. Since they are academia's standard, attempting to replace ruthenium(II) and iridium(III) photocatalysts will be extremely difficult; however, four first-row transition metals offer viable solutions. Chromium(III), iron(II), copper(I), and zinc(II) complexes all have the characteristics to suggest that they could usurp ruthenium(II) and iridium(III) as standard photocatalysts. Chromium(III) should be investigated as an alternative photooxidant since the Cr(IV) oxidation state is unknown. The excited-state reduction potentials of chromium(III) complexes can be tuned accordingly. Overall, investigations into utilizing chromium(III) as a photocatalyst are underwhelming and warrant more scientific study. Iron(II), copper(I), and zinc(II) all share similar photophysical properties. Most of these complexes have both excited-state reduction and oxidation potentials. That said, only copper(I) photocatalysis has been thoroughly investigated. Iron(II) photocatalysis has started becoming a more prominent area of research; however, it is still somewhat limited. The use of zinc(II) complexes as photocatalysts has never been investigated and could provide a unique niche within the photocatalysis community. Due to limited resources, transitioning from ruthenium(II) or iridium(III) photocatalysts to a more prudent choice of chromium(III), iron(II), copper(I), or zinc(II) photocatalysts could represent a novel approach in the ever-expanding field of photocatalysis.

1.7 References and Notes

[1] For reviews on photoredox catalysis see: a) Prier, C. K.; Rankic, D. A.; MacMillan, D. W. C. *Chem. Rev.* **2013**, *113*, 5322-5363 b) Stephenson, C. R. J. *Chem. Soc. Rev.* **2011**, *40*, 102-113. c) Romero, N. A.; Nicewicz, D. A. *Chem. Rev.* **2016**, *116*, 10075-10166.

[2] a) Fagnoni, M.; Dondi, D.; Ravelli, D.; Albini, A. *Chem. Rev.* **2007**, *107*, 2725-2746. b) Xi, Y.; Yi, H.; Lei, A. *Org. Biomol. Chem*. **2013**, *11*, 2387-2403.

[3] a) Ikezawa, H.; Kutal, C.; Yasufuku, K.; Yamazaki, H. *J. Am. Chem. Soc.* **1986**, *108*, 1589-1594. b) Wrighton, M.; Markham, J. *J. Phys. Chem.* **1973**, *77*, 3042-3044. c) Islangulov, R. R.; Castellano, F. N. *Angew. Chem., Int. Ed.* **2006**, *45*, 5957-5959.

[4] For reviews on earth-abundant photocatalysis see: a) Larsen, C. B.; Wenger, O. S. *Chem. Eur. J*. **2018**, *24*, 2039-2058. b) Wenger, O. S. *J. Am. Chem. Soc.* **2018**, *140*, 13522-13533. c) Hockin, B. M.; Li, C.; Robertson, N.; Zysman-Colman, E. *Catal. Sci. Technol*. **2019**, *9*, 889-915.

[5] Fujishima, A.; Rao, T. N.; Tryk, D. A. *J. Photochem. Photobiol. C* **2000**, *1*, 1-21.

[6] Mühldorf, B.; Wolf, R. *Chem. Commun.* **2015**, *51*, 8425-8428.

[7] Pfennig, B. W.; Thompson, M. E.; Bocarsly, A. B. *Organometallics* **1993**, *12*, 649-655.

[8] For reviews on heterogenous metal-doped TiO_2 materials see: a) Khlyustova, A.; Sirotkin, N.; Kusova, T.; Kraev, A.; Titov, V.; Agafonov, A. *Mater. Adv.* **2020**, *1*, 1193-1201. b) Kumeravel, V.; Mathew, S.; Bartlett, J.; Pillai, S. C. *Appl. Catal. B* **2019**, *144*, 1021-1064. c) Di Paola, A.; Ikeda, S. Marci, G.; Ohtani, B.; Palmisano, L. *Int. J. Photoenergy* **2001**, *3*, 171-176.

[9] Akçay, H. T.; Bayrak, R.; Demirbas, U.; Koca, A.; Kantekin, H.; Degirmencioglu, I. *Dye Pigm.* **2013**, *96*, 483-494.

[10] a) Tau, P.; Nyokong, T. *Polyhedron* **2006**, *25*, 1802-1810. b) Silver, J.; Lukes, P.; Hey, P.; Ahmet, M. T. *J. Mater. Chem.* **1991**, *1*, 881-888.

[11] Zhang, Y.; Peterson, J. L.; Milsmann, C. *J. Am. Chem. Soc.* **2016**, *138*, 13115-13118.

[12] Gazi, S.; Dokic, M.; Moeljadi, A. M. P.; Ganguly, R.; Hirao, H.; Soo, H. S. *ACS Catal.* **2017**, *7*, 4682-4691.

[13] Marek, I. *Chem. Rev.* **2021**, *121*, 1-2.

[14] Choing, S. N.; Francis, A. J.; Clendenning, G.; Schuurman, M. S.; Sommer, R. D.; Tamblyn, I.; Weare, W. W.; Cuk, T. *J. Phys. Chem. C* **2015**, *119*, 17029-17038.

[15] a) Stevenson, S. M.; Shores, M. P.; Ferreira, E. M. *Angew. Chem. Int. Ed.* **2015**, *127*, 6606-6610. b) Stevenson, S. M.; Higgins, R. F.; Shores, M. P.; Ferreira, E. M. *Chem. Sci.* **2017**, *8*, 654-660. c) Sarabia, F. J.; Ferreira, E. M. *Org. Lett.* **2017**, *19*, 2865-2868. d) Sarabia, F. J.; Li, Q.; Ferreira, E. M. *Angew. Chem. Int. Ed.* **2018**, *57*, 11015-11019.

[16] Serpone, N.; Jamieson, M. A.; Henry, M. S.; Hoffman, M. Z.; Bolletta, F.; Maestri, M. *J. Am. Chem. Soc.* **1979**, *101*, 2907-2916.

[17] Young, R. C.; Nagle, J. K.; Meyer, T. J.; Whitten, D. G. *J. Am. Chem. Soc.* **1978**, *100*, 4773-4778.

[18] McDaniel, A. M.; Tseng, H.-W.; Damrauer, N. H.; Shores, M. P. *Inorg. Chem.* **2010**, *49*, 7981-7991.

[19] Otto, S.; Grabolle, M.; Förster, C.; Kreitner, C.; Resch-Genger, U.; Heinze, K. *Angew. Chem. Int. Ed.* **2015**, *54*, 11572-11576.

[20] Jiménez, J.-R.; Doistau, B.; Besnard, C.; Piguet, C. *Chem. Commun.* **2018**, *54*, 13228-13231.

[21] Gall, B. K.; Morrison, T.; Shores, M. P.; Ferreira, E. M. *Manuscript in Preparation.*

[22] Gall, B. K.; Smith, A. K.; Ferreira, E. M. *Manscript in Preparation.*

[23] McDaniel, A. M.; Tseng, H.-W.; Hill, E. A.; Damrauer, N. H.; Rappé, A. K.; Shores, M. P. *Inorg. Chem.* **2013**, *52*, 1368-1378.

[24] Ramasami, T.; Endicott, J. F.; Brubaker, G. R. *J. Phys. Chem.* **1983**, *87*, 5057-5059.

[25] Comba, P.; Creaser, I. I.; Gahan, L. R.; Harrowfield. J. M.; Lawrance, G. A.; Martin, L. L.; Mau, A. W. H.; Sargeson, A. M.; Sasse, W. H. F.; Snow, M. R. *Inorg. Chem*. **1986**, *25*, 384-389.

[26] Brown, K. N.; Beue, R. J.; Sargeson, A. M.; Moran, G.; Ralph, S. F.; Reisen, H. *Chem. Commun.* **1998**, 2291-2292.

[27] Büldt, L. A.; Guo, X.; Vogel, R.; Prescimone, A.; Wenger, O. S. *J. Am. Chem. Soc.* **2017**, *139*, 985-992.

[28] Sharma, N.; Jung, J.; Ohkubo, K.; Lee, Y.-M.; El-Khouly, M. E.; Nam, W.; Fukuzumi, S. *J. Am. Chem. Soc.* **2018**, *140*, 8405-8409.

[29] Chábera P.; Kjaer, K. S.; Prakash, O.; Honarfar, A.; Liu, Y.; Fredin, L. A.; Harlang, T. C. B.; Lidin, S.; Uhlig, J.; Sundström, V.; Lomoth, R.; Persson, P.; Wärnmark, K. *J. Phys. Chem. Lett*. **2018**, *9*, 459–463.

[30] a) Palmer, R. A.; Piper, T. S. *Inorg. Chem.* **1966**, *5*, 864-878. b) Van Meter, F. M.; Neumann, H. M. *J. Am. Chem. Soc*. **1976**, *98*, 1382-1388.

[31] Parisien-Collette, S.; Hernandez-Perez, A. C.; Collins, S. K. *Org. Lett.* **2016**, *18*, 4994-4997.

[32] Huynh, H. V. *Chem. Rev*. **2018**, *118*, 9457-9492.

[33] Liu, Y.; Harlang, T.; Canton, S.; Charbera, P. Suárez-Alcántara, K; Fleckhaus, A.; Vithanage, D. A.; Göransson, E.; Corani, A.; Lomoth, R.; Sundström, V.; Wärnmark, K. *Chem. Commun.* **2013**, *49*, 6412-6414.

[34] Zimmer, P.; Burkhardt, L.; Freidrich, A.; Steube, J.; Neuba, A.; Schepper, R.; Müller, P.; Flörke, U.; Huber, M.; Lockbrunner, S.; Bauer, M. *Inorg. Chem.* **2018**, *57*, 360-373.

[35] Zhang, J.; Campolo, D.; Dumur, F.; Xiao, P.; Fouassier, J. P.; Gigmes, D.; Lalevée, J. *ChemCatChem* **2016**, *8*, 2227-2233.

[36] Pal, A. K.; Li, C.; Hanan, G. S.; Zysman-Colman, E. *Angew. Chem. Int. Ed.* **2018**, *57*, 8027-8031.

[37] Saracini, C.; Malik, D. D.; Sankaralingam, M.; Lee, Y.-M.; Nam, W.; Fukuzumi, S. *Inorg. Chem.* **2018**, *57*, 10945-10952.

[38] Welin, E. R.; Le, C.; Arias-Rotondo, D. M.; McCusker, J. K.; MacMillan, D. W. C. *Science* **2017**, *355*, 380-384.

[39] Grübel, M.; Bosque, I.; Altmann, P. J.; Bach, T.; Hess, C. R. *Chem. Sci.* **2018**, *9*, 3313-3317.

[40] a) Büldt, L. A.; Larsen, C. B.; Wenger, O. S. *Chem. Eur. J.* **2017**, *23*, 8577-8580. b) Büldt, L. A.; Wenger, O. S. *Dalton Trans*. **2017**, *46*, 15175-15177.

[41] Marion, R.; Sguerra, F.; Di Meo, F.; Sauvegeot, J.-F.; Daniellou, R.; Renaud, J.-L.; Linares, M.; Hamel, M.; Gaillard, S. *Inorg. Chem.* **2014**, *53*, 9181-9191.

[42] Moudam, O.; Kaesar, A.; Delavaux-Nicot, B.; Duhayon, C.; Holler, M.; Accorsi, G.; Armaroli, N.; Séguy, I.; Navarro, J.; Destruel, P.; Nierengarten, J.-F. *Chem. Commun.* **2007**, 3077-3079.

[43] Kaesar, A.; Moudam, O.; Accorsi, G.; Séguy, I.; Navarro, J.; Belbakra, A.; Duhayon, C.; Armaroli, N.; Delavaux-Nicot, B.; Nierengarten, J.-F. *Eur. J. Inorg. Chem.* **2014**, 1345-1355.

[44] a) Xiao, P.; Dumur, F.; Zhang, J. Fouassier, J. P.; Gigmes, D.; Lalevée, J. *Macromolecules* **2014**, *47*, 3837-3844. b) Mejia, E.; Luo, S. P.; Karnahl, M.; Friedrich, A.; Tschierlei, S.; Surkus, A. E.; Junge, H.; Gladiali, S.; Lochbrunner, S.; Beller, M. *Chem. Eur. J.* **2013**, *19*, 15972-15978. c) Andrés-Tomé, I.; Fyson, J.; Baiao Dias, F.; Monkman, A. P.; Iacobellis, G.; Coppo, P. *Dalton Trans.* **2012**, *41*, 8669-8674. d) Zhang, Y.; Heberle, M.; Wächtler, M.; Karnahl, M.; Dietzek, B. *RSC Adv*. **2016**, *6*, 105801-105805. e) Pirtsch, M.; Paria, S.; Matsuno, T.; Isobe, H.; Reiser, O. *Chem. Eur. J.* **2012**, *18*, 7336-7340. f) Cuttell, D. G.; Kuang, S. M.; Fanwick, P. E.; McMillin,

D. R.; Walton, R. A. *J. Am. Chem. Soc.* **2002**, *124*, 6-7. g) Michelet, B.; Deldaele, C.; Kajouj, S.; Moucheron, C.; Evano, G. *Org. Lett.* **2017**, *19*, 3576-2579.

[45] Wang, B.; Shelar, D. P.; Han, X. Z.; Li, T. T.; Guan, X.; Lu, W.; Liu, K.; Chen, Y.; Fu, F.; Che, C. M. *Chem. Eur. J.* **2015**, *21*, 1184-1190.

[46] Femoni, C.; Muzzioli, S.; Palazzi, A.; Stagni, S.; Zacchini, S.; Monti, F.; Accorsi, G.; Bolognesi, M.; Armaroli, N.; Massi, M.; Valenti, G.; Marcaccio, M. *Dalton Trans.* **2013**, *42*, 997-1010.

[47] Bizzarri, C.; Strabler, C,; Prock, J.; Trettenbrein, B.; Ruggenthaler, M.; Yang, C. H.; Polo, F.; Iordache, A.; Brüggeller, P.; De Cola, L. *Inorg. Chem.* **2014**, *53*, 10944-10951.

[48] Kern, J.-M.; Sauvage, J.-P. *J. Chem. Soc., Chem. Commun.* **1987**, 546-548.

[49] a) Knorn, M.; Rawner, T.; Czerwieniec, R.; Reiser, O. *ACS Catal* **2015**, *5*, 5186-5193. b) Paria, S.; Pirtsch, M.; Kais, V.; Reiser, O. *Synthesis* **2013**, *45*, 2689-2698. c) Bagal, D. B.; Kachkovskyi, G.; Knorn, M.; Rawner, T.; Bhanage, B. M.; Reiser, O. *Angew. Chem. Int. Ed.* **2015**, *54*, 6999-7002. d) Rawner, T.; Knorn, M.; Lutsker, E.; Hossain, A.; Reiser, O. *J. Org. Chem*. **2016**, *81*, 7139-7147. f) Pagire, S. K.; Paria, S.; Reiser, O. *Org. Lett.* **2016**, *18*, 2106-2109.

[50] Smith, C. S.; Mann, K. R. *J. Am. Chem. Soc*. **2012**, *134*, 8786-8789.

[51] Knorn, M.; Rawner, T.; Czerwieniec, R.; Reiser, O. *ACS Catal*. **2015**, *5*, 5186-5193.

[52] Son, H.-J.; Han, W.-S.; Chun, J.-Y.; Kang, B.-K.; Kwon, S.-N.; Ko, J.; Han, S. J.; Le, C.; Kim, S. J.; Kang, S. O. *Inorg. Chem*. **2008**, *47*, 5666-5676.

[53] Xu, H.; Xu, Z.-F.; Yue, Z.-Y.; Yan, P.-F.; Wang, B.; Jia, L.-W.; Li, G. M.; Sun, W.-B.; Zhang, J.-W. *J. Phys. Chem. C* **2008**, *112*, 15517-15525.

[54] Shanmugan, S.; Xu, J.; Boyer, C. *J. Am. Chem. Soc.* **2015**, *137*, 9174-9185.

[55] Akçay, H. T.; Bayrak, R.; Demirbas, U.; Koca, A.; Kantekin, H.; Degirmencioglu, I. *Dyes Pigm.* **2013**, *96*, 483-494.

[56] Janghouri, M.; Mohajerani, E.; Amini, M. M.; Majafi, E. *J. Lumin.* **2014**, *154*, 465-474.

[57] Xie, Y.-Z.; Shan, G.-G.; Zhou, Z.-Y.; Su, Z.-M. *Dyes Pigm.* **2013**, *96*, 467-474.

[58] For selected papers on aminium photocatalysts see: a) Bellville, D. J.; Wirth, D. D.; Bauld, N. L. *J. Am. Chem. Soc.* **1981**, *103*, 718-720. b) Pabon, R. A.; Bellville, D. J.; Bauld, N. L. *J. Am. Chem. Soc.* **1983**, *105*, 5158-5159. c) Bauld, N. L.; Bellville, D. J.; Gardner, S. A.; Migron, Y.; Cogswell, G. *Tetrahedron Lett.* **1982**, *23*, 825-828. d) Ghosh, S.; Bauld, N. L. *J. Catal.* **1985**, *95*, 300-304. e) Bauld, N. L.; Bellville, D. J.; Pabon, R.; Chelsky, R.; Green, G. *J. Am. Chem. Soc.* **1983**, *105*, 2378-2382. f) Lorenz, K. T.; Bauld, N. L. *J. Am. Chem. Soc.* **1987**, *109*, 1157-1160. g) Bauld, N. L. *Tetrahedron* **1989**, *45*, 5307-5363.

[59] Sakamoto, R.; Iwasima, T.; Kögel, J. F.; Kusaka, S.; Yasutaka, M.; Kitagawa, Y.; Nishihara, H. *J. Am. Chem. Soc.* **2016**, *138*, 5666-5677.

[60] a) Kusaka, S.; Sakamoto, R.; Kitagawa, Y.; Okumura, M.; Nishihara, H. *Chem. Asian J.* **2012**, *7*, 907−910. b) Kusaka, S.; Sakamoto, R.; Nishihara, H. *Inorg. Chem.* **2014**, *53*, 3275−3277.

CHAPTER 2

DESIGN, SYNTHESIS, AND PHOTOPHYSICAL ANALYSIS OF NEW CHROMIUM(III) PHOTOCATALYSTS

2.1 Introduction

In 1979, Serpone and co-workers investigated bipyridyl and phenanthroline-derived chromium(III) complexes for their photophysical properties (Figure 2.1).[1] Most importantly toward use in photocatalysis, Serpone and co-workers analyzed the excited-state behaviors of these chromium(III) complexes. The excited-state lifetimes of the chromium(III) compounds were two to three times longer (*vide infra*) when compared to analogous ruthenium(II) complexes. Substitution on the ligands of the chromium(III) complex greatly affected the absorbance and redox potentials, shifting absorbance up to 50 nm. The addition of electron withdrawing groups on the ligands saw a red-shift occur in the overall absorbance of the chromium(III) complex from 455 nm to 466 nm. Given these advantages, synthetic chemists interested in photoredox catalysis could potentially utilize the ligand tunability of these complexes in the search for new photocatalysts and reaction methodology. The addition of phenyl substituents in Serpone and co-workers' chromium(III) complexes shifted the absorption from 458 nm to 484 nm. Lastly, chromium(III) complexes were stable in acidic media with no substitution or ligand loss. This stability of the chromium(III) complexes, along with the photophysical properties, make them

ideal candidates for photocatalysts. These chromium(III) complexes laid the foundation for the future of chromium(III) photocatalysis.

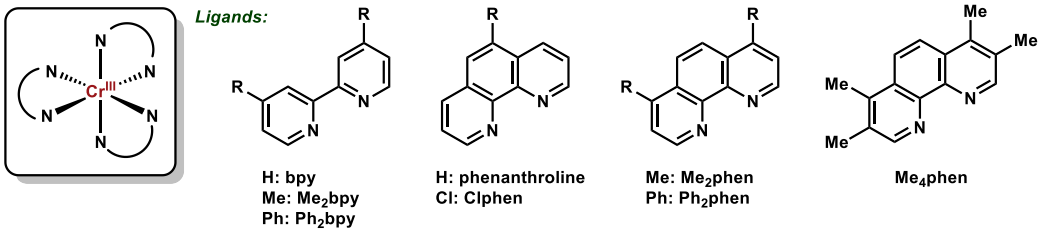

Figure 2.1. Cr(III) polypyridyl complexes studied by Serpone.

Just over a decade ago, McDaniel and co-workers started investigating the photophysical properties of related homo- and heteroleptic chromium(III) complexes (Figure 2.2).[2] It is worth noting that previous syntheses ligand scrambling was observed upon activation of the chromium metal center.[3] Once synthesized and characterized, the photophysical properties of the homo- and heteroleptic chromium(III) complexes could be analyzed. All homo- and heteroleptic chromium(III) complexes absorb in the near-UV (NUV) to visible regions (398 – 491 nm). Typically, a red-shift in absorbance occurs upon the addition of electron withdrawing and electron donating groups to a compound.[4] Another photophysical property analyzed was the excited-state lifetime of these complexes. The excited-state lifetimes exhibited a reverse trend in comparison to the absorbance (*vide infra*). The addition of the electron withdrawing groups on the ligands of the chromium(III) complexes decreased the excited-state lifetime (*vide infra*). The longest excited-state lifetime was $[Cr(Ph_2phen)_3]^{3+}$, which exhibited a lifetime of 425 μs. With the decrease in excited-state lifetimes comes an increase in excited-state reduction potential. Homoleptic $[Cr(dmcbpy)_3]^{3+}$ has the highest excited-state reduction potential, making it a potent photooxidant. The removal of the electron withdrawing groups sees the excited-state reduction potentials of the chromium(III) complexes decrease. Degradation of these complexes was also not

noted in acidic media, making McDaniel's chromium(III) complexes potentially useful as photosensitizers.

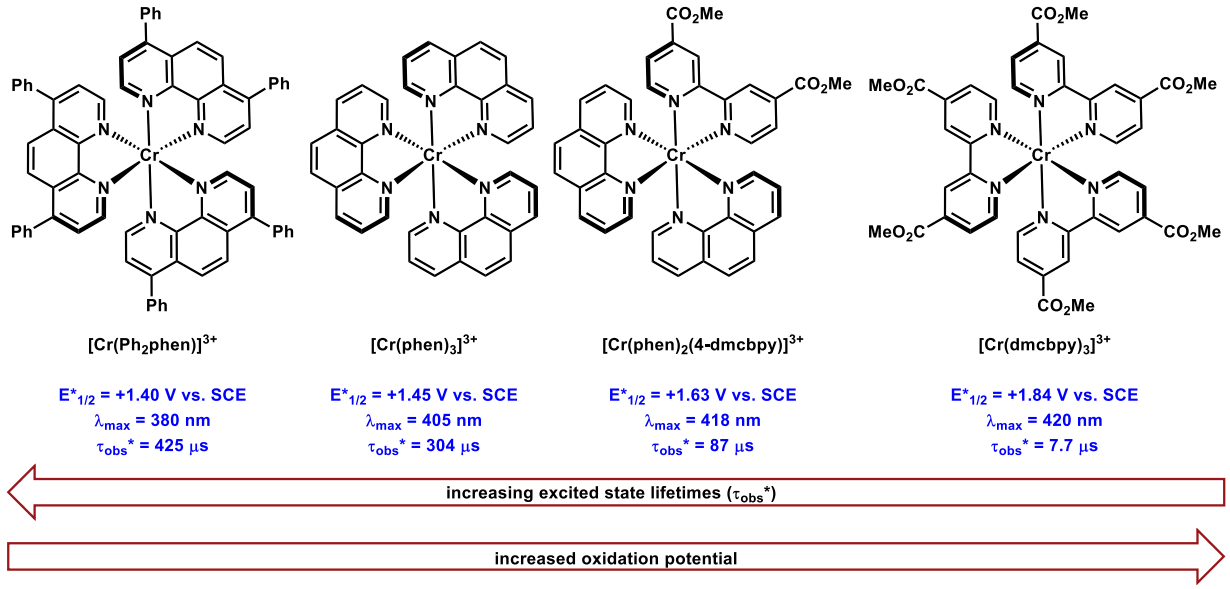

Figure 2.2. Selected Cr(III) complexes from McDaniel and co-workers.

To utilize McDaniel's chromium(III) complexes as a proof of concept, in 2015 our group reported the use of bipyridyl and phenanthroline-derived chromium(III) complexes as photocatalysts in a radical-cation Diels-Alder reaction via a single-electron transfer (SET) process (Scheme 2.1).[5] Using NUV light, along with catalytic $[Cr(Ph_2phen)_3]^{3+}$, these reactions proceeded to the desired (4+2) cycloadducts open to the air. The scope of the transformation showed the need for an electron donating group on the alkene and was also determined to be stereoconvergent. Mixtures of cis- and trans-alkenes only yielded anti cyclohexene products. In comparison to Yoon's results[6] with $[Ru(bpz)_3]^{2+}$ (up to 98% yields in under 2 h), $[Cr(Ph_2phen)_3]^{3+}$ provided similar yields, differentiating only by reaction times. To our knowledge, this was the first report using a chromium(III) complex as a photocatalyst for a synthetic transformation.

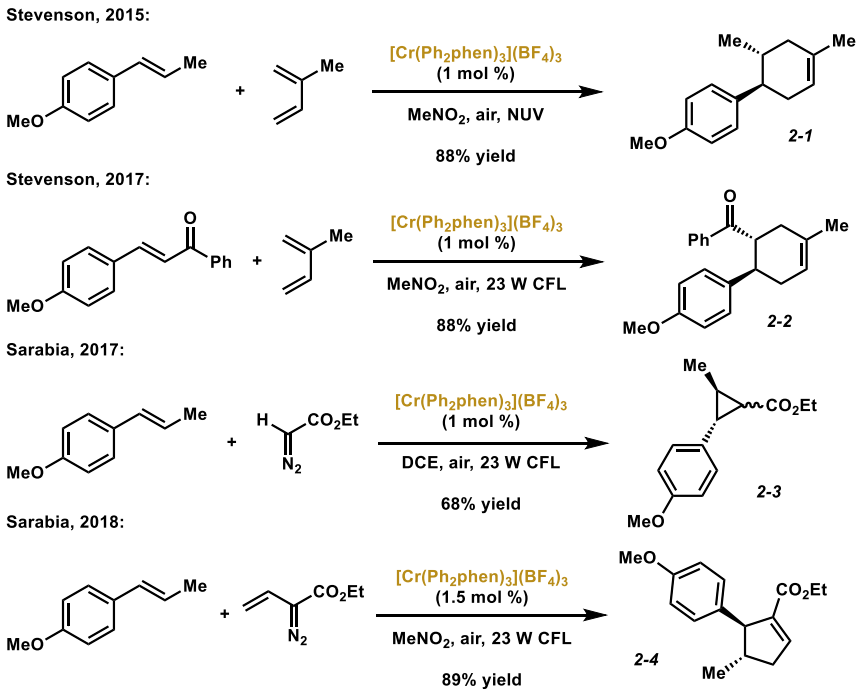

Scheme 2.1. Cr(III)-photocatalyzed transformations.

The proposed mechanism of Stevenson's reported (4+2) cycloaddition was studied further by Higgins and co-workers and is illustrated in Figure 2.3.[7] Irradiation of [Cr^{3+}] generated the excited-state species, [*Cr^{3+}], which has an excited-state reduction potential of +1.40 V vs. SCE, and can oxidize *trans*-anethole (E_{ox} = +1.10 V vs. SCE). The resulting radical-cation alkene can react with isoprene, creating the radical-cation (4+2) product **2-5**. Previously, Stevenson and co-workers proposed two different quenching pathways, using either [Cr^{2+}] to oxidize back to [Cr^{3+}] or another equivalent of *trans*-anethole in a radical chain process. Upon further examination, Higgins and co-workers suggest two operable pathways, with the favored pathway depicted. Despite a low quantum yield, a radical chain pathway was still possible; however, an oxygen-mediated reaction mechanism was determined. Singlet oxygen ($^1O_2$) oxidized [Cr^{2+}] to [Cr^{3+}] and generated superoxide (O_2^-) as a result. Superoxide then provides the electron needed to yield (4+2) cycloadduct **2-1** from radical-cation **2-6** and triplet oxygen ($^3O_2$). The excited-state quench of [*Cr^{3+}] to the ground state [Cr^{3+}] complex can react with $^3O_2$ and form singlet oxygen ($^1O_2$) in the

process. These dual cycles both contribute to the overall formation of the desired (4+2) cycloadduct.

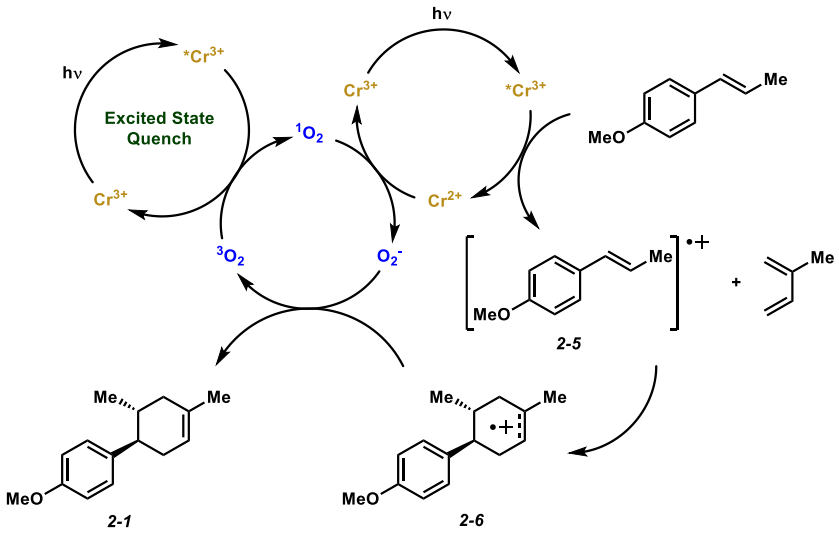

Figure 2.3. Proposed mechanism for the (4+2) photocatalyzed Diels-Alder reaction.

Stevenson and co-workers reported a (4+2) cycloaddition with electron deficient alkenes using chromium(III) photocatalysis (Scheme 2.1).[8] The (4+2) cycloaddition with electron deficient alkenes proceeds with visible light. Many functional groups were tolerated, with chalcone derivatives providing the best results. Higgins and co-workers determined that the mechanism of this reaction relied on an energy transfer process from the chromium(III) complex to facilitate a vinylcyclobutane rearrangement, affording the desired (4+2) cycloadduct.[9] Our group followed this up with a report with (2+1)[10] and (3+2)[11] cycloaddition reactions using electron rich alkenes and different diazo species (Scheme 2.1). Diazoesters reacted with the radical-cation intermediate to form the desired (2+1) cyclopropane products, while vinyl diazoacetates reacted to form the (3+2) cyclopentene products. Both of these transformations relied on the electron rich alkene; however, different diazo species were well tolerated.

2.2 Experimental Design

In 2013, the Catalysis Collaboratory for Light-activated Earth Abundant Reagents (C-CLEAR) was formed to develop photocatalysts from earth-abundant metals. Typical photocatalysts are ruthenium(II)- or iridium(III)- based, which are precious metals. Designing photocatalysts from earth-abundant metals, such as Cr[12], Fe[13], Cu[14], or Zn[15], has been a popular area of research over the past few years. Our group has been focused on developing methods using chromium(III) complexes as photocatalysts. As previously discussed, we have developed two different (4+2) cycloaddition reactions, a (2+1) cyclopropanation and a (3+2) cyclopentene-forming reaction.

There are a few drawbacks to using chromium(III) photocatalysis. The need for an electron rich substrate that can be easily oxidized is a significant hurdle for reactivity. Nitrogen-based substrates such as imines are unreactive in typical Diels-Alder conditions because of the potential oxidation of the nitrogen moiety. Reaction times in chromium(III)-photocatalyzed conditions are also typically longer. In comparison with $[Ru(bpz)_3]^{2+}$ in the electron rich Diels-Alder reaction, $[Cr(Ph_2phen)_3]^{3+}$ was considerably slower for almost all comparable substrates.[6] This phenomenon can also be seen in the (3+2) cycloaddition reaction. In an attempt to expand chromium(III) photocatalysis and close the gap on ruthenium(II)- and iridium(III)- based photocatalysts, we synthesized a series of new new chromium(III) photocatalysts (Figure 2.4).

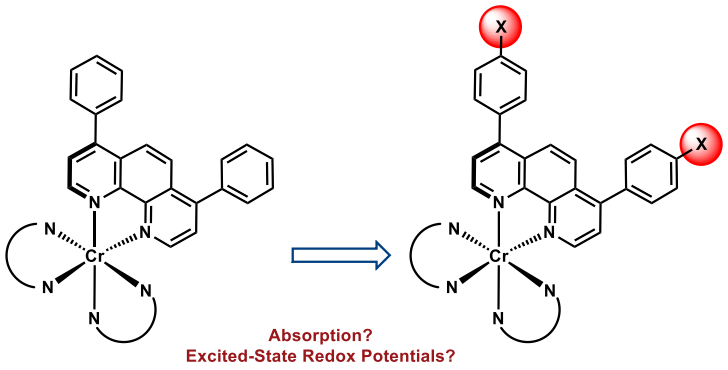

Figure 2.4. Changing ligand electronics on bathophenanthroline.

The photocatalyst that our group has utilized for different synthetic transformations has been $[Cr(Ph_2phen)_3]^{3+}$. The electrochemical and photophysical properties of $[Cr(Ph_2phen)_3]^{3+}$ have been extensively studied.[2] Understanding these properties, the addition of electronically different groups to the ligands could change the catalyst's characteristics. Most importantly, the absorbance, excited-state redox potentials, and excited-state lifetimes could all change. The addition of electron withdrawing groups in homoleptic chromium(III) complexes exhibited a noticeable trend. With this knowledge, we theorized that the addition of electron withdrawing or electron donating groups to the bathophenanthroline ligands would change the photophysical properties and potentially lead to the development of a comprehensive chromium(III) photocatalyst.

2.3 Ligands and Catalyst Synthesis

In 2006, Altman and Buchwald published a useful synthesis of 4,7-dichloro-1,10-phenanthroline (Scheme 2.2).[16] Starting from Meldrum's acid and 1,2-diaminobenzene, a series of three scalable steps produces 4,7-dichloro-1,10-phenanthroline in good yield. Suzuki coupling of aryl boronic acids with 4,7-dichloro-1,10-phenanthroline creates a series of electronically different ligands. Electron donating and electron withdrawing groups were added to the extended

phenyl ring. The naphthyl derivative adds an extended π-system that could facilitate electron transfer from π-stacking interactions with potential aryl substrates.

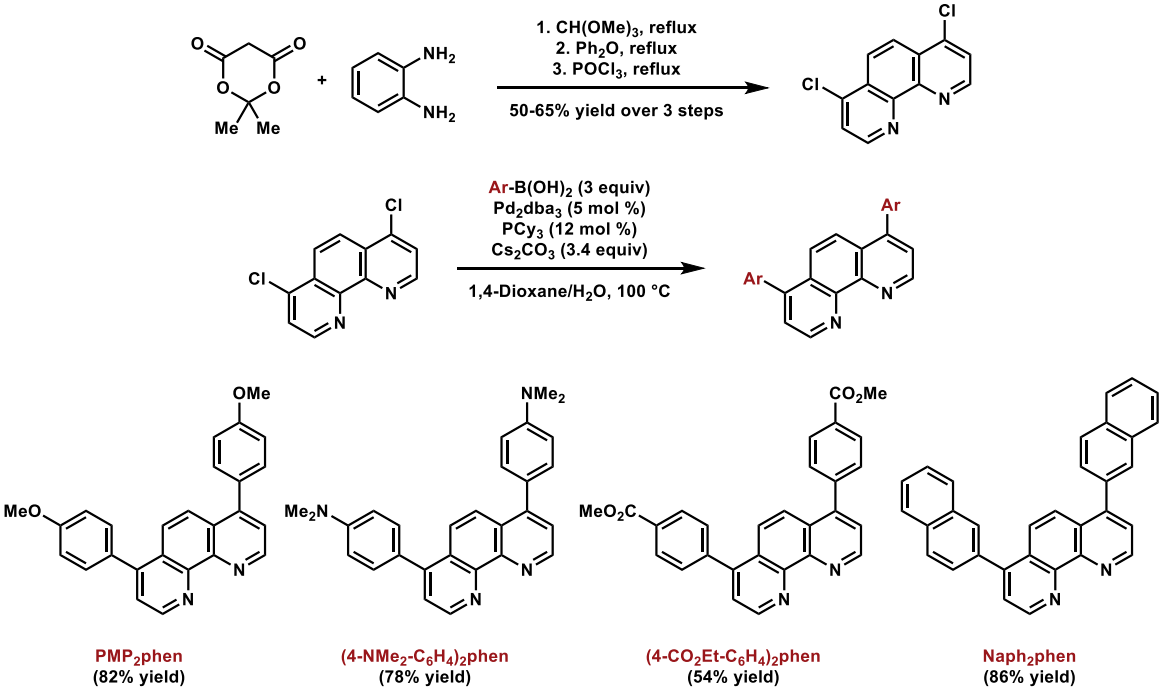

Scheme 2.2. Bathophenanthroline-derived ligands synthesized.

With the ligands synthesized, the chromium(II) precatalyst, $[Cr(NCCH_3)_4](BF_4)_2$, was synthesized from Cr(0) powder in two steps (Scheme 2.3).[17] $[Cr(NCCH_3)_4](BF_4)_2$ is extremely air-sensitive and must be handled in an argon-filled glovebox. The addition of the synthesized ligands and $AgBF_4$ generates the desired chromium(III) complexes. These complexes are best used after recrystallization from acetonitrile/diethyl ether. Images of the different chromium(III) complexes in solution can be seen in Figure 2.5.

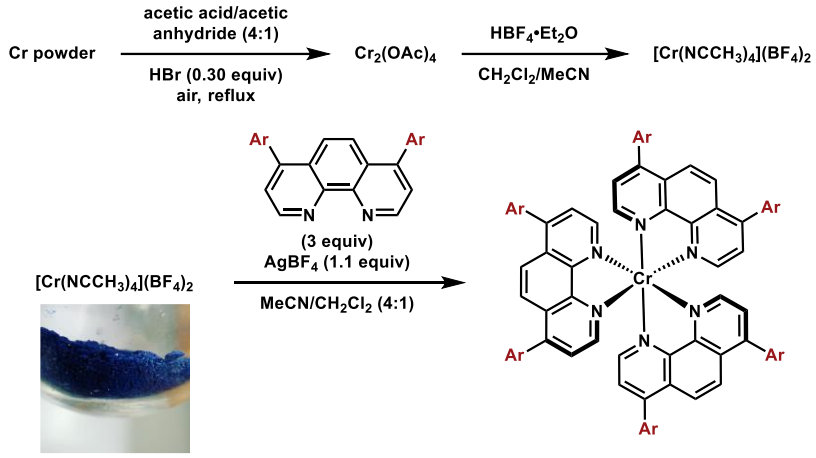

Scheme 2.3. Cr(III) complexes synthesized.

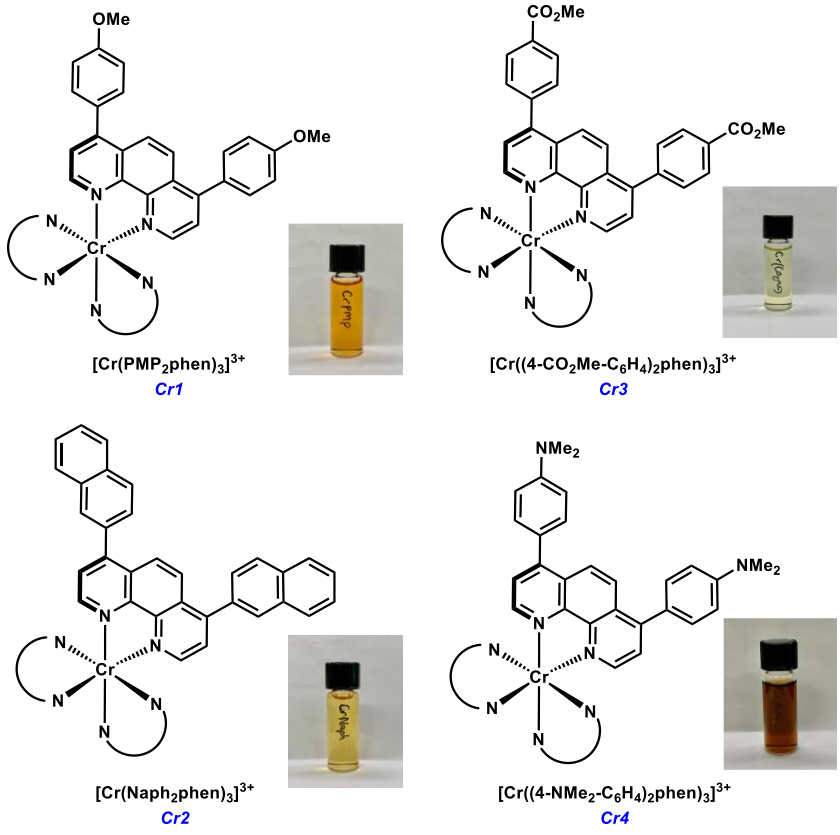

Figure 2.5. Cr(III) photocatalysts in solution.

2.4 Photophysical Properties of New Cr(III) Complexes

Once synthesized, the photophysical and electrochemical properties of each photocatalyst were investigated. Initially, the absorbance of each complex was analyzed in MeCN (Figure 2.6).

Each complex absorbs in the visible region, with $[Cr((4\text{-}NMe_2\text{-}C_6H_4)_2phen)_3](BF_4)_3$ having the highest λ_{max} at ~650 nm. Upon further investigation, the potential for ligand loss and complex degradation was prevalent, so other solvents were analyzed. Each complex and the corresponding ligand were dissolved in acetonitrile, dichloromethane, or tetrahydrofuran, and the absorbance were measured (Figures 2.7-2.10). If the absorption spectrum of the catalyst was identical to the analogous ligand, we assumed potential dissociation of the ligands had occurred. The only catalyst that showed potential ligand loss was $[Cr(Naph_2phen)_3](BF_4)_3$. Investigations into the absorption properties of the ligands and catalysts are currently ongoing by collaborators at Colorado State University.

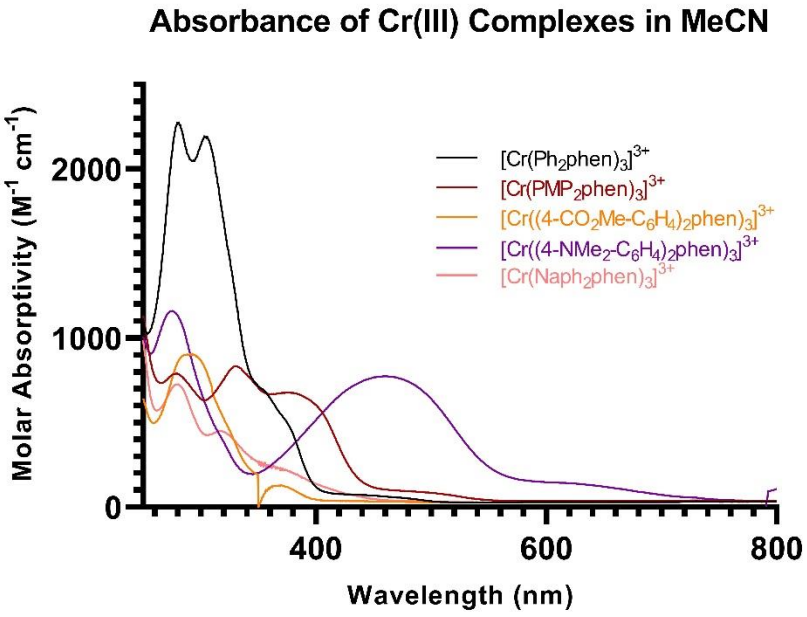

Figure 2.6. Absorbance of the Cr(III) complexes in acetonitrile at 0.001 M.

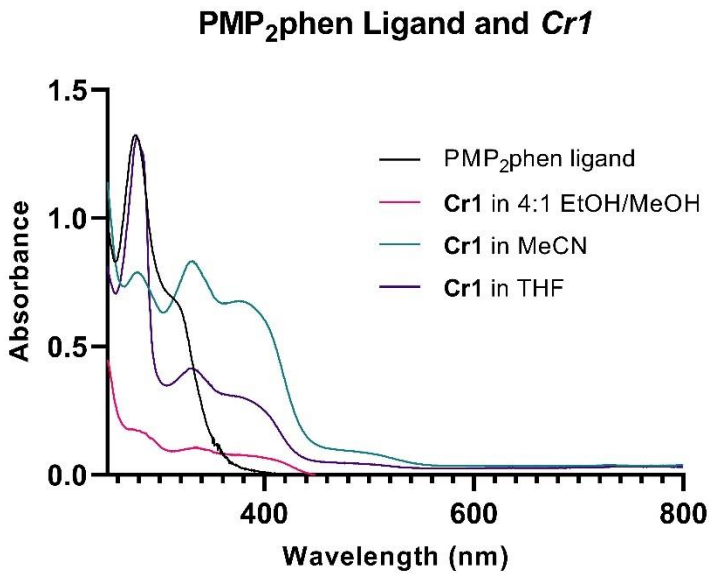

Figure 2.7. PMP_2phen ligand and catalyst (**Cr1**) in various solvent at 0.001 M.

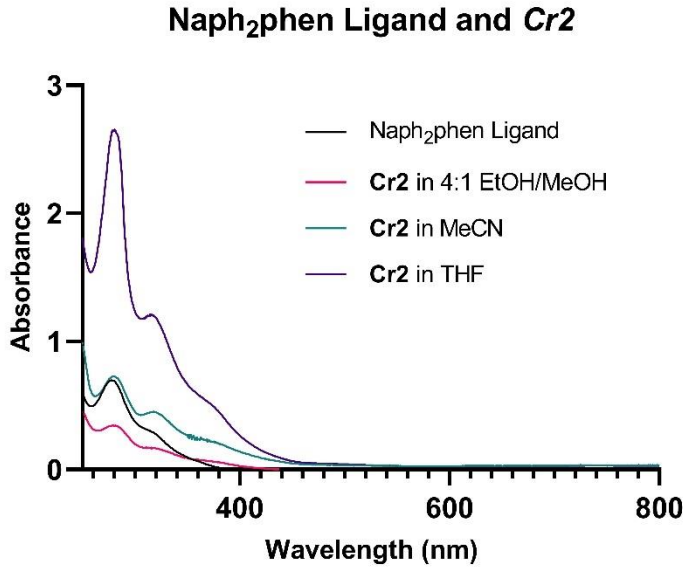

Figure 2.8. $Naph_2$phen ligand and catalyst (**Cr2**) in various solvents at 0.001 M.

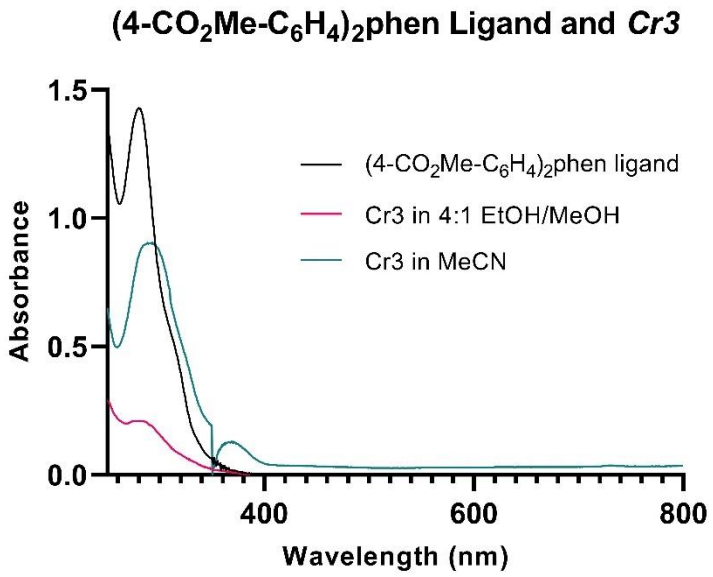

Figure 2.9. (4-CO_2Me-C_6H_4)$_2$phen ligand and catalyst (**Cr3**) in various solvents at 0.001 M.

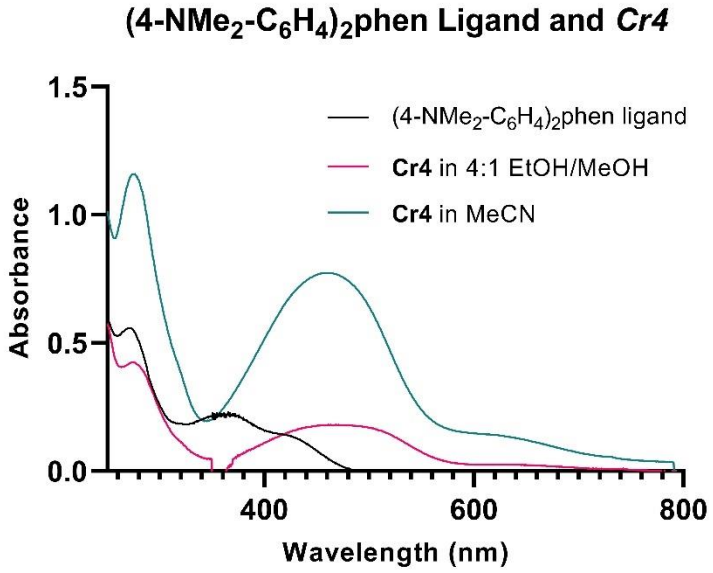

Figure 2.10. (4-NMe_2-C_6H_4)$_2$phen ligand and catalyst (**Cr4**) in various solvents at 0.001 M.

To simulate a photoreaction, the absorbance of [Cr(Ph_2phen)$_3$](BF_4)$_3$ and [Cr(PMP_2phen)$_3$](BF_4)$_3$ was measured over time while being irradiated with a 23 W CFL bulb in acetonitrile or dichloromethane (Figures 2.11-2.13). The resulting data showed that dissociation is not prevalent with either complex under simulated conditions. Due to the vast difference in

irradiated versus non-irradiated samples, investigations of $[Cr(PMP_2phen)_3](BF_4)_3$ to understand this phenomenon are ongoing by collaborators.

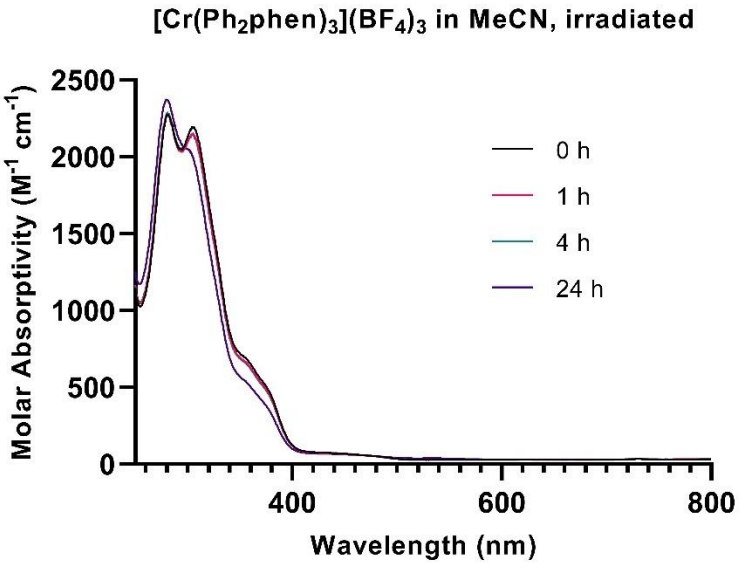

Figure 2.11. $[Cr(Ph_2phen)_3](BF_4)_3$ dissociation experiments in MeCN at 0.001 M.

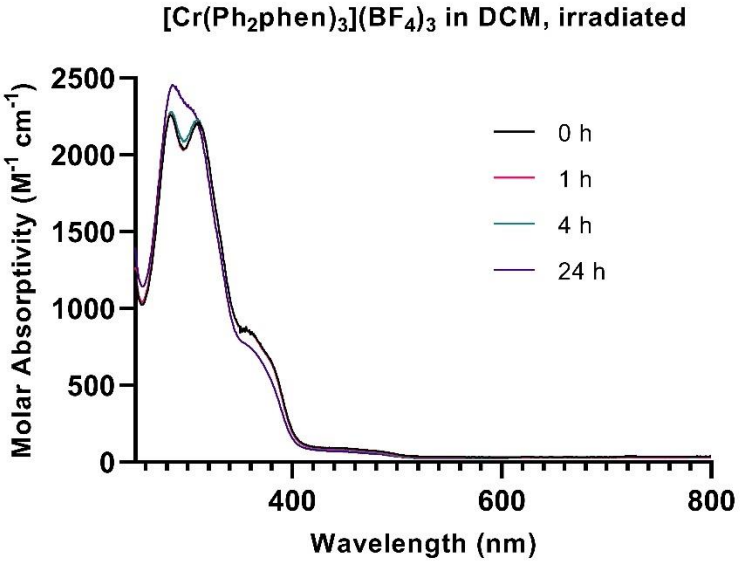

Figure 2.12. $[Cr(Ph_2phen)_3](BF_4)_3$ dissociation experiments in DCM 0.001 M.

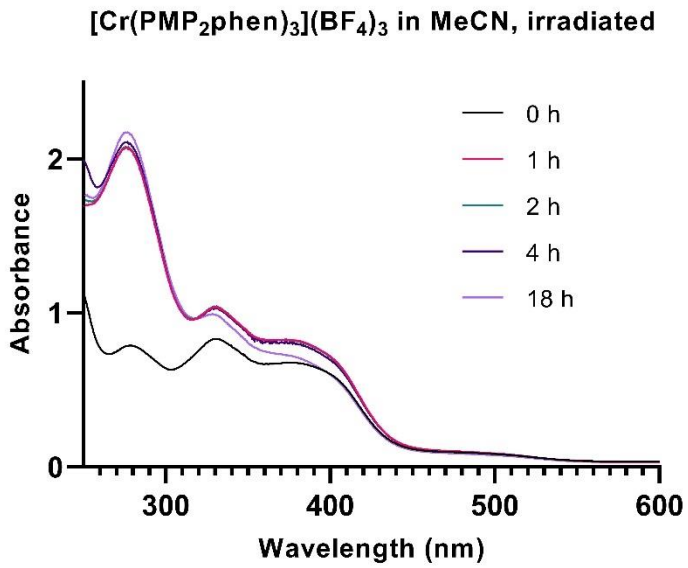

Figure 2.13. $[Cr(PMP_2phen)_3](BF_4)_3$ dissociation experiments in MeCN 0.001 M.

Of the new tris-homoleptic chromium(III) complexes synthesized, $[Cr(PMP_2phen)_3](BF_4)_3$, $[Cr(Naph_2phen)_3](BF_4)_3$, and $[Cr((4\text{-}CO_2Me\text{-}C_6H_4)_2phen)_3](BF_4)_3$ are emissive at room temperature following electronic excitation. Emission spectra for these complexes, shown in Figure 2.14, are measured in thoroughly deoxygenated acetonitrile following excitation at various wavelengths. The emission λ_{max} is needed for the calculation of the excited-state redox potentials for these complexes.

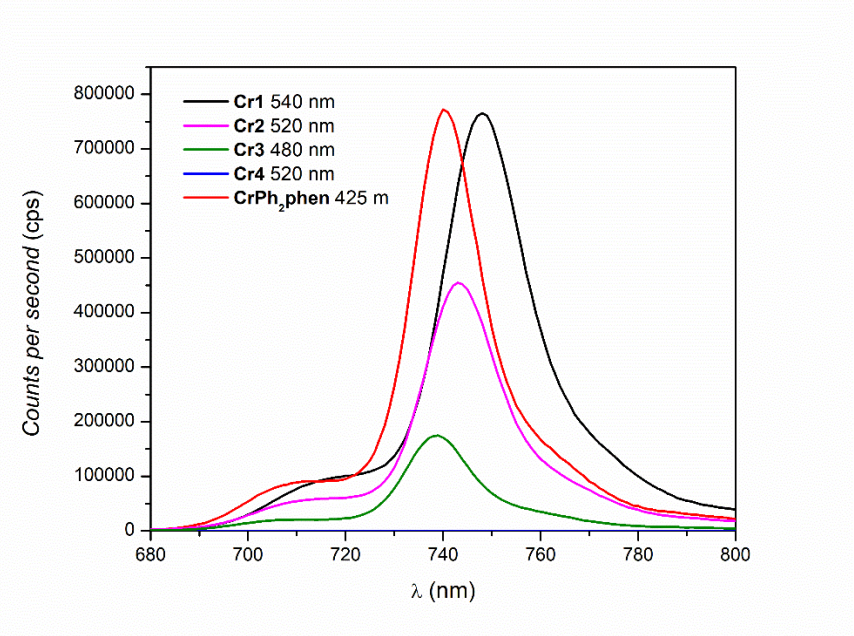

Figure 2.14. Emission data for Cr(III) complexes. **Cr1** = $[Cr(PMP_2phen)_3](BF_4)_3$; **Cr2** = $[Cr(Naph_2phen)_3](BF_4)_3$; **Cr3** = $[Cr((4\text{-}CO_2Me\text{-}C_6H_4)_2phen)_3](BF_4)_3$; **Cr4** = $[Cr((4\text{-}NMe_2\text{-}C_6H_4)_2phen)_3](BF_4)_3$ (did not emit, trace is on baseline); **CrPh$_2$phen** = $[Cr(Ph_2phen)_3](BF_4)_3$.

Along with the emission data, the second critical component for determining the excited-state redox potentials is determining the ground state $Cr^{III/II}$ and $Cr^{IV/III}$ redox couples (Table 2.1). Each of these complexes exhibits at least three reversible $1e^-$ reductions in acetonitrile. The $Cr^{IV/III}$ couples for these complexes are not observed due to being outside the acetonitrile oxidation window. The ground-state redox potentials for each chromium(III) complex can be seen in Table 2.2.

$$E_{00} = E_0 + (\Delta v)^2/16k_BT \ln (2) \qquad (1)$$

Using equation 1, the ΔG stored in the excited state (E_{00}) can be calculated and are seen for each of the catalysts where E_0 = λ_{max} of emission data, Δv = width of the vibronic transition, k_B = Boltzmann's constant, and T = temperature in K. The excited-state reduction potentials were then calculated using E_{00} and the ground state redox potentials for Cr(3+/2+) using equation 2 and can be seen in Table 2.2.

$$E_{1/2}(Cr^{*III/II}) = E_{00} + E_{1/2}(Cr^{III/II}) \qquad (2)$$

$[Cr((4\text{-}NMe_2\text{-}C_6H_4)_2phen)_3](BF_4)_3$ does not emit, most likely from the dimethylamino groups quenching the emission; therefore, the excited-state reduction potential could not be calculated. The excited stat

Complex	Solvent	3+/2+	2+/1+	1+/0	0/1-	1-/2-	2-/3-	3-/4-
$[Cr(Ph_2phen)_3](BF_4)_3$	MeCN	-0.69	-1.13	-1.64	-2.09	-2.32		
$[Cr(PMP_2phen)_3](BF_4)_3$	MeCN	-0.74	-1.17	-1.55	-1.63	-2.23		
$[Cr((4\text{-}CO_2Me\text{-}C_6H_4)_2phen)_3](BF_4)_3$	MeCN	-0.63	-1.05	-1.31	-1.50	-1.90	-2.06	-2.27
$[Cr((4\text{-}NMe_2\text{-}C_6H_4)_2phen)_3](BF_4)_3$	MeCN	-0.90	-1.31	-1.55	-1.80			
$[Cr(Naph_2phen)_3](BF_4)_3$	MeCN	-0.68	-1.12	-1.36	-1.51	-2.28		

Table 2.1. Ground-state redox potentials for Cr(III) complexes.

Previously, McDaniel noticed a trend between the electronics on the ligands of chromium(III) homo- and heteroleptic complexes and their excited-state reduction potential and absorbance. In the chromium(III) complexes that we have synthesized, a similar trend is seen (Table 2.2). The addition of the electron donating methoxy group makes the complex less oxidizing, therefore decreasing the excited-state reduction potential, which is consistent with McDaniel's trend. The inverse is seen with the addition of an electron withdrawing group on the ligand, which makes the complex more oxidizing and increases the excited-state reduction potential. The addition of either an electron withdrawing or electron donating group exhibits a red-shift in absorbance, which is also consistent within the literature.[4] The addition of the extra phenyl group in $[Cr(Naph_2phen)_3](BF_4)_3$ did not change the excited-state reduction potential in comparison to $[Cr(Ph_2phen)_3](BF_4)_3$.

Complex	*3+/2+
$[Cr(Ph_2phen)_3](BF_4)_3$	+1.401
$[Cr(PMP_2phen)_3](BF_4)_3$	+1.325
$[Cr(Naph_2phen)_3](BF_4)_3$	+1.395
$[Cr((4\text{-}NMe_2\text{-}C_6H_4)_2phen)_3](BF_4)_3$	--
$[Cr((4\text{-}CO_2Me\text{-}C_6H_4)_2phen)_3](BF_4)_3$	+1.454

Table 2.2. Excited-state reduction potentials of Cr(III) complexes.

To further characterize these complexes, the excited-state lifetimes would have to be explored. Due to the 2020 COVID pandemic, the possibility to work with our collaborators and acquire this data did not happen. For further understanding of these complexes, this data should be obtained. We would assume that a similar trend to McDaniel's report would be seen. The addition of the electron donating groups would increase the excited-state lifetimes, while the electron withdrawing groups would exhibit a decrease. Increased excited-state lifetimes give the catalyst a better chance to react within a photoreaction.

2.5 Reaction Comparisons

To determine whether these chromium(III) complexes were compatible photocatalysts, we subjected the series to our previously developed chromium(III) photocatalyzed cycloaddition reactions. With these photoreactions, a baseline was set by using the parent catalyst of $[Cr(Ph_2phen)_3](BF_4)_3$ and a ruthenium baseline catalyst of $[Ru(bpz)_3](PF_6)_2$. Each complex was analyzed as the photocatalyst within the reaction. In the case of electron rich olefins, *trans*-anethole and isoprene were reacted with visible light and photosensitizer. $[Cr(Ph_2phen)_3](BF_4)_3$ and $[Ru(bpz)_3](PF_6)_2$ both catalyzed the reaction to the (4+2) cycloadduct **2-1** in 84% and 98% yield in 24 h and 30 min, respectively (Scheme 2.4, entries 1 and 2). The $[Ru(bpz)_3](PF_6)_2$ was consistent with Yoon's previous report. $[Cr(PMP_2phen)_3](BF_4)_3$ gave the cycloadduct in 89% yield in just 2 h, a significant decrease in reaction time from the $[Cr(Ph_2phen)_3](BF_4)_3$ result (Scheme 2.4, entry 3). Since we were aiming to close the large gap between chromium(III) and ruthenium(II) photocatalysts, $[Cr(PMP_2phen)_3](BF_4)_3$ gives a compelling result toward this generalized goal. $[Cr((4\text{-}CO_2Me\text{-}C_6H_4)_2phen)_3](BF_4)_3$ was sluggish in the reaction, with a 69% yield in 24 h (Scheme 2.4, entry 4), while $[Cr((4\text{-}NMe_2\text{-}C_6H_4)_2phen)_3](BF_4)_3$ did not yield the

desired cycloadduct in 24 h (Scheme 2.4, entry 5). $[Cr(Naph_2phen)_3](BF_4)_3$ also increased reactivity in relation to the parent catalyst, affording **2-1** in a 92% yield in 7 h (Scheme 2.4, entry 6).

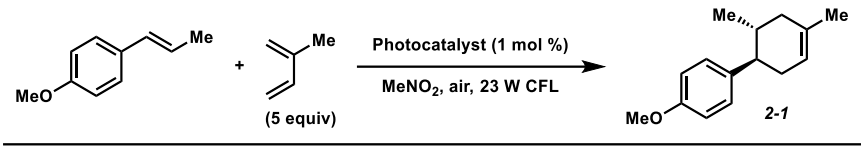

Entry	Photocatalyst	Time (h)	NMR yield
1	$[Cr(Ph_2phen)_3)][(BF_4)_3$	24	84%
2	$[Ru(bpz)_3](PF_6)_2$	0.5	98%
3	$[Cr(PMP_2phen)_3](BF_4)_3$	2	89%
4	$[Cr((4\text{-}CO_2Me\text{-}C_6H_4)_2phen)_3](BF_4)_3$	24	69%
5	$[Cr((4\text{-}NMe_2\text{-}C_6H_4)_2phen)_3](BF_4)_3$	24	0%
6	$[Cr(Naph_2phen)_3](BF_4)_3$	7	92%

Scheme 2.4. (4+2) Cycloaddition reaction with electron rich dienophiles.

With electron deficient dienophiles, 4-methoxychalcone and isoprene were used as model substrates. The benchmarks of $[Cr(Ph_2phen)_3](BF_4)_3$ and $[Ru(bpz)_3](PF_6)_2$ afforded (4+2) cycloadduct **2-2** in 81% yield in 3 h and 55% yield in 6 h, respectively (Scheme 2.5, entries 1 and 2). $[Cr(PMP_2phen)_3](BF_4)_3$ furnishes **2-2** in 30 min with a 92% yield (Scheme 2.5, entry 3). $[Cr(PMP_2phen)_3](BF_4)_3$ outcompetes the parent catalyst and the Ru(II) benchmarks. Again, $[Cr((4\text{-}CO_2Me\text{-}C_6H_4)_2phen)_3](BF_4)_3$ was sluggish in the reaction with a 51% yield in 24 h (Scheme 2.5, entry 4), while $[Cr((4\text{-}NMe_2\text{-}C_6H_4)_2phen)_3](BF_4)_3$ did not yield the cycloadduct (Scheme 2.5, entry 5). $[Cr(Naph_2phen)_3](BF_4)_3$ exhibited longer reaction times than $[Cr(Ph_2phen)_3](BF_4)_3$ and $[Ru(bpz)_3](PF_6)_2$, but increased the overall yield of the reaction (Scheme 2.5, entry 6).

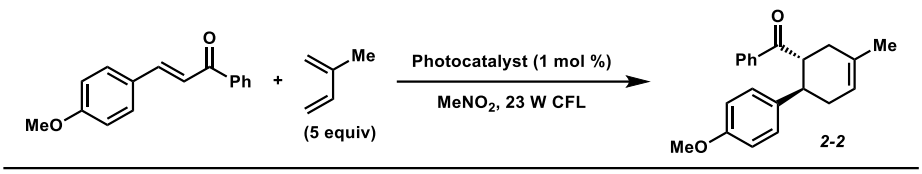

Entry	Photocatalyst	Time (h)	% yield
1	$[Cr(Ph_2phen)_3](BF_4)_3$	3	81
2	$[Ru(bpz)_3](PF_6)_2$	6	55
3	$[Cr(PMP_2phen)_3](BF_4)_3$	0.5	92
4	$[Cr((4\text{-}CO_2Me\text{-}C_6H_4)_2phen)_3](BF_4)_3$	24	51
5	$[Cr((4\text{-}NMe_2\text{-}C_6H_4)_2phen)_3](BF_4)_3$	24	0
6	$[Cr(Naph_2phen)_3](BF_4)_3$	7	90

Scheme 2.5. (4+2) Cycloaddition reaction with electron deficient dienophiles.

After two test reactions, it is clear that the addition of the electron donating methoxy group had a significant impact on catalyzing these photoreactions. This could stem from several different reasons. The addition of the methoxy groups on the ligands changed the absorbance properties of the catalyst and is now a better light absorber in the visible region in comparison to $[Cr(Ph_2phen)_3](BF_4)_3$. The excited-state redox potential could now have a significant overlap with the substrates, allowing for electron transfer to occur more readily. The excited-state lifetimes could also play a key role in reactivity. In McDaniel's report, the addition of the electron donating groups increased the excited-state lifetimes of the catalysts. If this trend holds, the addition of the methoxy groups could increase the excited-state lifetimes, therefore increasing overall reactivity of the photocatalyst. Lastly, the new catalyst could promote a different mechanistic pathway more effectively, like radical-chain propagation.

Developed by Sarabia and Ferreira, the chromium(III)-photocatalyzed cyclopropanation reaction with electron rich alkenes and diazoesters exemplifies differential reactivity in comparison to Stevenson's (4+2) cycloadditions.[10] *trans*-Anethole can react with ethyl diazoacetate in the presence of a photosensitizer and visible light to form cyclopropane **2-3**. With $[Cr(Ph_2phen)_3](BF_4)_3$ as the photocatalyst, **2-3** is furnished in 66% yield in 14 h (Scheme 2.6, entry

1); however, with $[Ru(bpz)_3](PF_6)_2$, cyclopropane **2-3** was not isolated (Scheme 2.6, entry 2). $[Cr(PMP_2phen)_3](BF_4)_3$ produces **2-3** in an 80% yield in 2 h (Scheme 2.6, entry 3), a noteworthy difference in comparison to $[Cr(Ph_2phen)_3](BF_4)_3$. Like previous results, $[Cr((4\text{-}CO_2Me\text{-}C_6H_4)_2phen)_3](BF_4)_3$ showed limited reactivity, with a 38% yield in 24 h (Scheme 2.6, entry 4), while $[Cr((4\text{-}NMe_2\text{-}C_6H_4)_2phen)_3](BF_4)_3$ did not yield the cycloadduct (Scheme 2.6, entry 5). $[Cr(Naph_2phen)_3](BF_4)_3$ produced **2-3** in comparable quantity to $[Cr(Ph_2phen)_3](BF_4)_3$ (Scheme 2.6, entry 6). Like previous photoreactions, $[Cr(PMP_2phen)_3](BF_4)_3$ outcompetes the parent catalyst handily.

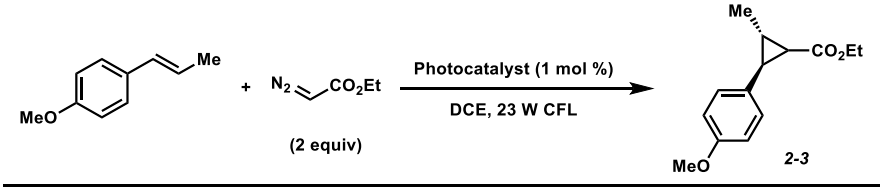

Entry	Photocatalyst	Time (h)	% yield
1	$[Cr(Ph_2phen)_3)](BF_4)_3$	14	66
2	$[Ru(bpz)_3](PF_6)_2$	24	<10
3	$[Cr(PMP_2phen)_3](BF_4)_3$	2	80
4	$[Cr((4\text{-}CO_2Me\text{-}C_6H_4)_2phen)_3](BF_4)_3$	36	38
5	$[Cr((4\text{-}NMe_2\text{-}C_6H_4)_2phen)_3](BF_4)_3$	12	0
6	$[Cr(Naph_2phen)_3](BF_4)_3$	6.5	62

Scheme 2.6. (2+1) Cycloaddition reaction with electron rich alkenes.

The last photoreaction analyzed is the chromium(III)-photocatalyzed (3+2) cycloaddition reaction using electron rich alkenes and vinyl diazoesters. Using *trans*-anethole and ethyl vinyldiazoacetate as starting materials, photocatalysts were varied with visible light. Sarabia and co-workers reported that both $[Cr(Ph_2phen)_3](BF_4)_3$ and $[Ru(bpz)_3](PF_6)_2$ produced cyclopentene **2-4** in 93% yield (Scheme 2.7, entry 1 and 2), with the reaction time using $[Ru(bpz)_3](PF_6)_2$ significantly quicker. $[Cr(PMP_2phen)_3](BF_4)_3$ produces **2-4** in a 92% yield in 30 min (Scheme 2.7, entry 3), faster than both reactions using $[Cr(Ph_2phen)_3](BF_4)_3$ or$[Ru(bpz)_3](PF_6)_2$. $[Cr((4\text{-}CO_2Me\text{-}C_6H_4)_2phen)_3](BF_4)_3$ and $[Cr(Naph_2phen)_3](BF_4)_3$ yielded cycloadduct **2-4** in 48% yield

in 48 h and 90% yield in 24 h, respectively, while $[Cr((4\text{-}NMe_2\text{-}C_6H_4)_2phen)_3](BF_4)_3$ did not yield the cycloadduct (Scheme 2.7, entries 4-6).

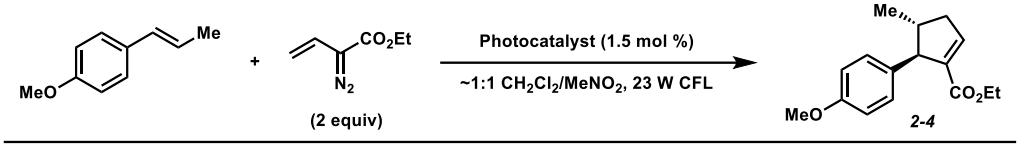

Entry	Photocatalyst	Time (h)	% yield
1	$[Cr(Ph_2phen)_3)](BF_4)_3$	16	93
2	$[Ru(bpz)_3](PF_6)_2$	1.5	93
3	$[Cr(PMP_2phen)_3](BF_4)_3$	0.5	92
4	$[Cr((4\text{-}CO_2Me\text{-}C_6H_4)_2phen)_3](BF_4)_3$	48	48
5	$[Cr((4\text{-}NMe_2\text{-}C_6H_4)_2phen)_3](BF_4)_3$	24	0
6	$[Cr(Naph_2phen)_3](BF_4)_3$	24	90

Scheme 2.7. (3+2) Cycloaddition reaction with electron rich alkenes.

Due to the immense difference in reaction times in the (3+2) photocatalyzed cycloaddition reaction between $[Cr(Ph_2phen)_3](BF_4)_3$ and $[Cr(PMP_2phen)_3](BF_4)_3$, a gas chromatography study was performed (Figure 2.15). The yield of the product is correlated to time in the reaction. Noticeably, within 20 min of starting the reaction, $[Cr(PMP_2phen)_3](BF_4)_3$ catalyzes the reaction to about a 90% yield of **2-4**, while $[Cr(Ph_2phen)_3](BF_4)_3$ proceeded around 5% yield. This disparity is also noted in the reaction times. $[Cr(PMP_2phen)_3](BF_4)_3$ takes 40 min to go to completion, whereas $[Cr(Ph_2phen)_3](BF_4)_3$ takes 42 h. Because of the large difference in reaction times, further investigation into the reaction and its mechanism using $[Cr(PMP_2phen)_3](BF_4)_3$ as the photocatalyst was needed.

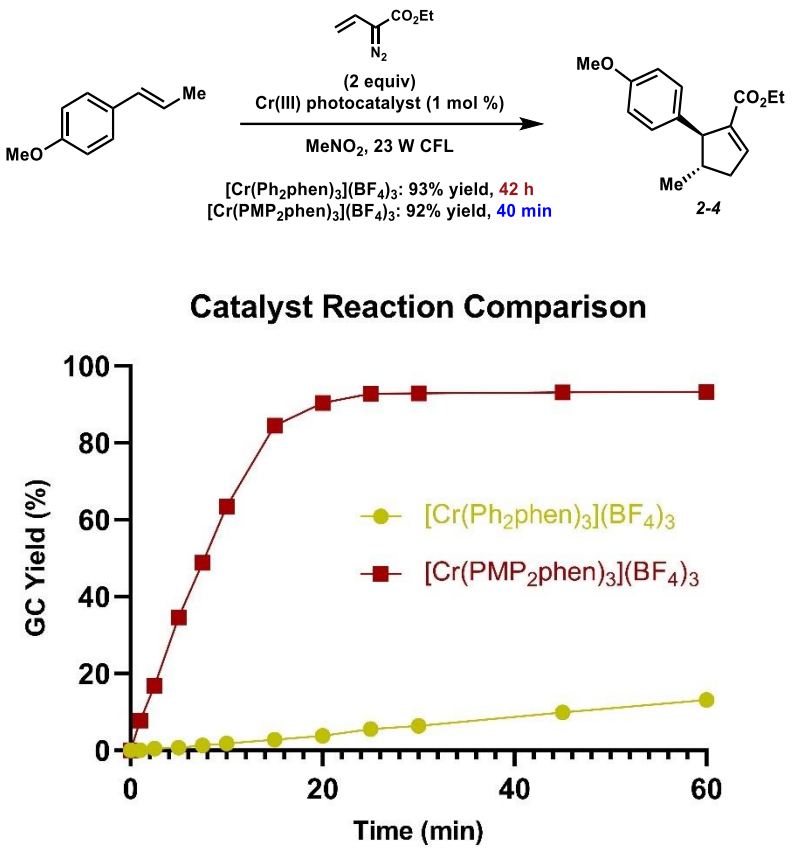

Figure 2.15. Reaction comparison of $[Cr(Ph_2phen)_3](BF_4)_3$ and $[Cr(PMP_2phen)_3](BF_4)_3$.

Sarabia's proposed mechanism employs a $Cr^{III/II}$ cycle. The ground state chromium(III) photocatalyst is irradiated by light and generates the excited-state chromium(III) complex. The excited-state photocatalyst abstracts an electron from *trans*-anethole, producing radical-cation intermediate **2-5**. Radical cation intermediate **2-5** can then react in two different pathways. First, a direct formation of the cyclopentene could occur from the addition of vinyldiazoacetate **2-7** to form radical-cation **2-9**. However, a 4-exo cyclization process could also generate radical-cation cyclobutene **2-8**, which also constructs radical-cation **2-9** upon ring expansion. Radical-cation **2-9** can be reduced in two different methods to form the desired cyclopentene **2-4**. A metal-centered reduction, where the chromium(III) catalyst is oxidized, reducing radical-cation **2-9** to the desired

cyclopentene. Alternatively, a radical-chain process could occur. *trans*-Anethole could act as an electron donor, causing a new radical-cation **2-5** and cyclopentene **2-4**.

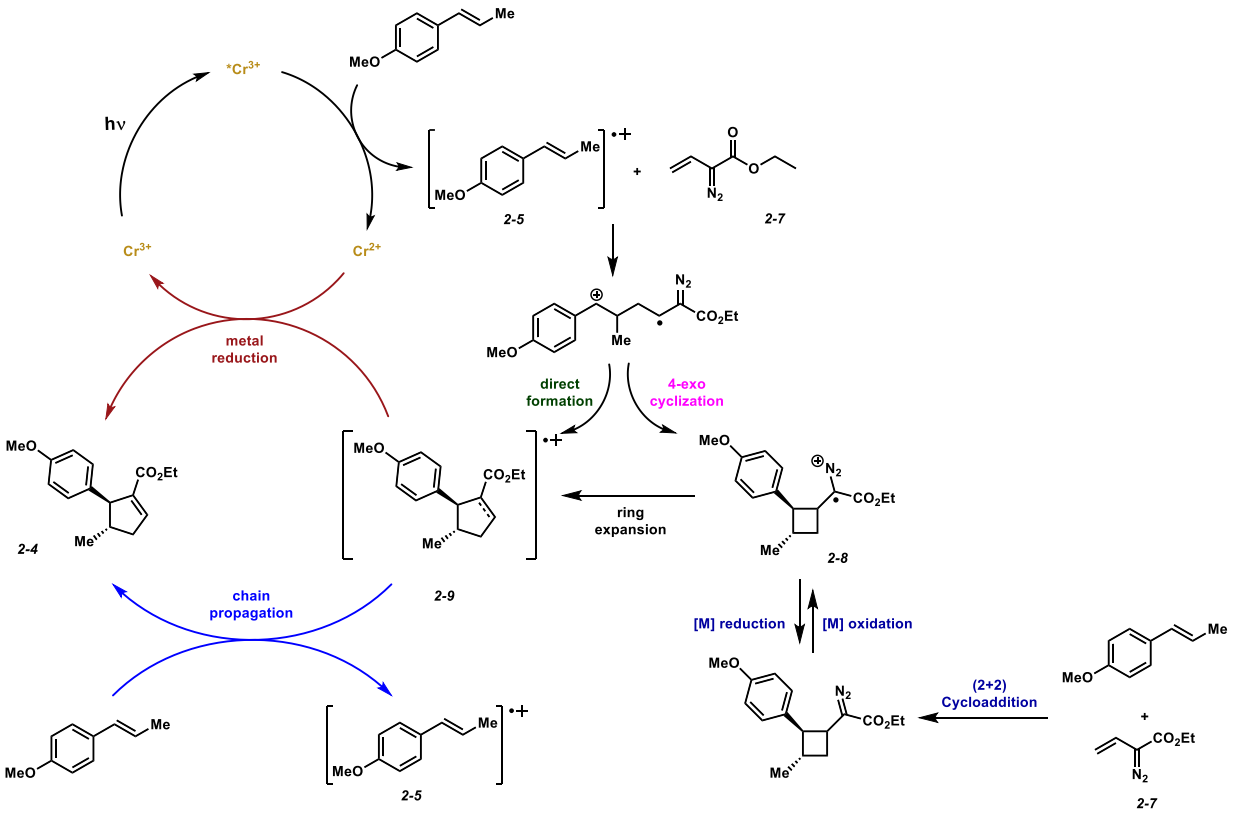

Scheme 2.8. Sarabia's proposed photocatalyzed (3+2) cycloaddition mechanism.

To probe the mechanism of the (3+2) photocatalyzed cycloaddition, quantum yield experiments were performed. Reaction quantum yields are utilized to identify the relationship between the photocatalyst and reaction mechanism. The amount of photons absorbed by the photocatalyst is relative to the amount of product produced in the reaction. The quantum yield can be determined to help identify a reaction mechanism. A quantum yield under one signifies that a radical-chain propagation mechanism cannot be ruled out. A radical chain propagation mechanism must be occurring to some extent if the quantum yield over one. Radical chain propagation utilizes another equivalent of starting alkene as the electron donor to generate the desired cycloadduct and a new radical-cation intermediate. In the case of the (3+2) photocatalyzed cycloaddition, the

quantum yield helps determine whether the photocatalyst (SET) or another equivalent of alkene (radical-chain propagation) is acting as the electron donor in the final reduction step. Using the decomposition of potassium ferrioxalate, a well-established actinometer, the quantum yield for the (3+2) photocatalyzed cycloaddition can be measured (see Experimental Section 2.7.7). $[Cr(Ph_2phen)_3](BF_4)_3$ has a calculated quantum yield of 0.9665, which is less than one. $[Cr(PMP_2phen)_3](BF_4)_3$ has a measured quantum yield of 2.118. Since the calculated quantum yield is greater than one, radical-chain processes are plausible in the mechanism. However, the catalyst can still act as an electron donor for the final reduction to the cyclopentene. As a baseline, $[Ru(bpz)_3](PF_6)_2$ was also analyzed within the reaction and the quantum yield was measured at 8.854, which is greater than $[Cr(PMP_2phen)_3](BF_4)_3$, Using $[Ru(bpz)_3](PF_6)_2$ as the photocatalyst suggests that a chain process is prevalent in the reaction mechanism and both mechanistic pathways are operable, with chain processes predominant.

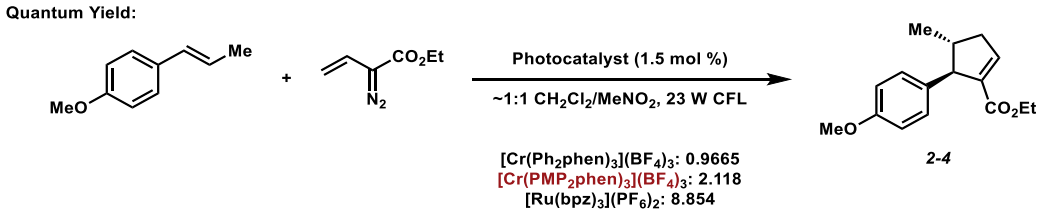

Scheme 2.9. Quantum yield studies.

2.6 Conclusions

In summary, we developed a series of new substituted bathophenanthroline ligands and corresponding chromium(III) complexes. These chromium(III) complexes were extensively characterized via their absorbances, emission data, and their excited-state reduction potentials. Examination of known photocatalyzed reactions using the new chromium(III) complexes showed that $[Cr(PMP_2phen)_3](BF_4)_3$ was vastly superior to other catalysts. In comparison to the parent $[Cr(Ph_2phen)_3](BF_4)_3$, $[Cr(PMP_2phen)_3](BF_4)_3$ outcompetes it in all all known chromium(III)

photocatalyzed reactions. To expand chromium(III) photocatalysis, new reactivity using these complexes has to be explored.[18]

2.7 Experimental Procedures

2.7.1 Materials and Methods

Reactions were performed under argon atmosphere unless otherwise noted. Deionized water was used for the coupling reactions. All other solvents and reagents were used as received unless otherwise noted. Commercially available chemicals and reagents were purchased from Alfa Aesar (Ward Hill, MA), MilliporeSigma (St. Louis, MO), Oakwood Products (West Columbia, SC), and Acros Organics (Geel, Belgium). Qualitative TLC analysis was performed on 250 mm thick, 60 Å, glass backed, F254 silica (SiliCycle, Quebec City, Canada). Visualization was accomplished with UV light and/or exposure to *p*-anisaldehyde or $KMnO_4$ stain solutions followed by heating. Flash chromatography was performed using SiliCycle silica gel (230-400 mesh). ^1H NMR spectra were acquired on a Varian Mercury Plus NMR (at 400 MHz) and are reported relative to $SiMe_4$ (δ 0.00). ^{13}C NMR spectra were acquired on a Varian Mercury Plus NMR (at 100 MHz) and are reported relative to $SiMe_4$ (δ 0.0). All IR spectra were obtained on an ATR-ZnSe as thin films with a Nicolet iS-50 FT-IR or Shimadzu IRPrestige-21 FT-IR spectrometer and are reported in wavenumbers (ν). High resolution mass spectrometry (HRMS) data were acquired by the Proteomics and Mass Spectrometry Facility at the University of Georgia on a Thermo Orbitrap Elite. Voltammograms were recorded with a CH Instrument 1230A under a nitrogen atmosphere. All experiments used 0.1 M tetrabutylammonium hexafluorophosphate (Bu_4NPF_6) solution in an acetonitrile with a 0.25 mm glassy carbon disk working electrode, Ag wire quasi-reference electrode, and a Pt wire auxiliary electrode. Reported potentials are referenced to the

ferrocenium/ferrocene ($[C_5H_5)_2Fe]^+/[(C_5H_5)_2Fe]$, $Fc^{+/0}$) redox couple and were determined by adding ferrocene as an internal standard at the conclusion of each electrochemical experiment. To convert the potentials from V vs. Fc^+/Fc to V vs. SCE, 0.400 was added to the potentials taken in acetonitrile.[19] Static emission spectra were taken on a Horiba Jobin-Yvon FluoroLog-3 spectrofluorometer. All samples were set to have an absorbance between 0.10 and 0.15 AU at the excitation wavelength in an air-free quartz cuvette. Emission spectra were measured with 4 mm entrance slits, 1 mm exit slits and 0.1 s integration time; excitation spectra were measured with 1 mm entrance slits, 4 mm exit slits and 0.1 s integration time. Quantum yield was calculated according to the procedure of Yoon[20] with data acquired by a Horiba Jobin Yvon FluoroMax-3 spectrophotometer with a 150 W Xe lamp used as the light source and a Varian Cary 100 Bio UV-Visible spectrophotometer.

2.7.2 Ligand Syntheses

General Procedure 1 (*GP1*): *Synthesis of Ligands*[21]

A mixture of 4,7-dichloro-1,10-phenanthroline (1.00 equiv), boronic acid (3.00 equiv), Cs_2CO_3 (3.40 equiv), $Pd_2(dba)_3$ (5 mol %), and PCy_3 (12 mol %) in a 3:1 mixture of 1,4-dioxane/H_2O (0.20 M in substrate) was degassed with argon for 15 min at 23 °C. The reaction mixture was then heated to 100 °C and stirred for 3-5 h. Upon completion, the reaction mixture was diluted with $CHCl_3$, poured into H_2O, and the layers were separated. The aqueous layer was then extracted with $CHCl_3$ (3x). The combined organic layers were washed sequentially with H_2O, sat. aq. Na_2CO_3, 10% aq. NaOH, H_2O, and brine, and then dried over Na_2SO_4, and concentrated in vacuo. The crude material was purified by recrystallization to afford bisarylated phenanthroline.

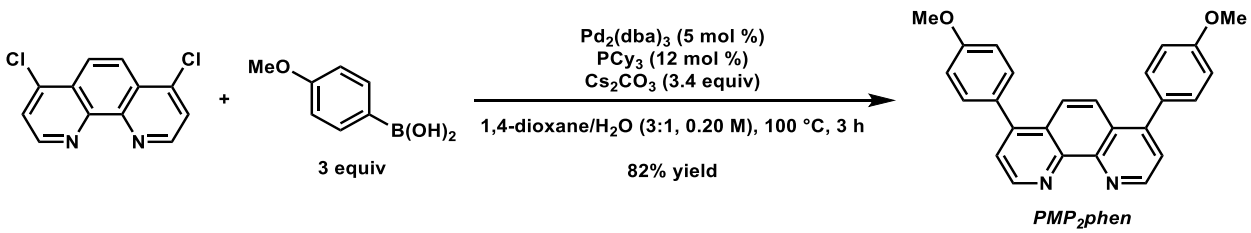

4,7-bis(4-methoxyphenyl)-1,10-phenanthroline (**PMP_2phen**)

According to GP1, 4,7-dichloro-1,10-phenanthroline (30.7 mg, 0.123 mmol) was subjected to the coupling with 4-methoxyphenylboronic acid (56.1 mg, 0.370 mmol), Cs_2CO_3 (136 mg, 0.419 mmol), $Pd_2(dba)_3$ (5.6 mg, 0.00616 mmol), and PCy_3 (4.1 mg, 0.0148 mmol) in 3:1 1,4-dioxane/H_2O (0.60 mL). The reaction mixture was then heated to 100 °C and stirred for 3 h. Upon completion, the reaction mixture was cooled to room temperature and then diluted with $CHCl_3$ (10 mL) and poured into H_2O (10 mL), and then the layers were separated. The aqueous layer was extracted with $CHCl_3$ (3 x 15 mL). The combined organic layers were washed sequentially with H_2O (25 mL), sat. aq. Na_2CO_3 (25 mL), 10% aq. NaOH (25 mL), H_2O (25 mL), and brine (25 mL),

and then dried over Na_2SO_4 and concentrated in vacuo. The crude residue was purified by recrystallization (hexanes) to afford **PMP$_2$phen** (39.6 mg, 82% yield) as an off-white solid.

R_f: 0.15 in 3:1 EtOAc/hexanes.

^{1}H NMR (400 MHz, $CDCl_3$): δ 9.18 (d, *J* = 4.5 Hz, 2H), 7.88 (s, 2H), 7.54 (d, *J* = 4.5 Hz, 2H), 7.46 (d, *J* = 8.6 Hz, 4H), 7.05 (d, *J* = 8.6 Hz, 4H), 3.88 (s, 6H).

^{13}C NMR (100 MHz, $CDCl_3$): δ 159.9, 149.8, 148.2, 147.0, 131.1, 130.3, 126.6, 124.1, 123.6, 114.2, 55.5.

IR (ATR, neat): 2935, 1605, 1502, 1246, 1175, 815 cm^{-1}.

HRMS (ESI+): *m/z* calc'd for $(M + H)^+$ $[C_{26}H_{20}N_2O_2 + H]^+$: 393.1600, found 393.1598.

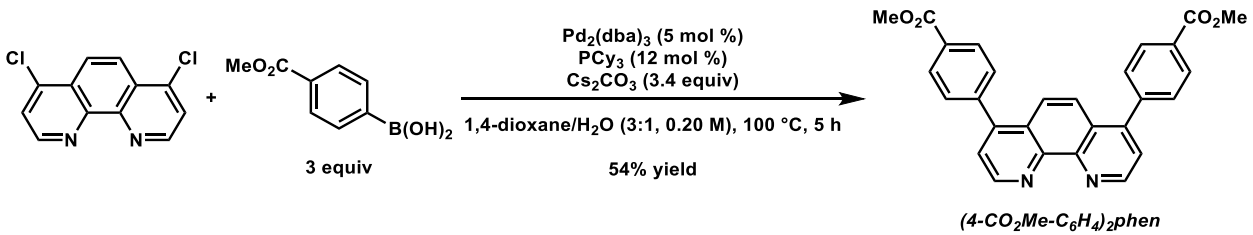

4,7-bis(4-methoxycarbonylbenzene)-1,10-phenanthroline (**(4-CO_2Me-C_6H_4)$_2$phen**)

According to GP1, 4,7-dichloro-1,10-phenanthroline (51.0 mg, 0.205 mmol) was subjected to the coupling with 4-(methoxycarbonyl)phenylboronic acid (111 mg, 0.617 mmol), Cs_2CO_3 (226 mg, 0.694 mmol), $Pd_2(dba)_3$ (9.4 mg, 0.0102 mmol), and PCy_3 (7.0 mg, 0.249 mmol) in 3:1 1,4-dioxane/H_2O (1.0 mL). The reaction mixture was then heated to 100 °C and stirred for 5 h. Upon completion, the reaction mixture was cooled to room temperature and then diluted with $CHCl_3$ (10 mL) and poured into H_2O (10 mL), and then the layers were separated. The aqueous layer was extracted with $CHCl_3$ (3 x 15 mL). The combined organic layers were washed sequentially with H_2O (25 mL), sat. aq. Na_2CO_3 (25 mL), 10% aq. NaOH (25 mL), H_2O (25 mL), and brine (25 mL), and then dried over Na_2SO_4 and concentrated in vacuo. The crude residue was purified by recrystallization (hexanes) to afford **(4-CO_2Me-C_6H_4)$_2$phen** (49.5 mg, 54% yield) as a light-brown solid.

R_f: 0.15 in 6:1 EtOAc/hexanes.

^{1}H NMR (400 MHz, $CDCl_3$): δ 9.29 (d, *J* = 4.5 Hz, 2H), 8.22 (d, *J* = 8.2 Hz, 4H), 7.80 (s, 2H), 7.62 (d, *J* = 8.2 Hz, 4H), 7.61 (d, *J* = 4.5 Hz, 2H), 3.99 (s, 6H).

^{13}C NMR (100 MHz, $CDCl_3$): δ 166.8, 150.1, 147.5, 147.0, 142.5, 130.5, 130.1, 129.9, 126.2, 124.2, 123.6, 52.5.

IR (ATR, neat): 2948, 1712, 1270, 1101, 845, 771 cm^{-1}.

HRMS (ESI+): *m/z* calc'd for $(M + H)^+$ $[C_{28}H_{20}N_2O_4 + H]^+$: 449.1496, found 449.1497.

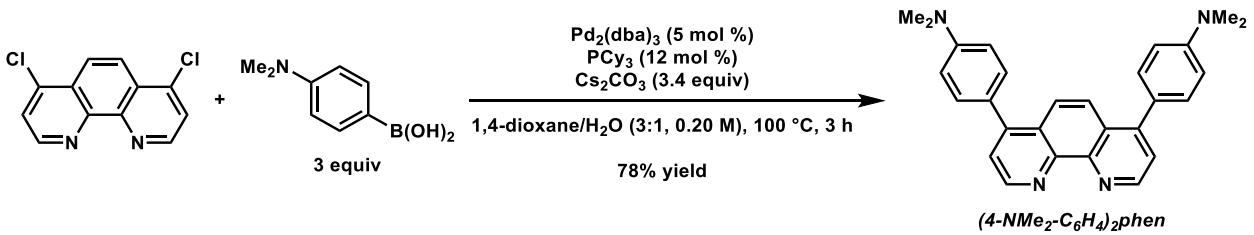

4,7-bis(4-(dimethylamino)phenyl)-1,10-phenanthroline (**(4-NMe$_2$-C$_6$H$_4$)$_2$phen**)

According to GP1, 4,7-dichloro-1,10-phenanthroline (49.3 mg, 0.198 mmol) was subjected to the coupling with 4-(dimethylamino)phenylboronic acid (98.0 mg, 0.593 mmol), Cs_2CO_3 (220 mg, 0.673 mmol), $Pd_2(dba)_3$ (9.0 mg, 0.00989 mmol), and PCy_3 (6.7 mg, 0.0239 mmol) in 3:1 1,4-dioxane/H_2O (1.0 mL). The reaction mixture was then heated to 100 °C and stirred for 3 h. Upon completion, the reaction mixture was cooled to room temperature and then diluted with $CHCl_3$ (10 mL) and poured into H_2O (10 mL), and then the layers were separated. The aqueous layer was extracted with $CHCl_3$ (3 x 15 mL). The combined organic layers were washed sequentially with H_2O (25 mL), sat. aq. Na_2CO_3 (25 mL), 10% aq. NaOH (25 mL), H_2O (25 mL), and brine (25 mL), and then dried over Na_2SO_4 and concentrated in vacuo. The crude residue was recrystallized (hexanes) to afford **(4-NMe$_2$-C$_6$H$_4$)$_2$phen** (64.6 mg, 78% yield) as an orange solid.

R_f: 0.18 in 6:1 EtOAc/hexanes.

^{1}H NMR (400 MHz, $CDCl_3$): δ 9.16 (d, *J* = 4.5 Hz, 2H), 7.99 (s, 2H), 7.54 (d, *J* = 4.5 Hz, 2H), 7.45 (d, *J* = 8.8 Hz, 4H), 6.86 (d, *J* = 8.8 Hz, 4H), 3.06 (s, 12H).

^{13}C NMR (100 MHz, $CDCl_3$): δ 150.6, 149.7, 148.8, 147.2, 130.9, 126.7, 125.7, 124.1, 123.3, 112.3, 40.6.

IR (ATR, neat): 2920, 2890, 1603, 1524, 1324, 815 cm^{-1}.

HRMS (ESI+): *m/z* calc'd for $(M + H)^+$ $[C_{28}H_{26}N_4 + H]^+$: 419.2230, found 419.2232.

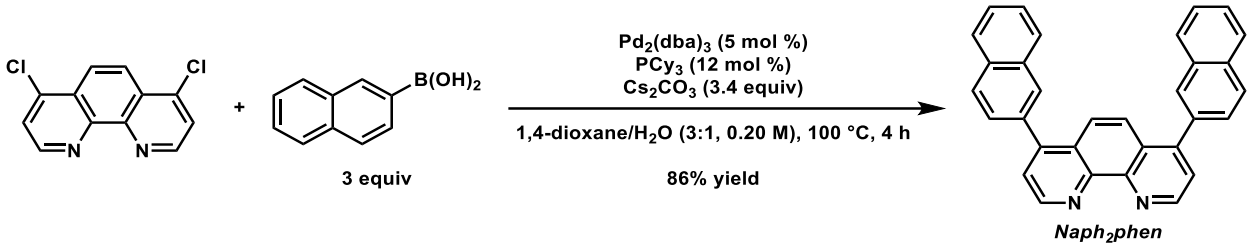

4,7-di(naphthalen-2-yl)-1,10-phenanthroline (**Naph$_2$phen**)

According to GP1, 4,7-dichloro-1,10-phenanthroline (50.5 mg, 0.202 mmol) was subjected to the coupling with 2-naphthylboronic acid (105 mg, 0.608 mmol), Cs_2CO_3 (225 mg, 0.689 mmol), $Pd_2(dba)_3$ (9.3 mg, 0.0101 mmol), and PCy_3 (6.8 mg, 0.0243 mmol) in 3:1 1,4-dioxane/H_2O (1.0 mL). The reaction mixture was then heated to 100 °C and stirred for 4 h. Upon completion, the reaction mixture was cooled to room temperature and then diluted with $CHCl_3$ (10 mL) and poured into H_2O (10 mL), and then the layers were separated. The aqueous phase was extracted with $CHCl_3$ (3 x 15 mL). The combined organic layers were washed sequentially with H_2O (25 mL), sat. aq. Na_2CO_3 (25 mL), 10% aq. NaOH (25 mL), H_2O (25 mL), and brine (25 mL), and then dried over Na_2SO_4 and concentrated in vacuo. The crude residue was purified by recrystallization (hexanes) to afford **Naph$_2$phen** (75.4 mg, 86% yield) as a grey solid.

R_f: 0.12 in 3:1 EtOAc/hexanes.

^{1}H NMR (400 MHz, $CDCl_3$): δ 9.29 (d, *J* = 4.5 Hz, 2H), 8.02 (s, 2H), 7.99 (d, *J* = 8.4 Hz, 2H), 7.96-7.92 comp. m, 4H), 7.91 (s, 2H), 7.70 (d, *J* = 4.5 Hz, 2H), 7.66-7.64 (dd, *J* = 8.4, 2.4 Hz, 2H), 7.60-7.55 (comp. m, 4H).

^{13}C NMR (100 MHz, $CDCl_3$): δ 149.9, 148.5, 147.0, 135.4, 133.3, 133.1, 129.0, 128.4, 128.3, 127.9, 127.4, 126.9 (2C), 126.6, 124.3, 123.9.

IR (ATR, neat): 3054, 1554, 1499, 828, 750 cm^{-1}.

HRMS (ESI+): *m/z* calc'd for $(M + H)^+$ $[C_{32}H_{20}N_2 + H]^+$: 433.1699, found 433.1702.

2.7.3 Catalyst Syntheses

General Procedure 2 (*GP2*): *Synthesis of Chromium(III) Photocatalysts*[2]

In an argon-filled glove box, a solution of $[Cr(NCCH_3)_4](BF_4)_2$ (1.0 equiv) in CH_3CN (0.12 M) was added to a mixture of ligand (4.0 equiv) in CH_3CN (0.20 M) and CH_2Cl_2 (0.30 M) at 28 °C. The reaction mixture was stirred for 2 h, and then $AgBF_4$ (1.0 equiv) was added, resulting in a brownish-colored mixture. The reaction vessel was then sealed and removed from the glove box, and the reaction mixture was stirred sealed under argon the atmosphere overnight. The mixture was then filtered over celite by vacuum filtration, washing with the minimal amount of CH_3CN. Et_2O was added to the filtrate while stirring, causing a solid to precipitate. After 10 min stirring, the solid was collected by vacuum filtration, rinsed with Et_2O, and then dried under vacuum overnight, yielding $[Cr(ligand)_3](BF_4)_3$ complexes as solids. The crude material was purified by recrystallization Methods A or B. Chromium(III) photocatalysts are air stable and were stored in a desiccator.

Typical Procedures for Recrystallization:

Method A: *Solvent Diffusion*

Crude catalyst (500 mg) was completely dissolved in CH_3CN (100 mL). Et_2O was then slowly added to the CH_3CN solution by pipetting the Et_2O down the sides of the flask so that two layers were formed. After a certain amount of Et_2O was added, the top layer started to become cloudy. In total, ~300 mL Et_2O were added. The flask was left to rest for 30 min and was not shaken or swirled, so as to not combine the layers. The top layer, which contained a precipitate, was then removed by pipette and filtered by vacuum filtration. The collected solid was then washed with Et_2O and dried under vacuum. More Et_2O could be added to the remaining CH_3CN solution to precipitate additional amounts of the pure catalyst.

Method B: *Vapor Diffusion*

In a scintillation vial, crude catalyst (~100 mg) was completely dissolved in CH_3CN (~4 mL). The vial was placed in a 150 mL beaker filled with Et_2O (30 mL). A watchglass was placed on top of the beaker, and the system was only disturbed to replenish Et_2O each day, maintaining approximately 30 mL in volume. After 10 d, the vial was decanted and the solid was washed with excess Et_2O. The solid was then collected and dried under vacuum.

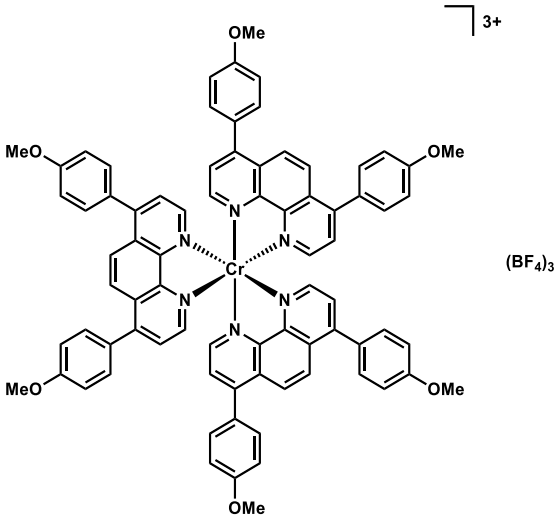

[Cr(PMP$_2$phen)$_3$](BF$_4$)$_3$ (Cr1):

According to GP2, [Cr(NCCH$_3$)$_4$](BF$_4$)$_2$ (0.218 g, 0.559 mmol) in CH$_3$CN (4.60 mL) was added to a solution of **PMP$_2$phen** (0.650 g, 1.66 mmol) in CH$_3$CN (2.70 mL) and CH$_2$Cl$_2$ (1.85 mL), and the resulting mixture was stirred for 2 h at 28 °C. AgBF$_4$ (0.110 g, 0.565 mmol) was then added to the reaction mixture, and the mixture was stirred overnight. The mixture was then vacuum filtered over celite, washing with CH$_3$CN (15 mL). Et$_2$O (150 mL) was added to the resulting filtrate while stirring, and the precipitated catalyst was collected by vacuum filtration and dried under vacuum overnight. The crude solid was recrystallized by **Method A** to afford **Cr1** (0.571 g, 68% yield) as a red solid.

HRMS (ESI+): *m/z* calc'd for $(M - 3BF_4)^{3+}$: $[C_{78}H_{60}CrN_6O_6]^{3+}$: 409.4655, found 409.4671.

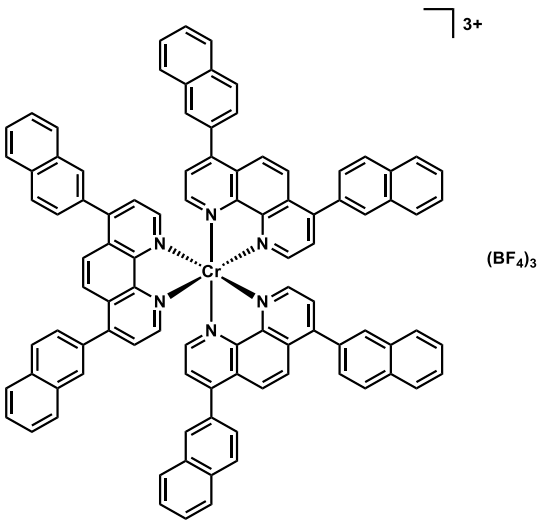

[Cr(Naph$_2$phen)$_3$](BF$_4$)$_3$ (Cr2):

According to GP2, [Cr(NCCH$_3$)$_4$](BF$_4$)$_2$ (0.270 g, 0.693 mmol) in CH$_3$CN (5.80 mL) was added to a solution of **Naph$_2$phen** (0.890 g, 2.06 mmol) in CH$_3$CN (3.50 mL) and CH$_2$Cl$_2$ (2.30 mL), and the resulting mixture was stirred for 2 h at 28 °C. AgBF$_4$ (0.135 g, 0.693 mmol) was then added, and the reaction mixture was stirred overnight. The mixture was then vacuum filtered over celite, washing with CH$_3$CN (20 mL). Et$_2$O (150 mL) was added to the resulting filtrate, and the precipitated catalyst was collected by vacuum filtration and dried under vacuum overnight. The crude solid was recrystallized by **Method B** to afford **Cr2** (0.901 g, 80% yield) as a red solid.

HRMS (ESI+): *m/z* calc'd for (M – 3BF$_4$)$^{3+}$: [C$_{96}$H$_{60}$CrN$_6$]$^{3+}$: 449.8100, found 449.8099.

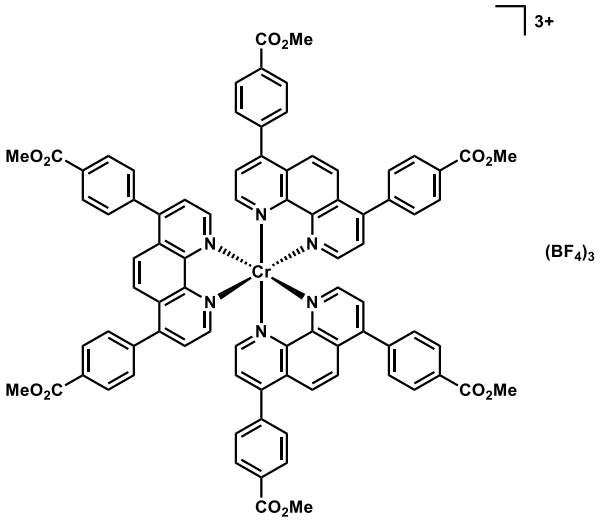

[Cr((4-CO_2Me-C_6H_4)$_2$phen)$_3$](BF_4)$_3$ (Cr3):

According to GP2, [Cr($NCCH_3$)$_4$](BF_4)$_2$ (0.150 g, 0.385 mmol) in CH_3CN (3.20 mL) was added to a solution of **(4-CO_2Me-C_6H_4)$_2$phen** (0.518 g, 1.15 mmol) in CH_3CN (2.00 mL) and CH_2Cl_2 (1.30 mL), and the resulting mixture was stirred for 2 h at 28 °C. $AgBF_4$ (0.075 g, 0.385 mmol) was then added, and the reaction mixture was stirred overnight. The mixture was then vacuum filtered over celite, washing with CH_3CN (8 mL). Et_2O (100 mL) was added to the resulting filtrate while stirring, and the precipitated catalyst was collected by vacuum filtration and dried under vacuum overnight. The crude solid was recrystallized by **Method B** to afford **Cr3** (0.370 g, 58% yield) as a light brown solid.

HRMS (ESI+): *m/z* calc'd for $(M - 3BF_4)^{3+}$: $[C_{84}H_{60}CrN_6O_{12}]^{3+}$: 466.1238, found 466.1236.

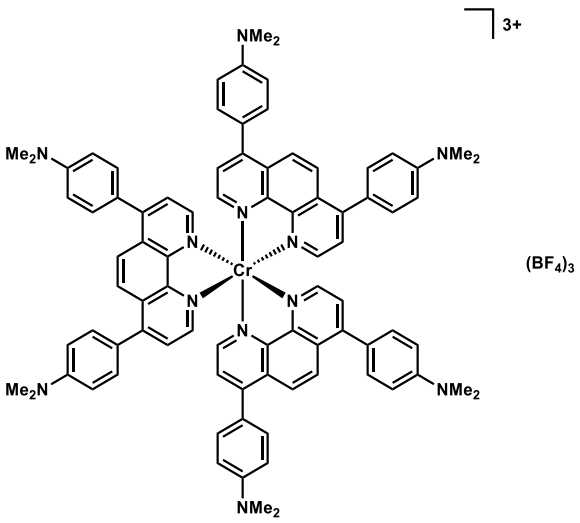

[Cr((4-NMe$_2$-C$_6$H$_4$)$_2$phen)$_3$](BF$_4$)$_3$ (Cr4):

According to GP2, [Cr(NCCH$_3$)$_4$](BF$_4$)$_2$ (0.200 g, 0.513 mmol) in CH$_3$CN (4.30 mL) was added to a solution of **(4-NMe$_2$-C$_6$H$_4$)$_2$phen** (0.649 g, 1.55 mmol) in CH$_3$CN (2.60 mL) and CH$_2$Cl$_2$ (1.70 mL), and the resulting mixture was stirred for 2 h at 28 °C. AgBF$_4$ (0.100 g, 0.514 mmol) was then added, and the reaction mixture was stirred overnight. The mixture was then vacuum filtered over celite, washing with CH$_3$CN (15 mL). Et$_2$O (200 mL) was added to the resulting filtrate, and the precipitated catalyst was collected by vacuum filtration and dried under vacuum overnight. The crude solid was recrystallized by **Method B** to afford **Cr4** (0.498 g, 62% yield) as a dark purple solid.

HRMS (ESI+): *m/z* calc'd for (M – 3BF$_4$)$^{3+}$: [C$_{84}$H$_{78}$CrN$_{12}$]$^{3+}$: 435.5288, found 435.5292.

2.7.4 Catalyst Characterization

Absorbance Analysis: Each catalyst was dissolved in the appropriate solvent (concentration = 0.001 M) and analyzed by UV/Vis spectroscopy. The data is compiled into different charts for each catalyst. Photodissociation experiments were carried out using the designed photobox and analyzing the solutions at different timepoints.

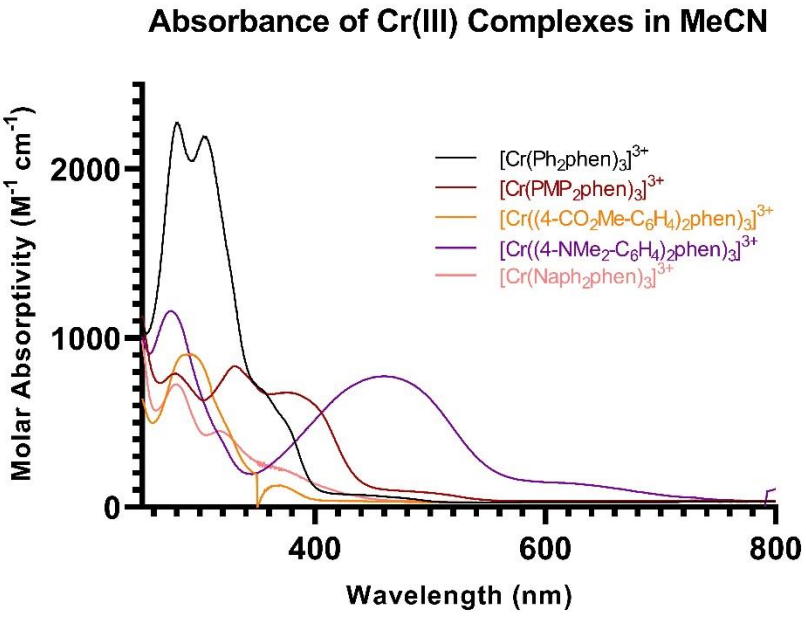

Figure S2.1. Absorbance of chromium(III) complexes in MeCN at 0.001 M.

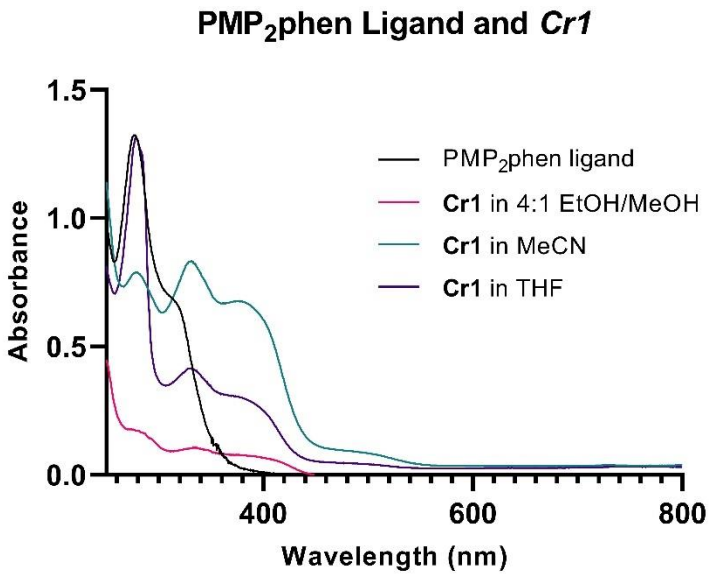

Figure S2.2. Absorbance of PMP-ligand and $[Cr(PMP_2phen)_3](BF_4)_3$ in various solvents 0.001 M.

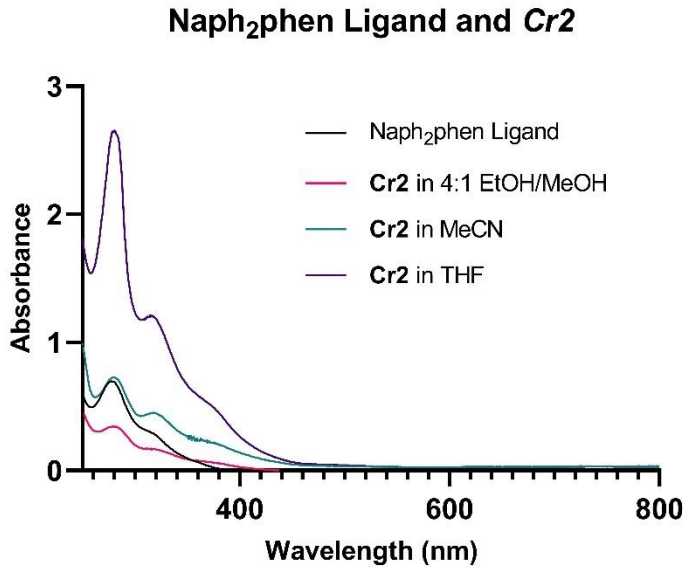

Figure S2.3. Absorbance of PMP-ligand and $[Cr(Naph_2phen)_3](BF_4)_3$ in various solvents 0.001 M.

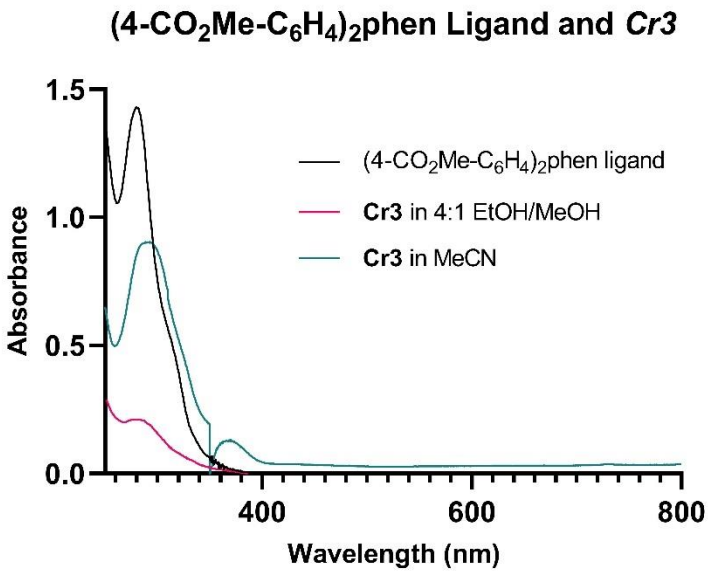

Figure S2.4. Absorbance of PMP-ligand and $[Cr((4\text{-}CO_2Me\text{-}C_6H_4)_2phen)_3](BF_4)_3$ in various solvents 0.001 M.

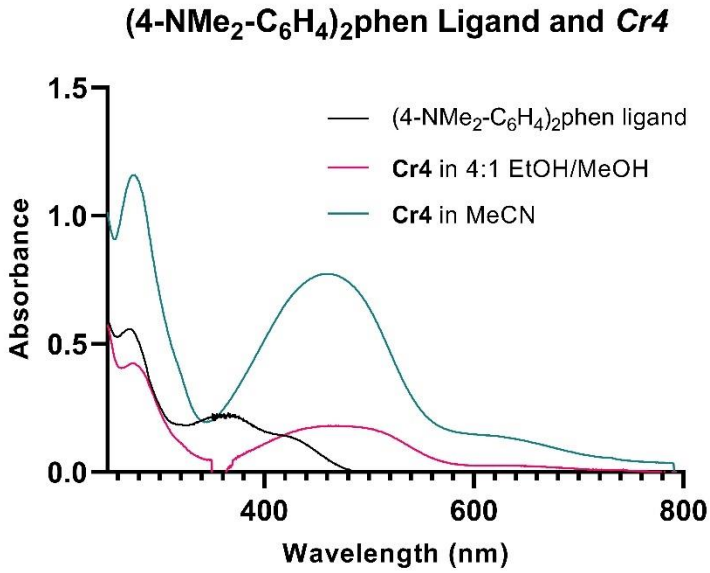

Figure S2.5. Absorbance of PMP-ligand and $[Cr((4\text{-}NMe_2\text{-}C_6H_4)_2phen)_3](BF_4)_3$ in various solvents 0.001 M.

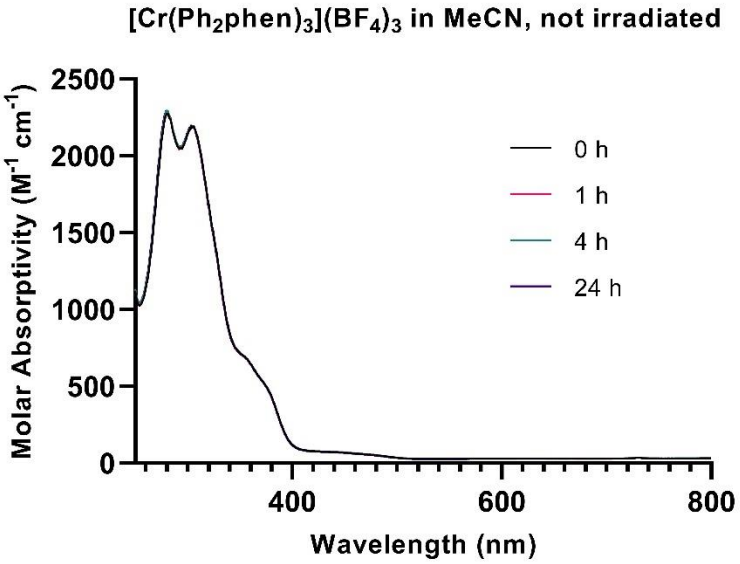

Figure S2.6. Photodissociation of $[Cr(Ph_2phen)_3](BF_4)$ in MeCN without irradiation 0.001 M.

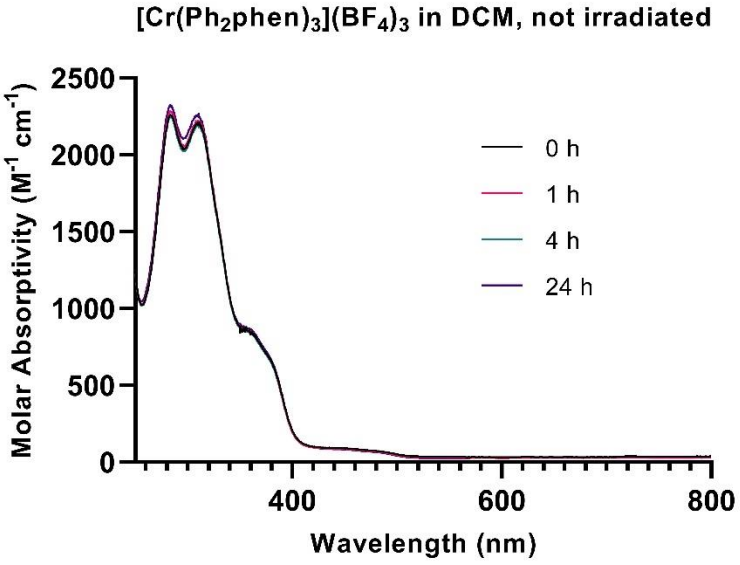

Figure S2.7. Photodissociation of $[Cr(Ph_2phen)_3](BF_4)$ in DCM without irradiation 0.001 M.

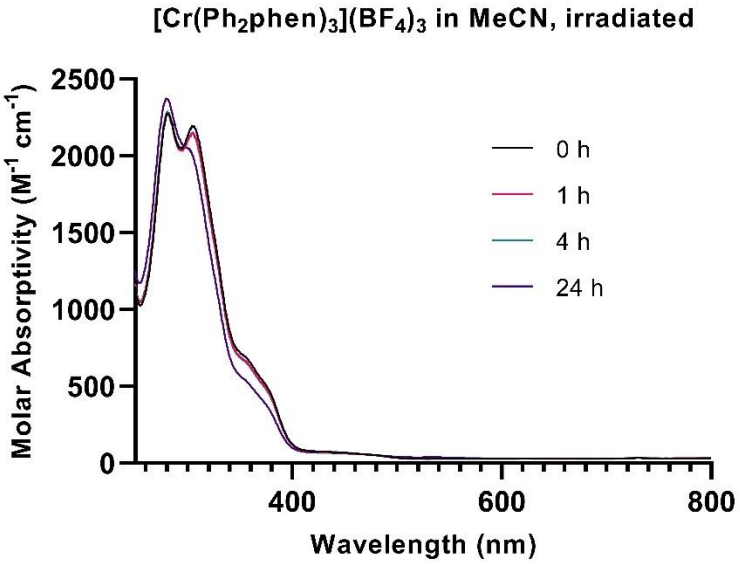

Figure S2.8. Photodissociation of $[Cr(Ph_2phen)_3](BF_4)$ in MeCN with irradiation from a 23 W CFL bulb 0.001 M.

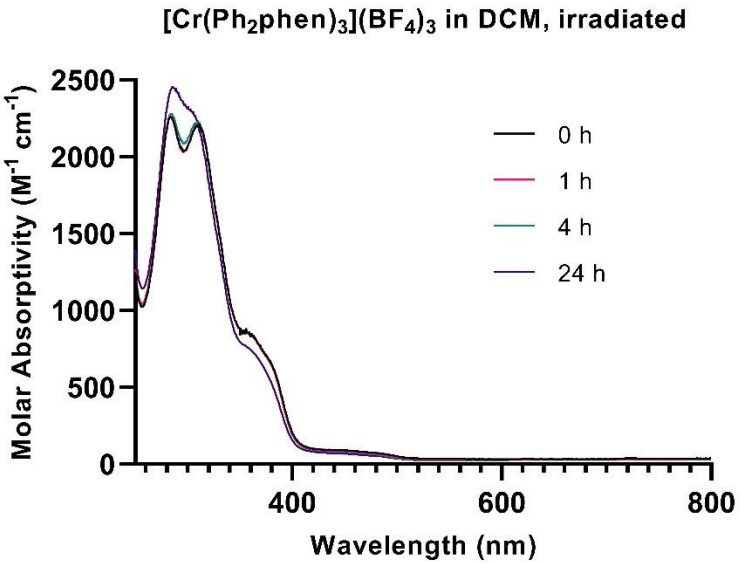

Figure S2.9. Photodissociation of $[Cr(Ph_2phen)_3](BF_4)$ in DCM with irradiation from a 23 W CFL bulb 0.001 M.

.

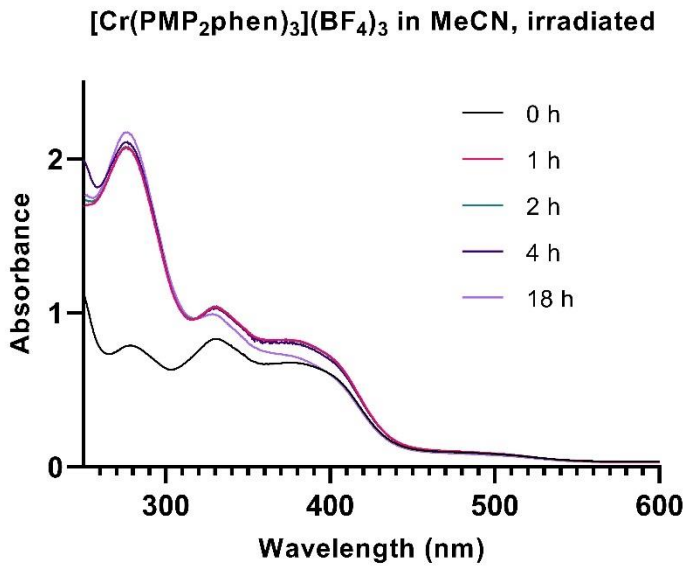

Figure S2.10. Photodissociation of $[Cr(PMP_2phen)_3](BF_4)$ in MeCN with irradiation from a 23 W CFL bulb 0.001 M.

Cyclic Voltammetry: All electrochemical experiments were performed in a dinitrogen atmosphere using degassed solvents. Electrochemical data were recorded with a CH Instruments potentiostat (Model 1230A or 660C) using a 0.25 mm glassy carbon disk working electrode, Ag+/Ag reference electrode, and a Pt wire auxiliary electrode in a 0.1 M Bu_4NPF_6 solution. Scans were collected at a rate of 100 mV/s. Square wave voltammograms were measured with a 25 mV amplitude at 15 Hz. Reported potentials are referenced to the $[Cp_2Fe]^+/[Cp_2Fe]$ (Fc^+/Fc) redox couple, where Cp = cyclopentadienyl, and were determined by adding ferrocene (which was sublimed before use) as an internal standard at the conclusion of each electrochemical experiment.

Complex charge	Solvent	($E_{1/2}$ vs Fc^+/Fc, V) +3/2+	2+/1+	1+/0	0/1-	1-/2-	2-/3-	3-/4-
$[Cr(Ph_2phen)_3](BF_4)_3$	CH_3CN	-0.69	-1.13	-1.64	-2.09	-2.32		
	THF	-0.90	-1.28	-1.80	-2.38	-2.59		
Cr1	CH_3CN	-0.74	-1.17	-1.55 (ir)	-1.63	-2.23		
	THF	-0.98	-1.49	-2.22	-2.94			
Cr2	CH_3CN	-0.68	-1.12	-1.36*	-1.51	-2.28 (qr)		
	THF	-0.74	-1.13	-1.41	-1.62	-2.17	-2.37	
Cr3	CH_3CN	-0.63	-1.05	-1.31*	-1.50	-1.90 (qr)	-2.06	-2.27
	THF	-0.68 (qr)	-1.00	-1.44	-1.92 (qr)	-2.09	-2.39	-2.68
Cr4	CH_3CN	-0.90*	-1.31 (qr)	-1.55	-1.80			
	THF	-1.39 (ir)	-1.90 (ir)	-2.49 (ir)	-2.68 (qr)	-2.85 (ir)		

Table S2.1. Ground-state redox potentials for Cr(III) photocatalysts. **Cr1** = $[Cr(PMP_2phen)_3](BF_4)_3$, **Cr2** = $[Cr((4\text{-}CO_2Me\text{-}C_6H_4)_2phen)_3](BF_4)_3$, **Cr3** = $[Cr((4\text{-}NMe_2\text{-}C_6H_4)_2phen)_3](BF_4)_3$, **Cr4** = $[Cr(Naph_2phen)_3](BF_4)_3$.

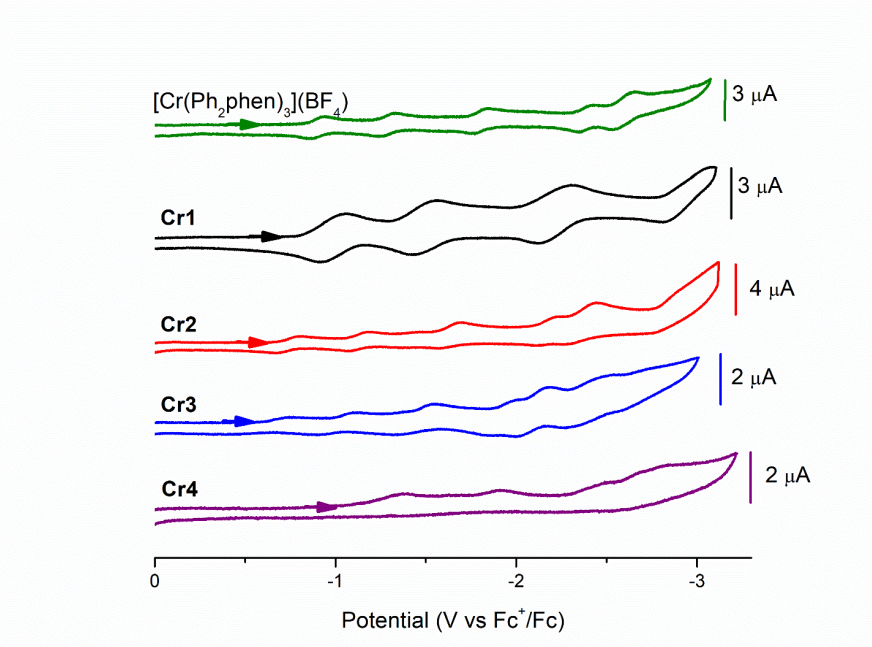

Figure S2.11. Cyclic voltammograms of $[Cr(Ph_2phen)_3](BF_4)$ and compounds **Cr1**-**Cr4**, obtained in THF using a glassy carbon working electrode, a silver wire pseudo-reference electrode, and a platinum counter electrode. Potentials are reported against the Fc^+/Fc couple. Arrows represent the starting points and directions of the initial scans.

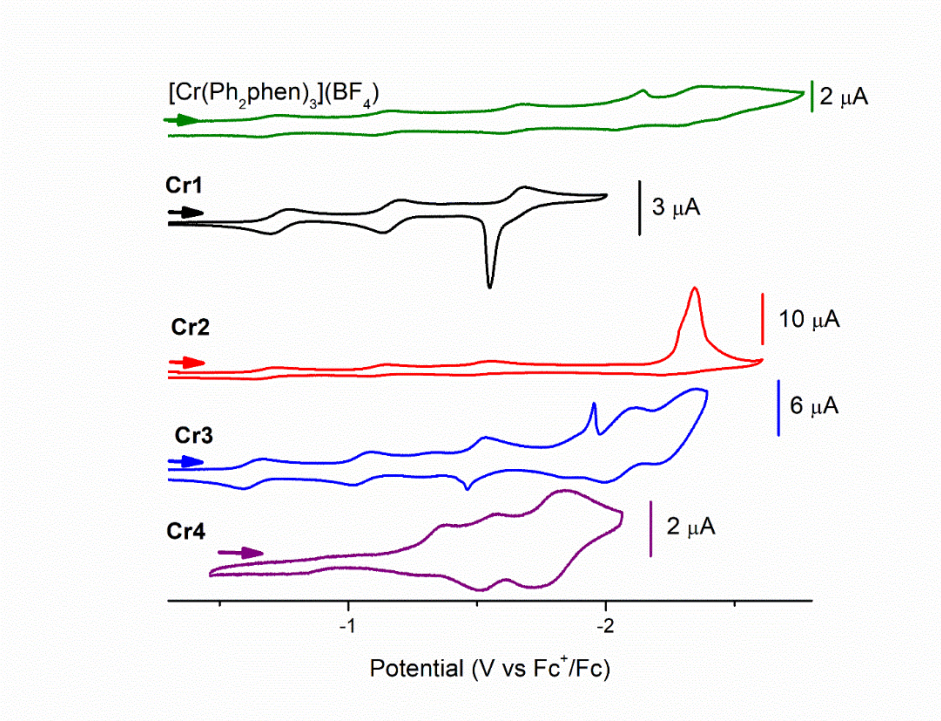

Figure S2.12. Cyclic voltammograms of $[Cr(Ph_2phen)_3](BF_4)$ and **Cr1**-**Cr4**, obtained in CH_3CN using a glassy carbon working electrode, a silver wire pseudo-reference electrode, and a platinum counter electrode. Potentials are reported against the Fc^+/Fc couple. Arrows represent the starting points and directions of the initial scans.

Static Emission: Static emission spectra were taken on a Horiba Jobin-Yvon FluoroLog-3 spectrofluorometer. All samples were set to have an absorbance between 0.10 and 0.15 AU at the excitation wavelength in an air-free quartz cuvette. Emission spectra were measured with 4 mm entrance slits, 1 mm exit slits and 0.1 s integration time; excitation spectra were measured with 1 mm entrance slits, 4 mm exit slits and 0.1 s integration time.

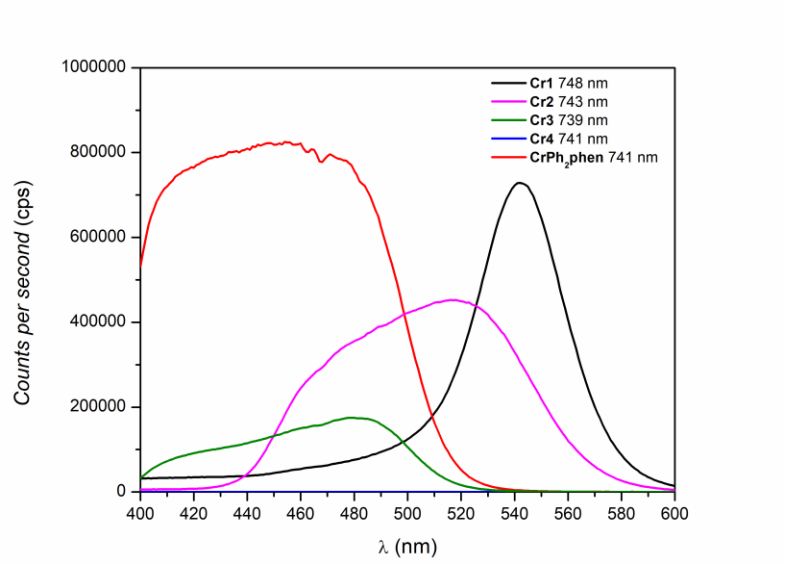

Figure S2.13. Raw mission data for all chromium(III) complexes for determining λ_{max}.

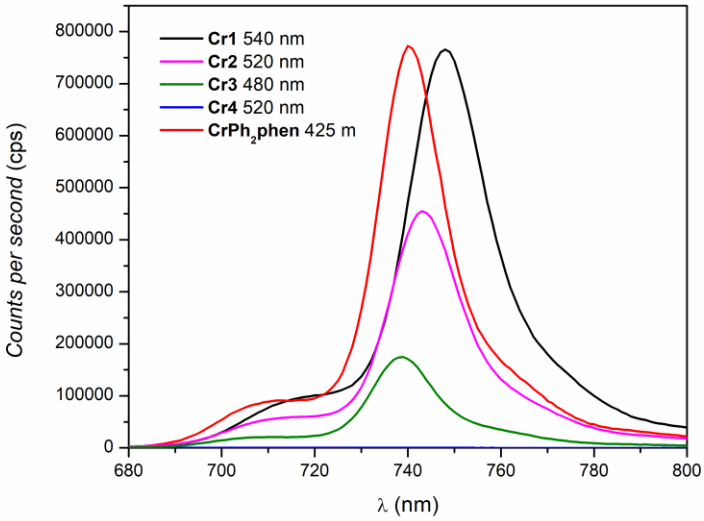

Figure S2.14. Emission data for all chromium(III) complexes for determining $\Delta\upsilon$.

2.7.5 Photocatalyzed Cycloaddition Reactions

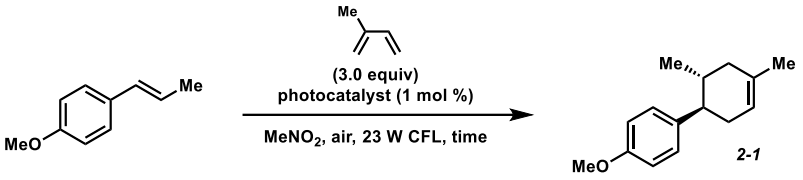

Entry	Photocatalyst	Time (h)	NMR Yield
1	$[Ru(bpz)_3](PF_6)_2$	0.5	98%
2	$[Cr(Ph_2phen)_3](BF_4)_3$	23	84%
3	Cr1	2	89%
4	Cr2	24	92%
5	Cr3	24	69%
6	Cr4	8	0%

General Procedure 3 (GP3): To a flame-dried 1-dram borosilicate vial open to air, *trans*-anethole (0.100 mmol, 1.0 equiv) and the respective [Cr] or [Ru] photocatalyst (1 mol %) were dissolved in $MeNO_2$ (1.00 mL, 0.10 M). Isoprene (0.300 mmol, 3.0 equiv) was then added, and the vial was sealed. The reaction mixture was irradiated with a 23 W compact fluorescent bulb (CFL) bulb while stirring for the listed time, and then concentrated via rotary evaporation. The yield of the crude product (**2-1**) was determined by ^1H NMR using CH_2Br_2 as an internal standard.

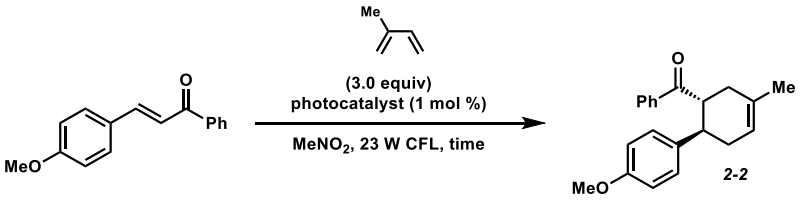

Entry	Photocatalyst	Time (h)	Isolated Yield
1	$[Ru(bpz)_3](PF_6)_2$	0.5	55%
2	$[Cr(Ph_2phen)_3](BF_4)_3$	23	81%
3	Cr1	2	92%
4	Cr2	24	90%
5	Cr3	24	51%
6	Cr4	8	0%

General Procedure 4 (GP4): To a flame-dried 1-dram borosilicate vial open to air, 4-methoxychalcone (0.100 mmol, 1.0 equiv) and the respective [Cr] or [Ru] photocatalyst (1 mol %) were dissolved in $MeNO_2$ (1.00 mL, 0.10 M). Isoprene (0.300 mmol, 3.0 equiv) was then added, and the vial was sealed. The reaction mixture was irradiated with a 23 W CFL bulb while stirring for the listed time, and then concentrated via rotary evaporation. The crude residue was purified by silica gel flash chromatography (9:1 hexanes/Et_2O eluent) to afford cycloadduct **2-2** as a colorless oil.

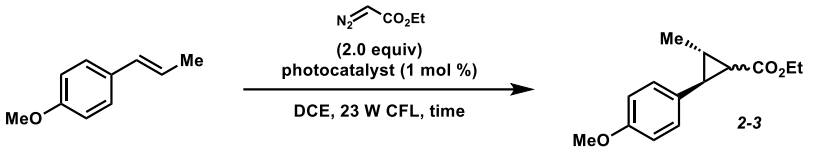

Entry	Photocatalyst	Time (h)	Isolated Yield
1	$[Ru(bpz)_3](PF_6)_2$	0.5	< 10%
2	$[Cr(Ph_2phen)_3](BF_4)_3$	23	66%
3	Cr1	2	80%
4	Cr2	24	62%
5	Cr3	24	38%
6	Cr4	8	0%

General Procedure 5 (GP5): To a flame-dried 1-dram borosilicate vial open to air, trans-anethole (0.100 mmol, 1.0 equiv) and the respective [Cr] or [Ru] photocatalyst (1 mol %) were dissolved in dichloroethane (1.00 mL, 0.10 M). Ethyl diazoacetate (0.200 mmol, 85% by weight in CH_2Cl_2, 2.0 equiv) was then added, and the vial was sealed. The reaction mixture was irradiated with a 23 W CFL bulb while stirring for the listed time, and then concentrated via rotary evaporation. The crude residue was purified by silica gel flash column chromatography (100% hexanes → 9:1 hexanes/EtOAc eluent) to afford cyclopropane **2-3** as a colorless oil.

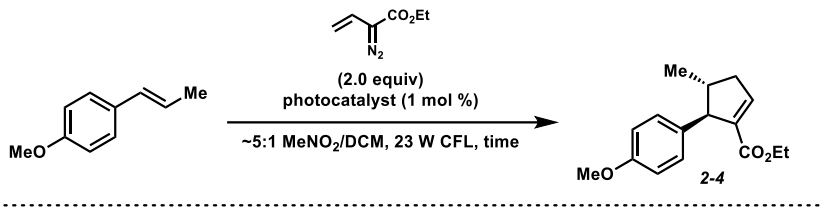

Entry	Photocatalyst	Time (h)	Isolated Yield
1	$[Ru(bpz)_3](PF_6)_2$	0.5	93%
2	$[Cr(Ph_2phen)_3](BF_4)_3$	23	93%
3	Cr1	2	92%
4	Cr2	24	90%
5	Cr3	24	48%
6	Cr4	8	0%

General Procedure 6 (GP6): To a flame-dried 1-dram borosilicate vial open to air, trans-anethole (0.100 mmol, 1.0 equiv) and the respective [Cr] or [Ru] photocatalyst (1 mol %) were dissolved in dichloroethane (1.00 mL, 0.10 M). Ethyl 2-diazobut-3-enoate (0.200 mmol, 1.0 M in CH_2Cl_2, 2.0 equiv) was then added, and the vial was sealed. The reaction mixture was irradiated with a 23 W CFL bulb while stirring for the listed time, and then concentrated via rotary evaporation. The crude residue was purified by silica gel flash column chromatography (100% hexanes → 9:1 hexanes/EtOAc eluent) to afford cyclopropentene **2-4** as a colorless oil.

2.7.6 GC Experiments

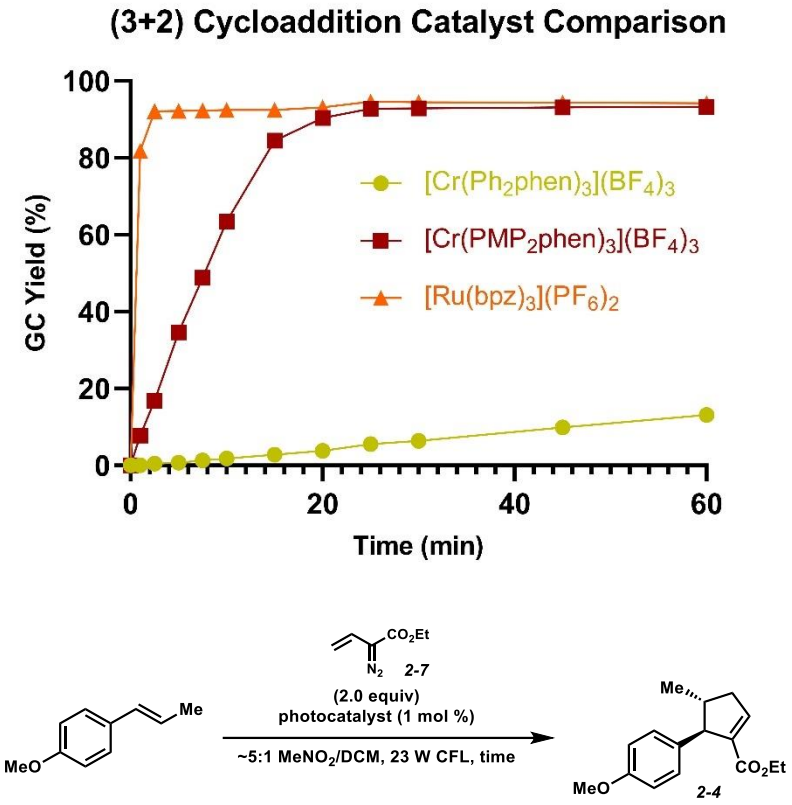

According to **GP6**, a solution of *trans*-anethole (19.6 mg, 1.38 mmol), tridecane (33.6 µL, 1.38 mmol), diazoester **2-7** (0.275 mL, 1.0 M solution in CH_2Cl_2, 2.75 mmol), **Cr1** (3.1 mg, 0.0206 mmol) in CH_3NO_2 (1.37 mL) was irradiated while withdrawing aliquots at various timepoints over 1 h.

According to **GP6**, a solution of *trans*-anethole (20.3 mg, 1.42 mmol), tridecane (34.8 µL, 1.42 mmol), diazoester **2-7** (0.285 mL, 1.0 M solution in CH_2Cl_2, 2.85 mmol), $[Cr(Ph_2phen)_3](BF_4)_3$ (2.8 mg, 0.0214 mmol) in CH_3NO_2 (1.42 mL) was irradiated while withdrawing aliquots at various timepoints over 1 h.

According to **GP6**, a solution of *trans*-anethole (17.4 mg, 1.22 mmol), tridecane (29.8 μL, 1.22 mmol), diazoester **2-7** (0.245 mL, 1.0 M solution in CH_2Cl_2, 2.45 mmol), $[Ru(bpz)_3](PF_6)_2$ (1.6 mg, 0.0184 mmol) in CH_3NO_2 (1.22 mL) was irradiated while withdrawing aliquots at various timepoints over 1 h.

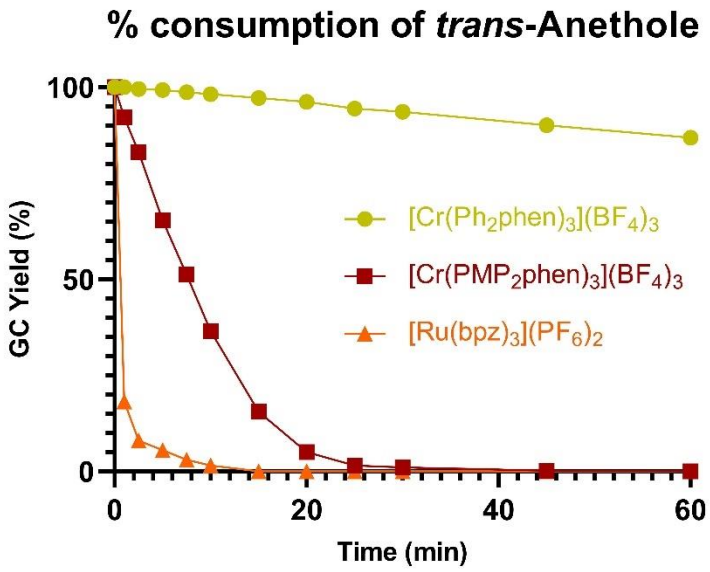

Figure S2.15. Consumption of trans-anethole using $[Cr(Ph_2phen)_3](BF_4)_3$, $[Cr(PMP_2phen)_3](BF_4)_3$, or $[Ru(bpz)_3](PF_6)_2$.

2.7.7 Quantum Yield Determination

The photon flux of the fluorimeter was determined by using standard ferrioxalate actinometry.[22] Ferrioxalate and phenanthroline buffer solutions were prepared according to Yoon.[20] 2.21 g potassium ferrioxalate hydrate was dissolved in 30 mL 0.05 M aq. H_2SO_4 to generate a 0.15 M ferrioxalate solution. 50 mg phenanthroline and 11.25 g sodium acetate were dissolved in 50 mL 0.5 M aq. H_2SO_4 to generate a phenanthroline buffer solution. These solutions were stored in the dark.

The photon flux of the fluorimeter was determined by adding 2.5 mL of the ferrioxalate solution to a quartz cuvette and irradiating for 90.0 seconds at λ = 419 nm with an emissions slit width at 10.0 nm. After 90 seconds, 0.5 mL of phenanthroline buffer was added and the solution was left to rest for 1 h to allow for complete coordination of phenanthroline to ferrous ions. The absorbance was then measured at 510 nm and recorded as the irradiated ferrioxalate solution. Concurrently, a non-irradiated sample was also prepared. 2.5 mL of ferrioxalate solution was added a to quartz cuvette, followed by 0.5 mL of phenanthroline buffer solution. The solution was allowed to rest for 1 h and the absorbance at 510 nm was then measured. The difference in absorbance between the irradiated ferrioxalate solution and the non-irradiated ferrioxalate solution was calculated and then used in Equation 1.

Equation 1 determines the moles of Fe^{2+}:

$$\text{mol } Fe^{2+} = \frac{V \cdot \Delta A}{l \cdot \varepsilon} \quad (1)$$

V = total volume of the solution (0.0030 L) after the addition of phenanthroline buffer solution

ΔA = difference in absorbance at 510 nm between the irradiated (at 419 nm) and non-irradiated ferrioxalate solutions after the addition of the phenanthroline buffer solution

l = pathlength of the quartz cuvette (1.000 cm)

ε = molar absorptivity at 510 nm (11,100 L mol^{-1} cm^{-1})

The photon flux can be calculated using equation 2:

$$\text{photon flux} = \frac{\text{mol } Fe^{2+}}{\phi \cdot t \cdot f} \quad (2)$$

Φ = quantum yield for the ferrioxalate actinometer (1.13 for a 0.15 M solution at λ = 419 nm)[23]

t = time of irradiation at 419 nm (90.0 seconds)

f = the fraction of light absorbed at 419 nm by the non-irradiated ferrioxalate solution (0.9996)

The fraction of light absorbed (f) is calculated by measuring the absorbance of the non-irradiated ferrioxalate solution at 419 nm (*Abs*) and using equation 3:

$$f = 1 - 10^{-Abs} \quad (3)$$

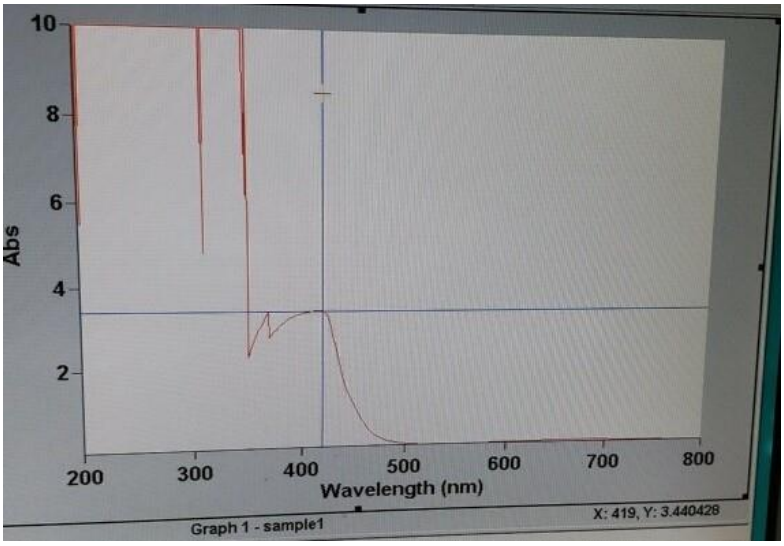

The photon flux was calculated (average of three experiments) to be 6.05 x 10^{-9} einsteins/sec.

Sample Calculation:

$$\text{mol } Fe^{2+} = \frac{0.003 \text{ L} \cdot 2.27465}{1.000 \text{ cm} \cdot 11{,}100 \text{ L mol}^{-1} \text{ cm}^{-1}} = 6.15 \times 10^{-7} \text{ mol}$$

$$\text{photon flux} = \frac{6.14 \times 10^{-7}\ \text{mol}}{1.13\ \cdot 90.0\ \text{s}\ \cdot 0.9996} = 6.05 \times 10^{-9}\ \text{einstein}\ \text{s}^{-1}$$

Determination of Quantum Yield:

A cuvette was charged with *trans*-anethole (1.0 equiv), ethyl 2-diazobut-3-enoate (2.0 equiv), photocatalyst (1.5 mol %) and CH_3NO_2 (0.10 M). The cuvette was then capped with a PTFE stopper. The solution was irradiated (λ = 419 nm, emissions slit width = 10.0 nm) for 1800 seconds (30 min). After irradiation, the solution was passed through a silica plug (eluent: Et_2O) and concentrated in vacuo. The yield of the product was determined by ^1H NMR using CH_2Br_2 as an internal standard. The quantum yield was determined using equation 4. To determine the incident light of the reaction mixture (f), an absorbance was taken of the catalyst at the reaction concentration in nitromethane.

$$\phi = \frac{\text{mol product}}{\text{flux} \cdot \text{t} \cdot \text{f}} \qquad (4)$$

mol product = using the NMR yield, the total amount of product can be calculated in moles

flux = determined by equation 2 (6.05 x 10^{-9} einsteins/sec)

t = time the reaction was run (1800 seconds)

f = incident light as determined by equation 3 of the actual reaction mixture (>.999)

The fraction of light absorbed (f) is calculated by measuring the absorbance of the catalyst at the reaction concentration (0.10 M) at 419 nm (*Abs*) and using equation 3:

$$\text{f} = 1 - 10^{-Abs}$$

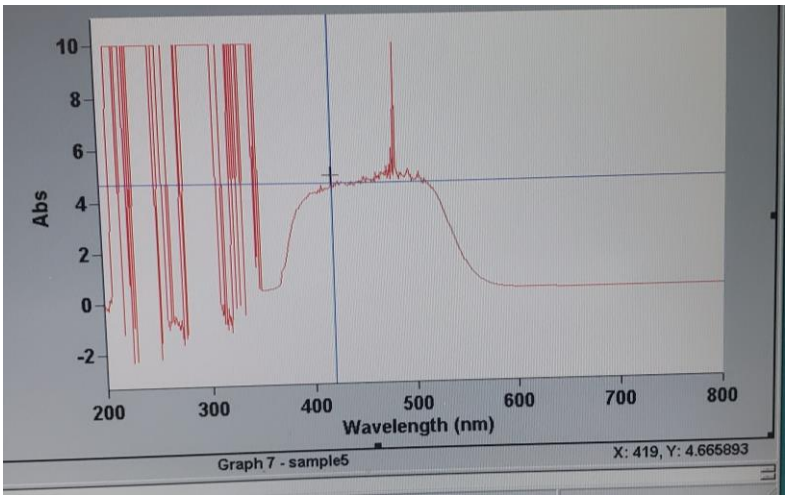

Cr-1 experiment: anethole (21.7 mg, 0.152 mmol), diazoester **2-7** (0.305 mL, 1.00 M solution in CH_2Cl_2, 0.305 mmol), **Cr-1** (3.4 mg, 0.00228 mmol) in 1.52 mL of CH_3NO_2. After 1800 seconds, 15.7% yield of (3+2) cycloaddition product **2-4** formed. Φ(15.9%)

Cr-1 experiment: anethole (22.9 mg, 0.155 mmol), diazoester **2-7** (0.309 mL, 1.00 M solution in CH_2Cl_2, 0.309 mmol), **Cr-1** (3.4 mg, 0.00232 mmol) in 1.55 mL of CH_3NO_2. After 1800 seconds, 16.4% yield of (3+2) cycloaddition product **2-4** formed. Φ(16.4%)

Cr-1 experiment: anethole (23.4 mg, 0.158 mmol), diazoester **2-7** (0.315 mL, 1.00 M solution in CH_2Cl_2, 0.315 mmol), **Cr-1** (3.5 mg, 0.00236 mmol) in 1.58 mL of CH_3NO_2. After 1800 seconds, 13.1% yield of (3+2) cycloaddition product **2-4** formed. Φ(13.1%)

$$average\ mol\ of\ product\ formed = 2.310 \times 10^{-5}$$

$$\Phi = 2.118$$

[Cr(Ph$_2$phen)$_3$](BF$_4$)$_3$ experiment: anethole (22.3 mg, 0.156 mmol), diazoester **2-7** (0.314 mL, 1.00 M solution in CH_2Cl_2, 0.314 mmol), $[Cr(Ph_2phen)_3](BF_4)_3$ (3.0 mg, 0.00228 mmol) in 1.56 mL of CH_3NO_2. After 1800 seconds, 7.89% yield of (3+2) cycloaddition product **2-4** formed. Φ(7.89%)

[Cr(Ph$_2$phen)$_3$](BF$_4$)$_3$ experiment: anethole (23.5 mg, 0.158 mmol), diazoester **2-7** (0.317 mL, 1.00 M solution in CH_2Cl_2, 0.317 mmol), $[Cr(Ph_2phen)_3](BF_4)_3$ (3.1 mg, 0.00237 mmol) in 1.58

mL of CH_3NO_2. After 1800 seconds, 6.70% yield of (3+2) cycloaddition product **2-4** formed. Φ(6.70%)

[Cr(Ph$_2$phen)$_3$](BF$_4$)$_3$ experiment: anethole (24.0 mg, 0.162 mmol), diazoester **2-7** (0.323 mL, 1.00 M solution in CH_2Cl_2, 0.323 mmol), [Cr(Ph$_2$phen)$_3$](BF$_4$)$_3$ (3.2 mg, 0.00243 mmol) in 1.62 mL of CH_3NO_2. After 1800 seconds, 5.61% yield of (3+2) cycloaddition product **2-4** formed. Φ(5.61%)

$$average\ mol\ of\ product\ formed = 1.052 \times 10^{-5}$$

$$\Phi = 0.9665$$

[Ru(bpz)$_3$](PF$_6$)$_2$ experiment: anethole (23.3 mg, 0.157 mmol), diazoester **2-7** (0.314 mL, 1.00 M solution in CH_2Cl_2, 0.314 mmol), [Ru(bpz)$_3$](PF$_6$)$_2$ (2.0 mg, 0.00236 mmol) in 1.57 mL of CH_3NO_2. After 1800 seconds, 64.1% yield of (3+2) cycloaddition product **2-4** formed. Φ(64.1%)

[Ru(bpz)$_3$](PF$_6$)$_2$ experiment: anethole (24.8 mg, 0.167 mmol), diazoester **2-7** (0.334 mL, 1.00 M solution in CH_2Cl_2, 0.334 mmol), [Ru(bpz)$_3$](PF$_6$)$_2$ (2.2 mg, 0.00251 mmol) in 1.67 mL of CH_3NO_2. After 1800 seconds, 54.2% yield of (3+2) cycloaddition product **2-4** formed. Φ(54.2%)

[Ru(bpz)$_3$](PF$_6$)$_2$ experiment: anethole (22.7 mg, 0.153 mmol), diazoester **2-7** (0.306 mL, 1.00 M solution in CH_2Cl_2, 0.306 mmol), [Ru(bpz)$_3$](PF$_6$)$_2$ (1.9 mg, 0.00230 mmol) in 1.53 mL of CH_3NO_2. After 1800 seconds, 63.8% yield of (3+2) cycloaddition product **2-4** formed. Φ(63.8%)

$$average\ mol\ of\ product\ formed = 9.641 \times 10^{-5}$$

$$\Phi = 8.854$$

2.7.8 Starting Material Synthesis

$[Cr(Ph_2phen)_3](BF_4)_3$ was prepared according to the procedure of Higgins et al.[7]

4,7-dichloro-1,10-phenanthroline was prepared according to the procedure of Altman and Buchwald.[16] The spectroscopic data were in agreement with the reported data.

4-(dimethylamino)phenylboronic acid was prepared according to the procedure of Oesch and Luedtke.[24] The spectroscopic data were in agreement with the reported data.

Ethyl 2-diazobut-3-enoate was prepared according to the procedure of Sarabia and Ferreira.[11] The spectroscopic data were in agreement with the reported data.

2.8 Notes and References

[1] Serpone, N.; Jamieson, M. A.; Henry, M. S.; Hoffman, M. Z.; Bolletta, F.; Maestri, M. *J. Am. Chem. Soc.* **1979**, *101*, 2907–2916.

[2] McDaniel, A. M.; Tseng, H.-W.; Damrauer, N. H.; Shores, M. P. *Inorg. Chem.* **2010**, *49*, 7981-7991.

[3] Barker, K. D.; Barnett, K. A.; Connell, S. M.; Glaeser, J. W.; Wallace, A. J.; Wildsmith, J.; Herbert, B. J.; Wheeler, J. F.; Kane-Maguire, N. A. P. *Inorg. Chim. Acta.* **2001**, *316*, 41–49.

[4] For a recent example see: Abou-Hatab, S.; Spata, V.; Matsika, S. *J. Phys. Chem. A* **2017**, *121*, 1213-1222.

[5] Stevenson, S. M.; Shores, M. P.; Ferreira, E. M. *Angew. Chem., Int. Ed.* **2015**, *54*, 6506−6510.

[6] Lin, S.; Ischay, M. A.; Fry, C. G.; Yoon, T. P. *J. Am. Chem. Soc.* **2011**, *133*, 19350-19353.

[7] Higgins, R. F.; Fatur, S. M.; Shepard, S. G.; Stevenson, S. M.; Boston, D. J.; Ferreira, E. M.; Damrauer, N. H.; Rappé, A. K.; Shores, M. P. *J. Am. Chem. Soc.* **2016**, *138*, 5451-5464.

[8] Stevenson, S. M.; Higgins, R. F.; Shores, M. P.; Ferreira, E. M. *Chem. Sci.* **2017**, *8*, 654-660.

[9] Higgins, R. F.; Fatur, S. M.; Damrauer, N. H.; Ferreira, E. M.; Rappé, A. K.; Shores, M. P. *ACS Catal.* **2018**, *8*, 9216-9225.

[10] Sarabia, F. J.; Ferreira, E. M. *Org. Lett.* **2017**, *19*, 2865-2868.

[11] Sarabia, F. J.; Li, Q.; Ferreira, E. M. *Angew. Chem. Int. Ed.* **2018**, *130*, 11181-11185.

[12] a) Kirk, A. D.; Porter, G. B. *J. Phys. Chem.* **1980**, *84*, 887-891. b) Serpone, N.; Jamieson, M. A.; Henry, M. S.; Hoffman, M. Z.; Bolletta, F.; Maestri, M. *J. Am. Chem. Soc.* **1979**, *101*, 2907-2916. c) Young, R. C.; Nagle, J. K.; Meyer, T. J.; Whitten, D. G. *J. Am. Chem. Soc.* **1978**, *100*, 4773-4778. d) Otto, S.; Grabolle, M.; Förster, C.; Kreitner, C.; Resch-Genger, U.; Heinze, K. *Angew. Chem. Int. Ed.* **2015**, *54*, 11572-11576. e) Jiménez, J-R.; Doistau, B.; Besnard, C.; Piguet,

C. *Chem. Commun.* **2018**, *54*, 13228-13231. f) Gall, B. K.; Morrison, T.; Shores, M. P.; Ferreira, E. M. *Manuscript in Preparation.* g) Gall, B. K.; Smith, A. K.; Ferreira, E. M. *Manscript in Preparation.* h) McDaniel, A. M.; Tseng, H.-W.; Hill, E. A.; Damrauer, N. H.; Rappé, A. K.; Shores, M. P. *Inorg. Chem.* **2013**, *52*, 1368-1378. i) Ramasami, T.; Endicott, J. F.; Brubaker, G. R. *J. Phys. Chem.* **1983**, *87*, 5057-5059. j) Comba, P. Creaser, I. I.; Gaha, L. R.; Harrowfield. J. M.; Lawrance, G. A.; Martin, L. L.; Mau, A. W. H.; Sargeson, A. M.; Sasse, W. H. F.; Snow, M. R. *Inorg. Chem*. **1986**, *25*, 384-389. k) Brown, K. N.; Beue, R. J.; Sargeson, A. M.; Moran, G.; Ralph, S. F.; Reisen, H. *Chem. Commun.* **1998**, 2291-2292.

[13] a) Chábera, P.; Kjaer, K. S.; Prakash O.; Honarfar, A.; Liu, Y.; Fredin, L. A.; Harlang, T. C. B.; Lidin, S.; Uhlig, J.; Sundström, V.; Lomoth, R.; Persson, P.; Wärnmark, K. *J. Phys. Chem. Lett*. **2018**, *9*, 459–463. b) Palmer, R. A.; Piper, T. S. *Inorg. Chem.* **1966**, *5*, 864-878. c) Van Meter, F. M.; Neumann, H. M. *J. Am. Chem. Soc*. **1976**, *98*, 1382-1388. d) Parisien-Collette, S.; Hernandez-Perez, A. C.; Collins, S. K. *Org. Lett.* **2016**, *18*, 4994-4997. e) Huynh, H. V. *Chem. Rev*. **2018**, *118*, 9457-9492. f) Liu, Y.; Harlang, T.; Canton, S.; Charbera, P.; Suárez-Alcántara, K; Fleckhaus, A.; Vithanage, D. A.; Göransson, E.; Corani, A.; Lomoth, R.; Sundström, V.; Wärnmark, K. *Chem. Commun.* **2013**, *49*, 6412-6414. g) Zimmer, P.; Burkhardt, L.; Freidrich, A.; Steube, J.; Neuba, A.; Schepper, R.; Müller, P.; Flörke, U.; Huber, M.; Lockbrunner, S.; Bauer, M. *Inorg. Chem.* **2018**, *57*, 360-373. h) Zhang, J.; Campolo, D.; Dumur, F.; Xiao, P.; Fouassier, J. P.; Gigmes, D.; Lalevée, J. *ChemCatChem* **2016**, *8*, 2227-2233.

[14] a) Marion, R.; Sguerra, F.; Di Meo, F.; Sauvegeot, J.-F.; Daniellou, R.; Renaud, J.-L.; Linares, M.; Hamel, M.; Gaillard, S. *Inorg. Chem.* **2014**, *53*, 9181-9191. b) Moudam, O.; Kaesar, A.; Delavaux-Nicot, B.; Duhayon, C.; Holler, M.; Accorsi, G.; Armaroli, N.; Séguy, I.; Navarro, J.; Destruel, P.; Nierengarten, J.-F. *Chem. Commun.* **2007**, 3077-3079. c) Kaesar, A.; Moudam, O.;

Accorsi, G.; Séguy, I.; Navarro, J.; Belbakra, A.; Duhayon, C.; Armaroli, N.; Delavaux-Nicot, B.; Nierengarten, J.-F. *Eur. J. Inorg. Chem.* **2014**, 1345-1355. d) Xiao, P.; Dumur, F.; Zhang, J. Fouassier, J. P.; Gigmes, D.; Lalevée, J. *Macromolecules* **2014**, *47*, 3837-3844. e) Mejia, E.; Luo, S. P.; Karnahl, M.; Friedrich, A.; Tschierlei, S.; Surkus, A. E.; Junge, H.; Gladiali, S.; Lochbrunner, S.; Beller, M. *Chem. Eur. J.* **2013**, *19*, 15972-15978. f) Andrés-Tomé, I.; Fyson, J.; Baiao Dias, F.; Monkman, A. P.; Iacobellis, G.; Coppo, P. *Dalton Trans.* **2012**, *41*, 8669-8674. g) Zhang, Y.; Heberle, M.; Wächtler, M.; Karnahl, M.; Dietzek, B. *RSC Adv.* **2016**, *6*, 105801-105805. h) Pirtsch, M.; Paria, S.; Matsuno, T.; Isobe, H.; Reiser, O. *Chem. Eur. J.* **2012**, *18*, 7336-7340. i) Cuttell, D. G.; Kuang, S. M.; Fanwick, P. E.; McMillin, D. R.; Walton, R. A. *J. Am. Chem. Soc.* **2002**, *124*, 6-7. j) Michelet, B.; Deldaele, C.; Kajouj, S.; Moucheron, C.; Evano, G. *Org. Lett.* **2017**, *19*, 3576-2579. k) Wang, B.; Shelar, D. P.; Han, X. Z.; Li, T. T.; Guan, X.; Lu, W.; Liu, K.; Chen, Y.; Fu, F.; Che, C. M. *Chem. Eur. J.* **2015**, *21*, 1184-1190. l) Femoni, C.; Muzzioli, S.; Palazzi, A.; Stagni, S.; Zacchini, S.; Monti, F.; Accorsi, G.; Bolognesi, M.; Armaroli, N.; Massi, M.; Valenti, G.; Marcaccio, M. *Dalton Trans.* **2013**, *42*, 997-1010. m) Bizzarri, C.; Strabler, C.; Prock, J.; Trettenbrein, B.; Ruggenthaler, M.; Yang, C. H.; Polo, F.; Iordache, A.; Brüggeller, P.; De Cola, L. *Inorg. Chem.* **2014**, *53*, 10944-10951. n) Kern, J.-M.; Sauvage, J.-P. *J. Chem. Soc., Chem. Commun.* **1987**, 546-548. o) Knorn, M.; Rawner, T.; Czerwieniec, R.; Reiser, O. *ACS Catal* **2015**, *5*, 5186-5193. p) Paria, S.; Pirtsch, M.; Kais, V.; Reiser, O. *Synthesis* **2013**, *45*, 2689-2698. q) Bagal, D. B.; Kachkovskyi, G.; Knorn, M.; Rawner, T.; Bhanage, B. M.; Reiser, O. *Angew. Chem. Int. Ed.* **2015**, *54*, 6999-7002. r) Rawner, T.; Knorn, M.; Lutsker, E.; Hossain, A.; Reiser, O. *J. Org. Chem.* **2016**, *81*, 7139-7147. s) Pagire, S. K.; Paria, S.; Reiser, O. *Org. Lett.* **2016**, *18*, 2106-2109. t) Smith, C. S.; Mann, K. R. *J. Am. Chem. Soc.* **2012**, *134*, 8786-8789.

[15] a) Son, H.-J.; Han, W.-S.; Chun, J.-Y.; Kang, B.-K.; Kwon, S.-N.; Ko, J.; Han, S. J.; Le, C.; Kim, S. J.; Kang, S. O. *Inorg. Chem*. **2008**, *47*, 5666-5676. b) Xu, H.; Xu, Z.-F.; Yue, Z.-Y.; Yan, P.-F.; Wang, B.; Jia, L.-W.; Li, G. M.; Sun, W.-B.; Zhang, J.-W. *J. Phys. Chem. C* **2008**, *112*, 15517-15525. c) Shanmugan, S.; Xu, J.; Boyer, C. *J. Am. Chem. Soc.* **2015**, *137*, 9174-9185. d) Akçay, H. T.; Bayrak, R.; Demirbas, U.; Koca, A.; Kantekin, H.; Degirmencioglu, I. *Dyes Pigm.* **2013**, *96*, 483-494. e) Gazi, S.; Dokic, M.; Moeljadi, A. M. P.; Ganguly, R.; Hirao, H.; Soo, H. S. *ACS Catal.* **2017**, *7*, 4682-4691. f) Xie, Y.-Z.; Shan, G.-G.; Zhou, Z.-Y.; Su, Z.-M. *Dyes Pigm.* **2013**, *96*, 467-474. g) Sakamoto, R.; Iwasima, T.; Kögel, J. F.; Kusaka, S.; Yasutaka, M.; Kitagawa, Y.; Nishihara, H. *J. Am. Chem. Soc.* **2016**, *138*, 5666-5677. h) Kusaka, S.; Sakamoto, R.; Kitagawa, Y.; Okumura, M.; Nishihara, H. *Chem. Asian J.* **2012**, *7*, 907−910. i) Kusaka, S.; Sakamoto, R.; Nishihara, H. *Inorg. Chem.* **2014**, *53*, 3275−3277.

[16] Altman, R. A.; Buchwald, S. L. *Org Lett*. **2006**, *8*, 2779-2782.

[17] Henriques, R. T.; Herdtweck, E.; Kühn, F. E.; Lopes, A. D.; Mink, J.; Romão, C. C. *J. Chem. Soc., Dalton Trans.* **1998**, *8*, 1293-1297.

[18] Selected work discussed in this chapter is to be submitted for publication.

[19] Connelly, N. G. Geiger, W. E. *Chem. Rev.* **1996**, *96*, 877-910.

[20] Cismesia, M. A.; Yoon, T. P. *Chem. Sci.* **2015**, *6*, 5426-5434.

[21] Edwards, A. C.; Geist, A.; Müllich, U.; Sharrad C. A.; Pritchard, R. G.; Whitehead, R. C.; Harwood, L. M. *Chem. Sci.* **2017**, *53*, 8160-8163.

[22] a) Hatchard, C. G.; Parker, C. A. *Proc. Roy. Soc.* (London) **1956**, *A235*, 518–536. b) Kuhn, H. J.; Braslavsky, S. E.; Schmidt, R. *Pure Appl. Chem.* **2004**, *76*, 2105–2146. c) Monalti, M., et. al. Chemical Actinometry. *Handbook of Photochemistry, 3rd Ed*; Taylor & Francis Group, LLC. Boca Raton, FL, **2006**, 601–616.

[23] Monalti, M. et. al. Chemical Actinometry. *Handbook of Photochemistry, 3rd Ed*; Taylor & Francis Group, LLC. Boca Raton, FL, **2006**, 601–616.

[24] Oesch, D.; Luedtke, N. W. *Chem. Commun.* **2015**, *51*, 12641-12644.

CHAPTER 3

DEAROMATIVE (3+2) CYCLOADDITION OF INDOLES AND VINYL DIAZOACETATES USING CHROMIUM(III) PHOTOCATALYSIS

3.1 Introduction

Over the past few decades, photoredox catalysis has emerged as a robust tool for new bond formation.[1] Acting as an oxidant or a reductant, an excited-state metal complex can generate highly reactive radical intermediates via a single-electron transfer process using a simple light source. Commonly used transition metal photocatalysts are complexes of ruthenium(II) or iridium(III), two of the rarest and most expensive transition metals. Due to their natural abundance, first-row transition metals as photocatalysts would provide an alternative approach to transition metal photocatalysis. First-row transition metal photocatalysts have been developed using chromium[2], iron[3], cobalt[4], nickel[5], and copper[6]. To expand first-row transition metal photocatalysis, Shores and coworkers investigated the photophysical properties of homo- and heteroleptic chromium(III) complexes.[7] These Cr(III) complexes feature relatively high excited-state reduction potentials and lifetimes while absorbing in the visible region. In 2015, our group and collaborators developed a chromium(III) photocatalyzed Diels-Alder cycloaddition reaction via a radical cation intermediate.[2a] Expanding on this cycloaddition reaction, Cr(III) photocatalysis has now been employed in (2+1) and (3+2) cycloaddition reactions using electron

rich alkenes and diazo or vinyl diazo reagents, respectively.[2c] To broaden Cr(III) photocatalysis's feasibility, indole represented a new class of electron rich alkenes for potential functionalization.

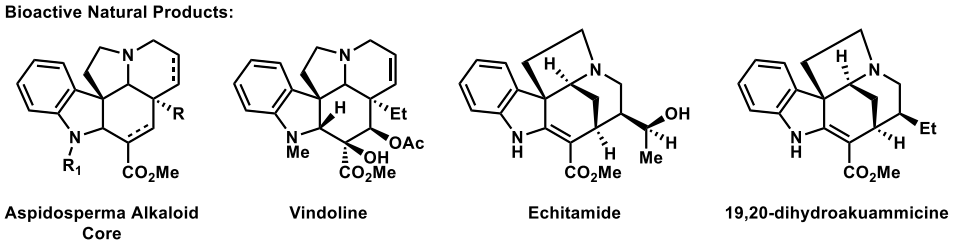

Figure 3.1. Indoline-containing bioactive natural products.

In nature, tryptophan and tryptamine serve as starting points for the biosynthesis of differently constructed indolines. The indoline structural motif is prevalent in many natural products with unique biological and pharmacological activity (Figure 3.1). Methods to synthesize indolines are widely known; however, very few photocatalyzed reactions have been developed. In 1990, Geiseler and coworkers discovered a (4+2) photocatalyzed cycloaddition using a pyrylium photocatalyst, indole as the dienophile, and cyclic dienes (Scheme 3.1).[8] Their method favors endo-cyclization products but requires electron rich dienophiles. Notably, their optimized reaction conditions were performed under air-free conditions and needed a protecting group to yield the desired product. Mechanistically, an abstraction of an electron from indole (E_{ox} = +1.26 V vs. Ag/Ag^+) by the excited-state pyrylium photocatalyst (E^*_{red} = +2.51 V vs. Ag/Ag^+) generates radical cation intermediate **3-2**. Radical-radical coupling of the radical-cation intermediate with cyclohexadiene forms a new radical-cation intermediate **3-3**. Reduction of **3-3** by the pyrylium photocatalyst and subsequent nucleophilic attack onto the iminium yields the unprotected (4+2) cycloadduct **3-4**. The need for the protecting group and base in the reaction is shown in this step. Cycloadduct **3-4** has an oxidation potential of +0.7 to +0.8 V vs. Ag/Ag^+ while indole has a oxidation potential of +1.26 V vs. Ag/Ag^+, meaning that oxidation of **3-4** is going to be preferential over oxidation of the starting material. The protection of cycloadduct **3-4** from the acetyl

chloride/$NaHCO_3$ conditions to form **3-1** pulls the oxidation potential of the desired cycloadduct out of range, leaving the pyrylium photocatalyst to favor oxidation of the starting indole. Geiseler, Steckhan, and Yoon have since updated reaction conditions and used different catalysts or dienes to perform the photocatalyzed (4+2) cycloaddition with indole.[9]

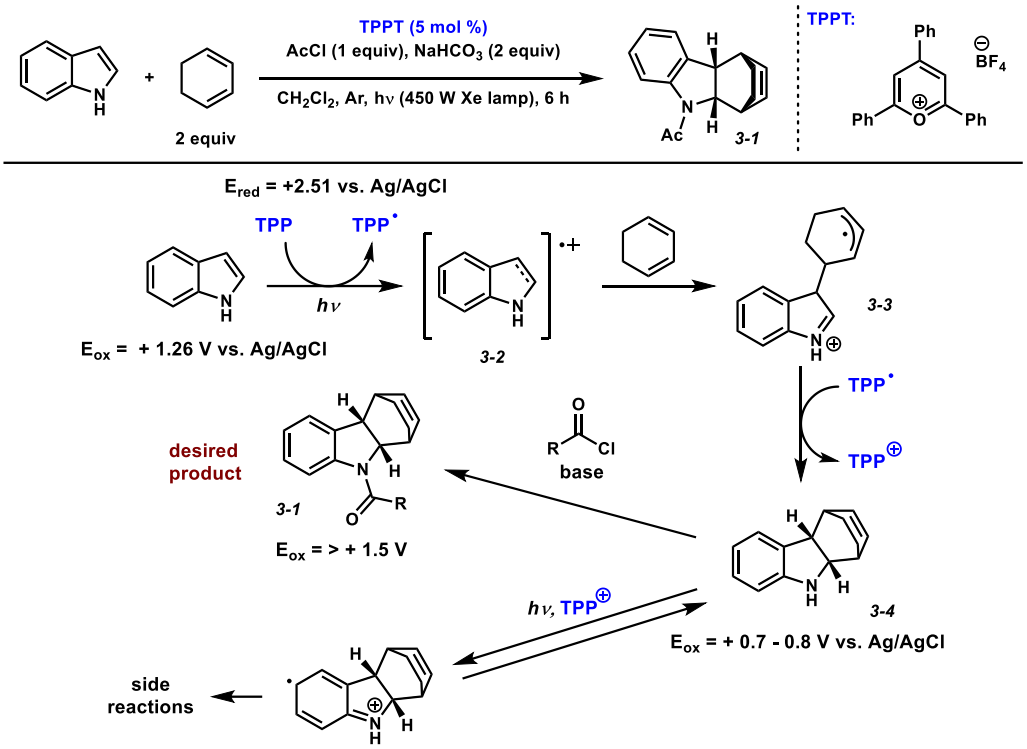

Scheme 3.1. Geiseler's reaction and proposed mechanism.

In 2018, Sarabia and coworkers developed a (3+2) cycloaddition of electron rich alkenes and vinyl diazoacetates using chromium(III) or ruthenium(II) photocatalysis.[2d] The requirement of electron rich alkenes limited the overall scope of the transformation. Ruthenium(II) photocatalyzed examples, in comparison to chromium(III) as the photocatalyst, tend to have faster reaction times. Using *trans*-anethole, isoprene, and a chromium(III) photocatalyst as model substrates, the mechanism of this reaction can be seen in Scheme 3.2. The ground-state Cr(III) catalyst can be excited by light to excited-state *Cr(III), which can abstract an electron from *trans*-anethole to form radical-cation intermediate **3-5**. Intermediate **3-5** then reacts with the vinyl

diazoacetate **3-6** in two different pathways, direct formation or a 4-exo cyclization. Direct construction yields (3+2) cycloadduct **3-7**, while the 4-exo cyclization product **3-8** can then undergo a ring expansion to form **3-7**. Cycloaddition product **3-8** can be formed from an oxidation of (2+2) cycloadduct **3-9**, which is formed from *trans*-anethole and vinyl diazoacetate **3-6**. Two different pathways can reduce radical-cation **3-7**. A metal reduction from the Cr(II) species generated previously yields cycloadduct **3-10** and Cr(III), the latter which can continue in the catalytic cycle. Alternatively, a chain propagation pathway could occur. Radical-cation **3-7** can abstract an electron from *trans*-anethole, forming **3-10** and the radical-cation **3-5**, the latter which can continue in the catalytic cycle. Using Geiseler's optimized conditions and our understanding of the chromium(III) photocatalyzed (3+2) reaction, we theorized that we could trap the indole radical-cation generated by chromium(III) photocatalysis with a vinyl diazoacetate to yield substituted indoline products.

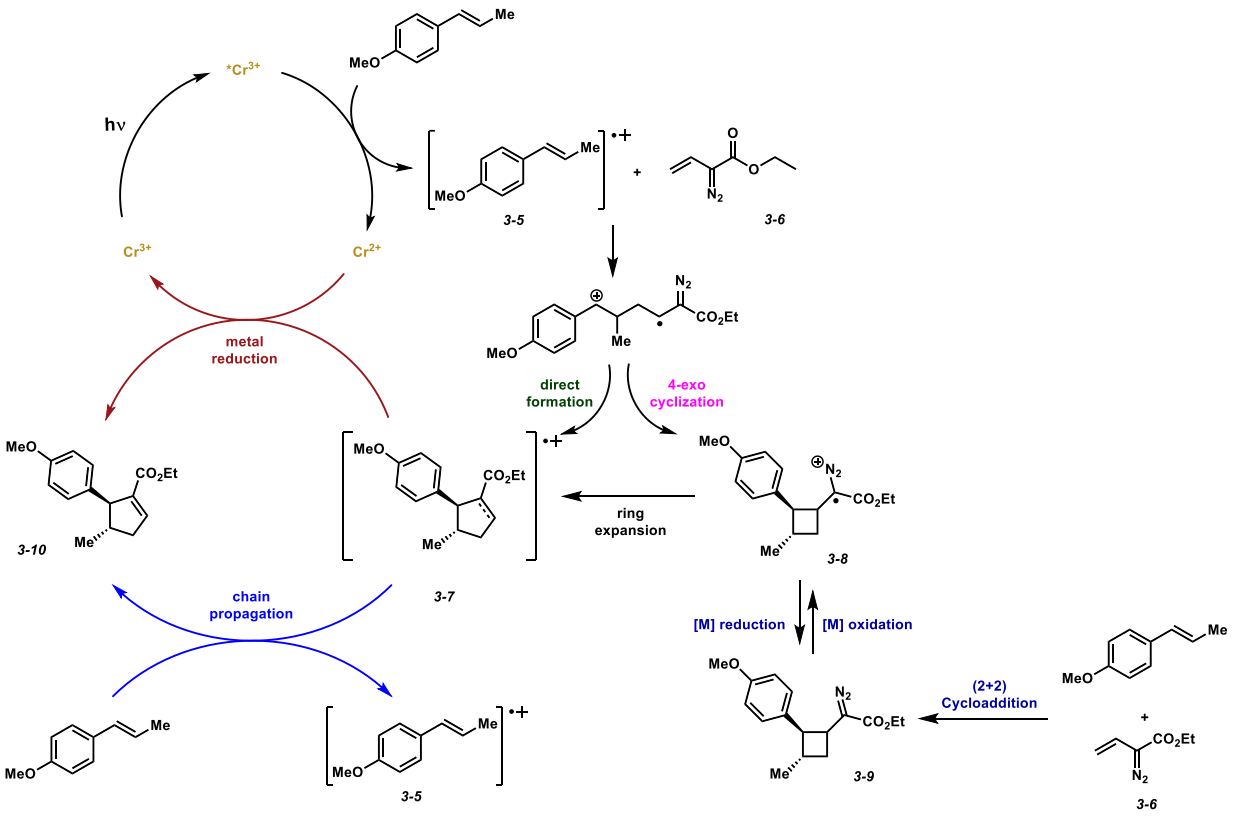

Scheme 3.2. Sarabia and coworkers' example reaction and proposed mechanism.

3.2 Early Optimization Experiments

Initially, Geiseler's conditions yielded the desired (3+2) cycloadduct in low yield (Table 3.1). In an independent experiment, acetyl chloride decomposed the vinyl diazoacetate. In the presence of base and light, acyl chlorides can form ketenes, which can react with alkenes.[10] In the presence of $NaHCO_3$ and visible light, acetyl chloride could generate a ketene in situ that can react with the vinyl diazoacetate, therefore decomposing the reagent. To avoid this decomposition, benzoyl chloride was used for catalyst optimization (Table 3.1). $[Cr(Ph_2phen)_3](BF_4)_3$ formed the desired cycloadduct in 26% yield (entry 1) in 24 h. Running the reaction for longer does not increase the yield of the cycloadduct. Catalyst decomposition, along with decomposition of the starting materials could occur, hindering reactivity. Seeking to improve on the $[Cr(Ph_2phen)_3](BF_4)_3$ result, other organic and transition metal photocatalysts were analyzed.

Pyrylium-based photocatalysts provided an increased yield to 43% (entries 2-3). Acridinium photocatalyst, Mes-Acr^{+}, yielded similar results to the pyrylium photocatalysts, with a 46% yield of the desired product (entry 4). $[Ru(bpy)_3]Cl_2$ with and without an oxidative quencher decreased the overall yield of the reaction (entries 5-6). In previously developed (3+2) cycloadditions, using $[Ru(bpz)_3](PF_6)_2$ increased yields while decreasing reaction times. In this reaction, $[Ru(bpz)_3](PF_6)_2$ produced similar results to the organic photocatalysts (entry 7); however, noticeable non-specific decomposition occurred within the reaction.

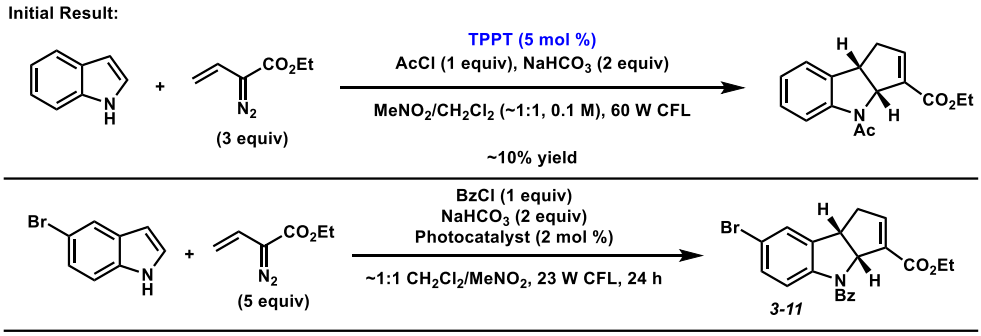

Entry	Catalyst	NMR yield
1	$[Cr(Ph_2phen)_3](BF_4)_3$	26%
2	TPPT	41%
3	$(OMe)_3$TPPT	43%
4	Mes-Acr	46%
5	$[Ru(bpy)_3]Cl_2$	10%
6	$[Ru(bpy)_3]Cl_2$ + MV	trace
7	$[Ru(bpz)_3](PF_6)_2$	44%
8	$[Ir(dFCF_3ppy)_2(5,5'\text{-}dCF_3bpy)](PF_6)$	62%

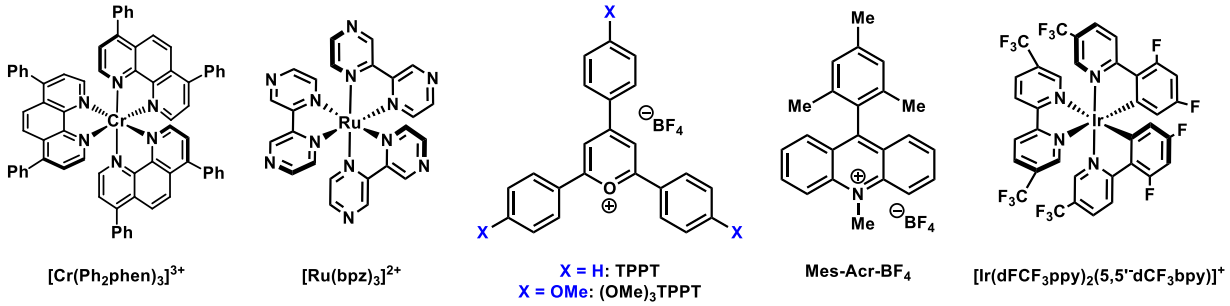

Table 3.1. Initial result and catalyst optimization. (MV = methyl viologen dichloride hydrate)

We theorized that the basicity of the pyrazine ligands on $[Ru(bpz)_3](PF_6)_2$ was reacting with benzoyl chloride, rendering the catalyst poisoned. Investigations into this phenomenon occurred by using UV-vis experiments. Treating $[Ru(bpz)_3](PF_6)_2$ with the simulated reaction conditions of 300 equivalents of benzoyl chloride while irradiating with visible light showed that $[Ru(bpz)_3](PF_6)_2$ decomposed over time into a different complex. These results can help explain the significant decomposition within the (3+2) reaction if catalyst poisoning or erosion into another entity is occurring. Lastly, we analyzed a highly oxidizing iridium(III) photocatalyst, which increased the overall yield of the reaction. There are two takeways from the iridium(III) results. First, this catalyst does not alight with our project goals to use first-row, earth-abundant transition metals as photocatalysts. Second, we believed that we could do better than the iridium(III) complex's results using a chromium(III) complex.

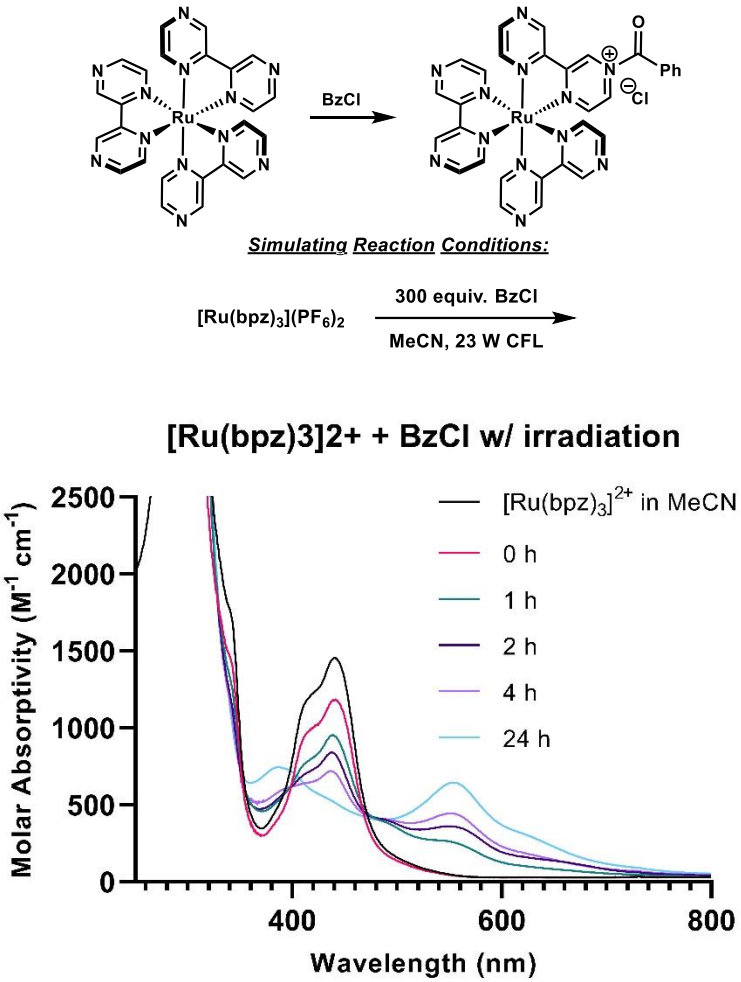

Figure 3.2. Degradation of $[Ru(bpz)_3](PF_6)_2$.

3.3 Catalyst Design and Synthesis

Design, synthesis, and characterization of new ligands and the corresponding chromium(III) complexes are explained in a previous chapter.[11] The chromium(III) complexes were also analyzed in different photoreactions, where $[Cr(PMP_2phen)_3](BF_4)_3$ outperformed the parent catalyst of $[Cr(Ph_2phen)_3](BF_4)_3$. $[Cr(PMP_2phen)_3](BF_4)_3$ was utilized as the photocatalyst for the (3+2) cycloaddition between indoles and vinyl ethyl diazoacetate using visible light. To our delight, using $[Cr(PMP_2phen)_3](BF_4)_3$ yields the desired cycloadduct **3-11** in 75% yield. For this reaction, we successfully outperformed iridium(III) and ruthenium(II) cases.

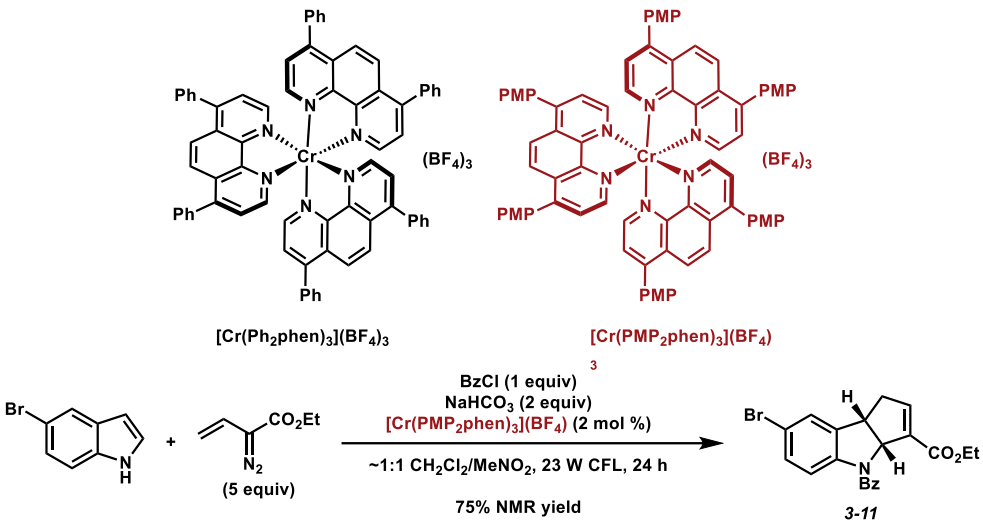

Scheme 3.3. $[Cr(PMP_2phen)_3](BF_4)_3$ photocatalyzed (3+2) cycloaddition.

3.4 Optimization and 5-Substituted Indole Scope of the Reaction

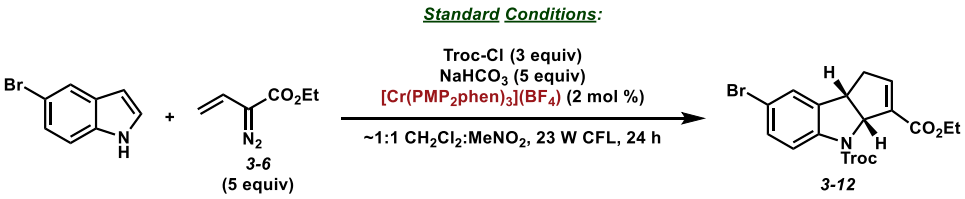

Entry	Deviation from Standard Conditions	NMR yield
1	none	95%
2	BzCl	94%
3	$KHCO_3$	51%
4	390 nm irradiation	28%
5	NUV irradiation	39%
6	Ar or O_2 atmosphere	>90%
7	2 equiv *3-6*	73%
8	0.5 mol % photocatalyst	76%
9	no base	45%
10	no acylating agent, catalyst, or light	0%

Table 3.2. Deviation from the standard conditions.

Extensive optimization of the reaction occurred while using $[Cr(PMP_2phen)_3](BF_4)_3$ as the photocatalyst. The protecting group, stoichiometry, irradiation source, and atmosphere are critical variables to this reaction. We found that using 2,2,2-trichloroethoxycarbonyl chloride (Troc-Cl) as the acylating agent and $NaHCO_3$ as the base gave the best results. Upon examining

stoichiometry, 3 equiv of an acylating agent and 5 equiv of base increased the overall yield of the reaction. The optimized, standard conditions for this reaction can be seen in Table 3.2, furnishing a 95% yield (entry 1). Deviations from these conditions are noted. Benzoyl chloride (BzCl) as the acylating agent showed comparable yield (entry 2); however, across a wide range of electronically different indoles, using BzCl as the acylating agenT saw diminished yields of cycloadducts. Troc-Cl was found to be more consistent; we therefore used that acylating agent for further reactions. Potassium bicarbonate ($KHCO_3$) instead of sodium bicarbonate ($NaHCO_3$) decreased the overall yield of the reaction (entry 3). Different light sources decreased the overall yield of the reaction (entries 4 and 5). An argon or oxygen atmosphere did not play a critical role in this reaction (entry 6). This information is critical in the mechanistic understanding of this reaction. Different stoichiometry, lower catalyst loading, or absent reagents showed diminished yields of cycloadduct **3-12** (entries 7, 8, and 9). Lastly, experiments without acylating agent, photocatalyst, or light did not yield the desired cycloadduct (entry 10).

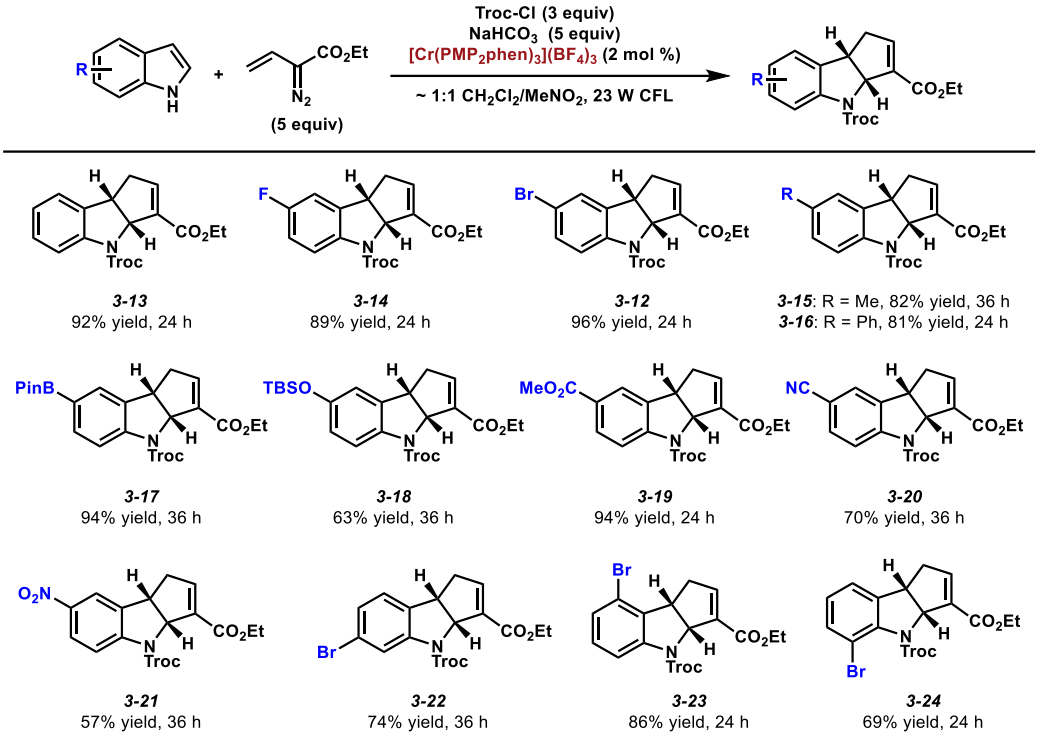

Scheme 3.4. 5-Substituted indole scope.

With the optimized conditions in hand, the scope of the reaction was analyzed. Initially, 5-substituted indoles with electron donating or electron withdrawing groups were investigated (Scheme 3.4). Indoles having halides, alkyl, or aryl substituents all reacted and afforded the desired cycloadduct in excellent yields (**3-12 – 3-16**). A boronic ester was also compatible in the reaction, which provides a valuable handle for further diversification (**3-17**). A silyl ether, ester, nitrile, or nitro groups on the indole also gave the desired cycloadduct in good yields (**3-18 – 3-21**). Differently substituted bromo-indoles were also analyzed, generating the desired cycloadducts in good yield (**3-22 – 3-24**).

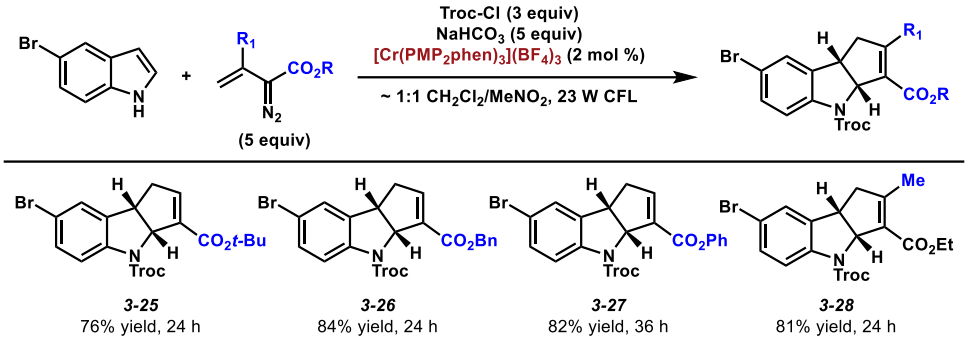

Scheme 3.5. Diazoester scope.

Different vinyl diazoesters or acylating agents were effective in affording the desired cycloadducts (Schemes 3.5-3.6). The highly activated phenyl ester (**3-27**) or even β-alkyl substitution (**3-28**) on the vinyl diazo reagent were tolerated. Benzoyl chloride derivatives with electron withdrawing and electron donating groups were compatible within the reaction and yielded the desired cycloadducts (**3-29 - 3-32**). Other alkoxylcarbonyl chlorides can be used to protect the desired indoline product (**3-33 – 3-34**). Overall, electronically diverse 5-substituted indoles, as well as different vinyl diazoesters and acylating agents, were compatible within the reaction.

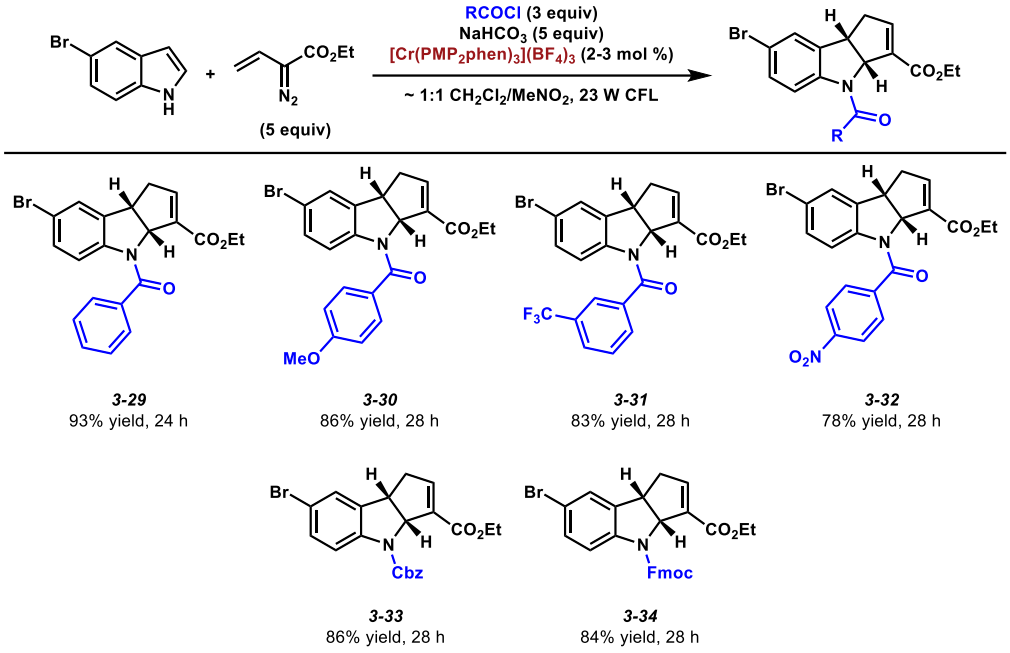

Scheme 3.6. Acylating agent scope.

3.5 2,3-Disubstituted Indole Optimization and Reaction Scope

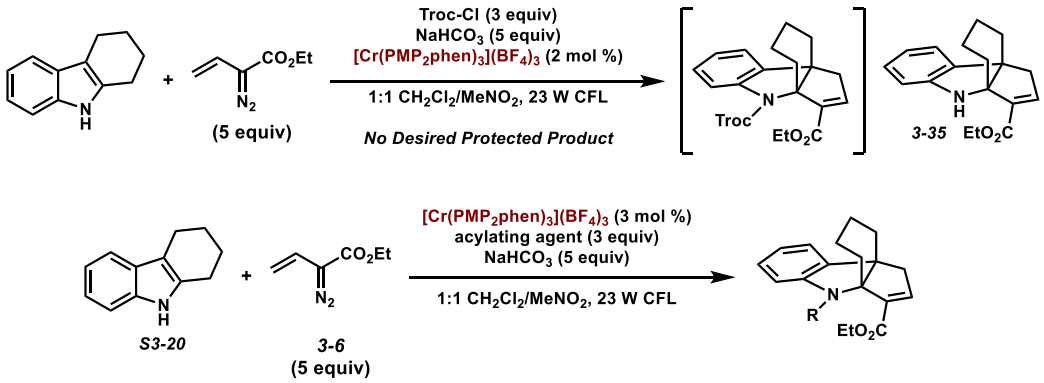

Acylating Agent/Electrophile	NMR yield (%)
BzCl	0
AcCl	0
Ac_2O	0
TFAA	0
Boc_2O	0
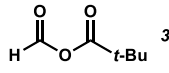 *3-36*	30
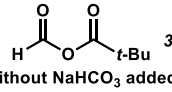 *3-36* (without $NaHCO_3$ added)	93

Scheme 3.7. 2,3-Disubstituted indole optimization.

Analysis of 2,3-disubstituted indoles with the optimized reaction conditions showed little to no desired product formation (Scheme 3.7). The majority of product isolated from the reaction mixture was unprotected (3+2) cycloadduct **3-35**, where the yield was low. Steckhan and coworkers proposed a competitive oxidation process between the unprotected indoline product and the starting indole in the presence of the excited state photosensitizer.[8] To overcome this issue, we analyzed different acylating agents or alternative electrophiles. Other acyl chlorides or anhydrides offered no desired protected product formation. To our delight, mixed anhydride **3-36** produced the desired formylated cycloadduct in 30% yield and generates pivalic acid as the primary byproduct of the reaction. We theorized that the base could assist in an irreversible deprotonation event at the nitrogen center or at the C2α-position, which is specific to 2-substituted indoles (Scheme 3.8). These new intermediates could lead to unwanted or hindered reactivity or product formation. Without the addition of $NaHCO_3$, conditions using mixed anhydride **3-36** as the acylating agent yielded formylated cycloadduct in 93% yield (Scheme 3.7).

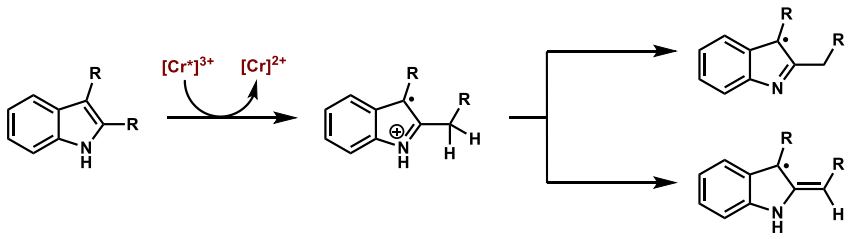

Scheme 3.8. Deprotonation of 2-substituted indoles.

Using **3-36** as the formylating agent, 2- and 3-substituted indoles with alkyl or aryl substituents all yielded the desired formylated cycloadduct in moderate yields (Scheme 3.9). A protected tryptamine derivative generated **3-41** in a modest yield. 2,3-Disubstituted indoles and fused-ring indoles (**3-37 – 3-46**) all reacted to yield the formylated cycloadduct. A different vinyl diazo reagent was also compatible with the formylating conditions (**3-47**).

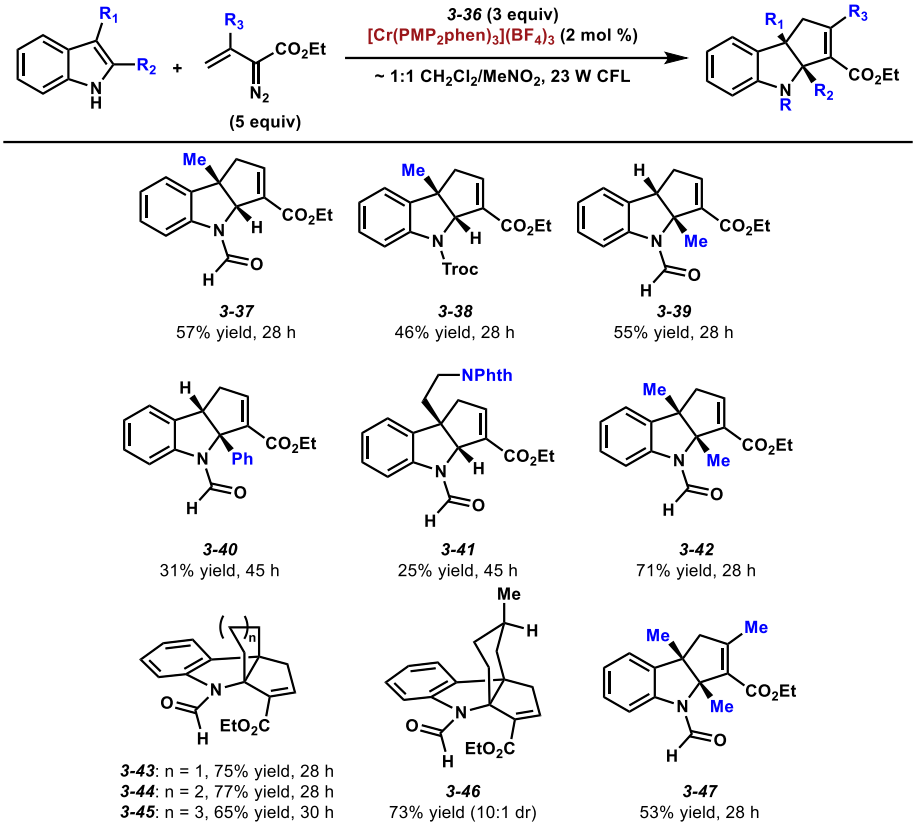

Scheme 3.9. 2-Substituted, 3-substituted, and 2,3-disubstituted indole scope.

3.6 Mechanistic Experiments and Proposed Mechanism

To determine whether this reaction is dependent upon the oxidation potentials of the substrates, competition experiments were investigated (Scheme 3.10). Equivalent amounts of two electronically different or similar indoles were mixed, subjected to standard 5-substituted indole conditions, and analyzed at timepoints to determine the yields of the products. The mixture of 5-bromoindole (E_{ox} = +1.30 V vs. SCE) and 5-methylindole (E_{ox} = +1.18 V vs. SCE) showed that 5-methylindole exclusively reacts to form the desired cycloadduct over 5-bromoindole. This would indicate that the oxidation potentials of the indole play a role in the reaction. 5-bromoindole (E_{ox} = +1.30 V vs. SCE) and 5-CO_2Me-indole (E_{ox} = +1.33 V vs. SCE) are more electronically equivalent. In this mixture, both indoles react equally, and the yields of the desired cycloadducts are similar. Mixtures of reactive alkenes and indoles were also accessed under standard 5-

substituted indole conditions. *trans*-Anethole (E_{ox} = +1.11 V vs. SCE[2a]) and 5-bromoindole (E_{ox} = +1.30 V vs. SCE) mixture yielded the desired cycloadducts in similar quantities, with cyclopentene formation from trans-anethole slightly favored. $[Cr(PMP_2phen)_3](BF_4)_3$ catalyzes cyclopentene formation between *trans*-anethole and ethyl vinyl diazoacetate using visible light in under 1 h. This experiment shows a direct comparison of the speeds of two different reactions within the same pot. All of this information helps guide the understanding of the reaction mechanism.

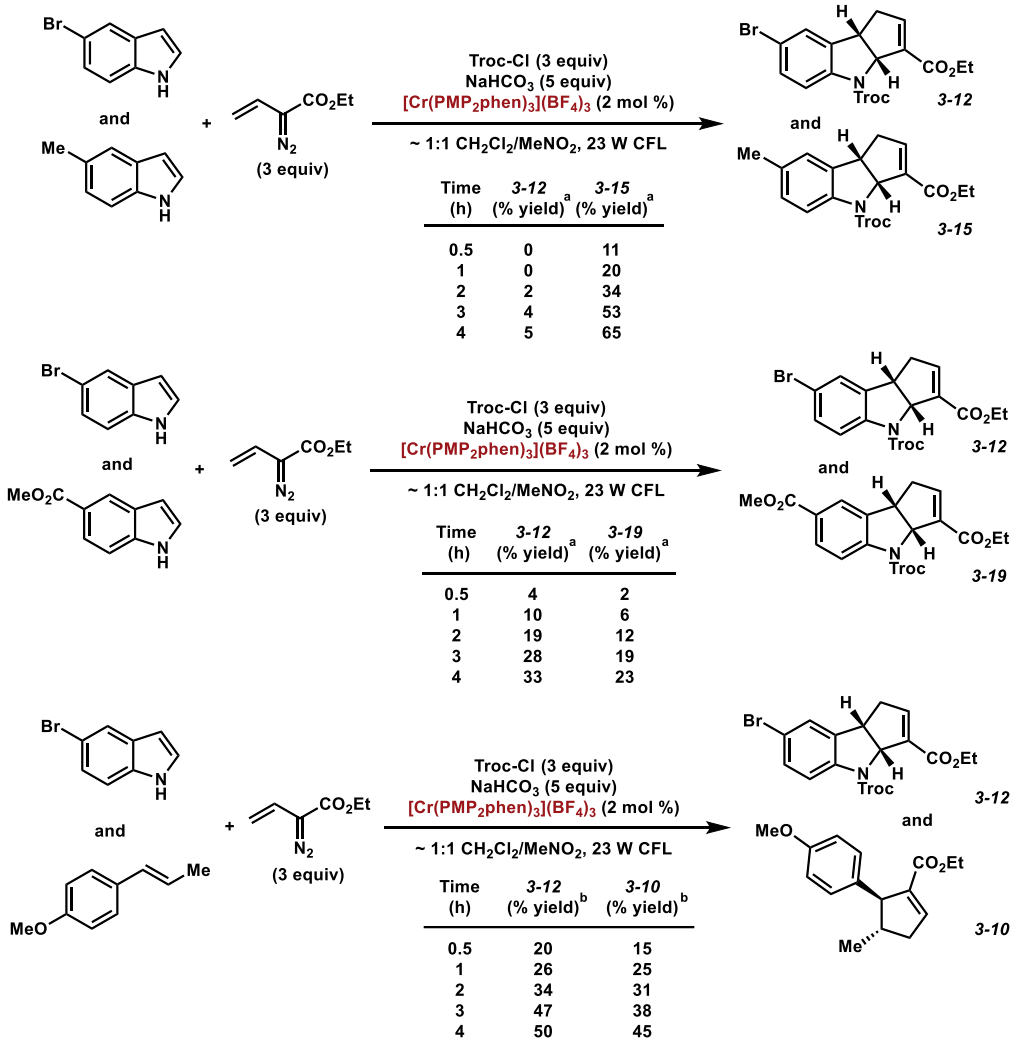

Scheme 3.10. Competition experiments. [a]Yields determined by GC analysis with 4,4'-di-*t*-butylbiphenyl as the internal standard, [b]1H NMR yields determined using dodecyl acetate as the internal standard, PMP = 4-$MeOC_6H_4$.

To analyze the regioselectivity of the vinyl diazoacetate addition to the indole in this reaction, intramolecular substrates were synthesized and subjected to the two different reaction conditions developed (Scheme 3.11). With all the 5-substituted indole cases, the regioselectivity of vinyl diazoacetate addition occurs exclusively at the benzylic position (3-position) of the indole. Substituted indoles with the vinyl diazoacetate tethers at either the 2- or 3-positions were investigated (**S3-31** and **S3-34)**. In the 3-substituted intramolecular example (Scheme 3.11), treatment to either reaction conditions did not produce the desired cycloadducts **3-48** or **3-49**. This is consistent with the regioselectivity that is seen within the reaction, where radical addition occurs at the 3-position. **S3-34** also poses conformation issues with addition, potentially generating a macrocyclic ring that would be unfavorable. In the 2-substituted intramolecular example, both conditions provided complex mixtures of products (**3-50** and **3-51**). We are confident that cycloaddition occurred; however, upon further analysis, we believe that the intermolecular cycloaddition reaction occurred. Regioselectivity of intermolecular product showed addition at the 3-position of **S3-31**.

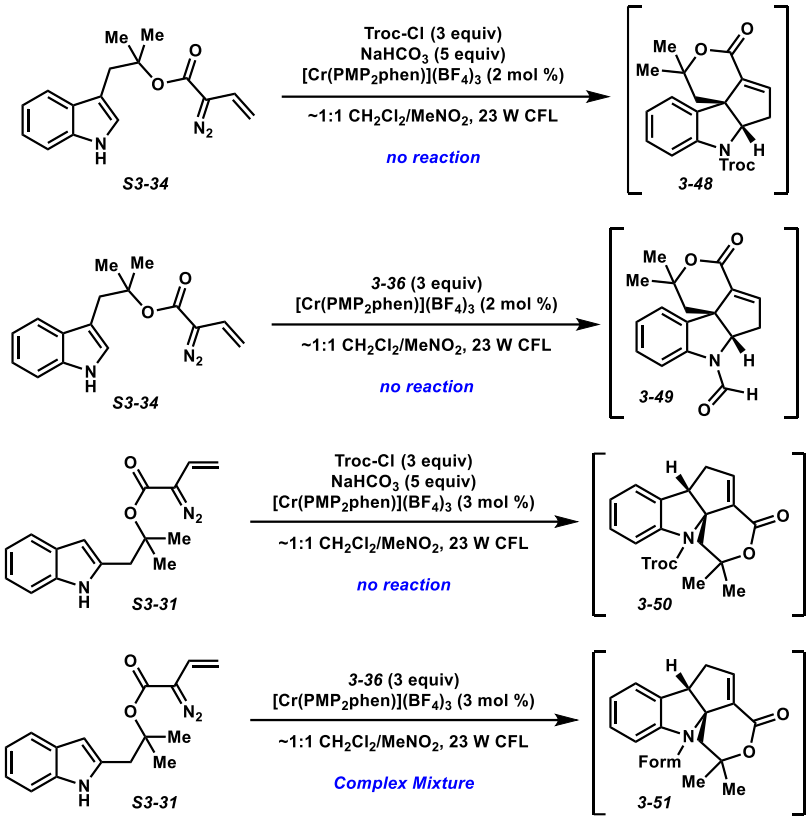

Scheme 3.11. Intramolecular examples.

The proposed mechanism can be seen in Figure 3.3 using indole and a chromium(III) photocatalyst as model substrates. The ground-state Cr(III) can be irradiated by light to the excited-state *Cr(III) catalyst. *Cr(III) can then abstract an electron from indole **3-52**, generating radical-cation intermediate **3-A** and Cr(II). Radical addition with the alkene of the vinyl diazoacetate forms a new radical-cation intermediate **3-B**. It cannot be ruled out that a (2+2) cycloaddition, similar to what Sarabia proposed, can occur, followed by a ring expansion to yield intermediate **3-C**. Along this route, loss of nitrogen followed by reduction from the Cr(II) forms unprotected indoline **3-D** and regenerates the Cr(III) catalyst. Indoline **3-D** can be protected by the acylating group to prevent competitive oxidation and to form cycloadduct **3-53**. Alternatively, a cyclization could occur, producing intermediate **3-C**. Loss of N_2 and subsequent reduction

generates intermediate **3-D**, which in the presence of the acylating agent and base forms cycloadduct **3-53**.

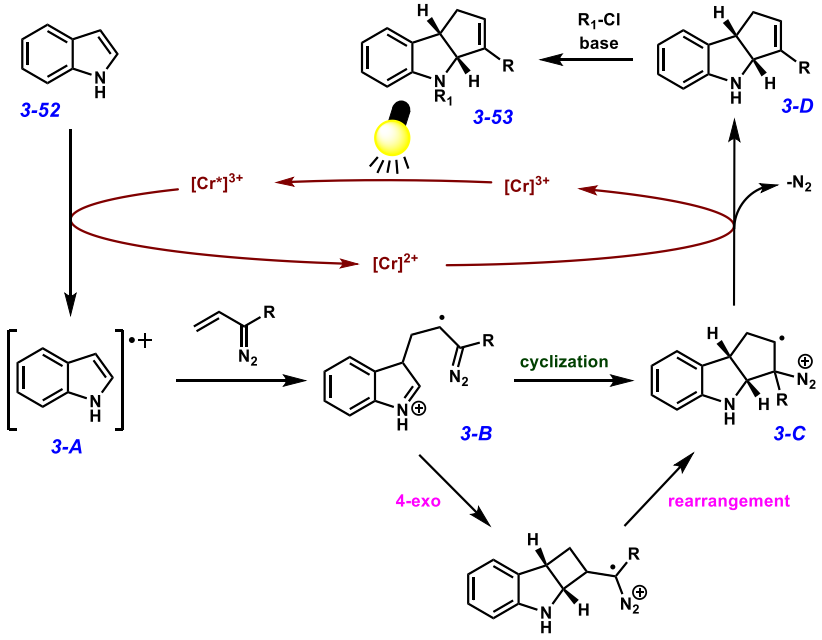

Figure 3.3. Proposed reaction mechanism.

3.7 Product Diversification

The indoline cycloaddition products can be readily diversified with transformations seen in Scheme 3.12. Deprotection of the Troc or formyl[12] group proceeded in excellent yield to the free indoline products **3-36** and **3-54** (Scheme 3.12). An N-heterocycle (**3-55**) and an electron rich arene (**3-56**) can be coupled to the product in good yield. Treatment of **3-12** with DIBAL-H yielded a reductive cyclization product **3-57** in excellent yield. Allylic oxidation using a pyridinium dichromate (PDC)/*t*-BuOOH system gave ketone **3-58** in good yield.[13] Dihydroxylation or conjugate reduction[14] of **3-12** each produces **3-59** and **3-60** in 94% yield with moderatre diastereoselectivity. Other cycloaddition reactions can also be performed. A (3+2) cyclization using imine **3-62** mediated by AgOAc yielded strictly endo product **3-61** in excellent yield.[15] The diastereoselectivity of this reaction was determined to be 5:1 endo/exo after

trifluoroacetate protection of the secondary amine. These transformations show the synthetic utility of the indoline products.

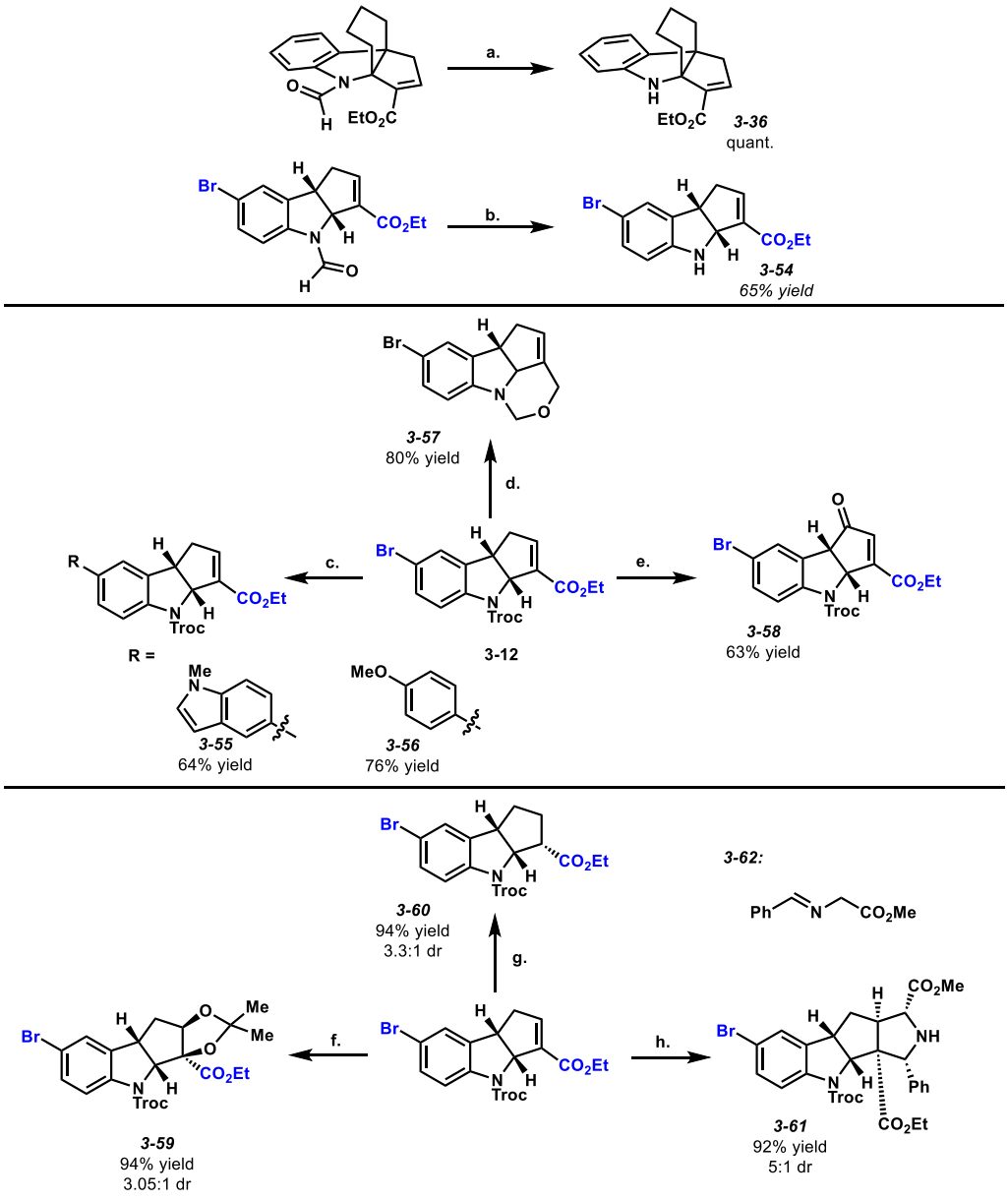

a) Zn dust, AcOH. b) methanolic HCl. c) $PdCl_2$(dppf), K_3PO_4, boronic acid or ester. d) DIBAL-H. e. PDC, *t*-BuOOH. f) OsO_4, NMO. g) Fe(tpp)Cl, $NaBH_4$. h) *3-62*, AgOAc, PPh_3, Et_3N.

Scheme 3.12. Product diversifications.

3.8 Conclusions

In summary, we have developed a Cr(III) photocatalyzed (3+2) cycloaddition between indoles and vinyl diazo compounds using a novel Cr(III) photocatalyst. The cycloadducts can be

readily diversified, expanding the utility of this transformation. To our knowledge, this is the first report of the vinyl diazo species reacting with an indole radical-cation intermediate. We anticipate this reaction could serve as a platform for accessing an array of indoline-based compounds. Further mechanistic studies, expansion toward enantioselective variants, and applications in chemical synthesis are currently underway.

3.9 Experimental Procedures

3.9.1 Materials and Methods

$[Ru(bpz)_3](PF_6)_2$ was prepared according to the procedure by Yoon and coworkers.[16] Reactions were performed under argon atmosphere unless otherwise noted. Dichloromethane, tetrahydrofuran, dimethylformamide, and toluene were purified by passing through activated alumina columns. Nitromethane (99%) and 1,4-dioxane were used as received. Commercially available chemicals were purchased from Alfa Aesar (Ward Hill, MA), Sigma-Aldrich (St. Louis, MO), Oakwood Products, (West Columbia, SC), Strem (Newburport, MA), and TCI America (Portland, OR). Qualitative TLC analysis was performed on 250 mm thick, 60 Å, glass backed, F254 silica (SiliCycle, Quebec City, Canada). Visualization was accomplished with UV light and/or exposure to cerium ammonium molybdate (Hanessian's Stain), $KMnO_4$, or *p*-anisaldehyde stain solutions followed by heating. Flash chromatography was performed using SiliCycle silica gel (230-400 mesh). ^1H NMR spectra were acquired on a Bruker AVANCE III HD NMR (at 400 MHz) and are reported relative to $SiMe_4$ (δ 0.00). ^{13}C NMR spectra were acquired on a Bruker AVANCE III HD NMR (at 100 MHz) and are reported relative to $SiMe_4$ (δ 0.0). ^{19}F NMR spectra were acquired on a Bruker AVANCE III HD NMR (at 376 MHz) and are reported relative to $CFCl_3$ (δ 0.0). Variable Temperature (VT) ^1H NMR was acquired on a Varian INOVA (at 500 MHz) and are reported relative to $SiMe_4$ (δ 0.00). Variable Temperature (VT) ^{13}C NMR was acquired on a Varian INOVA (at 125 MHz) and are reported relative to $SiMe_4$ (δ 0.00). All IR spectra were obtained Thermo Nicolet iS10 spectrometer and are reported in wavenumbers (ν). High resolution mass spectrometry (HRMS) data were acquired via electrospray ionization (ESI) using a ThermoFisher Orbitrap Q-Exactive. Cyclic voltammetry (CV) measurements were performed with a WaveDriver 40 Bipotentiostat/Galvanostat from the Pine Research Instrument

Company using non-aqueous Ag/Ag^+ reference electrode (Ag wire immersed in CH3CN containing 0.25 M Bu_4NPF_6), Pt wire counter electrode, and a stationary glassy-carbon working milli-electrode (3 mm diameter). Measurements were performed at ambient temperature under argon atmosphere using 5 mM analyte in CH_3CN containing 0.25 M Bu_4NPF_6 as the supporting analyte. Analyte potentials were referenced against 5 mM ferrocene internal standard under identical conditions, where $E_{1/2}$ = 0.275 V in CH_3CN vs the reported non-aqueous Ag/Ag^+ electrode. Potential is referenced to Fc^+/Fc. Scans were performed at 100 mV/s scan rate in 0.25 M Bu_4NPF_6. To convert potentials from V vs. Fc^+/Fc to V vs. SCE, 0.400 was added to the potentials taken in CH_3CN.[17] Reactions under near-UV irradiation (NUV) were performed in a Luzchem photoreactor (LZC-ORG) equipped with 10 lamps of wavelengths 419, 350, and 300 nm. Reactions under blue LED irradiation were performed using a 390 nm Kessil PR160L LED PhotoReaction light. Irradiation with visible light was performed with one 23 W compact fluorescent light bulb (EcoSmart 23 W bright white CFL spiral bulb, 1600 lumens). Cycloadditions using all modes of irradiation were performed using flame-dried borosilicate vials. The internal temperature of the photobox was maintained at 30 °C.

3.9.2 Optimization Experiments:

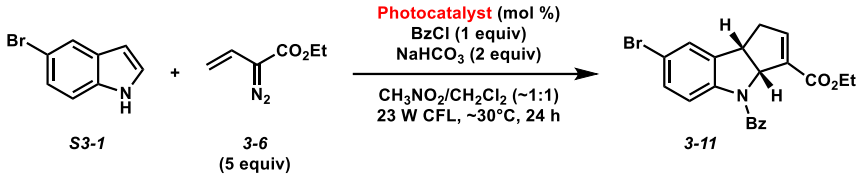

S3-1 + *3-6* (5 equiv) → *3-11*

Entry	Photocatalyst (mol %)	NMR yield (%)
1	$[Cr(Ph_2phen)_3](BF_4)_3$ (2)	26
2	TPPT (5)	41
3	$(OMe)_3$TPPT (5)	43
4	DCB (5)	0
5	DCA (5)	23
6	Mes-Acr-BF_4 (2)	46
7	4-CzIPN (2)	trace
8	$[Ru(bpy)_3]Cl_2$ (2)	10
9	$[Ru(bpy)_3]Cl_2$ + MV (2 + 10)	trace
10	$[Ru(bpz)_3](PF_6)_2$ (2)	44
11	$[Ir(dFCF_3ppy)_2(bpy)]$ (2)	0
12	$[Ir(dFCF_3ppy)_2(5,5'\text{-}dCF_3bpy))](PF_6)$ (2)	62
13	$[Cr(PMP_2phen)_3](BF_4)_3$ (2)	75
14	$[Cr(PMP_2phen)_3](BF_4)_3$ (2, no light)	0
15	none	0

General procedure for CATALYST optimization:

5-Bromoindole (0.100 mmol), $NaHCO_3$ (0.200 mmol), and photocatalyst (half of indicated amount in table) were added to a flame-dried 1-dram borosilicate vial open to air. The reagents were suspended in nitromethane (0.500 mL), and then benzoyl chloride (0.100 mmol) and vinyl diazoacetate reagent **3-6** (0.300 mmol, 1.0 M solution in CH_2Cl_2) were added. The vial was then capped, and the reaction mixture was irradiated with a 23 W CFL bulb while stirring. After 8 h, second charges of vinyl diazoacetate **3-6** (0.200 mmol, 1.0 M solution in CH_2Cl_2) and photocatalyst (half of indicated amount in table) were added, and the reaction mixture was irradiated for another 16 h. At the 24 h timepoint, the solvent was removed by rotary evaporation. The crude residue was then dissolved in CH_2Cl_2 (~1 mL), and the solution was passed through a

SiO_2 plug (0.5 x 3 cm), using CH_2Cl_2 as eluent (~8 mL). The filtrate was concentrated in vacuo, and the crude residue was analyzed by ^1H NMR using CH_2Br_2 as an internal standard.

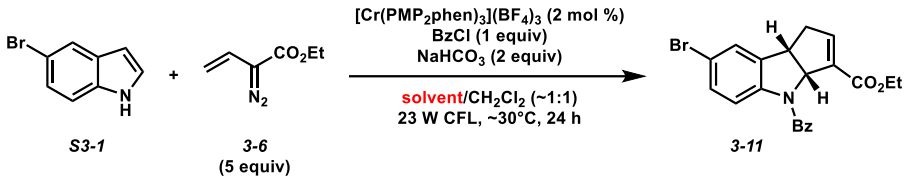

Entry	Solvent	NMR yield (%)
1	CH_3NO_2	75
2	CH_3CN	54
3	acetone	61
4	CH_2Cl_2	62

General procedure for SOLVENT optimization:

5-Bromoindole (0.100 mmol), $NaHCO_3$ (0.200 mmol), and $[Cr(PMP_2phen)_3](BF_4)_3$ (0.00100 mmol) were added to a flame-dried 1-dram borosilicate vial open to air. The reagents were suspended in solvent (0.500 mL), and then benzoyl chloride (0.100 mmol) and vinyl diazoacetate reagent **3-6** (0.300 mmol, 1.0 M solution in CH_2Cl_2) were added. The vial was then capped, and the reaction mixture was irradiated with a 23 W CFL bulb while stirring. After 8 h, second charges of vinyl diazoacetate **3-6** (0.200 mmol, 1.0 M solution in CH_2Cl_2) and $[Cr(PMP_2phen)_3](BF_4)_3$ (0.00100 mmol) were added, and the reaction mixture was irradiated for another 16 h. At the 24 h timepoint, the solvent was removed by rotary evaporation. The crude residue was then dissolved in CH_2Cl_2 (~1 mL), and the solution was passed through a SiO_2 plug (0.5 x 3 cm), using CH_2Cl_2 as eluent (~8 mL). The filtrate was concentrated in vacuo, and the crude residue was analyzed by ^1H NMR using CH_2Br_2 as an internal standard.

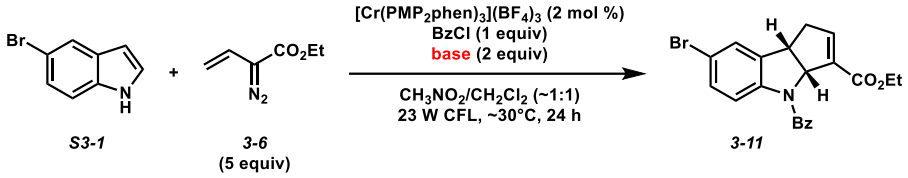

Entry	Base	NMR yield (%)
1	$NaHCO_3$	75
2	$KHCO_3$	51
3	NaH_2PO_4	18
4	Na_2HPO_4	32
5	pyridine	0
6	Et_3N	0

General procedure for BASE optimization:

5-Bromoindole (0.100 mmol), base (for entries 1-4, 0.200 mmol), and $[Cr(PMP_2phen)_3](BF_4)_3$ (0.00100 mmol) were added to a flame-dried 1-dram borosilicate vial open to air. The reagents were suspended in nitromethane (0.500 mL), and then benzoyl chloride (0.100 mmol), base (for entries 5-6, 0.200 mmol) and vinyl diazoacetate reagent **3-6** (0.300 mmol, 1.0 M solution in CH_2Cl_2) were added. The vial was then capped, and the reaction mixture was irradiated with a 23 W CFL bulb while stirring. After 8 h, second charges of vinyl diazoacetate **3-6** (0.200 mmol, 1.0 M solution in CH_2Cl_2) and $[Cr(PMP_2phen)_3](BF_4)_3$ (0.00100 mmol) were added, and the reaction mixture was irradiated for another 16 h. At the 24 h timepoint, the solvent was removed by rotary evaporation. The crude residue was then dissolved in CH_2Cl_2 (~1 mL), and the solution was passed through a SiO_2 plug (0.5 x 3 cm), using CH_2Cl_2 as eluent (~8 mL). The filtrate was concentrated in vacuo, and the crude residue was analyzed by ^1H NMR using CH_2Br_2 as an internal standard.

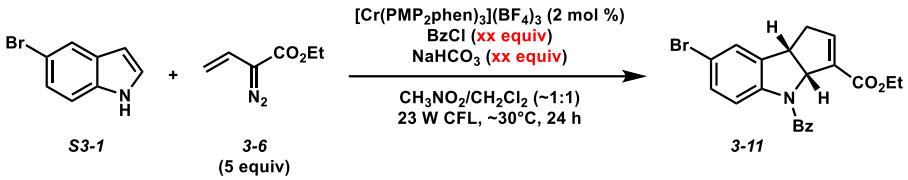

Entry	BzCl equiv	$NaHCO_3$ equiv	NMR yield (%)
1	1.0	2.0	75
2	2.0	4.0	79
3	3.0	5.0	88
4	5.0	5.0	85

General procedure for STOICHIOMETRY optimization:

5-Bromoindole (0.100 mmol), base (see table for equivalents), and $[Cr(PMP_2phen)_3](BF_4)_3$ (0.00100 mmol) were added to a flame-dried 1-dram borosilicate vial open to air. The reagents were suspended in nitromethane (0.500 mL), and then benzoyl chloride (see table for equivalents) and vinyl diazoacetate reagent **3-6** (0.300 mmol, 1.0 M solution in CH_2Cl_2) were added. The vial was then capped, and the reaction mixture was irradiated with a 23 W CFL bulb while stirring. After 8 h, second charges of vinyl diazoacetate **3-6** (0.200 mmol, 1.0 M solution in CH_2Cl_2) and $[Cr(PMP_2phen)_3](BF_4)_3$ (0.00100 mmol) were added, and the reaction mixture was irradiated for another 16 h. At the 24 h timepoint, the solvent was removed by rotary evaporation. The crude residue was then dissolved in CH_2Cl_2 (~1 mL), and the solution was passed through a SiO_2 plug (0.5 x 3 cm), using CH_2Cl_2 as eluent (~8 mL). The filtrate was concentrated in vacuo, and the crude residue was analyzed by ^1H NMR using CH_2Br_2 as an internal standard.

3.9.3 Protecting Groups Analyzed with 5-substituted Indoles:

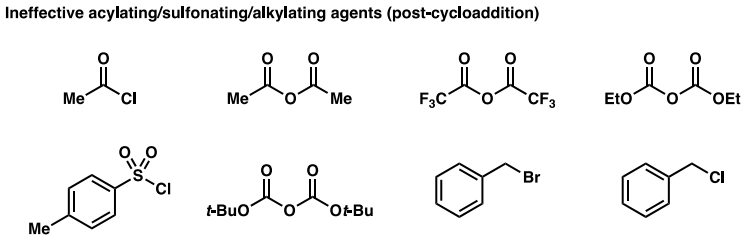

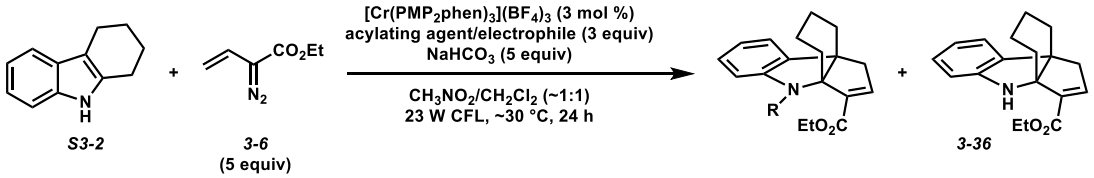

Entry	Acylating agent/Electrophile	NMR yield (%)
1	BzCl	0
2	(*p*-OMe)BzCl	0
3	(*p*-NO_2)BzCl	0
4	(*m*-CF_3)BzCl	0
5	(3,5-(NO_2)$_2$)BzCl	55
6	AcCl	0
7	Ac_2O	0
8	TFAA	0
9	Boc_2O	0
10	TsCl	0
11	BnBr	0
12	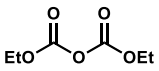	0
13	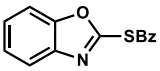	0
14	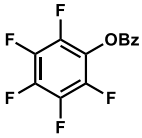	0
15	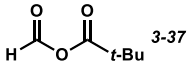 *3-37*	30
16	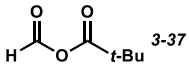 *3-37* (without $NaHCO_3$ added)	93

General Procedure for 2,3-disubstituted indoline acylating agent optimization:

Indole **S3-2** (0.100 mmol), $NaHCO_3$ (0.200 mmol), and $[Cr(PMP_2phen)_3](BF_4)_3$ (0.00100 mmol) were added to a flame-dried 1-dram borosilicate vial open to air. The reagents were suspended in nitromethane (0.500 mL), and then acylating agent/electrophile (0.300 mmol) and vinyl diazoacetate reagent **3-6** (0.300 mmol, 1.0 M solution in CH_2Cl_2) were added. The vial was then capped, and the reaction mixture was irradiated with a 23 W CFL bulb while stirring. After 8 h,

second charges of vinyl diazoacetate **3-6** (0.200 mmol, 1.0 M solution in CH_2Cl_2) and $[Cr(PMP_2phen)_3](BF_4)_3$ (0.00100 mmol) were added, and the reaction mixture was irradiated for another 16 h. At the 24 h timepoint, the solvent was removed by rotary evaporation. The crude residue was then dissolved in CH_2Cl_2 (~1 mL), and the solution was passed through a SiO_2 plug (0.5 x 3 cm), using CH_2Cl_2 as eluent (~8 mL). The filtrate was concentrated in vacuo, and the crude residue was analyzed by ^1H NMR using CH_2Br_2 as an internal standard.

3.9.4 Degradation of $[Ru(bpz)_3]^{2+}$ Experiments:

Procedure: $[Ru(bpz)_3](PF_6)_2$ (8.6 mg, 0.010 μmol) was dissolved in acetonitrile (50 mL). A baseline UV-Vis measurement was then taken. BzCl (0.35 mL, 0.0030 mmol, 300 equiv) was then added to the mixture, and another baseline measurement (0 h timepoint) was taken. Half of the solution (25 mL) was then placed in the photobox and irradiated by a 23 W CFL bulb for 18 h, withdrawing aliquots of the solution at 1, 2, 4, and 18 h timepoints, and measuring their UV-Vis absorbances. The other half of the solution (25 mL) was kept in the dark for 18 h, withdrawing aliquots at the same timepoints and measuring their UV-Vis absorbances. The data is recorded below.

Figure S3.1. $[Ru(bpz)_3](PF_6)_2$ and 300 equiv of BzCl in acetonitrile **irradiated** with a 23 W CFL bulb over time.

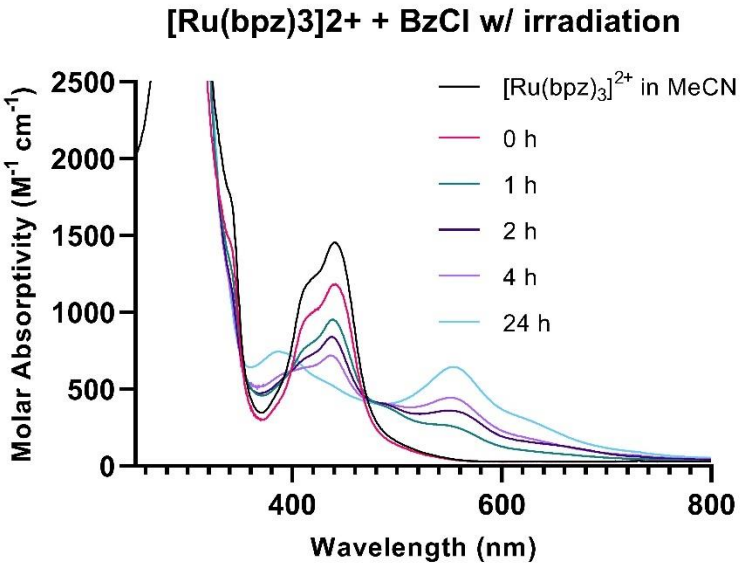

Figure S3.2. $[Ru(bpz)_3](PF_6)_2$ and 300 equiv of BzCl in acetonitrile over time.

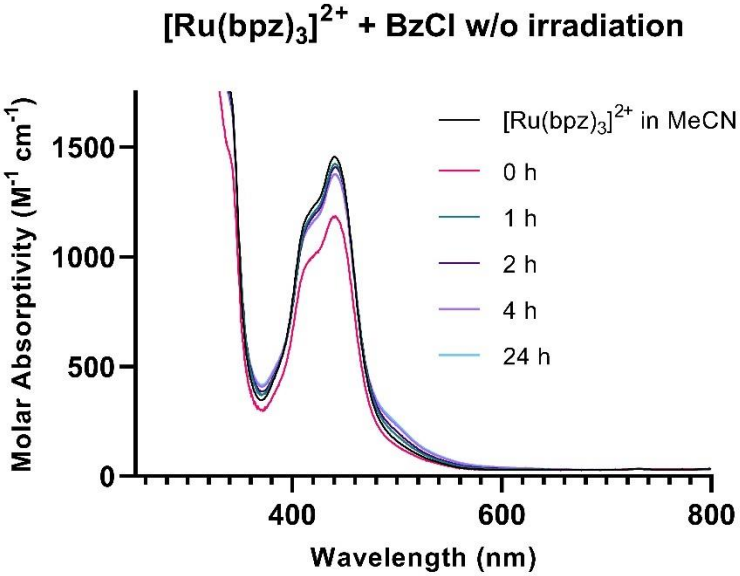

A solution of benzoyl chloride (0.35 mL, 0.0030 mmol) in acetonitrile (50 mL) was irradiated over the course of 24 h. No change between the 0 h timepoint and 24 h timepoint was observed.

Figure S3.3. BzCl in acetonitrile irradiated with a 23 W CFL bulb over 24 h. (Lines are overlapping.)

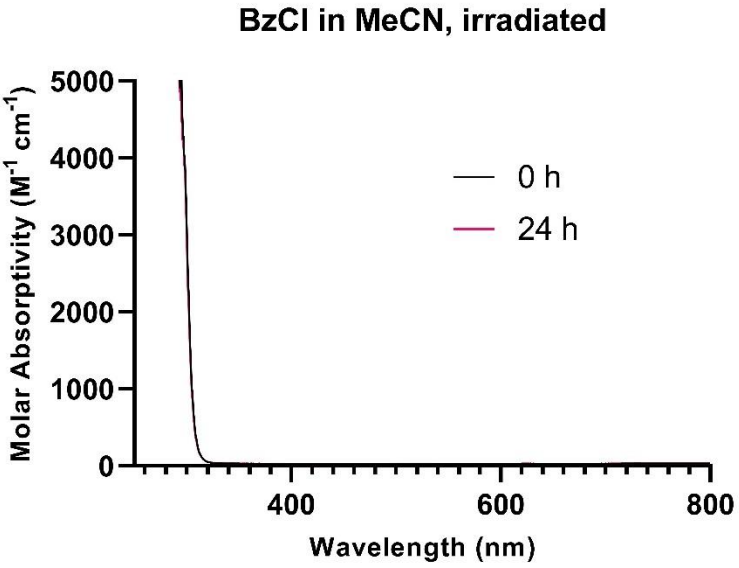

3.9.5 Photocatalyzed Cycloaddition Reactions

General Procedure A:

Indole (1.0 equiv), $NaHCO_3$ (5.0 equiv), and $[Cr(PMP_2phen)_3](BF_4)_3$ (1.0 mol %) were added to a flame-dried 1-dram borosilicate vial open to air. The reagents were suspended in CH_3NO_2 (0.20 M), and to this suspension were added 2,2,2-trichloroethoxycarbonyl chloride (3.0 equiv) and vinyl diazoacetate reagent (3.00 equiv, 1.0 M solution in CH_2Cl_2). The vial was then capped, and the reaction mixture was irradiated with a 23 W CFL bulb while stirring. After 8 h, second charges of vinyl diazoacetate reagent (2.0 equiv) and $[Cr(PMP_2phen)_3](BF_4)_3$ (1.0 mol %) were added, and irradiation was continued. Reaction progress was monitored by TLC. When determined complete, the solvent was removed by rotary evaporation. The crude residue was then dissolved in CH_2Cl_2 (~1 mL), and the solution was passed through a SiO_2 plug (0.5 x 3 cm), using CH_2Cl_2 as eluent (~8 mL). The filtrate was concentrated in vacuo, and the crude residue was purified by silica gel flash chromatography to afford pure indoline product.

General Procedure B:

In a flame-dried 1-dram borosilicate vial open to air, trimethylacetic formic anhydride (3.0 equiv) was dissolved in CH_3NO_2 (0.20 M). To this solution were added indole (1.0 equiv), $[Cr(PMP_2phen)_3](BF_4)_3$ (1.0 mol %), and vinyl diazoacetate reagent (3.0 equiv, 1.0 M solution in CH_2Cl_2). The vial was then capped, and the reaction mixture was irradiated with a 23 W CFL bulb while stirring. After 8 h, extra charges of vinyl diazoacetate reagent (2.0 equiv) and $[Cr(PMP_2phen)_3](BF_4)_3$ (1.0 mol %) were added, and irradiation was continued. At the 24 hour timepoint, extra charges of vinyl diazoacetate reagent (1.0 equiv) and $[Cr(PMP_2phen)_3](BF_4)_3$ (1.0 mol %) were added, and irradiation was continued. Reaction progress was monitored by TLC. When determined complete, the solvent was removed by rotary evaporation. The crude residue

was then dissolved in CH_2Cl_2 (~1 mL), and the solution was passed through a SiO_2 plug (0.5 x 3 cm), using CH_2Cl_2 as eluent (~8 mL). The filtrate was concentrated in vacuo, and the crude residue was purified by silica gel flash chromatography to afford pure indoline product.

Note for General Procedures A&B: In some cases, a third charge of vinyl diazo reagent and/or Cr photocatalyst were required for the reaction to proceed to completion, as monitored by TLC.

Note about characterization: Several compounds, particularly the Troc-protected indolines, required high temperature NMR for ^{13}C characterization due to rotameric complications. Even with this extra measure, 1-2 carbons were not detected in some cases.

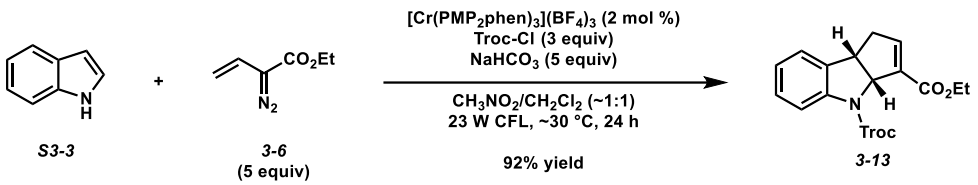

S3-3 + *3-6* (5 equiv) → *3-13*

Indoline 3-13. According to a modified General Procedure A, indole (**S3-3**, 25.0 mg, 0.213 mmol), $NaHCO_3$ (89.5 mg, 1.07 mmol), and $[Cr(PMP_2phen)_3](BF_4)_3$ (3.2 mg, 0.00213 mmol) were added to a flame-dried 1-dram borosilicate vial. The reagents were suspended in CH_3NO_2 (1.07 mL), and to this suspension were added 2,2,2-trichloroethoxycarbonyl chloride (88.1 µL, 0.640 mmol) and vinyl diazoacetate **3-6** (0.640 mL, 1.0 M in CH_2Cl_2, 0.640 mmol). The reaction mixture was irradiated with a 23 W CFL bulb while stirring. After 8 h, second charges of vinyl diazoacetate **3-6** (0.426 mL, 1.0 M in CH_2Cl_2, 0.426 mmol) and $[Cr(PMP_2phen)_3](BF_4)_3$ (3.2 mg, 0.00213 mmol) were added, and irradiation was continued. At the 24 h timepoint, the solvent was removed via rotary evaporation. The crude residue was dissolved in CH_2Cl_2 (~1 mL), and the solution was passed through a SiO_2 plug (0.5 x 3 cm), using CH_2Cl_2 as eluent (~8 mL). The filtrate was concentrated in vacuo, and the residue was purified by silica gel flash chromatography (4:1 hexanes/Et_2O eluent) to afford indoline **3-13** (79.4 mg, 92% yield) as a white solid.

TLC R_f: 0.50 in 1:1 hexanes/Et_2O, visualized by UV, stained blue in Hanessian's stain.

^{1}H NMR (400 MHz, $CDCl_3$): δ 7.90-7.60 (br. m, 1H), 7.24 (app. t, *J* = 7.8 Hz, 1H), 7.19 (d, *J* = 7.5 Hz, 1H), 7.07 (app. t, *J* = 7.4 Hz, 1H), 6.86 (app. s, 1H), 5.89 (app. d, *J* = 6.1 Hz, 1H), 5.40-4.50 (br. m, 2H), 4.24-4.11 (comp. m, 3H), 3.03 (app. ddt, *J* = 18.4, 7.7, 2.0 Hz, 1H), 2.79 (app. d, *J* = 18.4 Hz, 1H), 1.26 (t, *J* = 7.1 Hz, 3H).

^{13}C NMR (125 MHz, 50 °C, $CDCl_3$): δ 163.9, 151.8, 144.7, 140.7, 135.3, 128.5, 124.2, 117.2, 95.6, 75.7, 68.9, 60.5, 43.9, 37.8, 14.3 (*2 carbons not detected*).

IR (ATR, neat): 2981, 1723, 1628, 1198, 755 cm^{-1}.

HRMS (ESI+): *m/z* calc'd for $(M + H)^+$ $[C_{17}H_{16}Cl_3NO_4 + H]^+$: 404.0218, found 404.0199.

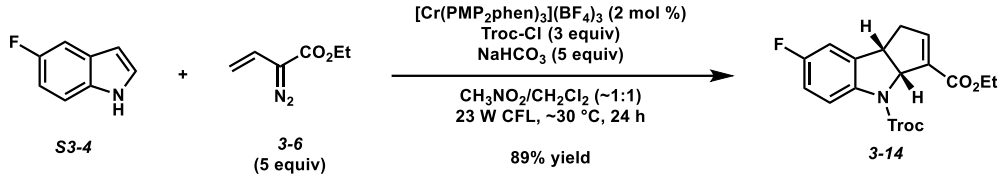

Indoline 3-14. According to a modified General Procedure A, 5-fluoroindole (**S3-4**, 27.5 mg, 0.203 mmol), $NaHCO_3$ (85.5 mg, 1.02 mmol), and $[Cr(PMP_2phen)_3](BF_4)_3$ (3.0 mg, 0.00203 mmol) were added to a flame-dried 1-dram borosilicate vial. The reagents were suspended in CH_3NO_2 (1.02 mL), and to this suspension were added 2,2,2-trichloroethoxycarbonyl chloride (84.0 µL, 0.610 mmol) and vinyl diazoacetate **3-6** (0.610 mL, 1.0 M in CH_2Cl_2, 0.610 mmol). The reaction mixture was irradiated with a 23 W CFL bulb while stirring. After 8 h, second charges of vinyl diazoacetate **3-6** (0.406 mL, 1.0 M in CH_2Cl_2, 0.406 mmol) and $[Cr(PMP_2phen)_3](BF_4)_3$ (3.0 mg, 0.00203 mmol) were added, and irradiation was continued. At the 24 h timepoint, the solvent was removed via rotary evaporation. The crude residue was dissolved in CH_2Cl_2 (~1 mL), and the solution was passed through a SiO_2 plug (0.5 x 3 cm), using CH_2Cl_2 as eluent (~8 mL). The filtrate was concentrated in vacuo, and the residue was purified by silica gel flash chromatography (4:1 hexanes/Et_2O eluent) to afford indoline **3-14** (76.5 mg, 89% yield) as a white solid.

TLC R_f: 0.43 in 1:1 hexanes/Et_2O, visualized by UV, stained blue in Hanessian's stain.

^{1}H NMR (400 MHz, $CDCl_3$): δ 7.80-7.50 (br. m, 1H), 6.96-6.82 (comp. m, 3H), 5.90 (app. d, J = 6.6 Hz, 1H), 5.30-4.50 (br. m, 2H), 4.26-4.05 (comp. m, 3H), 3.03 (app. ddt, J = 18.4, 7.8, 2.0 Hz, 1H), 2.74 (app. d, J = 18.4 Hz, 1H), 1.26 (t, J = 7.2 Hz, 3H).

^{13}C NMR (125 MHz, 50 °C, $CDCl_3$): δ 163.7, 160.9, 159.0, 151.8, 144.5, 136.7, 136.3 (d, J = 268 Hz), 135.2, 118.1, 114.9 (d, J = 23.0 Hz), 111.4 (d, J = 23.9 Hz), 95.5, 75.7, 69.3, 60.6, 43.9, 37.7, 14.3.

^{19}F NMR (376 MHz, $CDCl_3$): δ -119.0.

IR (ATR, neat): 2981, 1720, 1630, 1487, 1103, 747 cm^{-1}.

HRMS (ESI+): *m/z* calc'd for $(M + H)^+$ $[C_{17}H_{15}Cl_3FNO_4 + H]^+$: 422.0123, found 422.0113.

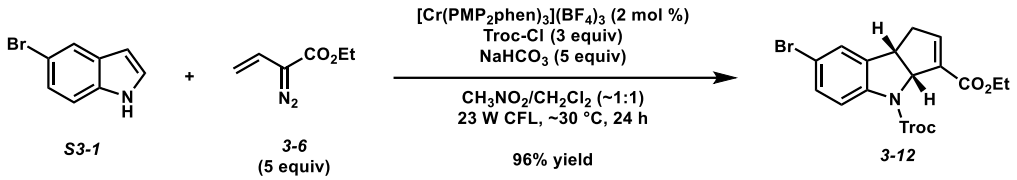

Indoline 3-12. According to a modified General Procedure A, 5-bromoindole (**S3-1**, 29.0 mg, 0.148 mmol), $NaHCO_3$ (62.1 mg, 0.740 mmol), and $[Cr(PMP_2phen)_3](BF_4)_3$ (2.2 mg, 0.00148 mmol) were added to a flame-dried 1-dram borosilicate vial. The reagents were suspended in CH_3NO_2 (0.74 mL), and to this suspension were added 2,2,2-trichloroethoxycarbonyl chloride (61.1 µL, 0.444 mmol) and vinyl diazoacetate **3-6** (0.444 mL, 1.0 M in CH_2Cl_2, 0.444 mmol). The reaction mixture was irradiated with a 23 W CFL bulb while stirring. After 8 h, second charges of vinyl diazoacetate **3-6** (0.296 mL, 1.0 M in CH_2Cl_2, 0.296 mmol) and $[Cr(PMP_2phen)_3](BF_4)_3$ (2.2 mg, 0.00148 mmol) were added, and irradiation was continued. At the 24 h timepoint, the solvent was removed via rotary evaporation. The crude residue was dissolved in CH_2Cl_2 (~1 mL), and the solution was passed through a SiO_2 plug (0.5 x 3 cm), using CH_2Cl_2 as eluent (~8 mL). The filtrate was concentrated in vacuo, and the residue was purified by silica gel flash chromatography (2:1 hexanes/Et_2O eluent) to afford indoline **3-12** (68.7 mg, 96% yield) as a white solid.

TLC R_f: 0.50 in 1:1 hexanes/Et_2O, visualized by UV, stained blue in Hanessian's stain.

^{1}H NMR (400 MHz, $CDCl_3$): δ 7.72-7.48 (br. m, 1H), 7.33 (d, *J* = 8.4 Hz, 1H), 7.30 (s, 1H), 6.86 (app. s, 1H), 5.87 (app. d, *J* = 6.7 Hz, 1H), 5.35-4.50 (br. m, 2H), 4.25-4.08 (comp. m, 3H), 3.03 (app. ddt, *J* = 18.4, 7.7, 2.0 Hz, 1H), 2.75 (app. d, *J* = 18.4 Hz, 1H), 1.26 (t, *J* = 7.2 Hz).

^{13}C NMR (125 MHz, 50 °C, $CDCl_3$): δ 163.7, 151.7, 144.6, 140.0, 137.7, 135.1, 131.5, 127.5, 118.6, 116.7, 95.4, 75.8, 69.2, 60.6, 43.8, 37.7, 14.3.

IR (ATR, neat): 2980, 1720, 1630, 1478, 1102, 746 cm^{-1}.

HRMS (ESI+): *m/z* calc'd for $(M + H)^+$ $[C_{17}H_{15}BrCl_3NO_4 + H]^+$: 481.9323 found 481.9313.

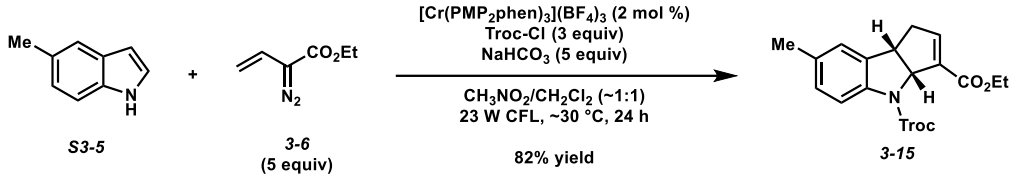

Indoline 3-15. According to a modified General Procedure A, 5-methylindole (**S3-5**, 25.0 mg, 0.191 mmol), $NaHCO_3$ (80.0 mg, 0.953 mmol), and $[Cr(PMP_2phen)_3](BF_4)_3$ (2.8 mg, 0.00191 mmol) were added to a flame-dried 1-dram borosilicate vial. The reagents were suspended in CH_3NO_2 (0.953 mL), and to this suspension were added 2,2,2-trichloroethoxycarbonyl chloride (78.9 µL, 0.573 mmol) and vinyl diazoacetate **3-6** (0.573 mL, 1.0 M in CH_2Cl_2, 0.573 mmol). The reaction mixture was irradiated with a 23 W CFL bulb while stirring. After 8 h, second charges of vinyl diazoacetate **3-6** (0.381 mL, 1.0 M in CH_2Cl_2, 0.381 mmol) and $[Cr(PMP_2phen)_3](BF_4)_3$ (2.8 mg, 0.00191 mmol) were added, and irradiation was continued. At the 24 h timepoint, the solvent was removed via rotary evaporation. The crude residue was dissolved in CH_2Cl_2 (~1 mL), and the solution was passed through a SiO_2 plug (0.5 x 3 cm), using CH_2Cl_2 as eluent (~8 mL). The filtrate was concentrated in vacuo, and the residue was purified by silica gel flash chromatography (4:1 hexanes/Et_2O eluent) to afford indoline **3-15** (65.4 mg, 82% yield) as a white solid.

TLC R_f: 0.46 in 1:1 hexanes/Et_2O, visualized by UV, stained blue in Hanessian's stain.

^{1}H NMR (400 MHz, $CDCl_3$): δ 7.75-7.50 (br. m, 1H), 7.05 (d, *J* = 8.2 Hz, 1H), 7.00 (s, 1H), 6.85 (app. s, 1H), 5.87 (app. d, *J* = 6.0 Hz, 1H), 5.30-4.50 (comp. m, 2H), 4.23-4.10 (comp. m, 2H), 4.09 (app. t, *J* = 7.2 Hz, 1H), 3.00 (app. ddt, *J* = 18.4, 7.8, 2.0 Hz, 1H), 2.77 (app. d, *J* = 18.4 Hz, 1H), 2.31 (s, 3H), 1.26 (t, *J* = 7.1 Hz, 3H).

^{13}C NMR (125 MHz, 50 °C, $CDCl_3$): δ 164.0, 151.9, 144.7, 138.4, 135.3, 133.8, 129.0, 124.8, 117.0, 95.6, 75.7, 69.0, 60.5, 43.9, 37.8, 21.1, 14.3 (*1 carbon not detected*).

IR (ATR, neat): 2980, 1720, 1626, 1491, 1102, 817 cm^{-1}.

HRMS (ESI+): *m/z* calc'd for $(M + H)^+$ $[C_{18}H_{18}Cl_3NO_4 + H]^+$: 418.0374, found 418.0362.

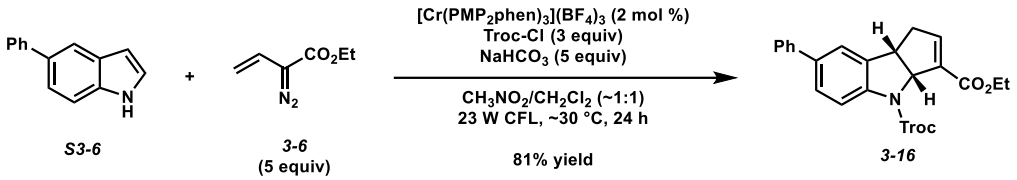

Indoline 3-16. According to a modified General Procedure A, 5-phenylindole (**S3-6**, 28.0 mg, 0.145 mmol), $NaHCO_3$ (60.8 mg, 0.724 mmol), and $[Cr(PMP_2phen)_3](BF_4)_3$ (2.2 mg, 0.00145 mmol) were added to a flame-dried 1-dram borosilicate vial. The reagents were suspended in CH_3NO_2 (0.725 mL), and to this suspension were added 2,2,2-trichloroethoxycarbonyl chloride (59.8 µL, 0.435 mmol) and vinyl diazoacetate **3-6** (0.435 mL, 1.0 M in CH_2Cl_2, 0.435 mmol). The reaction mixture was irradiated with a 23 W CFL bulb while stirring. After 8 h, second charges of vinyl diazoacetate **3-6** (0.290 mL, 1.0 M in CH_2Cl_2, 0.290 mmol) and $[Cr(PMP_2phen)_3](BF_4)_3$ (2.2 mg, 0.00145 mmol) were added, and irradiation was continued. At the 24 h timepoint, the solvent was removed via rotary evaporation. The crude residue was dissolved in CH_2Cl_2 (~1 mL), and the solution was passed through a SiO_2 plug (0.5 x 3 cm), using CH_2Cl_2 as eluent (~8 mL). The filtrate was concentrated in vacuo, and the residue was purified by silica gel flash chromatography (4:1 hexanes/Et_2O eluent) to afford indoline **3-16** (56.4 mg, 81% yield) as a white solid.

TLC R_f: 0.43 in 1:1 hexanes/Et_2O, visualized by UV, stained blue in Hanessian's stain.

^{1}H NMR (400 MHz, $CDCl_3$): δ 7.93-7.67 (br. m, 1H), 7.55 (d, *J* = 7.2 Hz, 2H), 7.49 (d, *J* = 8.4 Hz, 1H), 7.44-7.41 (comp. m, 3H), 7.33 (t, *J* = 7.3 Hz, 1H), 6.90 (app. s, 1H), 5.94 (app. d, *J* = 6.2 Hz, 1H), 5.40-4.47 (br. m, 2H), 4.26-4.13 (comp m, 3H), 3.07 (app. ddt, *J* = 18.4, 7.7, 1.9 Hz, 1H), 2.86 (app. d, *J* = 18.4 Hz, 1H), 1.28 (t, *J* = 7.1 Hz, 3H).

^{13}C NMR (125 MHz, 50 °C, $CDCl_3$): δ 163.9, 151.9, 144.8, 141.0, 140.1, 137.7, 136.0, 135.3, 128.9, 127.6, 127.2, 127.1, 123.0, 117.4, 95.6, 75.8, 69.2, 60.6, 44.0, 37.9, 14.4.

IR (ATR, neat): 2980, 1720, 1628, 1102, 833 cm^{-1}.

HRMS (ESI+): *m/z* calc'd for $(M + H)^+$ $[C_{23}H_{20}Cl_3NO_4 + H]^+$: 480.0531, found 480.0520.

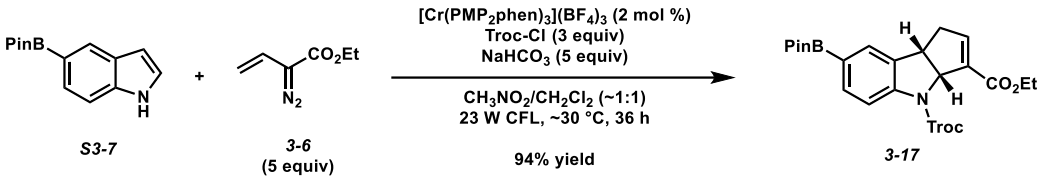

Indoline 3-17. According to a modified General Procedure A, indole (**S3-7**, 30.2 mg, 0.124 mmol), $NaHCO_3$ (52.2 mg, 0.621 mmol), and $[Cr(PMP_2phen)_3](BF_4)_3$ (1.9 mg, 0.00124 mmol) were added to a flame-dried 1-dram borosilicate vial. The reagents were suspended in CH_3NO_2 (0.621 mL), and to this suspension were added 2,2,2-trichloroethoxycarbonyl chloride (51.3 µL, 0.373 mmol) and vinyl diazoacetate **3-6** (0.373 mL, 1.0 M in CH_2Cl_2, 0.373 mmol). The reaction mixture was irradiated with a 23 W CFL bulb while stirring. After 8 h, second charges of vinyl diazoacetate **3-6** (0.248 mL, 1.0 M in CH_2Cl_2, 0.248 mmol) and $[Cr(PMP_2phen)_3](BF_4)_3$ (1.9 mg, 0.00124 mmol) were added, and irradiation was continued. At the 36 h timepoint, the solvent was removed via rotary evaporation. The crude residue was dissolved in CH_2Cl_2 (~1 mL), and the solution was passed through a SiO_2 plug (0.5 x 3 cm), using CH_2Cl_2 as eluent (~8 mL). The filtrate was concentrated in vacuo, and the residue was purified by silica gel flash chromatography (4:1 hexanes/Et_2O eluent) to afford indoline **3-17** (62.0 mg, 94% yield) as a white solid.

TLC R_f: 0.48 in 2:1 hexanes/Et_2O, visualized by UV, stained blue in Hanessian's stain.

^{1}H NMR (400 MHz, $CDCl_3$): δ 7.80-7.71 (comp. m, 2H), 7.64 (s, 1H), 6.84 (app. s, 1H), 5.88 (app. d, *J* = 6.0 Hz, 1H), 5.30-4.50 (br. m, 2H), 4.23-4.09 (comp. m, 3H), 3.01 (app. ddt, *J* = 18.4, 6.1, 2.0 Hz, 1H), 2.87 (app. d, *J* = 18.4 Hz, 1H), 1.33 (s, 6H), 1.32 (s, 6H), 1.25 (t, *J* = 7.1 Hz, 1H).

^{13}C NMR (125 MHz, 50 °C, $CDCl_3$): δ 164.0, 151.8, 145.0, 143.3, 135.8, 135.2, 134.7, 130.6, 124.7 (br, *C*-BPin), 116.5, 95.5, 83.9, 75.8, 69.1, 60.5, 43.7, 37.8, 25.1, 25.0, 14.4.

IR (ATR, neat): 2978, 1724, 1607, 1433, 856 cm^{-1}.

HRMS (ESI+): *m/z* calc'd for $(M + H)^+$ $[C_{23}H_{27}BCl_3NO_6 + H]^+$: 530.1070, found 530.1071.

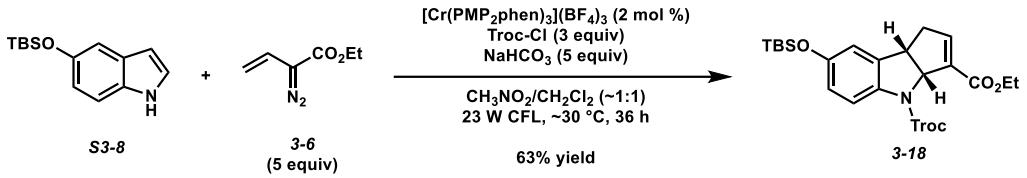

Indoline 3-18. According to a modified General Procedure A, 5-(*tert*-butyl-dimethyl-silanyloxy)-1*H*-indole (**S3-8**, 31.3 mg, 0.127 mmol), $NaHCO_3$ (53.1 mg, 0.633 mmol), and $[Cr(PMP_2phen)_3](BF_4)_3$ (1.9 mg, 0.00127 mmol) were added to a flame-dried 1-dram borosilicate vial. The reagents were suspended in CH_3NO_2 (0.633 mL), and to this suspension were added 2,2,2-trichloroethoxycarbonyl chloride (52.2 µL, 0.380 mmol) and vinyl diazoacetate **3-6** (0.380 mL, 1.0 M in CH_2Cl_2, 0.380 mmol). The reaction mixture was irradiated with a 23 W CFL bulb while stirring. After 8 h, second charges of vinyl diazoacetate **3-6** (0.253 mL, 1.0 M in CH_2Cl_2, 0.253 mmol) and $[Cr(PMP_2phen)_3](BF_4)_3$ (1.9 mg, 0.00127 mmol) were added, and irradiation was continued. At the 24 h timepoint, the solvent was removed via rotary evaporation. The crude residue was dissolved in CH_2Cl_2 (~1 mL), and the solution was passed through a SiO_2 plug (0.5 x 3 cm), using CH_2Cl_2 as eluent (~8 mL). The filtrate was concentrated in vacuo, and the residue was purified by silica gel flash chromatography (9:1 → 4:1 hexanes/Et_2O eluent) to afford indoline **3-18** (42.6 mg, 63% yield) as a yellow solid.

TLC R_f: 0.64 in 2:1 hexanes/Et_2O, visualized by UV, stained blue in Hanessian's stain.

^{1}H NMR (400 MHz, $CDCl_3$): δ 7.70-7.40 (br. m, 1H), 6.84 (s, 1H), 6.69 (d, *J* = 8.6 Hz, 1H), 6.65 (app. s, 1H), 5.87 (app. d, *J* = 6.3 Hz, 1H), 5.35-4.45 (br. m, 2H), 4.24-4.12 (comp. m, 2H), 4.07 (app. t, *J* = 7.3 Hz, 1H), 2.99 (app. dd, *J* = 18.4, 6.1 Hz, 1H), 2.72 (app. d, *J* = 18.4 Hz, 1H), 1.26 (t, *J* = 7.2 Hz, 3H), 0.97 (s, 9H), 0.17 (s, 6H).

^{13}C NMR (125 MHz, 50 °C, $CDCl_3$): δ 164.0, 152.7, 151.9, 144.6, 136.7, 135.4, 134.6, 119.6, 117.9, 115.9, 95.7, 75.7, 69.2, 60.6, 43.9, 37.9, 25.9, 18.3, 14.4, -4.26, -4.28.

IR (ATR, neat): 2955, 2929, 1721, 1635, 1266, 839 cm^{-1}.

HRMS (ESI+): *m/z* calc'd for $(M + H)^+$ $[C_{23}H_{30}Cl_3NO_5Si + H]^+$: 534.1032, found 534.1019.

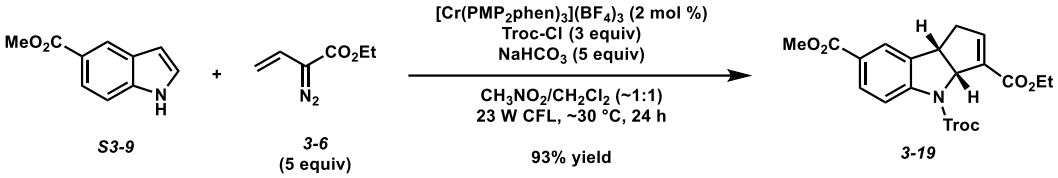

Indoline 3-19. According to a modified General Procedure A, methyl 1*H*-indole-5-carboxylate (**S3-9**, 28.0 mg, 0.160 mmol), $NaHCO_3$ (67.1 mg, 0.799 mmol), and $[Cr(PMP_2phen)_3](BF_4)_3$ (2.4 mg, 0.00160 mmol) were added to a flame-dried 1-dram borosilicate vial. The reagents were suspended in CH_3NO_2 (0.800 mL), and to this suspension were added 2,2,2-trichloroethoxycarbonyl chloride (66.0 µL, 0.479 mmol) and vinyl diazoacetate **3-6** (0.479 mL, 1.0 M in CH_2Cl_2, 0.479 mmol). The reaction mixture was irradiated with a 23 W CFL bulb while stirring. After 8 h, second charges of vinyl diazoacetate **3-6** (0.320 mL, 1.0 M in CH_2Cl_2, 0.320 mmol) and $[Cr(PMP_2phen)_3](BF_4)_3$ (2.4 mg, 0.00160 mmol) were added, and irradiation was continued. At the 24 h timepoint, the solvent was removed via rotary evaporation. The crude residue was dissolved in CH_2Cl_2 (~1 mL), and the solution was passed through a SiO_2 plug (0.5 x 3 cm), using CH_2Cl_2 as eluent (~8 mL). The filtrate was concentrated in vacuo, and the residue was purified by silica gel flash chromatography (4:1 hexanes/Et_2O eluent) to afford indoline **3-19** (69.1 mg, 93% yield, 4.7 mg of pyrazole unable to be separated from the pure product) as a white solid.

TLC R_f: 0.40 in 2:1 hexanes/Et_2O, visualized by UV, stained blue in Hanessian's stain.

^{1}H NMR (400 MHz, $CDCl_3$): δ 7.95 (d, *J* = 8.5 Hz, 1H), 7.87 (s, 1H), 7.78 (br. s, 1H), 6.86 (app. s, 1H), 5.92 (d, *J* = 6.0 Hz, 1H), 5.20-4.60 (br. m, 2H), 4.20-4.10 (comp. m, 3H), 3.88 (s, 3H), 3.04 (app. dd, *J* = 18.5, 6.2 Hz, 1H), 2.84 (app. d, *J* = 18.5 Hz, 1H), 1.25 (t, *J* = 7.2 Hz, 1H).

^{13}C NMR (125 MHz, 50 °C, $CDCl_3$): δ 166.7, 163.8, 151.7, 144.9, 135.6, 135.0, 132.6, 130.9, 126.1, 125.9, 116.5, 95.3, 75.9, 69.5, 60.7, 52.1, 43.6, 37.8, 14.3.

IR (ATR, neat): 2982, 1717, 1610, 1276, 1187 cm^{-1}.

HRMS (ESI+): *m/z* calc'd for $(M + H)^+$ $[C_{19}H_{18}Cl_3NO_6 + H]^+$: 462.0272, found 462.0257.

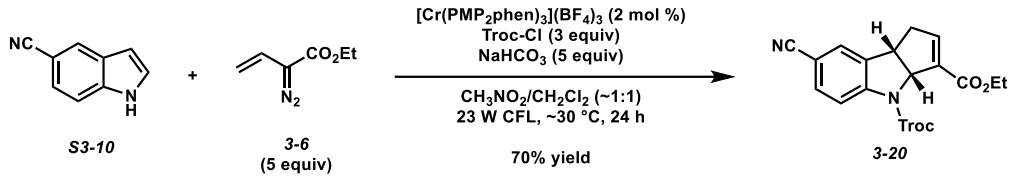

Indoline 3-20. According to a modified General Procedure A, 5-cyanoindole (**S3-10**, 29.2 mg, 0.205 mmol), $NaHCO_3$ (86.3 mg, 1.03 mmol), and $[Cr(PMP_2phen)_3](BF_4)_3$ (3.1 mg, 0.00205 mmol) were added to a flame-dried 1-dram borosilicate vial. The reagents were suspended in CH_3NO_2 (1.03 mL), and to this suspension were added 2,2,2-trichloroethoxycarbonyl chloride (84.8 µL, 0.616 mmol) and vinyl diazoacetate **3-6** (0.616 mL, 1.0 M in CH_2Cl_2, 0.616 mmol). The reaction mixture was irradiated with a 23 W CFL bulb while stirring. After 8 h, second charges of vinyl diazoacetate **3-6** (0.411 mL, 1.0 M in CH_2Cl_2, 0.411 mmol) and $[Cr(PMP_2phen)_3](BF_4)_3$ (3.1 mg, 0.00205 mmol) were added, and irradiation was continued. At the 24 h timepoint, the solvent was removed via rotary evaporation. The crude residue was dissolved in CH_2Cl_2 (~1 mL), and the solution was passed through a SiO_2 plug (0.5 x 3 cm), using CH_2Cl_2 as eluent (~8 mL). The filtrate was concentrated in vacuo, and the residue was purified by silica gel flash chromatography (2:1 hexanes/Et_2O eluent) to afford indoline **3-20** (61.7 mg, 70% yield) as a yellow oil.

TLC R_f: 0.32 in 2:1 hexanes/Et_2O, visualized by UV, stained blue in Hanessian's stain.

^{1}H NMR (400 MHz, $CDCl_3$): δ 7.88-7.78 (br. m, 1H), 7.55 (d, *J* = 8.4 Hz, 1H), 7.46 (s, 1H), 6.87 (app. s, 1H), 5.92 (d, *J* = 6.0 Hz, 1H), 5.20-4.60 (br. m, 2H), 4.23-4.11 (comp. m, 3H), 3.08 (app. dd, *J* = 18.3, 6.2 Hz, 1H), 2.78 (app. d, *J* = 18.3 Hz, 1H), 1.26 (t, *J* = 7.2 Hz, 1H).

^{13}C NMR (125 MHz, 50 °C, $CDCl_3$): δ 163.6, 151.4, 144.7, 136.6, 134.8, 133.4, 128.1, 119.0, 117.3, 107.4, 95.2, 75.9, 69.3, 60.8, 43.6, 37.7, 14.3 (*1 carbon not detected*).

IR (ATR, neat): 2982, 2224, 1720, 1628, 1484, 832 cm^{-1}.

HRMS (ESI+): *m/z* calc'd for $(M + H)^+$ $[C_{18}H_{15}Cl_3N_2O_4 + H]^+$: 429.0170, found 429.0160.

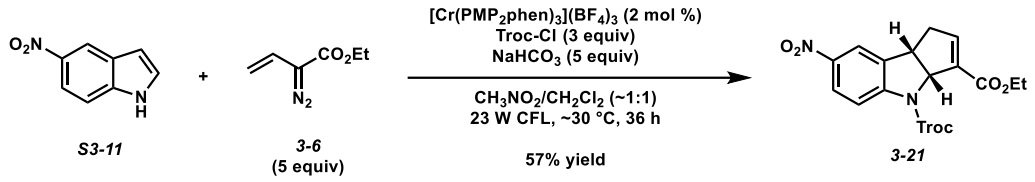

Indoline 3-21. According to a modified General Procedure A, 5-nitroindole (**S3-11**, 22.5 mg, 0.139 mmol), $NaHCO_3$ (58.3 mg, 0.694 mmol), and $[Cr(PMP_2phen)_3](BF_4)_3$ (2.1 mg, 0.00139 mmol) were added to a flame-dried 1-dram borosilicate vial. The reagents were suspended in CH_3NO_2 (0.694 mL), and to this suspension were added 2,2,2-trichloroethoxycarbonyl chloride (57.3 µL, 0.416 mmol) and vinyl diazoacetate **3-6** (0.416 mL, 1.0 M in CH_2Cl_2, 0.416 mmol). The reaction mixture was irradiated with a 23 W CFL bulb while stirring. After 8 h, second charges of vinyl diazoacetate **3-6** (0.278 mL, 1.0 M in CH_2Cl_2, 0.278 mmol) and $[Cr(PMP_2phen)_3](BF_4)_3$ (2.1 mg, 0.00139 mmol) were added, and irradiation was continued. At the 36 h timepoint, the solvent was removed via rotary evaporation. The crude residue was dissolved in CH_2Cl_2 (~1 mL), and the solution was passed through a SiO_2 plug (0.5 x 3 cm), using CH_2Cl_2 as eluent (~8 mL). The filtrate was concentrated in vacuo, and the residue was purified by silica gel flash chromatography (9:1:1 hexanes/Et_2O/CH_2Cl_2 eluent) to afford indoline **3-21** (35.6 mg, 57% yield) as a white solid.

TLC R_f: 0.42 in 1:1 hexanes/Et_2O, visualized by UV, stained blue in Hanessian's stain.

^{1}H NMR (400 MHz, $CDCl_3$): δ 8.18 (d, *J* = 8.7 Hz, 1H), 8.07 (s, 1H), 7.94-7.82 (br. m, 1H), 6.90 (app. s, 1H), 5.97 (d, *J* = 7.0 Hz, 1H), 5.20-4.60 (br. m, 2H), 4.27-4.13 (comp. m, 3H), 3.12 (app. dd, *J* = 18.5, 7.6 Hz, 1H), 2.87 (app. d, *J* = 18.5 Hz, 1H), 1.27 (t, *J* = 7.1 Hz, 1H).

^{13}C NMR (125 MHz, 50 °C, $CDCl_3$): δ 163.6, 151.5, 144.8, 144.5, 136.7, 134.8, 125.4, 120.3, 116.5, 95.1, 76.0, 69.9, 60.8, 43.6, 37.7, 14.4 (*1 carbon not detected*).

IR (ATR, neat): 2925, 1720, 1518, 1479, 832 cm^{-1}.

HRMS (ESI+): *m/z* calc'd for $(M + H)^+$ $[C_{17}H_{15}Cl_3N_2O_6 + H]^+$: 449.0068, found 449.0062.

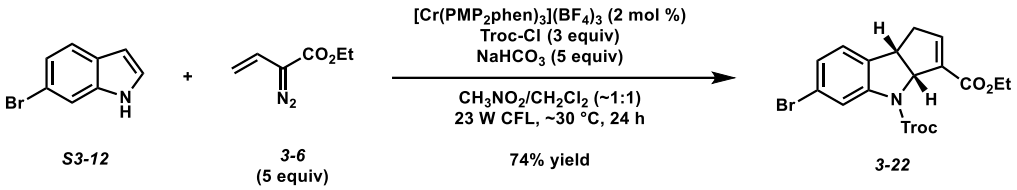

Indoline 3-22. According to a modified General Procedure A, 6-bromoindole (**S3-12**, 27.9 mg, 0.142 mmol), $NaHCO_3$ (59.8 mg, 0.712 mmol), and $[Cr(PMP_2phen)_3](BF_4)_3$ (2.1 mg, 0.00142 mmol) were added to a flame-dried 1-dram borosilicate vial. The reagents were suspended in CH_3NO_2 (0.712 mL), and to this suspension were added 2,2,2-trichloroethoxycarbonyl chloride (58.8 µL, 0.427 mmol) and vinyl diazoacetate **3-6** (0.427 mL, 1.0 M in CH_2Cl_2, 0.427 mmol). The reaction mixture was irradiated with a 23 W CFL bulb while stirring. After 8 h, second charges of vinyl diazoacetate **3-6** (0.285 mL, 1.0 M in CH_2Cl_2, 0.285 mmol) and $[Cr(PMP_2phen)_3](BF_4)_3$ (2.1 mg, 0.00142 mmol) were added, and irradiation was continued. At the 24 h timepoint, the solvent was removed via rotary evaporation. The crude residue was dissolved in CH_2Cl_2 (~1 mL), and the solution was passed through a SiO_2 plug (0.5 x 3 cm), using CH_2Cl_2 as eluent (~8 mL). The filtrate was concentrated in vacuo, and the residue was purified by silica gel flash chromatography (2:1 hexanes/Et_2O eluent) to afford indoline **3-22** (50.9 mg, 74% yield) as a white solid.

TLC R_f: 0.40 in 1:1 hexanes/Et_2O, visualized by UV, stained blue in Hanessian's stain.

^{1}H NMR (400 MHz, $CDCl_3$): δ 8.05-7.83 (br. m, 1H), 7.18 (dd, *J* = 8.0, 1.7 Hz, 1H), 7.04 (d, *J* = 8.0 Hz, 1H), 6.85 (app. s, 1H), 5.88 (app. d, *J* = 6.3 Hz, 1H), 5.35-4.45 (br. m, 2H), 4.23-4.12 (comp. m, 2H), 4.06 (app. t, *J* = 7.5 Hz, 1H), 3.02 (app. ddt, *J* = 18.4, 6.2, 2.0 Hz, 1H), 2.74 (app. d, *J* = 18.4 Hz, 1H), 1.26 (t, *J* = 7.2 Hz, 1H).

^{13}C NMR (125 MHz, 50 °C, $CDCl_3$): δ 163.8, 151.6, 144.7, 142.1, 135.1, 134.4, 127.1, 125.3, 121.9, 120.5, 95.4, 75.8, 69.3, 60.7, 43.6, 37.7, 14.4.

IR (ATR, neat): 2981, 1720, 1630, 1479, 778 cm^{-1}.

HRMS (ESI+): *m/z* calc'd for $(M + H)^+$ $[C_{17}H_{15}BrCl_3NO_4 + H]^+$: 481.9323, found 481.9312.

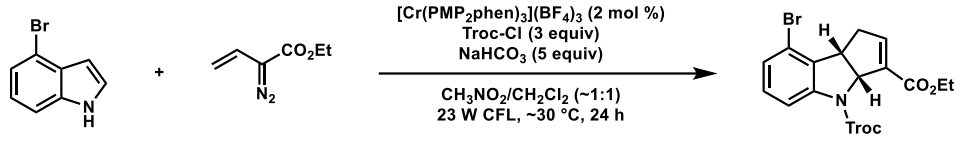

Indoline 3-23. According to a modified General Procedure A, 4-bromoindole (**S3-13**, 25.5 mg, 0.130 mmol), $NaHCO_3$ (54.6 mg, 0.650 mmol), and $[Cr(PMP_2phen)_3](BF_4)_3$ (2.0 mg, 0.00130 mmol) were added to a flame-dried 1-dram borosilicate vial. The reagents were suspended in CH_3NO_2 (0.650 mL), and to this suspension were added 2,2,2-trichloroethoxycarbonyl chloride (53.7 µL, 0.390 mmol) and vinyl diazoacetate **3-6** (0.390 mL, 1.0 M in CH_2Cl_2, 0.390 mmol). The reaction mixture was irradiated with a 23 W CFL bulb while stirring. After 8 h, second charges of vinyl diazoacetate **3-6** (0.260 mL, 1.0 M in CH_2Cl_2, 0.260 mmol) and $[Cr(PMP_2phen)_3](BF_4)_3$ (2.0 mg, 0.00130 mmol) were added, and irradiation was continued. At the 24 h timepoint, the solvent was removed via rotary evaporation. The crude residue was dissolved in CH_2Cl_2 (~1 mL), and the solution was passed through a SiO_2 plug (0.5 x 3 cm), using CH_2Cl_2 as eluent (~8 mL). The filtrate was concentrated in vacuo, and the residue was purified by silica gel flash chromatography (2:1 hexanes/Et_2O eluent) to afford indoline **3-23** (54.1 mg, 86% yield) as a white solid.

TLC R_f: 0.67 in 1:1 hexanes/Et_2O, visualized by UV, stained blue in Hanessian's stain.

^{1}H NMR (400 MHz, $CDCl_3$): δ 7.71 (br. d, *J* = 7.6 Hz, 1H), 7.19 (d, *J* = 8.0 Hz, 1H), 7.10 (app. t, *J* = 8.0 Hz, 1H), 6.84 (app. d, *J* = 1.5 Hz, 1H), 5.90 (dd, *J* = 8.3, 1.5 Hz, 1H), 5.23-4.60 (br. m, 2H), 4.31-4.10 (comp. m, 3H), 3.13 (app. d, *J* = 17.4 Hz, 1H), 3.04 (app. dd, *J* = 17.4, 8.0 Hz, 1H), 1.28 (t, *J* = 7.1 Hz, 3H).

^{13}C NMR (125 MHz, 50 °C, $CDCl_3$): δ 164.1, 151.8, 144.8, 142.5, 135.1, 134.3, 129.9, 127.6, 119.6, 116.0, 95.4, 75.8, 68.4, 60.6, 45.4, 37.5, 14.4.

IR (ATR, neat): 2980, 1723, 1633, 1453, 848 cm^{-1}.

HRMS (ESI+): *m/z* calc'd for $(M + Na)^+$ $[C_{17}H_{15}BrCl_3NO_4 + Na]^+$: 503.9142, found 503.9125.

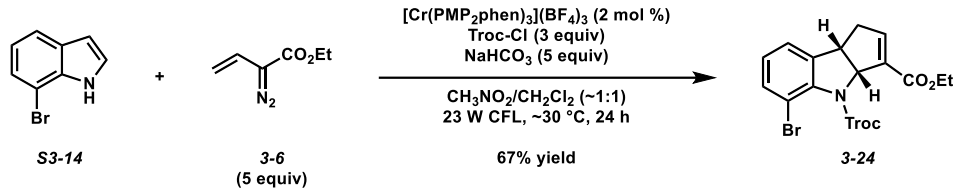

S3-14 + *3-6* (5 equiv) — 67% yield — *3-24*

Indoline 3-24. According to a modified General Procedure A, 7-bromoindole (**S3-14**, 28.3 mg, 0.144 mmol), $NaHCO_3$ (60.6 mg, 0.722 mmol), and $[Cr(PMP_2phen)_3](BF_4)_3$ (2.2 mg, 0.00144 mmol) were added to a flame-dried 1-dram borosilicate vial. The reagents were suspended in CH_3NO_2 (0.722 mL), and to this suspension were added 2,2,2-trichloroethoxycarbonyl chloride (59.6 µL, 0.433 mmol) and vinyl diazoacetate **3-6** (0.433 mL, 1.0 M in CH_2Cl_2, 0.433 mmol). The reaction mixture was irradiated with a 23 W CFL bulb while stirring. After 8 h, second charges of vinyl diazoacetate **3-6** (0.288 mL, 1.0 M in CH_2Cl_2, 0.288 mmol) and $[Cr(PMP_2phen)_3](BF_4)_3$ (2.2 mg, 0.00144 mmol) were added, and irradiation was continued. At the 24 h timepoint, the solvent was removed via rotary evaporation. The crude residue was dissolved in CH_2Cl_2 (~1 mL), and the solution was passed through a SiO_2 plug (0.5 x 3 cm), using CH_2Cl_2 as eluent (~8 mL). The filtrate was concentrated in vacuo, and the residue was purified by silica gel flash chromatography (2:1 hexanes/Et_2O eluent) to afford indoline **3-24** (47.6 mg, 68% yield, 1.7 mg of pyrazole unable to be separated from the pure product) as a white solid.

TLC R_f: 0.35 in 1:1 hexanes/Et_2O, visualized by UV, stained blue in Hanessian's stain

^{1}H NMR (400 MHz, $CDCl_3$): δ 7.42 (d, *J* = 8.0 Hz, 1H), 7.14 (d, *J* = 7.5 Hz, 1H), 7.01 (app. t, *J* = 7.8 Hz, 1H) 6.88-6.80 (m, 1H), 6.00-5.90 (m, 1H), 5.10 (d, *J* = 12.0 Hz, 1H), 4.79 (d, *J* = 12.0 Hz, 1H), 4.29 (dq, *J* = 14.2, 7.1 Hz, 1H), 4.23-4.12 (comp. m, 2H), 2.97 (app. ddt, *J* = 18.4, 7.6, 2.2 Hz, 1H), 2.69 (app. d, *J* = 18.4 Hz, 1H), 1.29 (t, *J* = 7.1 Hz, 3H).

^{13}C NMR (125 MHz, 50 °C, $CDCl_3$): δ 163.6, 152.7, 144.7, 140.8, 140.4, 135.5, 133.1, 127.1, 123.0, 114.2, 95.6, 75.7, 71.5, 60.6, 45.2, 37.7, 14.4.

IR (ATR, neat): 2981, 1724, 1636, 1478, 794 cm^{-1}.

HRMS (ESI+): *m/z* calc'd for $(M + H)^+$ $[C_{17}H_{15}BrCl_3NO_4 + H]^+$: 481.9323, found 481.9316.

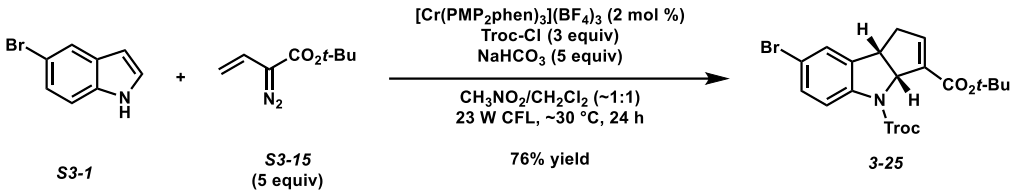

Indoline 3-25. According to a modified General Procedure A, 5-bromoindole (**S3-1**, 28.0 mg, 0.143 mmol), $NaHCO_3$ (60.0 mg, 0.714 mmol), and $[Cr(PMP_2phen)_3](BF_4)_3$ (2.1 mg, 0.00143 mmol) were added to a flame-dried 1-dram borosilicate vial. The reagents were suspended in CH_3NO_2 (0.714 mL), and to this suspension were added 2,2,2-trichloroethoxycarbonyl chloride (59.0 µL, 0.428 mmol) and vinyl diazoacetate **S3-15** (0.428 mL, 1.0 M in CH_2Cl_2, 0.428 mmol). The reaction mixture was irradiated with a 23 W CFL bulb while stirring. After 8 h, second charges of vinyl diazoacetate **S3-15** (0.286 mL, 1.0 M in CH_2Cl_2, 0.286 mmol) and $[Cr(PMP_2phen)_3](BF_4)_3$ (2.1 mg, 0.00143 mmol) were added, and irradiation was continued. At the 24 h timepoint, the solvent was removed via rotary evaporation. The crude residue was dissolved in CH_2Cl_2 (~1 mL), and the solution was passed through a SiO_2 plug (0.5 x 3 cm), using CH_2Cl_2 as eluent (~8 mL). The filtrate was concentrated in vacuo, and the residue was purified by silica gel flash chromatography (4:1 hexanes/Et_2O eluent) to afford indoline **3-25** (55.5 mg, 76% yield) as a yellow oil.

TLC R_f: 0.72 in 1:1 hexanes/Et_2O, visualized by UV, stained blue in Hanessian's stain.

^{1}H NMR (400 MHz, $CDCl_3$): δ 7.75-7.43 (br. m, 1H), 7.34 (d, *J* = 8.6 Hz, 1H), 7.29 (s, 1H), 6.73 (app. s, 1H), 5.84 (app. d, *J* = 6.8 Hz, 1H), 5.31-4.40 (br. m, 2H), 4.09 (app. t, *J* = 7.5 Hz, 1H), 2.98 (app. ddt, *J* = 18.3, 7.7, 2.0 Hz, 1H), 2.72 (app. d, *J* = 18.3 Hz, 1H), 1.45 (s, 9H).

^{13}C NMR (125 MHz, 50 °C, $CDCl_3$): δ 163.1, 151.7, 143.4, 140.0, 137.9, 136.5, 131.4, 127.4, 118.7, 116.7, 95.4, 81.2, 75.8, 69.2. 43.8, 37.5, 28.3.

IR (ATR, neat): 2978, 1716, 1629, 1478, 1161 cm^{-1}.

HRMS (ESI+): *m/z* calc'd for $(M + Na)^+$ $[C_{19}H_{19}BrCl_3NO_4 + Na]^+$: 531.9455, found 531.9443.

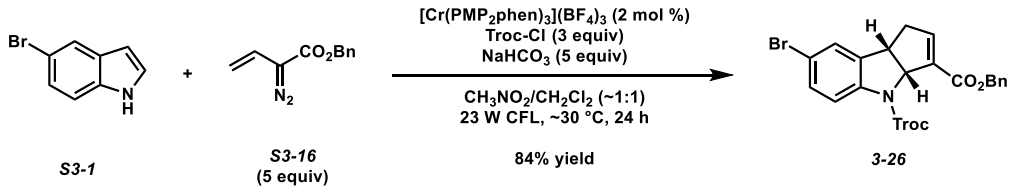

Indoline 3-26. According to a modified General Procedure A, 5-bromoindole (**S3-1**, 27.9 mg, 0.142 mmol), $NaHCO_3$ (59.8 mg, 0.712 mmol), and $[Cr(PMP_2phen)_3](BF_4)_3$ (2.1 mg, 0.00142 mmol) were added to a flame-dried 1-dram borosilicate vial. The reagents were suspended in CH_3NO_2 (0.712 mL), and to this suspension were added 2,2,2-trichloroethoxycarbonyl chloride (58.8 µL, 0.427 mmol) and vinyl diazoacetate **S3-16** (0.427 mL, 1.0 M in CH_2Cl_2, 0.427 mmol). The reaction mixture was irradiated with a 23 W CFL bulb while stirring. After 8 h, second charges of vinyl diazoacetate **S3-16** (0.284 mL, 1.0 M in CH_2Cl_2, 0.284 mmol) and $[Cr(PMP_2phen)_3](BF_4)_3$ (2.1 mg, 0.00142 mmol) were added, and irradiation was continued. At the 24 h timepoint, the solvent was removed via rotary evaporation. The crude residue was dissolved in CH_2Cl_2 (~1 mL), and the solution was passed through a SiO_2 plug (0.5 x 3 cm), using CH_2Cl_2 as eluent (~8 mL). The filtrate was concentrated in vacuo, and the residue was purified by silica gel flash chromatography (4:1 hexanes/Et_2O eluent) to afford indoline **3-26** (65.2 mg, 84% yield) as a white solid.

TLC R_f: 0.53 in 1:1 hexanes/Et_2O, visualized by UV, stained blue in Hanessian's stain.

^{1}H NMR (400 MHz, $CDCl_3$): δ 7.78-7.44 (br. m, 1H), 7.44-7.27 (comp. m, 7H), 6.94 (app. s, 1H), 5.89 (d, J = 6.7 Hz, 1H), 5.20-4.60 (br. m, 2H), 5.15 (ABq, J = 12.3 Hz, Δν = 35.1 Hz, 2H), 4.13 (app. t, J = 7.6 Hz, 1H), 3.03 (app. dd, J = 18.5, 7.7 Hz, 1H), 2.76 (app. d, J = 18.5 Hz, 1H).

^{13}C NMR (125 MHz, 50 °C, $CDCl_3$): δ 163.6, 151.6, 145.5, 140.0, 137.6, 136.0, 134.8, 131.5, 128.8, 128.6, 128.5, 127.5, 118.6, 116.7, 95.4, 75.5, 69.1, 66.6, 43.9, 37.7.

IR (ATR, neat): 2951, 1720, 1629, 1477, 819 cm^{-1}.

HRMS (ESI+): *m/z* calc'd for $(M + H)^+$ $[C_{22}H_{17}BrCl_3NO_4 + H]^+$: 543.9479, found 543.9471.

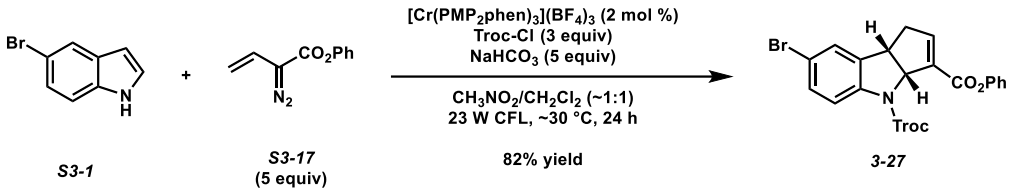

Indoline 3-27. According to a modified General Procedure A, 5-bromoindole (**S3-1**, 28.1 mg, 0.143 mmol), $NaHCO_3$ (60.2 mg, 0.717 mmol), and $[Cr(PMP_2phen)_3](BF_4)_3$ (2.2 mg, 0.00143 mmol) were added to a flame-dried 1-dram borosilicate vial. The reagents were suspended in CH_3NO_2 (0.717 mL), and to this suspension were added 2,2,2-trichloroethoxycarbonyl chloride (59.2 µL, 0.430 mmol) and vinyl diazoacetate **S3-17** (0.430 mL, 1.0 M in CH_2Cl_2, 0.430 mmol). The reaction mixture was irradiated with a 23 W CFL bulb while stirring. After 8 h, second charges of vinyl diazoacetate **S3-17** (0.287 mL, 1.0 M in CH_2Cl_2, 0.287 mmol) and $[Cr(PMP_2phen)_3](BF_4)_3$ (2.2 mg, 0.00143 mmol) were added, and irradiation was continued. At the 24 h timepoint, the solvent was removed via rotary evaporation. The crude residue was dissolved in CH_2Cl_2 (~1 mL), and the solution was passed through a SiO_2 plug (0.5 x 3 cm), using CH_2Cl_2 as eluent (~8 mL). The filtrate was concentrated in vacuo, and the residue was purified by silica gel flash chromatography (4:1 hexanes/Et_2O eluent) to afford indoline **3-27** (62.5 mg, 82% yield) as a white solid.

TLC R_f: 0.53 in 1:1 hexanes/Et_2O, visualized by UV, stained blue in Hanessian's stain.

^{1}H NMR (400 MHz, $CDCl_3$): δ 7.80-7.45 (br. m, 1H), 7.44-7.30 (comp. m, 4H), 7.22 (t, *J* = 7.4 Hz, 1H), 7.17-7.02 (comp. m, 3H), 6.00 (d, *J* = 6.7 Hz, 1H), 5.25-4.35 (br. m, 2H), 4.21 (app. t, *J* = 7.5 Hz, 1H), 3.13 (app. dd, *J* = 18.7, 7.8 Hz, 1H), 2.86 (app. d, *J* = 18.7 Hz, 1H).

^{13}C NMR (125 MHz, 50 °C, $CDCl_3$): δ 161.8, 151.7, 150.8, 147.1, 140.0, 137.5, 134.5, 131.6, 129.6, 127.5, 126.0, 121.7, 118.7, 116.9, 95.4, 75.7, 69.1, 44.0, 38.0.

IR (ATR, neat): 2924, 1724, 1628, 1478, 1190, 817 cm^{-1}.

HRMS (ESI+): *m/z* calc'd for $(M + H)^+$ $[C_{21}H_{15}BrCl_3NO_4 + H]^+$: 529.9323, found 529.9315.

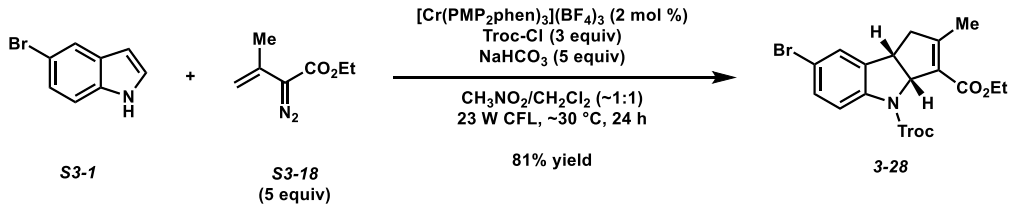

S3-1 *S3-18* (5 equiv) *3-28*

Indoline 3-28. According to a modified General Procedure A, 5-bromoindole (**S3-1**, 28.5 mg, 0.145 mmol), $NaHCO_3$ (61.1 mg, 0.727 mmol), and $[Cr(PMP_2phen)_3](BF_4)_3$ (2.2 mg, 0.00145 mmol) were added to a flame-dried 1-dram borosilicate vial. The reagents were suspended in CH_3NO_2 (0.727 mL), and to this suspension were added 2,2,2-trichloroethoxycarbonyl chloride (60.0 µL, 0.436 mmol) and vinyl diazoacetate **S3-18** (0.436 mL, 1.0 M in CH_2Cl_2, 0.436 mmol). The reaction mixture was irradiated with a 23 W CFL bulb while stirring. After 8 h, second charges of vinyl diazoacetate **S3-18** (0.291 mL, 1.0 M in CH_2Cl_2, 0.291 mmol) and $[Cr(PMP_2phen)_3](BF_4)_3$ (2.2 mg, 0.00145 mmol) were added, and irradiation was continued. At the 30 h timepoint, the solvent was removed via rotary evaporation. The crude residue was dissolved in CH_2Cl_2 (~1 mL), and the solution was passed through a SiO_2 plug (0.5 x 3 cm), using CH_2Cl_2 as eluent (~8 mL). The filtrate was concentrated in vacuo, and the residue was purified by silica gel flash chromatography (2:1 hexanes/Et_2O eluent) to afford indoline **3-28** (58.6 mg, 81% yield) as a colorless oil.

TLC R_f: 0.61 in 1:1 hexanes/Et_2O, visualized by UV, stained blue in Hanessian's stain.

^{1}H NMR (400 MHz, $CDCl_3$): δ 7.68-7.47 (br. m, 1H), 7.34 (d, *J* = 8.6 Hz, 1H), 7.29 (s, 1H), 5.88 (d, *J* = 6.4 Hz, 1H), 5.30-4.40 (br. m, 2H), 4.24-4.15 (comp. m, 2H), 3.97 (app. t, *J* = 7.6 Hz, 1H), 3.01 (dd, *J* = 17.7, 8.0 Hz, 1H), 2.66 (app. d, *J* = 17.7 Hz, 1H), 2.01 (s, 3H), 1.28 (t, *J* = 7.1 Hz, 1H).

^{13}C NMR (125 MHz, 50 °C, $CDCl_3$): δ 165.4, 153.9, 151.6, 140.0, 138.1, 131.3, 127.5, 127.3, 118.8, 116.7, 111.9, 95.4, 75.7, 71.3, 60.4, 44.3, 42.0, 16.5, 14.4.

IR (ATR, neat): 2975, 1723, 1643, 1478, 1104, 821 cm^{-1}.

HRMS (ESI+): *m/z* calc'd for $(M + H)^+$ $[C_{18}H_{17}BrCl_3NO_4 + H]^+$: 495.9479, found 495.9467.

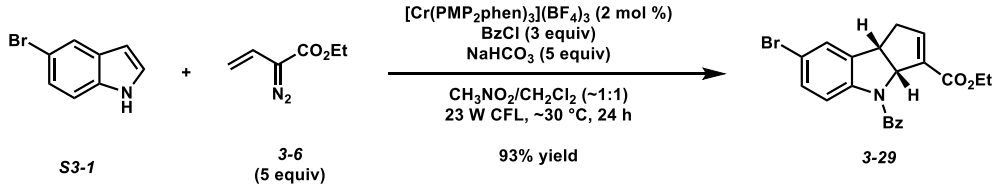

Indoline 3-29. According to General Procedure A, 5-bromoindole (**S3-1**, 28.5 mg, 0.145 mmol), $NaHCO_3$ (61.1 mg, 0.727 mmol) and $[Cr(PMP_2phen)_3](BF_4)_3$ (2.2 mg, 0.00145 mmol) were added to a flame-dried 1-dram borosilicate vial. The reagents were suspended in CH_3NO_2 (0.727 mL), and to this suspension were added benzoyl chloride (50.7 µL, 0.436 mmol) and vinyl diazoacetate **3-6** (0.436 mL, 1.0 M in CH_2Cl_2, 0.436 mmol). The reaction mixture was irradiated with a 23 W CFL bulb while stirring. After 8 h, extra charges of vinyl diazoacetate **3-6** (0.291 mL, 1.0 M in CH_2Cl_2, 0.291 mmol) and $[Cr(PMP_2phen)_3](BF_4)_3$ (2.2 mg, 0.00145 mmol) were added, and irradiation was continued. At the 28 h timepoint, the solvent was removed via rotary evaporation. The crude residue was dissolved in CH_2Cl_2 (~1 mL), and the solution was passed through a SiO_2 plug (0.5 x 3 cm), using CH_2Cl_2 as eluent (~8 mL). The filtrate was concentrated in vacuo, and the residue was purified by silica gel flash chromatography (4:1 hexanes/EtOAc eluent) to afford indoline **3-29** (55.7 mg, 93% yield) as a white solid.

TLC: R_f = 0.28 in 4:1 hexanes/EtOAc, visualized by UV.

^{1}H NMR (400 MHz, $CDCl_3$): δ 7.57 (d, *J* = 8.0 Hz, 2H), 7.50-7.40 (comp. m, 3H), 7.31 (s, 1H), 7.18 (d, *J* = 8.5 Hz, 1H), 7.18-6.96 (br. m, 1H), 6.86-6.80 (m, 1H), 6.02 (app. d, *J* = 5.9 Hz, 1H), 4.20-4.09 (comp. m, 3H), 2.99 (app. ddt, *J* = 18.3, 7.4, 2.0 Hz, 1H), 2.77 (app. d, *J* = 18.3 Hz, 1H), 1.22 (t, *J* = 7.1 Hz, 3H).

^{13}C NMR (100 MHz, $CDCl_3$): δ 170.0, 163.7, 144.7, 141.2, 138.1, 136.9, 135.0, 131.0, 130.5, 128.5, 128.0, 127.5, 118.3, 116.6, 69.6, 60.7, 43.6, 37.4, 14.3.

IR (ATR, neat): 2980, 1715, 1651, 1469, 1378, 728 cm^{-1}.

HRMS (ESI+): *m/z* calc'd for $(M + Na)^+$ $[C_{21}H_{18}BrNO_3 + Na]^+$: 434.0362, found 434.0358.

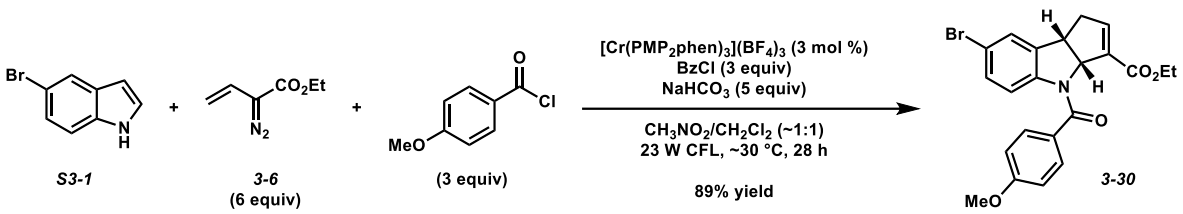

Indoline 3-30. According to a modified General Procedure A, 5-bromoindole (**S3-1**, 24.8 mg, 0.126 mmol), $NaHCO_3$ (53.1 mg, 0.632 mmol), and $[Cr(PMP_2phen)_3](BF_4)_3$ (1.9 mg, 0.00126 mmol) were added to a flame-dried 1-dram borosilicate vial. The reagents were suspended in CH_3NO_2 (0.630 mL), and to this suspension were added 4-methoxybenzoyl chloride (51.2 µL, 0.378 mmol) and vinyl diazoacetate **3-6** (0.378 mL, 1.0 M in CH_2Cl_2, 0.378 mmol). The reaction mixture was irradiated with a 23 W CFL bulb while stirring. After 8 h, second charges of vinyl diazoacetate **3-6** (0.252 mL, 1.0 M in CH_2Cl_2, 0.252 mmol) and $[Cr(PMP_2phen)_3](BF_4)_3$ (1.9 mg, 0.00126 mmol) were added, and irradiation was continued. At the 20 h timepoint, third charges of vinyl diazoacetate **3-6** (0.126 mL, 1.0 M in CH_2Cl_2, 0.126 mmol) and $[Cr(PMP_2phen)_3](BF_4)_3$ (1.9 mg, 0.00126 mmol) were added, and irradiation was continued. At the 28 h timepoint, the solvent was removed via rotary evaporation. The crude residue was dissolved in CH_2Cl_2 (~1 mL), and the solution was passed through a SiO_2 plug (0.5 x 3 cm), using CH_2Cl_2 as eluent (~8 mL). The filtrate was concentrated in vacuo, and the residue was purified by silica gel flash chromatography (2:1 hexanes/Et_2O eluent) to afford indoline **3-30** (48.3 mg, 86% yield, impurity not included in this total weight) as a colorless oil.

TLC: R_f = 0.21 in 4:1 hexanes/EtOAc, visualized by UV.

^{1}H NMR (400 MHz, $CDCl_3$): δ 7.56 (d, *J* = 8.7 Hz, 2H), 7.31 (s, 1H), 7.22-7.12 (comp. m, 2H), 6.94 (d, *J* = 8.7 Hz, 2H), 6.85-6.80 (m, 1H), 6.03 (dd, *J* = 7.2, 1.6 Hz, 1H), 4.13 (app. q, *J* = 7.1, 3H), 3.86 (s, 3H), 2.99 (app. ddt, *J* = 18.3, 7.5, 2.0 Hz, 1H), 2.77 (app. d, *J* = 18.3 Hz, 1H), 1.20 (t, *J* = 7.1 Hz, 3H).

^{13}C NMR (100 MHz, $CDCl_3$): δ 170.0, 163.8, 161.4, 144.6, 141.5, 138.0, 135.1, 131.0, 130.2, 129.2, 127.5, 118.1, 116.3, 113.7, 69.7, 60.6, 55.5, 43.6, 37.5, 14.3.

IR (ATR, neat): 2933, 1715, 1644, 1606, 1252, 877 cm^{-1}.

HRMS (ESI+): *m/z* calc'd for $(M + Na)^+$ $[C_{22}H_{20}BrNO_4 + Na]^+$: 464.0468, found 464.0469.

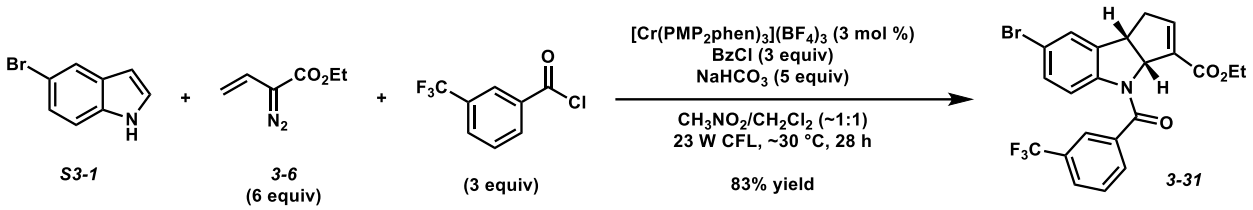

Indoline 3-31. According to a modified General Procedure A, 5-bromoindole (**S3-1**, 26.3 mg, 0.134 mmol), $NaHCO_3$ (56.3 mg, 0.671 mmol), and $[Cr(PMP_2phen)_3](BF_4)_3$ (2.0 mg, 0.00134 mmol) were added to a flame-dried 1-dram borosilicate vial. The reagents were suspended in CH_3NO_2 (0.670 mL), and to this suspension were added 3-(trifluoromethyl)benzoyl chloride (59.9 µL, 0.397 mmol) and vinyl diazoacetate **3-6** (0.402 mL, 1.0 M in CH_2Cl_2, 0.402 mmol). The reaction mixture was irradiated with a 23 W CFL bulb while stirring. After 8 h, second charges of vinyl diazoacetate **3-6** (0.268 mL, 1.0 M in CH_2Cl_2, 0.268 mmol) and $[Cr(PMP_2phen)_3](BF_4)_3$ (2.0 mg, 0.00134 mmol) were added, and irradiation was continued. At the 20 h timepoint, third charges of vinyl diazoacetate **3-6** (0.134 mL, 1.0 M in CH_2Cl_2, 0.134 mmol) and $[Cr(PMP_2phen)_3](BF_4)_3$ (2.0 mg, 0.00134 mmol) were added, and irradiation was continued. At the 28 h timepoint, the solvent was removed via rotary evaporation. The crude residue was dissolved in CH_2Cl_2 (~1 mL), and the solution was passed through a SiO_2 plug (0.5 x 3 cm), using CH_2Cl_2 as eluent (~8 mL). The filtrate was concentrated in vacuo, and the residue was purified by silica gel flash chromatography (6:1 hexanes/EtOAc eluent) to afford indoline **3-31** (53.2 mg, 83% yield) as a yellow oil.

TLC: R_f = 0.45 in 4:1 hexanes/EtOAc, visualized by UV.

^{1}H NMR (400 MHz, $CDCl_3$): δ 7.87 (s, 1H), 7.81 (d, *J* = 7.7 Hz, 1H), 7.73 (d, *J* = 7.7 Hz, 1H), 7.58 (app. t, *J* = 7.7 Hz, 1H), 7.53-7.22 (br. m, 1H), 7.35 (s, 1H), 7.29-7.21 (m, 1H), 6.85-6.80 (m, 1H), 5.85 (app. d, *J* = 5.5 Hz, 1H), 4.18-4.09 (comp. m, 3H), 3.00 (app. ddt, *J* = 18.4, 7.3, 2.0 Hz, 1H), 2.79 (app. d, *J* = 18.4 Hz, 1H), 1.21 (t, *J* = 7.1 Hz, 3H).

^{13}C NMR (100 MHz, $CDCl_3$): δ 168.5, 163.4, 145.0, 140.9, 137.9, 137.7, 134.4, 131.7, 131.3, 130.8 (q, *J* = 32.4 Hz), 129.0, 127.6, 127.0 (q, *J* = 3.7 Hz), 126.6 (q, *J* = 271 Hz), 125.1 (q, *J* = 3.7 Hz), 118.5, 117.1, 70.0, 60.7, 43.7, 37.3, 14.3.

IR (ATR, neat): 2983, 1715, 1651, 1470, 1384, 822 cm^{-1}.

HRMS (ESI+): *m/z* calc'd $(M + H)^+$ $[C_{22}H_{17}BrF_3NO_3 + H]^+$: 480.0417 found 480.0414.

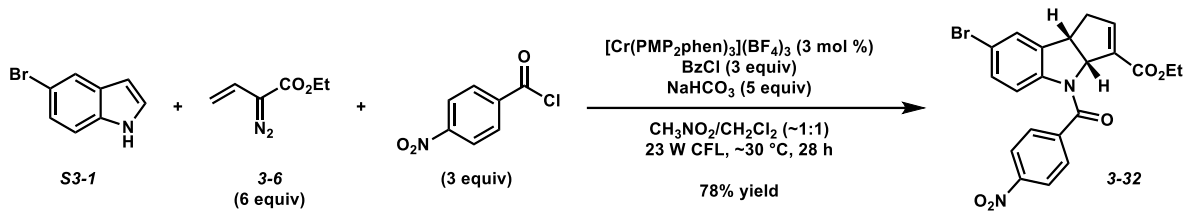

Indoline 3-32. According to a modified General Procedure A, 5-bromoindole (**S3-1**, 26.6 mg, 0.136 mmol), $NaHCO_3$ (57.1 mg, 0.680 mmol), and $[Cr(PMP_2phen)_3](BF_4)_3$ (2.0 mg, 0.00136 mmol) were added to a flame-dried 1-dram borosilicate vial. The reagents were suspended in CH_3NO_2 (0.680 mL), and to this suspension were added 4-nitrobenzoyl chloride (75.7 mg, 0.408 mmol) and vinyl diazoacetate **3-6** (0.408 mL, 1.0 M in CH_2Cl_2, 0.408 mmol). The reaction mixture was irradiated with a 23 W CFL bulb while stirring. After 8 h, second charges of vinyl diazoacetate **3-6** (0.272 mL, 1.0 M in CH_2Cl_2, 0.272 mmol) and $[Cr(PMP_2phen)_3](BF_4)_3$ (2.0 mg, 0.00136 mmol) were added, and irradiation was continued. At the 20 h timepoint, third charges of vinyl diazoacetate **3-6** (0.136 mL, 1.0 M in CH_2Cl_2, 0.136 mmol) and $[Cr(PMP_2phen)_3](BF_4)_3$ (2.0 mg, 0.00136 mmol) were added, and irradiation was continued. At the 28 h timepoint, the solvent was removed via rotary evaporation. The crude residue was dissolved in CH_2Cl_2 (~1 mL), and the solution was passed through a SiO_2 plug (0.5 x 3 cm), using CH_2Cl_2 as eluent (~8 mL). The filtrate was concentrated in vacuo, and the residue was purified by silica gel flash chromatography (2:1 hexanes/Et_2O eluent) to afford indoline **3-32** (48.3 mg, 78% yield) as a white solid.

TLC: R_f = 0.27 in 4:1 hexanes/EtOAc, visualized by UV.

^{1}H NMR (400 MHz, $CDCl_3$): δ 8.31 (d, *J* = 8.5 Hz, 2H), 7.80 (d, *J* = 8.5 Hz, 2H), 7.70-7.41 (br. m, 1H), 7.36 (s, 1H), 7.30 (d, *J* = 7.6 Hz, 1H), 6.85-6.80 (m, 1H), 5.79 (br. s, 1H), 4.22-4.08 (comp. m, 3H), 3.00 (app. ddt, *J* = 18.4, 7.3, 2.0 Hz, 1H), 2.81 (app. d, *J* = 18.4 Hz, 1H), 1.22 (t, *J* = 7.1 Hz, 3H).

^{13}C NMR (100 MHz, $CDCl_3$): δ 163.4, 148.7, 145.2, 142.9, 140.7, 137.8, 134.0, 131.4, 129.4, 127.6, 123.7, 118.7, 117.4, 70.1, 60.8, 43.7, 37.4, 14.3 (*1 carbon not detected*).

IR (ATR, neat): 2925, 1713, 1652, 1521, 1346, 734 cm^{-1}.

HRMS (ESI+): *m/z* calc'd for $(M + Na)^+$ $[C_{21}H_{17}BrN_2O_5 + Na]^+$: 479.0213, found 479.0216.

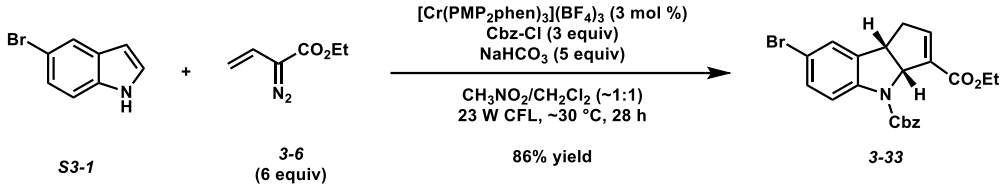

S3-1 *3-6* (6 equiv) 86% yield *3-33*

Indoline 3-33. According to a modified General Procedure A, 5-bromoindole (**S3-1**, 25.3 mg, 0.129 mmol), $NaHCO_3$ (54.2 mg, 0.645 mmol), and $[Cr(PMP_2phen)_3](BF_4)_3$ (2.0 mg, 0.00129 mmol) were added to a flame-dried 1-dram borosilicate vial. The reagents were suspended in CH_3NO_2 (0.645 mL), and to this suspension were added benzyl chloroformate (55.3 µL, 0.387 mmol) and vinyl diazoacetate **3-6** (0.387 mL, 1.0 M in CH_2Cl_2, 0.387 mmol). The reaction mixture was irradiated with a 23 W CFL bulb while stirring. After 8 h, second charges of vinyl diazoacetate **3-6** (0.258 mL, 1.0 M in CH_2Cl_2, 0.258 mmol) and $[Cr(PMP_2phen)_3](BF_4)_3$ (2.0 mg, 0.00129 mmol) were added, and irradiation was continued. At the 20 h timepoint, third charges of vinyl diazoacetate **3-6** (0.129 mL, 1.0 M in CH_2Cl_2, 0.129 mmol) and $[Cr(PMP_2phen)_3](BF_4)_3$ (2.0 mg, 0.00129 mmol) were added, and irradiation was continued. At the 28 h timepoint, the solvent was removed via rotary evaporation. The crude residue was dissolved in CH_2Cl_2 (~1 mL), and the solution was passed through a SiO_2 plug (0.5 x 3 cm), using CH_2Cl_2 as eluent (~8 mL). The filtrate was concentrated in vacuo, and the residue was purified by silica gel flash chromatography (6:1 hexanes/EtOAc eluent) to afford indoline **3-33** (49.0 mg, 86% yield) as a yellow oil.

TLC: R_f = 0.45 in 4:1 hexanes/EtOAc, visualized by UV.

^{1}H NMR (400 MHz, $CDCl_3$): δ 7.69-7.38 (br. m, 1H), 7.45 (d, *J* = 6.9 Hz, 2H), 7.41-7.23 (comp. m, 5H), 6.83 (app. s, 1H), 5.83 (d, *J* = 6.6 Hz, 1H), 5.38 (d, *J* = 12.0 Hz, 1H), 5.23 (br. d, *J* = 12.0 Hz, 1H), 4.23-4.08 (comp. m, 2H), 4.06 (app. t, *J* = 7.6 Hz, 1H), 2.98 (app. dd, *J* = 18.4, 7.6 Hz, 1H), 2.72 (app. d, *J* = 18.4 Hz, 1H), 1.23 (t, *J* = 7.1 Hz, 3H).

^{13}C NMR (125 MHz, $CDCl_3$, 50 °C): δ 164.0, 153.5, 144.1, 140.8, 137.5, 136.5, 135.7, 131.3, 128.7, 128.4, 128.3, 127.3, 118.4, 116.0, 69.0, 67.9, 60.6, 43.9, 37.8, 14.3.

IR (ATR, neat): 2979, 1709, 1629, 1477, 1280, 752 cm^{-1}.

HRMS (ESI+): *m/z* calc'd for $(M + Na)^+$ $[C_{22}H_{20}BrNO_4 + Na]^+$: 464.0468 found 464.0466.

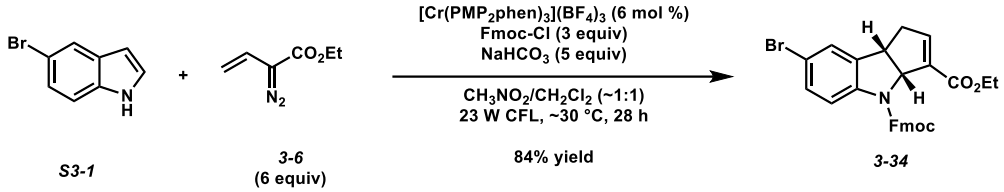

Indoline 3-34. According to a modified General Procedure A, 5-bromoindole (**S3-1**, 25.5 mg, 0.130 mmol), $NaHCO_3$ (54.6 mg, 0.650 mmol), and $[Cr(PMP_2phen)_3](BF_4)_3$ (2.0 mg, 0.00130 mmol) were added to a flame-dried 1-dram borosilicate vial. The reagents were suspended in CH_3NO_2 (0.650 mL), and to this suspension were added 9-fluorenylmethyl chloroformate (101 mg, 0.390 mmol) and vinyl diazoacetate **3-6** (0.390 mL, 1.0 M in CH_2Cl_2, 0.390 mmol). The reaction mixture was irradiated with a 23 W CFL bulb while stirring. After 8 h, second charges of vinyl diazoacetate **3-6** (0.260 mL, 1.0 M in CH_2Cl_2, 0.260 mmol) and $[Cr(PMP_2phen)_3](BF_4)_3$ (2.0 mg, 0.00130 mmol) were added, and irradiation was continued. At the 20 h timepoint, third charges of vinyl diazoacetate **3-6** (0.130 mL, 1.0 M in CH_2Cl_2, 0.130 mmol) and $[Cr(PMP_2phen)_3](BF_4)_3$ (2.0 mg, 0.00130 mmol) were added, and irradiation was continued. At the 28 h timepoint, the solvent was removed via rotary evaporation. The crude residue was then dissolved in CH_2Cl_2 (~1 mL), and the solution was passed through a SiO_2 plug (0.5 x 3 cm), using CH_2Cl_2 as eluent (~8 mL). The filtrate was concentrated in vacuo, and the crude residue was purified by silica gel flash chromatography (6:1 hexanes/EtOAc eluent) to afford indoline **3-34** (58.1 mg, 84% yield) as a white solid.

TLC: R_f = 0.36 in 4:1 hexanes/EtOAc, visualized by UV.

^{1}H NMR (400 MHz, $CDCl_3$): δ 7.78 (app. t, *J* = 6.6 Hz, 2H), 7.65-7.57 (comp. m, 2H), 7.41 (app. q, *J* = 6.6 Hz, 2H), 7.35-7.27 (comp. m, 3H), 7.27-7.08 (br. m, 1H), 7.24 (s, 1H), 6.83 (app. s, 1H), 5.82 (dd, *J* = 7.6, 1.6 Hz, 1H), 4.80-4.50 (br. m, 2H), 4.36 (app. t, *J* = 6.1 Hz, 1H), 4.26-3.98

(comp. m, 3H), 3.00 (app. dd, J = 18.0, 7.9 Hz, 1H), 2.72 (app. d, J = 18.0 Hz, 1H), 1.20 (t, J = 7.1 Hz, 3H).

^{13}C NMR (100 MHz, $CDCl_3$): δ 163.9, 153.5, 144.8, 144.1, 141.5, 131.1, 127.9, 127.7, 127.3, 127.24, 127.20, 125.1, 120.21, 120.17, 120.1, 115.9, 68.7, 67.8, 60.6, 50.5, 47.3, 37.7, 14.3.

IR (ATR, neat): 2955, 1713, 1635, 1477, 757 cm^{-1}.

HRMS (ESI+): *m/z* calc'd for $(M + Na)^+$ $[C_{29}H_{24}BrNO_4 + Na]^+$: 552.0781, found 552.0784.

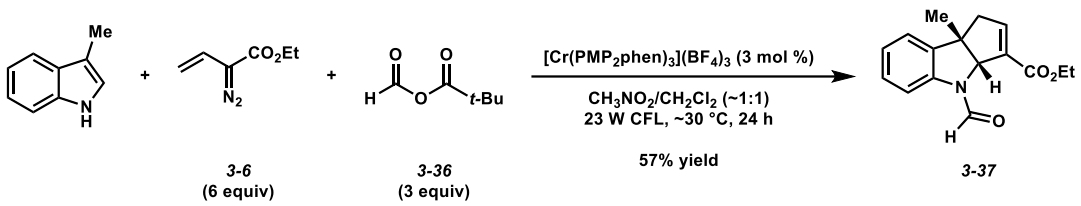

Indoline 3-37. According to General Procedure B, in a flame-dried 1-dram borosilicate vial, trimethylacetic formic anhydride (**3-36**, 60.5 mg, 0.465 mmol) was dissolved in CH_3NO_2 (0.775 mL). To this solution were added 3-methylindole (20.3 mg, 0.155 mmol), $[Cr(PMP_2phen)_3](BF_4)_3$ (2.3 mg, 0.00155 mmol), and vinyl diazoacetate **3-6** (0.465 mL, 1.0 M in CH_2Cl_2, 0.465 mmol). The reaction mixture was irradiated with a 23 W CFL bulb while stirring. After 8 h, second charges of vinyl diazoacetate **3-6** (0.310 mL, 1.0 M in CH_2Cl_2, 0.310 mmol) and $[Cr(PMP_2phen)_3](BF_4)_3$ (2.3 mg, 0.00155 mmol) were added, and irradiation was continued. At the 24 h timepoint, third charges of vinyl diazoacetate **3-6** (0.155 mL, 1.0 M in CH_2Cl_2, 0.155 mmol) and $[Cr(PMP_2phen)_3](BF_4)_3$ (2.3 mg, 0.00155 mmol) were added, and irradiation was continued. At the 28 h timepoint, the solvent was removed via rotary evaporation. The crude residue was dissolved in CH_2Cl_2 (~1 mL), and the solution was passed through a SiO_2 plug (0.5 x 3 cm), using CH_2Cl_2 as eluent (~8 mL). The filtrate was concentrated in vacuo, and the residue was purified by silica gel flash chromatography (2:1 hexanes/Et_2O eluent) to afford indoline **3-37** (24.1 mg, 57% yield) as a yellow oil.

TLC: R_f = 0.25 in 3:1 hexanes/EtOAc, visualized by UV.

^{1}H NMR (400 MHz, $CDCl_3$): δ 8.89 (s, 1H), 8.03 (d, *J* = 8.0 Hz, 1H), 7.25-7.18 (comp. m, 2H), 7.10 (app. td, *J* = 7.3, 1.0 Hz, 1H), 6.87 (app. s, 1H), 5.15-5.10 (m, 1H), 4.22 (app. qd, *J* = 7.1, 2.0 Hz, 2H), 2.99 (app. dt, *J* = 18.9, 2.2 Hz, 1H), 2.79 (app. dt, *J* = 18.9, 2.2 Hz, 1H), 1.50 (s, 3H), 1.30 (t, *J* = 7.1 Hz, 3H).

^{13}C NMR (100 MHz, $CDCl_3$): δ 164.0, 161.9, 146.3, 139.9, 139.1, 134.5, 128.5, 125.1, 122.9, 117.6, 74.5, 61.0, 51.7, 46.5, 26.6, 14.3.

IR (ATR, neat): 2959, 1711, 1676, 1484, 756 cm^{-1}.

HRMS (ESI+): *m/z* calc'd for $(M + Na)^+$ $[C_{16}H_{17}NO_3 + Na]^+$: 294.1101, found 294.1096.

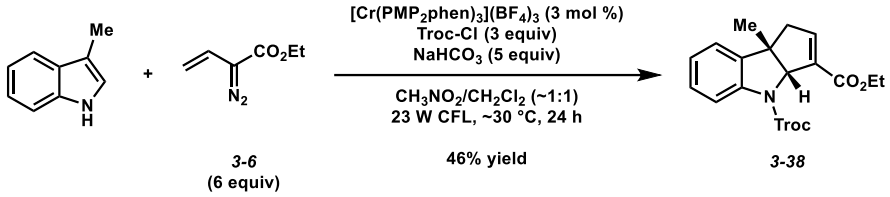

3-6 (6 equiv) — 46% yield — *3-38*

Indoline 3-38. According to a modified General Procedure A, 3-methylindole (20.5 mg, 0.156 mmol), $NaHCO_3$ (65.6 mg, 0.781 mmol), and $[Cr(PMP_2phen)_3](BF_4)_3$ (2.3 mg, 0.00156 mmol) were added to a flame-dried 1-dram borosilicate vial. The reagents were suspended in CH_3NO_2 (0.780 mL), and to this suspension were added 2,2,2-trichloroethoxycarbonyl chloride (64.4 µL, 0.468 mmol) and vinyl diazoacetate **3-6** (0.468 mL, 1.0 M in CH_2Cl_2, 0.468 mmol). The reaction mixture was irradiated with a 23 W CFL bulb while stirring. After 8 h, second charges of vinyl diazoacetate **3-6** (0.312 mL, 1.0 M in CH_2Cl_2, 0.312 mmol) and $[Cr(PMP_2phen)_3](BF_4)_3$ (2.3 mg, 0.00156 mmol) were added, and irradiation was continued. At the 20 h timepoint, a third charge of $[Cr(PMP_2phen)_3](BF_4)_3$ (2.3 mg, 0.00156 mmol) was added, and irradiation was continued. At the 28 h timepoint, the solvent was removed via rotary evaporation. The crude residue was dissolved in CH_2Cl_2 (~1 mL), and the solution was passed through a SiO_2 plug (0.5 x 3 cm), using CH_2Cl_2 as eluent (~8 mL). The filtrate was concentrated in vacuo, and the residue was purified by silica gel flash chromatography (2:1 hexanes/Et_2O eluent) to afford indoline **3-38** (30.3 mg, 46% yield) as a yellow oil.

TLC: R_f = 0.52 in 4:1 hexanes/EtOAc, visualized by UV.

^{1}H NMR (400 MHz, $CDCl_3$): δ 7.84-7.63 (br. m, 1H), 7.24 (app. t, *J* = 8.0 Hz, 1H), 7.19 (d, *J* = 7.3 Hz, 1H), 7.08 (app. t, *J* = 7.3 Hz, 1H), 6.81 (app. s, 1H), 5.48 (s, 1H), 5.37-4.44 (br. m, 2H), 4.26-4.10 (comp. m, 2H), 2.95 (app. d, *J* = 18.2 Hz, 1H), 2.75 (app. d, *J* = 18.2 Hz, 1H), 1.46 (s, 1H), 1.26 (t, *J* = 7.1 Hz, 3H).

^{13}C NMR (125 MHz, 50 °C, $CDCl_3$): δ 163.9, 152.2, 144.9, 140.1, 135.3, 128.5, 124.3, 122.8, 117.3, 95.7, 75.7, 75.0, 60.5, 44.9, 29.0, 25.9, 14.4 (*1 carbon not detected*).

IR (ATR, neat): 2957, 1720, 1628, 1463, 1242, 736 cm^{-1}.

HRMS (ESI+): *m/z* calc'd for $(M + Na)^+$ $[C_{18}H_{18}Cl_3NO_4 + Na]^+$: 440.0194, found 440.0192.

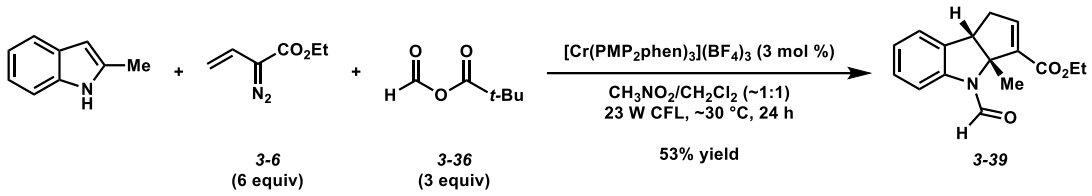

Indoline 3-39. According to General Procedure B, in a flame-dried 1-dram borosilicate vial, trimethylacetic formic anhydride (**3-36**, 60.5 mg, 0.465 mmol) was dissolved in CH_3NO_2 (0.775 mL). To this solution were added 2-methylindole (20.3 mg, 0.155 mmol), $[Cr(PMP_2phen)_3](BF_4)_3$ (2.3 mg, 0.00155 mmol), and vinyl diazoacetate **3-6** (0.465 mL, 1.0 M in CH_2Cl_2, 0.465 mmol). The reaction mixture was irradiated with a 23 W CFL bulb while stirring. After 8 h, second charges of vinyl diazoacetate **3-6** (0.310 mL, 1.0 M in CH_2Cl_2, 0.310 mmol) and $[Cr(PMP_2phen)_3](BF_4)_3$ (2.3 mg, 0.00155 mmol) were added, and irradiation was continued. At the 24 h timepoint, third charges of vinyl diazoacetate **3-6** (0.155 mL, 1.0 M in CH_2Cl_2, 0.155 mmol) and $[Cr(PMP_2phen)_3](BF_4)_3$ (2.3 mg, 0.00155 mmol) were added, and irradiation was continued. At the 28 h timepoint, the solvent was removed via rotary evaporation. The crude residue was dissolved in CH_2Cl_2 (~1 mL), and the solution was passed through a SiO_2 plug (0.5 x 3 cm), using CH_2Cl_2 as eluent (~8 mL). The filtrate was concentrated in vacuo, and the residue was purified by silica gel flash chromatography (2:1 hexanes/Et_2O eluent) to afford indoline **3-39** (23.2 mg, 55% yield) as a pink oil.

TLC: R_f = 0.24 in 3:1 hexanes/EtOAc, visualized by UV.

^{1}H NMR (400 MHz, $CDCl_3$): δ 9.03 (s, 1H), 8.18 (d, *J* = 8.0 Hz, 1H), 7.24 (app. t, *J* = 8.0 Hz, 1H), 7.16 (d, *J* = 7.3 Hz, 1H), 7.08 (app. t, *J* = 7.3 Hz, 1H), 6.89 (app. t, *J* = 2.2 Hz, 1H), 4.20 (q, *J* = 7.1 Hz, 2H), 3.77 (d, *J* = 7.9 Hz, 1H), 3.07 (ddd, *J* = 18.9, 7.9, 2.2 Hz, 1H), 2.73 (app. d, *J* = 18.9 Hz, 1H), 1.91 (s, 3H), 1.29 (t, *J* = 7.1 Hz, 3H).

^{13}C NMR (100 MHz, $CDCl_3$): δ 163.6, 161.5, 145.4, 140.8, 137.1, 133.1, 128.5, 124.6, 123.9, 117.4, 76.8, 60.8, 53.3, 37.4, 24.2, 14.3.

IR (ATR, neat): 2922, 1709, 1669, 1483, 755 cm^{-1}.

HRMS (ESI+): *m/z* calc'd for $(M + Na)^+$ $[C_{16}H_{17}NO_3 + Na]^+$: 294.1101, found 294.1098.

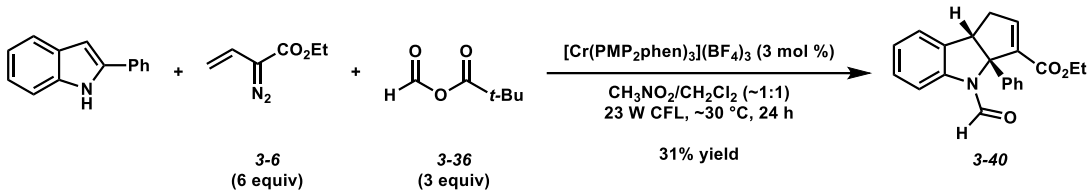

Indoline 3-40. According to General Procedure B, in a flame-dried 1-dram borosilicate vial, trimethylacetic formic anhydride (**3-36**, 62.1 µL, 0.477 mmol) was dissolved in CH_3NO_2 (0.795 mL). To this solution were added 3-phenylindole (30.7 mg, 0.159 mmol), $[Cr(PMP_2phen)_3](BF_4)_3$ (2.4 mg, 0.00159 mmol), and vinyl diazoacetate **3-6** (0.477 mL, 1.0 M in CH_2Cl_2, 0.477 mmol). The reaction mixture was irradiated with a 23 W CFL bulb while stirring. After 8 h, second charges of vinyl diazoacetate **3-6** (0.318 mL, 1.0 M in CH_2Cl_2, 0.318 mmol) and $[Cr(PMP_2phen)_3](BF_4)_3$ (2.4 mg, 0.00159 mmol) were added, and irradiation was continued. At the 24 h timepoint, third charges of vinyl diazoacetate **3-6** (0.159 mL, 1.0 M in CH_2Cl_2, 0.159 mmol) and $[Cr(PMP_2phen)_3](BF_4)_3$ (2.4 mg, 0.00159 mmol) were added, and irradiation was continued. At the 45 h timepoint, the solvent was removed via rotary evaporation. The crude residue was dissolved in CH_2Cl_2 (~1 mL), and the solution was passed through a SiO_2 plug (0.5 x 3 cm), using CH_2Cl_2 as eluent (~8 mL). The filtrate was concentrated in vacuo, and the residue was purified by silica gel flash chromatography (2:1 hexanes/Et_2O eluent) to afford indoline **3-40** (16.2 mg, 31% yield) as a yellow oil.

TLC: R_f = 0.38 in 3:1 hexanes/EtOAc, visualized by UV.

^{1}H NMR (400 MHz, $CDCl_3$): δ 8.66 (s, 1H), 8.31 (d, *J* = 8.0 Hz, 1H), 7.42-7.34 (comp. m, 2H), 7.35-7.26 (comp. m, 5H), 7.17-7.12 (comp. m, 2H), 4.20 (q, *J* = 7.1 Hz, 2H), 3.97 (d, *J* = 7.9 Hz, 1H), 3.03 (ddd, *J* = 18.8, 7.9, 2.1 Hz, 1H), 2.75 (app. dd, *J* = 18.8, 3.1 Hz, 1H), 1.25 (t, *J* = 7.1 Hz, 3H).

^{13}C NMR (100 MHz, $CDCl_3$): δ 163.5, 163.2, 149.1, 141.4, 141.3, 135.1, 132.4, 129.2, 128.7, 128.1, 126.3, 124.9, 123.9, 117.2, 82.5, 61.0, 57.9, 37.5, 14.3.

IR (ATR, neat): 2979, 1712, 1672, 1483, 736 cm^{-1}.

HRMS (ESI+): *m/z* calc'd for $(M + Na)^+$ $[C_{21}H_{19}NO_3 + Na]^+$: 356.1257, found 356.1254.

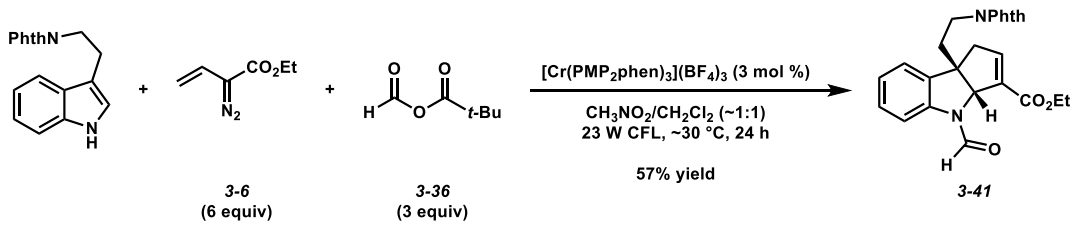

Indoline 3-41. According to General Procedure B, in a flame-dried 1-dram borosilicate vial, trimethylacetic formic anhydride (**3-36**, 41.4 mg, 0.318 mmol) was dissolved in CH_3NO_2 (0.530 mL). To this solution were added *N*-phthalimidotryptamine (30.8 mg, 0.106 mmol), $[Cr(PMP_2phen)_3](BF_4)_3$ (1.6 mg, 0.00106 mmol), and vinyl diazoacetate **3-6** (0.318 mL, 1.0 M in CH_2Cl_2, 0.318 mmol). The reaction mixture was irradiated with a 23 W CFL bulb while stirring. After 8 h, second charges of vinyl diazoacetate **3-6** (0.212 mL, 1.0 M in CH_2Cl_2, 0.212 mmol) and $[Cr(PMP_2phen)_3](BF_4)_3$ (1.6 mg, 0.00106 mmol) were added, and irradiation was continued. At the 24 h timepoint, third charges of vinyl diazoacetate **3-6** (0.106 mL, 1.0 M in CH_2Cl_2, 0.106 mmol) and $[Cr(PMP_2phen)_3](BF_4)_3$ (1.6 mg, 0.00106 mmol) were added, and irradiation was continued. At the 45 h timepoint, the solvent was removed via rotary evaporation. The crude residue was dissolved in CH_2Cl_2 (~1 mL), and the solution was passed through a SiO_2 plug (0.5 x 3 cm), using CH_2Cl_2 as eluent (~8 mL). The filtrate was concentrated in vacuo, and the residue was purified by silica gel flash chromatography (2:1 hexanes/EtOAc eluent) to afford indoline **3-41** (11.6 mg, 25% yield) as a yellow oil.

TLC: R_f = 0.31 in 2:1 hexanes/EtOAc, visualized by UV.

^{1}H NMR (400 MHz, $CDCl_3$): δ 8.94 (s, 1H), 8.03 (d, *J* = 8.0 Hz, 1H), 7.83-7.75 (comp. m, 2H), 7.72-7.64 (comp. m, 2H), 7.27 (d, *J* = 7.1 Hz, 1H), 7.22 (app. t, *J* = 8.0 Hz, 1H), 7.11 (app. t, *J* = 7.1 Hz, 1H), 6.88 (app. s, 1H), 5.45 (s, 1H), 4.30-4.17 (comp. m, 2H), 3.68-3.57 (m, 1H), 3.56-3.44 (m, 1H), 2.99 (app. d, *J* = 19.1 Hz, 1H), 2.88 (app. d, *J* = 19.1 Hz, 1H), 2.36-2.26 (m, 1H), 2.18-2.07 (m, 1H), 1.32 (t, *J* = 7.1 Hz, 3H).

^{13}C NMR (100 MHz, $CDCl_3$): δ 168.1, 163.8, 161.7, 145.7, 139.7, 136.7, 134.5, 134.2, 132.1, 128.9, 125.3, 123.4, 117.8, 72.2, 61.1, 54.1, 45.7, 37.6, 34.2, 14.3 (*1 carbon not detected*).

IR (ATR, neat): 2927, 1771, 1712, 1677, 1483, 721 cm^{-1}.

HRMS (ESI+): *m/z* calc'd for $(M + Na)^+$ $[C_{25}H_{22}N_2O_5 + Na]^+$: 453.1421, found 453.1418.

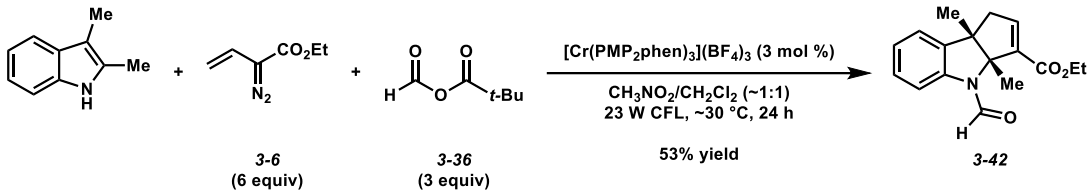

Indoline 3-42. According to General Procedure B, in a flame-dried 1-dram borosilicate vial, trimethylacetic formic anhydride (**3-36**, 78.1 mg, 0.600 mmol) was dissolved in CH_3NO_2 (1.00 mL). To this solution were added 2,3-dimethylindole (29.1 mg, 0.200 mmol), $[Cr(PMP_2phen)_3](BF_4)_3$ (3.0 mg, 0.00200 mmol), and vinyl diazoacetate **3-6** (0.600 mL, 1.0 M in CH_2Cl_2, 0.600 mmol). The reaction mixture was irradiated with a 23 W CFL bulb while stirring. After 8 h, second charges of vinyl diazoacetate **3-6** (0.400 mL, 1.0 M in CH_2Cl_2, 0.400 mmol) and $[Cr(PMP_2phen)_3](BF_4)_3$ (3.0 mg, 0.00200 mmol) were added, and irradiation was continued. At the 24 h timepoint, third charges of vinyl diazoacetate **3-6** (0.200 mL, 1.0 M in CH_2Cl_2, 0.200 mmol) and $[Cr(PMP_2phen)_3](BF_4)_3$ (3.0 mg, 0.00200 mmol) were added, and irradiation was continued. At the 28 h timepoint, the solvent was removed via rotary evaporation. The crude residue was dissolved in CH_2Cl_2 (~1 mL), and the solution was passed through a SiO_2 plug (0.5 x 3 cm), using CH_2Cl_2 as eluent (~8 mL). The filtrate was concentrated in vacuo, and the residue was purified by silica gel flash chromatography (4:1 hexanes/EtOAc eluent) to afford indoline **3-42** (40.6 mg, 71% yield) as a colorless oil.

TLC: R_f = 0.23 in 3:1 hexanes/EtOAc, visualized by UV.

^{1}H NMR (400 MHz, $CDCl_3$): δ 8.91 (s, 1H), 8.14 (d, *J* = 8.0 Hz, 1H), 7.25-7.15 (comp. m, 2H), 7.08 (t, *J* = 7.3 Hz, 1H), 6.86-6.82 (m, 1H), 4.22-4.11 (comp. m, 2H), 2.95 (app. dd, *J* = 18.5, 3.1 Hz, 1H), 2.64 (app. d, *J* = 18.5 Hz, 1H), 1.75 (s, 3H), 1.28 (s, 3H), 1.27 (t, *J* = 7.1 Hz, 3H).

^{13}C NMR (100 MHz, $CDCl_3$): δ 163.4, 161.6, 144.7, 139.6, 138.5, 137.6, 128.4, 124.6, 122.5, 117.3, 77.3, 60.7, 55.4, 43.9, 22.6, 19.0, 14.2.

IR (ATR, neat): 2978, 1709, 1669, 1414, 757 cm^{-1}.

HRMS (ESI+): *m/z* calc'd for $(M+H)^+$ $[C_{17}H_{19}NO_3 + H]^+$: 286.1438, found 286.1434.

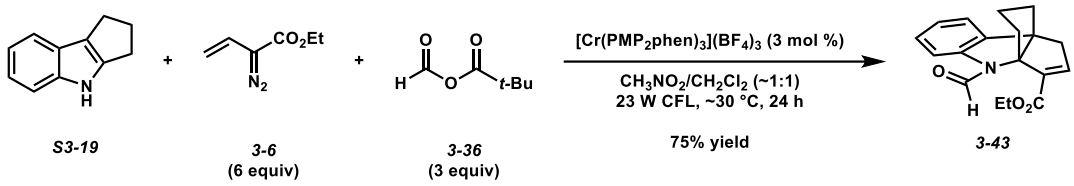

S3-19 + *3-6* (6 equiv) + *3-36* (3 equiv) → *3-43*

Indoline 3-43. According to General Procedure B, in a flame-dried 1-dram borosilicate vial, trimethylacetic formic anhydride (**3-36**, 67.1 mg, 0.516 mmol) was dissolved in CH_3NO_2 (0.860 mL). To this solution were added indole **S3-19** (27.1 mg, 0.172 mmol), $[Cr(PMP_2phen)_3](BF_4)_3$ (2.6 mg, 0.00172 mmol), and vinyl diazoacetate **3-6** (0.516 mL, 1.0 M in CH_2Cl_2, 0.516 mmol). The reaction mixture was irradiated with a 23 W CFL bulb while stirring. After 8 h, second charges of vinyl diazoacetate **3-6** (0.344 mL, 1.0 M in CH_2Cl_2, 0.344 mmol) and $[Cr(PMP_2phen)_3](BF_4)_3$ (2.6 mg, 0.00172 mmol) were added, and irradiation was continued. At the 24 h timepoint, third charges of vinyl diazoacetate **3-6** (0.172 mL, 1.0 M in CH_2Cl_2, 0.172 mmol) and $[Cr(PMP_2phen)_3](BF_4)_3$ (2.6 mg, 0.00172 mmol) were added, and irradiation was continued. At the 28 h timepoint, the solvent was removed via rotary evaporation. The crude residue was dissolved in CH_2Cl_2 (~1 mL), and the solution was passed through a SiO_2 plug (0.5 x 3 cm), using CH_2Cl_2 as eluent (~8 mL). The filtrate was concentrated in vacuo, and the residue was purified by silica gel flash chromatography (4:1 hexanes/EtOAc eluent) to afford indoline **3-43** (38.3 mg, 75% yield) as a colorless oil.

TLC: R_f = 0.37 in 3:1 hexanes/EtOAc, visualized by UV.

^{1}H NMR (400 MHz, $CDCl_3$): δ 9.12 (s, 1H), 8.17 (d, *J* = 8.0 Hz, 1H), 7.25-7.15 (comp. m, 2H), 7.10 (app. t, *J* = 7.3 Hz, 1H), 6.86 (app. t, *J* = 2.4 Hz, 1H), 4.30-4.17 (comp. m, 2H), 2.91 (dd, *J* = 19.5, 2.4 Hz, 1H), 2.79 (dd, *J* = 19.5, 2.4 Hz, 1H), 2.48-2.30 (comp. m, 2H), 2.10-1.93 (comp. m, 2H), 1.83-1.64 (comp. m, 2H), 1.31 (t, *J* = 7.1 Hz, 3H).

^{13}C NMR (100 MHz, $CDCl_3$): δ 164.0, 162.5, 146.7, 141.3, 137.5, 136.7, 128.3, 125.1, 123.3, 117.3, 87.8, 65.5, 61.0, 47.2, 41.6, 40.7, 26.7, 14.3.

IR (ATR, neat): 2957, 1709, 1671, 1240, 700 cm^{-1}.

HRMS (ESI+): *m/z* calc'd for $(M + Na)^+$ $[C_{18}H_{19}NO_3 + Na]^+$: 320.1257, found 320.1255.

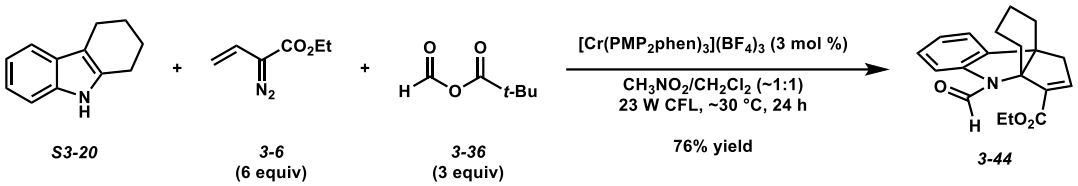

Indoline 3-44. According to General Procedure B, in a flame-dried 1-dram borosilicate vial, trimethylacetic formic anhydride (**3-36**, 70.3 mg, 0.540 mmol) was dissolved in CH_3NO_2 (0.90 mL). To this solution were added tetrahydrocarbazole **S3-20** (30.9 mg, 0.180 mmol), $[Cr(PMP_2phen)_3](BF_4)_3$ (2.7 mg, 0.00180 mmol), and vinyl diazoacetate **3-6** (0.540 mL, 1.0 M in CH_2Cl_2, 0.540 mmol). The reaction mixture was irradiated with a 23 W CFL bulb while stirring. After 8 h, second charges of vinyl diazoacetate **3-6** (0.360 mL, 1.0 M in CH_2Cl_2, 0.360 mmol) and $[Cr(PMP_2phen)_3](BF_4)_3$ (2.7 mg, 0.00180 mmol) were added, and irradiation was continued. At the 24 h timepoint, third charges of vinyl diazoacetate **3-6** (0.180 mL, 1.0 M in CH_2Cl_2, 0.180 mmol) and $[Cr(PMP_2phen)_3](BF_4)_3$ (2.7 mg, 0.00180 mmol) were added, and irradiation was continued. At the 28 h timepoint, the solvent was removed via rotary evaporation. The crude residue was dissolved in CH_2Cl_2 (~1 mL), and the solution was passed through a SiO_2 plug (0.5 x 3 cm), using CH_2Cl_2 as eluent (~8 mL). The filtrate was concentrated in vacuo, and the residue was purified by silica gel flash chromatography (4:1 hexanes/EtOAc eluent) to afford indoline **3-44** (42.9 mg, 77% yield) as a yellow oil.

TLC: R_f = 0.28 in 3:1 hexanes/EtOAc, visualized by UV.

^{1}H NMR (400 MHz, $CDCl_3$): δ 8.93 (s, 1H), 8.16 (d, *J* = 8.0 Hz, 1H), 7.23 (app. t, *J* = 8.0 Hz, 1H), 7.15 (d, *J* = 7.1 Hz, 1H), 7.08 (app. t, *J* = 7.1 Hz, 1H), 6.91 (app. s, 1H), 4.18 (q, *J* = 7.1 Hz, 2H), 2.85 (app. d, *J* = 18.7 Hz, 1H), 2.75 (app. d, *J* = 18.7 Hz, 1H), 2.59 (app. dt, *J* = 15.0, 5.0 Hz, 1H), 2.11-1.99 (m, 1H), 1.92-1.83 (m, 1H), 1.72-1.62 (m, 1H), 1.57-1.30 (comp. m, 4H), 1.28 (t, *J* = 7.1 Hz, 3H).

^{13}C NMR (100 MHz, $CDCl_3$): δ 163.7, 161.7, 145.7, 140.2, 138.5, 137.5, 128.3, 124.7, 122.4, 117.5, 60.7, 55.0, 43.0, 32.4, 29.0, 18.7, 17.7, 14.5, 14.3.

IR (ATR, neat): 2935, 1709, 1669, 1481, 1379, 753 cm^{-1}.

HRMS (ESI+): *m/z* calc'd for $(M + H)^+$ $[C_{19}H_{21}NO_3 + H]^+$: 312.1594, found 312.1591.

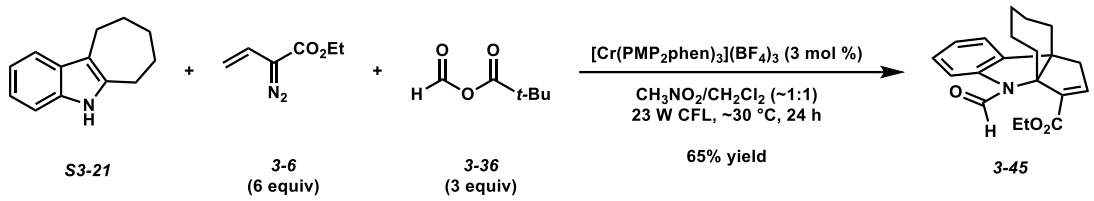

Indoline 3-45. According to General Procedure B, in a flame-dried 1-dram borosilicate vial, trimethylacetic formic anhydride (**3-36**, 54.3 mg, 0.417 mmol) was dissolved in CH_3NO_2 (0.695 mL). To this solution were added indole **S3-21** (25.7 mg, 0.139 mmol), $[Cr(PMP_2phen)_3](BF_4)_3$ (2.1 mg, 0.00139 mmol), and vinyl diazoacetate **3-6** (0.417 mL, 1.0 M in CH_2Cl_2, 0.417 mmol). The reaction mixture was irradiated with a 23 W CFL bulb while stirring. After 8 h, second charges of vinyl diazoacetate **3-6** (0.278 mL, 1.0 M in CH_2Cl_2, 0.278 mmol) and $[Cr(PMP_2phen)_3](BF_4)_3$ (2.1 mg, 0.00139 mmol) were added, and irradiation was continued. At the 24 h timepoint, third charges of vinyl diazoacetate **3-6** (0.139 mL, 1.0 M in CH_2Cl_2, 0.139 mmol) and $[Cr(PMP_2phen)_3](BF_4)_3$ (2.1 mg, 0.00139 mmol) were added, and irradiation was continued. At the 28 h timepoint, the solvent was removed via rotary evaporation. The crude residue was dissolved in CH_2Cl_2 (~1 mL), and the solution was passed through a SiO_2 plug (0.5 x 3 cm), using CH_2Cl_2 as eluent (~8 mL). The filtrate was concentrated in vacuo, and the residue was purified by silica gel flash chromatography (4:1 hexanes/EtOAc eluent) to afford indoline **3-45** (29.3 mg, 65% yield) as a white solid.

TLC: R_f = 0.40 in 3:1 hexanes/EtOAc, visualized by UV.

^{1}H NMR (400 MHz, $CDCl_3$): δ 8.97 (s, 1H), 8.26 (d, *J* = 8.0 Hz, 1H), 7.23 (app. td, *J* = 8.0, 2.0 Hz, 1H), 7.16-7.06 (comp. m, 2H), 6.92 (app. t, *J* = 2.6 Hz, 1H), 4.17 (q, *J* = 7.1 Hz, 2H), 2.82 (app. d, *J* = 2.6 Hz, 2H), 2.78-2.69 (m, 1H), 2.28-2.15 (m, 1H), 2.13 (app. dd, *J* = 9.5, 5.2 Hz, 1H) 1.86 (app. dd, *J* = 9.5, 5.2 Hz, 1H), 1.64-1.47 (comp. m, 4H), 1.46-1.35 (m, 1H), 1.26 (t, *J* = 7.1 Hz, 3H), 0.99 (app. q, *J* = 9.5 Hz, 1H).

^{13}C NMR (100 MHz, $CDCl_3$): δ 163.7, 162.6, 145.6, 140.7, 137.9, 136.9, 128.4, 124.7, 122.9, 117.2, 82.5, 60.7, 60.6, 46.9, 39.9, 32.9, 30.8, 24.6, 24.0, 14.3.

IR (ATR, neat): 2928, 1709, 1668, 1483, 756 cm^{-1}.

HRMS (ESI+): *m/z* calc'd for $(M + H)^+$ $[C_{20}H_{23}NO_3 + H]^+$: 326.1751, found 326.1745.

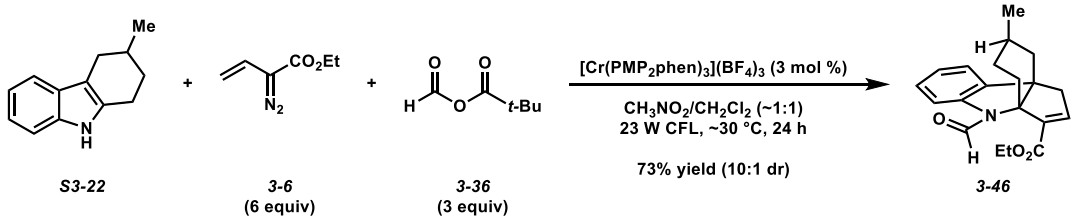

S3-22 | *3-6* (6 equiv) | *3-36* (3 equiv) | *3-46*

Indoline 3-46. According to General Procedure B, to a flame-dried 1-dram borosilicate vial, trimethylacetic formic anhydride (**3-36**, 64.0 mg, 0.492 mmol) was dissolved in CH_3NO_2 (0.82 mL). To this solution were added tetrahydrocarbazole **S3-22** (30.4 mg, 0.164 mmol), $[Cr(PMP_2phen)_3](BF_4)_3$ (2.5 mg, 0.00164 mmol), and vinyl diazoacetate **3-6** (0.492 mL, 1.0 M in CH_2Cl_2, 0.492 mmol). The reaction mixture was irradiated with a 23 W CFL bulb while stirring. After 8 h, second charges of vinyl diazoacetate **3-6** (0.328 mL, 1.0 M in CH_2Cl_2, 0.328 mmol) and $[Cr(PMP_2phen)_3](BF_4)_3$ (2.5 mg, 0.00164 mmol) were added, and irradiation was continued. At the 24 h timepoint, third charges of vinyl diazoacetate **3-6** (0.164 mL, 1.0 M in CH_2Cl_2, 0.164 mmol) and $[Cr(PMP_2phen)_3](BF_4)_3$ (2.5 mg, 0.00164 mmol) were added, and irradiation was continued. At the 28 h timepoint, the solvent was removed via rotary evaporation. The crude residue was dissolved in CH_2Cl_2 (~1 mL), and the solution was passed through a SiO_2 plug (0.5 x 3 cm), using CH_2Cl_2 as eluent (~8 mL). The filtrate was concentrated in vacuo, and the crude ^1H NMR indicated a >10:1 dr of the indoline cycloadduct. The material was purified by silica gel flash chromatography (4:1 hexanes/EtOAc eluent) to afford indoline **3-46** (38.8 mg, 73% yield, >10:1 dr) as a colorless oil. The major diastereomer was further isolated by preparatory TLC (6:1 hexanes/EtOAc eluent) for analytical characterization.

TLC: R_f = 0.33 in 3:1 hexanes/EtOAc, visualized by UV.

^{1}H NMR (400 MHz, $CDCl_3$):

Major Diastereomer: δ 8.92 (s, 1H), 8.16 (d, *J* = 8.0 Hz, 1H), 7.22 (app. t, *J* = 8.0 Hz, 1H), 7.13 (d, *J* = 7.1 Hz, 1H), 7.06 (app. t, *J* = 7.1 Hz, 1H), 6.82 (app. s, 1H), 4.22-4.11 (comp. m, 2H), 2.92-

2.72 (comp. m, 3H), 1.98 (dd, *J* = 13.8, 2.6 Hz, 1H), 1.93-1.84 (m, 1H), 1.76-1.48 (comp. m, 2H), 1.27 (t, *J* = 7.1 Hz, 3H), 1.14-0.97 (comp. m, 2H), 0.91 (d, *J* = 6.3 Hz, 3H).

Minor Diastereomer: Identified by a methyl doublet at 0.85 ppm.

^{13}C NMR (100 MHz, $CDCl_3$): δ 163.5, 161.4, 144.2, 139.7, 139.5, 138.5, 128.2, 124.6, 121.7, 117.6, 76.4, 60.7, 55.4, 42.1, 39.9, 30.2, 27.4, 27.2, 22.2, 14.2.

IR (ATR, neat): 2925, 1709, 1669, 1480, 753 cm^{-1}.

HRMS (ESI+): *m/z* calc'd for $(M + H)^+$ $[C_{20}H_{23}NO_3 + H]^+$: 326.1751, found 326.1747.

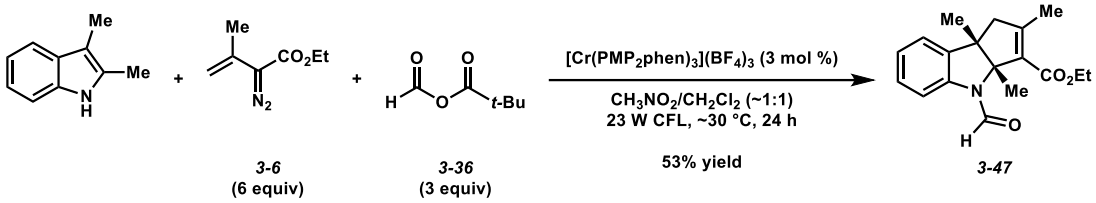

Indoline 3-47. According to General Procedure B, in a flame-dried 1-dram borosilicate vial, trimethylacetic formic anhydride (**3-36**, 53.5 mg, 0.411 mmol) was dissolved in CH_3NO_2 (0.685 mL). To this solution were added 2,3-dimethylindole (19.9 mg, 0.137 mmol), $[Cr(PMP_2phen)_3](BF_4)_3$ (2.1 mg, 0.00137 mmol), and vinyl diazoacetate **3-6** (0.411 mL, 1.0 M in CH_2Cl_2, 0.411 mmol). The reaction mixture was irradiated with a 23 W CFL bulb while stirring. After 8 h, second charges of vinyl diazoacetate **3-6** (0.274 mL, 1.0 M in CH_2Cl_2, 0.274 mmol) and $[Cr(PMP_2phen)_3](BF_4)_3$ (2.1 mg, 0.00137 mmol) were added, and irradiation was continued. At the 24 h timepoint, third charges of vinyl diazoacetate **3-6** (0.137 mL, 1.0 M in CH_2Cl_2, 0.137 mmol) and $[Cr(PMP_2phen)_3](BF_4)_3$ (2.1 mg, 0.00137 mmol) were added, and irradiation was continued. At the 28 h timepoint, the solvent was removed via rotary evaporation. The crude residue was dissolved in CH_2Cl_2 (~1 mL), and the solution was passed through a SiO_2 plug (0.5 x 3 cm), using CH_2Cl_2 as eluent (~8 mL). The filtrate was concentrated in vacuo, and the residue was purified by silica gel flash chromatography (4:1 hexanes/EtOAc eluent) to afford indoline **3-47** (21.6 mg, 53% yield) as a white solid.

TLC: R_f = 0.23 in 3:1 hexanes/EtOAc, visualized by UV.

^{1}H NMR (400 MHz, $CDCl_3$): δ 8.81 (s, 1H), 8.10 (d, *J* = 8.0 Hz, 1H), 7.22 (app. t, *J* = 8.0 Hz, 1H), 7.17 (d, *J* = 7.3 Hz, 1H), 7.07 (app. t, *J* = 7.3 Hz, 1H), 4.29-4.13 (comp. m, 2H), 2.86 (d, *J* = 17.9 Hz, 1H), 2.67 (d, *J* = 17.9 Hz, 1H), 2.03 (s, 3H), 1.74 (s, 3H), 1.31 (t, *J* = 7.1 Hz, 3H), 1.22 (s, 3H).

^{13}C NMR (100 MHz, $CDCl_3$): δ 164.6, 161.5, 156.7, 139.7, 138.9, 129.8, 128.3, 124.5, 122.4, 117.4, 79.1, 60.4, 53.2, 50.4, 22.4, 19.2, 17.5, 14.3.

IR (ATR, neat): 2977, 1701, 1669, 1597, 757 cm^{-1}.

HRMS (ESI+): *m/z* calc'd for $(M + Na)^+$ $[C_{18}H_{21}NO_3 + Na]^+$: 322.1414, found 322.1407.

3.9.6 Synthesis of $[Cr(PMP_2phen)_3](BF_4)_3$:

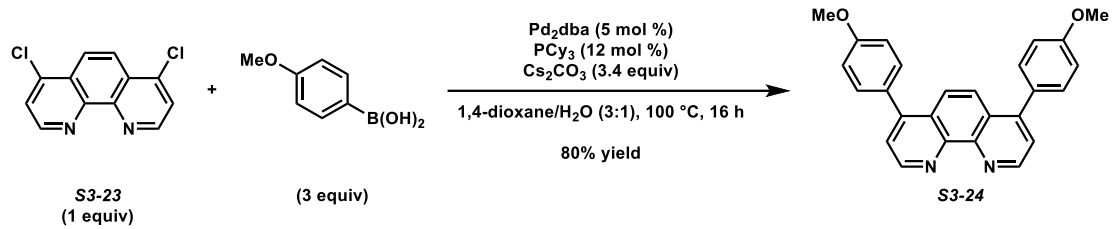

4,7-Bis(4-methoxyphenyl)-1,10-phenanthroline (**S3-24**). A flame-dried flask charged with 4,7-dichloro-1,10-phenanthroline (**S3-23**, 0.500 g, 2.01 mmol), 4-methoxyphenylboronic acid (0.916 g, 6.03 mmol), Cs_2CO_3 (2.22 g, 6.82 mmol), $Pd_2(dba)_3$ (91.9 mg, 0.100 mmol), and PCy_3 (67.5 mg, 0.241 mmol) in 3:1 1,4-dioxane/H_2O (10 mL) was degassed with argon for 15 min at 23 °C. The reaction mixture was then heated to 100 °C and stirred for 16 h. Upon completion, the reaction mixture was cooled to room temperature, diluted with $CHCl_3$, (50 mL), and poured into H_2O (25 mL). The layers were separated, and the aqueous layer was extracted with $CHCl_3$ (3 x 50 mL). The combined organic layers were washed sequentially with H_2O (200 mL), sat. aq. Na_2CO_3 (200 mL), 10% aq. NaOH (200 mL), H_2O (200 mL), and brine (200 mL), and then dried over Na_2SO_4 and concentrated in vacuo. The crude residue was triturated with hexanes (50 mL), and the solid was collected and rinsed with hexanes to afford phenanthroline **S3-24** (630 mg, 80% yield) as an off-white solid.

TLC: R_f = 0.15 in 3:1 EtOAc/hexanes.

^{1}H NMR (400 MHz, $CDCl_3$): δ 9.18 (d, *J* = 4.5 Hz, 2H), 7.88 (s, 2H), 7.54 (d, *J* = 4.5 Hz, 2H), 7.46 (d, *J* = 8.6 Hz, 4H), 7.05 (d, *J* = 8.6 Hz, 4H), 3.88 (s, 6H).

^{13}C NMR (100 MHz, $CDCl_3$): δ 160.0, 149.8, 148.2, 147.0, 131.1, 130.3, 126.6, 124.0, 123.6, 114.2, 55.5.

IR (ATR, neat): 2935, 1605, 1502, 1246, 1175, 815 cm^{-1}.

HRMS (ESI+): *m/z* calc'd for $(M + H)^+$ $[C_{26}H_{20}N_2O_2 + H]^+$: 393.1598 found 393.1600.

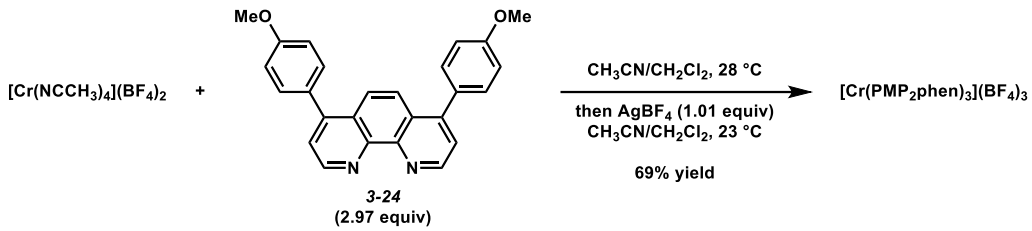

[Cr(PMP$_2$phen)$_3$](BF$_4$)$_3$: In an argon-filled glove box at 28 °C, a solution of [Cr(NCCH$_3$)$_4$](BF$_4$)$_2$ (0.218 g, 0.559 mmol) in CH$_3$CN (4.60 mL) was added to a solution of phenanthroline **S3-24** (0.650 g, 1.66 mmol) in CH$_3$CN (2.70 mL) and CH$_2$Cl$_2$ (1.85 mL). The reaction mixture was stirred for 2 h, and then AgBF$_4$ (0.110 g, 0.565 mmol) was added, resulting in a brownish-colored mixture. The reaction vessel was then sealed and removed from the glove box, and the reaction mixture was stirred in the hood under an argon atmosphere overnight at 23 °C. The mixture was then filtered over celite by vacuum filtration, washing with the minimal amount of CH$_3$CN (15 mL). Et$_2$O (300 mL) was added to the filtrate while stirring, causing an orange solid to precipitate. After 10 min stirring, the solid was collected by vacuum filtration, rinsed with Et$_2$O, and then dried under vacuum overnight, yielding the [Cr(PMP$_2$phen)$_3$](BF$_4$)$_3$ complex as an orange solid. The crude material was purified by recrystallization using vapor diffusion. In a scintillation vial, crude catalyst (~100 mg) was completely dissolved in CH$_3$CN (~5 mL). The vial was placed in a 150 mL beaker filled with Et$_2$O (30 mL). A watchglass was placed on top of the beaker, and the system was only disturbed to replenish Et$_2$O each day, maintaining approximately 30 mL in volume. After 7 d, the vial was decanted and the solid was washed with excess Et$_2$O. The solid was then collected and dried under vacuum to afford pure [Cr(PMP$_2$phen)$_3$](BF$_4$)$_3$ (0.571 g, 69% yield) as a red solid. **HRMS** (ESI+): *m/z* calc'd for (M – 3BF$_4$)$^{3+}$: [C$_{78}$H$_{60}$CrN$_6$O$_6$]$^{3+}$: 409.4654, found 409.4673.

3.9.7 Cycloaddition Product Diversification

Deprotection of Formyl Group

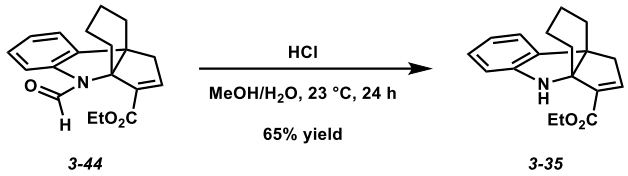

3-44 *3-35*

N-H Indoline 3-36. According to a modification of a procedure by Sheehan and Yang,[12] in a flame-dried flask under argon, indoline **3-44** (36.5 mg, 0.117 mmol) was dissolved in a 12:1 mixture of MeOH/conc. HCl (0.500 mL) at 23 °C. The reaction mixture was stirred for 24 h. The mixture was then neutralized with sat. aq. $NaHCO_3$ (2 mL) and extracted with EtOAc (3 x 10 mL). The combined organic extracts were washed with brine (20 mL), dried over $MgSO_4$, and concentrated in vacuo. The crude residue was purified by flash chromatography (4:1 hexanes/EtOAc eluent) to afford N-H indoline **3-36** (21.5 mg, 65% yield) as a yellow oil.

TLC: R_f = 0.43 in 4:1 hexanes/EtOAc, visualized by UV.

^{1}H NMR (400 MHz, $CDCl_3$): δ 7.03 (app. t, *J* = 7.4 Hz, 2H), 6.76 (app. s, 1H), 6.71 (app. t, *J* = 7.4 Hz, 1H), 6.62 (d, *J* = 7.4 Hz, 1H), 4.77 (br. s, 1H), 4.15 (q, *J* = 7.1 Hz, 2H), 2.81-2.69 (comp. m, 2H), 2.38 (app. d, *J* = 13.0 Hz, 1H), 1.92 (app. d, *J* = 13.0 Hz, 1H), 1.62-1.34 (comp. m, 6H), 1.27 (t, *J* = 7.1 Hz, 3H).

^{13}C NMR (100 MHz, $CDCl_3$): δ 164.5, 148.8, 142.6, 139.8, 138.5, 127.8, 122.4, 118.7, 109.9, 74.4, 60.3, 53.3, 41.3, 33.7, 32.6, 20.8, 19.6, 14.4.

IR (ATR, neat): 3376, 2930, 1700, 1242, 743 cm^{-1}.

HRMS (ESI+): *m/z* calc'd for $(M + H)^+$ $[C_{18}H_{21}NO_2 + H]^+$: 284.1645, found 284.1640.

Deprotection of Troc-Group

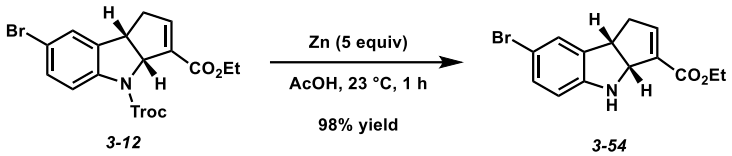

N-H Indoline 3-54. To a solution of indoline **3-12** (30.5 mg, 0.0631 mmol) in AcOH (0.631 mL) in a flame-dried vial under argon at 23 °C was added zinc dust (20.6 mg, 0.315 mmol), and the resulting mixture was stirred for 1 h. Upon completion, the reaction mixture was concentrated in vacuo. The crude residue was suspended in EtOAc (~2 mL), and the mixture was passed through a celite plug (0.5 x 2 cm), eluting with EtOAc (~10 mL). The filtrate was then washed sequentially with sat. aq. $NaHCO_3$ (20 mL), H_2O (20 mL), and brine (20 mL), and then dried over Na_2SO_4 and concentrated in vacuo. The crude residue was then purified by flash chromatography (4:1 hexanes/EtOAc eluent) to afford N-H indoline **3-54** (19.0 mg, 98% yield) as a yellow oil.

TLC R_f: 0.54 in 2:1 hexanes/Et_2O, visualized by UV, stained blue in Hanessian's stain.

^{1}H NMR (400 MHz, $CDCl_3$): δ 7.16 (s, 1H), 7.10 (d, *J* = 8.3 Hz, 1H), 6.86 (app. s, 1H), 6.46 (d, *J* = 8.3 Hz, 1H), 5.02 (d, *J* = 8.4 Hz, 1H), 4.60 (br. s, 1H), 4.22 (q, *J* = 7.1 Hz, 2H), 4.04 (app. t, *J* = 8.2 Hz, 1H), 3.05 (app. dd, *J* = 18.7, 8.2 Hz, 1H), 2.69 (app. d, *J* = 18.7 Hz, 1H), 1.30 (t, *J* = 7.1 Hz, 1H).

^{13}C NMR (100 MHz, $CDCl_3$): δ 164.7, 148.7, 144.5, 136.0, 134.6, 130.9, 127.5, 111.1, 109.9, 67.9, 60.7, 44.5, 40.1, 14.4.

IR (ATR, neat): 3391, 2926, 1704, 1478, 808 cm^{-1}.

HRMS (ESI+): *m/z* calc'd for $(M + H)^+$ $[C_{14}H_{14}BrNO_2 + H]^+$: 308.0281, found 308.0273.

Suzuki Coupling - Indole

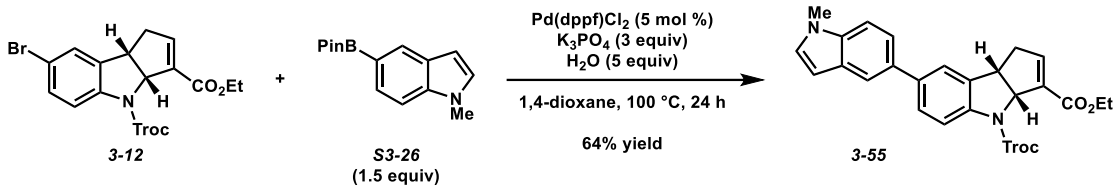

Coupling product 3-55. A vial charged with indoline **3-12** (35.6 mg, 0.0736 mmol), *N*-Me indole boronate **S3-26** (28.4 mg, 0.110 mmol), K_3PO_4 (46.9 mg, 0.221 mmol), and $Pd(dppf)Cl_2$ (2.7 mg, 0.00368 mmol) in 1,4-dioxane (0.294 mL) and H_2O (6.6 µL, 0.368 mmol) was degassed with argon for 15 min at 23 °C. The reaction mixture was then heated to 100 °C and stirred for 24 h, at which point the reaction had proceeded to completion as determined by TLC. The reaction mixture was diluted with EtOAc (2 mL) and filtered through a celite plug (0.5 x 2 cm), eluting with EtOAc (15 mL). The filtrate was washed sequentially with H_2O (3 x 10 mL) and brine (10 mL). The organic layer was dried over Na_2SO_4 and concentrated in vacuo. The crude reside was purified by flash chromatography (2:1 hexanes/EtOAc eluent) to afford coupling product **3-55** (25.1 mg, 64% yield) as a white solid.

TLC R_f: 0.46 in 2:1 hexanes/EtOAc, visualized by UV, stained blue in Hanessian's stain.

^{1}H NMR (500 MHz, 50 °C, C_6D_6): δ 8.21-8.08 (br. m, 1H), 7.89 (s, 1H), 7.55 (d, *J* = 8.4 Hz, 1H), 7.49 (dd, *J* = 8.5, 1.4 Hz, 1H), 7.32 (s, 1H), 7.11 (d, *J* = 8.5 Hz, 1H), 6.63 (d, *J* = 3.0 Hz, 1H), 6.54 (d, *J* = 3.0 Hz, 1H), 6.48 (m, 1H), 5.87 (d, *J* = 7.1 Hz, 1H), 5.35-5.05 (m, 2H), 4.76 (d, *J* = 11.9 Hz, 1H), 4.08-3.92 (comp. m, 3H), 3.51 (app. t, *J* = 5.4 Hz, 1H), 3.04 (s, 3H), 2.32-2.24 (comp. m, 2H), 1.00 (t, *J* = 7.0 Hz, 3H).

^{13}C NMR (125 MHz, 50 °C, C_6D_6): δ 163.7, 151.9, 144.5, 139.9, 139.4, 136.9, 136.1, 135.5, 133.2, 129.9, 129.4, 123.3, 121.7, 119.8, 117.5, 109.7, 101.9, 96.3, 75.9, 69.4, 60.3, 44.0, 37.7, 32.2, 14.3 (*1 carbon not detected*).

IR (ATR, neat): 2980, 2950, 1716, 1633, 1479 cm^{-1}.

HRMS (ESI+): *m/z* calc'd for $(M + H)^+$ $[C_{25}H_{21}Cl_3N_2O_4 + H]^+$: 533.0796, found 533.0802.

Suzuki Coupling - 4-methoxyphenylboronic acid

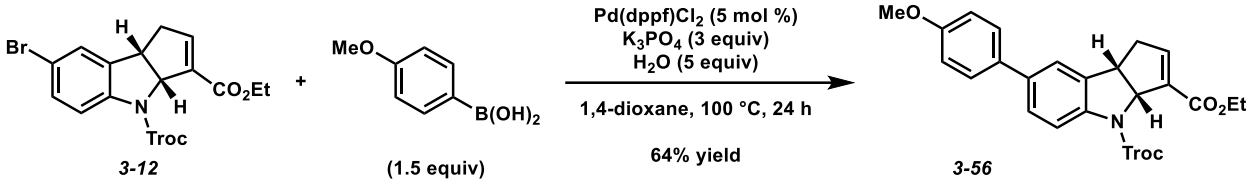

Coupling product 3-56. A vial charged with indoline **3-12** (39.1 mg, 0.0809 mmol), 4-methoxyphenylboronic acid (18.4 mg, 0.121 mmol), K_3PO_4 (51.5 mg, 0.243 mmol), and Pd(dppf)Cl_2 (3.0 mg, 0.00404 mmol) in 1,4-dioxane (0.323 mL) and H_2O (7.3 µL, 0.404 mmol) was degassed with argon for 15 min at 23 °C. The reaction mixture was then heated to 100 °C and stirred for 24 h, at which point the reaction had proceeded to completion as determined by TLC. The reaction mixture was diluted with EtOAc (2 mL) and filtered through a celite plug (0.5 x 2 cm), eluting with EtOAc (15 mL). The filtrate was washed sequentially with H_2O (3 x 10 mL) and brine (10 mL). The organic layer was dried over Na_2SO_4 and concentrated in vacuo. The crude reside was purified by flash chromatography (2:1 hexanes/Et_2O eluent) to afford coupling product **3-56** (28.1 mg, 68% yield) as a white solid.

TLC R_f: 0.38 in 1:1 hexanes/Et_2O, visualized by UV, stained blue in Hanessian's stain

^{1}H NMR (400 MHz, $CDCl_3$): δ 7.89-7.62 (br. m, 1H), 7.47 (d, *J* = 8.8 Hz, 2H), 7.43 (d, *J* = 8.4 Hz, 1H), 7.36 (s, 1H), 6.96 (d, *J* = 8.8 Hz, 2H), 6.86 (app. s, 1H), 5.93 (app. d, *J* = 6.2 Hz, 1H), 5.38-4.53 (comp. m, 2H), 4.26-4.11 (comp. m, 3H), 3.85 (s, 3H), 3.06 (app. ddt, *J* = 18.3, 7.7, 2.0 Hz, 1H), 2.85 (app. d, *J* = 18.3 Hz, 1H), 1.27 (t, *J* = 7.1 Hz, 3H).

^{13}C NMR (125 MHz, 50 °C, $CDCl_3$): δ 164.0, 159.4, 151.9, 144.8, 139.6, 137.4, 136.0, 135.3, 133.7, 128.1, 127.1, 122.6, 117.4, 114.5, 95.6, 75.8, 69.2, 60.6, 55.5, 44.0, 37.9, 14.4.

IR (ATR, neat): 2953, 1720, 1609, 1485, 1254, 822 cm^{-1}.

HRMS (ESI+): *m/z* calc'd for $(M + H)^+$ $[C_{24}H_{22}Cl_3NO_5 + H]^+$: 510.0636, found 510.0628.

Reduction

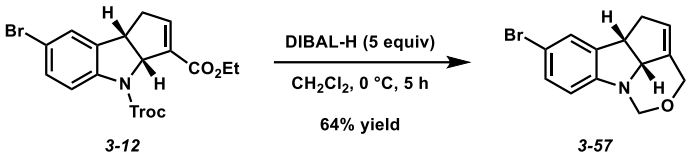

3-12 *3-57*

Alcohol 3-57. In a flame-dried flask under argon, to a solution of indoline **3-12** (30.0 mg, 0.0620 mmol) in CH_2Cl_2 (0.620 mL) at 0 °C was added DIBAL-H (0.310 mL, 1.0 M in hexanes, 0.310 mmol). The reaction mixture was stirred at 0 °C for 5 h, at which point the starting material was consumed as determined by TLC. The reaction mixture was diluted with Et_2O (15 mL) and quenched by the addition of sat. aq. Rochelle's salt (15 mL). The biphasic mixture was stirred for 1 h at room temperature. The layers were then separated, and the aqueous layer was extracted with Et_2O (3 x 10 mL). The combined organic extracts were washed with brine (15 mL), dried over Na_2SO_4, and concentrated in vacuo. The crude residue was purified by flash chromatography (4:1 hexanes/Et_2O eluent) to afford aminal **3-57** (11.0 mg, 64% yield) as a white solid.

TLC R*f*: 0.43 in 2:1 hexanes/Et_2O, visualized by UV, stained blue in Hanessian's stain.

^{1}H NMR (400 MHz, $CDCl_3$): δ 7.25 (s, 1H), 7.24 (d, *J* = 8.4 Hz, 1H), 6.59 (d, *J* = 8.4 Hz, 1H), 5.68-5.57 (m, 1H), 5.20 (d, *J* = 11.5 Hz, 1H), 4.77 (d, *J* = 11.5 Hz, 1H), 4.64 (d, *J* = 6.8 Hz, 1H), 4.46 (d, *J* = 12.2 Hz, 1H), 4.29 (d, *J* = 12.2 Hz, 1H), 3.80 (app. t, *J* = 6.8 Hz, 1H), 2.95-2.85 (m, 1H), 2.49 (app. d, *J* = 16.4 Hz, 1H).

^{13}C NMR (100 MHz, $CDCl_3$): δ 148.1, 138.0, 136.0, 131.0, 128.2, 125.2, 111.9, 111.6, 76.5, 70.4, 67.5, 43.5, 38.5.

IR (ATR, neat): 2919, 2849, 1473, 1027, 810 cm^{-1}.

HRMS (ESI+): *m/z* calc'd for $(M + H)^+$ $[C_{13}H_{12}BrNO + H]^+$: 278.0175, found 278.0172.

Allylic Oxidation

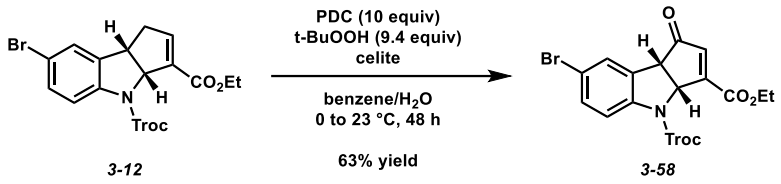

Enone 3-58. According to a modification of a procedure by Guandalini and coworkers,[13] indoline **3-12** (45.2 mg, 0.0934 mmol), celite (0.163 g, 1.75 g/mmol of **3-12**), and PDC (0.176 g, 0.467 mmol) were dissolved in benzene (1.00 mL) and cooled to 0 °C. *t*-BuOOH (60.1 µL, 70% wt. in H_2O, 0.439 mmol) was then added at 0 °C with vigorous stirring. The reaction mixture was allowed to warm to 23 °C and stir for 24 h. After 24 h, second charges of PDC (0.176 g, 0.467 mmol) and *t*-BuOOH (60.1 µL, 70% wt. in H_2O, 0.439 mmol) were added at 23 °C, and the mixture was stirred for an additional 24 h. After 48 h total, the reaction mixture was diluted with Et_2O (~ 20 mL), and the solids were removed by vacuum filtration using a Buchner funnel, rinsing with Et_2O (~ 20 mL). The filtrate was then dried over $MgSO_4$ and concentrated in vacuo. The crude residue was purified by flash chromatography (2:1 hexanes/Et_2O eluent) to afford enone **3-58** (29.3 mg, 63% yield) as a white solid.

TLC R_f: 0.47 in 1:1 hexanes/Et_2O, visualized by UV, stained blue in Hanessian's stain.

^{1}H NMR (400 MHz, $CDCl_3$): δ 7.60 (br. s, 1H), 7.58 (s, 1H), 7.42 (dd, *J* = 8.7, 1.4 Hz, 1H), 6.68 (d, *J* = 1.0 Hz, 1H), 5.97 (dd, *J* = 6.7, 1.0 Hz, 1H), 5.33-4.49 (br. m, 2H), 4.32 (q, *J* = 7.1 Hz, 2H), 4.24 (d, *J* = 6.7 Hz, 1H), 1.34 (t, *J* = 7.1 Hz, 3H).

^{13}C NMR (125 MHz, 50 °C, $CDCl_3$): δ 201.6, 163.6, 160.5, 151.6, 139.6, 137.2, 132.7, 128.7, 128.1, 118.8, 117.5, 95.0, 76.0, 63.5, 62.3, 52.2, 14.2.

IR (ATR, neat): 2982, 1725, 1613, 1477, 1250, 820 cm^{-1}.

HRMS (ESI+): *m/z* calc'd for $(M + H)^+$ $[C_{17}H_{13}BrCl_3NO_5 + H]^+$: 495.9115, found 495.9106.

Dihydroxylation

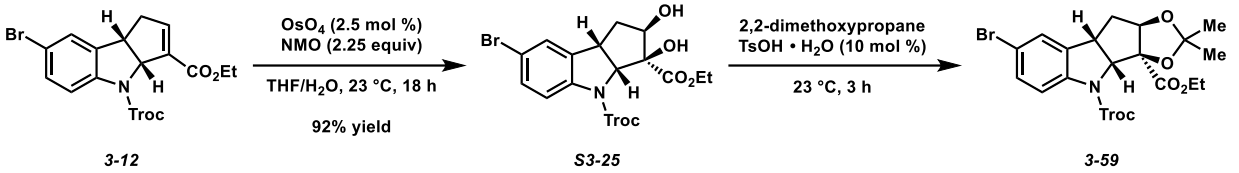

Acetal 3-59. In a flask under argon, to a solution of indoline **3-12** (40.1 mg, 0.0829 mmol) in THF (0.332 mL) at room temperature was added aq. NMO (38.8 µL, 50% w/w, 0.187 mmol) and OsO_4 (0.5 mg, 0.00207 mmol) sequentially. After 18 h, sat. aq. $NaHSO_3$ (~2 mL) was added, and the reaction mixture was stirred for 1 h. The THF was removed by rotary evaporation, and the resulting aqueous mixture was then extracted with EtOAc (5 x 10 mL). The combined organic extracts were washed sequentially with H_2O (20 mL) and brine (20 mL), and then dried over $MgSO_4$ and concentrated in vacuo. The crude residue was purified by flash chromatography (2:1 hexanes/EtOAc eluent) to afford diol **S3-25** (39.5 mg, 92% yield, 3.1:1 dr) as a colorless oil. Diol **S3-25** (39.5 mg, 0.0763 mmol) was immediately dissolved in 2,2-dimethoxypropane (0.305 mL) at room temperature open to air. *p*-TsOH·H_2O (1.4 mg, 0.00763 mmol) was then added, and the mixture was stirred until full consumption of starting material, as determined by TLC. After 3 h, the reaction mixture was concentrated in vacuo, and the crude residue was dissolved in EtOAc (20 mL). The organic layer was washed sequentially with 1 M aq. HCl (20 mL), sat. aq. $NaHCO_3$ (20 mL), and brine (20 mL), and then dried over Na_2SO_4 and concentrated in vacuo. The crude reside was purified by flash chromatography (9:1 hexanes/EtOAc eluent) to afford acetal **3-59** (40.9 mg, 96% yield) as a colorless oil, as a still inseparable 3.1:1 dr mixture.

TLC R_f (diol): 0.13 in 1:1 hexanes/Et_2O, visualized by UV, stained blue in Hanessian's stain.

TLC R_f (acetal): 0.52 in 2:1 hexanes/Et_2O, visualized by UV, stained blue in Hanessian's stain.

^{1}H NMR (400 MHz, $CDCl_3$):

Major diastereomer: δ 7.73 (d, *J* = 8.5 Hz, 1H), 7.33 (app. d, *J* = 8.5 Hz, 1H), 7.29 (app. s, 1H), 5.31 (d, *J* = 12.0 Hz, 1H), 5.15 (d, *J* = 9.0 Hz, 1H), 4.66 (d, *J* = 4.5 Hz, 1H), 4.38 (d, *J* = 12.0 Hz, 1H), 4.26 (dq, *J* = 10.2, 6.9 Hz, 2H), 4.10 (app. t, *J* = 8.5 Hz, 1H), 2.54 (app. d, *J* = 15.0 Hz, 1H), 2.46-2.33 (comp. m, 1H), 1.32 (t, *J* = 6.9 Hz, 1H), 1.27 (s, 3H), 0.77 (s, 3H).

Minor diastereomer: δ 7.53 (d, *J* = 8.5 Hz, 1H), 7.33 (app. d, *J* = 8.5 Hz, 1H), 7.29 (app. s, 1H), 5.09 (d, *J* = 9.2 Hz, 1H), 5.04 (d, *J* = 11.9 Hz, 1H), 4.86 (d, *J* = 11.9 Hz, 1H), 4.68 (t, *J* = 4.2 Hz, 1H), 4.28 (dq, *J* = 10.2, 7.2 Hz, 2H), 4.06 (app. t, *J* = 8.6 Hz, 1H), 2.54 (app. d, *J* = 15.0 Hz, 1H), 2.46-2.33 (comp. m, 1H), 1.35 (t, *J* = 7.2 Hz, 3H), 1.29 (s, 3H), 0.79 (s, 3H).

^{13}C NMR (125 MHz, 50 °C, $CDCl_3$): 173.0, 172.7, 151.8, 150.9, 141.3, 140.2, 137.3, 136.9, 136.3, 130.9, 130.7, 127.3, 126.9, 116.5, 116.3, 116.3, 116.2, 113.7, 113.6, 95.5, 95.0, 90.2, 90.0, 86.3, 86.3, 76.1, 74.7, 70.2, 69.6, 62.1, 61.9, 46.0, 45.3, 34.3, 34.1, 25.5, 25.5, 24.0 (2), 14.4, 13.9.

IR (ATR, neat): 2987, 1757, 1724, 1479, 824 cm^{-1}.

HRMS (ESI+): *m/z* calc'd for $(M + H)^+$ $[C_{20}H_{21}BrCl_3NO_6 + H]^+$: 555.9691, found 555.9682.

The relative stereochemistry of acetal **3-59** was confirmed by a reduction of the ester to the primary alcohol and subjected to 2D NOESY NMR analysis.

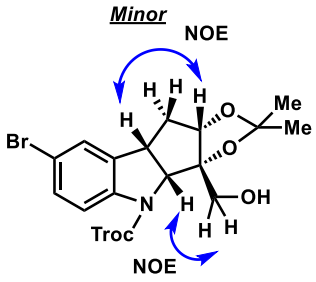

Conjugate Reduction

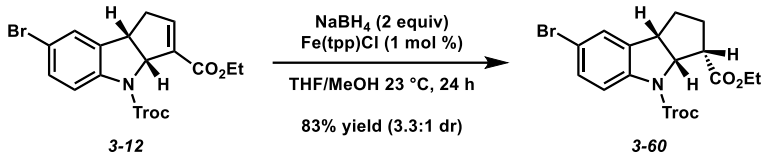

Saturated ester 3-60. According to a modification of a procedure by Sakaki and coworkers,[14] in an argon-filled glove box a 2-dram vial was charged with Fe(tpp)Cl (0.4 mg, 0.631 μmol). The vial was removed from the glovebox and equipped to a Schlenk line under argon. The Fe complex was then dissolved in THF (0.315 mL) and MeOH (0.315 mL, distilled over MS3Å) at 23 °C. In a separate flame-dried vial, indoline **3-12** (30.5 mg, 0.0631 mmol) and $NaBH_4$ (4.8 mg, 0.126 mmol) were suspended in THF (0.315 mL) at 23 °C. The solution of the Fe(tpp)Cl complex was then added dropwise to the indoline mixture over 15 min, and the resulting mixture was stirred at room temperature. After 24 h, the reaction mixture was quenched by the addition of sat. aq. NH_4Cl (10 mL), and the mixture was extracted with EtOAc (3 x 10 mL). The combined organic extracts were washed sequentially with H_2O (20 mL) and brine (20 mL), and then dried over Na_2SO_4 and concentrated in vacuo. The crude residue was purified by flash chromatography (9:1 hexane/Et_2O eluent) to afford saturated ester **3-60** (25.4 mg, 83% yield, 3.3:1 dr) as a colorless oil.

TLC R_f: 0.65 in 2:1 hexanes/Et_2O, visualized by UV, stained blue in Hanessian's stain.

^{1}H NMR (400 MHz, $CDCl_3$):

Major diastereomer: δ 7.70 (d, *J* = 8.6 Hz, 1H), 7.34 (app. d, *J* = 8.6 Hz, 1H), 7.28 (app. s, 1H), 5.23 (app. d, *J* = 8.6 Hz, 1H), 4.93 (d, *J* = 11.8 Hz, 1H), 4.75 (d, *J* = 11.8 Hz, 1H), 4.14 (app. q, *J* = 7.1 Hz, 2H), 4.01 (app. t, *J* = 7.9 Hz, 1H), 3.19 (app. d, *J* = 7.9 Hz, 1H), 2.20-2.07 (m, 1H), 2.03-1.86 (comp. m, 2H), 1.85-1.69 (comp. m, 1H), 1.27 (app. t, *J* = 7.1 Hz, 3H).

Minor diastereomer: δ 7.53 (d, *J* = 8.5 Hz, 1H), 7.34 (app. d, *J* = 8.5 Hz, 1H), 7.28 (app. s, 1H), 5.15-5.07 (m, 1H), 4.97-4.86 (comp. m, 2H), 4.20 (app. q, *J* = 7.2 Hz, 2H), 3.96-3.84 (m, 1H),

3.04-2.95 (m, 1H), 2.35-2.24 (br. m, 1H), 2.03-1.86 (comp. m, 2H), 1.85-1.69 (comp. m, 1H), 1.27 (app. t, *J* = 7.1 Hz, 3H).

^{13}C NMR (125 MHz, 50 °C, $CDCl_3$): δ 173.8, 150.7, 136.6, 131.0, 127.6, 116.5, 116.3, 95.2, 75.0, 67.0, 61.0, 52.4, 45.6, 32.8, 28.8, 14.4 (*1 carbon not detected*).

(*The minor diastereomer was not observed in the ^{13}C NMR.*)

IR (ATR, neat): 2956, 1723, 1479, 1396, 1136 cm^{-1}.

HRMS (ESI+): *m/z* calc'd for $(M + H)^+$ $[C_{17}H_{17}BrCl_3NO_4 + H]^+$: 483.9479, found 483.9472.

The relative stereochemistry of the major diastereomer of saturated ester **3-60** was confirmed through 2D NOESY NMR analysis.

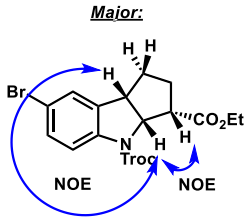

(3+2) Cycloaddition Reaction

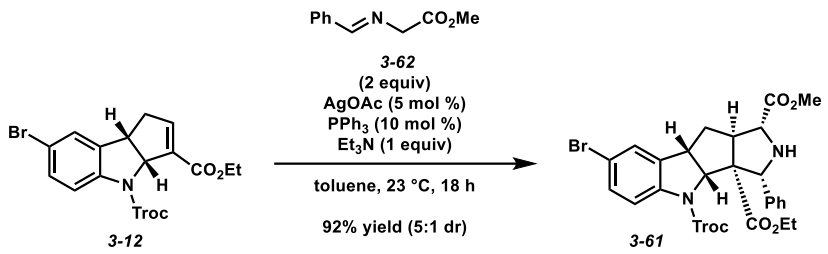

Cycloadduct 3-61. According to a modification of a procedure by Mancebo-Anacil and coworkers,[15] to a flame-dried flask wrapped in aluminum foil under argon, AgOAc (0.6 mg, 0.00367 mmol) and PPh_3 (1.9 mg, 0.00734 mmol) were suspended in toluene (0.734 mL) at 23 °C, and the suspension was stirred for 15 min. A solution of indoline **3-12** (35.5 mg, 0.0734 mmol) and imine **3-62** (26.0 mg, 0.147 mmol) in toluene (0.734 mL) at room temperature was then added dropwise to the stirring mixture of AgOAc/PPh_3 at room temperature over 10 min. Et_3N (10.2 µL, 0.0734 mmol) was then added to the reaction mixture, and the resulting mixture was stirred to reaction completion, as determined by TLC. The reaction mixture was diluted with EtOAc (2 mL) and filtered through a celite plug (0.5 x 2 cm, eluting with 10 mL EtOAc), and the filtrate was concentrated in vacuo. The crude residue was purified by flash chromatography (4:1 hexane/Et_2O eluent) to afford cycloadduct **3-61** (44.6 mg, 92% yield, 5:1 dr) as a colorless oil.

TLC R_f: 0.35 in 1:1 hexanes/Et_2O, visualized by UV, stained blue in Hanessian's stain.

^{1}H NMR (400 MHz, $CDCl_3$): δ 7.77-7.51 (br. m, 1H), 7.39 (s, 1H), 7.36 (d, *J* = 5.7 Hz, 1H), 7.30-7.20 (comp. m, 5H), 5.75 (d, *J* = 9.1 Hz, 1H), 5.33-4.63 (br. m, 2H), 4.39 (br. s, 1H), 4.17-4.07 (br. m, 1H), 3.75 (s, 3H), 3.75-3.56 (br. m, 2H), 3.44-3.32 (br. m, 1H), 2.96 (br. d, *J* = 8.8 Hz, 1H), 2.61 (br. s, 1H), 2.45-2.28 (br. m, 2H), 0.81 (t, *J* = 7.1 Hz, 3H).

^{13}C NMR (125 MHz, 50 °C, $CDCl_3$): δ 173.2, 172.7, 152.4, 140.8, 140.7, 138.4, 131.5, 128.2, 127.9, 127.6, 127.2, 118.8, 117.7, 95.2, 75.7, 72.7, 70.7, 66.8, 64.4, 61.4, 55.9, 52.3, 47.1, 32.9, 13.6.

IR (ATR, neat): 3356, 2953, 1727, 1477, 754 cm^{-1}.

HRMS (ESI+): *m/z* calc'd for $(M + H)^+$ $[C_{27}H_{26}BrCl_3N_2O_6 + H]^+$: 659.0113, found 659.0092.

The relative stereochemistry of cycloadduct **3-61** was confirmed through 2D NOESY NMR analysis of the TFA-protected amine.

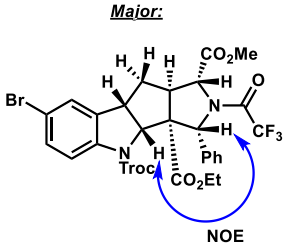

3.9.8 Characterization of Pyrazoles:

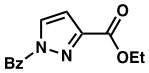

TLC R_f: 0.41 in 1:1 hexanes/Et_2O, visualized by UV, stained blue in Hanessian's stain.

^{1}H NMR (400 MHz, $CDCl_3$): δ 8.45 (d, *J* = 2.8 Hz, 1H), 8.19 (d, *J* = 8.6 Hz, 2H), 7.64 (t, *J* = 7.4 Hz, 1H), 7.52 (app. t, *J* = 7.9 Hz, 2H), 6.99 (d, *J* = 2.8 Hz, 1H), 4.42 (q, *J* = 7.1 Hz, 2H), 1.40 (t, *J* = 7.1 Hz, 3H).

^{13}C NMR (100 MHz, $CDCl_3$): δ 166.2, 161.7, 148.2, 133.9, 132.2, 131.9, 130.4, 128.5, 110.8, 61.8, 14.4.

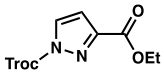

TLC R_f: 0.56 in 1:1 hexanes/Et_2O, visualized by UV, stained blue in Hanessian's stain.

^{1}H NMR (400 MHz, $CDCl_3$): δ 8.22 (d, *J* = 2.9 Hz, 1H), 6.96 (d, *J* = 2.9 Hz, 1H), 5.09 (s, 2H), 4.43 (q, *J* = 7.2 Hz, 2H), 1.40 (t, *J* = 7.2 Hz, 3H).

^{13}C NMR (100 MHz, $CDCl_3$): δ 161.3, 149.4, 147.5, 132.7, 111.5, 93.7, 76.6, 62.0, 14.4.

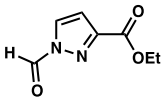

TLC R_f: 0.32 in 1:1 hexanes/Et_2O, visualized by UV, stained blue in Hanessian's stain.

^{1}H NMR (400 MHz, $CDCl_3$): δ 9.26 (s, 1H), 8.23 (d, *J* = 2.8 Hz, 1H), 7.01 (dd, *J* = 2.8, 1.1 Hz, 1H), 4.47 (q, *J* = 7.1 Hz, 2H), 1.43 (t, *J* = 7.1 Hz, 3H).

^{13}C NMR (100 MHz, $CDCl_3$): δ 161.2, 160.2, 149.4, 128.3, 112.2, 62.1, 14.4.

3.9.10 Mechanistic Experiments

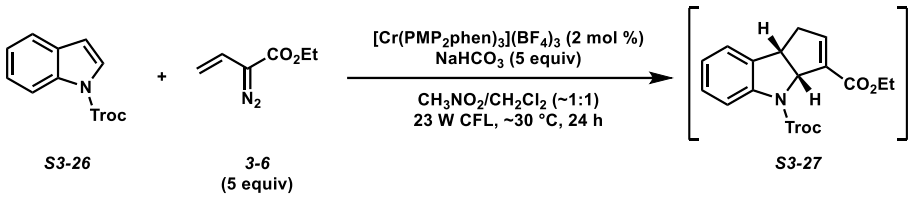

S3-26 *3-6* (5 equiv) *S3-27*

According to a modified General Procedure A, indole **S3-26** (30.0 mg, 0.103 mmol), $NaHCO_3$ (43.1 mg, 0.515 mmol), and $[Cr(PMP_2phen)_3](BF_4)_3$ (1.5 mg, 0.00103 mmol) were added to a flame-dried 1-dram borosilicate vial. The reagents were suspended in CH_3NO_2 (0.515 mL), and to this solution was added vinyl diazoacetate **3-6** (0.309 mL, 1.0 M in CH_2Cl_2, 0.309 mmol). The reaction mixture was irradiated with a 23 W CFL bulb while stirring. After 8 h, second charges of vinyl diazoacetate **3-6** (0.206 mL, 1.0 M in CH_2Cl_2, 0.206 mmol) and $[Cr(PMP_2phen)_3](BF_4)_3$ (1.5 mg, 0.00103 mmol) were added, and irradiation was continued. At the 24 h timepoint, the solvent was removed via rotary evaporation. The crude residue was dissolved in CH_2Cl_2 (~1 mL), and the solution was passed through a SiO_2 plug (0.5 x 3 cm), using CH_2Cl_2 as eluent (~8 mL). The filtrate was concentrated in vacuo, and the residue was analyzed by ^1H NMR using CH_2Br_2 as an internal standard, where there was a >95% recovery of indole **S3-26** and no formation of indoline **S3-27**.

Competition Experiments

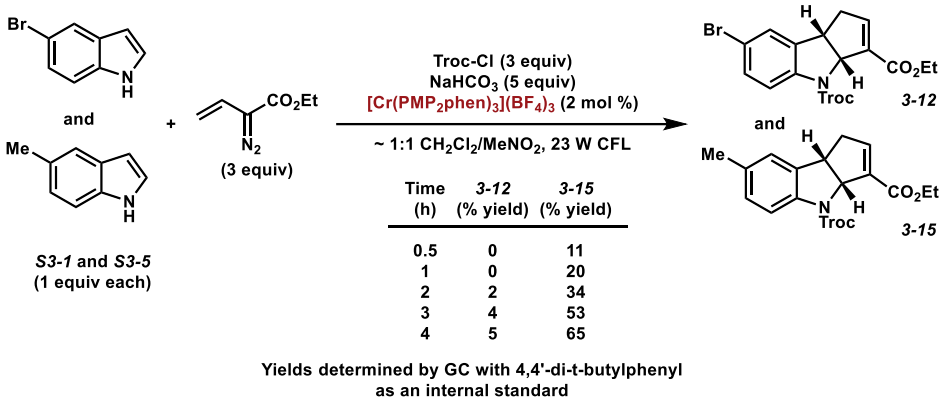

Procedure: According to General Procedure A, 5-methylindole (13.4 mg, 0.102 mmol), 5-bromoindole (20.0 mg, 0.102 mmol), $NaHCO_3$ (42.0 mg, 0.500 mmol), 4,4'-di-*tert*-butylbiphenyl (27.2 mg, 0.102 mmol) and $[Cr(PMP_2phen)_3](BF_4)_3$ (1.5 mg, 0.00102 mmol) were added to a flame-dried 1-dram borosilicate vial. The reagents were suspended in CH_3NO_2 (0.510 mL), and to this suspension were added 2,2,2-trichloroethoxycarbonyl chloride (42.1 µL, 0.306 mmol) and vinyl diazoacetate **3-6** (0.306 mL, 1.00 M in CH_2Cl_2, 0.306 mmol). The reaction mixture was irradiated with a 23 W CFL bulb while stirring. Aliquots of 25 µL were taken at various timepoints. Aliquots were dissolved in EtOAc (0.2 mL) and passed through a silica plug (0.5 x 0.5 cm), using EtOAc as eluent (2 mL). The aliquots were then directly analyzed via GC assay.

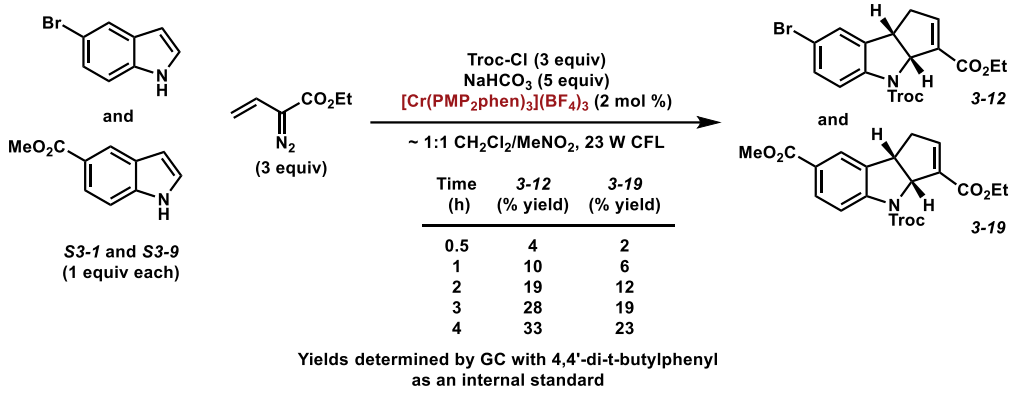

Procedure: According to General Procedure A, 5-bromoindole (20.0 mg, 0.102 mmol), 5-(CO_2Me)-indole (17.9 mg, 0.102 mmol), $NaHCO_3$ (42.0 mg, 0.500 mmol), 4,4'-di-*tert*-butylbiphenyl (27.2 mg, 0.102 mmol) and $[Cr(PMP_2phen)_3](BF_4)_3$ (1.5 mg, 0.00102 mmol) were added to a flame-dried 1-dram borosilicate vial. The reagents were suspended in CH_3NO_2 (0.510 mL), and to this suspension were added 2,2,2-trichloroethoxycarbonyl chloride (42.1 µL, 0.306 mmol) and vinyl diazoacetate **3-6** (0.306 mL, 1.00 M in CH_2Cl_2, 0.306 mmol). The reaction mixture was irradiated with a 23 W CFL bulb while stirring. Aliquots of 25 µL were taken at various timepoints. Aliquots were dissolved in EtOAc (0.2 mL) and passed through a silica plug (0.5 x 0.5 cm), using EtOAc as eluent (2 mL). The aliquots were then directly analyzed via GC assay.

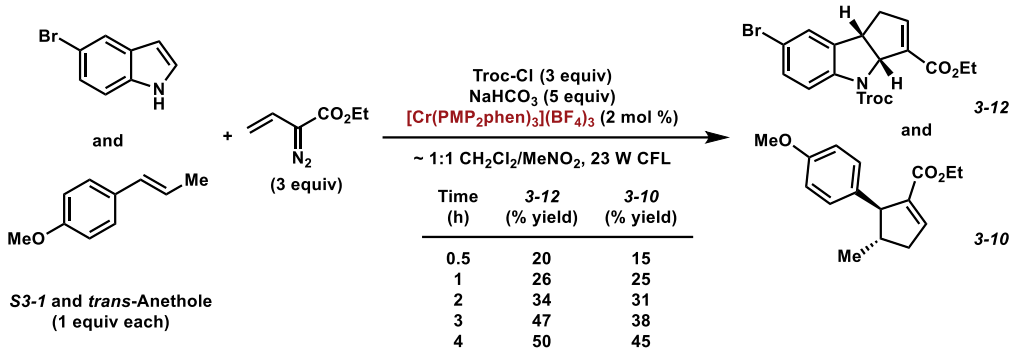

Time (h)	*3-12* (% yield)	*3-10* (% yield)
0.5	20	15
1	26	25
2	34	31
3	47	38
4	50	45

Yields determined by GC with 4,4'-di-t-butylphenyl as an internal standard

Procedure: According to General Procedure A, 5-bromoindole (30.0 mg, 0.153 mmol), $NaHCO_3$ (64.3 mg, 0.765 mmol), and $[Cr(PMP_2phen)_3](BF_4)_3$ (2.3 mg, 0.00153 mmol) were added to a flame-dried 1-dram borosilicate vial. The reagents were suspended in CH_3NO_2 (0.765 mL), and to this suspension were added *trans*-anethole (22.9 µL, 0.153 mmol), dodecyl acetate (40.4 µL, 0.153 mmol), 2,2,2-trichloroethoxycarbonyl chloride (63.2 µL, 0.459 mmol), and vinyl diazoacetate **3-6** (0.459 mL, 1.00 M in CH_2Cl_2, 0.459 mmol). The reaction mixture was irradiated with a 23 W CFL bulb while stirring. Aliquots of 50 µL were taken at various timepoints. Aliquots were dissolved in EtOAc (0.5 mL) and passed through a silica plug (0.5 x 0.5 cm), using EtOAc

as eluent (4 mL). The volatile materials were evaporated, and the crude residue was analyzed by ^{1}H NMR.

3.9.11 Cyclic Voltammetry of Corresponding Indoles:

Figure S3.4. Cyclic Volammogram of indole **S3-1** (5 mM) recorded at ambient temperature in CH_3CN containing 0.25 M Bu_4NPF_6, galssy carbon working electrode measured at a scan rate of 100 mV/s and referenced to Fc/Fc^+. The arrow displays the scan direction.

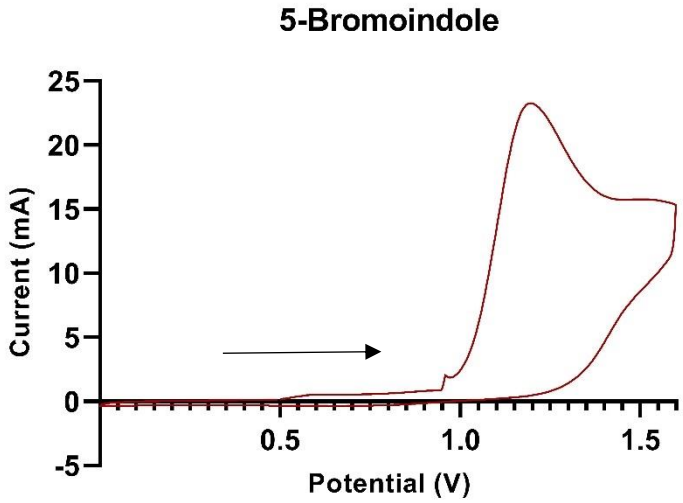

Figure S3.5. Cyclic Volammogram of indole **S3-5** (5 mM) recorded at ambient temperature in CH_3CN containing 0.25 M Bu_4NPF_6, galssy carbon working electrode measured at a scan rate of 100 mV/s and referenced to Fc/Fc^+. The arrow displays the scan direction.

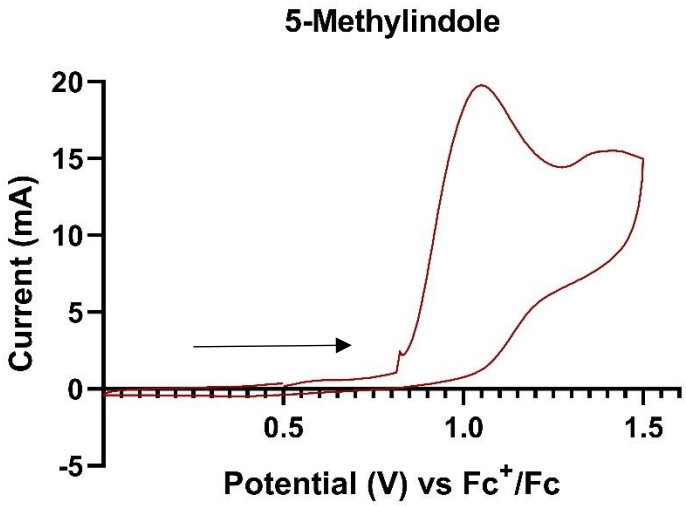

Figure S3.6. Cyclic Volammogram of indole **S3-9** (5 mM) recorded at ambient temperature in CH_3CN containing 0.25 M Bu_4NPF_6, galssy carbon working electrode measured at a scan rate of 100 mV/s and referenced to Fc/Fc^+. The arrow displays the scan direction.

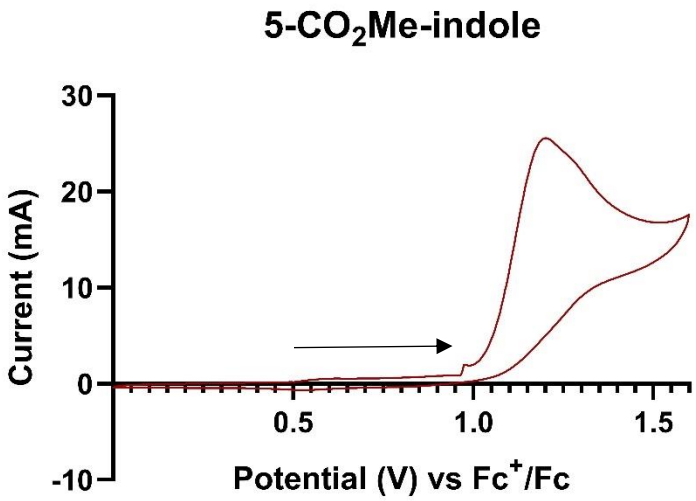

3.9.12 Intramolecular Cycloadditions

Substrate synthesis:

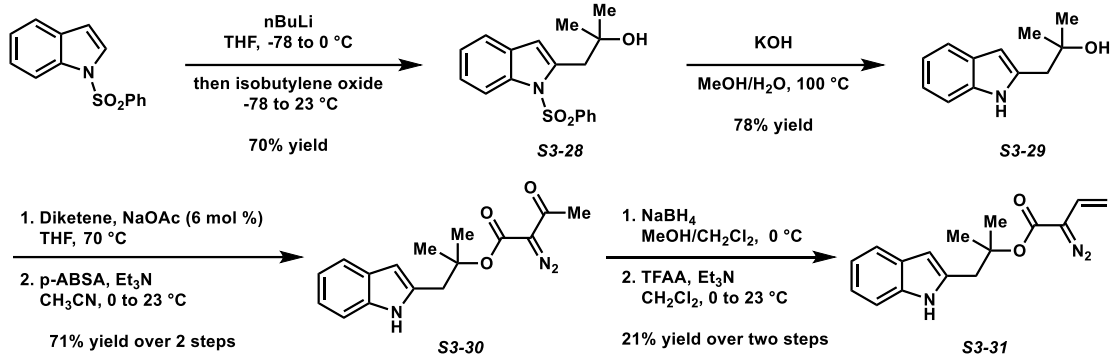

Alcohol S3-28. According to a modification of a reported procedure by Chikkade and coworkers,[18] to a solution of 1-phenylsulfonylindole (1.80 g, 6.99 mmol) in THF (27.9 mL, 0.250 M) cooled to -78 ºC was added *n*-butyllithium (3.36 mL, 2.5 M in hexanes, 8.39 mmol) dropwise over 10 min. The solution was stirred for 1.5 h at -78 ºC, and then was warmed to 0 ºC and stirred for 1 h. The solution was cooled back to -78 ºC, and isobutylene oxide (0.745 mL, 8.39 mmol) was added dropwise. The reaction mixture was warmed to room temperature and stirred overnight. After 16 h, the reaction mixture was quenched by the addition of sat. aq. NH_4Cl (10 mL). THF was removed by rotary evaporation, and the mixture was extracted with EtOAc (3 x 30 mL). The combined organic layers were washed sequentially with H_2O (10 mL) and brine (10 mL), and then dried over Na_2SO_4 and concentrated in vacuo. The crude residue was purified by silica gel flash chromatography (4:1 → 2:1 hexanes/EtOAc eluent) to afford the indolyl alcohol (**S3-28**, 1.60 g, 70% yield) as an orange oil (TLC: R_f = 0.16 in 4:1 hexanes/EtOAc).

A solution of sulfonylindole **S3-28** (6.79 g, 20.6 mmol) and KOH (5.78 g, 103 mmol) in MeOH/H_2O (3:1, 103 mL, 0.2 M) was refluxed for 8 h. The reaction mixture was cooled to 23 ºC and quenched by the addition of sat. aq. NH_4Cl (30 mL). The mixture was extracted with EtOAc (3 x 50 mL). The combined organic layers were washed sequentially with H_2O (30 mL) and brine

(30 mL), and then dried over Na_2SO_4 and concentrated in vacuo. The crude residue was purified via silica gel flash chromatography (3:1 hexanes/EtOAc eluent) to afford deprotected indole **S3-29** (3.04 g, 78% yield) as a pale yellow solid.

TLC: R_f = 0.35 in 2:1 hexanes/EtOAc, visualized by UV.

^{1}H NMR (400 MHz, $CDCl_3$): δ 8.63 (br. s, 1H), 7.55 (d, *J* = 7.9 Hz, 1H), 7.33 (d, *J* = 7.2 Hz, 1H), 7.13 (app. t, *J* = 7.2 Hz, 1H), 7.07 (app. t, *J* = 7.9 Hz, 1H), 6.26 (s, 1H), 2.91 (s, 2H), 1.29 (s, 6H).

Diazo S3-30. Following a procedure reported by Doyle and coworkers,[19] a solution of indole **S3-29** (3.04 g, 16.1 mmol) and NaOAc (79.0 mg, 0.963 mmol) in THF (4.60 mL) was heated to reflux. A solution of diketene (1.49 mL, 19.3 mmol) in THF (2.14 mL) was then added dropwise to the reaction mixture over 30 min. The reaction mixture was refluxed for 4 h, and then cooled to room temperature. The reaction mixture was then partitioned between Et_2O (25 mL) and brine (25 mL). The aqueous layer was extracted with Et_2O (3 x 25 mL), and the organic layers were combined, dried over $MgSO_4$, and concentrated in vacuo. The crude ketoester was taken forward without further purification (TLC: R_f = 0.41 in 4:1 hexanes/EtOAc).

To a stirring solution of the ketoester (assume 16.1 mmol) in acetonitrile (13.4 mL) at 0 ºC was added Et_3N (2.92 mL, 20.9 mmol) dropwise. A solution of *p*-ABSA (5.03 g, 20.9 mmol) in acetonitrile (10.7 mL) was then added dropwise to the reaction mixture over 30 min. The resulting mixture was then warmed to room temperature and stirred for 3 h. The reaction mixture was then filtered through a Buchner funnel to remove the *p*-ABSA byproducts, and the filtrate was concentrated in vacuo. The crude residue was purified via silica gel flash chromatography (4:1 hexanes/EtOAc eluent) to afford α-diazo ketoester **S3-30** (3.42 g, 71% yield over 2 steps) as a yellow oil.

TLC: R_f = 0.45 in 4:1 hexanes/EtOAc, visualized by UV.

^{1}H NMR (400 MHz, $CDCl_3$): δ 8.62 (br. s, 1H), 7.55 (d, *J* = 7.7 Hz, 1H), 7.34 (d, *J* = 7.3 Hz, 1H), 7.14 (app. t, *J* = 7.3 Hz, 1H), 7.07 (app. t, *J* = 7.7 Hz, 1H), 6.29 (s, 1H), 3.21 (s, 2H), 2.45 (s, 3H), 1.61 (s, 6H).

Diazoester 3-31. To a solution of α-diazo ketoester **S3-30** (300 mg, 1.00 mmol) in MeOH/CH_2Cl_2 (1:1, 4.0 mL) at 0 ºC was added $NaBH_4$ (45.4 mg, 1.20 mmol) portionwise. After addition, the reaction mixture was warmed to room temperature and stirred for 3 h, monitoring progress by TLC. The reaction mixture was then diluted with H_2O (10 mL) and extracted with EtOAc (3 x 10 mL). The combined organic layers were washed with brine (10 mL), dried over $MgSO_4$, and concentrated in vacuo. The crude alcohol product was taken forward without further purification (TLC: R_f = 0.20 in 3:1 hexanes/EtOAc).

According to a modification of a procedure by Rianelli and coworkers,[20] to a solution of the crude alcohol (assume 1.00 mmol) in CH_2Cl_2 (8.33 mL) at 0 °C was added triethylamine (0.697 mL, 5.00 mmol) and trifluoroacetic anhydride (0.153 mL, 1.10 mmol) sequentially. The reaction mixture was warmed to room temperature and stirred for 2 h. The reaction mixture was then concentrated in vacuo, and the crude residue was purified via silica gel flash chromatography (6:1 hexanes/Et_2O eluent) to afford vinyl diazoester **3-31** (59.2 mg, 21% yield over 2 steps) as an orange oil.

TLC: R_f = 0.55 in 4:1 hexanes/EtOAc, visualized by UV.

^{1}H NMR (400 MHz, $CDCl_3$): δ 7.98 (br. s, 1H), 7.56 (d, *J* = 7.7 Hz, 1H), 7.33 (d, *J* = 7.8 Hz, 1H), 7.15 (app. t, *J* = 7.7 Hz, 1H), 7.09 (app. t, *J* = 7.8 Hz, 1H), 6.33-6.28 (m, 1H), 6.14 (dd, *J* = 10.9, 17.4 Hz, 1H), 5.13 (d, *J* = 10.9 Hz, 1H), 4.86 (d, *J* = 17.4 Hz, 1H), 3.26 (s, 2H), 1.58 (s, 6H).

^{13}C NMR (100 MHz, $CDCl_3$): δ 136.0, 134.3, 128.6, 121.5, 120.5, 120.1, 119.8, 110.7, 107.8, 102.8, 83.7, 40.4, 26.6 (*2 carbons not detected: carbonyl and diazo*).

IR (ATR, neat): 3399, 2924, 2854, 2087, 1785, 1406, 1168, 740 cm^{-1}.

HRMS (ESI+): *m/z* calc'd for $(M + Na)^+$ $[C_{16}H_{17}N_3O_2 + Na]^+$: 306.1213, found 306.1209.

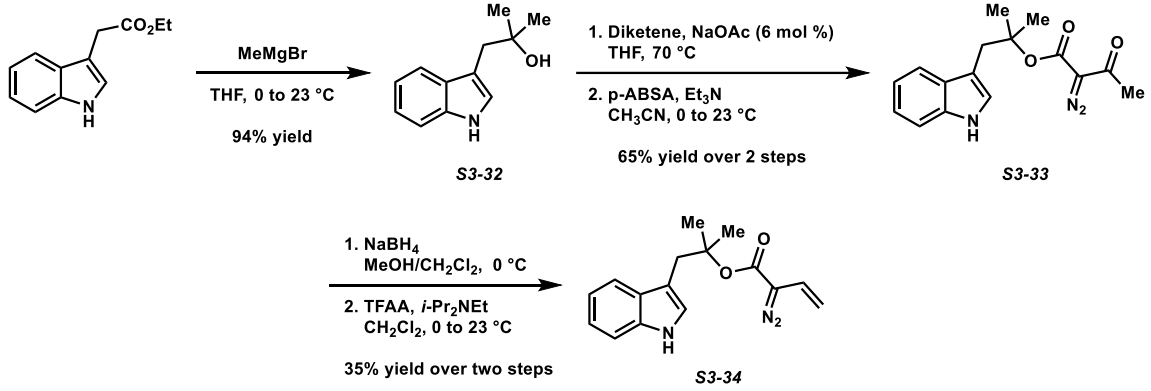

Alcohol S3-32: According to a known procedure by Maskeri and coworkers,[21] to a solution of ethyl 2-(1*H*-indol-3-yl)acetate (1.55 g, 7.63 mmol) in THF (25.4 mL) at 0 °C was added methylmagnesium bromide (8.13 mL, 3.0 M in Et_2O, 24.4 mmol) dropwise. The reaction mixture was then warmed to room temperature and stirred for 2 h. The reaction mixture was then quenched with sat. aq. NH_4Cl (20 mL), and the layers were separated. The aqueous layer was extracted with EtOAc (3 x 30 mL). The combined organic layers were washed with brine (20 mL), dried over $MgSO_4$, and concentrated in vacuo. The resulting alcohol (S**3-32**,1.31 g, 94% yield) required no further purification. The spectroscopic data was in accordance with the published values[21] (TLC: R_f = 0.24 in 4:1 hexanes/EtOAc).

Diazoester S3-33: Following a procedure reported by Doyle and coworkers,[19] a solution of indole **S3-32** (1.11 g, 5.89 mmol) and NaOAc (28.9 mg, 0.353 mmol) in THF (1.68 mL, 3.5 M) was heated to reflux. A solution of diketene (0.500 mL, 6.48 mmol) in THF (0.697 mL, 9.3 M) was then added dropwise to the reaction mixture over 30 min. The resulting mixture was refluxed for 4 h and then cooled to room temperature. The reaction mixture was partitioned between Et_2O (25 mL) and brine (25 mL). The aqueous layer was extracted with Et_2O (3 x 25 mL), and the organic

layers were combined, dried over $MgSO_4$, and concentrated in vacuo. A portion of crude ketoester was taken forward without further purification (TLC: R_f = 0.33 in 2:1 hexanes/EtOAc).

To a stirring solution of the crude ketoester (1.08 g, assume 3.95 mmol) in acetonitrile (3.29 mL) at 0 ºC was added Et_3N (0.716 mL, 5.14 mmol) dropwise. A solution of *p*-ABSA (1.23 g, 5.14 mmol) in acetonitrile (3.43 mL) was then added dropwise to the reaction mixture over 30 min. The resulting mixture was then warmed to room temperature and stirred for 3 h. The reaction mixture was then filtered through a Buchner funnel to remove the *p*-ABSA byproducts, and the filtrate was concentrated in vacuo. The crude residue was purified via silica gel flash chromatography (4:1 hexanes/EtOAc eluent) to afford α-diazo ketoester **S3-33** (1.08 g, 90% yield over 2 steps) as a yellow oil.

TLC: R_f = 0.56 in 2:1 hexanes/EtOAc, visualized by UV.

^{1}H NMR (400 MHz, $CDCl_3$): δ 8.08 (br. s, 1H), 7.61 (app. t, *J* = 7.9 Hz, 1H), 7.37 (d, *J* = 7.9 Hz, 1H), 7.23-7.08 (comp. m, 2H), 7.02 (d, *J* = 7.7 Hz, 1H), 3.29 (s, 2H), 2.44 (s, 3H), 1.59 (s, 6H).

Diazoester S3-34: To a solution of α-diazo ketoester **S3-33** (1.07 g, 3.57 mmol) in MeOH/CH_2Cl_2 (1:1, 14 mL) at 0 ºC was added $NaBH_4$ (162 mg, 4.29 mmol) portionwise. After addition, the reaction mixture was warmed to room temperature and stirred for 3 h, monitoring progress by TLC. The reaction mixture was then diluted with H_2O (20 mL) and extracted with EtOAc (3 x 20 mL). The combined organic layers were washed with brine (20 mL), dried over $MgSO_4$, and concentrated in vacuo. A portion of the crude alcohol product was taken forward without any further purification (TLC: R_f = 0.30 in 4:1 hexanes/EtOAc).

To a solution of the crude alcohol (690 mg, assume 2.29 mmol, 90% product alcohol, 10% diazoester S3-33) in CH_2Cl_2 (19 mL) at 0 °C was added *i*-Pr_2NEt (2.01 mL, 11.5 mmol) and MsCl (0.213 mL, 2.75 mmol) sequentially. The reaction mixture was warmed to room temperature and

stirred for 2 h. The reaction mixture was then concentrated in vacuo, and the crude residue was purified via silica gel flash chromatography (8:1 hexanes/Et_2O eluent) to afford vinyl diazoester **S3-34** (239 mg, 29% yield over 2 steps) as an orange oil.

TLC: R_f = 0.55 in 2:1 hexanes/Et_2O, visualized by UV.

^{1}H NMR (400 MHz, C_6D_6): δ 7.63-7.55 (m, 1H), 7.25-7.18 (comp. m, 2H), 7.08-7.00 (m, 1H), 6.74 (br. s, 1H), 6.52 (app. d, *J* = 2.4 Hz), 6.22 (dd, *J* = 17.4, 11.0 Hz, 1H), 4.84 (d, *J* = 11.0 Hz, 1H), 4.62 (d, *J* = 17.4 Hz, 1H), 3.18 (s, 2H), 1.46 (s, 6H).

^{13}C NMR (100 MHz, C_6D_6): δ 164.0, 136.3, 128.9, 123.7, 122.0, 121.3, 119.8, 119.7, 111.4, 111.3, 107.0, 84.7, 36.5, 26.4 (*1 carbon not detected: diazo*).

IR (ATR, neat): 3412, 2950, 2086, 1692, 1309, 1111, 743 cm^{-1}.

HRMS (ESI+): *m/z* calc'd for $(M + Na)^+$ $[C_{16}H_{17}N_3O_2 + Na]^+$: 306.1213, found 306.1209.

Intramolecular cycloaddition reactions

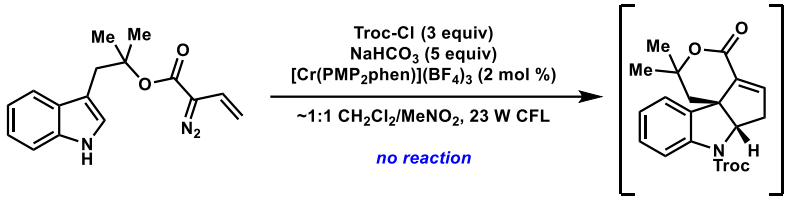

Procedure: A 0.8 M solution of diazoester **S3-34** (239 mg, 0.845 mmol) in CH_2Cl_2 (0.845 mL) was prepared for test reactions. In a 1-dram borosilicate vial, $[Cr(PMP_2phen)_3](BF_4)_3$ (1.1 mg, 0.000750 mmol) was dissolved in CH_3NO_2 (0.25 mL). 2,2,2-trichloroethoxycarbonyl chloride (20.6 μL, 0.150 mmol) and the solution of diazoester **S3-34** (0.0500 mL, 0.8 M in CH_2Cl_2, 0.0400 mmol) were added. The reaction mixture was irradiated with a 23 W CFL bulb while stirring. After 8 h, a second charge of $[Cr(PMP_2phen)_3](BF_4)_3$ (1.1 mg, 0.000750 mmol) was added. After 24 h total, the solvent was removed via rotary evaporation. The crude residue was dissolved in CH_2Cl_2 (~1 mL), and the solution was passed through a silica plug (0.5 x 3 cm), using

CH_2Cl_2/EtOAc as eluent (~10 mL, 1:1). The filtrate was concentrated in vacuo, and the residue was analyzed by ^1H NMR. Cycloadduct **3-48** was not observed.

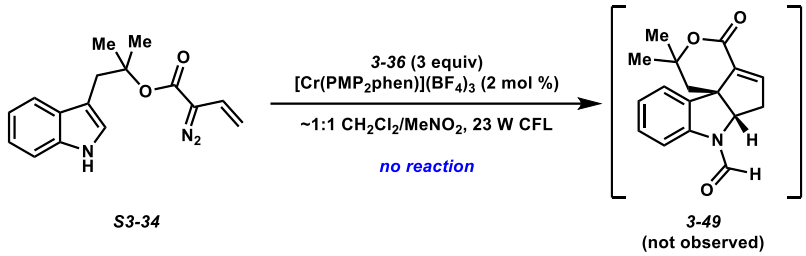

S3-34 *3-49* (not observed)

In a 1-dram borosilicate vial, trimethylacetic formic anhydride (19.5 mg, 0.150 mmol) was dissolved in CH_3NO_2 (0.250 mL). $[Cr(PMP_2phen)_3](BF_4)_3$ (1.1 mg, 0.000750 mmol) was then added, followed by the solution of diazoester **S3-34** (0.0500 mL, 0.8 M in CH_2Cl_2, 0.0400 mmol). The reaction mixture was irradiated with a 23 W CFL bulb while stirring. After 8 h, a second charge of $[Cr(PMP_2phen)_3](BF_4)_3$ (1.1 mg, 0.000750 mmol) was added. After 24 h total, the solvent was removed via rotary evaporation. The crude residue was dissolved in CH_2Cl_2 (~1 mL), and the solution was passed through a silica plug (0.5 x 3 cm), using CH_2Cl_2/EtOAc as eluent (~10 mL, 1:1). The filtrate was concentrated in vacuo, and the residue was analyzed by ^1H NMR. Cycloadduct **3-49** was not observed.

S3-31 *3-50* (not observed)

In a 1-dram borosilicate vial, $[Cr(PMP_2phen)_3](BF_4)_3$ (1.6 mg, 0.00106 mmol) was dissolved in CH_3NO_2 (0.250 mL). 2,2,2-trichloroethoxycarbonyl chloride (29.1 μL, 0.212 mmol) and the solution of diazoester **S3-31** (20.0 mg in 0.14 mL CH_2Cl_2, 0.0706 mmol) were added. The reaction mixture was irradiated with a 23 W CFL bulb while stirring. After 8 h, a second charge of $[Cr(PMP_2phen)_3](BF_4)_3$ (1.6 mg, 0.00106 mmol) was added. After 24 h total, the solvent was

removed via rotary evaporation. The crude residue was dissolved in CH_2Cl_2 (~1 mL), and the solution was passed through a silica plug (0.5 x 3 cm), using CH_2Cl_2/EtOAc as eluent (~10 mL, 1:1). The filtrate was concentrated in vacuo, and the residue was analyzed by ^1H NMR. Cycloadduct **3-50** was not observed.

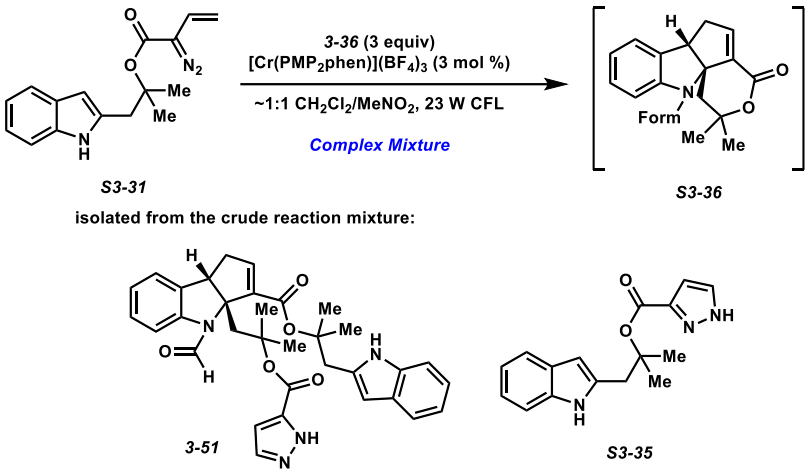

In a 1-dram borosilicate vial, trimethylacetic formic anhydride (52.4 mg, 0.402 mmol) was dissolved in CH_3NO_2 (0.670 mL). $[Cr(PMP_2phen)_3](BF_4)_3$ (3.0 mg, 0.00201 mmol) was then added, followed by a solution of diazoester **S3-31** (38.0 mg, 0.134 mmol) in CH_2Cl_2 (0.134 mL). The reaction mixture was irradiated with a 23 W CFL bulb while stirring. After 8 h, a second charge of $[Cr(PMP_2phen)_3](BF_4)_3$ (3.0 mg, 0.00201 mmol) was added. After 24 h total, the solvent was removed via rotary evaporation. The crude residue was dissolved in CH_2Cl_2 (~1 mL), and the solution was passed through a silica plug (0.5 x 3 cm), using CH_2Cl_2/EtOAc as eluent (~10 mL, 1:1). The filtrate was concentrated in vacuo, and the residue was purified via flash chromatography (4:1 → 2:1 EtOAc/hexanes eluent) to afford cycloadduct **S3-36** (9.0 mg, 12% yield) as a yellow oil, and a pyrazole byproduct (**S3-35,** 33% NMR yield using CH_2Br_2 (9.3 μL, 0.134 mmol) as the internal standard) as a beige solid.

S3-35 (pyrazole)

TLC R_f = 0.15 in 4:1 hexanes/EtOAc, visualized by UV.

^{1}H NMR (400 MHz, $CDCl_3$): δ 9.72 (br. s, 1H), 7.67 (d, *J* = 2.4 Hz, 1H), 7.55 (d, *J* = 7.5 Hz, 1H), 7.31 (d, *J* = 7.9 Hz, 1H), 7.10 (app. t, *J* = 7.5 Hz, 1H), 7.05 (app. t, *J* = 7.9 Hz, 1H), 6.91 (d, *J* = 2.4 Hz, 1H), 6.32 (s, 1H), 3.18 (s, 2H), 1.67 (s, 6H).

^{13}C NMR (100 MHz, $CDCl_3$): δ 160.7, 136.8, 135.4, 128.2, 121.1, 120.0, 119.4, 110.7, 108.4, 102.6, 83.8, 41.9, 25.5. (*2 carbons not detected)*

IR (ATR, neat): 3344, 2926, 1711, 1459, 1168, 740 cm^{-1}.

HRMS (ESI+): *m/z* calc'd for $(M + Na)^+$ $[C_{16}H_{17}N_3O_2 + Na]^+$: 306.1213, found 306.1209.

Intramolecular cycloadduct S3-36 was determined to not be the desired cycloadduct; however, intermolecular cycloadduct 3-51 was isolated from the reaction mixture.

3-51 (cycloadduct)

TLC R_f = 0.20 in 1:1 hexanes/EtOAc, visualized by UV.

^{1}H NMR (400 MHz, $CDCl_3$): δ δ 9.24 (s, 1H), 8.30 (d, *J* = 8.1 Hz, 1H), 7.98 (br. s, 1H), 7.64 (app. s, 1H), 7.50 (d, *J* = 7.8 Hz, 1H), 7.35-7.17 (comp. m, 2H), 7.16-6.98 (comp. m, 4H), 6.79 (app. s, 1H), 6.75 (app. s, 1H), 6.26 (s, 1H), 4.57 (app. d, *J* = 8.4 Hz, 1H), 3.38 (app. d, *J* = 14.6 Hz, 1H), 3.17 (app. d, *J* = 14.6 Hz, 1H), 3.09 (app. d, *J* = 16.0 Hz, 1H), 3.00 (app. dd, *J* = 18.2, 8.4 Hz, 1H), 2.89 (app. d, *J* = 16.0 Hz, 1H), 2.60 (app. d, *J* = 18.2, 8.4 Hz, 1H), 1.66 (s, 3H), 1.62 (s, 3H), 1.58 (s, 3H), 1.53 (s, 3H).

^{13}C NMR (100 MHz, $CDCl_3$): δ 164.0, 162.3, 146.9, 140.4, 138.4, 136.0, 134.2, 133.4, 128.63, 128.56, 124.9, 124.0, 121.5, 120.0, 119.8, 117.7, 110.8, 108.5, 102.8, 84.2, 83.5, 79.4, 48.9, 45.2, 39.6, 38.7, 31.1, 27.8, 27.4, 26.6 (*3 carbons not detected).*

IR (ATR, neat): 3716, 2928, 1710, 1658, 1547, 1241, 748 cm^{-1}.

HRMS (ESI+): *m/z* calc'd for $(M + H)^+$ $[C_{33}H_{34}N_4O_5 + H]^+$: 567.2602, found 567.2588.

3.9.13 Starting Material Synthesis

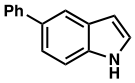

XX

Indole S3-6. Prepared according to the procedure reported by Shao and coworkers.[22]

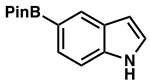

XX

Indole S3-7. Prepared according to the procedure reported by Prieto and coworkers.[23]

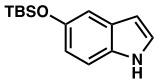

XX

Indole S3-8. Prepared according to the procedure reported by Ito and coworkers.[24]

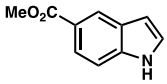

XX

Indole S3-9. Prepared according to the procedure reported by Kong and coworkers.[25]

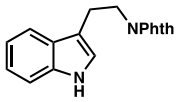

XX

***N*-phthalimidotryptamine**. Prepared according to the procedure reported by Feng and coworkers.[26]

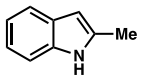

XX

2-methylindole. Prepared according to the procedure reported by Zhang and Yu.[27]

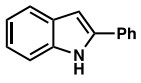

XX

2-phenylindole. Prepared according to the procedure reported by Gaikwad and coworkers.[28]

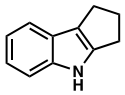

XX

Indole S3-19. Prepared according to the procedure reported by Matsumoto and coworkers.[29]

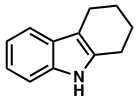

XX

Indole S3-20. Prepared according to the procedure reported by Dalvi and Lokhande.[30]

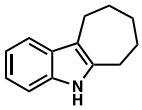

XX

Indole S3-21. Prepared according to the procedure reported by Matsumoto and coworkers.[29]

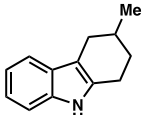

XX

Indole S3-22. Prepared according to the procedure reported by Matsumoto and coworkers.[29]

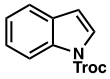

XX

Indole S3-26. Prepared according to the procedure reported by Yuan and coworkers.[31]

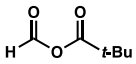

Trimethylacetic formic anhydride (3-36). Prepared according to the procedure reported by Vlietstra and coworkers.[32]

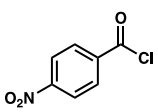

XX

4-Nitrobenzoyl chloride. Prepared according to the procedure reported by Otevrel and coworkers.[33]

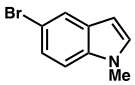

XX

5-bromo-1-methyl-indole. Prepared according to the procedure reported by Nemoto and coworkers.[34]

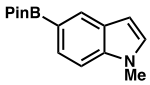

XX

1-methyl-5-(4,4,5,5-tetramethyl-1,3,2-dioxaborolan-2-yl)-1*H*-indole. Prepared according to the procedure reported by Ha and coworkers.[35]

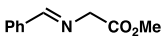

XX

Methyl 2-(benzylidienamino)acetate (3-62). Prepared according to the procedure reported by Lasch and Heinrich.[36]

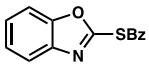

XX

5-(benzoxazole-2-yl)thiobenzoate. Prepared according to the procedure reported by Ueda and coworkers.[37]

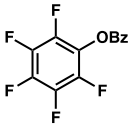

XX

Pentafluorophenyl benzoate. Prepared according to the procedure reported by Igolen and Morin.[38]

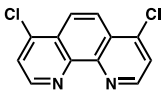

XX

4,7-dichloro-1,10-phenanthroline (S3-23). Prepared according to the procedure reported by Altman and Buchwald.[39]

Diazocarbonyl Synthesis:

General Notes: After synthesizing, vinyl diazocarbonyl compounds were stored in a -20 °C freezer as a 1.0 M solution in CH_2Cl_2. Diazo compounds are toxic, irritants, and many compounds are explosive. Care should be taken when handling and synthesizing diazo compounds. For several of these compounds, the ^{13}C NMR signal for the CN_2 carbon atom was not observed; this phenomenon is common and is due to the long relaxation time due to the enhanced negative partial charge on this atom.[40]

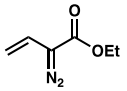

XX

Diazoester 3-6. Prepared according to the procedure reported by Davies and coworkers.[41]

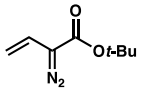

XX

Diazoester S3-15. Prepared according to the procedure reported by Schwartz and coworkers.[42]

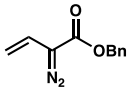

XX

Diazoester S3-16. Prepared according to the procedure reported by Sarabia and coworkers.[2d]

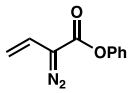

XX

Diazoester S3-17. Prepared according to the procedure reported by Sarabia and coworkers.[2d]

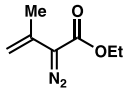

XX

Diazoester S3-18. Prepared according to the procedure reported by Jadhav and coworkers.[41c]

3.10 References and Notes

[1] a) Prier, C. K.; Rankic, D. A.; MacMillan, D. W. C. *Chem. Rev.* **2013**, *113*, 5322-5363. b) Romero, N. A.; Nicewicz, D. A. *Chem. Rev.* **2016**, *116*, 10075-10166. c) Narayanam, J. M. R.; Stephenson C. R. J. *Chem. Soc. Rev.* **2011**, *40*, 102-113.

[2] a) Stevenson, S. M.; Shores, M. P.; Ferreira, E. M. *Angew. Chem., Int. Ed.* **2015**, *54*, 6506−6510. b) Stevenson, S. M.; Higgins, R. F.; Shores, M. P.; Ferreira, E. M. *Chem. Sci.* **2017**, *8*, 654-660. c) Sarabia, F. J.; Ferreira, E. M. *Org. Lett.* **2017**, *19*, 2865-2868. d) Sarabia, F. J.; Li, Q.; Ferreira, E. M. *Angew. Chem. Int. Ed.* **2018**, *57*, 11015-11019. e) Büldt, L. A.; Guo, X.; Vogel, R.; Prescimone, A.; Wenger, O. S. *J. Am. Chem. Soc.* **2017**, *139*, 985−992. f) Treiling, S.; Wang, C.; Forster, C.; Reichenauer, F.; Kalmbach, J.; Boden, P.; Harris, J. P.; Carrella, L. M.; Rentschler, E.; Resch-Genger, U.; Reber, C.; Seitz, M.; Gerhards, M.; Heinze, K. *Angew. Chem. Int. Ed.* **2019**, *58*, 18075-18085.

[3] a) Gualandi, A.; Marchini, M.; Mengozzi, L.; Natali, M.; Lucarini, M.; Ceroni, P.; Cozzi, P. G. *ACS Catal.* **2015**, *5*, 5927−5931. b) Parisien-Collette, S.; Hernandez-Perez, A. C.; Collins, S. K. *Org. Lett.* **2016**, *18*, 4994−4997. c) Liu, L.; Duchanois, T.; Etienne, T.; Monari, A.; Beley, M.; Assfeld, X.; Haacke, S.; Gros, P. C. *Phys. Chem. Chem. Phys.* **2016**, *18*, 12550−12556. d) Fatur, S. M.; Shepard, S. G.; Higgins, R. F.; Shores, M. P.; Damrauer, N. H. *J. Am. Chem. Soc.* **2017**, *139*, 4493−4505. e) Kjær, K. S.; Kaul, N.; Prakash, O.; Chabera, P.; Rosemann, N. W.; Honarfar, A.; Gordivska, O.; Fredin,́ L. A.; Bergquist, K.-E.; Haggstro¨m, L.; Ericsson, T.; Lindh, L.; Yartsev, A.; Styring, S.; Huang, P.; Uhlig, J.; Bendix, J.; Strand, D.; Sundström, V.; Persson, P.; Lomoth, R.; Warnmark, K. *Science* **2019**, *363*, 249−253. f) Braun, J. D.; Lozada, I. B.; Kolodziej, C.; Burda, C.; Newman, K. M. E.; van Lierop, J.; Davis, R. L.; Herbert, D. E. *Nat. Chem.* **2019**, *11*, 1144−1150. g) Xia, S.; Hu, K.; Lei, C.; Jin, J. *Org. Lett.* **2020**, *22*, 1385-1389.

[4] Pal, A. K.; Li, C.; Hanan, G. S.; Zysman-Colman, E. *Angew. Chem., Int. Ed.* **2018**, *57*, 8027−8031.

[5] Grübel, M.; Bosque, I.; Altmann, P. J.; Bach, T.; Hess, C. R. *Chem. Sci.* **2018**, *9*, 3313−3317.

[6] a) Kern, J.-M.; Sauvage, J.-P.; J. Chem. Soc. *Chem. Commun.* **1987**, 546-548. b) Paria, S.; Reiser, O.; *ChemCatChem* **2014**, *6*, 2477-2483. c) Majek, M.; Jacobi von Wangelin, A. *Angew. Chem. Int. Ed.* **2013**, *52*, 5919-5921. d) Creutz, S. E.; Lotito, K. J.; Fu, G. C.; Peters, J. C. *Science* **2012**, *338*, 647-651. e) Pirtsch, M.; Paria, S.; Matsuno, T.; Isobe, H.; Reiser, O. *Chem. Eur. J.* **2012**, *18*, 7336-7340. f) Barelle, A.; Fensterbank, L.; Goddard, J.-P.; Ollivier, C. *Chem. Eur. J.* **2013**, *19*, 10809-10813. g) Paria, S.; Pirtsch, M.; Kaid, W.; Reiser O. *Synthesis* **2013**, *45*, 2689-2698. h) Tang, X.-J.; Dolbier, W. R. *Angew. Chem. Int. Ed.* **2015**, *54*, 4246-4249. i) Minozzi, C.; Caron, A.; Grenier-Petel, J.-C.; Santandrea, J.; Collins, S. K. *Angew. Chem., Int. Ed.* **2018**, *57*, 5477−5481. j) Hossain, A.; Bhattacharyya, A.; Reiser, O. *Science* **2019**, *364*, eaav9713.

[7] McDaniel, A. M.; Tsseng, H.-W.; Damrauer, N. H.; Shores, M. P. *Inorg. Chem.* **2010**, *49*, 7981-7991.

[8] Geiseler, A.; Steckhan, E.; Wiest, O.; Knoch, F. *J. Org Chem.* **1991**, *56*, 1405-1411.

[9] a) Gieseler, A.; Steckhan, E.; Wiest, O. *Synlett* **1990**, 275 −277. b) Wiest, O.; Steckhan, E. *Tetrahedron Lett.* **1993**, *34*, 6391 −6394. c) Peglow, T.; Blechert, S.; Steckhan, E. *Chem. Commun.* **1999**, 433 −434. d) Pitre, S. P.; Scaiano, J. C.; Yoon, T. P. *ACS Catal.* **2017**, *7*, 6440-6444.

[10] Allen, A. D.; Tidwell, T. T. *Eur. J. Org. Chem.* **2012**, *6*, 1081-1096.

[11] See Chapter 2, Section 2.3: Ligand and Catalyst Synthesis.

[12] Sheehan, J. C.; Yang, D.-D. H. *J. Am. Chem. Soc.* **1958**, *80*, 1154-1158.

[13] Guandalini, L.; Dei, S.; Gualtieri, F.; Romanelli, M. N.; Scapecchi, S.; Teodori, E.; Varani, K. *Helv. Chim. Acta.* **2002**, *85*, 96-107.

[14] Sakaki, S.; Kojima, T.; Arai, T. *J. Chem. Soc., Dalton Trans.* **1994**, 7-11.

[15] Mancebo-Aracil, J.; Martín-Rodríguez, M.; Nájera, C.; Sansano, J. M.; Costa, P. R. R.; Crizanto de Lima, E.; Dias, A. G. *Tetrahedron: Asymmetry* **2012**, *23*, 1596-1606.

[16] Schultz, D. M.; Sawicki, J. W.; Yoon, T. P. *Beilstein J. Org. Chem.* **2015**, *11*, 61-65.

[17] Connelly, N. G. Geiger, W. E. *Chem. Rev.* **1996**, *96*, 877-910.

[18] Chikkade, P. K.; Shimizu, Y.; Kanai, M. *Chem. Sci.* **2014**, *5*, 1585-1590.

[19] Doyle, M. P.; Winchester, W. R.; Protopopova, M. N.; Kazala, A. P.; Westrum, L. J. *Org. Synth.* **1996**, *73*, 13.

[20] Rianelli, R. d. S.; da Silva, F. d. C.; de Souza, M. C. B. V. Ferreira, V. F. *Letters in Organic Chemistry* **2006**, *3*, 73.

[21] Maskeri, M. A.; O'Connor, M. J.; Jaworski, A. A.; Davies, A. V.; Scheidt, K. A. *Angew. Chem. Int. Ed.* **2018**, *57*, 17225-17229.

[22] Shao, G.; Shi, G.; Zhang, Y., Pan, S.; Guan, X. *Org. Lett.* **2015**, *17*, 2652-2655.

[23] Prieto, M.; Zurita, E.; Rosa, E.; Muñoz, L.; Lloyd-Williams, P.; Giralt, E. *J. Org. Chem.* **2004**, *69*, 6812-6820.

[24] Ito, F.; Shudo, K.; Yamaguchi, K. *Tetrahedron* **2011**, *67*, 1805-1811.

[25] Kong, A.; Han, X.; Lu, X. *Org. Lett*. **2006**, *8*, 1339-1342.

[26] Feng, P.; Fan, Y.; Xue, F.; Liu, W.; Li, S.; Shi, Y. *Org. Lett.* **2011**, *13*, 5827-5829.

[27] Zhang, S.; Yu, Z. *Org. Biomol. Chem.* **2016**, *14*, 10511-10515.

[28] Gaikwad, R.; Bobde, Y.; Ganesh, R.; Patel, T.; Rathore, A.; Ghosh, B.; Das, K.; Gayen, S. *Synth. Commun.* **2019**, *49*, 2258-2269.

[29] (a) Matsumoto, K.; Tanaka, A.; Yukio, I.; Toda, M.; Bulman, R. A. *Heterocyclic Communications* **2003**, *9*, 9-12. (b) Bergès, J.; García, B.; Muñiz, K. *Angew. Chem. Int. Ed*. **2018**, *57*, 15891-15895.

[30] Dalvi, B. A.; Lokhande, P. D. *Tetrahedron Lett*. **2018**, *59*, 2145-2149.

[31] Yuan, Y.-A.; Lu, D.-F.; Chen, Y.-R.; Xu, H. *Angew. Chem. Int. Ed.* **2016**, *55*, 534-538.

[32] Vlietstra, E. J.; Zwikker, J. A.; Nolte, R. J. M.; Drenth, W. *Recl. Trav. Chim. Pays. Bas.* **1982**, *101*, 460-462.

[33] (a) Otevrel, J.; Mandelova, Z.; Pesko, M.; Gui, J.; Kralova, L.; Sersen, F.; Vejsova, M.; Kalinowski, D. S.; Kovacevic, Z.; Coffey, A.; Csollei, J.; Richardson, D. R.; Jampilek, J. *Molecules* **2010**, *15*, 8122-8142. (b) Zaragoza, F. *J. Org. Chem*. **2015**, *80*, 10370-10374.

[34] Nemoto, K.; Tanaka, S.; Konno, M.; Onozawa, S.; Chiba, M.; Tanaka, Y.; Sasaki, Y.; Okubo, R.; Hattori, T. *Tetrahedron* **2016**, *72*, 734-745.

[35] Ha, P. T.; Nguyen, O. T. K.; Huynh, K. D.; Phan, N. T. S. *Synlett* **2018**, *29*, 2031-2034.

[36] Lasch, R.; Heinrich, M. R. *Tetrahedron* **2015**, *71*, 4282-4295.

[37] (a) Ueda, M.; Seki, K.; Imai, Y. *Synthesis* **1981**, 991-993. (b) Nishio, T.; Shiwa, K. *Heterocycles* **2004**, *62*, 313-324.

[38] Igolen, J.; Morin, C. *J. Org. Chem.* **1980**, *45*, 4802-4804.

[39] Altman, R. A.; Buchwald, S. L. *Org. Lett.* **2006**, *8*, 2779-2782.

[40] (a) Kappe, T.; Lang, G.; Pongratz, E. *J. Chem. Soc., Chem Commun.* **1984**, 338–339. (b) Schmitz, A.; Kraatz, U.; Korte, F. *Heterocycles* **1978**, *10*, 199–205.

[41] (a) Davies, H. M. L.; Cantrell, W. R., Jr.; Romines, K. R.; Baum, J. S. *Org. Synth.* **1992**, *70*, 93. (b) Davies, H. M. L.; Houghland, P. W.; Cantrell, W. R., Jr. *Synth. Commun*. **1992**, *22*, 971-978. (c) Jadhav, A. M.; Pagar, V. V.; Liu, R. -S. *Angew. Chem. Int. Ed*. **2012**, *51*, 11809-11813.

[42] Schwartz, B. D.; Denton, J. R.; Lian, Y.; Davies, H. M. L.; Williams, C. M. *J. Am. Chem. Soc.* **2009**, *131*, 8329– 8332.

CHAPTER 4

DEVELOPMENT OF AN INTRAMOLECULAR BAEYER-VILLIGER REACTION TOWARD THE SYNTHESIS OF THE CRIPOWELLIN ALKALOIDS

4.1 Introduction

Amaryllidaceae is a family of flowering plants native to tropical and subtropical climates with a minimum of 1600 different species (Figure 4.1).[1] Amaryllidaceae have numerous subfamilies with different genuses. Among those genuses, the *Crinum* genus includes 180+ distinct species of plants. They possess large flowers and grow in moist areas, such as forests, river edges, and saltpans exclusively in Asia, Africa, the Americas, and the Pacific Islands.[2] *Crinum* extracts have typically used as treatments for swelling, fever, pain management, sores and other wounds, malaria, and even cancer. Alkaloids isolated from this species have shown a wide variety of biological activity in analgesic, antifungal, antiviral, antibacterial, and antimalarial assays.[3] Malaria disproportionately affects underdeveloped countries, so the need for new treatments that are also affordable can be considered a necessity.

Figure 4.1. *Crinum powellii* and *crinum erubescens* flowers.

4.2 Structural Analysis

Most alkaloids from the Amaryllidaceae family tend to exhibit similar structural motifs. The most common functionality among most compounds in the family is the benzodioxole core, which is in a variety of bioactive natural products and pharmaceuticals.[4] In the Amaryllidaceae family, the benzodioxole core is part of a fused ring system bearing additional functionality (Figure 4.2). This fused ring system is typically trans-fused, adding further complications toward the synthesis of these molecules. Most alkaloids also contain a substituted piperdine motif. This piperdine substructure is predominantly trisubstituted; however, disubstituted examples are also prominent. This trisubstituted piperdine adds to the overall difficulty in the synthesis of this family of alkaloids.

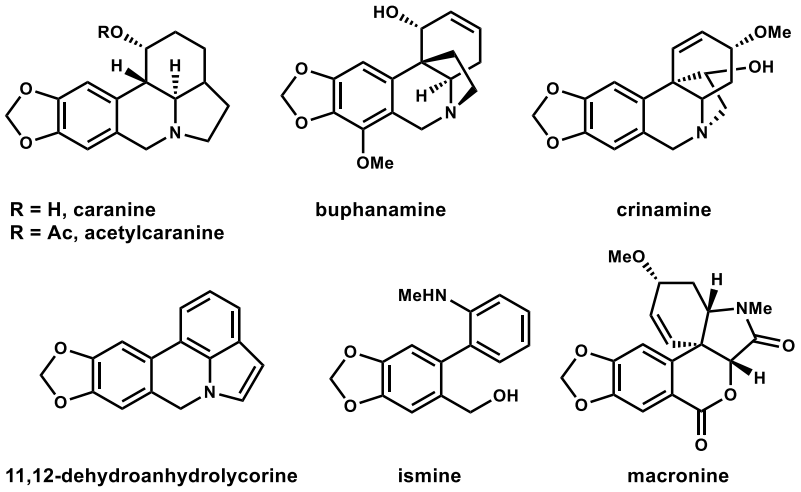

Figure 4.2. Natural products isolated from the Amaryllidaceae family.

In the *Crinum* genus, a series of alkaloids have been isolated from *crinum powellii* and *crinum erubescens* with unique structural characteristics like most in the Amaryllidaceae family. Cripowellin A-D were isolated from the methanolic extracts of the bulbs of *crinum powellii* and *crinum erubescens* by the Velten and Kingston groups, respectively (Scheme 4.1).[5] These alkaloids possess the benzodioxole structural motif as well as a fused ring system.[6] Typically, the Amaryllidaceae family has the 6,6-trans-fused ring system with a piperdine motif embedded

within;[4] however, the Cripowellin alkaloids have an azepane moiety. This 7-membered azepane connects directly to a 9-membered ring, now conjoined through a lactam ring. The 7,9-bicyclic structural motif is what makes the Cripowellin alkaloids so uncommon and synthetically interesting to organic chemists.

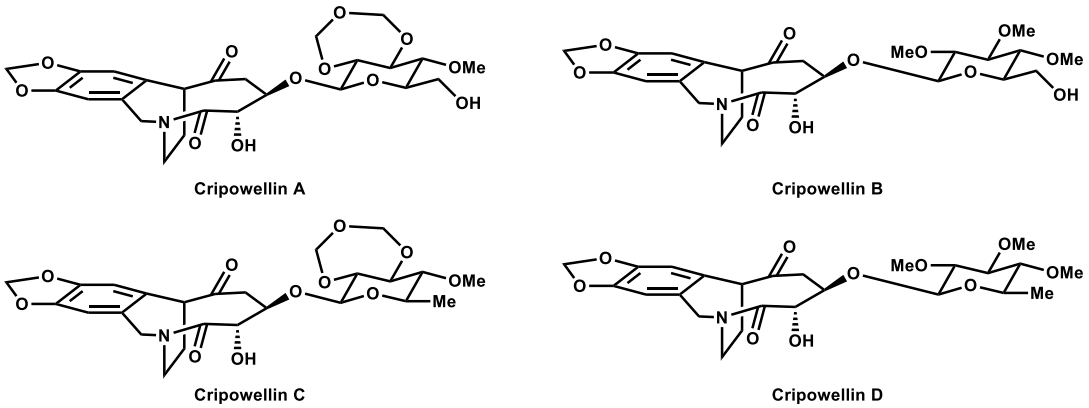

Natural Product	D2d Malaria Strain: IC_{50} values (nM):	Antiproliferation of A2780 HOC cells: IC_{50} values (nM):
Cripowellin A	30 ± 2	11.1 ± 0.4
Cripowellin B	180 ± 20	16.4 ± 0.1
Cripowellin C	26 ± 2	25.0 ± 2.0
Cripowellin D	260 ± 20	28.0 ± 2.0

Scheme 4.1. Structure and biological activity of the Cripowellin alkaloids.

4.3 Biological Activity of the Cripowellin Alkaloids

Along with being synthetically challenging, the Cripowellin alkaloids exhibit a range of biological activity. In 1997, Cripowellins A and B were shown to possess insecticidal activity.[7] With almost no investigation for ten years, in 2006, Kingston and coworkers reported that Cripowellin B had potent antiproliferation activity against various human cancer cell lines (Scheme 4.1).[8] Kingston and coworkers also analyzed Cripowellins A-D for antimalarial properties and antiproliferation capabilities in human ovarian cancer (HOC) cells. Cripowellins A and C were the most effective against malaria, with IC_{50} values of 30 ± 2 and 26 ± 2 nM, respectively. Cripowellins A and B were efficient in the antiproliferation of HOC cells with IC_{50}

values of 11.1 ± 0.4 and 16.4 ± 0.1 nM. Kingston and coworkers also noticed some antiplasmodial activity when analyzing different biological strains of malaria. They determined that the Cripowellin alkaloids would not be ideal candidates for antimalarial treatment since their antiplasmodial and antiproliferation activities cannot be separated.

4.4 Synthetic Approaches to the Cripowellin Alkaloids

Due to their biological activity and synthetic structural challenges, the Cripowellin alkaloids would represent a valuable class of natural products for synthetic chemists to target. However, the total synthesis of any of the Cripowellin alkaloids has never been reported. Enders and coworkers described a total asymmetric synthesis of the 1-*epi*-aglycon of the Cripowellin alkaloids, which is the portion of the molecule left after the sugar moiety is detached.[9] It is also the wrong epimer of the alkaloids, differentiating at the C1 and N1 positions (Figure 4.3). Enders and coworkers' convergent synthetic strategy comprises synthesizing two different parts and attaching them to complete the synthesis.

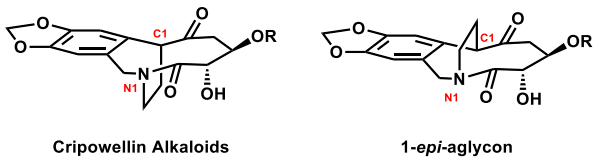

Figure 4.3. Cripowellin alkaloid aglycon vs. 1-*epi*-aglycon by Enders.

Enders and coworkers employed many different convergent synthesis strategies that were not productive, but eventually found one that was (Scheme 4.2). Protection of commercially available (*E*)-hexa-2,5-dien-1-ol with *p*-MeO-benzoyl chloride followed by a Sharpless asymmetric dihydroxylation yielded the desired diol **4-2** in 63% yield and >99% ee over two steps. Protection of this diol followed by deprotection of the *p*-MeO-benzoyl group using K_2CO_3 yielded

primary alcohol **4-3**. A Swern oxidation to the corresponding aldehyde and then oxidation to the carboxylic acid using Pinnick reaction conditions yielded the desired carboxylic acid **4-4**.

The other fragment starts with 6-bromo-piperonal, synthesized from the selective bromination of piperonal,[10] and a reductive amination with 3-butene-1-amine to formed amine **4-6** (Scheme 4.2). Amide formation between amine **4-6** and carboxylic acid **4-4** facilitated by FEP (2-fluoro-1-ethylpyridinium tetrafluoroborate) generated amide **4-7**. Structurally, amide **4-7** has two terminal alkenes, which formed macrocycle upon treatment with the Grubbs-II metathesis catalyst. The authors noted an instability with this compound and quickly subjected it to Heck reaction conditions to form alkene **4-8** in a 45% yield over two steps. Dihydroxylation of the alkene followed by Swern oxidation of the secondary alcohol, yields ketone **4-9** in 55% yield over two steps. Ketone **4-9** is subjected to a three-step sequence of radical deoxygenation, acetal deprotection, and acetate protection to yield the 1-*epi*-aglycon of cripowellin **4-10**. Enders and coworkers' synthesis is 16 total steps with an overall yield of 5.6%. A crystal structure of the 1-*epi*-aglycon was obtained, showing that both the ketone and the lactam carbonyl groups had the same spatial orientation as the actual alkaloids. It is conceivable that the 1-*epi* derivative would have a similar biological activity to the isolated alkaloids; however, the analysis of this hypothesis was not complete.

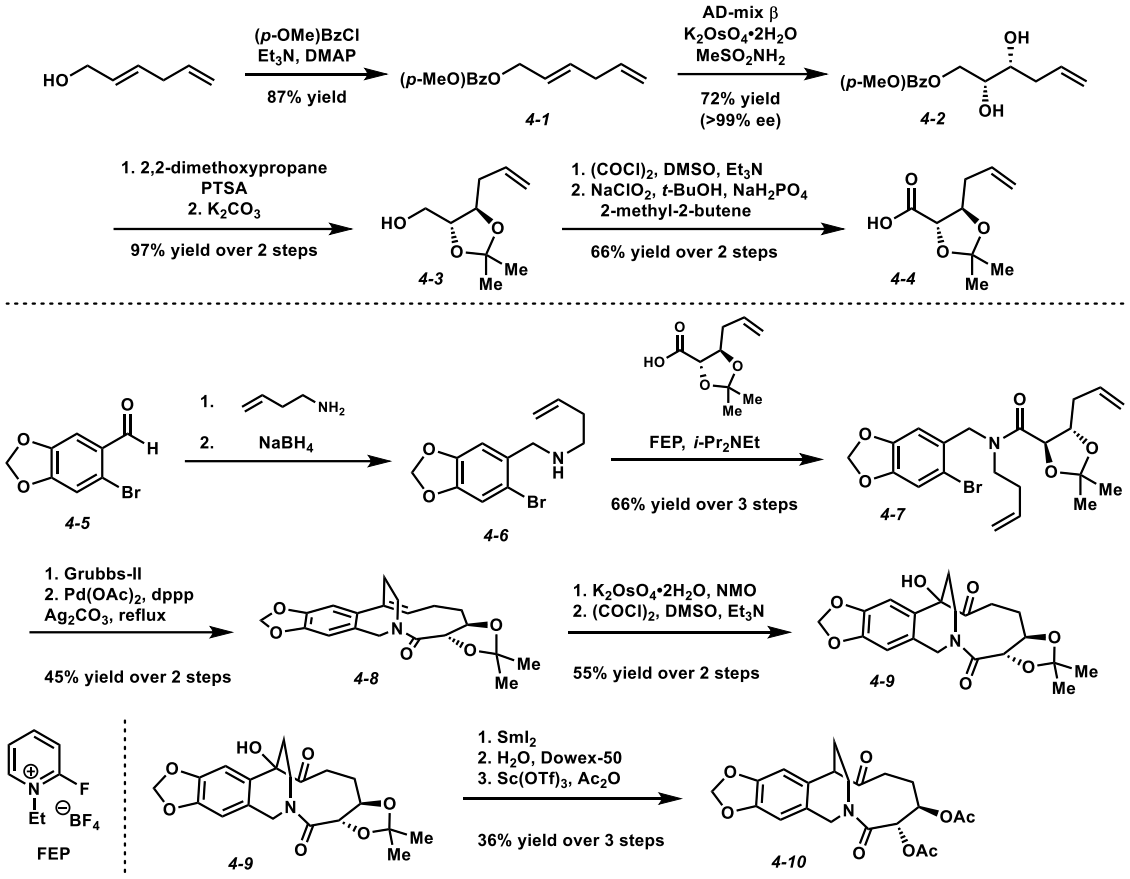

Scheme 4.2. Enders's synthesis of the 1-*epi*-aglycon of the Cripowellin alkaloids.

Enders and coworkers examined different approaches toward the synthesis of the Cripowellin alkaloids that did not work. These failed strategies must be considered and serve as the starting point for our synthesis of these molecules.

4.5 Experimental Design and Results

Further analysis of the Cripowellin alkaloids showed key disconnections. We envisioned lactam formation as the final step to synthesize the Cripowellin core, arises from carboxylic acid **4-11** in our initial retrosynthetic approach (Scheme 4.3). Carboxylic acid **4-11** bears a ketone functionality that quickly could be synthesized from a nitro group using the Nef reaction[11] from nitroalkane **4-12**. Nitroalkane **4-12** has a syn diol and a carboxylic acid, which could stem from a

metathesis reaction of an acrylate with a terminal alkene. This sequence creates azepane **4-13**. The formation of azepane **4-13** from a reductive amination and subsequent Shapiro reaction could generate the terminal alkene from benzylamine **4-14**. Benzylamine **4-14** has ketone and aldehyde functional groups generated through the oxidative cleavage of a trisubstituted alkene from cyclohexene **4-15**. Cyclohexene **4-15** formation from a potential photocatalyzed Diels-Alder reaction between nitroalkene **4-16** and isoprene would give the desired regioselectivity.

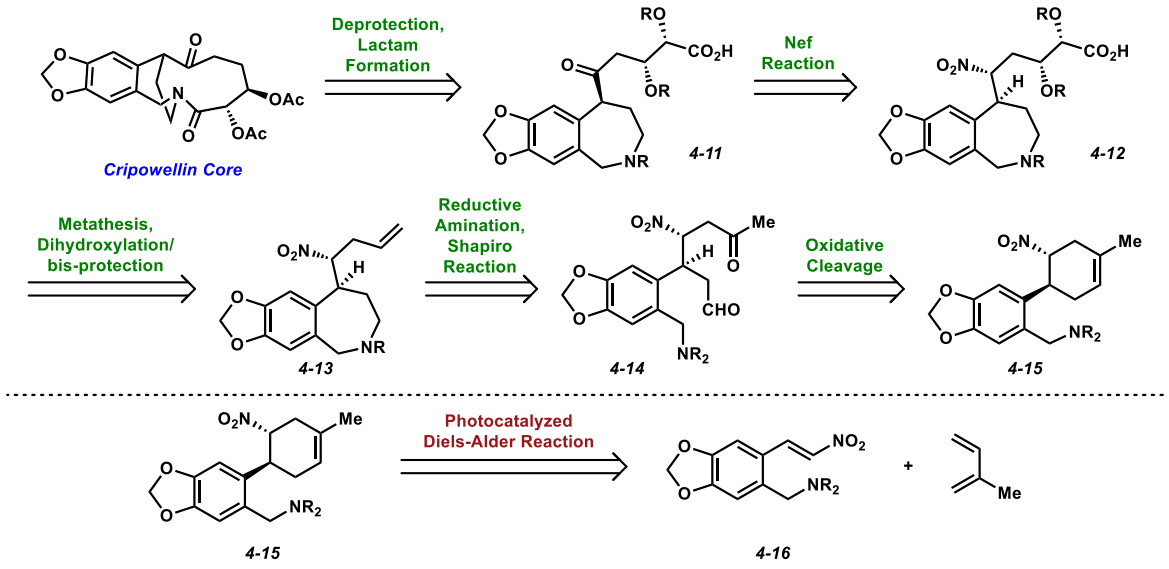

Scheme 4.3. Initial retrosynthetic approach toward the Cripowellin core.

Challenges within this synthesis are notable. The Nef reaction utilizes strongly acidic and basic conditions, so choosing the syn diol's protecting group(s) is essential. The Shapiro transformation could pose a real challenge due to the preference of disubstituted alkenes over monosubstituted alkenes.[12] Reductive amination from the benzylamine to form the azepane functionality could also be synthetically challenging. In reductive amination reactions, aldehydes and ketones react somewhat similarly.[13] The benzylamine could react with either the aldehyde or ketone in this molecule, forming a stable 7-membered ring product (reacts with aldehyde) or an 8-membered product (reactions with ketone). Another potential issue could be the photocatalytic

Diels-Alder reaction. Due to the proposed mechanisms by which this reaction proceeds, two different reactivity outcomes are possible. Oxidation of the benzylamine to the radical-cation would not yield the desired cycloadduct. Alternatively, a (2+2) cycloaddition can occur with the nitroalkene and diene, followed by a vinylcyclobutane rearrangement to yield the desired product. An energy-transfer pathway is also viable within this reaction. Overcoming the oxidation of the benzylamine by the excited-state photocatalyst to promote a different mechanistic pathway to yield the cycloadduct is the biggest challenge within this synthesis. The last major issue with this synthesis is the overall scalability. Batchwise protocols can consist of long reaction times and light penetration issues with could attribute to decreased yields. To get around this issue, photochemical flow reactors can provide an alternative approach. By using a flow reactor, light penetration is no longer a problem; however, the cost for the instrument is expensive.

In this approach to synthesize the Cripowellin alkaloids, the formation of the correct configuration of the cyclohexene rings relies on the regioselectivity of the Diels-Alder reaction. A trademark of the Diels-Alder reaction is its highly selective regiochemical outcomes (Figure 4.4). Electron withdrawing groups on a dienophile and an electron donating groups on the diene directly impact the overall regioselectivity of the reaction. The phenomenon is called the *ortho-para* rule. With this rule in mind, in a typical Diels-Alder reaction, "para-" products are favored over the formation of the "meta-". However, Stevenson and coworkers found that a chromium(III)-photocatalyzed Diels-Alder reaction with electron withdrawing groups on the dienophile and an electron donating groups on the diene provided inverse regioselectivity to classical methods.[14] Stevenson's approach favored the "meta-" products over the "para-".[15] In the synthesis of the Cripowellin alkaloids, the regioselectivity of the Diels-Alder reaction must prefer the "meta-" products for the synthesis to work. Using Stevenson's chromium(III)-photocatalyzed

Diels-Alder reaction as the basis for the total synthesis provides the desired regioselectivity needed to carry forward with this synthesis.

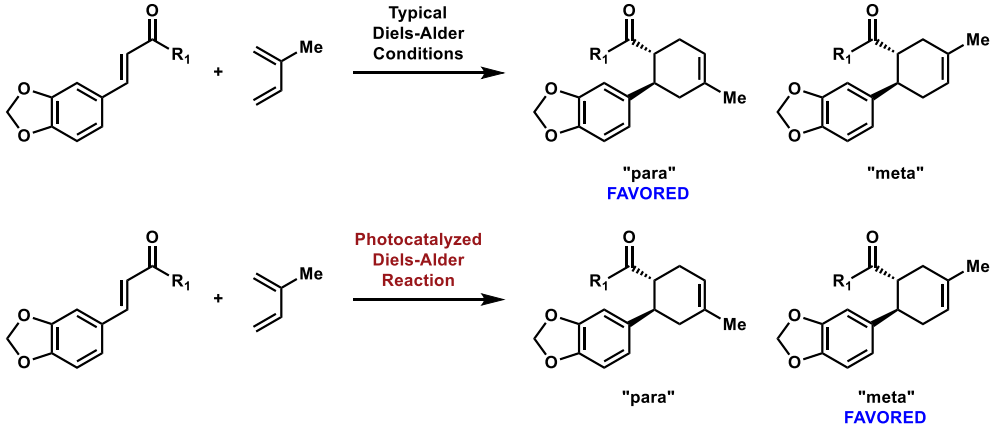

Figure 4.4. Regioselectivity of an electron deficient photocatalyzed Diels-Alder reaction.

A starting point for the synthesis was the creation of the dienophile with an electron withdrawing group. The nitroalkene provided the handle needed to utilize Stevenson's chromium(III) photocatalyzed Diels-Alder reaction. For the synthesis of the azepane ring, the inclusion of a protected benzylamine functional group was desired. Selective bromination of piperonylamine followed by bis-allyl protection of the benzylamine yields intermediate **4-17** in 85% yield over two steps (Scheme 4.4). Formylation of intermediate **4-17** using DMF yielded aldehyde **4-18** in a 91% yield. Synthesis of nitroalkene **4-19** via a Henry reaction and subsequent elimination from aldehyde **4-18** yielded the desired dienophile in 67% yield. The overall yield of this 4-step synthetic sequence was 52%. Analysis of the dienophile in photocatalytic conditions showed significant decomposition. This compound is not bench or solution stable and notable deterioration was seen in a matter of hours.[16] Conjugate addition of the amine with the nitroalkene could occur, causing decomposition of the dienophile. Because of the stability problems, an alternative solution needed to be found.

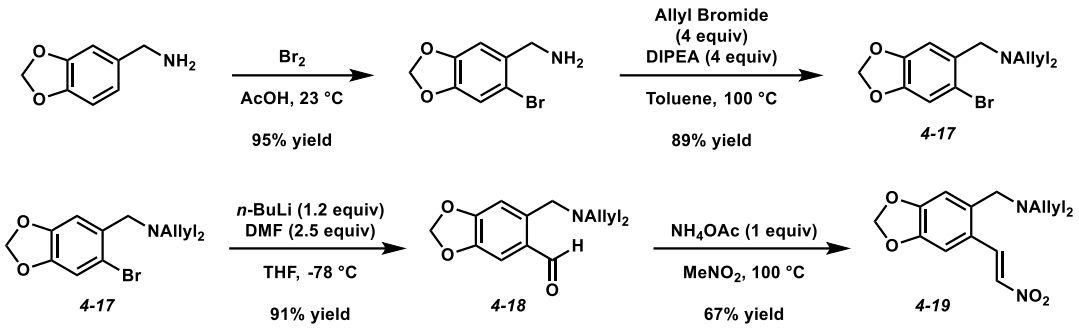

Scheme 4.4. Synthesis of the starting dienophile.

Because of this setback, a new strategy was developed (Scheme 4.5). Like the first strategy, lactam formation generates the Cripowellin core from the coming together of an amine and a carboxylic acid. Carboxylic acid **4-20** is synthesized from the deprotection and subsequent oxidation of protected alcohol from azepane **4-21**. The syn diol and carboxylic acid could stem from a metathesis-dihydroxylation pathway from terminal alkene **4-22**. A sequence of azepane then alkene formation would yield the desired intermediate. The use of reductive amination, then the Pictet-Spengler process produces the azepane functionality, and an ensuing Shapiro reaction from ketone **4-23** creates the desired alkene **4-22**. The synthesis of ketone **4-23** can arise from many different functional group conversions of -X, which can be several other functionalities. Oxidative cleavage of an alkene from cyclohexene **4-24** yields desired ketone **4-23**. A photocatalyzed Diels-Alder reaction synthesizes the desired cyclohexene **4-24** from alkene **4-25** and isoprene. The photocatalyzed Diels-Alder with alkene **4-25** would still yield the desired regioisomer for this synthesis if an electron withdrawing group were directly attached. A screen of different starting dienophiles with electron withdrawing groups could be helpful to understand overall reactivity to give the desired cycloadduct.

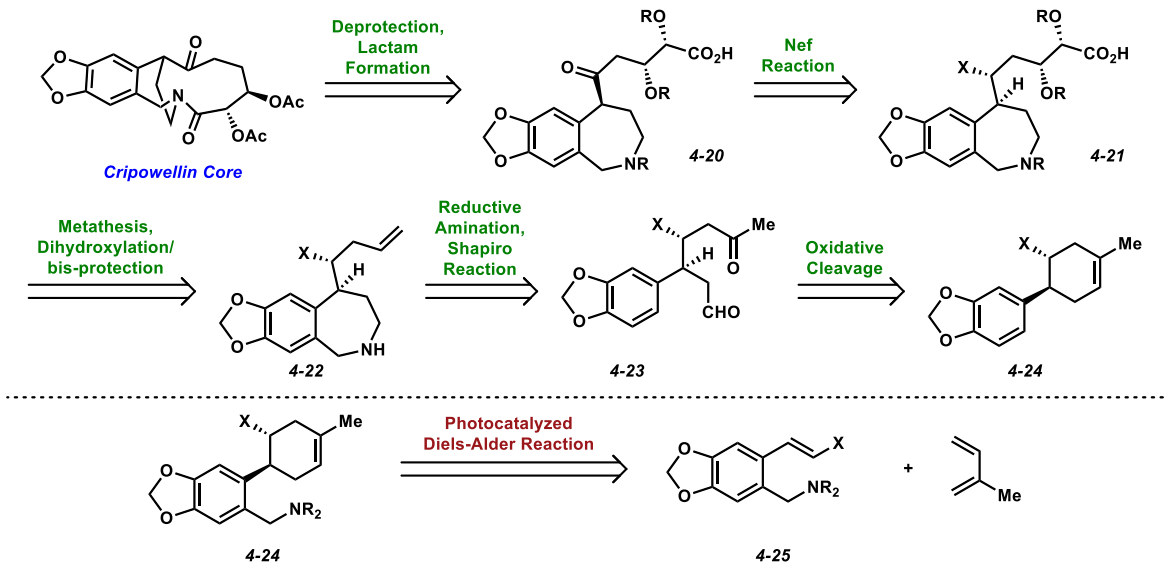

Scheme 4.5. A new potential strategy for the synthesis of the Cripowellin core.

We envisioned four potential functional groups that could yield us the desired cyclohexene derivatives for this synthesis. In working with the nitroalkenes previously, the use of a nitro group (**4-A** and **4-B**) is also plausible since it can be readily converted to a ketone using a Nef reaction. Next, we could use enone derivatives, more specifically, alkyl ketones (**4-C**). Baeyer-Villiger oxidation of the ketone to the corresponding ester derivative yields a pathway to the desired Cripowellin core. Lastly, an option was to use an α-ketoester (**4-D**). This functionality could also undergo a Baeyer-Villiger reaction.

In the proposed mechanism for this reaction, Stevenson and coworkers suggest a two-step sequence. The formation of a vinylcyclobutane, followed by a rearrangement to yield the desired [4+2] cycloadducts, was determined to be a possible reaction mechanism. Scheme 4.6 shows the different dienophiles analyzed in this two-step approach. The complete conversion of the [2+2] cycloadduct to the [4+2] product is limited in the single-step direct process. Chromatographic separation of the [2+2] cycloadduct from the desired [4+2] product was near impossible, so the

two-step route provides a workaround with the complete conversion of starting materials to maximize the formation of the product.

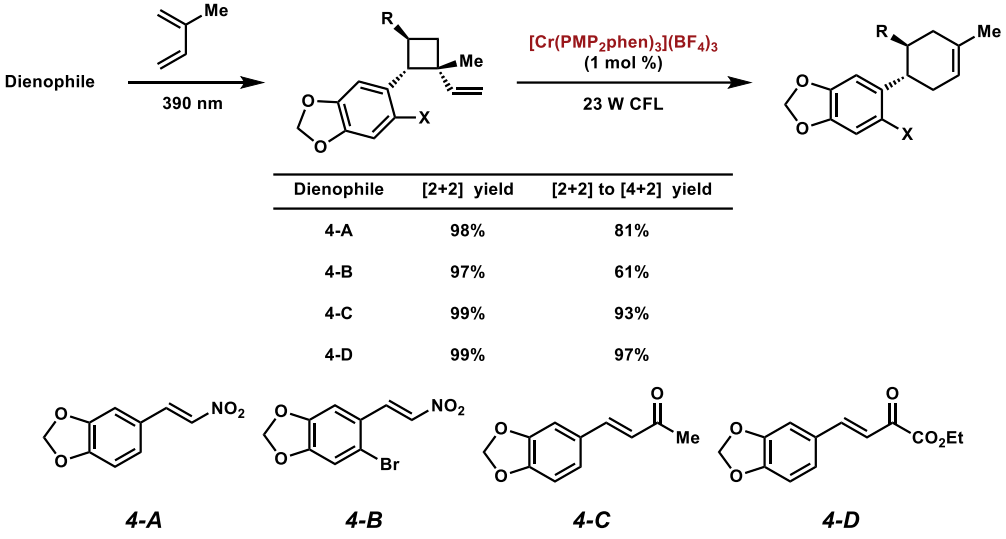

Dienophile	[2+2] yield	[2+2] to [4+2] yield
4-A	98%	81%
4-B	97%	61%
4-C	99%	93%
4-D	99%	97%

4-A *4-B* *4-C* *4-D*

Scheme 4.6. Dienophiles that were analyzed in this [2+2] to [4+2] reaction sequence.

Conversion of each dienophile to the corresponding [2+2] vinylcyclobutane intermediates proceeded in near quantitative yields using isoprene and visible light. Vinylcyclobutanes undergo the rearrangement using the photocatalyzed conditions of $[Cr(PMP_2phen)_3](BF_4)_3$ [17] and visible light in moderate to excellent yields (61-97% yield). The addition of the bromine atom on dienophile **4-B** severely hindered the formation of the [4+2] compound (61% yield), with the starting material recovered in 36% yield. Dienophiles **4-C** and **4-D** both yielded the [4+2] compound in excellent yields (93% and 97%). Using this data, we determined that dienophile **4-C** was the appropriate choice to start our synthesis. Dienophile **4-C** can be synthesized by a known literature prep using aldol conditions with acetone and piperonal, whereas dienophile **4-D** requires a three-step sequence.

As a model, in the reaction of electron deficient alkene and isoprene, four possible cyclobutanes can be formed (Scheme 4.7). The head-to-head and head-to-tail cyclobutanes between the dienophile and alkene *A* of the diene are one set of possibilities. The other set of

cyclobutanes deriving from head-to-head and head-to-tail addition with alkene *B* of isoprene. Only the head-to-tail isomers (**4-27** and **4-29**) have the vinyl group and the electron rich aryl group on adjacent carbons, allowing the rearrangement to occur to the corresponding cyclohexenes. Each cyclobutane product also has a mixture of diastereomers. Therefore, in a single reaction, there are 8 possible cyclobutane products that could form. Characterization of these products can become difficult when each head-to-tail product has a mixture of diastereomers. The major cyclohexene isomer (**4-30**) that is observed with the reversed Diels-Alder regioselectivity results from the rearrangement of cyclobutane **4-27**. The minor cyclohexene isomer (**4-31**) results from the rearrangement of the other head-to-tail product (**4-29**). It is presumed that the formation of **4-27** is likely favored over **4-29** because alkene *A* is more electron rich than alkene *B*.

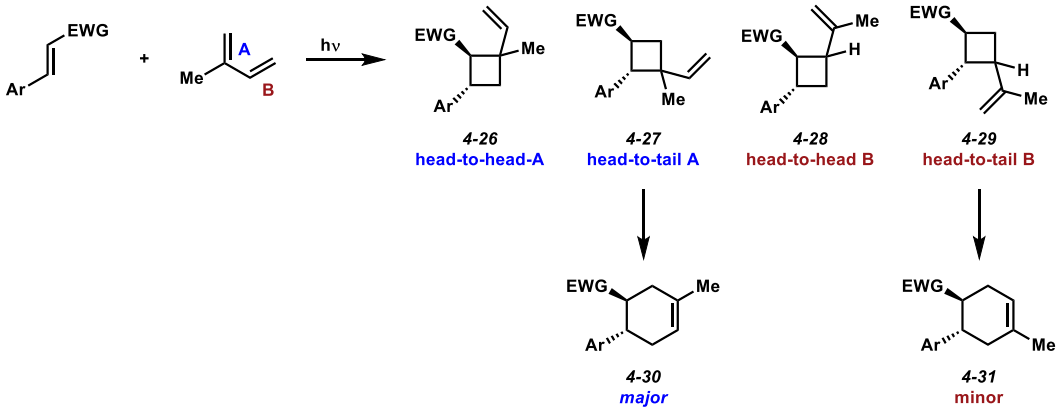

Scheme 4.7. Plausible regiochemical explanation of cyclohexene products.

The scalability of a photoreaction is often overlooked. There are two main methods to scale a photoreaction, batch-wise or flow.[18] Batch-wise synthesis of the [2+2] cycloadduct **4-32** has been completed on a 5-mmol scale. With a large amount of **4-32** in hand, optimization of the vinylcyclobutane rearrangement with different photocatalysts ensued. Using multiple Kessil BlueTuna LEDs for scalable photoreactions was not pursued due to overall cost; therefore using a CFL bulb was more advantageous and cost-effective. $[Cr(Ph_2phen)_3](BF_4)_3$, $[Cr(PMP_2phen)_3](BF_4)_3$, and $[Ru(bpz)_3](PF_6)_2$ [19] were all analyzed as the photocatalysts for the

vinylcyclobutane rearrangement with visible light (Scheme 4.8). $[Cr(Ph_2phen)_3](BF_4)_3$ and $[Cr(PMP_2phen)_3](BF_4)_3$ along with visible light were both competent in the reaction; however, prolonged reactions times and diminished yield were seen. $[Ru(bpz)_3](PF_6)_2$ catalyzed the rearrangement of **4-32** to **4-33** in 94% yield with visible light.

Continuous flow photocatalysis is a technique that has gathered increasing interest as means for scalability and production. In an academic setting, continuous flow photocatalysis is being utilized in reaction discovery and methodology. The most appealing quality of flow photocatalysis is the scalability of a photochemical reaction. To learn new laboratory techniques, the use of flow photocatalysis was attractive, especially in the scaleup efforts in a natural product synthesis. Given budgetary restrictions, continuous flow photocatalysis was not an option; however, using non-continuous flow methods was attainable with everyday laboratory items. The mechanical operator in a non-continuous flow setup can be a simple syringe pump, suited for anywhere from 1-60 mL syringes. Wrapping PFA tubing around an aluminum foil-covered 60 mL syringe provides the necessary pathway for the reaction mixture. We also bought a syringe-to-tubing adapter for Luer-lock syringes to help connect the syringe and tubing. A picture of the flow photocatalysis reactor is in Figure 4.5. The alternative to flow photocatalysis is a batch-wise process. The batch-wise reaction technique involves running a large-scale photoreaction in a single pot. Issues with the batch-wise process involve the transmittance of light throughout the solution and overall distance from the light. The further away from the light source, light penetration into the solution is decreased, therefore the amount of photons into solution is decreased, altering reactivity negatively. The use of flow photocatalysis allows for even light penetration and photons throughout the reaction mixture.

Figure 4.5. Flow photocatalysis setup developed.

$[Ru(bpz)_3](PF_6)_2$ can catalyze the direct formation of the desired [4+2] cycloadduct from enone **4-C** (Scheme 4.8). In the non-continuous flow setup on a 1-mmol scale, enone **4-C** was directly transformed to [4+2] cycloadduct **4-33** in 78% yield. About 15% of the [2+2] product **4-32** was able to be isolated from this reaction. On the same scale in a batch-wise process, the [2+2] cycloadduct **4-32** was isolated in 80% yield, while the desired [4+2] cycloadduct **4-33** was only isolated < 10% yield. This result is consistent with the issues previously discussed batch-wise synthesis. Both the flow pathway and the two-step sequence are operable in generating large quantities of [4+2] product **4-33**.

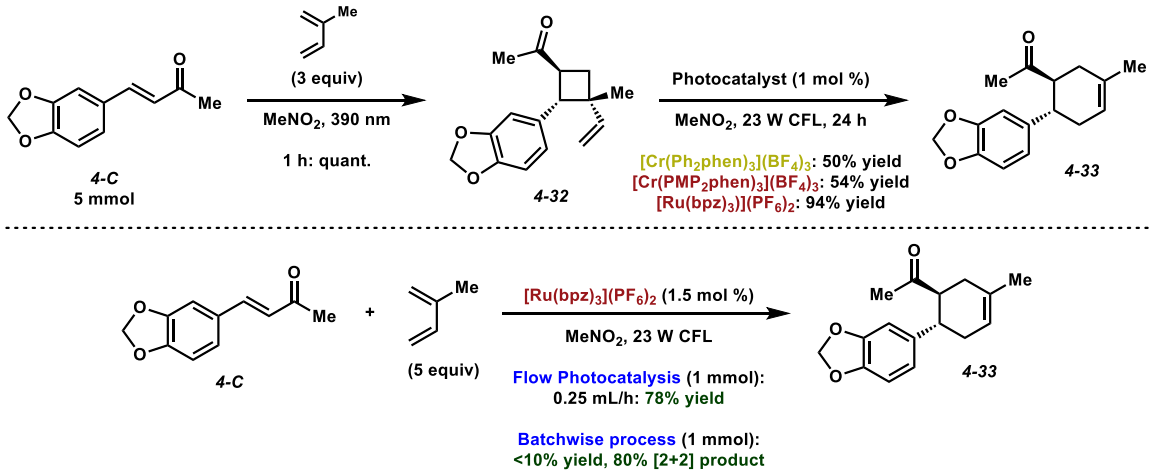

Scheme 4.8. Sequences toward the [4+2] product.

With a sizable amount of starting material generated, the focus shifted toward the Baeyer-Villiger oxidation of the ketone in the presence of the electron rich alkene.[20] The [4+2] cyclohexene product **4-33** has many potential oxidation sites, the ketone, electron rich alkene, or even the arene (Scheme 4.9A). Upon treatment with an oxidant, all three oxidation sites could react, making the choice of oxidant an important decision. In this example, we wanted the oxidation of the ketone in the presence of the electron rich alkene. Conditions that were developed to oxidize a ketone in the presence of an alkene were preferred and extensively analyzed (Scheme 4.9B). Significant decomposition of **4-33** was seen in most reactions; however, in a few cases, epoxidation of the alkene to **4-35** was favored. Lewis acids also did not help facilitate these reactions. Electrophilic aromatic substitution reactions could be favored when using an electron rich arene and Lewis acids, forming a stable 5-membered ring. Understanding the failure of this pathway, a new strategy had to be developed.

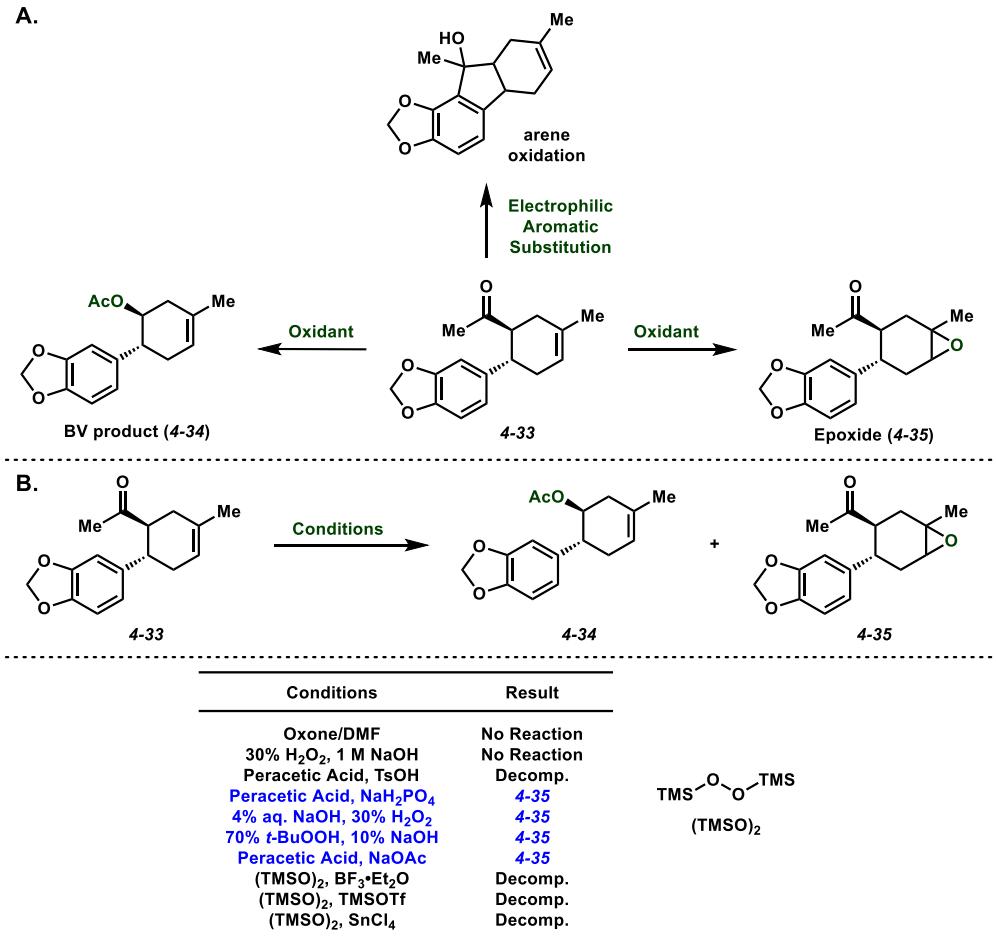

Scheme 4.9. A) Different oxidation possibilities. B) Conditions screened for reactivity.

4.6 Development of an Intramolecular Baeyer-Villiger Reaction

While reviewing the literature for potential Baeyer-Villiger conditions for the oxidation of a ketone in the presence of an electron rich alkene, there were few examples of this type of reactivity.[20] In our case, those conditions did not yield the desired Baeyer-Villiger product, with the epoxidation product favored. Since the use of an external oxidant formed the undesired epoxidation product, we theorized using an internal oxidant on the molecule.

In 1979, Corey and coworkers reported an epoxidation of an alkene from the *in situ* formation of a peracid chemoselectively (Scheme 4.10).[21] Corey and coworkers generated a peracid from a carboxylic acid as the key intermediate. Since the peracid is now in the proper

spatial arrangement, oxidation of the alkene will occur. Corey utilized this strategy in the synthesis of prostaglandin derivatives. The critical step of generating a peracid from a carboxylic acid could offer an alternative approach toward the synthesis of Cripowellin.

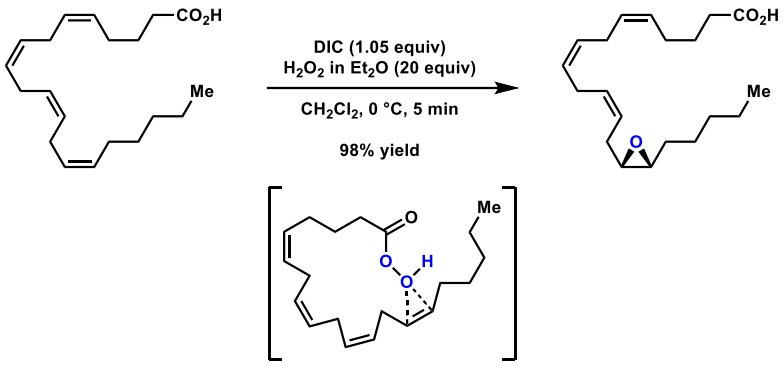

Scheme 4.10. Corey's intramolecular reaction sequence.

Using similar conditions to Corey, Miller and coworkers generate peracids on peptides in an enantioselective Baeyer-Villiger oxidation (Scheme 4.11).[22] Miller's proposed intermediate is the peptide peracid, which reacts with cyclohexanone derivatives. The Baeyer-Villiger rearrangement can then occur, yielding different lactone products. The selectivity of Miller's enantioselective Baeyer-Villiger reaction stems from hydrogen bonding with the protected amine. Other amine protecting groups showed that more H-bonding sites increased the overall yield of the transformation. In our case, the inability to use external oxidants to promote the Baeyer-Villiger oxidation of a ketone in the presence of the electron rich alkene prompted a change in strategy. Miller and Corey's work sparked a potential adjustment to our dienophile. The generation of an oxidant in situ for an intramolecular (Corey) or intermolecular (Miller) oxidation reaction provided a different approach to solve our reactivity problem.

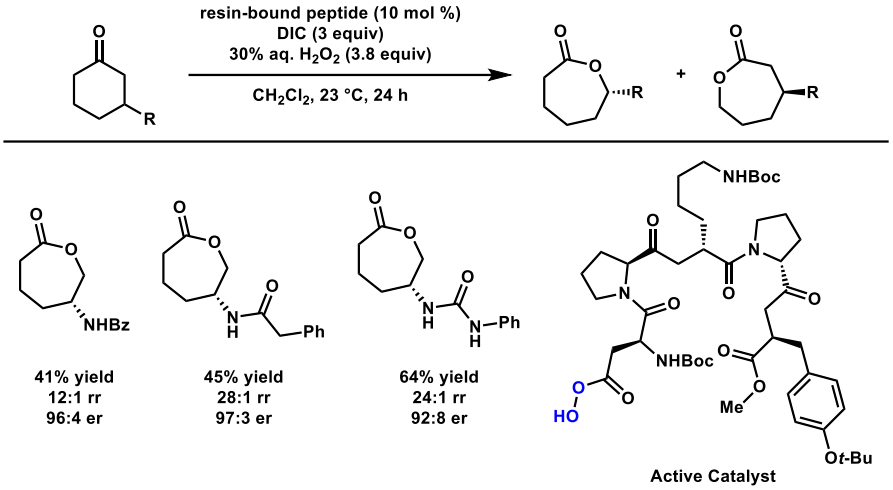

Scheme 4.11. Miller's enantioselective Baeyer-Villiger reaction.

Baeyer-Villiger oxidation of the methyl ketone in the presence of the electron rich alkene did not yield the desired products necessary to continue that strategy. However, changing the methyl ketone (**4-33**) to a benzoic acid derivative (**4-36**) would provide an alternative approach (Scheme 4.12A). With the addition of the benzoic acid derivative (**4-36**), the formation of a peracid (**4-38**) for the intramolecular Baeyer-Villiger reaction becomes possible. Once formed, the peracid has three plausible reaction pathways. First, the peracid could form the 6-membered ring intermediate, leading to the desired intramolecular Baeyer-Villiger product. Second, the peracid could intramolecularly oxidize the alkene; however, given the spatial arrangement of the molecule, the predicted product would be a macrocycle, which would be unlikely to occur. Similar to Corey's example, oxidation of the of the ketone over the formation of the epoxide would occur chemoselectively due to the spatial orientation of the molecule. Lastly, intermolecular oxidation of the ketone or alkene of a second cyclohexene molecule could occur. Because of intramolecular reactivity being favored over an intermolecular process and the formation of a stable 6-membered ring intermediate over potential macrocycle, this reaction should favor the formation of the Baeyer-Villiger product.

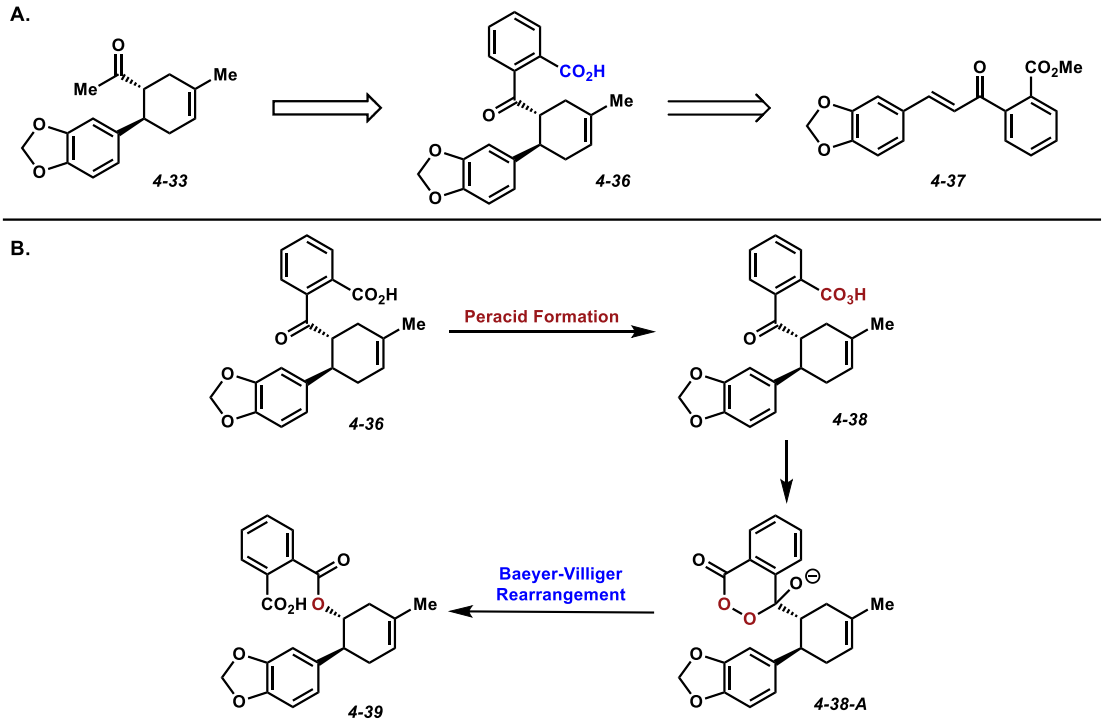

Scheme 4.12. A) Alternative approach for the Baeyer-Villiger reaction. B) Proposed intramolecular Baeyer-Villiger mechanism.

The proposed reaction mechanism appears in Scheme 4.12B. Peracid formation from carboxylic acid **4-36** generates **4-38**. Nucleophilic attack from peracid **4-38** onto the ketone produces a stable 6-membered ring intermediate. A Baeyer-Villiger rearrangement occurs, shifting the alkyl bond, creating desired ester product **4-39**. Our hypothesis was investigated by synthesizing a series of test substrates (Scheme 4.13). To our delight, acetyl benzoic acid derivatives treated with $(COCl)_2$ to form the acyl chloride followed by Na_2O_2 to form the peracid, yielded the corresponding Baeyer-Villiger products (**4-40** to **4-43**).

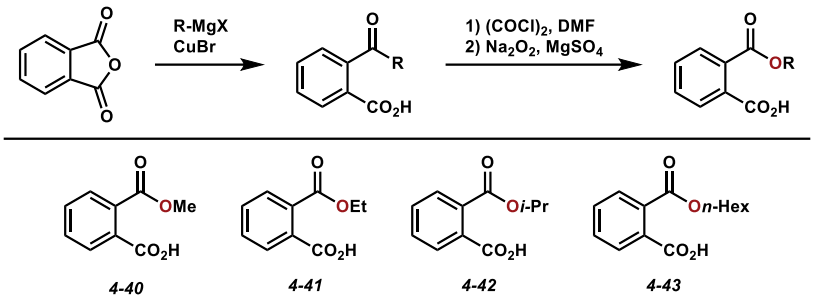

Scheme 4.13. Synthesis and analysis of test substrates for the intramolecular Baeyer-Villiger reaction.

With these results, synthesizing a new dienophile was needed (Scheme 4.14). To utilize the previously developed intramolecular Baeyer-Villiger conditions, a dienophile with a masked carboxylic acid group is preferred. Dienophile **4-37** was synthesized from piperonal in three steps. Like our previous strategy, dienophile **4-37** can either participate in a direct, single-step, or two-step sequence. In the single-step approach with isoprene as the diene, $[Cr(Ph_2phen)_3](BF_4)_3$ catalyzed formation of the [4+2] cycloadduct **4-44** from dienophile **4-37** in 76% yield. Using flow photocatalysis, the same reaction on a 1-mmol scale generates an 82% yield of [4+2] cycloadduct **4-44**. In the two-step sequence, the formation of vinylcyclobutane intermediate **4-45** proceeds in quantitative yield. $[Ru(bpz)_3](PF_6)_2$ can catalyze the subsequent vinylcyclobutane rearrangement to the desired [4+2] cycloadduct **4-44**. Saponification of the ester with lithium hydroxide yields the unmasked carboxylic acid [4+2] cycloadduct **4-46**. Treatment of carboxylic acid **4-46** to the intramolecular Baeyer-Villiger conditions produces **4-47** in 80% yield. Optimization of solvent, stoichiometry, and scalability could help provide the necessary information needed to determine the overall feasibility of this synthetic pathway.

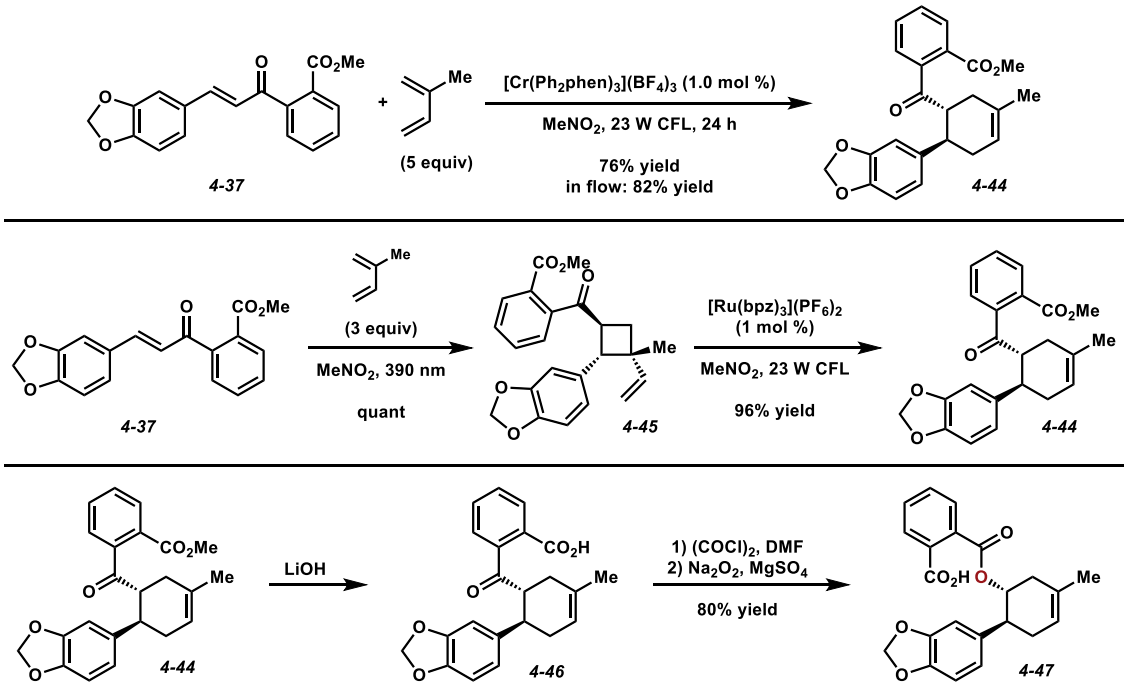

Scheme 4.14. Reaction sequence with dienophile **4-37** and intramolecular Baeyer-Villiger reaction.

4.7 Alternative Strategies and Conclusions

We are always thinking about new methods to help improve our overall route to the Cripowellin alkaloids. One potential strategy that is unexplored is a radical decarboxylative hydroxylation approach (Figure 4.6). Sun and coworkers and Xiao and coworkers both report a decarboxylative hydroxylation of secondary and tertiary carboxylic alcohols under photocatalytic conditions.[23] Sun and coworkers utilize an iridium(III) photocatalyst, while Xiao and coworkers use an organic photosensitizer. Mashima and coworkers report using a cerium photocatalyst under an oxygen atmosphere for a radical decarboxylative hydroxylation.[24] An enzymatic decarboxylation is also an option for this transformation.[25] There are plenty of other conditions not mentioned. This pathway provides a unique, alternative approach to the strategies discussed prior. In conclusion, we have developed unique synthetic design for the synthesis of the Cripowellin alkaloids. With the use of chromium(III) photocatalysis and the development of an

intramolecular Baeyer-Villiger reaction, we synthesized a product in our route in relatively good overall yield. The scalability of these reactions would need to be analyzed to carry forward on this synthetic route.

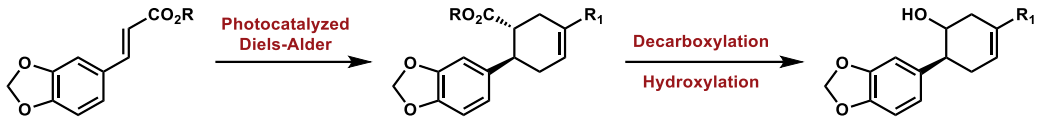

Figure 4.6. Alternative pathway toward the Cripowellin alkaloids.

4.8 Experimental Procedures

4.8.1 Materials and Methods

Reactions were performed under argon atmosphere unless otherwise noted. Dichloromethane, tetrahydrofuran, dimethylformamide, and toluene were purified by passing through activated alumina columns. Nitromethane (99%) and 1,4-dioxane (99.5%) was used as received. Commercially available chemicals were purchased from Alfa Aesar (Ward Hill, MA), Sigma-Aldrich (St. Louis, MO), Oakwood Products, (West Columbia, SC), Strem (Newburport, MA), and TCI America (Portland, OR). Qualitative TLC analysis was performed on 250 mm thick, 60 Å, glass backed, F254 silica (SiliCycle, Quebec City, Canada). Visualization was accomplished with UV light and/or exposure to cerium ammonium molybdate (Hanessian's Stain), $KMnO_4$, or *p*-anisaldehyde stain solutions followed by heating. Flash chromatography was performed using SiliCycle silica gel (230-400 mesh). ^{1}H NMR spectra were acquired on a Varian Mercury Plus NMR (at 400 MHz) and are reported relative to $SiMe_4$ (δ 0.00). ^{13}C NMR spectra were acquired on a Varian Mercury Plus NMR (at 100 MHz) and are reported relative to $SiMe_4$ (δ 0.0). Reactions under blue LED irradiation were performed using a 390 nm Kessil PR160L LED PhotoReaction light. Irradiation with visible light was performed with one 23 W compact fluorescent light bulb (EcoSmart 23 W bright white CFL spiral bulb, 1600 lumens) unless otherwise noted. Cycloadditions using all modes of irradiation were performed using flame-dried borosilicate vials. The internal temperature of the photobox was maintained at 30 °C.

4.8.2 General Procedures

General Prodecure A: [2+2] Cycloaddition Reaction

A flame-dried borosilicate vial was charged with dienophile (1.0 equiv) and $MeNO_2$ (0.25 M) open to air. Isoprene (3.0 equiv) was then added. The vial was then capped and irradiated by a 390 nm Kessil Lamp until full consumption of dienophile, as indicated by TLC. Upon completion, the reaction mixture was concentrated in vacuo and purified by silica gel flash chromatography affording the corresponding [2+2] cycloadduct.

General Procedure B: Vinylcyclobutane to Cyclohexane Rearrangement

A flame-dried borosilicate vial was charged with a [2+2] cycloadduct (1.0 equiv) and $MeNO_2$ (0.10 M) open to air. Photocatalyst (1 mol %) was then added to the reaction mixture. The vial was then capped and irradiated by a 23 W CFL bulb until TLC analysis indicated full consumption of the [2+2] cycloadduct. Upon completion, the reaction mixture was concentrated in vacuo and purified by silica gel flash chromatography to afford the [4+2] cycloadduct.

General Procedure C: Epoxidation

To flame-dried borosilicate vial under argon charged with a [4+2] cycloadduct (1.0 equiv) in CH_2Cl_2 (0.10 M) was added *m*CPBA (1.25 equiv). The reaction mixture was stirred at room temperature until TLC analysis indicated full consumption of starting material. Upon completion, the reaction mixture was quenched upon the addition of sat. aq. Na_2SO_3. The organic layer was separated, and the aqueous layer was extracted with CH_2Cl_2 (3x). The combined organic layers were washed sequentially with sat. aq. Na_2SO_3 (1x), sat. aq. $NaHCO_3$ (1x), and brine (1x), and then dried over Na_2SO_4 and concentrated in vacuo. The crude residue was purified by silica gel flash chromatography to afford epoxide products.

General Procedure D: Intramolecular BV Reaction

To a flame-dried borosilicate vial under argon charged with a carboxylic acid (1.0 equiv) in CH_2Cl_2 (0.10 M) and DMF (1-2 drops), cooled to 0 °C, was added oxalyl chloride (1.3 equiv) dropwise over 5 min. The reaction mixture was monitored by TLC. Upon completion, the reaction mixture was concentrated in vacuo. The crude residue was dissolved in benzene, stirred for 5 min, and then concentrated in vacuo. This process was repeated 2 more times. The crude residue was then dissolved in THF (0.10 M) and H_2O (0.10 M) and cooled to 0 °C. $MgSO_4$ (10 mol %) and Na_2O_2 (2.0 equiv) were added sequentially, and the reaction mixture was stirred to completion, as determined by TLC analysis. The reaction mixture was quenched with 20% aq. H_2SO_4 and extracted with $CHCl_3$ (3x). The combined organic layers were then dried over Na_2SO_4 and concentrated in vacuo. The crude residue was purified by silica gel flash chromatography to afford desired intramolecular BV products.

4.8.3 Synthesis of Nitroalkene 4-19

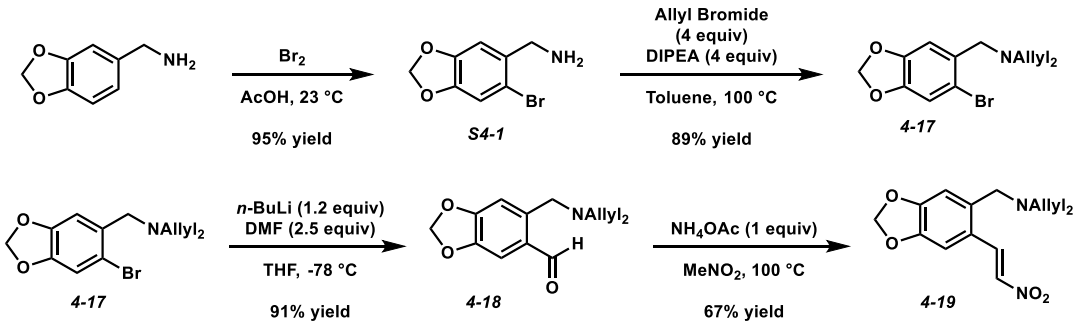

Scheme S4.1. Synthesis of Nitroalkene 4-19.

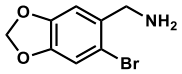

Benzylamine S4-1. Prepared according to a known literature procedure by Kalaitzakis and coworkers.[26]

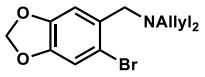

Allylamine 4-17. Prepared according to a known literature procedure by Enders and coworkers.[9]

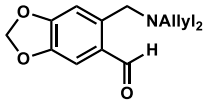

Aldehyde 4-18. Prepared according to a known literature procedure by Enders and coworkers.[9]

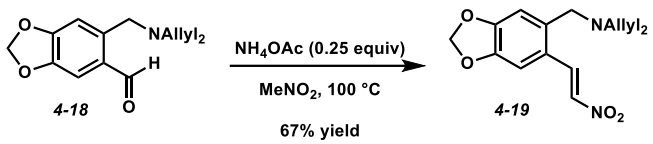

Nitroalkene 4-19. In a flame-dried flask equipped with a reflux condenser, aldehyde **4-18** (0.249 g, 0.960 mmol) and ammonium acetate (18.5 mg, 0.240 mmol) were dissolved in $MeNO_2$ (2.40 mL). The reaction mixture was then heated to 100 °C. After 2 h, the reaction mixture was cooled to room temperature and then concentrated in vacuo. The crude residue was dissolved in EtOAc (20 mL) and washed with H_2O (20 mL). The organic layer was dried over Na_2SO_4 and concentrated in vacuo. The crude residue was purified by silica gel flash chromatography (2:1 hexanes:Et_2O) to afford nitroalkene **4-19** (0.195 g, 67% yield) as a yellow solid.

TLC: R_f = 0.45 in 2:1 hexanes/Et_2O, visualized by UV.

^{1}H NMR (400 MHz, $CDCl_3$): δ 8.60 (d, *J* = 13.5 Hz, 1H), 7.40 (d, *J* = 13.5 Hz, 1H), 6.98 (s, 1H), 6.86 (s, 1H), 6.03 (s, 2H), 6.05-5.83 (comp. m, 6H), 5.22-5.17 (comp. m, 2H), 3.56 (s, 2H), 3.04 (d, *J* = 10.1 Hz, 4H).

^{13}C NMR (100 MHz, $CDCl_3$): δ 150.8, 147.6, 137.5, 137.1, 135.4, 135.3, 123.4, 118.3, 111.6, 106.5, 102.0, 56.6, 55.6.

4.8.4 Synthesis of Dienophiles

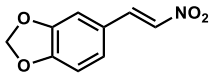

Dienophile 4-A. Prepared according to a known literature procedure by Vaccari and coworkers.[27]

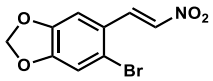

Dienophile 4-B. Prepared according to a known literature procedure by Kolarovic and coworkers.[28]

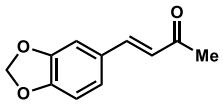

Dienophile 4-C. Prepared according to a known literature procedure by Glaskowski and coworkers.[29]

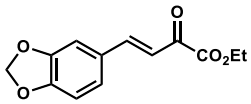

Dienophile 4-D. Prepared according to a known literature procedure by Joharapurker and coworkers.[30]

4.8.5 Synthesis of [2+2] Cycloadducts:

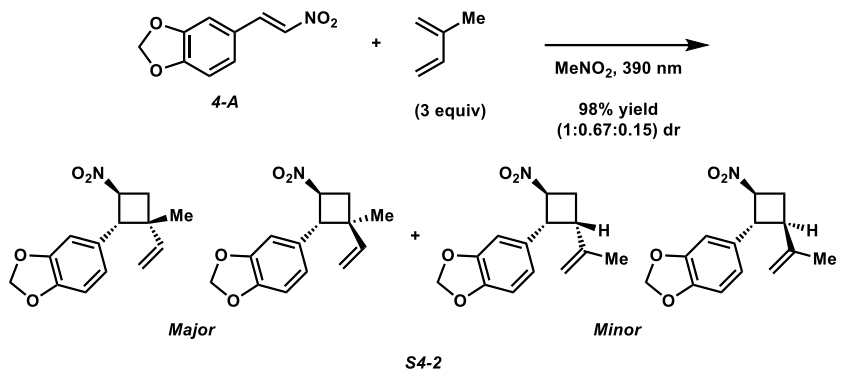

Cycloadducts S4-2. According to General Procedure A, dienophile **4-A** (35.0 mg, 0.181 mmol), isoprene (54.4 µL, 0.544 mmol) and $MeNO_2$ (0.906 mL) were added to a flame-dried vial. The vial was then capped and irradiated by a 390 nm Kessil Lamp until full consumption of dienophile, indicated by TLC. Upon completion, the reaction mixture was concentrated in vacuo and purified by silica gel flash chromatography (4:1 hexanes/EtOAc eluent) to afford cycloadducts **S4-2** (46.4 mg, 98% yield, 1 : 0.67 : 0.15 dr mixture) as a colorless oil.

TLC: R_f = 0.38 in 2:1 hexanes/Et_2O, visualized by UV, stained green in anisaldehyde. **^{1}H NMR** (400 MHz, $CDCl_3$): δ 6.80-6.54 (comp. m, 3H), 6.07 (dd, *J* = 17.3, 10.6 Hz, 1H), 5.94 (s, 2H), 5.25-5.01 (comp. m, 3H), 3.98 (d, *J* = 9.2 Hz, 1H), 2.69 (app. t, *J* = 9.6 Hz, 1H), 2.34 (app. t, *J* = 9.6 Hz, 1H), 0.93 (s, 3H).

^{13}C NMR (100 MHz, $CDCl_3$): δ 148.1, 147.92, 147.86, 147.0, 146.9, 146.8, 145.5, 144.7, 143.3, 140.6, 133.2, 130.7, 129.9, 129.5, 120.7, 120.4, 120.1, 119.8, 113.8, 113.1, 112.3, 111.0, 108.5, 108.4, 108.3, 108.2, 107.7, 107.6, 107.2, 107.1, 101.21, 101.16, 79.7, 79.3, 76.51, 76.45, 56.6, 54.2, 51.4, 48.7, 40.9, 40.6, 40.4, 39.2, 37.1, 35.4, 30.1, 28.3, 28.0, 22.4, 20.2, 20.1.

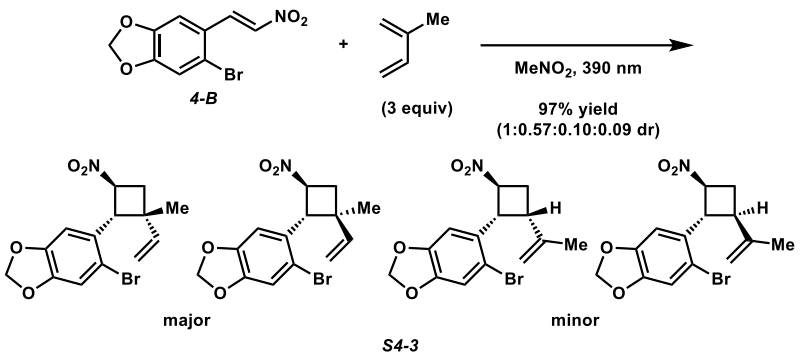

Cycloadducts S4-3. According to General Procedure A, dienophile **4-B** (30.0 mg, 0.110 mmol), isoprene (33.1 µL, 0.331 mmol) and $MeNO_2$ (0.551 mL) were added to a flame-dried vial. The vial was then capped and irradiated by a 390 nm Kessil Lamp until full consumption of dienophile, indicated by TLC. Upon completion, the reaction mixture was concentrated in vacuo and purified by silica gel flash chromatography (4:1 hexanes/EtOAc eluent) to afford cycloadducts **S4-3** (36.8 mg, 97% yield, 1 : 0.57 : 0.10 : 0.09 dr mixture) as a light, yellow oil.

TLC: R_f = 0.31 in 2:1 hexanes/Et_2O, visualized by UV.

^{1}H NMR (400 MHz, $CDCl_3$): δ 7.02 (s, 1H), 6.83 (s, 1H), 6.23 (dd, *J* = 17.3, 10.6 Hz, 1H), 6.01-5.98 (m, 2H), 5.22 (app. q, *J* = 8.6 Hz, 1H), 5.14-5.03 (comp. m, 3H), 2.78 (dd, *J* = 11.6, 8.6 Hz, 1H), 2.30 (dd, *J* = 11.6, 8.6 Hz, 1H), 0.98 (s, 3H).

^{13}C NMR (100 MHz, $CDCl_3$): δ 148.1, 147.9, 147.72, 147.69, 147.6, 147.5, 145.8, 144.3, 143.0, 140.5, 131.1, 128.9, 128.2, 128.1, 115.5, 115.4, 115.0, 114.1, 113.6, 113.24, 113.17, 112.9, 112.4, 112.1, 111.3, 108.8, 108.4, 108.1, 107.6, 102.2, 102.13, 102.08, 79.4, 77.6, 76.2, 76.1, 55.2, 54.7, 51.0, 49.3, 42.4, 41.0, 40.4, 39.4, 35.8, 34.4, 29.6, 29.1, 28.4, 22.6, 20.4, 20.2.

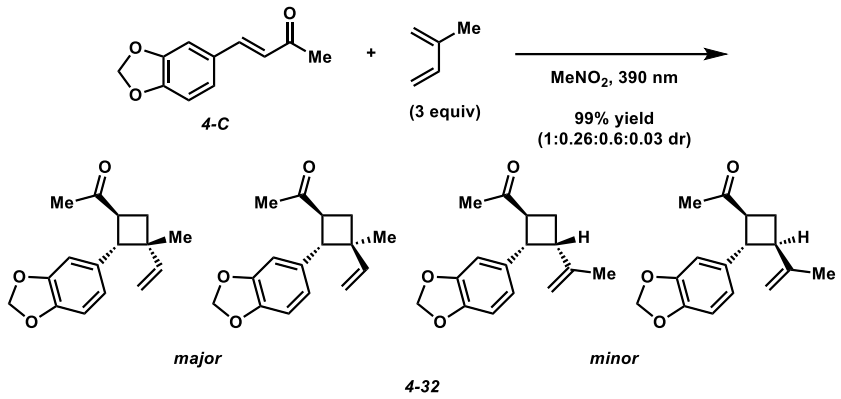

Cycloadducts 4-32. According to General Procedure A, dienophile **4-C** (35.0 mg, 0.184 mmol), isoprene (55.2 µL, 0.552 mmol) and $MeNO_2$ (0.920 mL) were added to a flame-dried vial. The vial was then capped and irradiated by a 390 nm Kessil Lamp until full consumption of dienophile, indicated by TLC. Upon completion, the reaction mixture was concentrated in vacuo and purified by silica gel flash chromatography (4:1 hexanes/EtOAc eluent) to afford cycloadducts **4-32** (47.1 mg, 99% yield, 1 : 0.26 : 0.06 : 0.03 dr mixture) as a colorless oil.

TLC: R_f = 0.40 in 2:1 hexanes/Et_2O, visualized by UV.

^{1}H NMR (400 MHz, $CDCl_3$): δ 6.74 (d, *J* = 7.9 Hz, 1H), 6.64-6.55 (comp. m, 2H), 5.99 (dd, *J* = 17.3, 10.7 Hz, 1H), 5.92 (s, 2H), 5.03-4.93 (comp. m, 2H), 3.51-3.44 (comp. m, 2H), 2.26-2.18 (m, 1H), 2.09 (s, 3H), 1.91-1.85 (m, 1H), 0.89 (s, 3H).

^{13}C NMR (100 MHz, $CDCl_3$): δ 209.1, 209.0, 208.9, 208.4, 147.9, 147.7, 147.6, 147.5, 146.7, 146.5, 146.32, 146.26, 144.6, 143.8, 142.1, 136.6, 134.1, 132.7, 132.5, 121.2, 120.7, 120.23, 120.19, 112.5, 111.7, 110.8, 109.6, 108.3, 108.2, 108.11, 108.06, 107.9, 107.8, 107.3, 100.99, 100.96, 100.9, 53.8, 50.8, 50.3, 49.5, 48.3, 45.9, 45.6, 44.77, 44.75, 43.1, 42.9, 41.5, 33.2, 31.4, 28.5, 28.4, 28.3, 28.2, 27.5, 26.1, 23.8, 22.5, 20.4, 20.1.

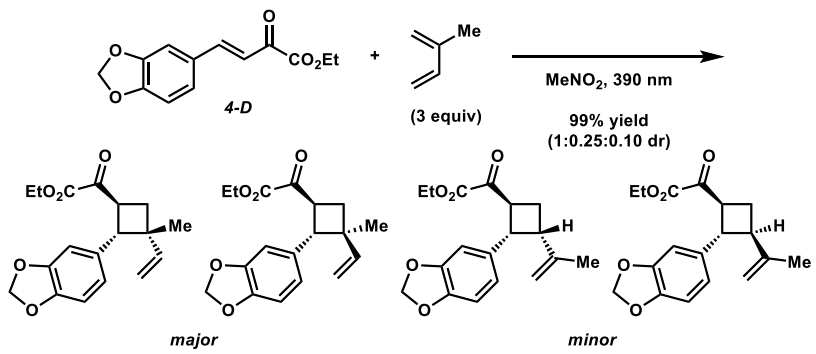

S4-4

Cycloadduct S4-4. According to General Procedure A, dienophile **4-D** (35.0 mg, 0.141 mmol), isoprene (42.3 µL, 0.423 mmol) and $MeNO_2$ (0.705 mL) were added to a flame-dried vial. The vial was then capped and irradiated by a 390 nm Kessil Lamp until full consumption of dienophile, indicated by TLC. Upon completion, the reaction mixture was concentrated in vacuo and purified by silica gel flash chromatography (4:1 hexanes/EtOAc eluent) to afford cycloadduct **S4-4** (44.2 mg, 99% yield, 1 : 0.25 : 0.10 dr mixture) as a colorless oil.

TLC: R_f = 0.42 in 2:1 hexanes/Et_2O, visualized by UV.

^{1}H NMR (400 MHz, $CDCl_3$): δ 6.73 (d, *J* = 7.9 Hz, 1H), 6.64-6.54 (comp. m, 2H), 6.01 (dd, *J* = 17.3, 10.6 Hz, 1H), 5.91 (s, 2H), 5.07-4.94 (comp. m, 2H), 4.27 (q, *J* = 7.1 Hz, 2H), 4.14 (app. q, *J* = 10.3 Hz, 1H), 3.64 (d, *J* = 10.3 Hz, 1H), 2.26 (app. t, *J* = 10.3 Hz, 1H), 2.01 (dd, *J* = 10.7, 9.0 Hz, 1H), 1.30 (t, *J* = 7.1 Hz, 3H), 0.94 (s, 3H).

^{13}C NMR (100 MHz, $CDCl_3$): δ 194.74, 194.70, 194.1, 161.38, 161.35, 161.1, 147.8, 147.6, 147.5, 146.5, 146.4, 146.3, 146.1, 141.8, 136.0, 132.2, 132.1, 120.7, 120.20, 120.17, 112.9, 112.2, 110.0, 108.2, 108.14, 108.05, 108.0, 107.8, 107.4, 101.0, 101.0, 62.6, 62.51, 62.45, 53.1, 50.2, 47.3, 46.4, 45.1, 43.6, 42.1, 41.6, 40.7, 34.2, 32.4, 27.6, 27.2, 20.3, 20.0, 14.03, 13.99.

4.8.6 Flow Photocatalysis Setup and Experimental

Mechanical Operator: Syringe Pump
PFA tubing (1/16th inch inner diameter)
Luerlock Tubing adapter
2 x 23 W CFL Bulbs
Typical photobox setup

Syringe Diameter matters…
Pump settings: 0.25-0.50 mL/h

Typical Flow Photocatalyzed Reaction: A flame-dried borosilicate vial was charged with dienophile (1.0 equiv), $[Ru(bpz)_3](PF_6)_2$ (1 mol %), isoprene (5 equiv), and $MeNO_2$ (0.20 M), open to air. The reaction mixture was drawn up into a syringe, washing the vial once with $MeNO_2$ (0.20 M, total concentration = 0.10 M). The syringe was equipped with the tubing adapter, hooked up to the PFA tubing, and then the syringe pump was input with the appropriate pump settings and flow rate. The syringe in the syringe pump was covered with aluminum foil and pumped to completion. Upon emptying the syringe, an acetone syringe was equipped at the same flow rate until all the reaction mixture was through the tubing. Upon completion, the reaction mixture was concentrated in vacuo and purified by silica gel flash chromatography to afford cyclohexene products.

4.8.7 Synthesis of Cyclohexene Products

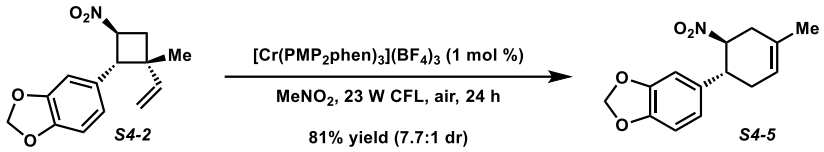

Cyclohexene S4-5. According to General Procedure B, cycloadduct **S4-2** (30.0 mg, 0.115 mmol) and $[Cr(PMP_2phen)_3](BF_4)_3$ (1.7 mg, 0.00115 mmol) were dissolved in $MeNO_2$ (1.15 mL). The vial was then capped and irradiated by a 23 W CFL bulb until TLC analysis indicated full consumption of the [2+2] cycloadduct. Upon completion, the reaction mixture was concentrated in vacuo and purified by silica gel flash chromatography (2:1 hexanes/Et_2O eluent) to afford cyclohexene **S4-5** (24.3 mg, 81% yield, 7.7:1 dr) yield as a colorless oil.

TLC: R_f = 0.40 in 2:1 hexanes/Et_2O, visualized by UV.

^{1}H NMR (400 MHz, $CDCl_3$): δ 6.79 (comp. m, 3H), 5.93 (s, 2H), 5.48 (app. s, 1H), 4.97-4.88 (app. td, *J* = 10.7, 5.5 Hz, 1H), 3.33-3.22 (app. td, *J* = 10.7, 5.5 Hz, 1H), 2.83-2.19 (comp. m, 4H), 1.75 (s, 3H).

^{13}C NMR (100 MHz, $CDCl_3$): δ 148.0, 147.0, 133.8, 130.4, 120.9, 120.7, 120.2, 111.1, 108.62, 108.58, 107.7, 107.2, 101.3, 101.2, 88.1, 79.4, 51.6, 44.1, 40.5, 35.8, 33.3, 30.2, 22.9, 20.3.

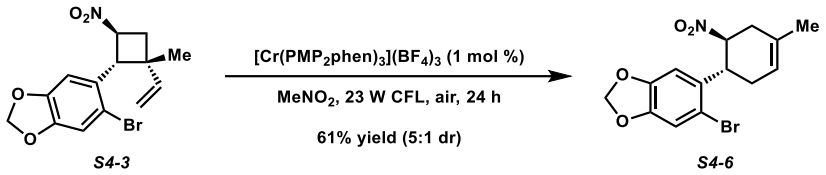

Cyclohexene S4-6. According to General Procedure B, cycloadduct **S4-3** (30.0 mg, 0.0882 mmol) and $[Cr(PMP_2phen)_3](BF_4)_3$ (1.3 mg, 0.000882 mmol) were dissolved in $MeNO_2$ (0.882 mL). The vial was then capped and irradiated by a 23 W CFL bulb until TLC analysis indicated full consumption of the [2+2] cycloadduct. Upon completion, the reaction mixture was concentrated in vacuo and purified by silica gel flash chromatography (2:1 hexanes/Et_2O eluent) to afford cyclohexene **S4-6** (18.3 mg, 61% yield, 5:1 dr) yield as a colorless oil.

TLC: R_f = 0.35 in 2:1 hexanes/Et_2O, visualized by UV.

^{1}H NMR (400 MHz, $CDCl_3$): δ 6.99 (s, 1H), 6.73 (s, 1H), 5.96 (app. dd, J = 4.9, 1.2 Hz, 2H), 5.48 (app. s, 1H), 5.06-4.93 (m, 1H), 4.01-3.89 (m, 1H), 2.83-2.71 (m, 1H), 2.65-2.42 (comp. m, 3H), 1.76 (s, 3H).

^{13}C NMR (100 MHz, $CDCl_3$): δ 148.1, 147.6, 140.6, 130.6, 120.5, 114.1, 113.4, 108.8, 102.1, 102.0, 85.9, 55.3, 42.5, 35.3, 34.4, 31.8, 29.2, 23.0.

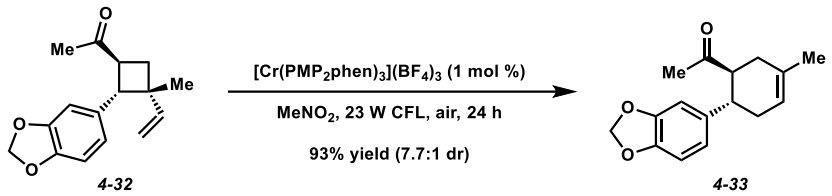

Cyclohexene 4-33. According to General Procedure B, cycloadduct **4-32** (35.0 mg, 0.135 mmol) and $[Cr(PMP_2phen)_3](BF_4)_3$ (2.0 mg, 0.00135 mmol) were dissolved in $MeNO_2$ (1.35 mL). The vial was then capped and irradiated by a 23 W CFL bulb until TLC analysis indicated full consumption of the [2+2] cycloadduct. Upon completion, the reaction mixture was concentrated in vacuo and purified by silica gel flash chromatography (2:1 hexanes/Et_2O eluent) to afford cyclohexene **4-33** (32.6 mg, 93% yield, 7.7:1 dr) yield as a colorless oil.

TLC: R_f = 0.42 in 2:1 hexanes/Et_2O, visualized by UV.

^{1}H NMR (400 MHz, $CDCl_3$): δ 6.74-6.60 (comp. m, 3H), 5.91 (s, 2H), 5.45 (app. s, 1H), 2.98 (app. td, *J* = 10.7, 5.5 Hz, 1H), 2.85 (app. td, *J* = 10.7, 5.5 Hz, 1H), 2.31-2.08 (comp. m, 4H), 1.88 (s, 3H), 1.71 (s, 3H).

^{13}C NMR (100 MHz, $CDCl_3$): δ 212.2, 208.5, 147.9, 147.8, 146.5, 146.4, 146.2, 138.1, 136.7, 132.3, 120.74, 120.65, 120.3, 109.7, 108.4, 108.3, 107.8, 107.4, 101.1, 101.0, 53.8, 50.4, 48.4, 44.9, 42.6, 34.3, 33.4, 30.0, 28.3, 26.1, 23.3, 20.4.

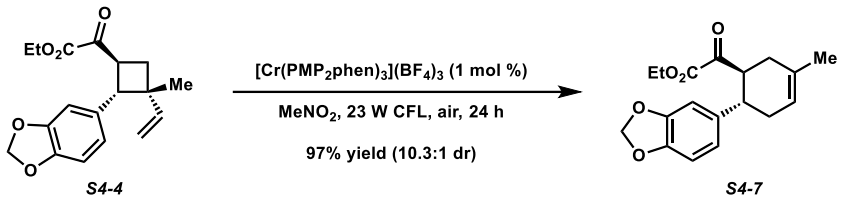

Cyclohexene S4-7. According to General Procedure B, cycloadduct **S4-4** (35.0 mg, 0.111 mmol) and $[Cr(PMP_2phen)_3](BF_4)_3$ (1.7 mg, 0.00111 mmol) were dissolved in $MeNO_2$ (1.11 mL). The vial was then capped and irradiated by a 23 W CFL bulb until TLC analysis indicated full consumption of the [2+2] cycloadduct. Upon completion, the reaction mixture was concentrated in vacuo and purified by silica gel flash chromatography (2:1 hexanes/Et_2O eluent) to afford cyclohexene **S4-7** (34.0 mg, 97% yield, 10.3:1 dr) yield as a colorless oil.

TLC: R_f = 0.44 in 2:1 hexanes/Et_2O, visualized by UV.

^{1}H NMR (400 MHz, $CDCl_3$): δ 6.71-6.60 (comp. m, 3H), 5.89 (s, 2H), 5.50 (app. s, 1H), 4.12 (q, *J* = 7.1 Hz, 2H), 3.77 (app. td, *J* = 10.7, 5.5 Hz, 1H), 2.95 (app. td, *J* = 10.7, 5.5 Hz, 1H), 2.39-2.10 (comp. m, 4H), 1.72 (s, 3H), 1.23 (t, *J* = 7.1 Hz, 3H).

^{13}C NMR (100 MHz, $CDCl_3$): δ 197.9, 194.1, 161.4, 161.2, 147.9, 147.8, 146.5, 146.3, 146.1, 137.0, 136.0, 132.0, 121.0, 120.7, 120.2, 110.1, 108.4, 108.3, 108.2, 107.4, 101.1, 101.0, 62.5, 62.3, 48.4, 47.4, 46.4, 45.2, 42.9, 42.7, 34.3, 33.0, 29.8, 27.2, 23.3, 20.3, 14.01, 13.97.

4.8.8 Synthesis of Epoxides

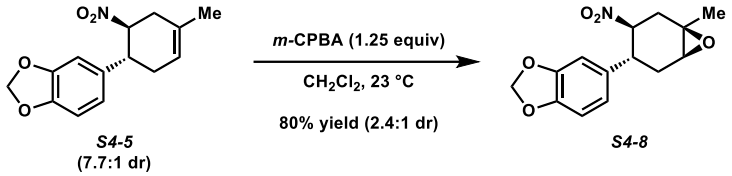

Epoxide S4-8. According to General Procedure C, to a flame-dried vial under argon, cyclohexene **S4-5** (40.0 mg, 0.153 mmol) was dissolved in CH_2Cl_2 (1.53 mL) and *m*-CPBA (44.0 mg, 75% by weight, 0.191 mmol) was added at room temperature. The reaction mixture was stirred at room temperature. Upon completion, the reaction mixture was quenched upon the addition of sat. aq. Na_2SO_3 (5 mL). The organic layer was separated, and the aqueous layer was extracted with CH_2Cl_2 (3 x 10 mL). The combined organic layers were washed sequentially with sat. aq. Na_2SO_3 (20 mL), sat. aq. $NaHCO_3$ (20 mL), and brine (20 mL), and then dried over Na_2SO_4 and concentrated in vacuo. The crude residue was purified by silica gel flash chromatography (2:1 hexanes/Et_2O eluent) to afford epoxide **S4-8** (34.0 mg, 80% yield, 2.4:1 dr) as a colorless oil.

TLC: R_f = 0.35 in 2:1 hexanes/Et_2O, visualized by UV.

^{1}H NMR (400 MHz, $CDCl_3$): δ 6.85-6.53 (comp. m, 3H), 5.92 (s, 2H), 4.85-4.60 (m, 1H), 3.35-3.01 (comp. m, 2H), 2.76-2.56 (m, 1H), 2.52-2.35 (comp. m, 2H), 2.17-2.20 (m, 1H), 1.44 (s, 3H).

^{13}C NMR (100 MHz, $CDCl_3$): δ 148.0, 147.2, 132.9, 132.4, 121.0, 108.73, 108.66, 107.7, 101.3, 87.0, 86.8, 59.3, 59.2, 58.1, 56.0, 43.7, 39.4, 36.0, 34.6, 33.0, 32.3, 23.9, 22.5.

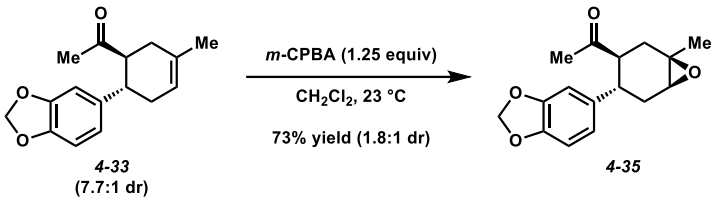

Epoxide 4-35. According to General Procedure C, to a flame-dried vial under argon, cyclohexene **4-33** (40.0 mg, 0.155 mmol) was dissolved in CH_2Cl_2 (1.55 mL) and *m*-CPBA (44.5 mg, 75% by weight, 0.194 mmol) was added at room temperature. The reaction mixture was stirred at room temperature. Upon completion, the reaction mixture was quenched upon the addition of sat. aq. Na_2SO_3 (5 mL). The organic layer was separated, and the aqueous layer was extracted with CH_2Cl_2 (3 x 10 mL). The combined organic layers were washed sequentially with sat. aq. Na_2SO_3 (20 mL), sat. aq. $NaHCO_3$ (20 mL), and brine (20 mL), and then dried over Na_2SO_4 and concentrated in vacuo. The crude residue was purified by silica gel flash chromatography (2:1 hexanes/Et_2O eluent) to afford epoxide **4-35** (31.0 mg, 73% yield, 1.8:1 dr) as a colorless oil.

TLC: R_f = 0.45 in 2:1 hexanes/Et_2O, visualized by UV.

^{1}H NMR (400 MHz, $CDCl_3$): δ 6.74-6.54 (comp. m, 3H), 5.92 (s, 2H), 3.16-3.03 (m, 1H), 3.01-2.88 (m, 1H), 2.71-2.60 (m, 1H), 2.38-2.25 (m, 1H), 2.17-2.07 (m, 1H), 2.03-1.96 (m,1H), 1.93-1.86 (m, 1H), 1.83 (s, 3H), 1.39 (s, 3H).

^{13}C NMR (100 MHz, $CDCl_3$): δ 210.8, 147.9, 146.4, 137.1, 136.7, 120.82, 120.75, 108.6, 108.5, 107.92, 107.87, 101.10, 101.08, 60.2, 58.9, 58.2, 56.5, 53.2, 50.3, 42.1, 37.7, 33.8, 33.6, 33.4, 31.9, 31.3, 28.8, 24.3, 22.9.

4.8.9 Intramolecular Baeyer-Villiger Reaction

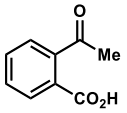

Benzoic Acid S4-9. Prepared according to a known literature procedure by Li and coworkers.[31]

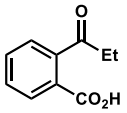

Benzoic Acid S4-10. Prepared according to a known literature procedure by Yang and coworkers.[32]

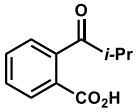

Benzoic Acid S4-11. Prepared according to a known literature procedure by Yang and coworkers.[32]

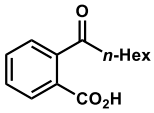

Benzoic Acid S4-12. Prepared according to a known literature procedure by Yang and coworkers.[32]

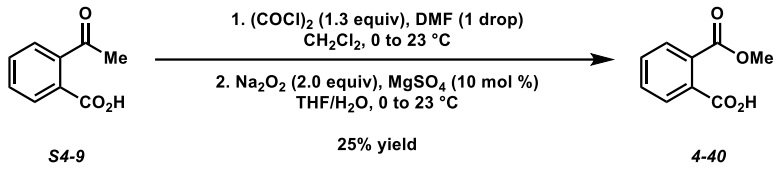

Ester 4-40. According to General Procedure D, to a flame-dried vial charged with benzoic acid **S4-9** (16.4 mg, 0.0999 mmol) in CH_2Cl_2 (0.999 mL) and DMF (1 drop), cooled to 0 °C, was added oxalyl chloride (11.1 µL, 0.130 mmol), and the reaction mixture was stirred at 0 °C. Upon completion, the reaction mixture was concentrated in vacuo. The crude residue was dissolved in benzene (1 mL), stirred for 5 min, and then concentrated in vacuo. This process was repeated 2 more times. The crude residue was then dissolved in THF (0.999 mL) and H_2O (0.999 mL) and cooled to 0 °C. $MgSO_4$ (1.2 mg, 0.00999 mmol) and Na_2O_2 (15.6 mg, 0.200 mmol) were added sequentially, and the reaction mixture was stirred to completion, as determined by TLC. The reaction mixture was quenched with 20% aq. H_2SO_4 (5 mL) and extracted with $CHCl_3$ (3 x 10 mL). The combined organic layers were then dried over Na_2SO_4 and concentrated in vacuo, affording analytically pure ester **4-40** (4.5 mg, 25% yield). The spectroscopic data were in agreement with the literature data.[33]

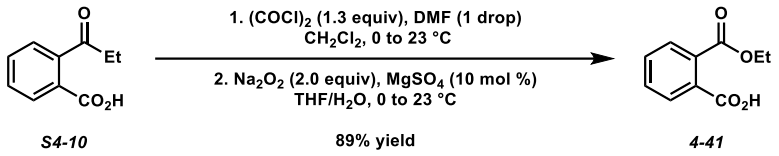

Ester 4-41. According to General Procedure D, to a flame-dried vial charged with benzoic acid **S4-10** (17.8 mg, 0.0999 mmol) in CH_2Cl_2 (0.999 mL) and DMF (1 drop), cooled to 0 °C, was added oxalyl chloride (11.1 µL, 0.130 mmol), and the reaction mixture was stirred at 0 °C. Upon completion, the reaction mixture was concentrated in vacuo. The crude residue was dissolved in benzene (1 mL), stirred for 5 min, and then concentrated in vacuo. This process was repeated 2 more times. The crude residue was then dissolved in THF (0.999 mL) and H_2O (0.999 mL) and cooled to 0 °C. $MgSO_4$ (1.2 mg, 0.00999 mmol) and Na_2O_2 (15.6 mg, 0.200 mmol) were added sequentially, and the reaction mixture was stirred to completion, as determined by TLC. The reaction mixture was quenched with 20% aq. H_2SO_4 (5 mL) and extracted with $CHCl_3$ (3 x 10 mL). The combined organic layers were then dried over Na_2SO_4 and concentrated in vacuo, affording analytically pure ester **4-41** (17.3 mg, 89% yield). The spectroscopic data were in agreement with the literature data.[33]

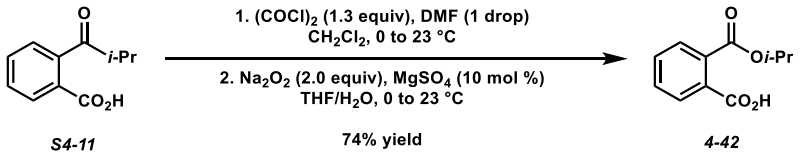

S4-11 *4-42*

Ester 4-42. According to General Procedure D, to a flame-dried vial charged with benzoic acid **S4-11** (19.2 mg, 0.0999 mmol) in CH_2Cl_2 (0.999 mL) and DMF (1 drop), cooled to 0 °C, was added oxalyl chloride (11.1 µL, 0.130 mmol), and the reaction mixture was stirred at 0 °C. Upon completion, the reaction mixture was concentrated in vacuo. The crude residue was dissolved in benzene (1 mL), stirred for 5 min, and then concentrated in vacuo. This process was repeated 2 more times. The crude residue was then dissolved in THF (0.999 mL) and H_2O (0.999 mL) and cooled to 0 °C. $MgSO_4$ (1.2 mg, 0.00999 mmol) and Na_2O_2 (15.6 mg, 0.200 mmol) were added sequentially, and the reaction mixture was stirred to completion. The reaction mixture was quenched with 20% aq. H_2SO_4 (5 mL) and extracted with $CHCl_3$ (3 x 10 mL). The combined organic layers were then dried over Na_2SO_4 and concentrated in vacuo, affording analytically pure ester **4-42** (15.4 mg, 74% yield). The spectroscopic data were in agreement with the literature data.[33]

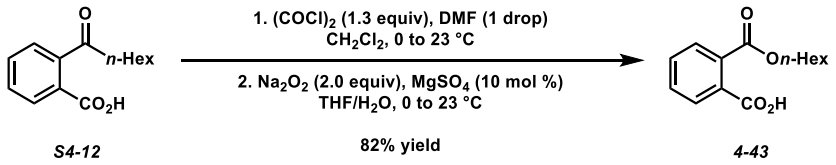

S4-12 *4-43*

Ester 4-43. According to General Procedure D, to a flame-dried vial charged with benzoic acid **S4-12** (23.0 mg, 0.0982 mmol) in CH_2Cl_2 (0.982 mL) and DMF (1 drop), cooled to 0 °C, was added oxalyl chloride (10.9 µL, 0.128 mmol), and the reaction mixture was stirred at 0 °C. Upon completion, the reaction mixture was concentrated in vacuo. The crude residue was dissolved in benzene (1 mL), stirred for 5 min, and then concentrated in vacuo. This process was repeated 2 more times. The crude residue was then dissolved in THF (0.982 mL) and H_2O (0.982 mL) and cooled to 0 °C. $MgSO_4$ (1.2 mg, 0.00982 mmol) and Na_2O_2 (15.3 mg, 0.196 mmol) were added sequentially, and the reaction mixture was stirred to completion. The reaction mixture was quenched with 20% aq. H_2SO_4 (5 mL) and extracted with $CHCl_3$ (3 x 10 mL). The combined organic layers were then dried over Na_2SO_4 and concentrated in vacuo, affording analytically pure ester **4-43** (20.1 mg, 82% yield). The spectroscopic data were in agreement with the literature data.[34]

4.8.10 IMBV toward Cripowellin

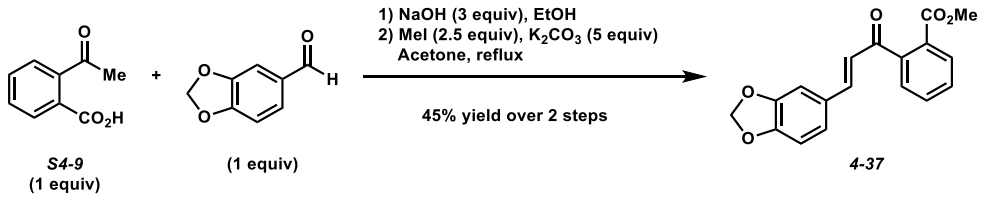

Dienophile 4-37. To a flask charge with benzoic acid **S4-9** (1.05 g, 6.40 mmol), piperonal (0.960 g, 6.40 mmol) in EtOH (12.8 mL) was added NaOH pellets (0.767 g, 19.2 mmol) at room temperature. After 24 h, the reaction mixture was concentrated in vacuo. The crude residue was dissolved in 1 M aq. HCl until pH = 2. The aqueous layer was then extracted with EtOAc (3 x 50 mL). The combined organic extracts were washed sequentially with H_2O (100 mL) and brine (100 mL), dried over Na_2SO_4, and concentrated in vacuo, affording a crude yellow solid. The crude yellow solid and K_2CO_3 (4.42 g, 32.0 mmol) were suspended in acetone (32.0 mL) and methyl iodide (0.995 mL, 16.0 mmol) was added. The mixture was heated to reflux for 8 h. Upon completion, the reaction mixture was cooled to room temperature, filtered through celite (acetone eluent), and concentrated in vacuo. The crude residue was dissolved in EtOAc (100 mL) and washed sequentially with H_2O (50 mL) and brine (50 mL), dried over Na_2SO_4, and concentrated in vacuo. The crude residue was purified by silica gel flash chromatography (4:1 hexanes/EtOAc eluent) to afford dienophile **4-37** (0.893 g, 45% yield over 2 steps) as an off-white solid.

TLC: R_f = 0.65 in 2:1 hexanes/EtOAc, visualized by UV.

^{1}H NMR (400 MHz, $CDCl_3$): δ 7.97 (dd, *J* = 7.5, 1.0 Hz, 1H), 7.61 (app. dt, *J* = 7.5, 1.3 Hz, 1H), 7.53 (app. dt, *J* = 7.5, 1.3 Hz, 1H), 7.43 (dd, *J* = 7.5, 1.0 Hz, 1H), 7.16 (d, *J* = 16.1 Hz, 1H), 7.04 (d, *J* = 1.6 Hz, 1H), 6.95 (dd, *J* = 8.0, 1.6 Hz, 1H), 6.86 (d, *J* = 16.1 Hz, 1H), 6.78 (d, *J* = 8.0 Hz, 1H), 6.00 (s, 2H), 3.81 (s, 3H).

^{13}C NMR (100 MHz, $CDCl_3$): δ 196.2, 167.1, 150.1, 148.6, 145.4, 142.1, 132.2, 130.2, 129.8, 129.6, 127.8, 125.4, 125.2, 108.7, 106.8, 101.8, 52.5.

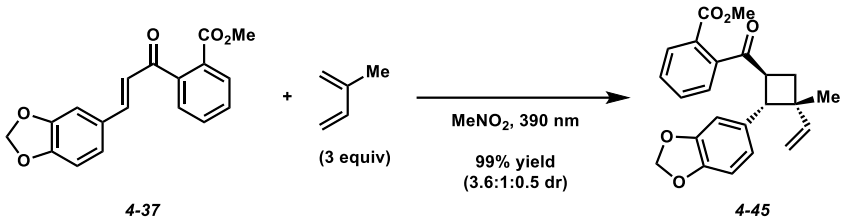

Cycloadduct 4-45. According to General Procedure A, dienophile **4-37** (50.0 mg, 0.161 mmol), isoprene (48.3 µL, 0.483 mmol) and $MeNO_2$ (0.806 mL) were added to a flame-dried vial. The vial was then capped and irradiated by a 390 nm Kessil Lamp until full consumption of dienophile, indicated by TLC. Upon completion, the reaction mixture was concentrated in vacuo and purified by silica gel flash chromatography (4:1 hexanes/EtOAc eluent) to afford cycloadduct **4-45** (60.4 mg, 99% yield, 3.6 : 1 : 0.5 dr) as a colorless oil.

TLC: R_f = 0.56 in 2:1 hexanes/Et_2O, visualized by UV.

^{1}H NMR (400 MHz, $CDCl_3$): δ 7.98-7.79 (m, 1H), 7.52-7.42 (comp. m, 2H), 7.28-7.19 (m, 1H), 6.69-6.64 (m, 1H), 6.57 (s, 1H), 6.52-6.46 (m, 1H), 6.05 (dd, *J* = 17.2, 10.7 Hz, 1H), 5.89 (s, 2H), 5.05-4.95 (comp. m, 2H), 3.94 (app. q, *J* = 8.9 Hz, 2H), 3.82 (s, 3H), 3.78-3.73 (m, 1H), 2.41 (app. t, *J* = 10.3 Hz, 1H), 1.96 (dd, *J* = 10.6, 8.7 Hz, 1H) , 0.91 (s, 3H).

^{13}C NMR (100 MHz, $CDCl_3$): δ 206.5, 206.3, 205.4, 167.3, 167.1, 167.0, 147.7, 147.5, 147.4, 147.3, 146.9, 146.5, 146.2, 146.13, 146.08, 144.8, 143.0, 142.8, 142.3, 142.0, 141.9, 136.6, 134.3, 132.9, 132.7, 132.3, 132.2, 132.1, 132.0, 130.1, 130.0, 129.9, 129.80, 129.77, 129.0, 128.4, 128.2, 126.74, 126.72, 126.5, 121.3, 120.7, 120.3, 120.2, 112.5, 111.9, 110.9, 109.8, 108.3, 108.2, 108.1, 108.0, 107.9, 107.8, 107.4, 101.0, 100.9, 53.7, 52.7, 52.64, 52.56, 51.0, 49.4, 48.7, 48.2, 46.0, 45.2, 45.0, 44.5, 43.4, 43.1, 35.1, 33.5, 27.9, 27.6, 25.6, 22.4, 20.4, 20.0.

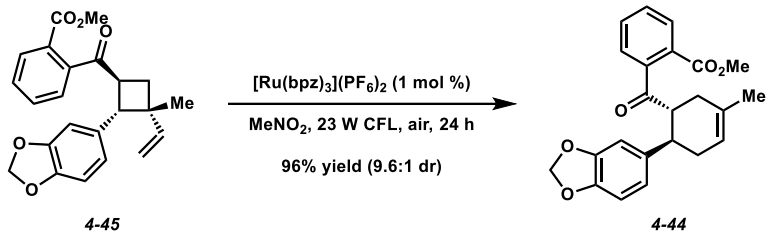

Cyclohexene 4-44. According to General Procedure B, cycloadduct **4-45** (50.0 mg, 0.132 mmol) and $[Ru(bpz)_3](PF_6)_2$ (1.1 mg, 0.00132 mmol) were dissolved in $MeNO_2$ (1.32 mL). The vial was then capped and irradiated by a 23 W CFL bulb until TLC analysis indicated full consumption of the [2+2] cycloadduct. Upon completion, the reaction mixture was concentrated in vacuo and purified by silica gel flash chromatography (4:1 hexanes/EtOAc) to afford cyclohexene **4-44** (48.0 mg, 96% yield, 9.6:1 dr) yield as a colorless oil.

TLC: R_f = 0.60 in 2:1 hexanes/Et_2O, visualized by UV.

^{1}H NMR (400 MHz, $CDCl_3$): δ 7.73 (d, *J* = 7.6 Hz, 1H), 7.37 (app. t, *J* = 7.6 Hz, 1H), 7.29 (app. t, *J* = 7.6 Hz, 1H), 6.82 (d, *J* = 7.6 Hz, 1H), 6.59-6.49 (comp. m, 2H), 6.51 (s, 1H), 5.82 (dd, *J* = 17.7, 1.3 Hz, 2H), 5.47 (app. s, 1H), 3.86 (s, 3H), 3.41 (app. td, *J* = 10.7, 5.5 Hz, 1H), 2.98 (app. td, *J* = 10.7, 5.5 Hz, 1H), 2.62-2.51 (m, 1H), 2.36-2.13 (comp. m, 3H), 1.73 (s, 3H).

^{13}C NMR (100 MHz, $CDCl_3$): δ 207.7, 167.8, 147.6, 146.1, 142.9, 138.2, 133.2, 131.5, 129.8, 129.5, 129.3, 127.6, 121.1, 120.1, 108.12, 108.09, 100.8, 52.8, 52.5, 43.5, 34.2, 33.9, 23.5.

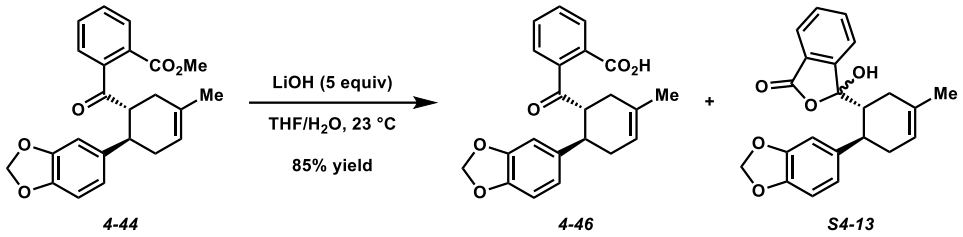

Benzoic Acid and Hemiacetal 4-46 and S4-13. Cyclohexene **4-44** (0.125 g, 0.330 mmol) was dissolved in THF (3.30 mL). LiOH (39.6 mg, 1.65 mmol) was dissolved in H_2O (3.30 mL). The solution of LiOH/H_2O was added dropwise over 5 min to the cyclohexene **4-44**/THF mixture, and the resulting mixture was stirred to completion, as determined by TLC analysis. Upon completion, the reaction mixture was diluted with 1 M aq. HCl until pH = 2. The aqueous layer was extracted with EtOAc (3 x 20 mL). The combined organic layers were washed sequentially with H_2O (30 mL) and brine (30 mL), dried over Na_2SO_4, and concentrated in vacuo. The crude residue was purified by silica gel flash chromatography (2:1 hexane/EtOAc with 1% AcOH) to afford a mixture of benzoic acid **4-46** and hemiacetal **S4-13** (0.102 g, 85% yield) as a white solid.

TLC: R_f = 0.30 in 2:1 hexanes/EtOAc with 1% AcOH, visualized by UV.

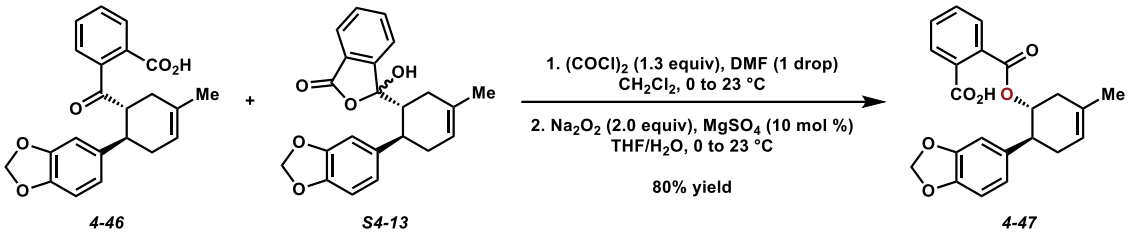

Ester 4-47. According to General Procedure D, to a flame-dried vial charged with a mixture of benzoic acid **4-46** and hemiacetal **S4-13** (35.0 mg, 0.0960 mmol) in CH_2Cl_2 (0.960 mL) and DMF (1 drop), cooled to 0 °C, was added oxalyl chloride (10.7 µL, 0.125 mmol), and the reaction mixture was stirred at 0 °C. Upon completion, the reaction mixture was concentrated in vacuo. The crude residue was dissolved in benzene (1 mL), stirred for 5 min, and then concentrated in vacuo. This process was repeated 2 more times. The crude residue was then dissolved in THF (0.960 mL) and H_2O (0.960 mL) and cooled to 0 °C. $MgSO_4$ (1.1 mg, 0.00960 mmol) and Na_2O_2 (15.0 mg, 0.192 mmol) were added sequentially, and the reaction mixture was stirred to completion. The reaction mixture was quenched with 20% aq. H_2SO_4 (5 mL) and extracted with $CHCl_3$ (3 x 10 mL). The combined organic layers were then dried over Na_2SO_4 and concentrated in vacuo. The crude residue was purified by silica gel flash chromatography (2:1 hexanes/EtOAc with 1% AcOH) to afford ester **4-47** (29.2 mg, 80% yield) as a while solid.

TLC: R_f = 0.53 in 2:1 hexane/EtOAc with 1% AcOH, visualized by UV.

^{1}H NMR (400 MHz, $CDCl_3$): δ 9.81-8.52 (br. m, 1H), 7.90-7.79 (m, 1H), 7.59-7.42 (comp. m, 2H), 7.21-7.14 (comp. m, 1H), 6.78 (app. s, 1H), 6.73 (app. s, 2H), 5.90 (s, 2H), 5.51-5.38 (comp. m, 2H), 3.09-2.97 (comp. m, 1H), 2.59-2.17 (comp. m, 4H), 1.68 (s, 3H).

^{13}C NMR (100 MHz, $CDCl_3$): δ 167.8, 147.7, 146.2, 136.3, 132.0, 131.7, 130.7, 129.9, 128.5, 121.1, 120.2, 108.2, 108.1, 101.0, 74.8, 44.3, 35.3, 32.9, 23.2

4.9 References and Notes

[1] a) Kilgore, M. B.; Kutchan, T. M. *Phytochem Rev*. **2016**, *15*, 317-337. b) https://www.britannica.com/plant/Amaryllidaceae.

[2] Snijman, D. A.; Linder, H. P. *Ann. Mo. Bot. Gard*. **1996**, *83*, 362-386.

[3] a) Fennell, C. W.; van Staden, J. *J. Ethnopharmacology* **2001**, *78*, 15-26. b) Anonymous *World Malaria* Report 2015; World Health Organization: Geneva, Switzerland, 2015.

[4] a) Bastida, J.; Berkov, S.; Torras, L.; Pigni, N. B.; de Andrade, J. P.; Martínez, V.; Viladomat, F. *In Recent Advances in Pharmaceutical Sciences*; Muñoz-Torrero, D., Ed.; Transworld Research Network: Kerala, India, 2011; p 65. b) Jin, Z.; Yao, G. *Nat. Prod. Rep*. **2019**, *36*, 1462-1488.

[5] a) Velten, R.; Erdelen, C.; Gehling, M.; Göhrt, A.; Gondol, D.; Lenz, J.; Lockhoff, O.; Wachendorff, U.; Wendisch, D. *Tetrahedron Lett.* **1998**, *39*, 1737-1740. b) Presley C. C.; Krai, P.; Dalal, S.; Su, Q.; Cassera, M.; Goetz, M.; Kingston, D. G. I. *Bioorg. Med. Chem.* **2016**, *24*, 5418-5422.

[6] Ka, S.; Kiorala, M.; Mérindol, N.; Desgagné-Penix, I. *Molecules* **2020**, *25*, 4901.

[7] Gehling, M.; Goehrt, A.; Gondol, D.; Lenz, J.; Lockhoff, O.; Moeschler, H.-F.; Velten, R.; Wendisch, D.; Andersch, W.; Erdelen, C.; Harder, A.; Mencke, N.; Turberg, A.; Wachendorff-Neumann, U. DE19610279A1, **1997**.

[8] Antonicek, H. -P.; Velten, R.; Jeschke, P. WO2006136309A1, **2006**.

[9] Enders, D.; Lenzen, A.; Backes, M.; Janeck, C.; Catlin, K.; Lannou, M.-I.; Runsink, J.; Raabe, G. *J. Org. Chem.* **2005**, *70*, 10538-10551.

[10] Beck, D. E.; Agama, K.; Marchand, C.; Chergui, A.; Pommier, Y.; Cushman, M. *J. Med. Chem.* **2014**, *57*, 1495-1512.

[11] Noland, W. E. *Chem. Rev*. **1955**, *55*, 137-155.

[12] a) Ghavre, M. *Asian J. Org. Chem.* **2020**, *9*, 1901-1923. b) Adlington, R. M.; Barrett, A. G. M. *Acc. Chem. Res.* **1983**, *16*, 55-59.

[13] a) Afanasyev, O. I.; Kuchuk, E.; Usanov, D. L.; Chusov, D. *Chem. Rev*. **2019**, *119*, 11857-11811. b) Baxter, E. W.; Reitz, A. B. *Org. React.* **2001**, *59*, 1-714.

[14] Stevenson, S. M.; Higgins, R. F.; Shores, M. P.; Ferreira, E. M. *Chem. Sci.* **2017**, *8*, 654-660.

[15] Adjusting molecular orbital coefficients occur in catalyzed vs. thermal/noncatalyzed processes, see: (a) Trost, B. M.; Ippen, J.; Vladuchick, W. C. *J. Am. Chem. Soc.* **1977**, *99*, 8116-8118. b) Stojanac, Z.; Dickinson, R. A.; Stojanac, N.; Woznow, R. J.; Valenta, Z. *Can. J. Chem*. **1975**, *53*, 616-618. c) Tou, J. S.; Reusch, W. *J. Org. Chem.* **1980**, *45*, 5012-5014. d) Alston, P. V.; Gordon, M. D.; Ottenbrite, R. M.; Cohen, T. *J. Org. Chem.* **1983**, *48*, 5051-5054.

[16] Compound **4-19** turned black within 3 h of isolation. The compound is presumably slightly acid sensitive, with deterioration seen within 20 min when subjected to $CHCl_3$.

[17] Synthesis of $[Cr(PMP_2phen)_3](BF_4)_3$ by Gall, B. K.; Ferreira, E. M. *Manuscript in Prep.*

[18] Sambiagio, C.; Noël, T. *Trends in Chemistry*, **2020**, *2*, 92-106.

[19] Synthesis of $[Ru(bpz)_3](PF_6)_2$ according to Schultz, D. M.; Sawicki, J. W.; Yoon, T. P. *Beilstein J. Org. Chem.* **2015**, *11*, 61-65.

[20] a) Krow, G. R. "The Baeyer-Villiger Oxidation of Ketones and Aldehydes" *Org. React.* **1993**, *43*, 251-798. b) ten Brink, G.-J.; Arends, I. W. C. E.; Sheldon, R. A. *Chem. Rev.* **2004**, *104*, 4105-4124.

[21] Corey, E. J.; Niwa, H.; Falck, J. R. *J. Am. Chem. Soc.* **1979**, *101*, 1586-1587.

[22] Romney D. K.; Colvin, S. M.; Miller, S. J. *J. Am. Chem. Soc.* **2014**, *136*, 14019-14022.

[23] a) Khan, S. N.; Zaman, M.; Li, R.; Sun, Z. *J. Org. Chem.* **2020**, *85*, 5019-5026. b) Song, H.-T.; Ding, W.; Zhou, Q.-Q.; Liu, J.; Lu, L-Q.; Xiao, W.-J. *J. Org. Chem.* **2016**, *81*, 7250-7255.

[24] Shirase, S.; Tamaki, S.; Shinohara, K.; Hirosawa, K.; Tsurugi, H.; Satoh, T.; Mashima, K. *J. Am. Chem. Soc.* **2020**, *142*, 5668-5675.

[25] Xu, J.; Arkin, M.; Peng, Y.; Xu, W.; Yu, H.; Lin, X.; Wu, Q. *Green Chem.* **2019**, *21*, 1907-1911.

[26] Kalaitzakis, D.; Bosveli, A.; Sfakianaki, K.; Montagnon, T.; Vassilikogiannokis, G. *Angew. Chem. Int. Ed.* **2021**, *60*, 4335-4341.

[27] Vaccari, D.; Davoli, P.; Ori, C.; Spaggiari, A.; Prati, F. *Synlett* **2008**, *18*, 2807-2810.

[28] Kolarovic, A.; Käslin, A.; Wennemers, H. *Org. Lett.* **2014**, *16*, 4236-4239.

[29] Glaskowski, W.; Gliszczyńska, A.; Siepka, M.; Czarnecka, M.; Maciejewska, G. *Tetrahedron: Asymmetry* **2015**, *26*, 702-709.

[30] Joharapurker, A.; Raval, S.; Patel, J. Z.; Soni, R.; Gite, A.; Goswami, A.; Sadhwani, N.; Gandhi, N.; Patel, H.; Mishra, B.; Solanki, M.; Pandey, B.; Jain, M. R.; Patel, P. R. *J. Med. Chem.* **2007**, *50*, 5951-5966.

[31] Li, J.; Zhao, Y.-F.; Yaun, Z.-Y.; Xu, J.-X.; Gong, P. *Molecules* **2006**, *11*, 574-582.

[32] Yang, G.; Shen, C.; Zhang, W. *Angew. Chem. Int. Ed.* **2012**, *51*, 9141-9145.

[33] Shi, J.; Niwayama, S. *Tetrahedron Lett*. **2018**, *59*, 799-802.

[34] Wang, D.; Liu, J.; Guodong, Y.; Yanjun, H.; Cheng, Z.; Wenli, X. CN111499529, **2020**.

APPENDIX A

NMR SPECTRA RELEVANT TO CHAPTER 2

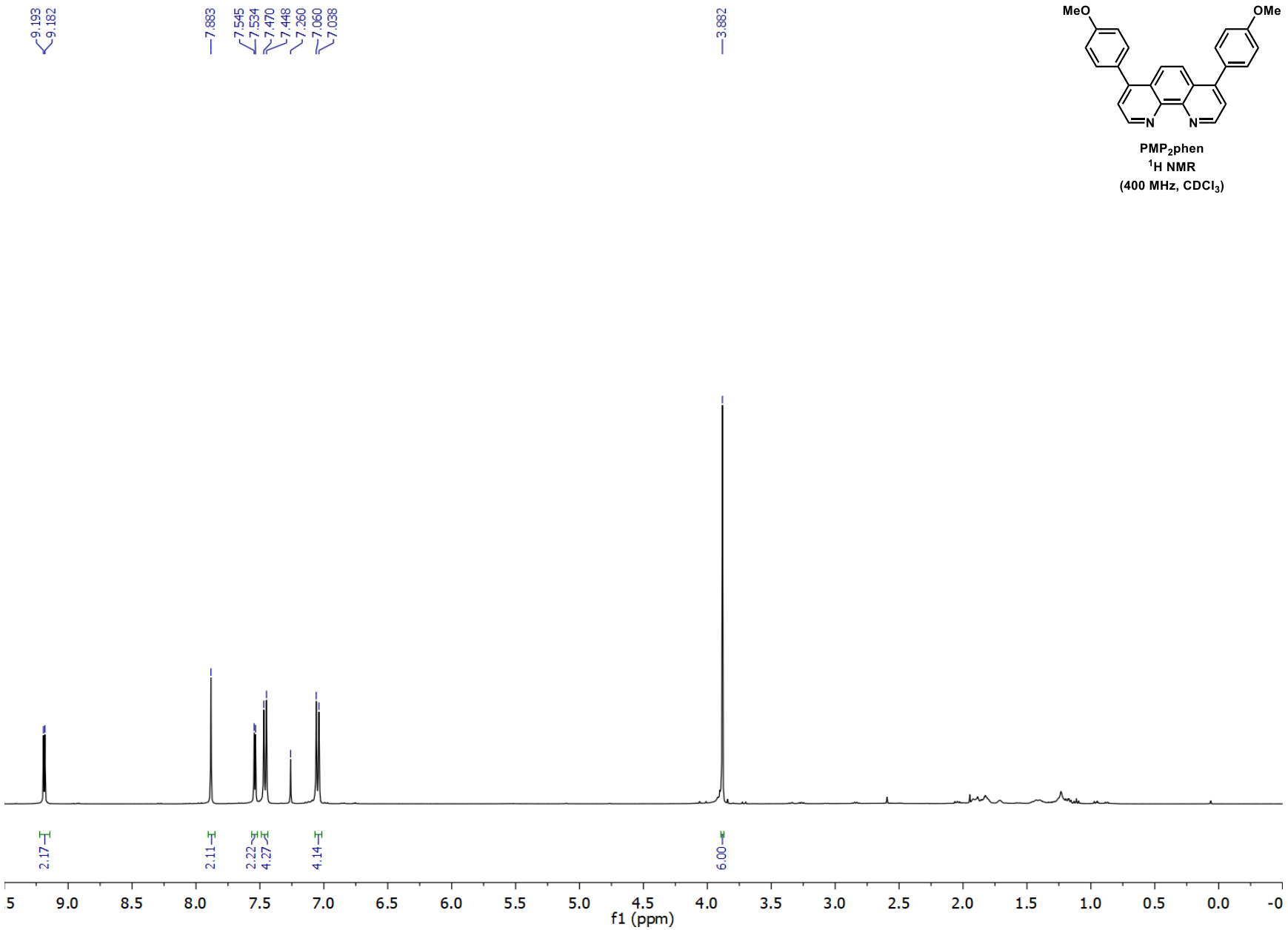
9.193
9.182
7.883
7.545
7.534
7.470
7.448
7.260
7.060
7.038
3.882
MeO
OMe
N
N
PMP2phen
1H NMR
(400 MHz, CDCl3)
2.17
2.11
2.22
4.27
4.14
6.00
f1 (ppm)

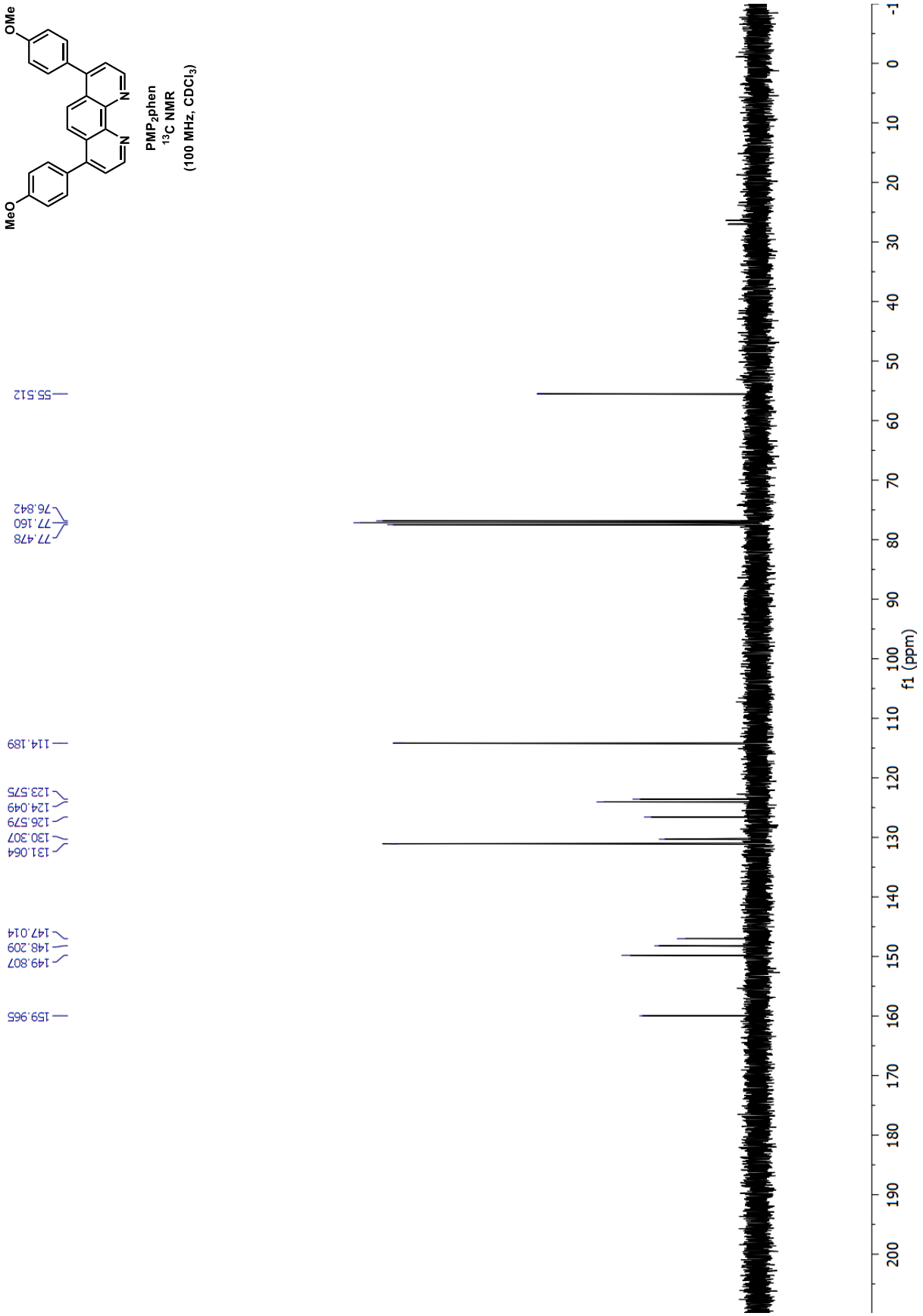
PMP2phen
13C NMR
(100 MHz, CDCl3)
OMe
MeO
N
N
55.512
76.842
77.160
77.478
114.189
123.575
124.049
126.579
130.307
131.064
147.014
148.209
149.807
159.965
f1 (ppm)

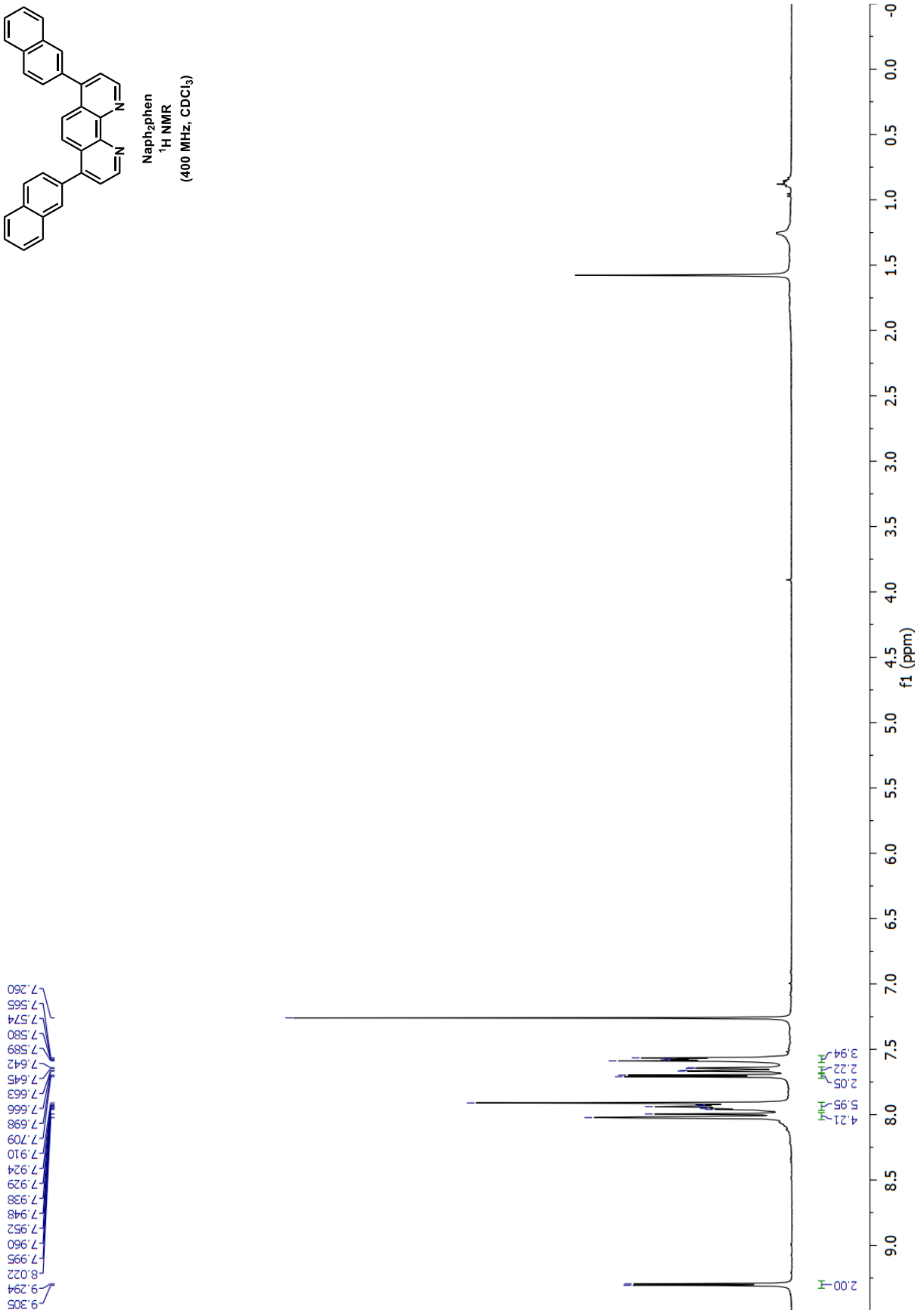
Naph2phen
1H NMR
(400 MHz, CDCl3)
9.305
9.294
8.022
7.995
7.960
7.952
7.948
7.938
7.929
7.924
7.910
7.709
7.698
7.666
7.663
7.645
7.642
7.589
7.580
7.574
7.565
7.260
2.00
4.21
5.95
2.05
2.22
3.94
f1 (ppm)

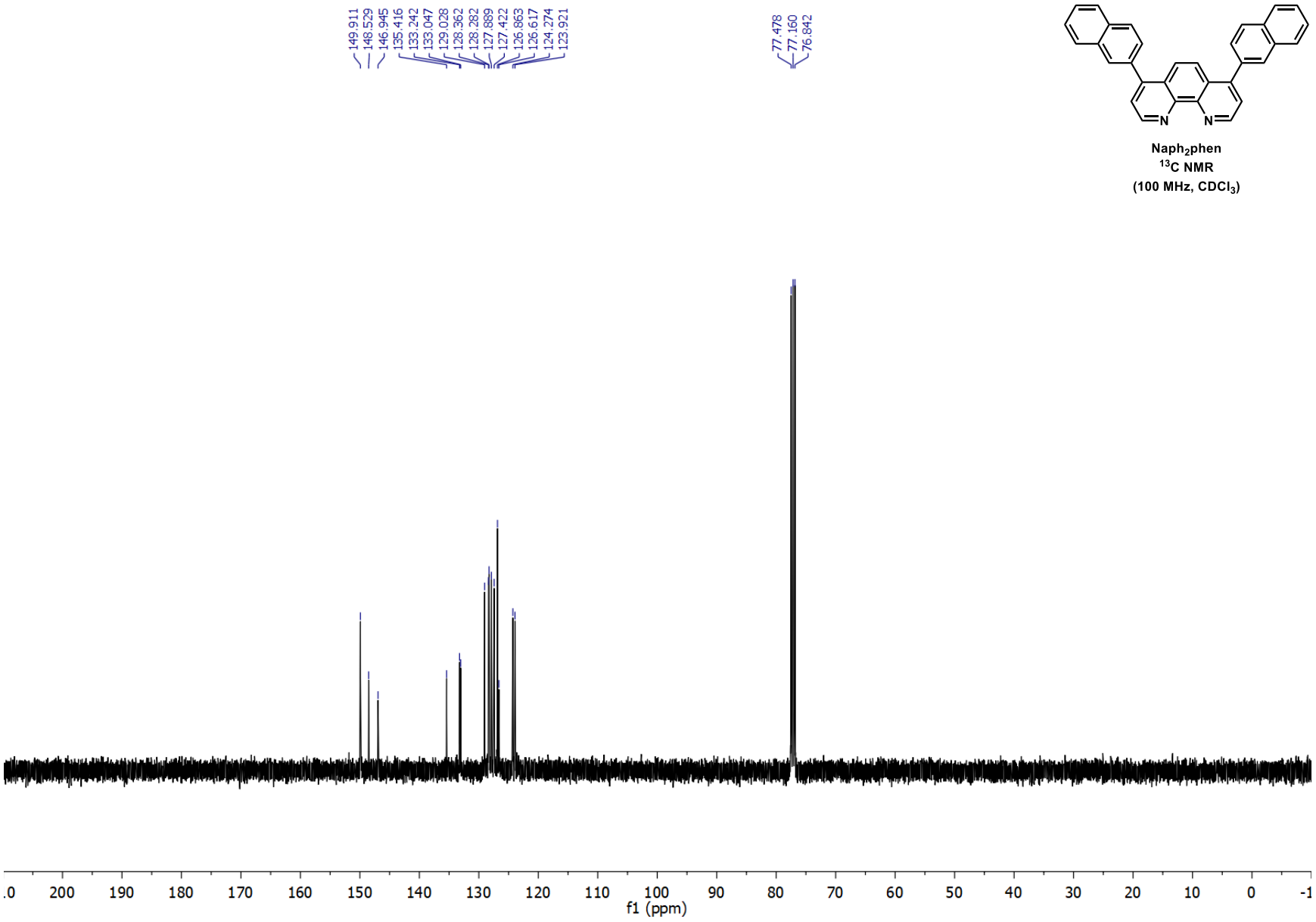
149.911
148.529
146.945
135.416
133.242
133.047
129.028
128.362
128.282
127.889
127.422
126.863
126.617
124.274
123.921
77.478
77.160
76.842
N
N
Naph2phen
13C NMR
(100 MHz, CDCl3)
f1 (ppm)

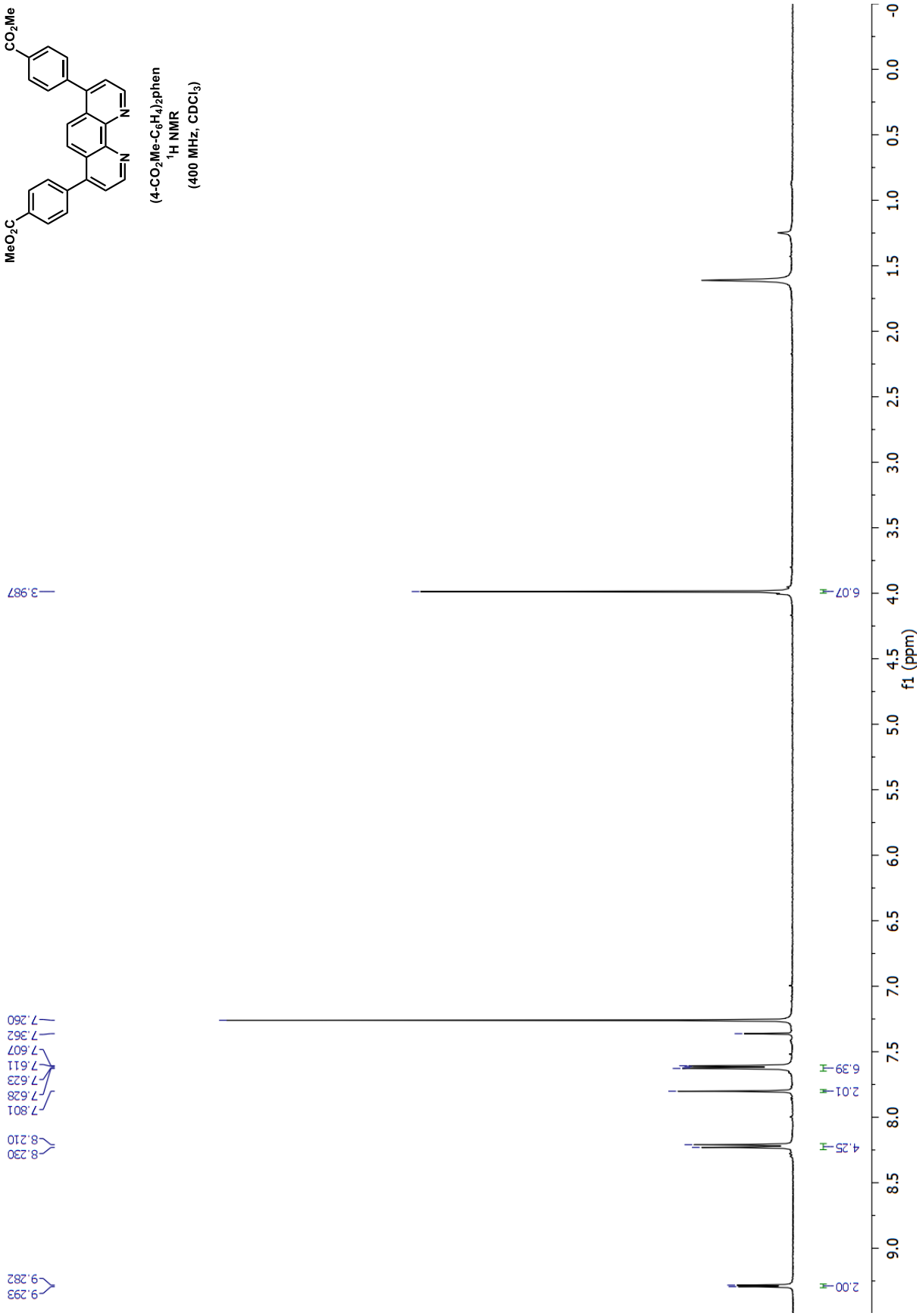
(4-CO2Me-C6H4)2phen
1H NMR
(400 MHz, CDCl3)
CO2Me
MeO2C
N
N
9.293
9.282
8.230
8.210
7.801
7.628
7.623
7.611
7.607
7.362
7.260
3.987
2.00
4.25
2.01
6.39
6.07
f1 (ppm)

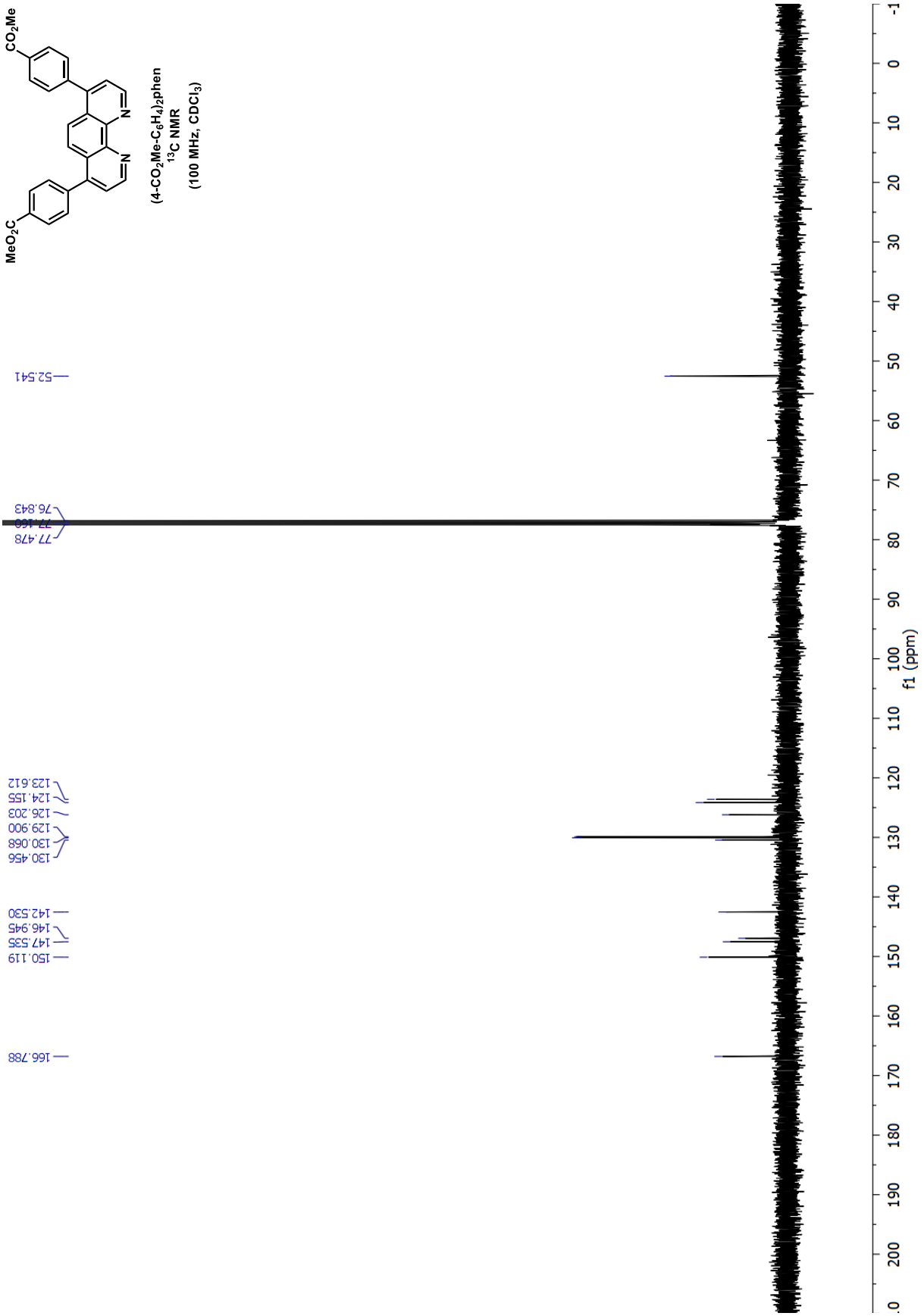
(4-CO2Me-C6H4)2phen
13C NMR
(100 MHz, CDCl3)
MeO2C
CO2Me
N
N
52.541
77.478
77.160
76.843
166.788
150.119
147.535
146.945
142.530
130.456
130.068
129.900
126.203
124.155
123.612
f1 (ppm)

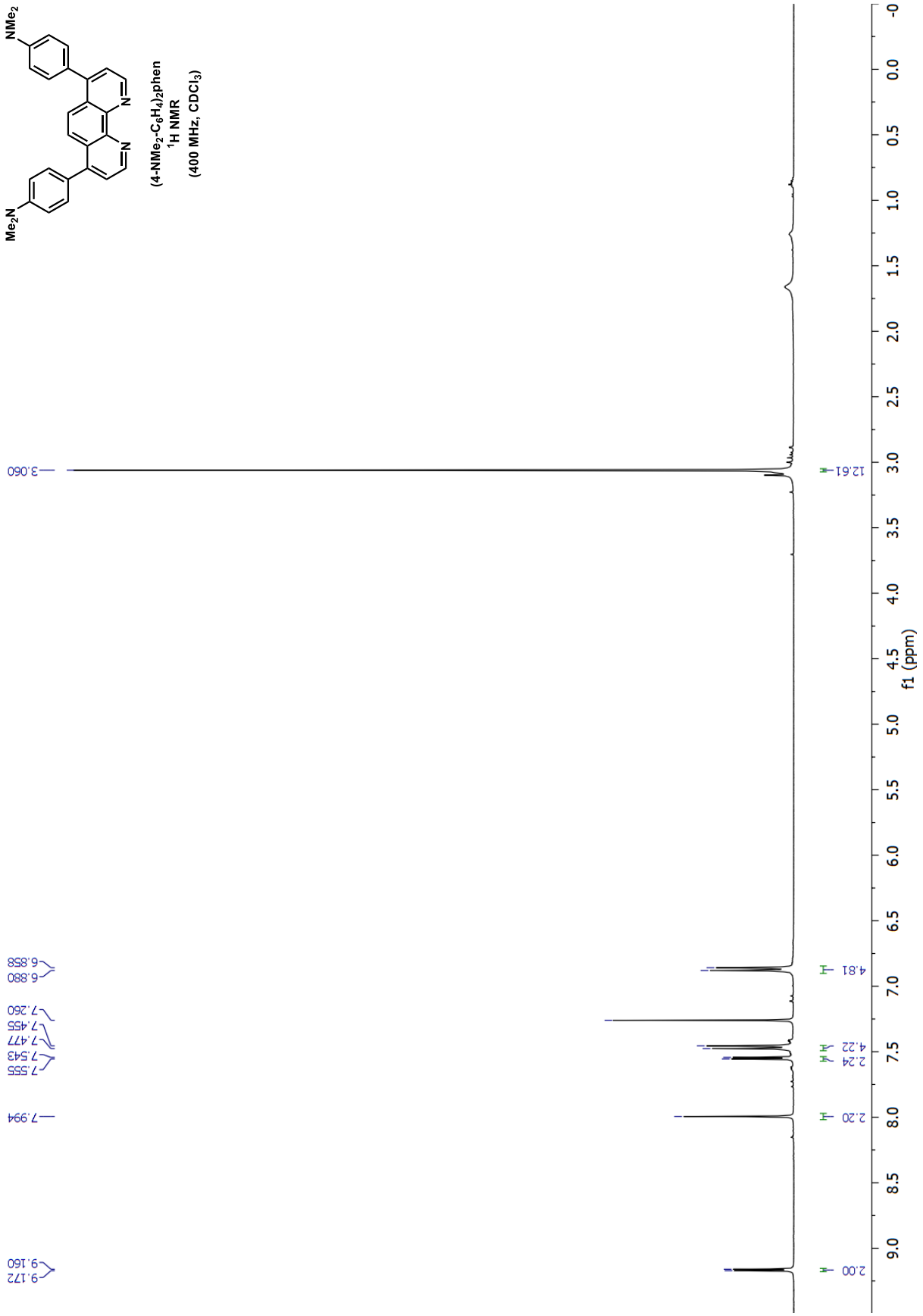
(4-NMe2-C6H4)2phen
1H NMR
(400 MHz, CDCl3)
NMe2
Me2N
9.172
9.160
7.994
7.555
7.543
7.477
7.455
7.260
6.880
6.858
3.060
2.00
4.81
2.20
2.24
4.22
12.61
f1 (ppm)

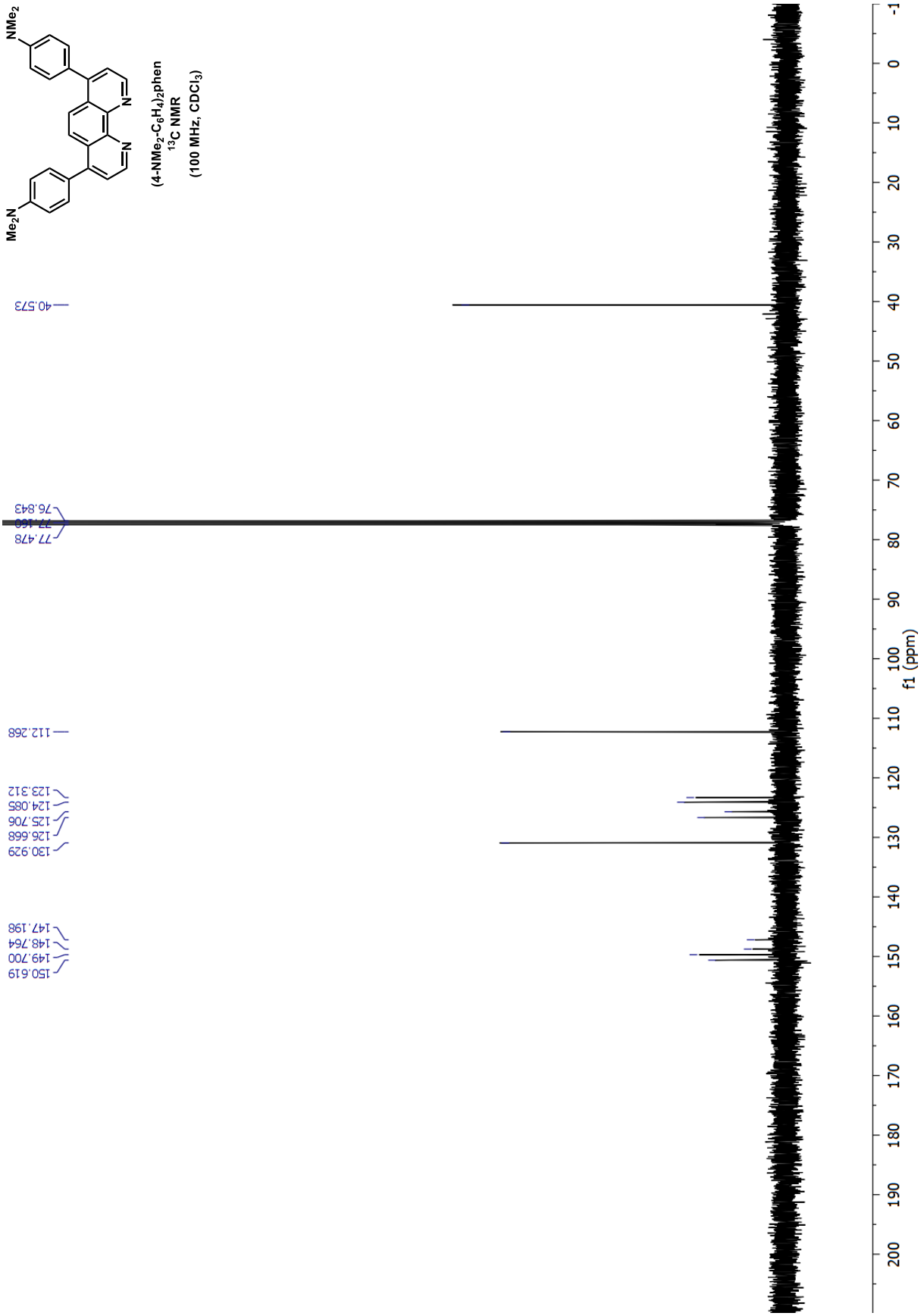
(4-NMe2-C6H4)2phen
13C NMR
(100 MHz, CDCl3)
NMe2
Me2N
N
N
40.573
76.843
77.160
77.478
112.268
123.312
124.085
125.706
126.668
130.929
147.198
148.764
149.700
150.619
f1 (ppm)

APPENDIX B

NMR SPECTRA RELEVANT TO CHAPTER 3

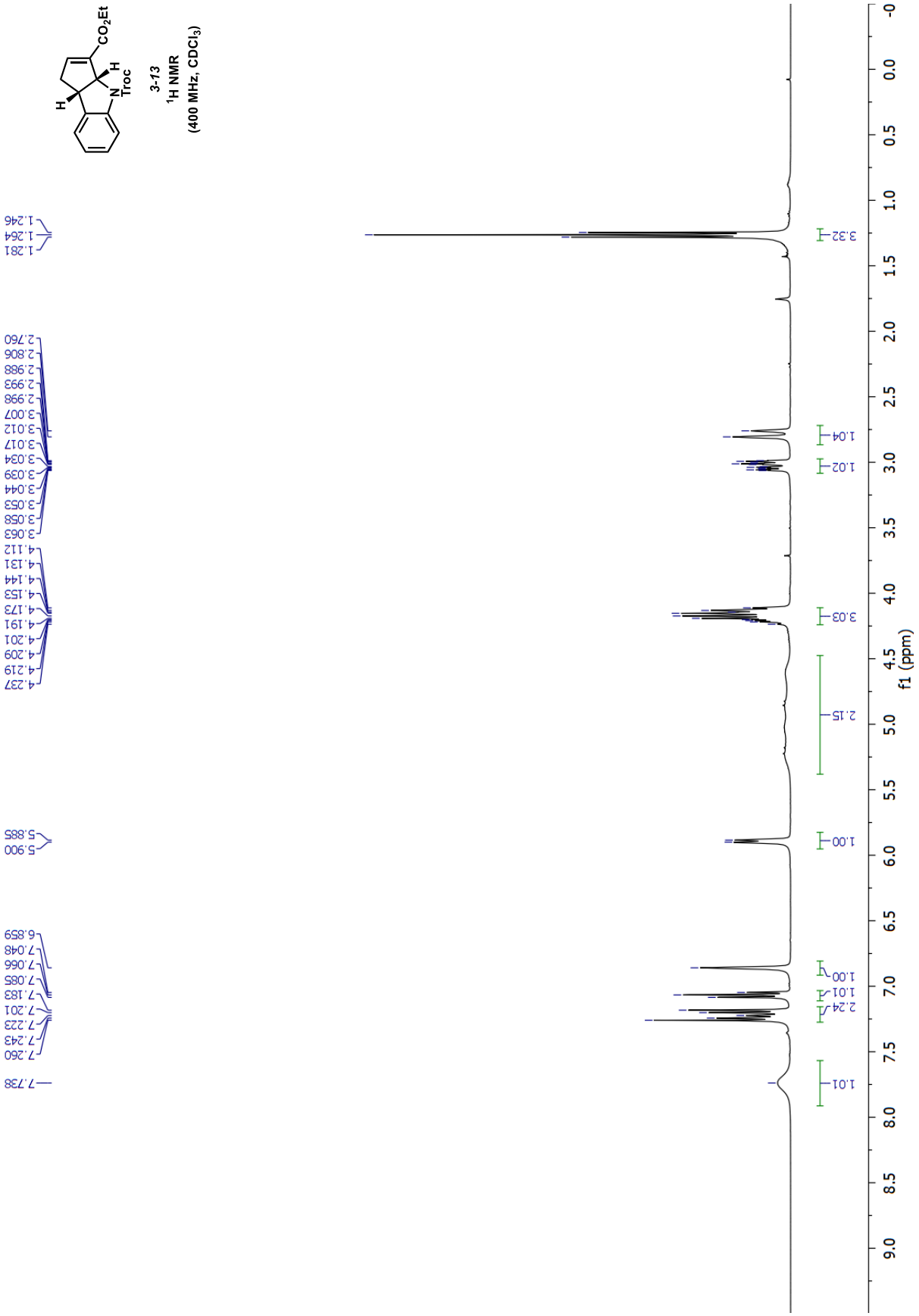
CO2Et
H
N
Troc
H
3-13
1H NMR
(400 MHz, CDCl3)
1.281
1.264
1.246
2.760
2.806
2.988
2.993
2.998
3.007
3.012
3.017
3.034
3.039
3.044
3.053
3.058
3.063
4.112
4.131
4.144
4.153
4.173
4.191
4.201
4.209
4.219
4.237
5.885
5.900
6.859
7.048
7.066
7.085
7.183
7.201
7.223
7.243
7.260
7.738
3.32
1.04
1.02
3.03
2.15
1.00
1.00
1.01
2.24
1.01
f1 (ppm)

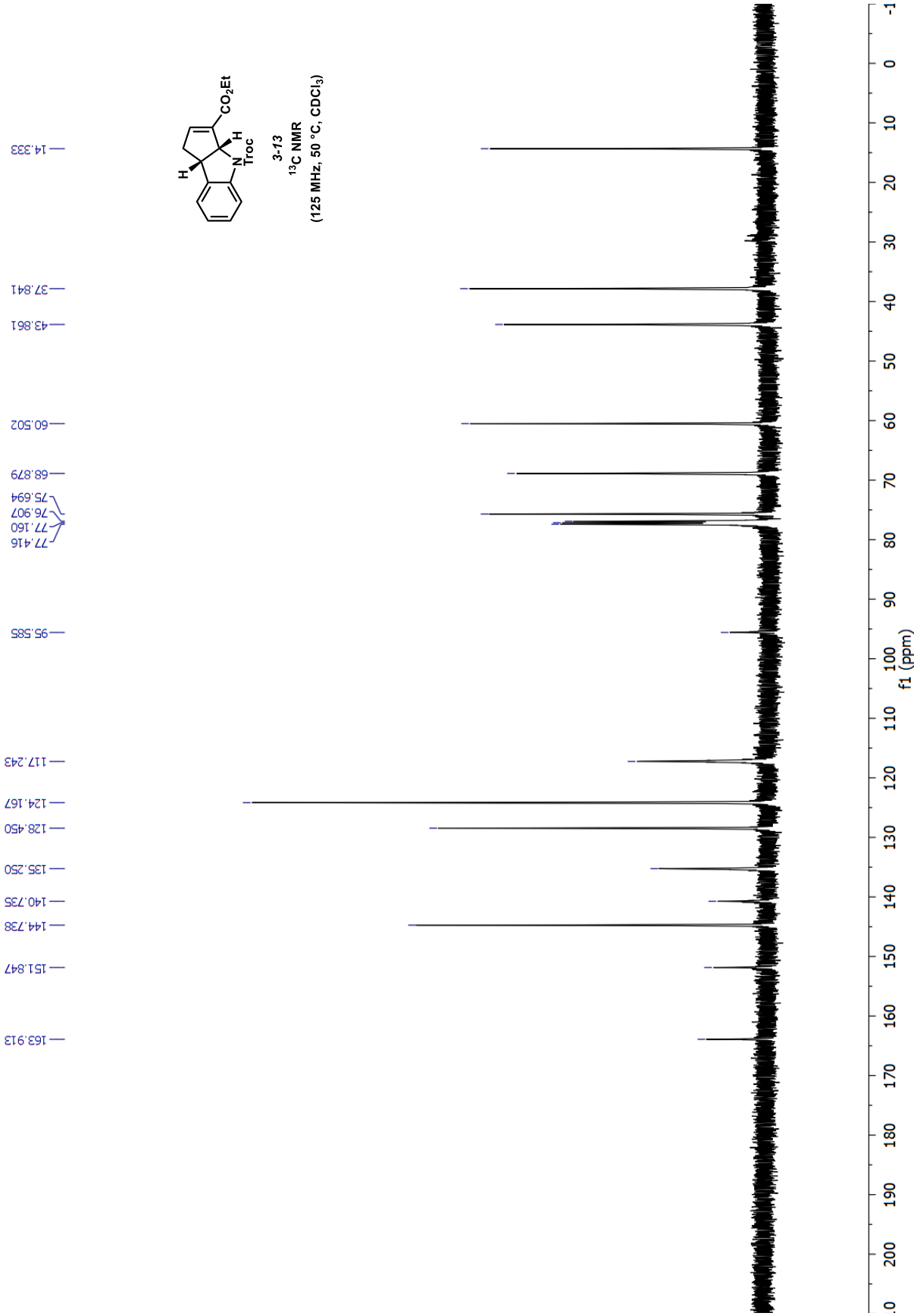
3-13
13C NMR
(125 MHz, 50 °C, CDCl3)
CO2Et
H
N
Troc
H
14.333
37.841
43.861
60.502
68.879
75.694
76.907
77.160
77.416
95.585
117.243
124.167
128.450
135.250
140.735
144.738
151.847
163.913
f1 (ppm)

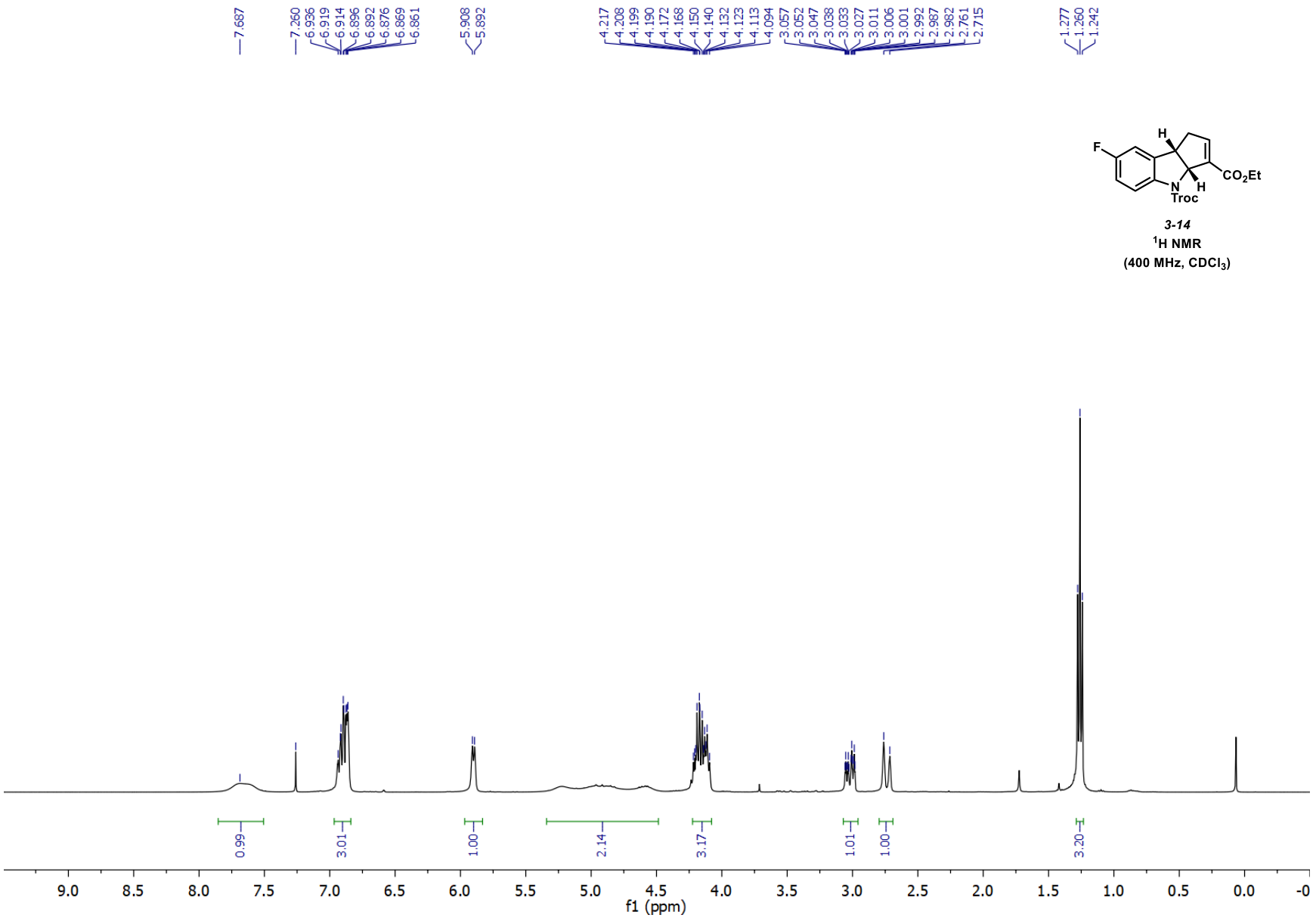
7.687
7.260
6.936
6.919
6.914
6.896
6.892
6.876
6.869
6.861
5.908
5.892
4.217
4.208
4.199
4.190
4.172
4.168
4.150
4.140
4.132
4.123
4.113
4.094
3.057
3.052
3.047
3.038
3.033
3.027
3.011
3.006
3.001
2.992
2.987
2.982
2.761
2.715
1.277
1.260
1.242
F
H
CO2Et
N
H
Troc
3-14
1H NMR
(400 MHz, CDCl3)
0.99
3.01
1.00
2.14
3.17
1.01
1.00
3.20
9.0
8.5
8.0
7.5
7.0
6.5
6.0
5.5
5.0
4.5
4.0
3.5
3.0
2.5
2.0
1.5
1.0
0.5
0.0
-0
f1 (ppm)

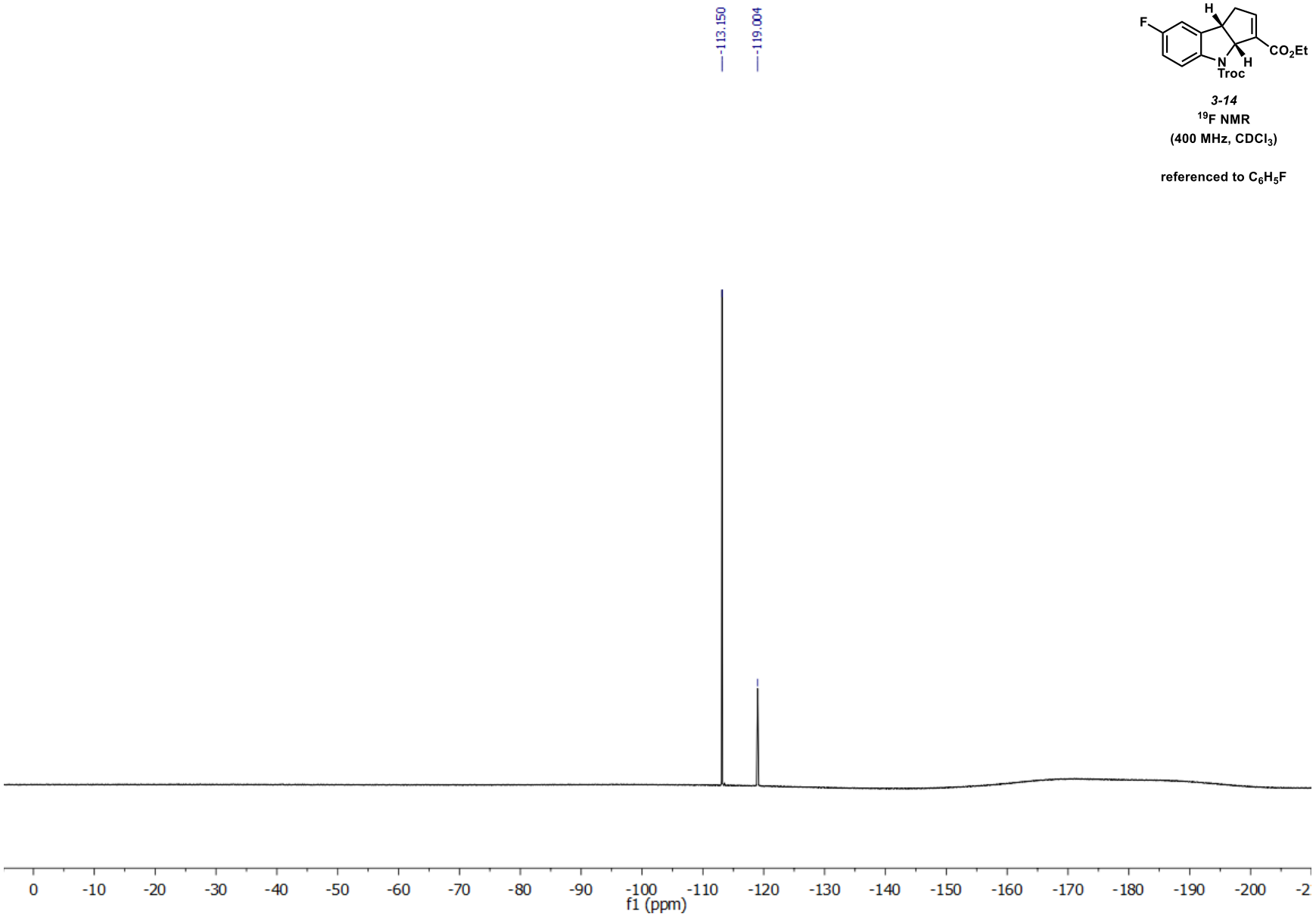
-113.150
-119.004
F
H
N
H
Troc
CO2Et
3-14
19F NMR
(400 MHz, CDCl3)
referenced to C6H5F
0
-10
-20
-30
-40
-50
-60
-70
-80
-90
-100
-110
-120
-130
-140
-150
-160
-170
-180
-190
-200
f1 (ppm)

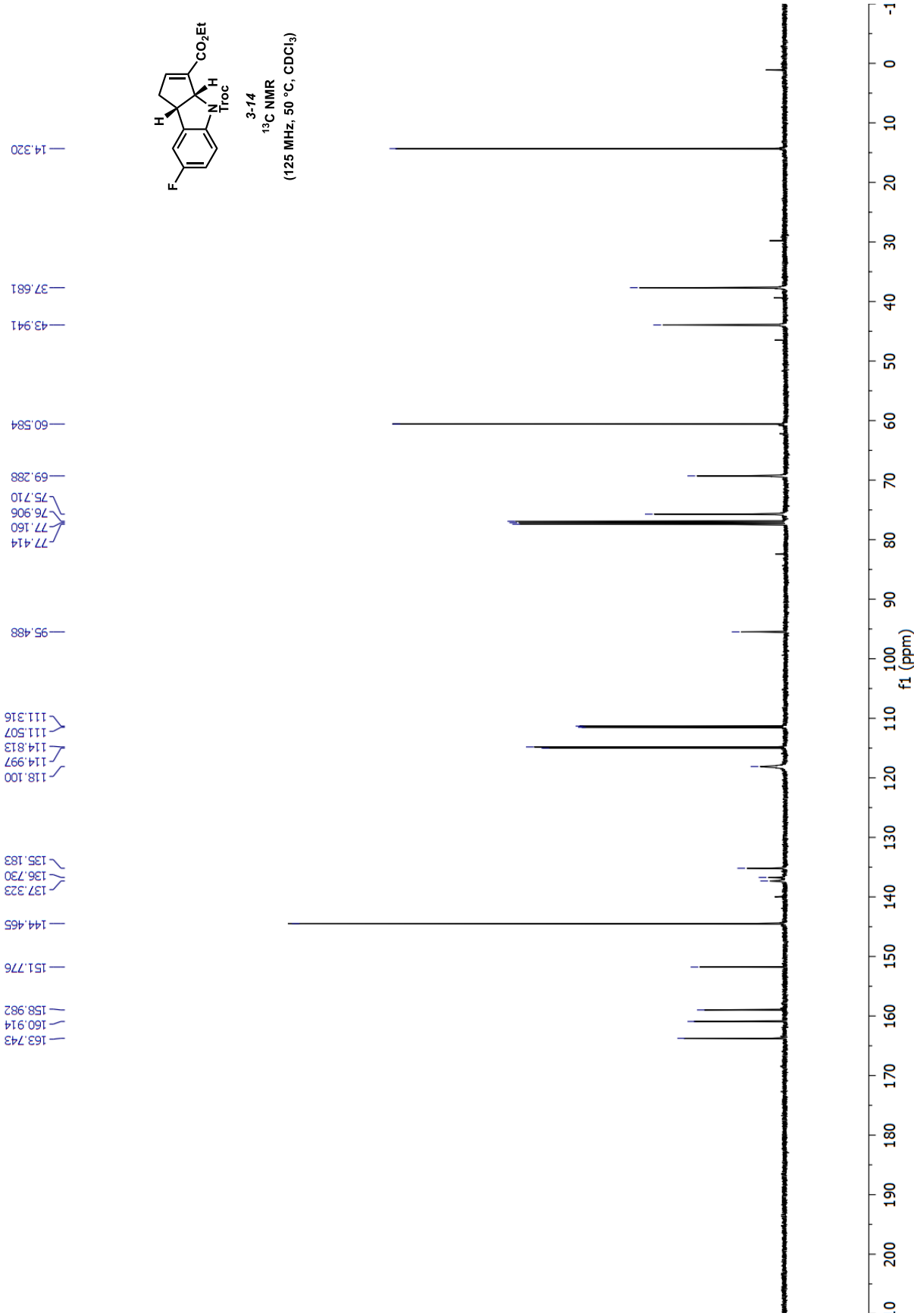
3-14
^{13}C NMR
(125 MHz, 50 °C, $CDCl_3$)
CO_2Et
H
N
Troc
H
F
14.320
37.681
43.941
60.584
69.288
75.710
76.906
77.160
77.414
95.488
111.316
111.507
114.813
114.997
118.100
135.183
136.730
137.323
144.465
151.776
158.982
160.914
163.743
f1 (ppm)

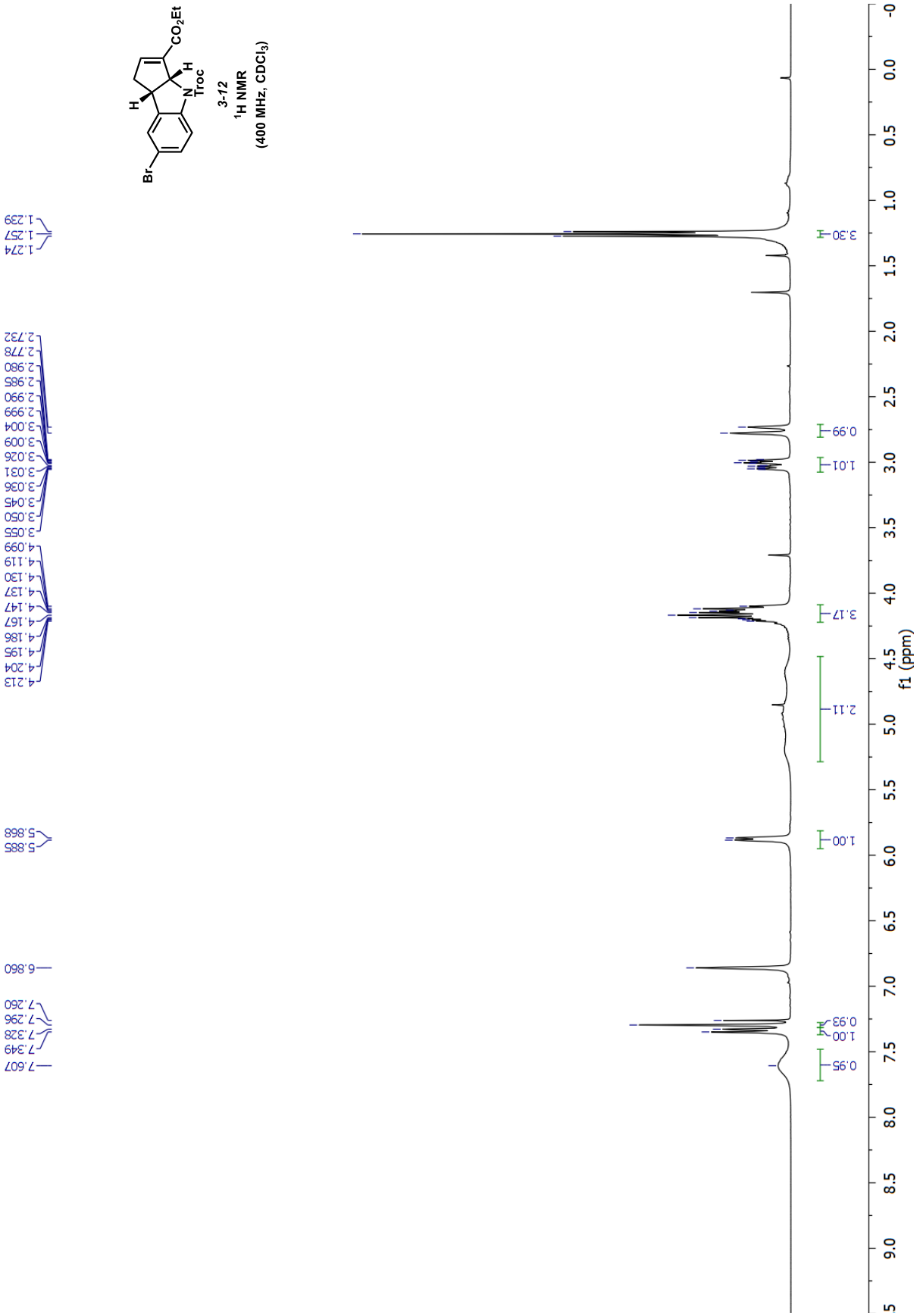
CO2Et
H
N
Troc
H
Br
3-12
1H NMR
(400 MHz, CDCl3)
1.274
1.257
1.239
2.732
2.778
2.980
2.985
2.990
2.999
3.004
3.009
3.026
3.031
3.036
3.045
3.050
3.055
4.099
4.119
4.130
4.137
4.147
4.167
4.186
4.195
4.204
4.213
5.885
5.868
6.860
7.260
7.296
7.328
7.349
7.607
3.30
0.99
1.01
3.17
2.11
1.00
0.93
1.00
0.95
f1 (ppm)

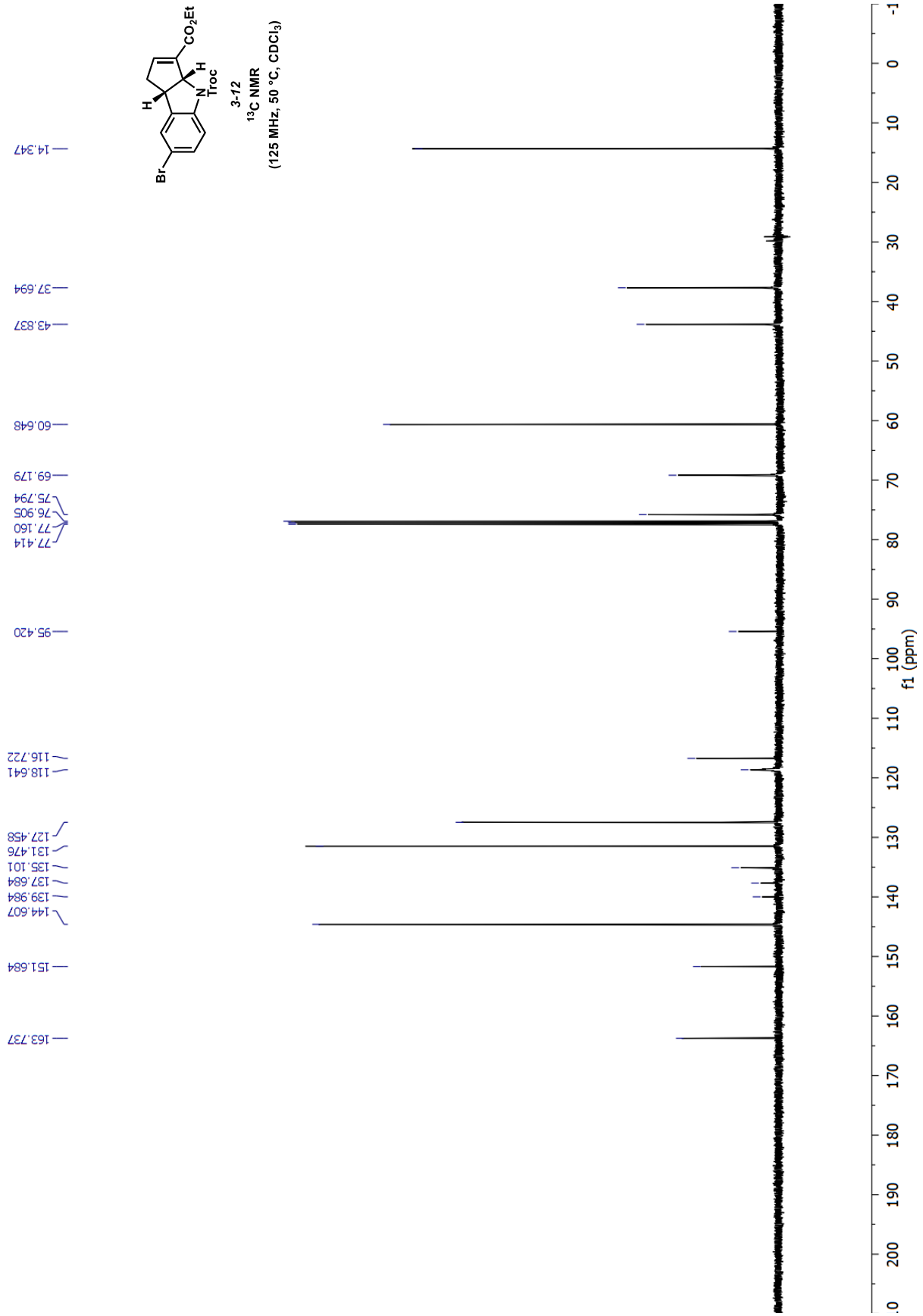
3-12
^{13}C NMR
(125 MHz, 50 °C, CDCl$_3$)
CO$_2$Et
H
Troc
N
H
Br
14.347
37.694
43.837
60.648
69.179
75.794
76.905
77.160
77.414
95.420
116.722
118.641
127.458
131.476
135.101
137.684
139.984
144.607
151.684
163.737
f1 (ppm)

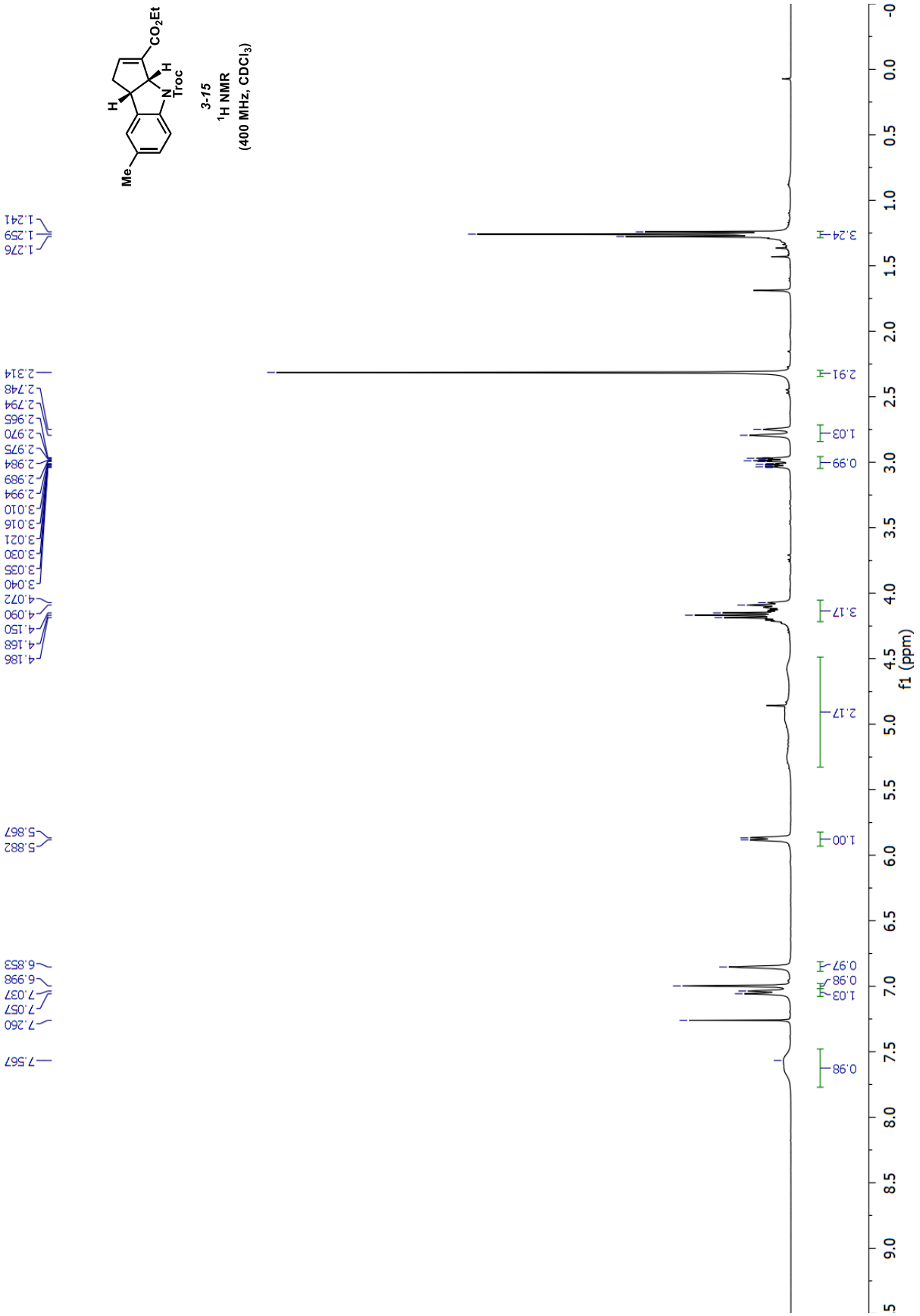
CO2Et
H
N
Troc
H
Me
3-15
1H NMR
(400 MHz, CDCl3)
1.276
1.259
1.241
2.314
2.748
2.794
2.965
2.970
2.975
2.984
2.989
2.994
3.010
3.016
3.021
3.030
3.035
3.040
4.072
4.090
4.150
4.168
4.186
5.882
5.867
6.853
6.998
7.037
7.057
7.260
7.567
3.24
2.91
1.03
0.99
3.17
2.17
1.00
0.97
0.98
1.03
0.98
f1 (ppm)

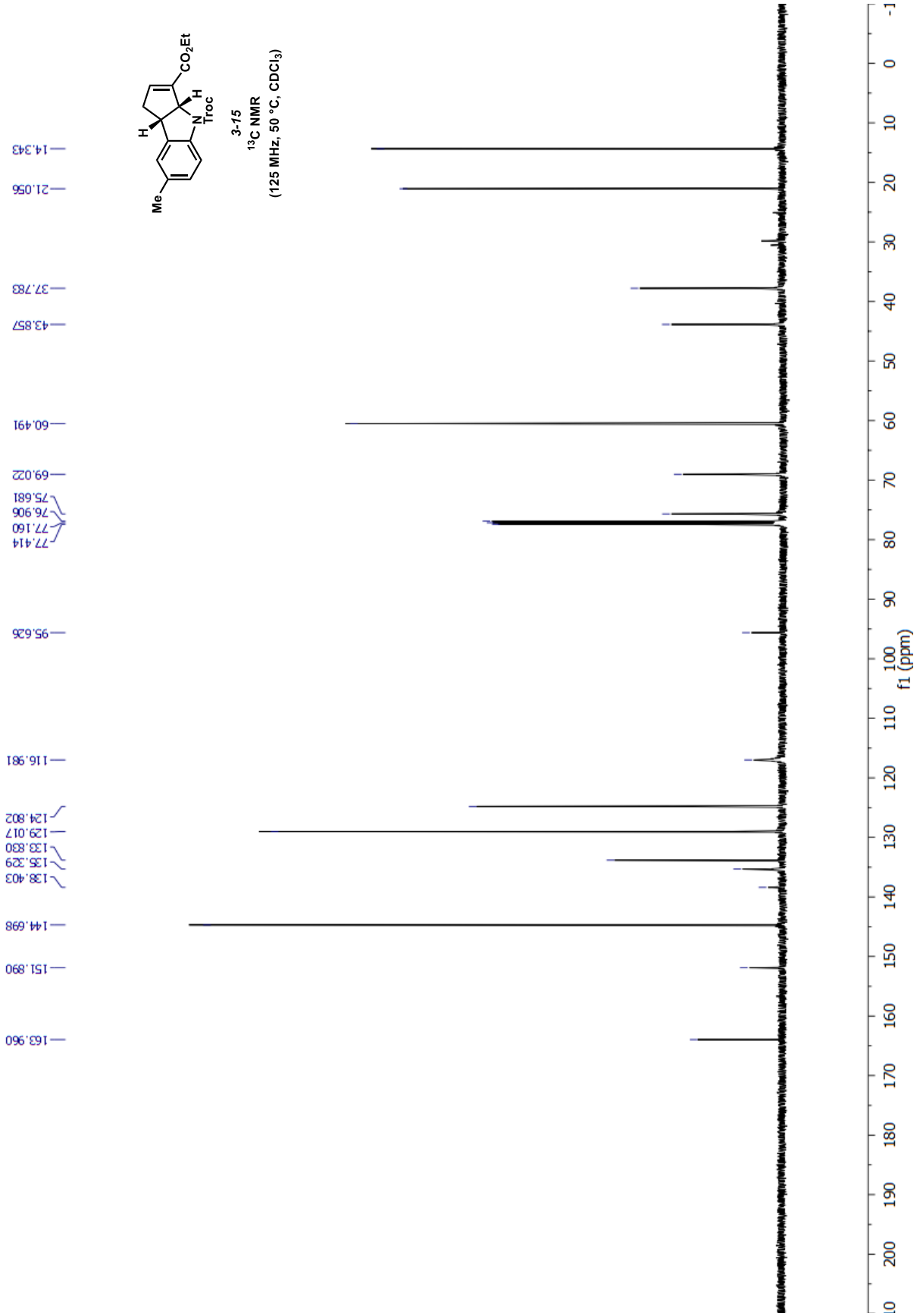
CO2Et
H
N
Troc
Me
3-15
13C NMR
(125 MHz, 50 °C, CDCl3)
14.343
21.056
37.783
43.857
60.491
69.022
75.681
76.906
77.160
77.414
95.636
116.981
124.802
129.017
133.830
135.329
138.403
144.698
151.890
163.960
f1 (ppm)

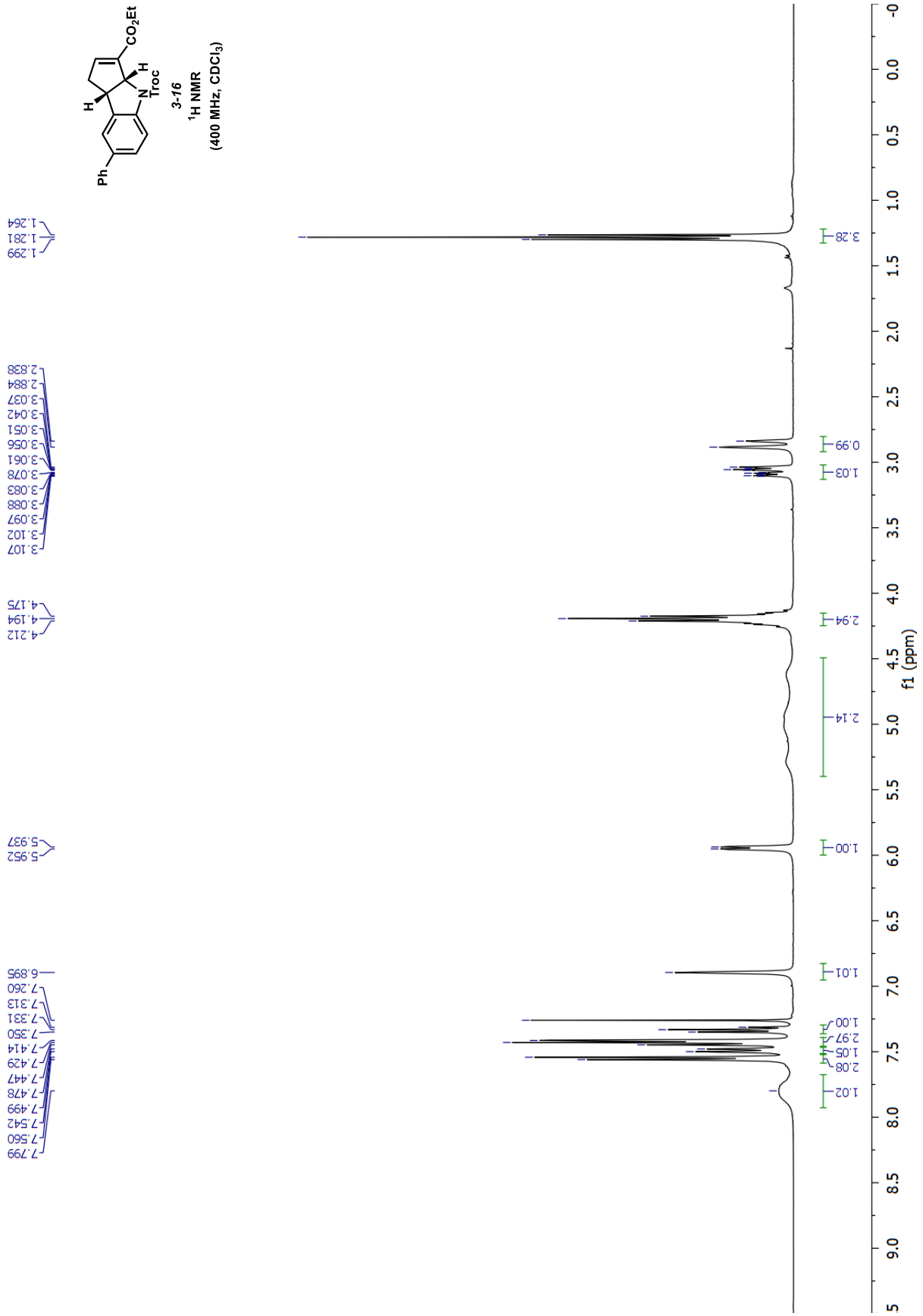
CO2Et
H
N
Troc
H
Ph
3-16
1H NMR
(400 MHz, CDCl3)
1.299
1.281
1.264
3.107
3.102
3.097
3.088
3.083
3.078
3.061
3.056
3.051
3.042
3.037
2.884
2.838
4.212
4.194
4.175
5.952
5.937
7.799
7.560
7.542
7.499
7.478
7.447
7.429
7.414
7.350
7.331
7.313
7.260
6.895
3.28
0.99
1.03
2.94
2.14
1.00
1.01
1.00
2.97
1.05
2.08
1.02
f1 (ppm)

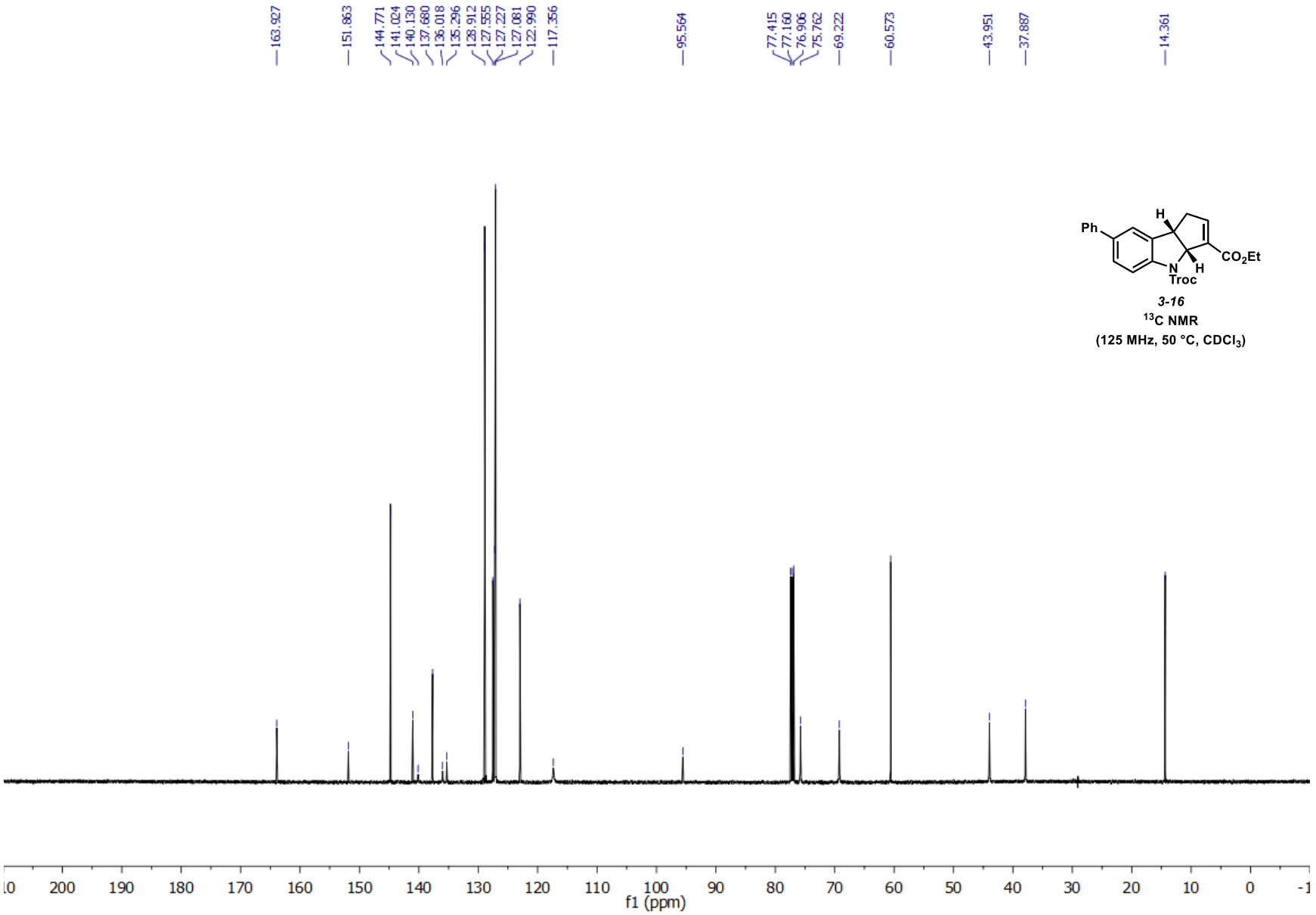
163.927
151.863
144.771
141.024
140.130
137.680
136.018
135.296
128.912
127.555
127.227
127.081
122.990
117.356
95.564
77.415
77.160
76.906
75.762
69.222
60.573
43.951
37.887
14.361
Ph
H
N
H
Troc
CO2Et
3-16
13C NMR
(125 MHz, 50 °C, CDCl3)
f1 (ppm)

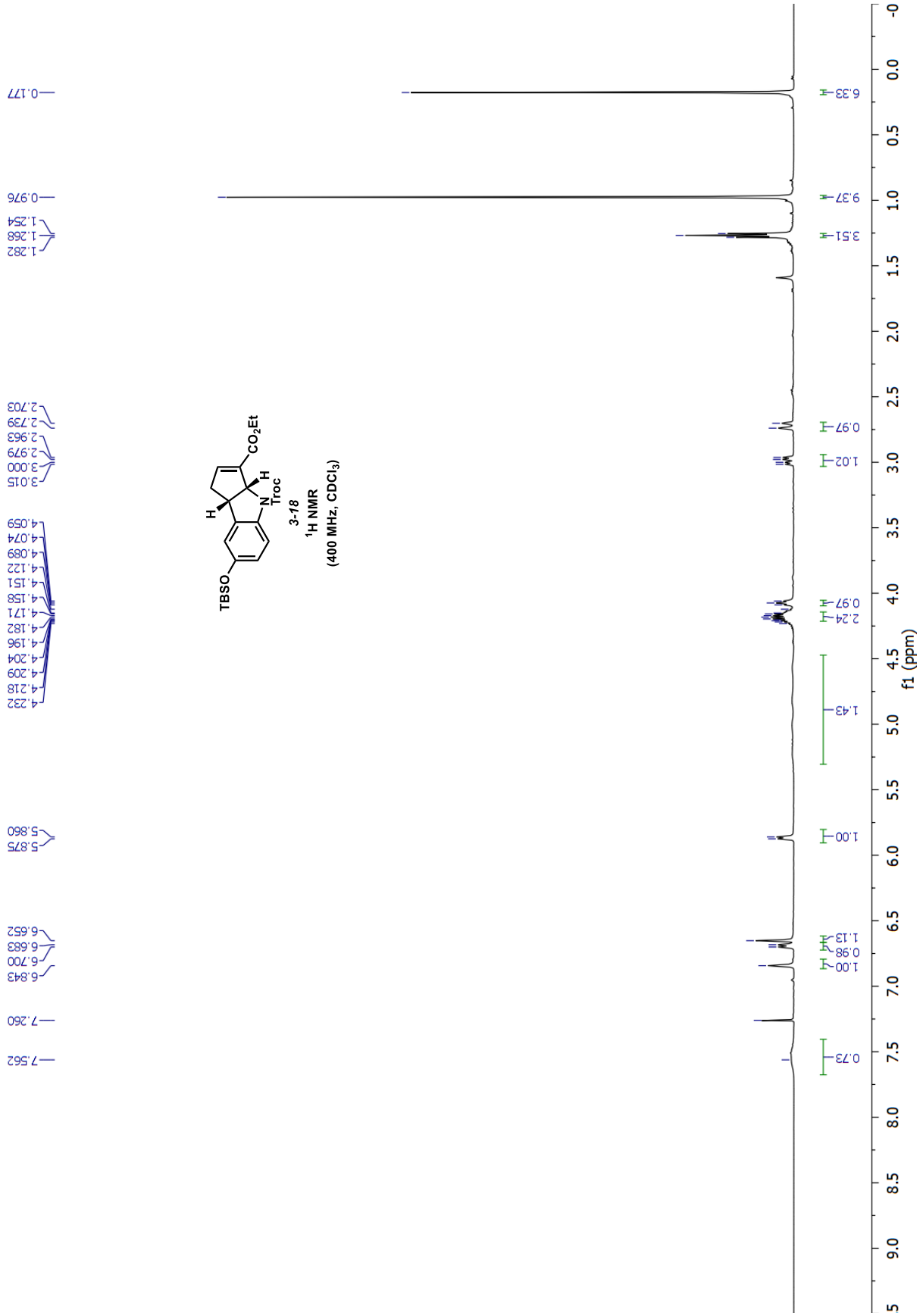
TBSO
CO2Et
H
N
Troc
H
3-18
1H NMR
(400 MHz, CDCl3)
f1 (ppm)

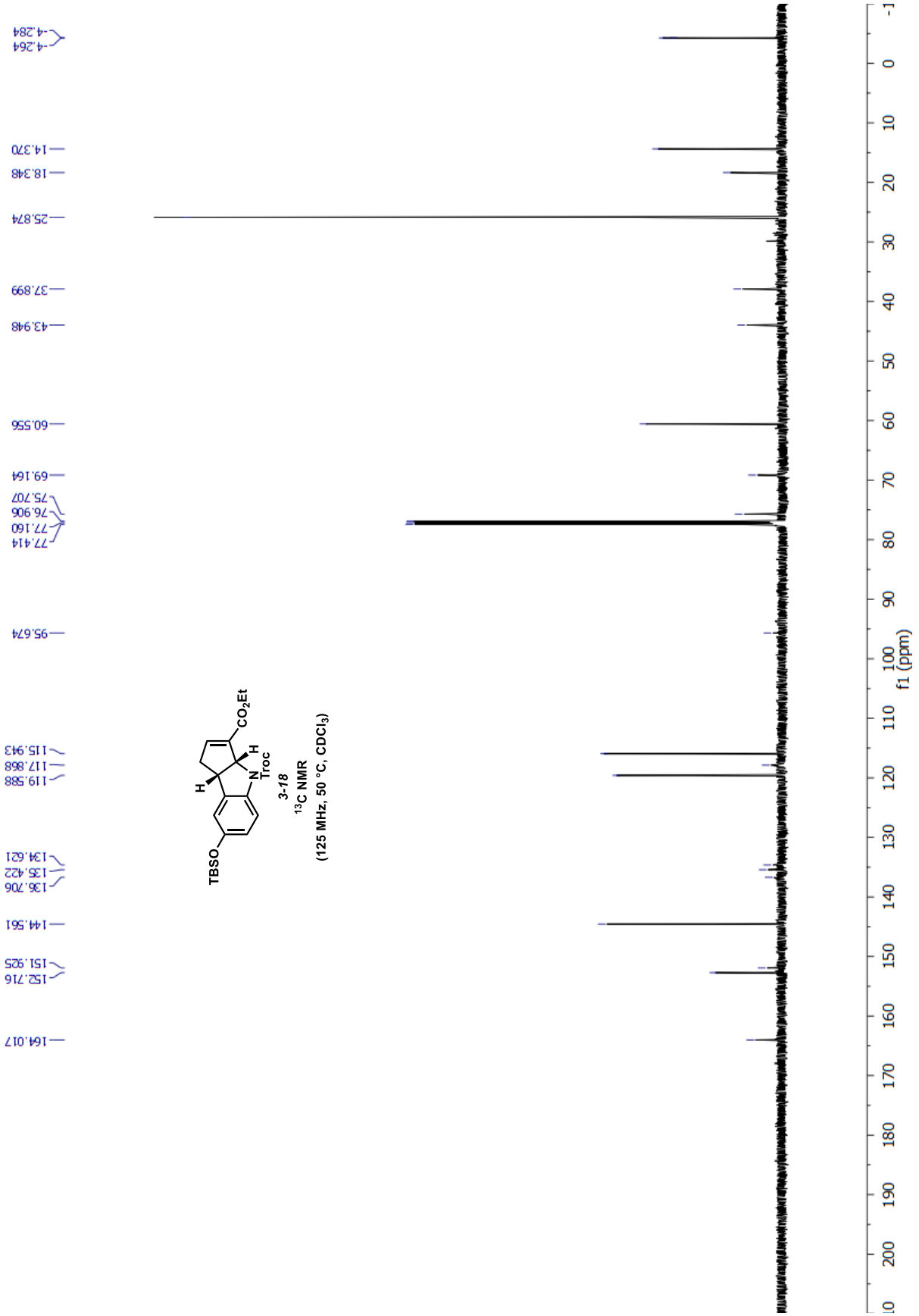
-4.284
-4.264
14.370
18.348
25.874
37.899
43.948
60.556
69.164
75.707
76.906
77.160
77.414
95.674
115.943
117.868
119.588
134.621
135.422
136.706
144.561
151.925
152.716
164.017
TBSO
H
N
Troc
H
CO2Et
3-18
13C NMR
(125 MHz, 50 °C, CDCl3)
f1 (ppm)

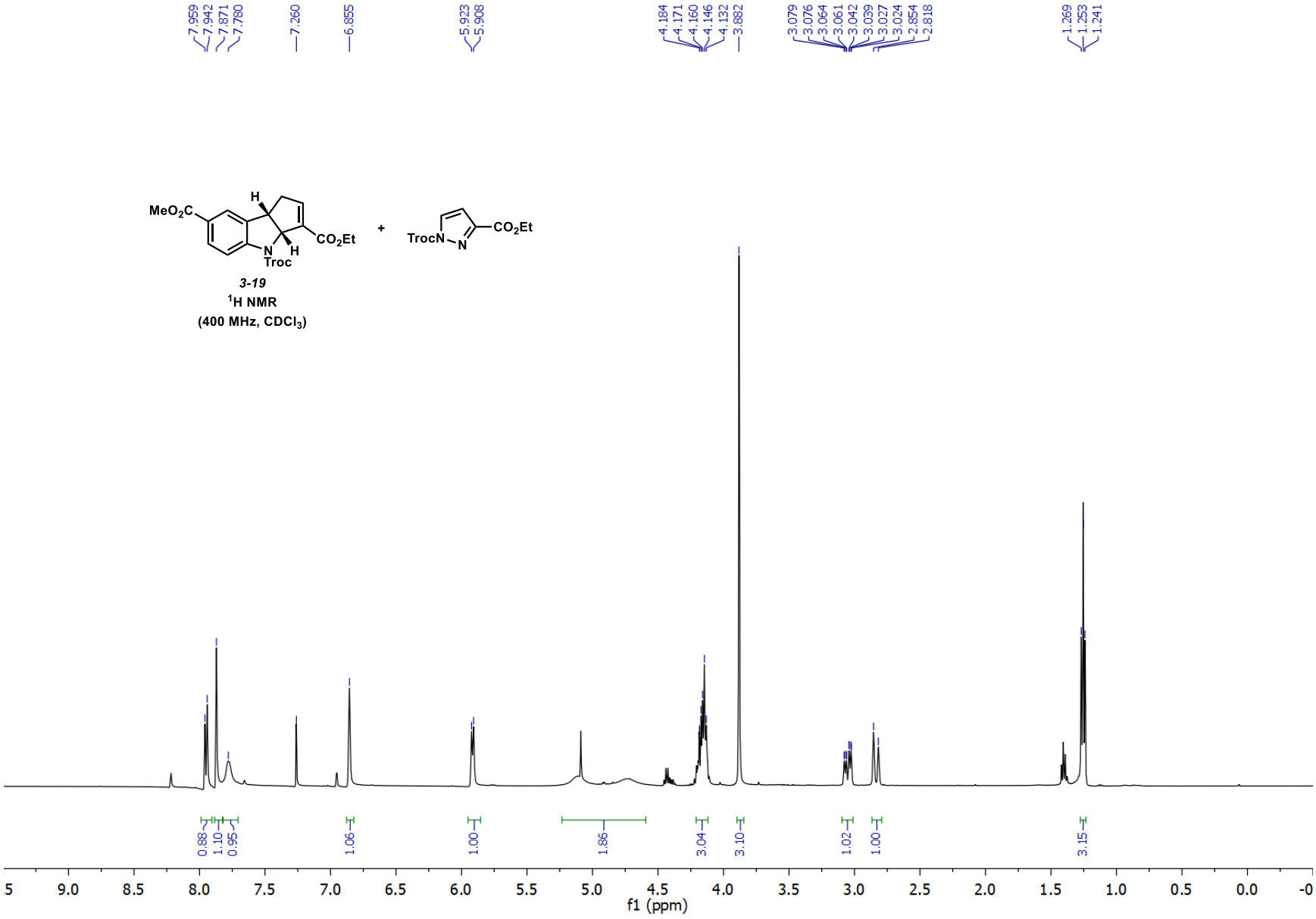
7.959
7.942
7.871
7.780
7.260
6.855
5.923
5.908
4.184
4.171
4.160
4.146
4.132
3.882
3.079
3.076
3.064
3.061
3.042
3.039
3.027
3.024
2.854
2.818
1.269
1.253
1.241
MeO2C
H
CO2Et
N
H
Troc
+
TrocN
N
CO2Et
3-19
1H NMR
(400 MHz, CDCl3)
0.88
1.10
0.95
1.06
1.00
1.86
3.04
3.10
1.02
1.00
3.15
f1 (ppm)

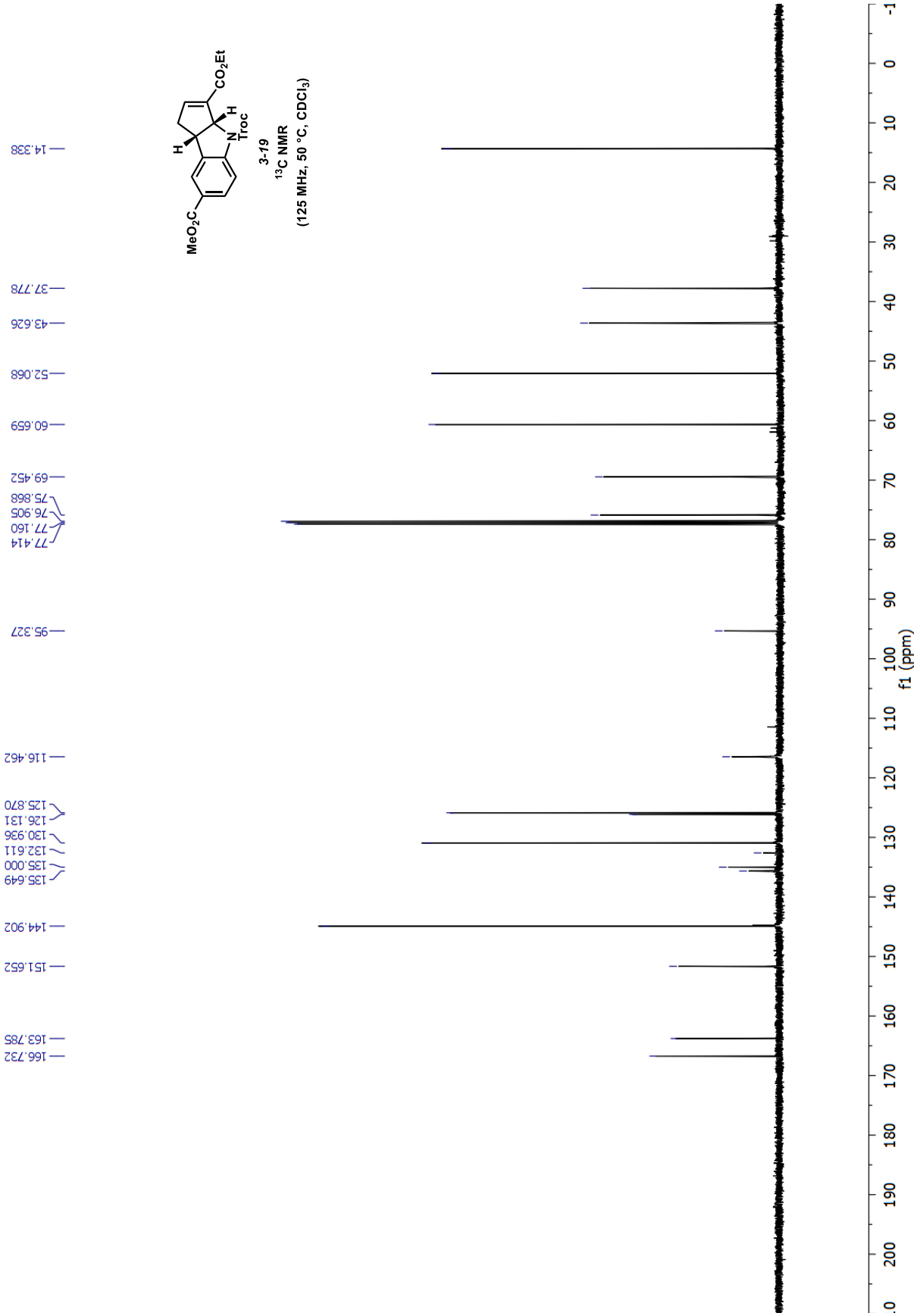
3-19
13C NMR
(125 MHz, 50 °C, CDCl3)
CO2Et
H
N
Troc
H
MeO2C
14.338
37.778
43.626
52.068
60.659
69.452
75.868
76.905
77.160
77.414
95.327
116.462
125.870
126.131
130.936
132.611
135.000
135.649
144.902
151.652
163.785
166.732
f1 (ppm)

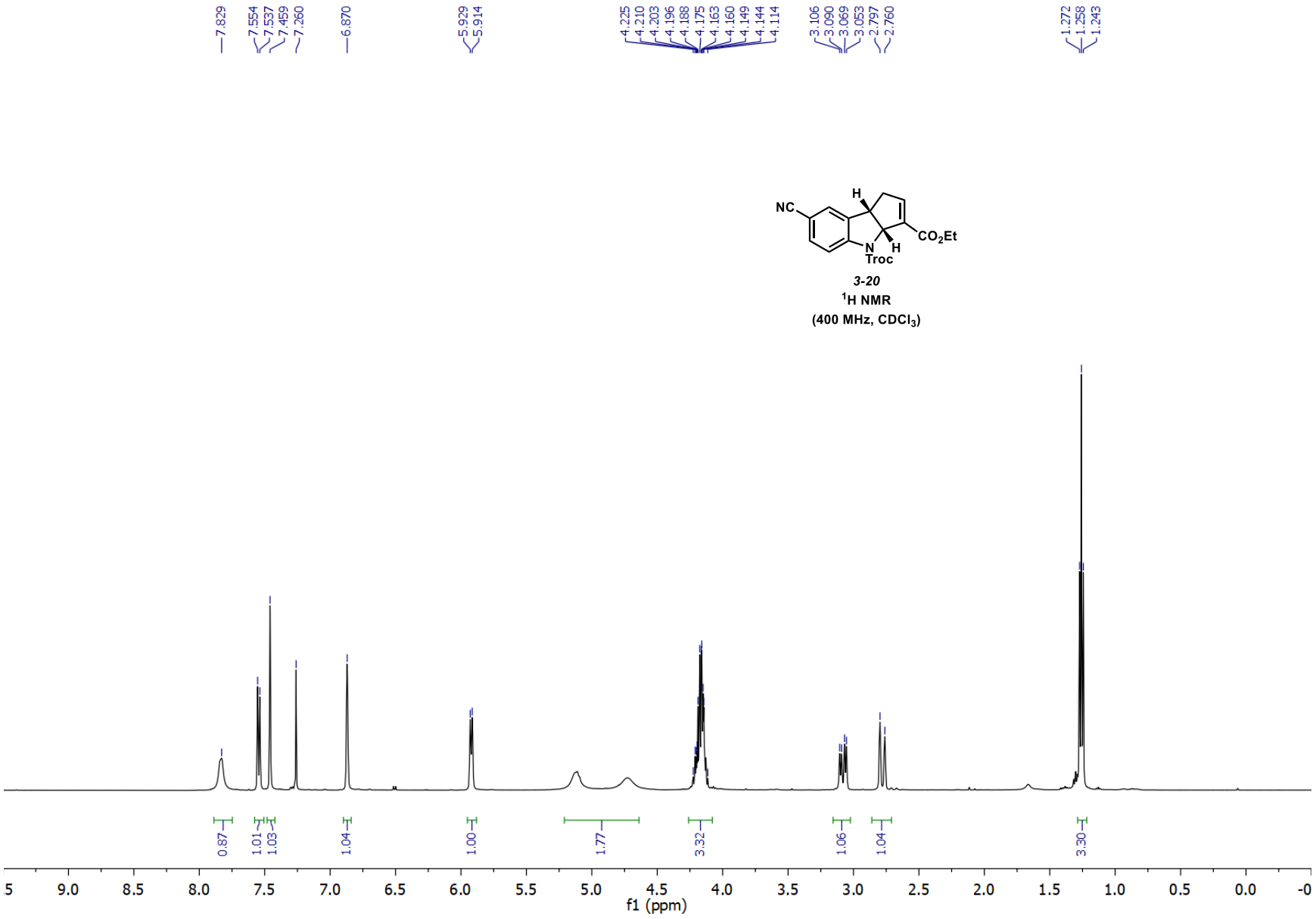
7.829
7.554
7.537
7.459
7.260
6.870
5.929
5.914
4.225
4.210
4.203
4.196
4.188
4.175
4.163
4.160
4.149
4.144
4.114
3.106
3.090
3.069
3.053
2.797
2.760
1.272
1.258
1.243
NC
H
CO2Et
N
H
Troc
3-20
1H NMR
(400 MHz, CDCl3)
0.87
1.01
1.03
1.04
1.00
1.77
3.32
1.06
1.04
3.30
f1 (ppm)

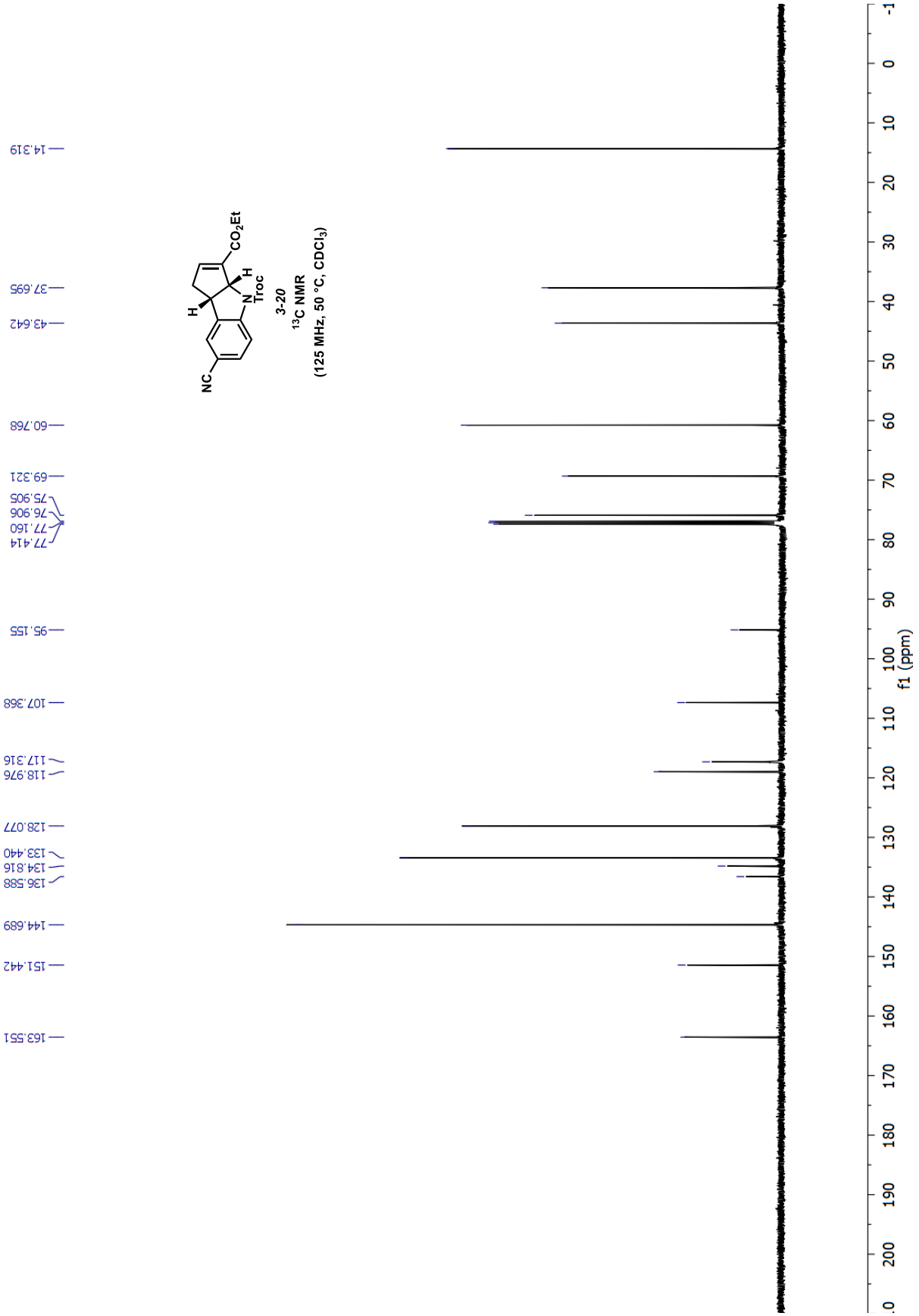
14.319
37.695
43.642
60.768
69.321
75.905
76.906
77.160
77.414
95.155
107.368
117.316
118.976
128.077
133.440
134.816
136.588
144.689
151.442
163.551
CO2Et
H
N
Troc
H
NC
3-20
13C NMR
(125 MHz, 50 °C, CDCl3)
f1 (ppm)

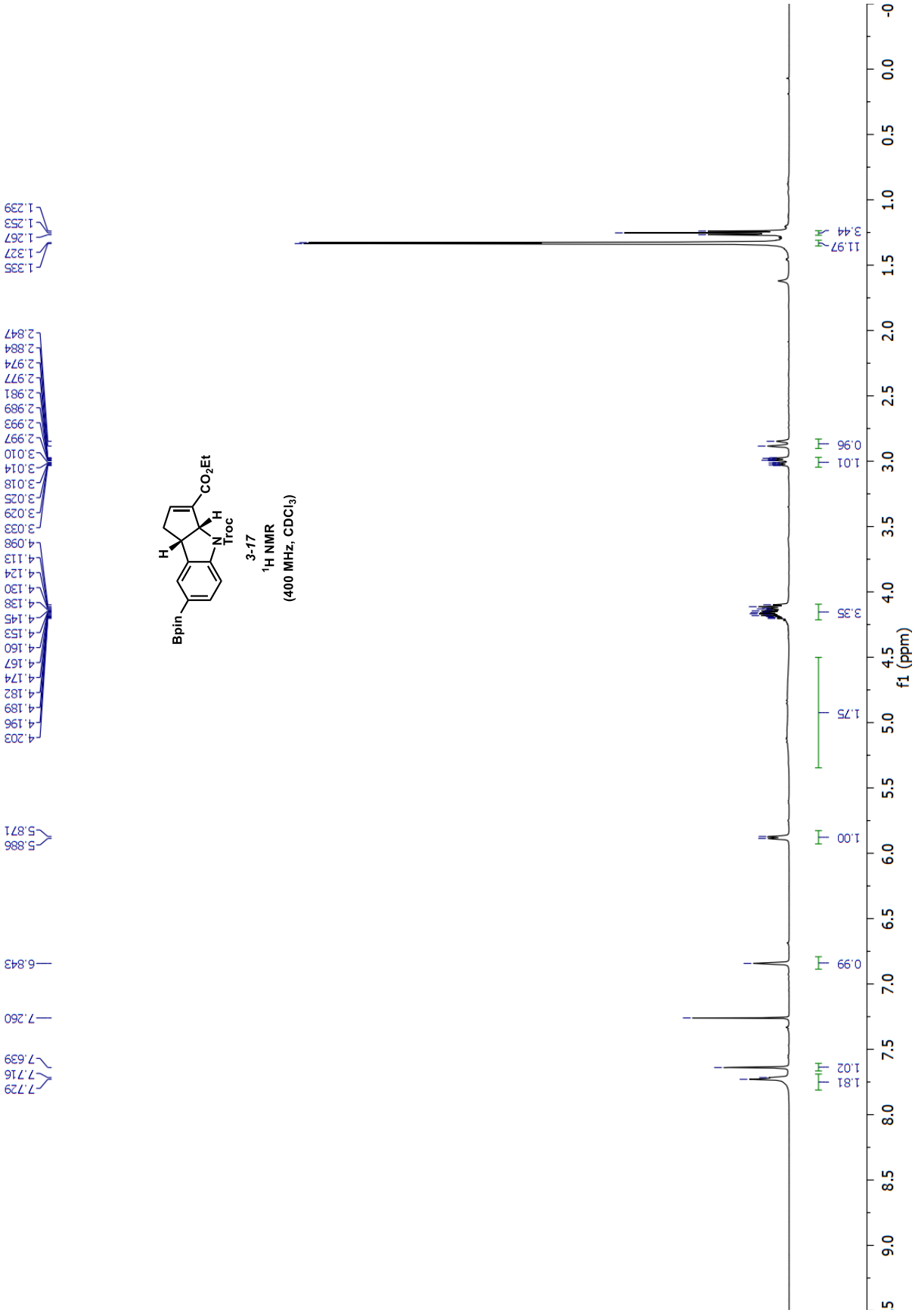
CO2Et
H
N
Troc
H
Bpin
3-17
1H NMR
(400 MHz, CDCl3)
f1 (ppm)

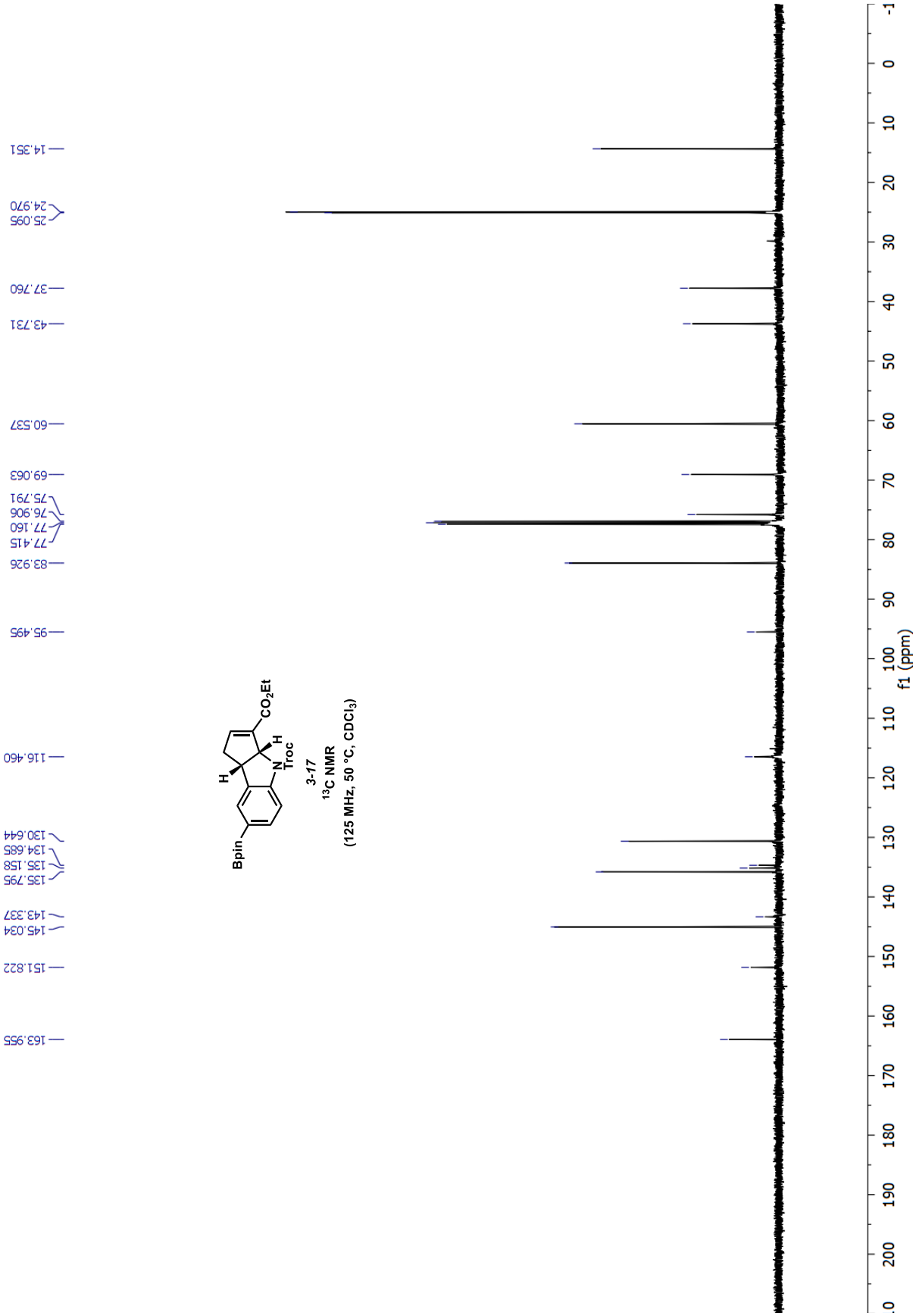
14.351
24.970
25.095
37.760
43.731
60.537
69.063
75.791
76.906
77.160
77.415
83.926
95.495
116.460
130.644
134.685
135.158
135.795
143.337
145.034
151.822
163.955
Bpin
H
N
Troc
H
CO2Et
3-17
13C NMR
(125 MHz, 50 °C, CDCl3)
f1 (ppm)

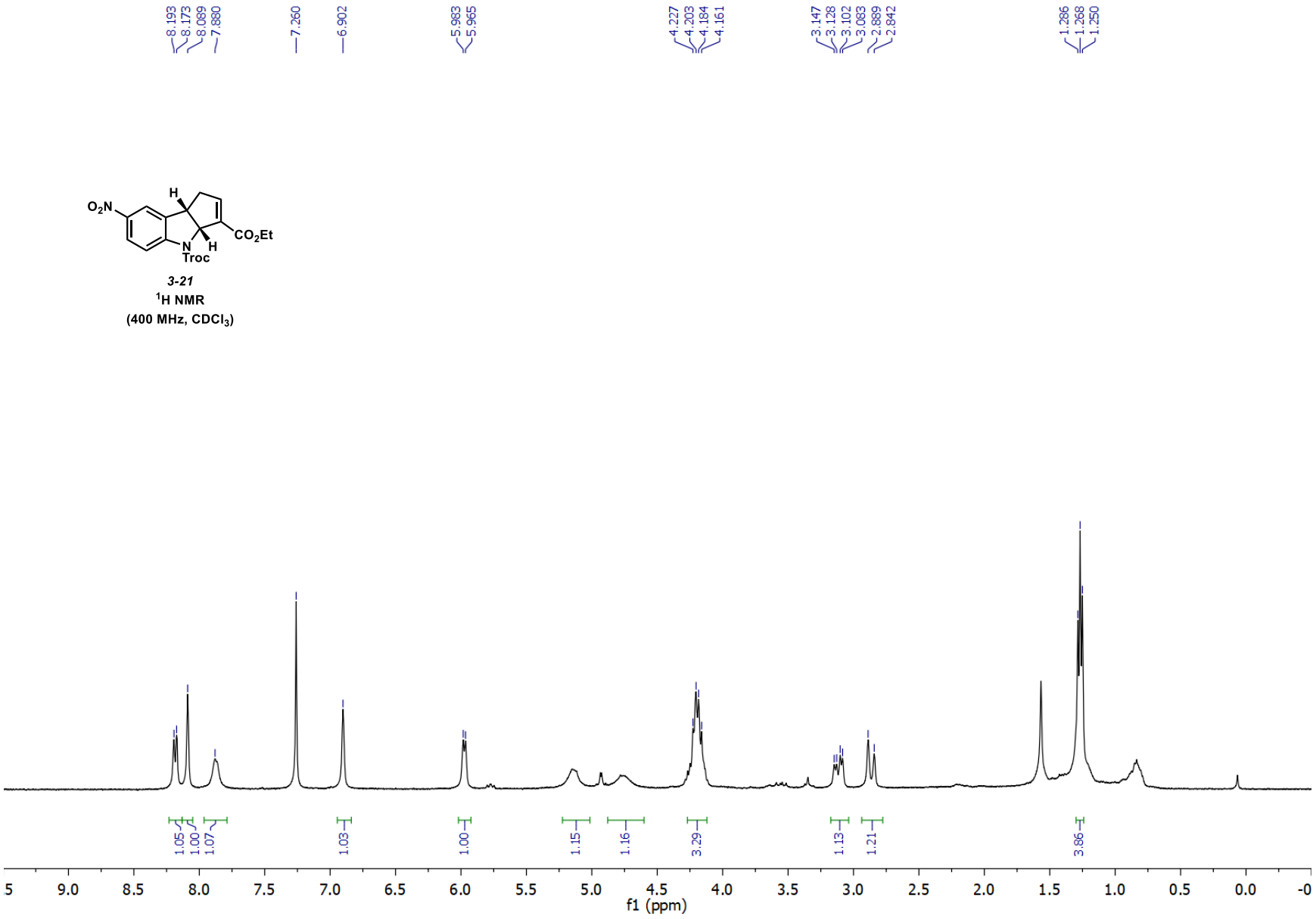
8.193
8.173
8.089
7.880
7.260
6.902
5.983
5.965
4.227
4.203
4.184
4.161
3.147
3.128
3.102
3.083
2.889
2.842
1.286
1.268
1.250
O2N
H
CO2Et
N
H
Troc
3-21
1H NMR
(400 MHz, CDCl3)
1.05
1.00
1.07
1.03
1.00
1.15
1.16
3.29
1.13
1.21
3.86
f1 (ppm)

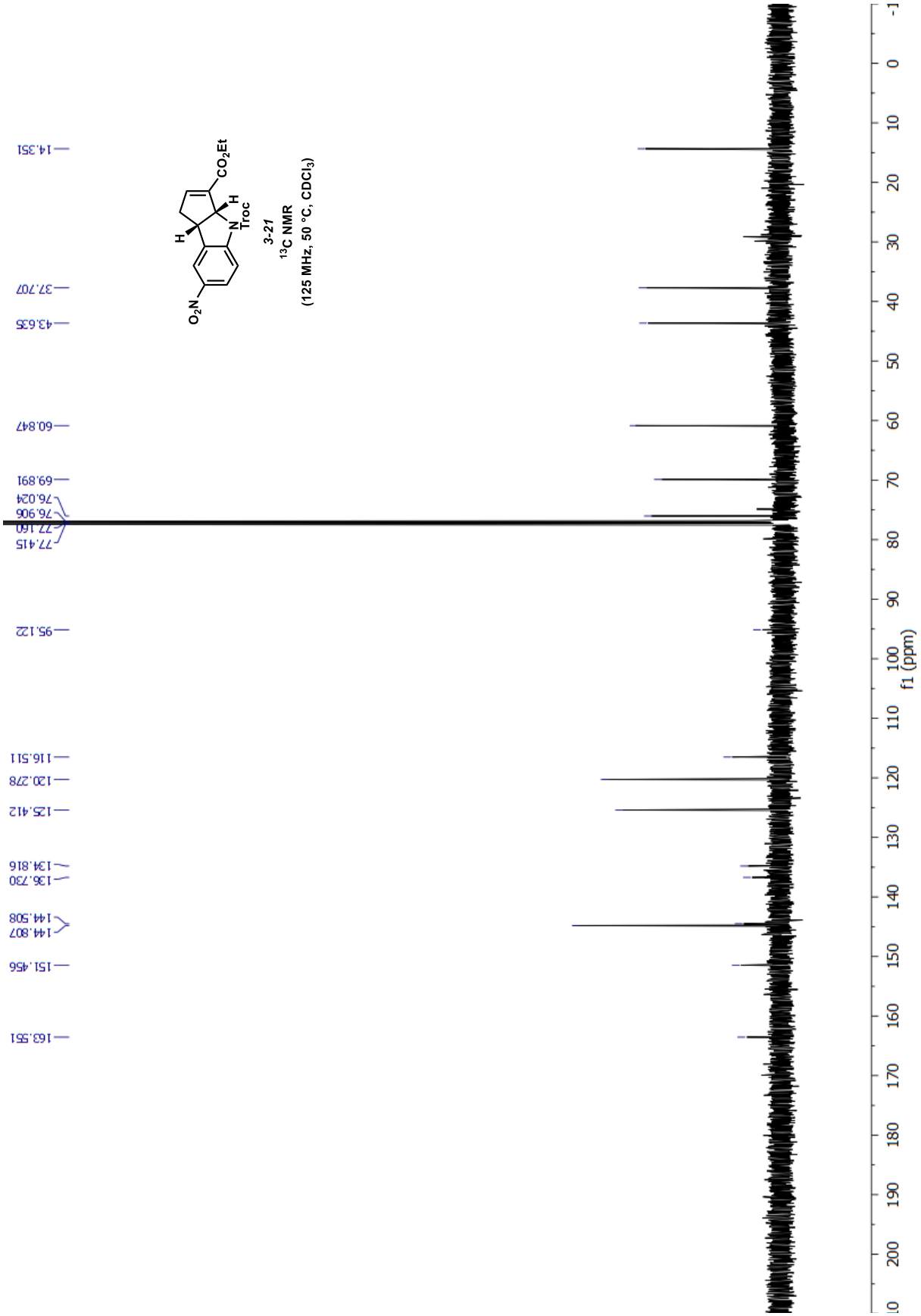
14.351
37.707
43.635
60.847
69.891
76.024
76.906
77.160
77.415
95.122
116.511
130.278
135.412
134.816
136.730
144.807
144.508
151.456
163.551
3-27
13C NMR
(125 MHz, 50 °C, CDCl3)
f1 (ppm)

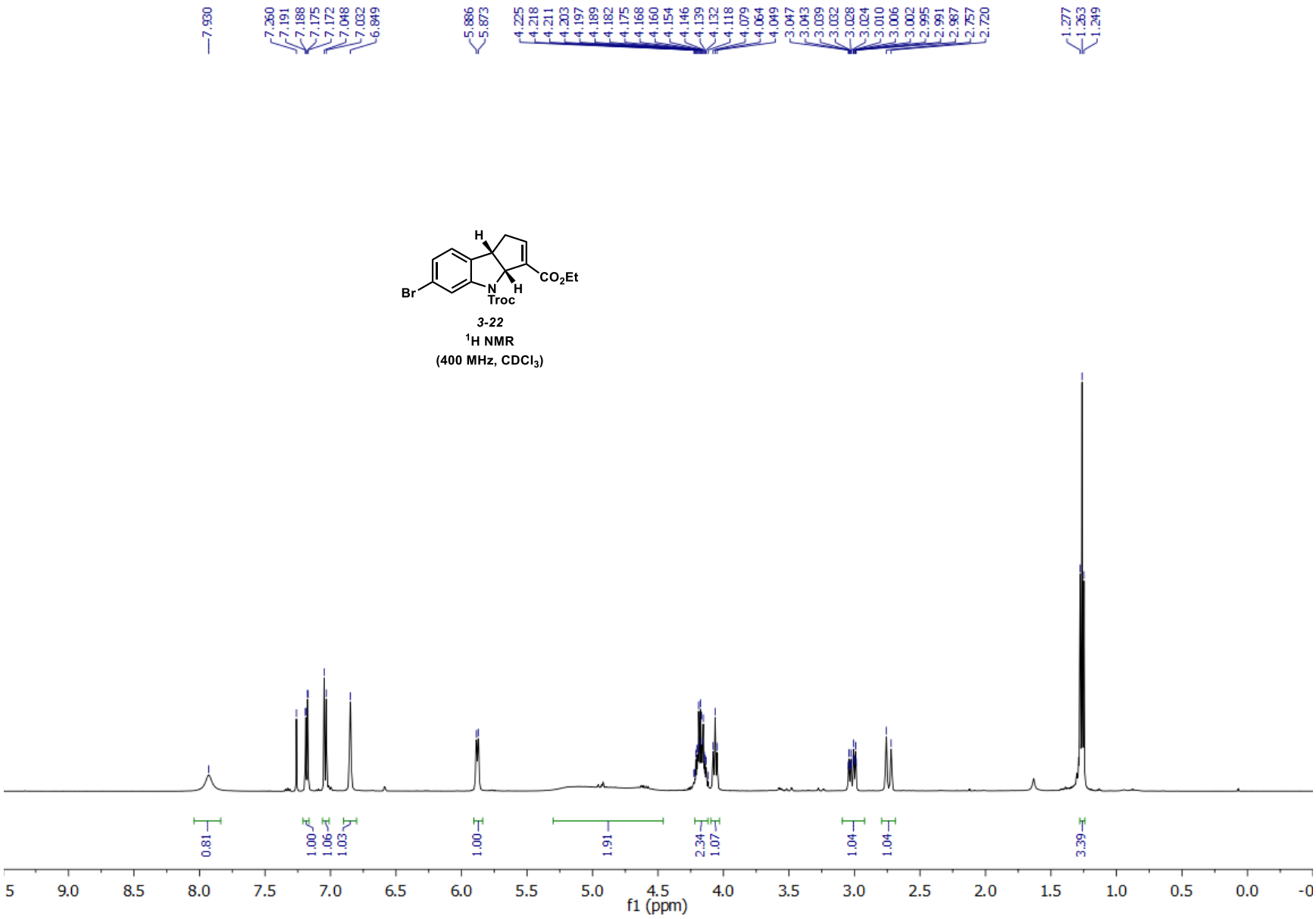
7.930
7.260
7.191
7.188
7.175
7.172
7.048
7.032
6.849
5.886
5.873
4.225
4.218
4.211
4.203
4.197
4.189
4.182
4.175
4.168
4.160
4.154
4.146
4.139
4.132
4.118
4.079
4.064
4.049
3.047
3.043
3.039
3.032
3.028
3.024
3.010
3.006
3.002
2.995
2.991
2.987
2.757
2.720
1.277
1.263
1.249
H
Br
N
Troc
H
CO2Et
3-22
1H NMR
(400 MHz, CDCl3)
0.81
1.00
1.06
1.03
1.00
1.91
2.34
1.07
1.04
1.04
3.39
f1 (ppm)

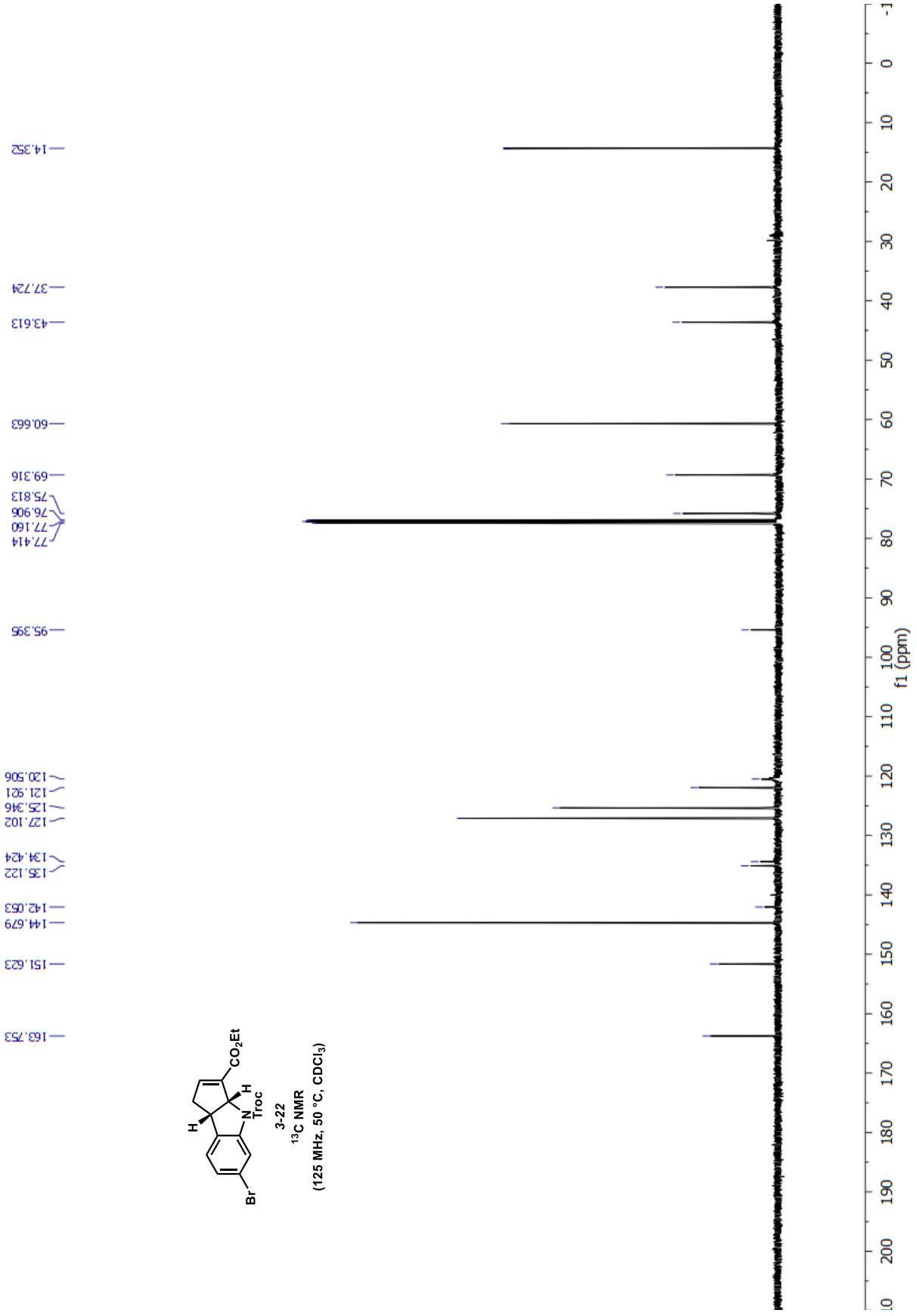
14.352
37.724
43.613
60.663
69.316
75.813
76.906
77.160
77.414
95.395
120.506
121.921
125.346
127.102
134.424
135.122
142.053
144.679
151.623
163.753
CO2Et
H
N
Troc
H
Br
3-22
13C NMR
(125 MHz, 50 °C, CDCl3)
f1 (ppm)

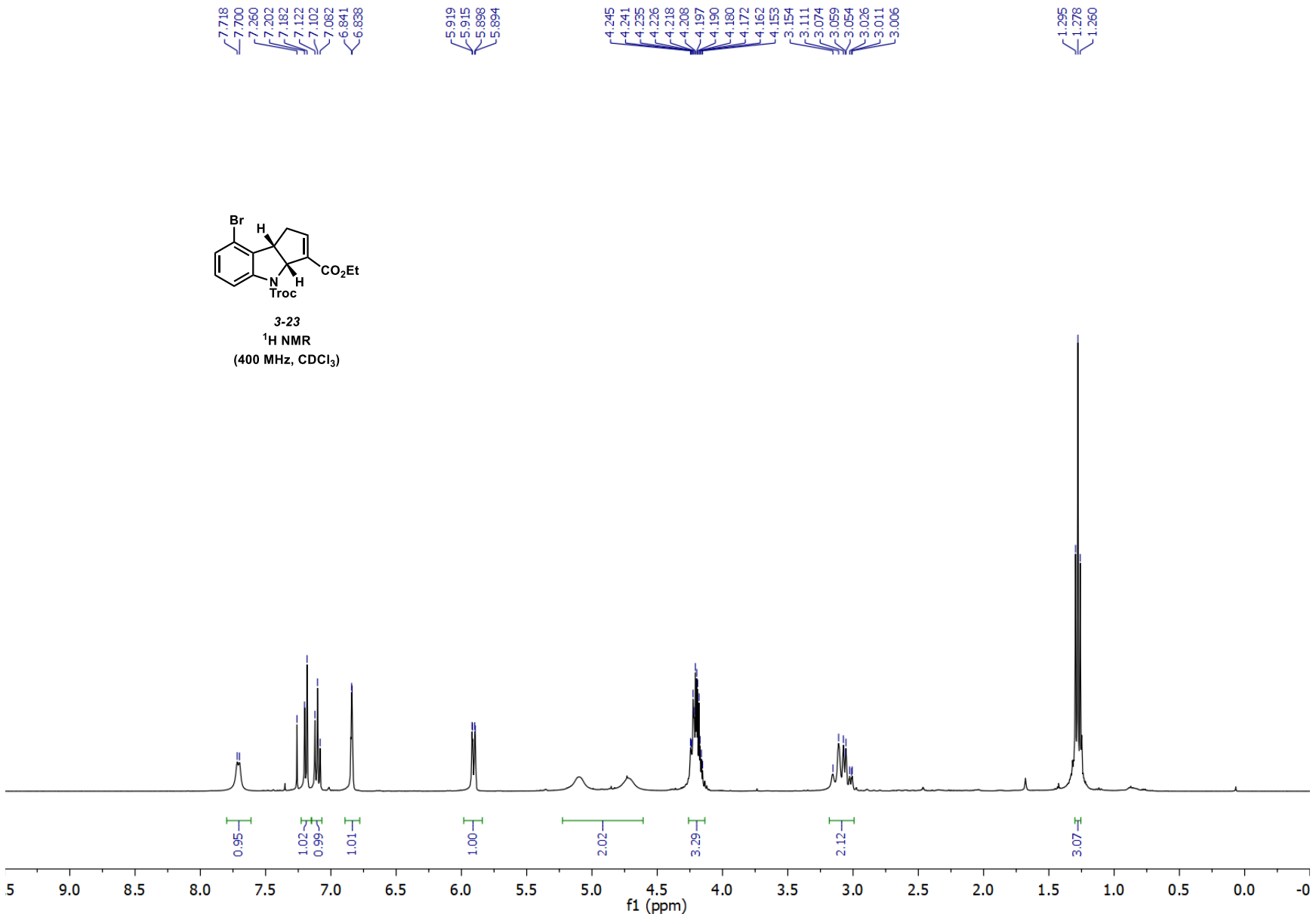
7.718
7.700
7.260
7.202
7.182
7.122
7.102
7.082
6.841
6.838
5.919
5.915
5.898
5.894
4.245
4.241
4.235
4.226
4.218
4.208
4.197
4.190
4.180
4.172
4.162
4.153
3.154
3.111
3.074
3.059
3.054
3.026
3.011
3.006
1.295
1.278
1.260
Br
H
CO2Et
N
H
Troc
3-23
1H NMR
(400 MHz, CDCl3)
0.95
1.02
0.99
1.01
1.00
2.02
3.29
2.12
3.07
f1 (ppm)

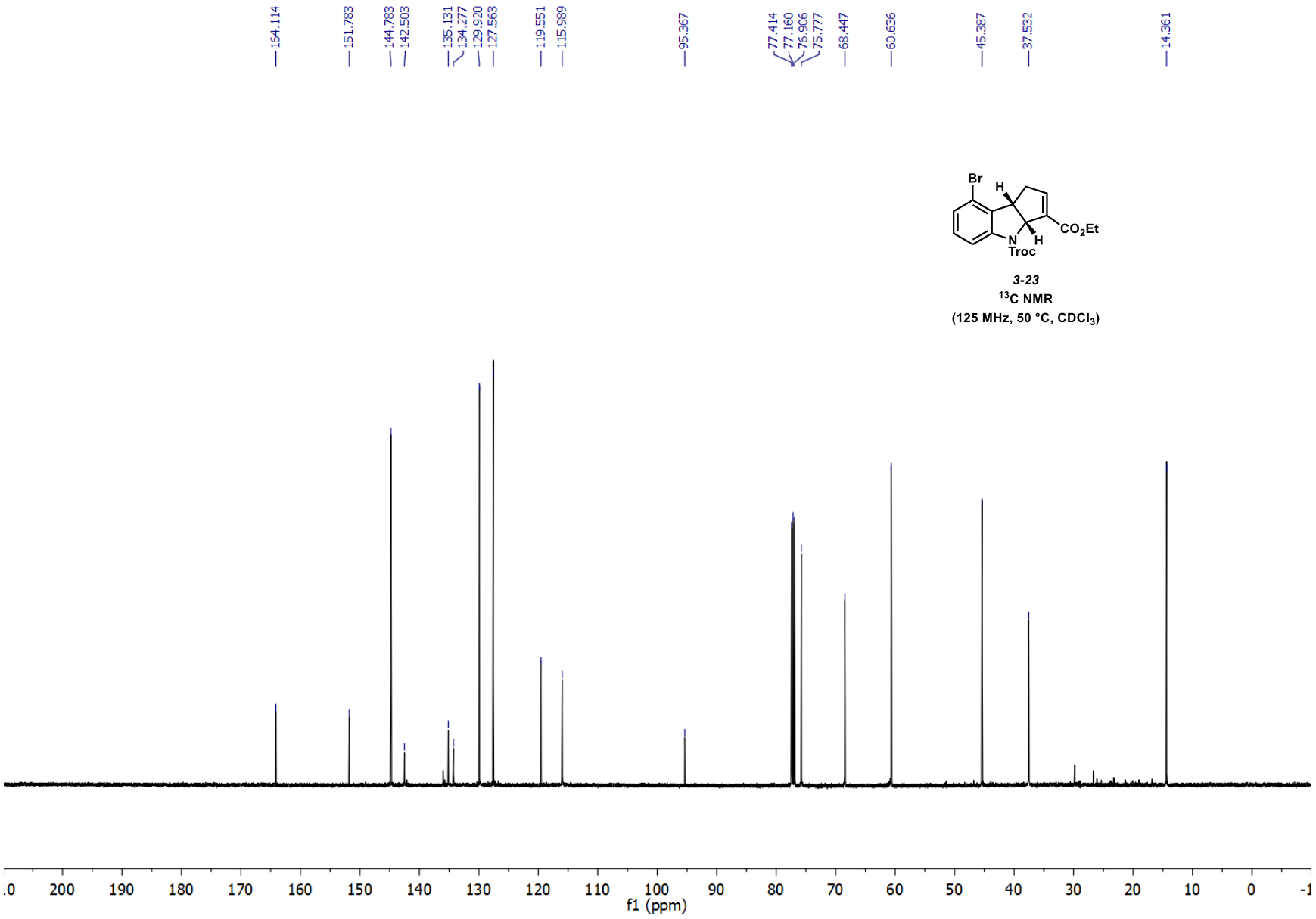
164.114
151.783
144.783
142.503
135.131
134.277
129.920
127.563
119.551
115.989
95.367
77.414
77.160
76.906
75.777
68.447
60.636
45.387
37.532
14.361
Br
H
CO2Et
N
H
Troc
3-23
13C NMR
(125 MHz, 50 °C, CDCl3)
f1 (ppm)

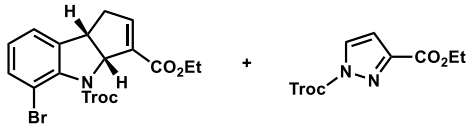

+

3-24

^{1}H NMR

(400 MHz, $CDCl_3$)

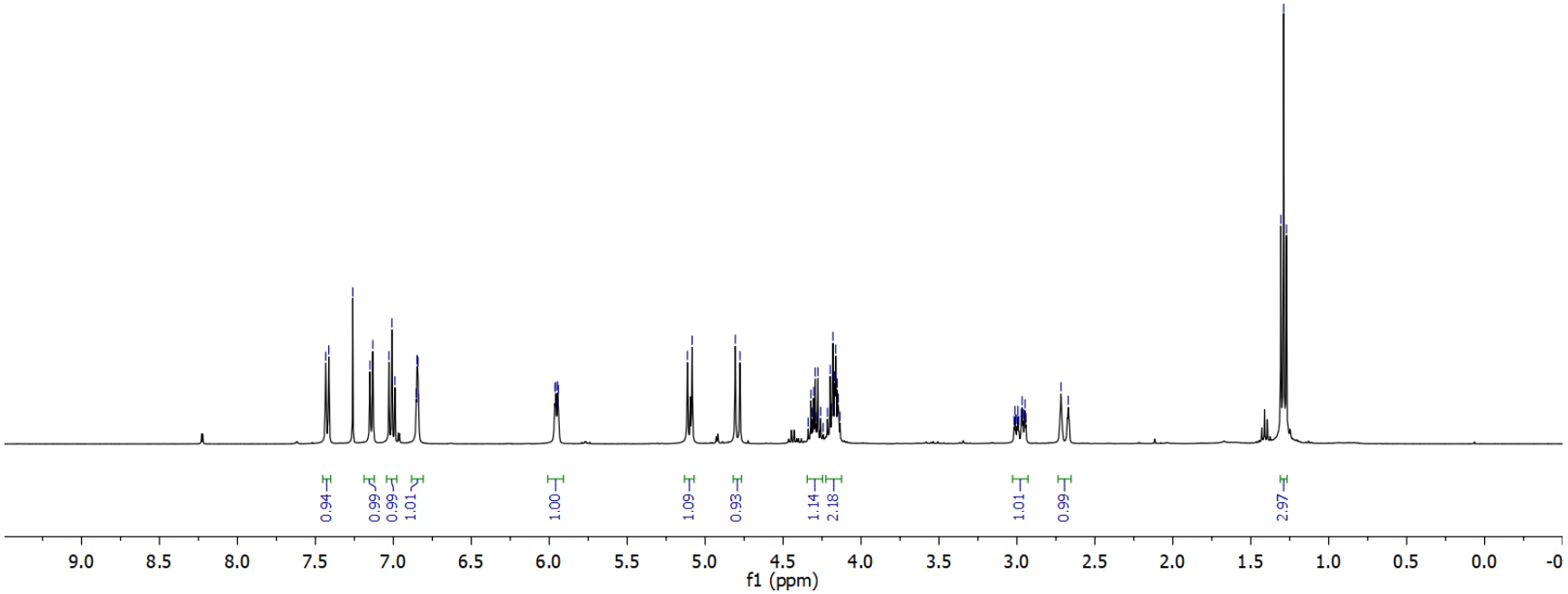

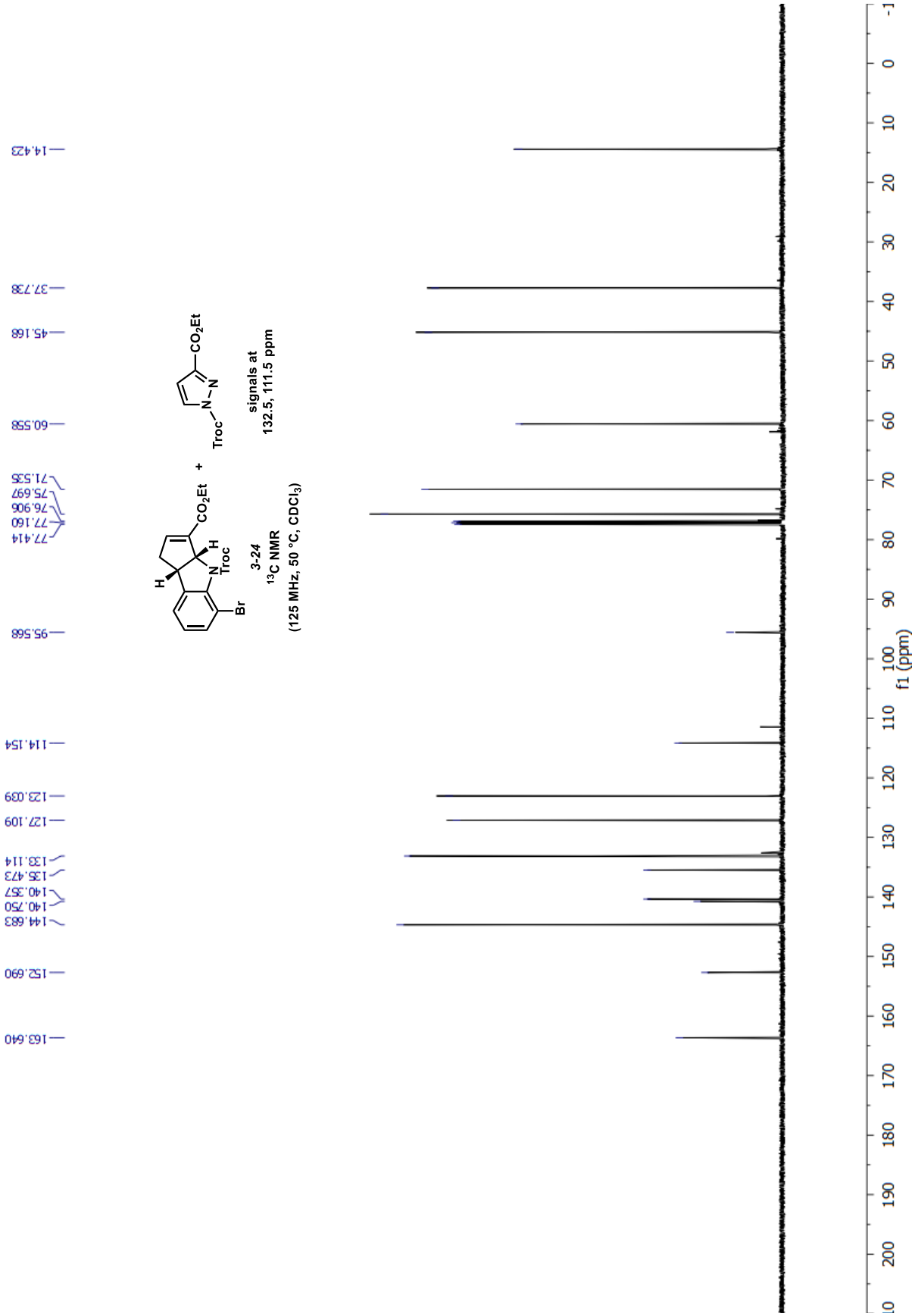
14.423
37.738
45.168
60.558
71.535
75.697
76.906
77.160
77.414
95.568
114.154
123.039
127.109
133.114
135.473
140.357
140.750
144.683
152.690
163.640
CO2Et
Troc
signals at
132.5, 111.5 ppm
+
CO2Et
H
Troc
N
H
Br
3-24
13C NMR
(125 MHz, 50 °C, CDCl3)
f1 (ppm)

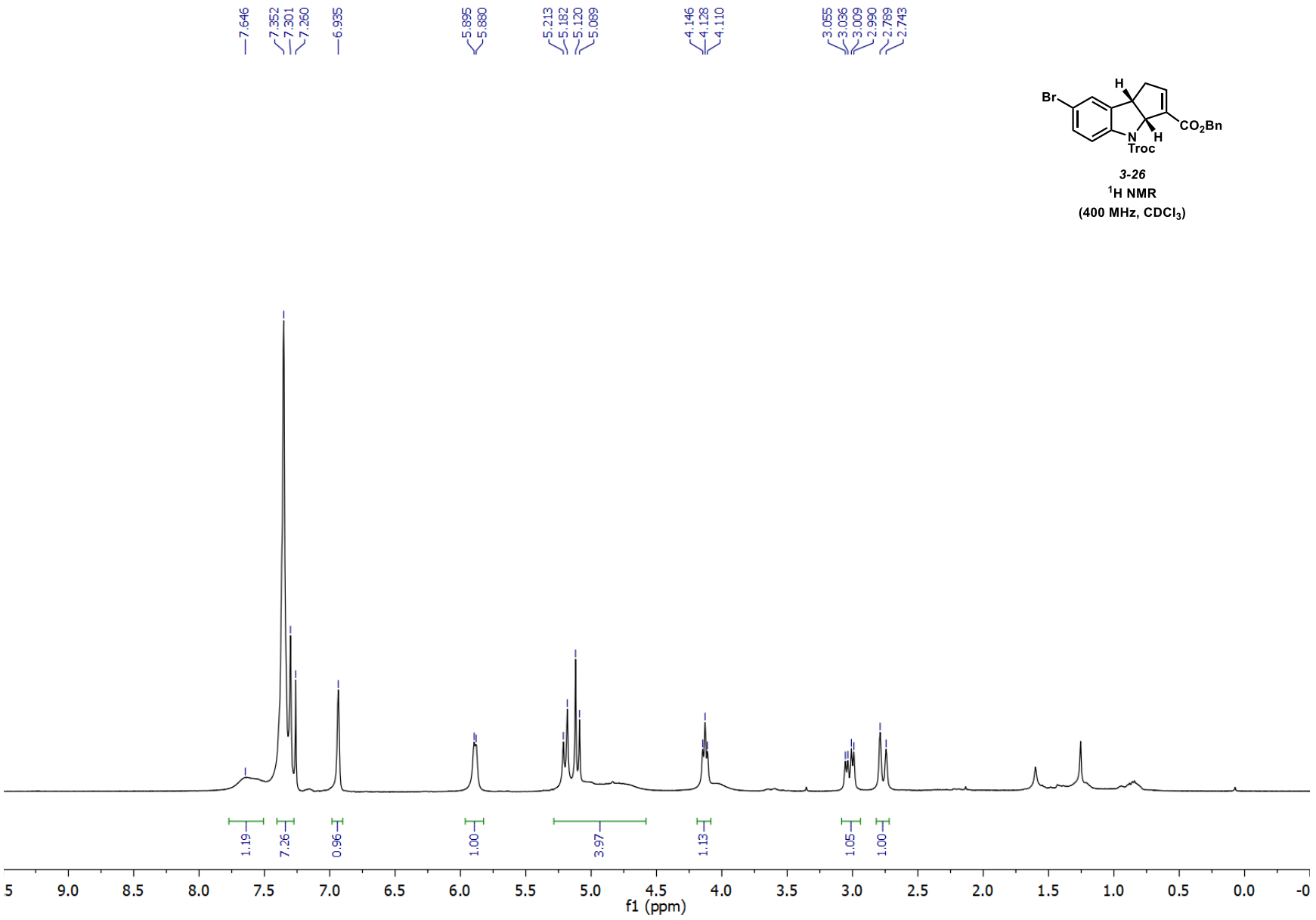
7.646
7.352
7.301
7.260
6.935
5.895
5.880
5.213
5.182
5.120
5.089
4.146
4.128
4.110
3.055
3.036
3.009
2.990
2.789
2.743
Br
H
N
H
Troc
CO2Bn
3-26
1H NMR
(400 MHz, CDCl3)
1.19
7.26
0.96
1.00
3.97
1.13
1.05
1.00
f1 (ppm)

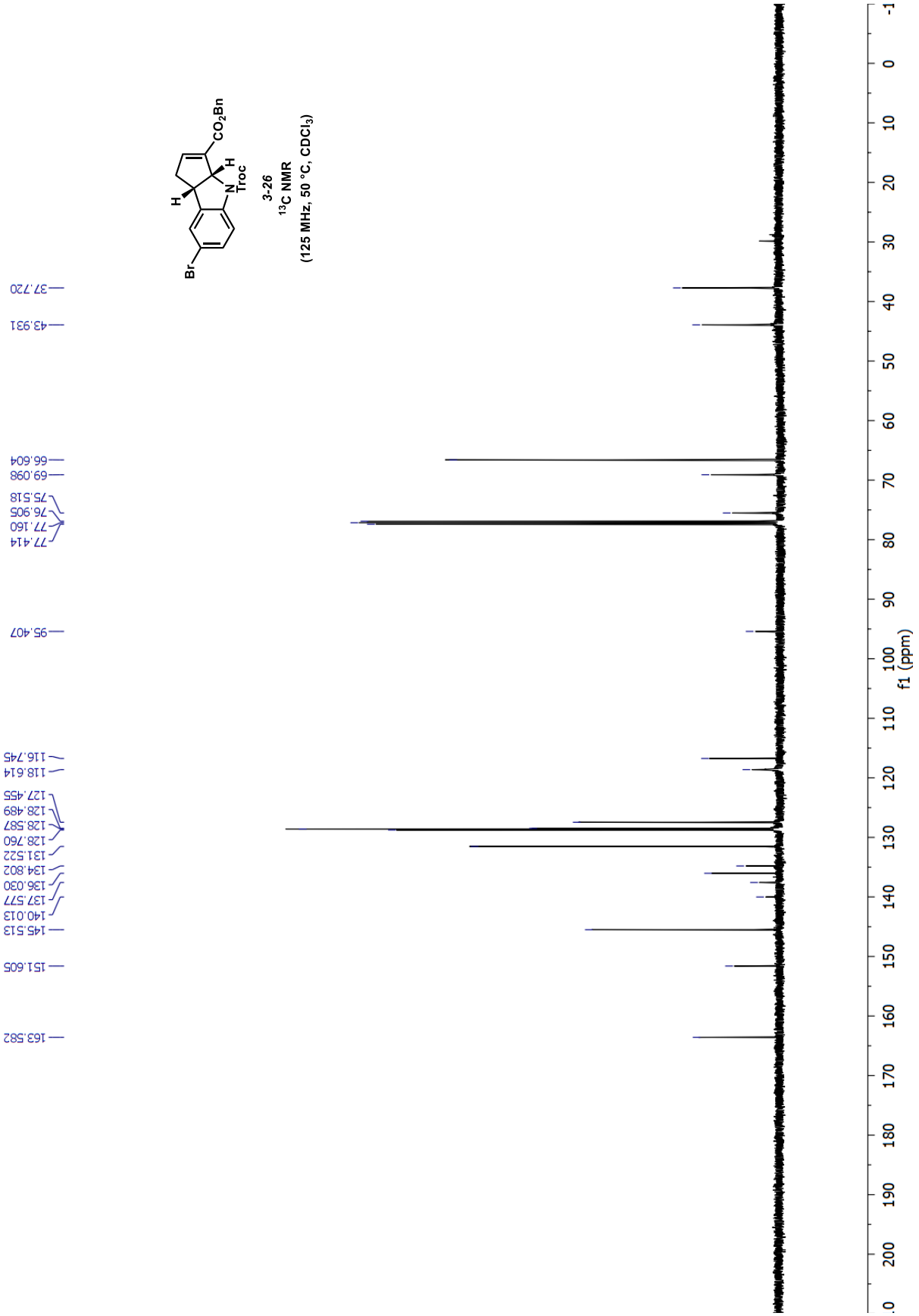
3-26
^{13}C NMR
(125 MHz, 50 °C, CDCl$_3$)
CO$_2$Bn
Troc
N
H
H
Br
37.720
43.931
66.604
69.098
75.518
76.905
77.160
77.414
95.407
116.745
118.614
127.455
128.489
128.587
128.760
131.522
134.802
136.030
137.577
140.013
145.513
151.605
163.582
f1 (ppm)

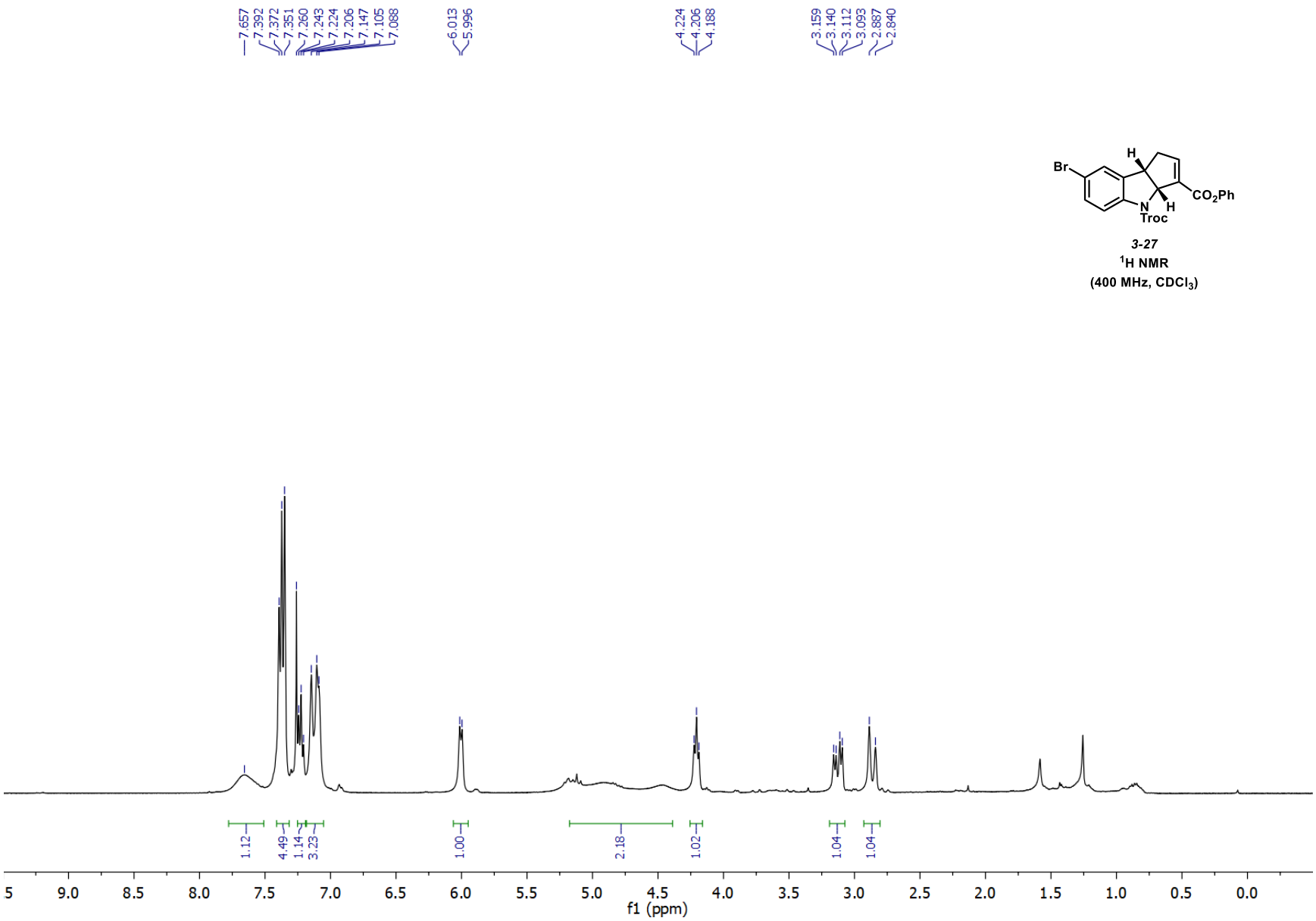

3-27
^{1}H NMR
(400 MHz, $CDCl_3$)

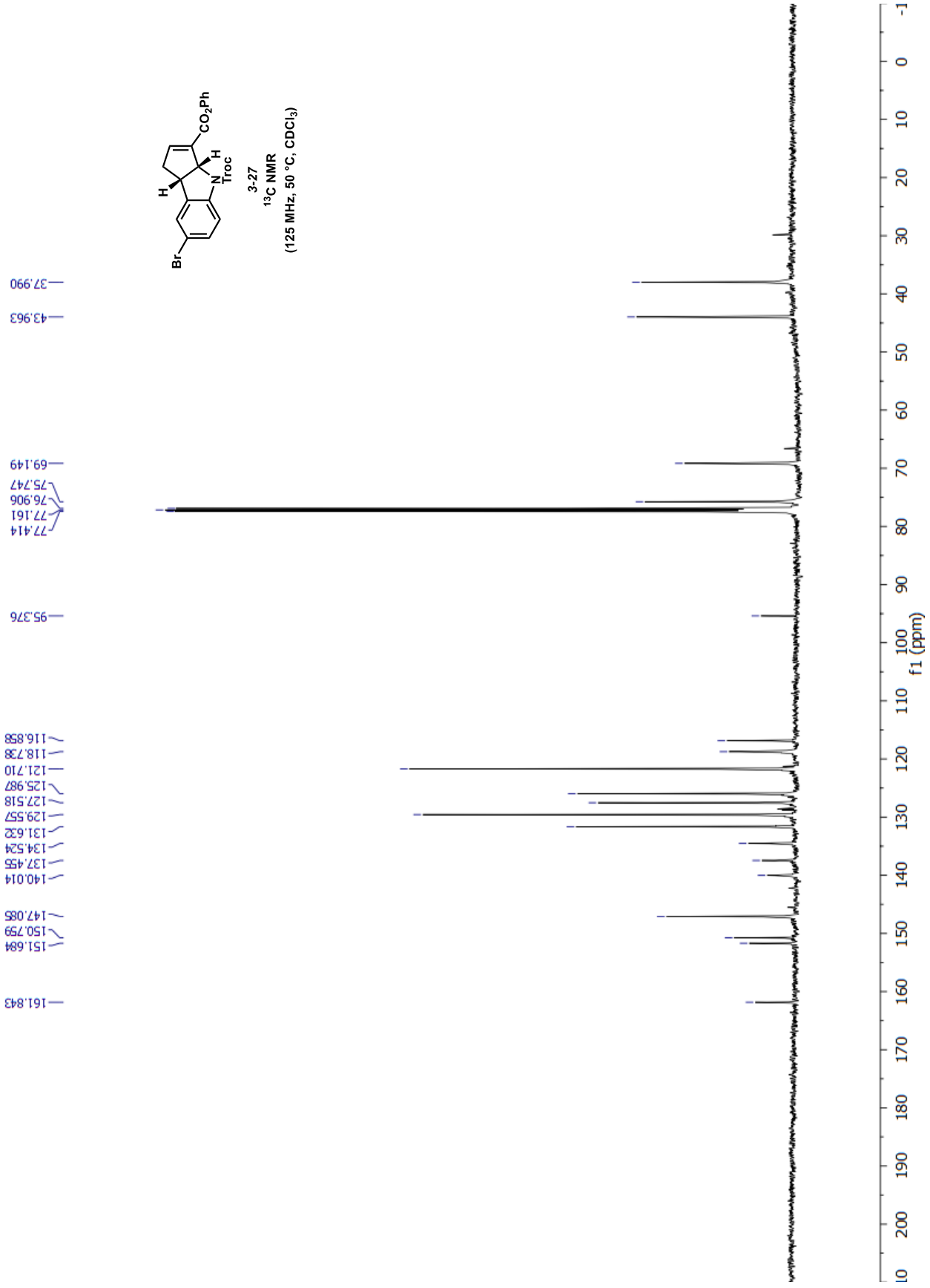
CO2Ph
H
N
Troc
H
Br
3-27
13C NMR
(125 MHz, 50 °C, CDCl3)
37.990
43.963
69.149
75.747
76.906
77.161
77.414
95.376
116.858
118.738
121.710
125.987
127.518
129.557
131.632
134.524
137.455
140.014
147.085
150.759
151.684
161.843
f1 (ppm)

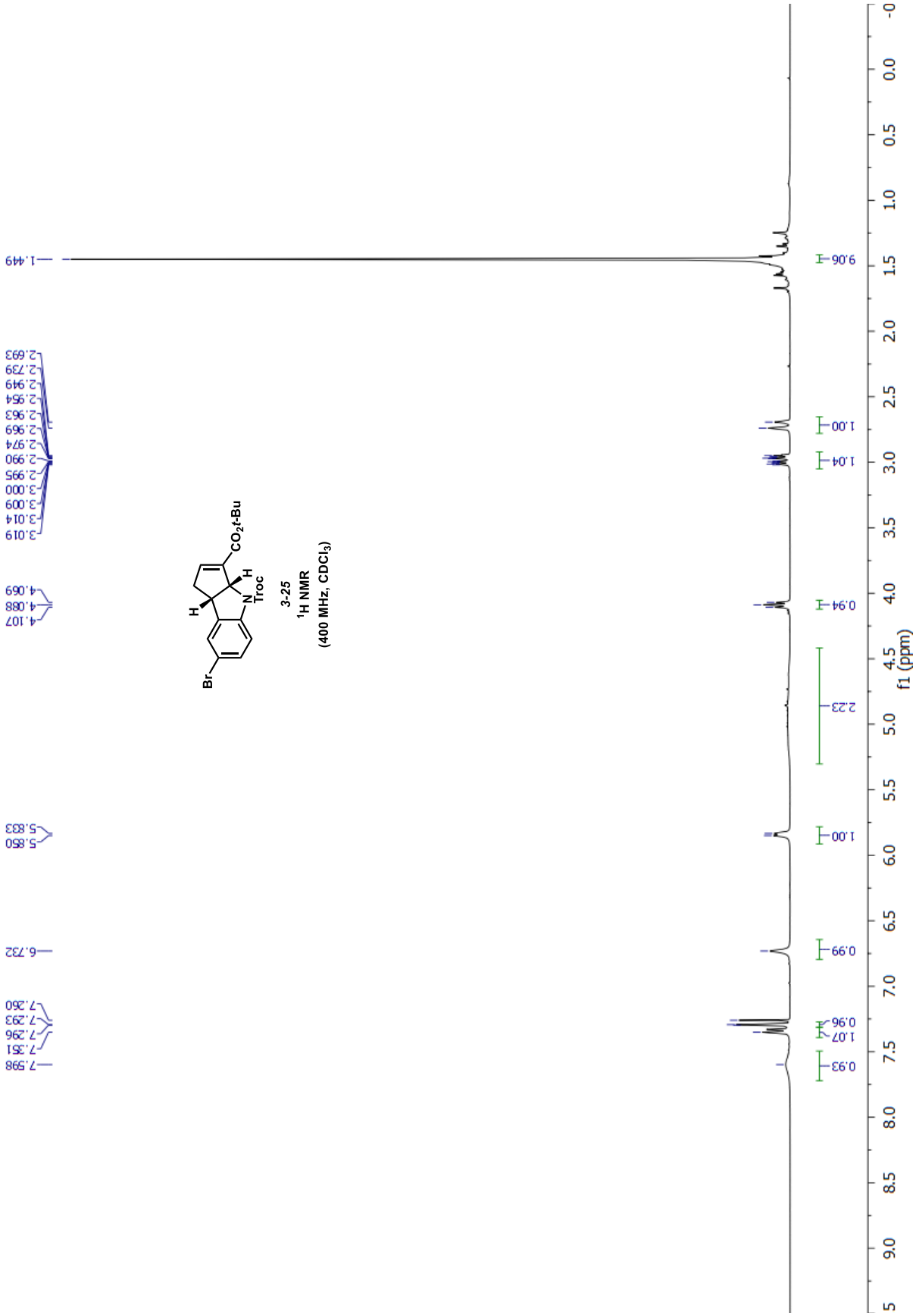
1.449
2.693
2.739
2.949
2.954
2.963
2.969
2.974
2.990
2.995
3.000
3.009
3.014
3.019
4.069
4.088
4.107
5.833
5.850
6.732
7.260
7.293
7.296
7.351
7.598
9.06
1.00
1.04
0.94
2.23
1.00
0.99
0.96
1.07
0.93
CO2t-Bu
H
N
Troc
H
Br
3-25
1H NMR
(400 MHz, CDCl3)
f1 (ppm)

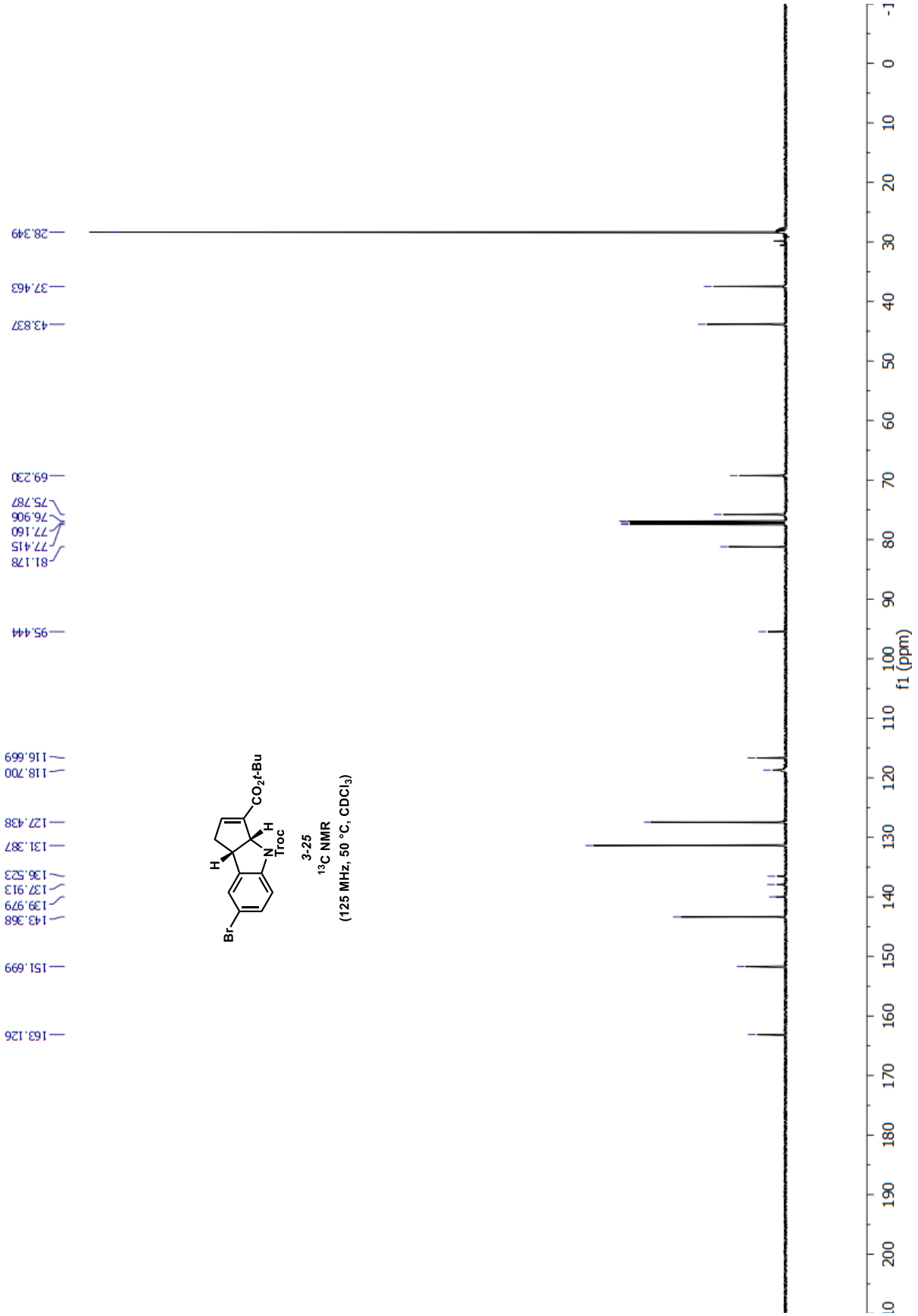
28.349
37.463
43.837
69.230
75.787
76.906
77.160
77.415
81.178
95.444
116.669
118.700
127.438
131.387
136.523
137.913
139.979
143.368
151.699
163.126
CO2t-Bu
H
N
Troc
H
Br
3-25
13C NMR
(125 MHz, 50 °C, CDCl3)
-10
0
10
20
30
40
50
60
70
80
90
100
110
120
130
140
150
160
170
180
190
200
f1 (ppm)

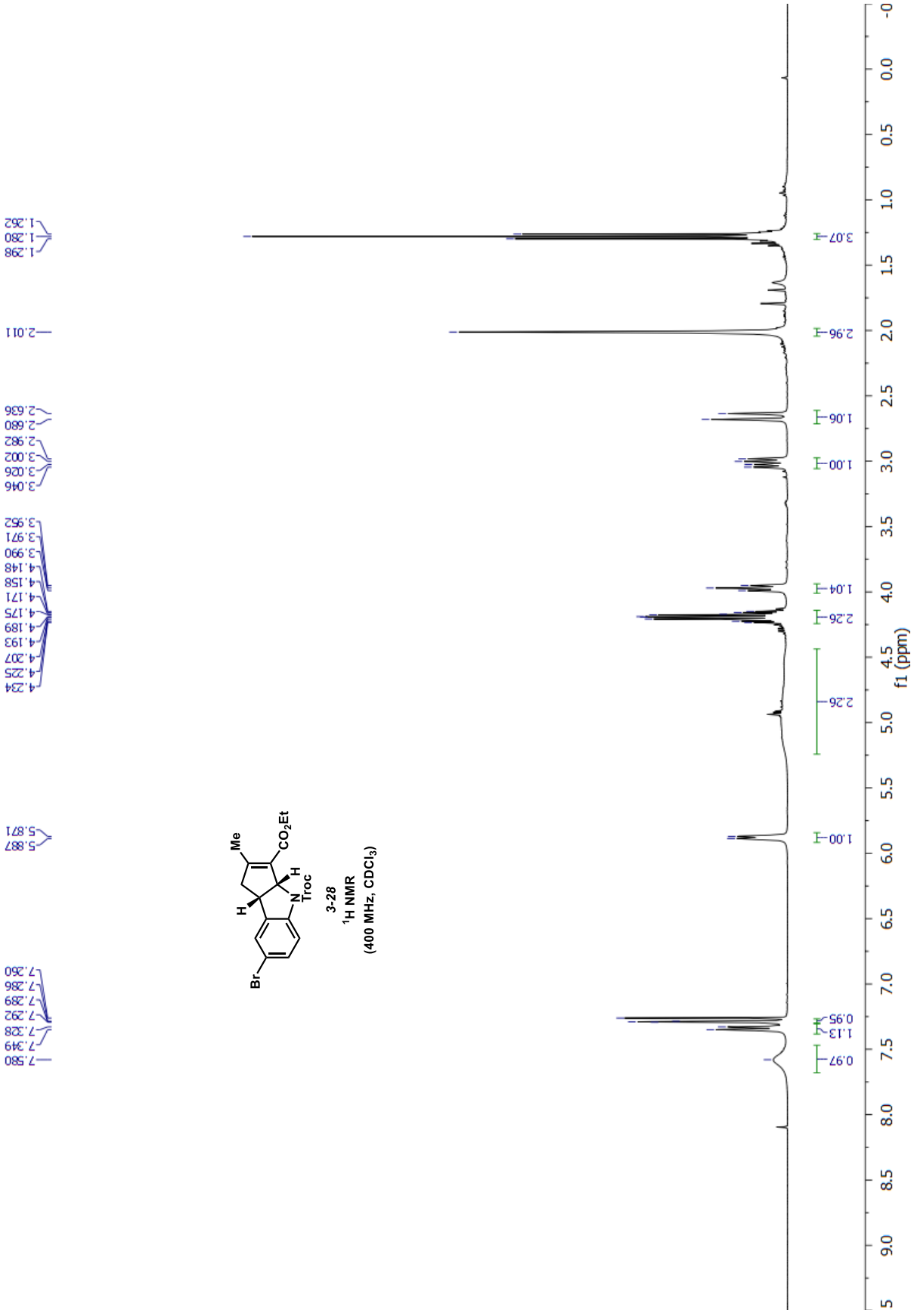
Me
CO2Et
H
Troc
N
H
Br
3-28
1H NMR
(400 MHz, CDCl3)
f1 (ppm)

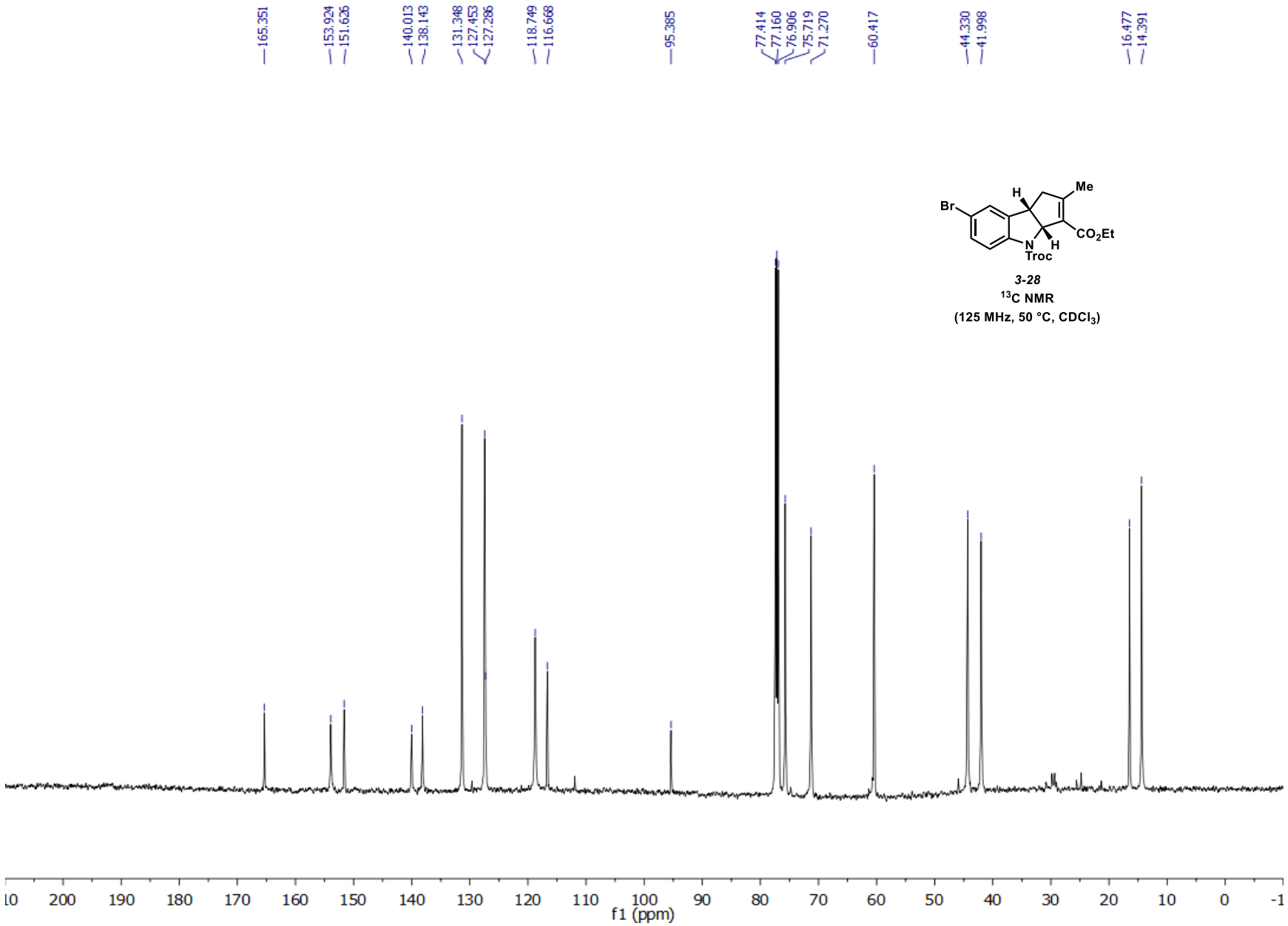
165.351
153.924
151.626
140.013
138.143
131.348
127.453
127.286
118.749
116.668
95.385
77.414
77.160
76.906
75.719
71.270
60.417
44.330
41.998
16.477
14.391
Br
H
Me
CO2Et
N
H
Troc
3-28
13C NMR
(125 MHz, 50 °C, CDCl3)
f1 (ppm)

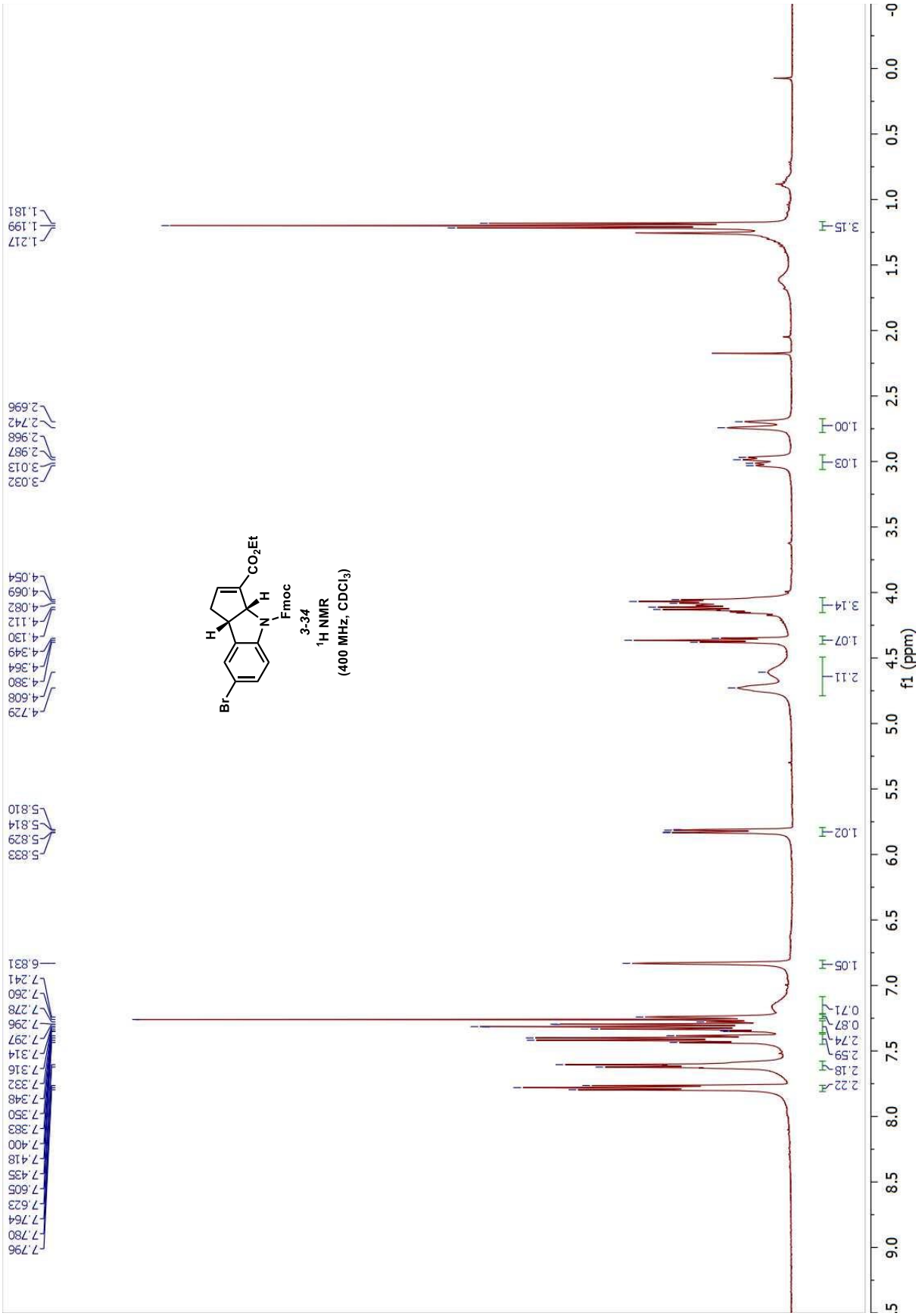
CO2Et
H
Fmoc
N
H
Br
3-34
1H NMR
(400 MHz, CDCl3)
f1 (ppm)

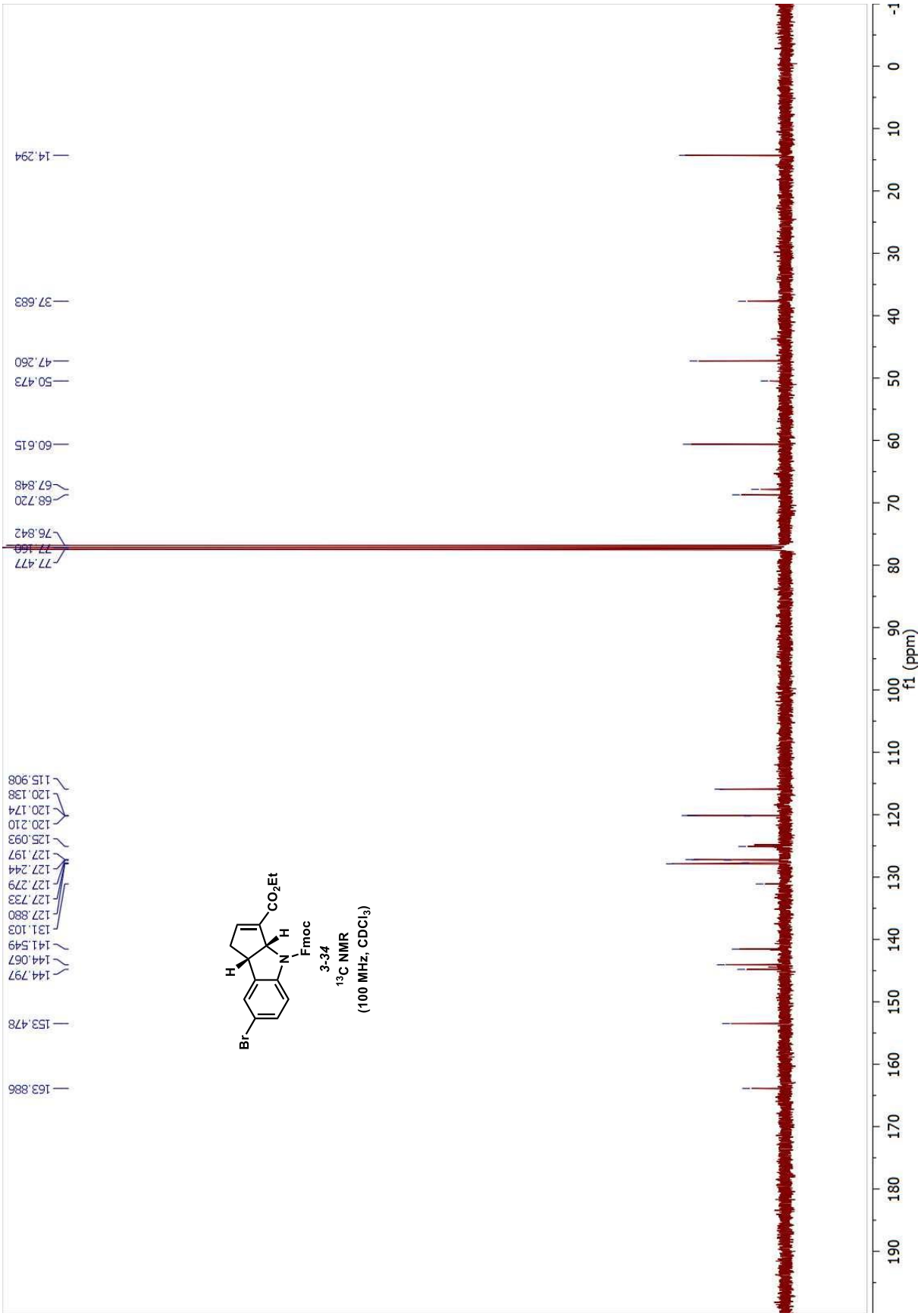
14.294
37.683
47.260
50.473
60.615
67.848
68.720
76.842
77.160
77.477
115.908
120.138
120.174
120.210
125.093
127.197
127.244
127.279
127.733
127.880
131.103
141.549
144.067
144.797
153.478
163.886
CO2Et
H
N
Fmoc
H
Br
3-34
13C NMR
(100 MHz, CDCl3)
f1 (ppm)

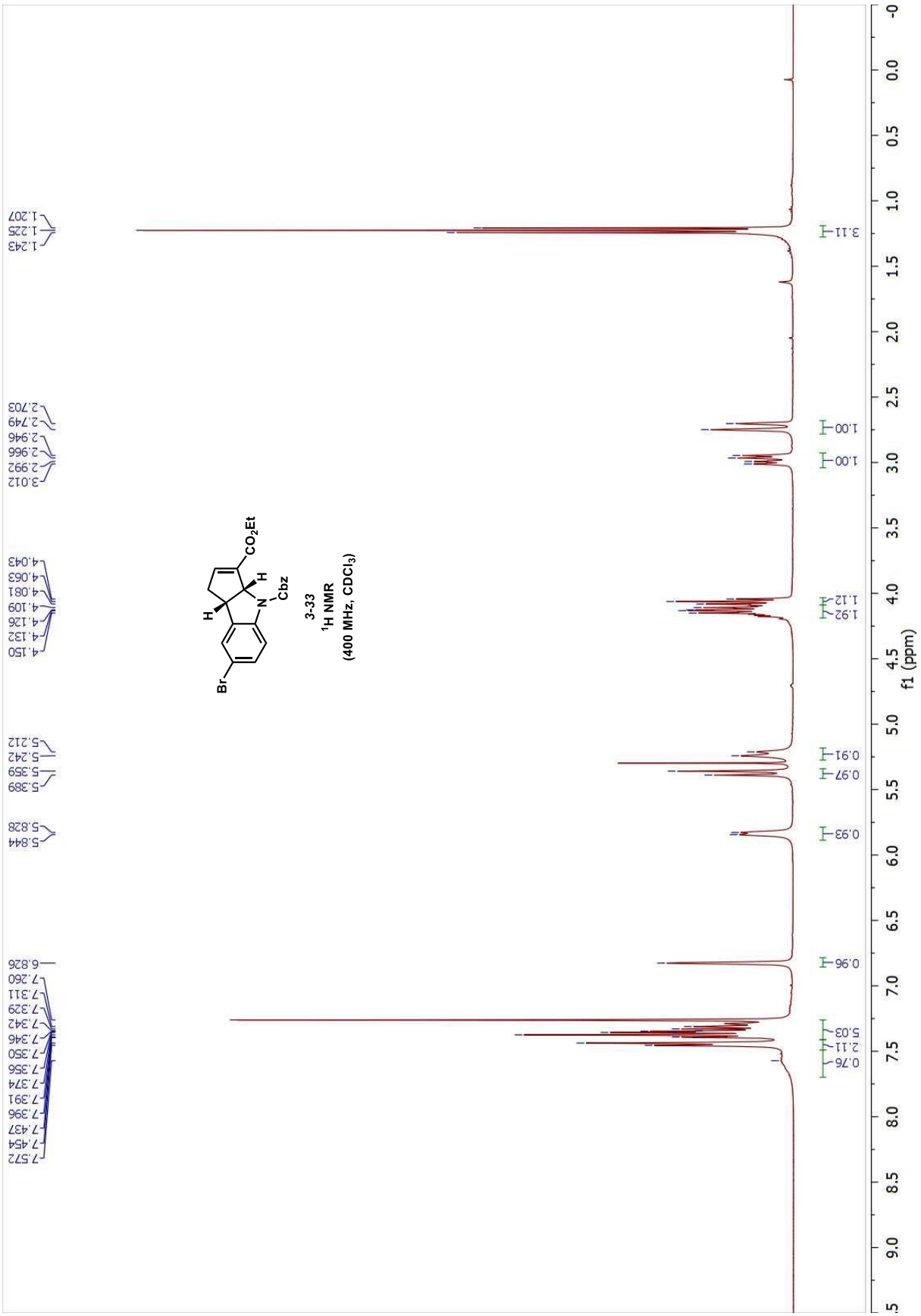
3-33
1H NMR
(400 MHz, CDCl3)
CO2Et
Cbz
Br
f1 (ppm)

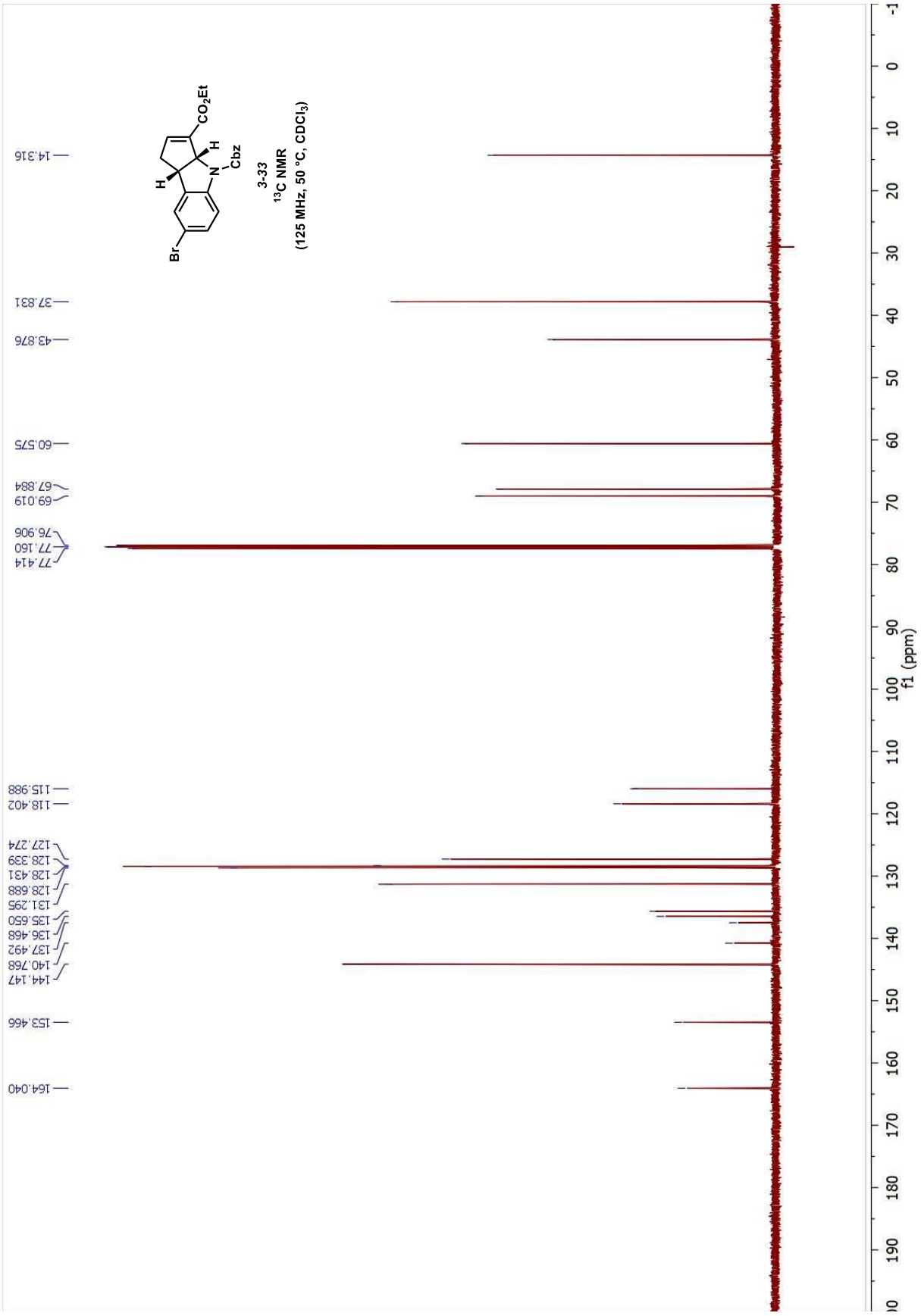
3-33
^{13}C NMR
(125 MHz, 50 °C, CDCl$_3$)
CO$_2$Et
H
N
Cbz
H
Br
14.316
37.831
43.876
60.575
67.884
69.019
76.906
77.160
77.414
115.988
118.402
127.274
128.339
128.431
128.688
131.295
135.650
136.468
137.492
140.768
144.147
153.466
164.040
f1 (ppm)

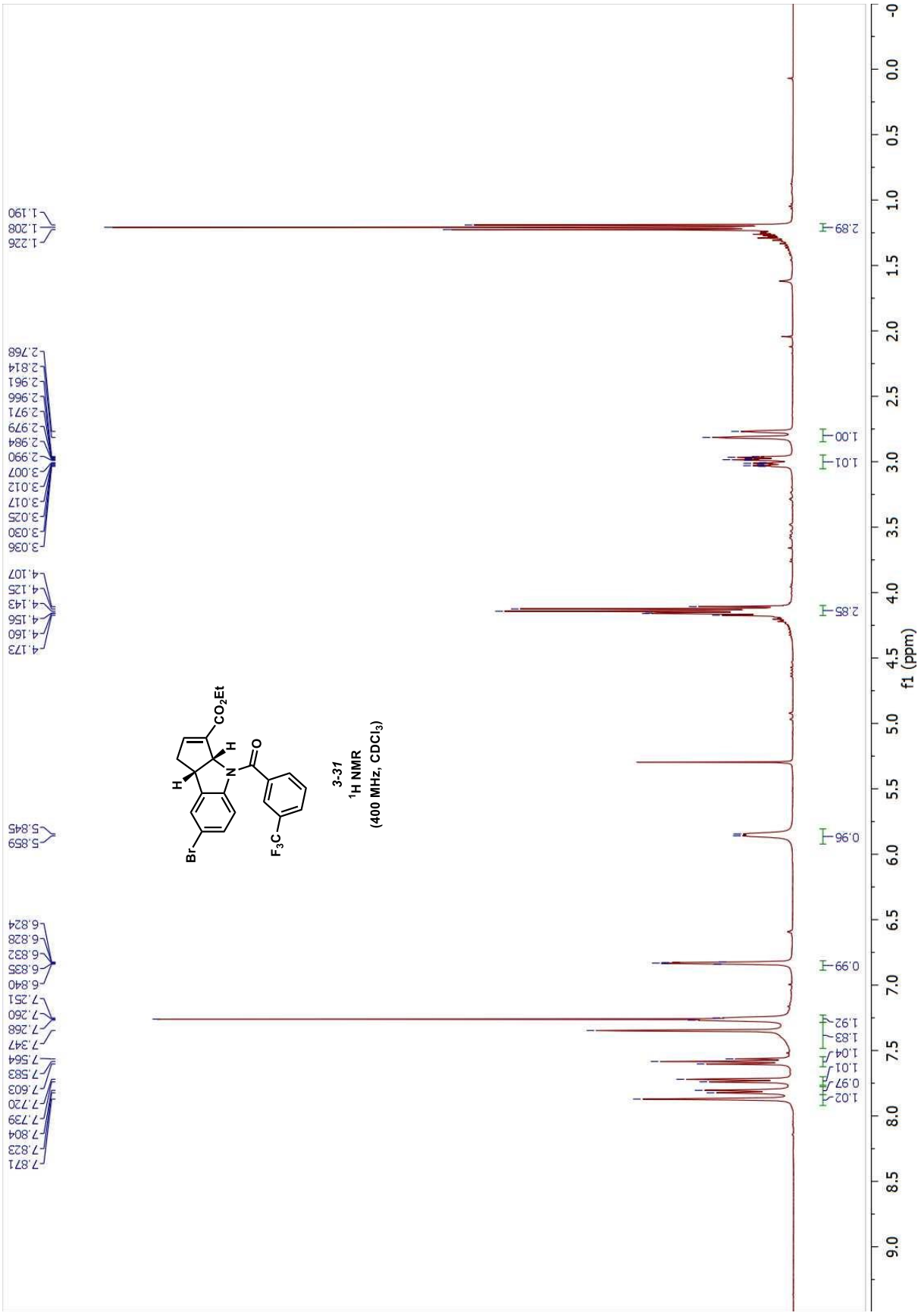
3-31
^{1}H NMR
(400 MHz, $CDCl_3$)
CO_2Et
H
H
N
O
Br
F_3C
f1 (ppm)

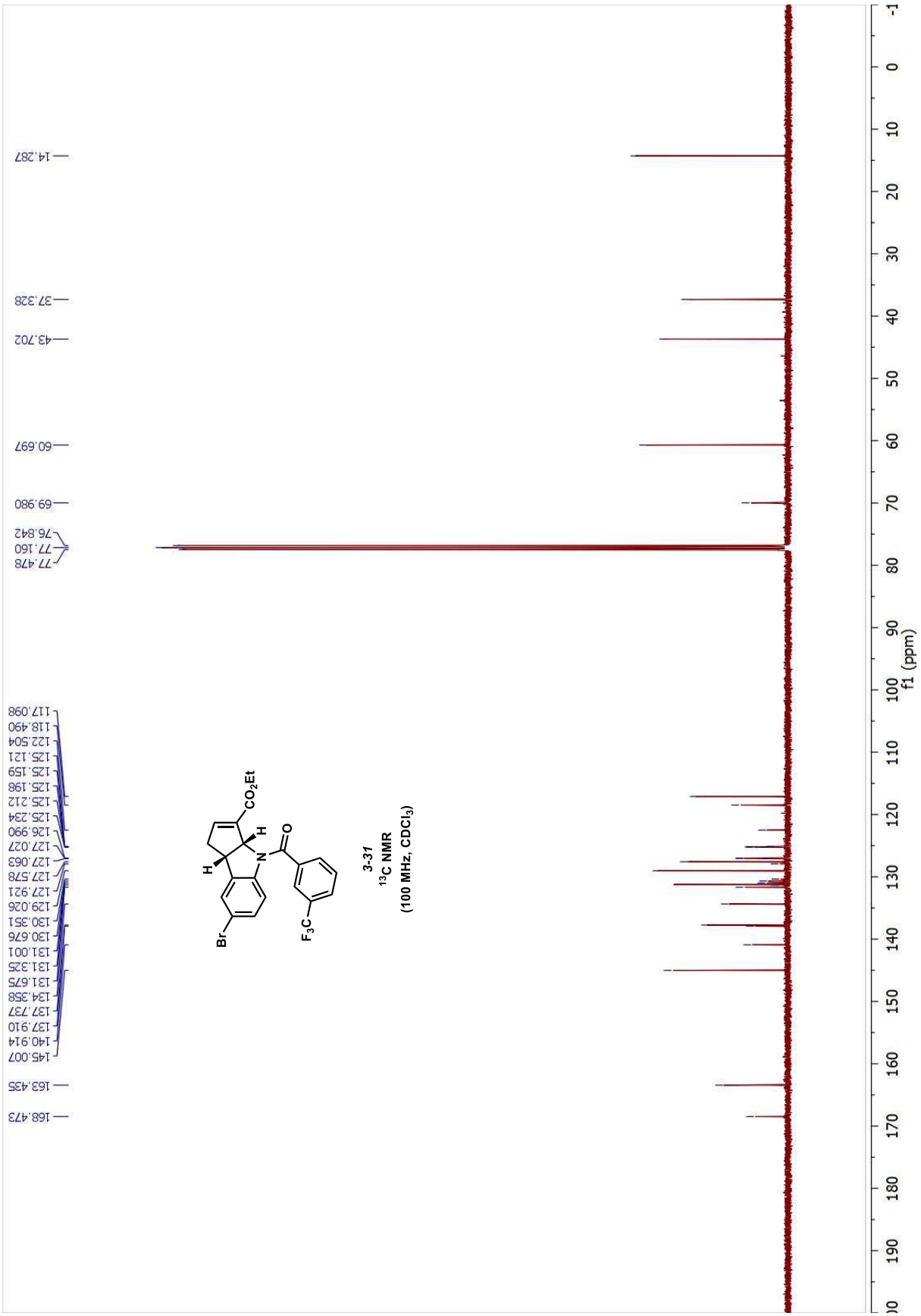
14.287
37.328
43.702
60.697
69.980
76.842
77.160
77.478
117.098
118.490
122.504
125.121
125.159
125.198
125.212
125.234
126.990
127.027
127.063
127.578
127.921
129.026
130.351
130.676
131.001
131.325
131.675
134.358
137.737
137.910
140.914
145.007
163.435
168.473
Br
CO2Et
F3C
3-31
13C NMR
(100 MHz, CDCl3)
f1 (ppm)

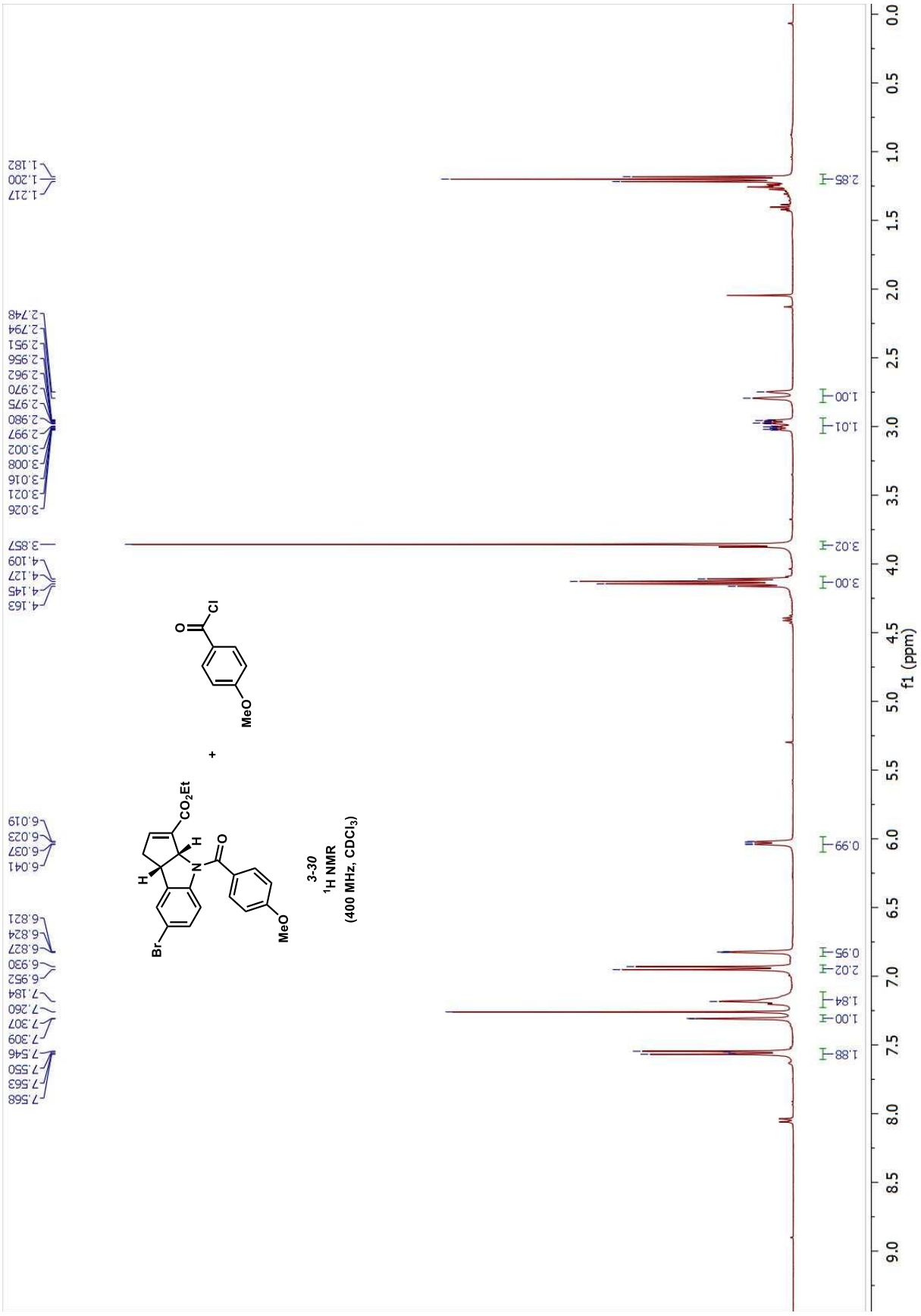
1.182
1.200
1.217
2.748
2.794
2.951
2.956
2.962
2.970
2.975
2.980
2.997
3.002
3.008
3.016
3.021
3.026
3.857
4.109
4.127
4.145
4.163
6.019
6.023
6.037
6.041
6.821
6.824
6.827
6.930
6.952
7.184
7.260
7.307
7.309
7.546
7.550
7.563
7.568
2.85
1.00
1.01
3.02
3.00
0.99
0.95
2.02
1.84
1.00
1.88
f1 (ppm)
0.0
0.5
1.0
1.5
2.0
2.5
3.0
3.5
4.0
4.5
5.0
5.5
6.0
6.5
7.0
7.5
8.0
8.5
9.0
CO2Et
H
N
O
Br
MeO
Cl
O
MeO
+
3-30
1H NMR
(400 MHz, CDCl3)

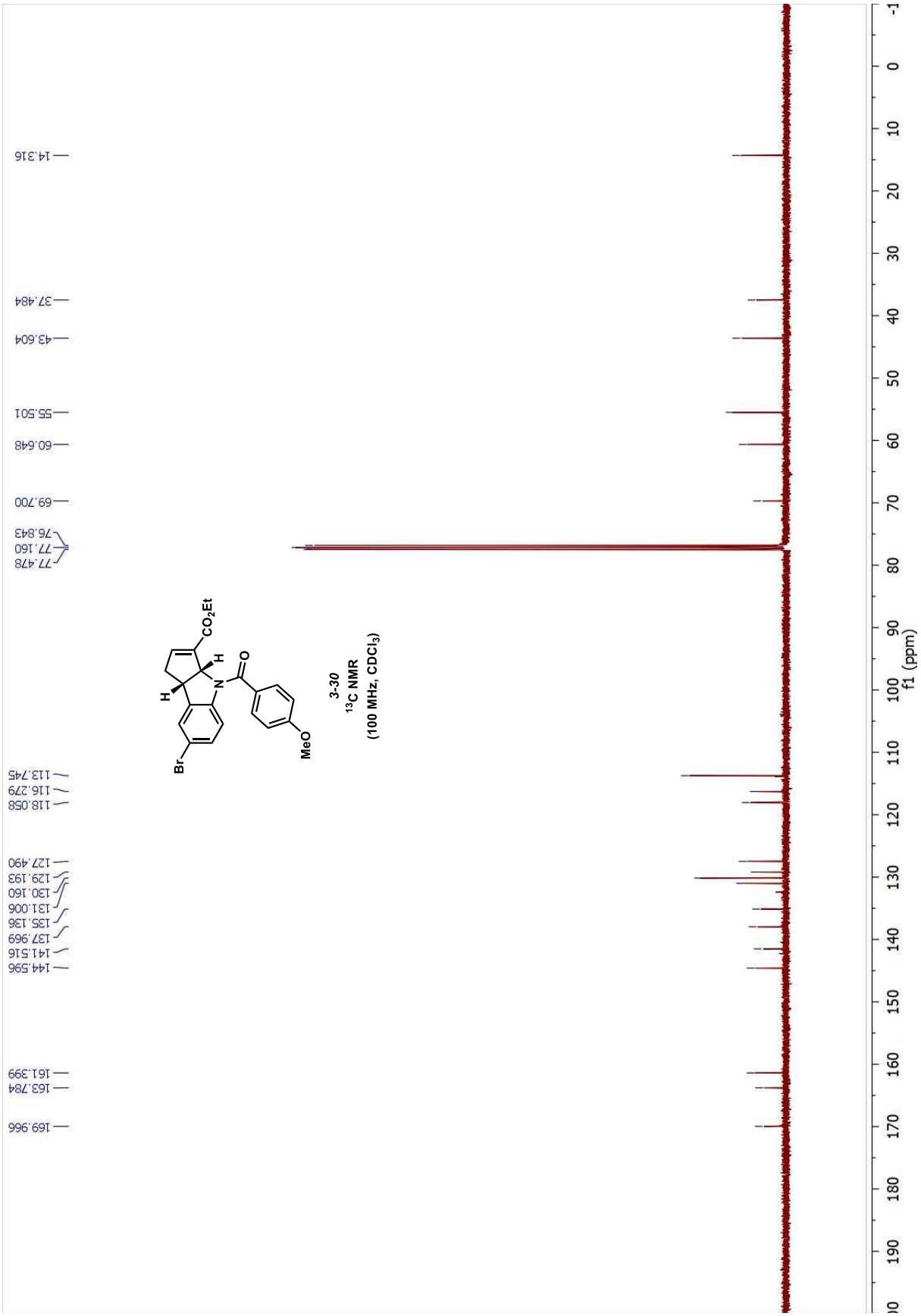
14.316
37.484
43.604
55.501
60.648
69.700
76.843
77.160
77.478
113.745
116.279
118.058
127.490
129.193
130.160
131.006
135.136
137.969
141.516
144.596
161.399
163.784
169.966
CO2Et
H
N
H
O
Br
MeO
3-30
13C NMR
(100 MHz, CDCl3)
f1 (ppm)

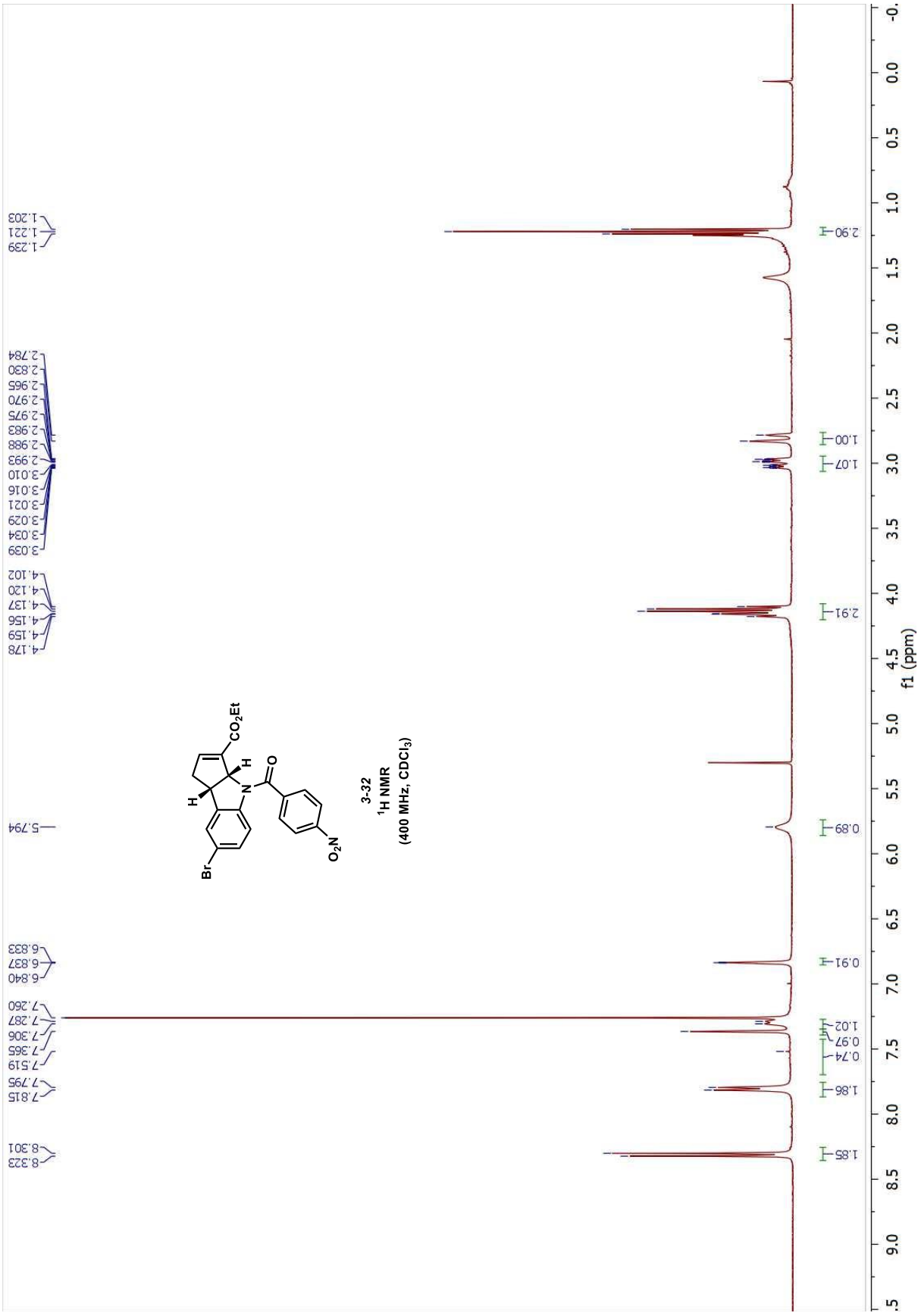
3-32
^{1}H NMR
(400 MHz, $CDCl_3$)
CO_2Et
H
H
N
O
Br
O_2N
8.323
8.301
7.815
7.795
7.519
7.365
7.306
7.287
7.260
6.840
6.837
6.833
5.794
4.178
4.159
4.156
4.137
4.120
4.102
3.039
3.034
3.029
3.021
3.016
3.010
2.993
2.988
2.983
2.975
2.970
2.965
2.830
2.784
1.239
1.221
1.203
2.90
1.00
1.07
2.91
0.89
0.91
1.02
0.97
0.74
1.86
1.85
f1 (ppm)

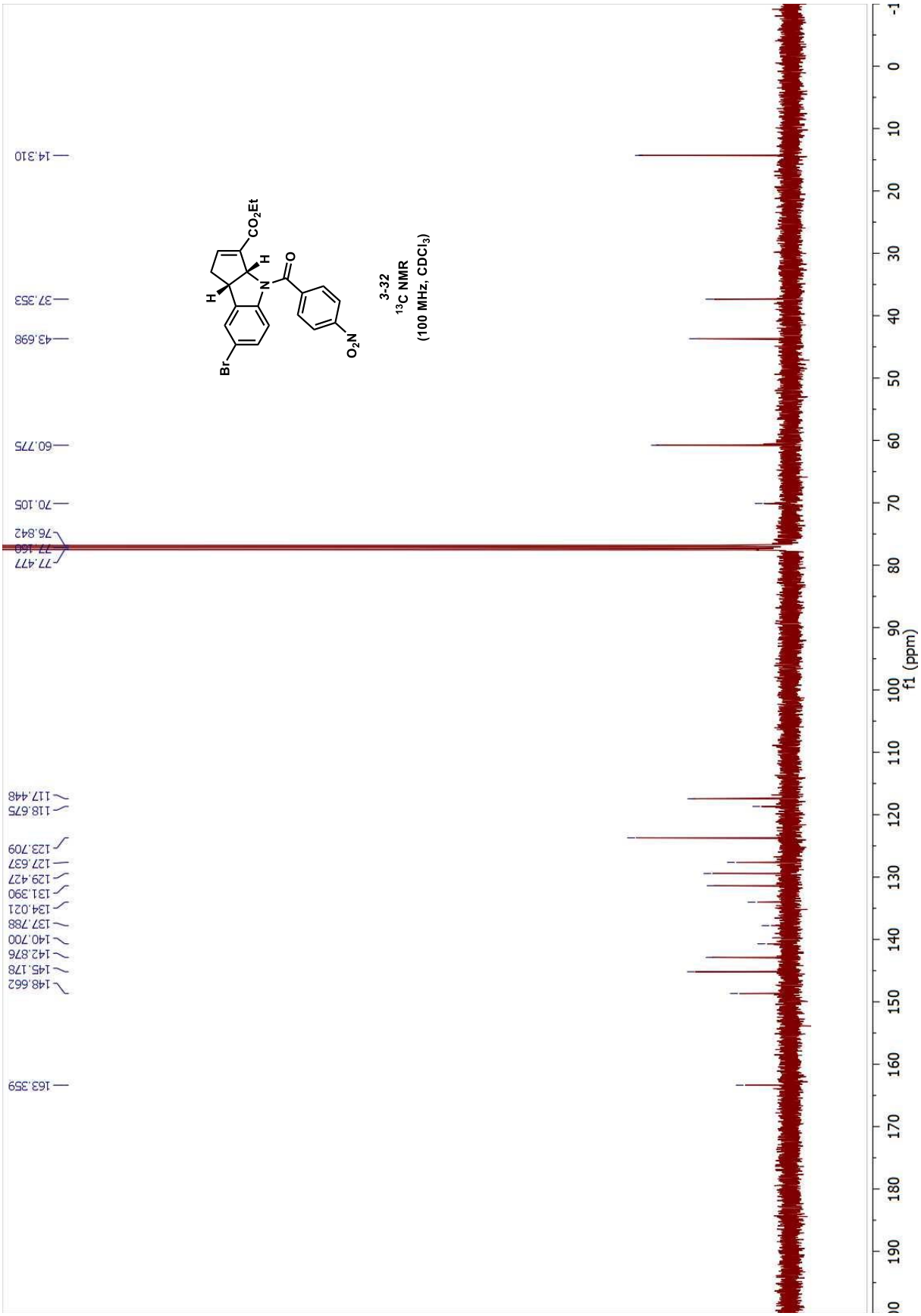
3-32
^{13}C NMR
(100 MHz, $CDCl_3$)
CO_2Et
H
H
N
O
Br
O_2N
14.310
37.353
43.698
60.775
70.105
76.842
77.160
77.477
117.448
118.675
123.709
127.637
129.427
131.390
134.021
137.788
140.700
142.876
145.178
148.662
163.359
f1 (ppm)

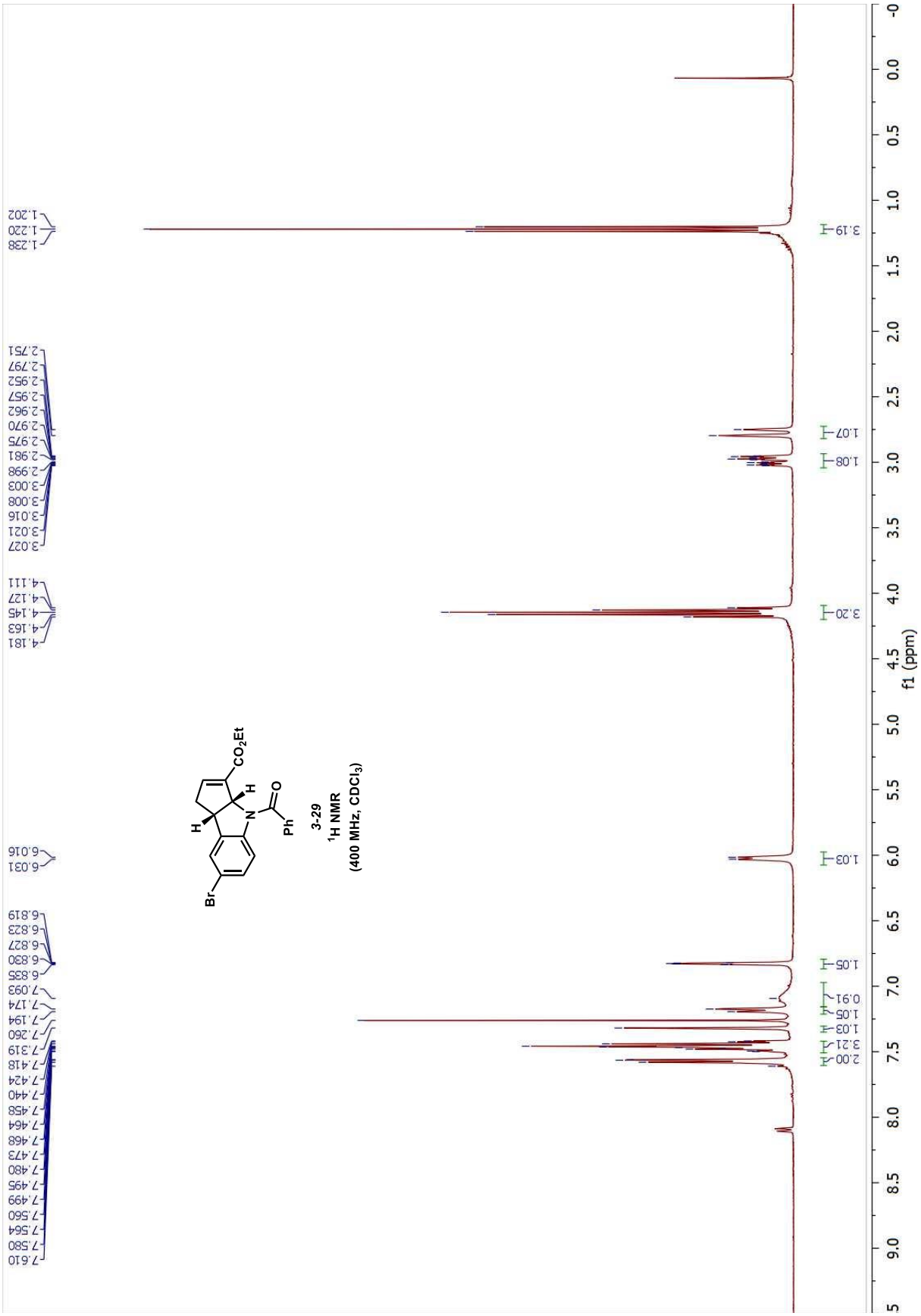
3-29
^{1}H NMR
(400 MHz, CDCl$_3$)
f1 (ppm)

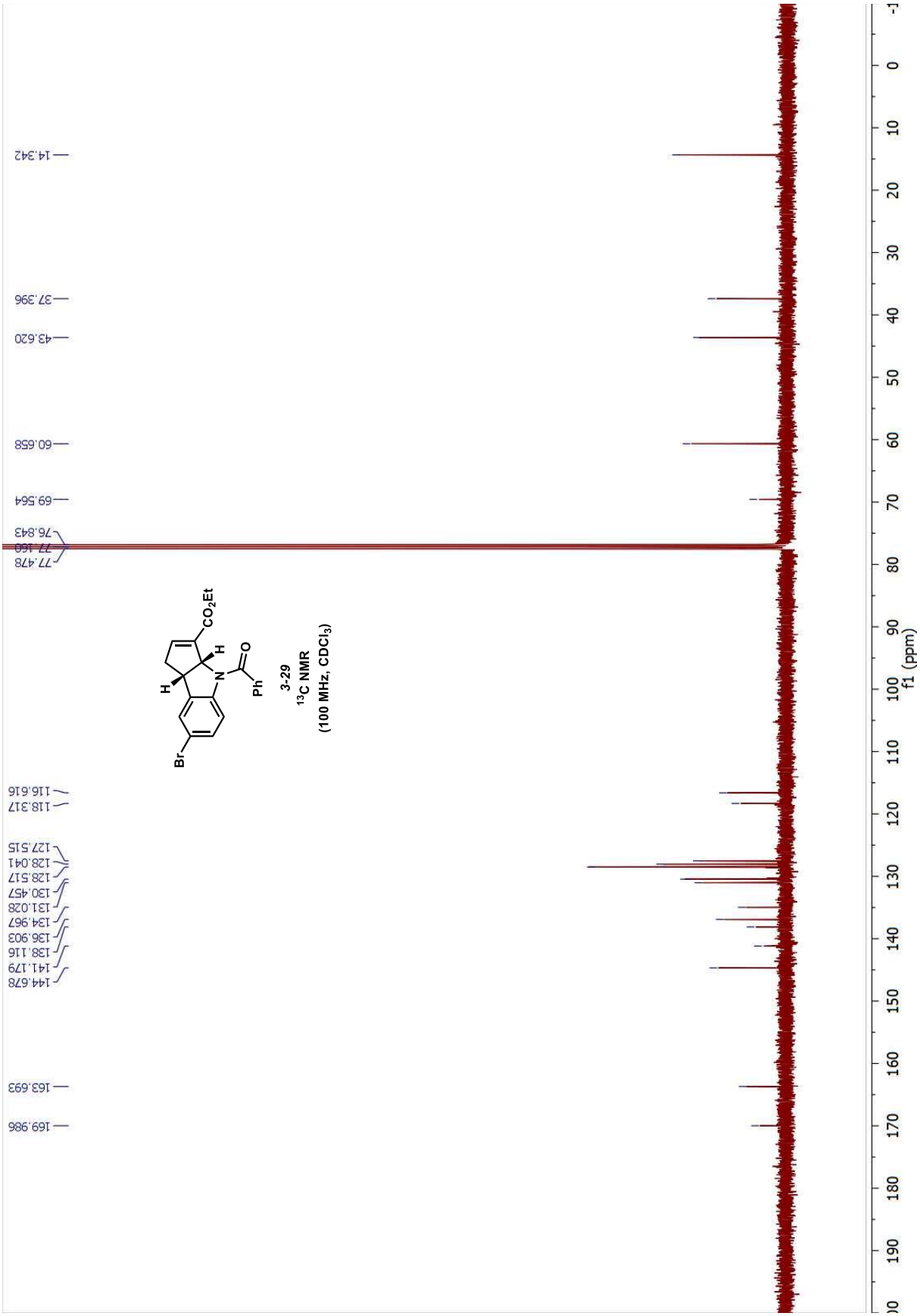
14.342
37.396
43.620
60.658
69.564
76.843
77.160
77.478
116.616
118.317
127.515
128.041
128.517
130.457
131.028
134.967
136.903
138.116
141.179
144.678
163.693
169.986
CO2Et
H
N
O
Ph
H
Br
3-29
13C NMR
(100 MHz, CDCl3)
f1 (ppm)

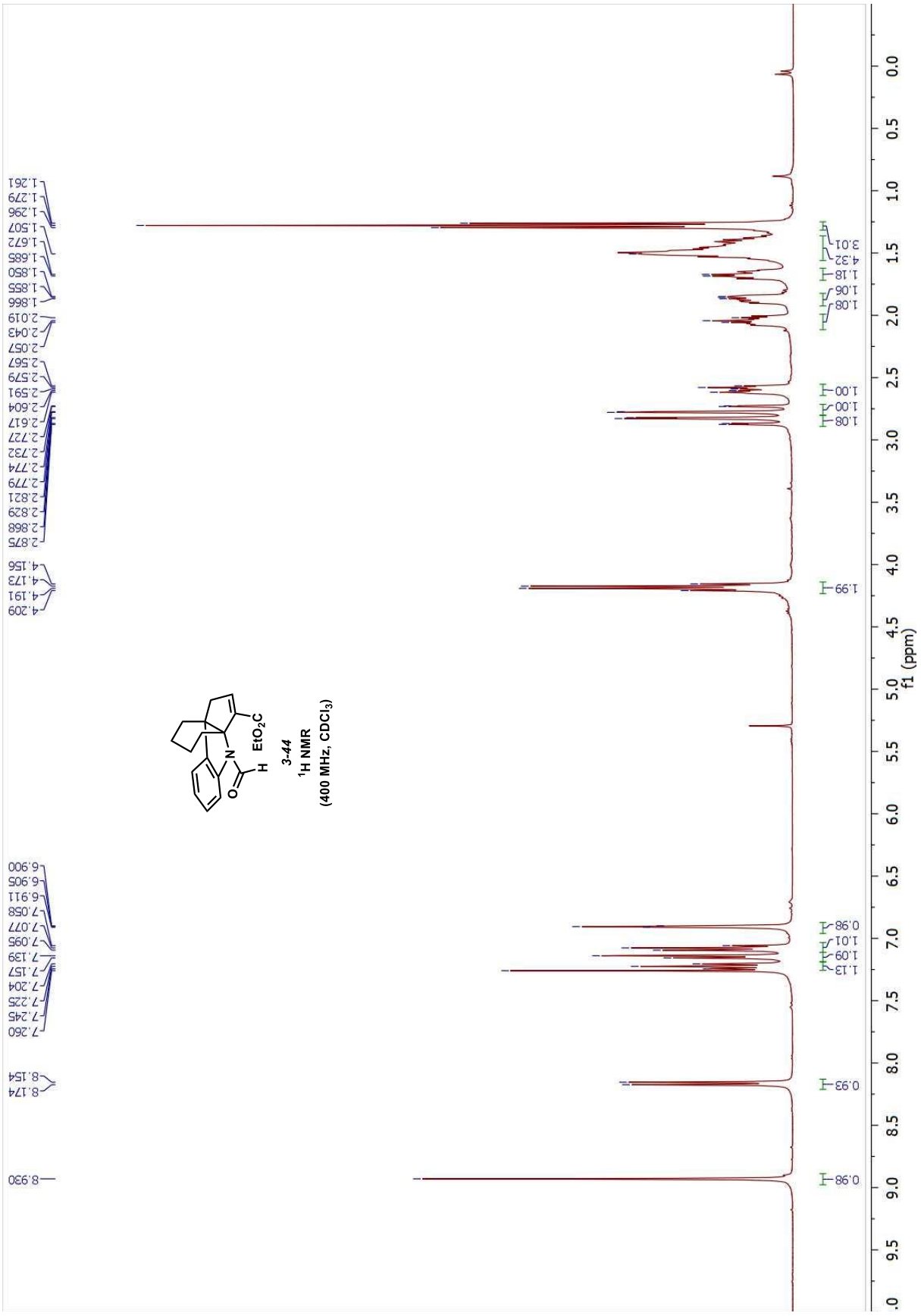
3-44
^{1}H NMR
(400 MHz, CDCl$_3$)
EtO$_2$C
H
N
O
f1 (ppm)

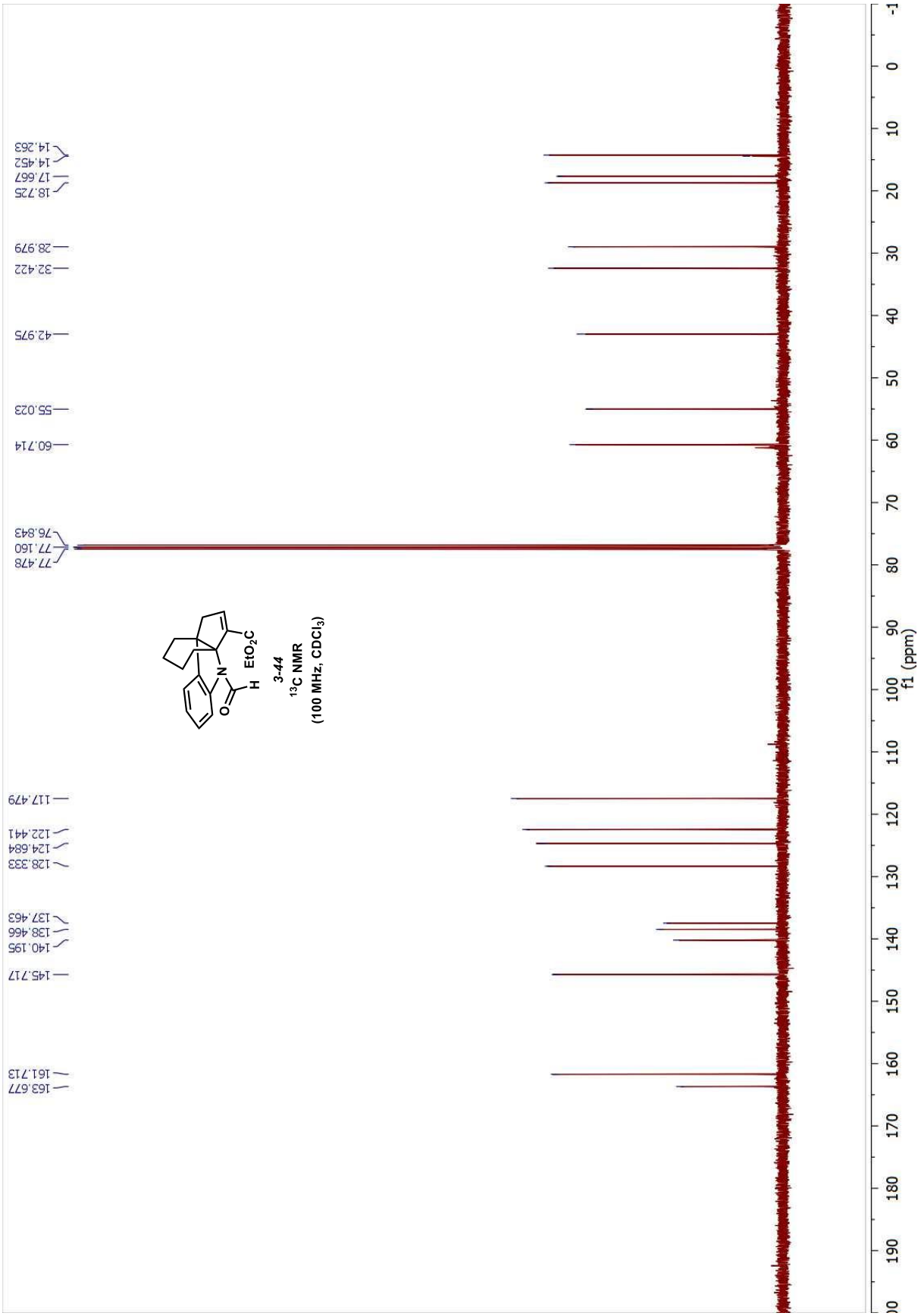
14.263
14.452
17.667
18.725
28.979
32.422
42.975
55.023
60.714
76.843
77.160
77.478
117.479
122.441
124.684
128.333
137.463
138.466
140.195
145.717
161.713
163.677
EtO2C
H
N
O
3-44
13C NMR
(100 MHz, CDCl3)
f1 (ppm)

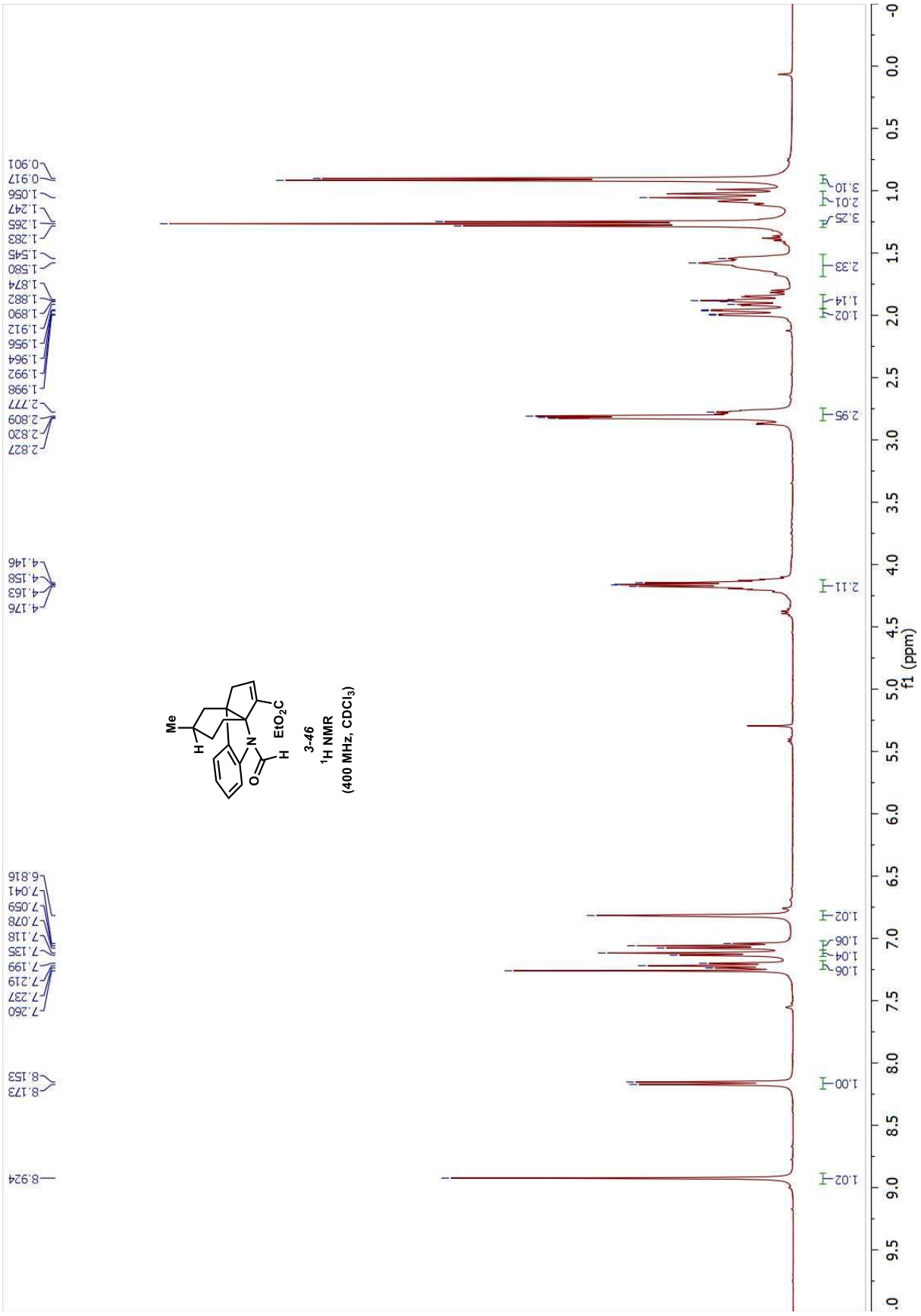
Me
H
N
O
H
EtO2C
3-46
1H NMR
(400 MHz, CDCl3)
f1 (ppm)

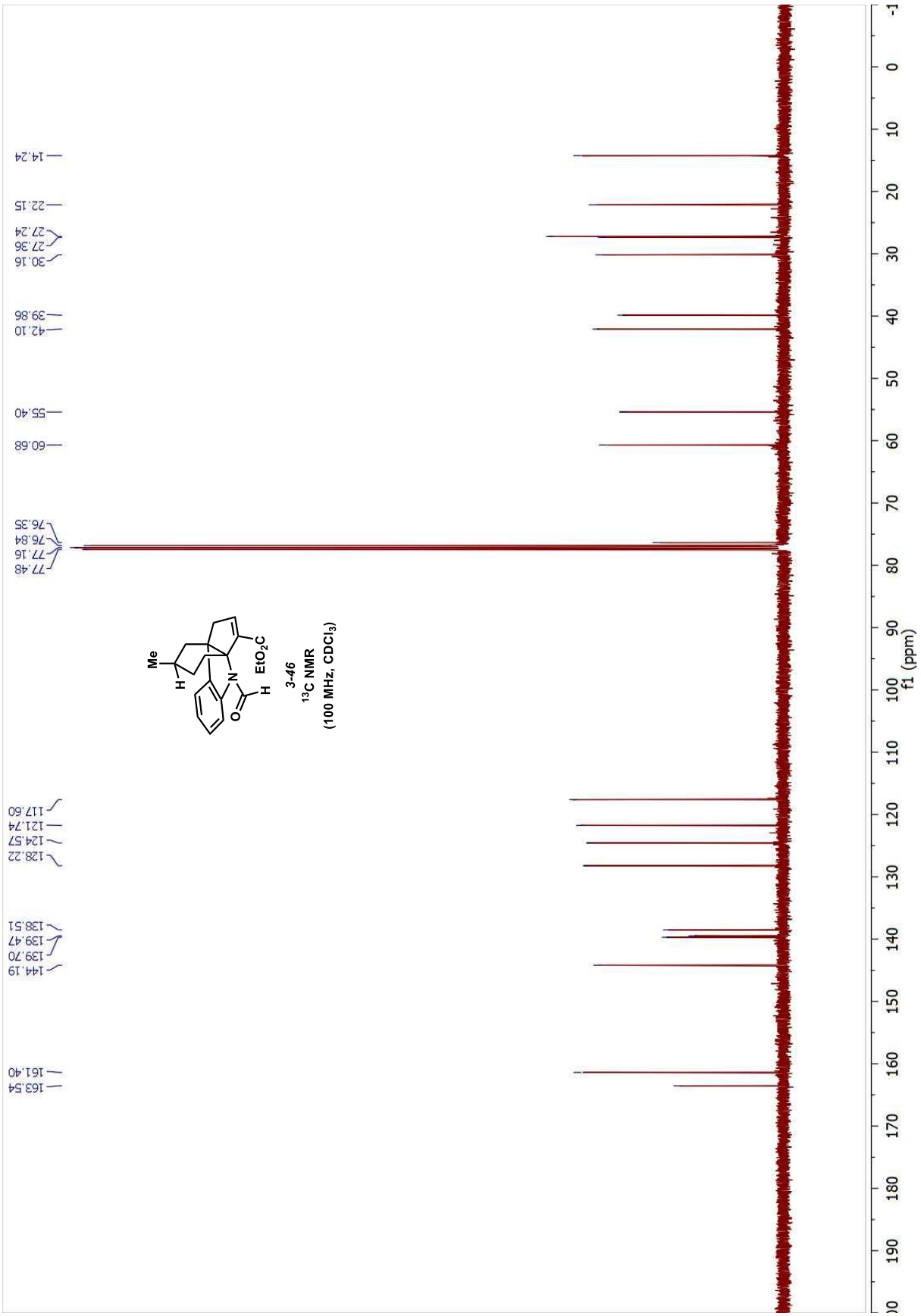
14.24
22.15
27.24
27.36
30.16
39.86
42.10
55.40
60.68
76.35
76.84
77.16
77.48
117.60
121.74
124.57
128.22
138.51
139.47
139.70
144.19
161.40
163.54
Me
H
N
O
H
EtO2C
3-46
13C NMR
(100 MHz, CDCl3)
f1 (ppm)

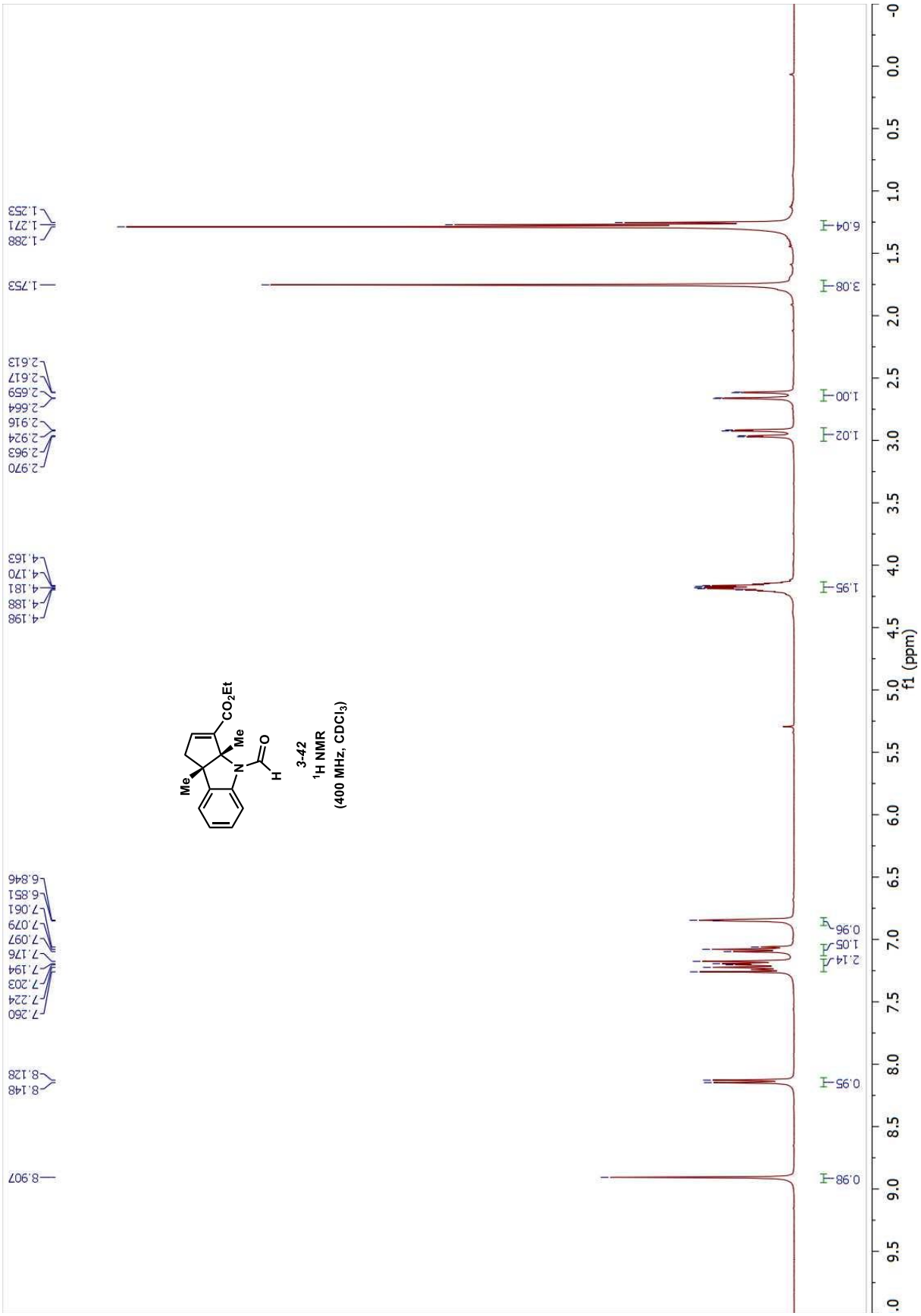
3-42
^{1}H NMR
(400 MHz, CDCl$_3$)
f1 (ppm)

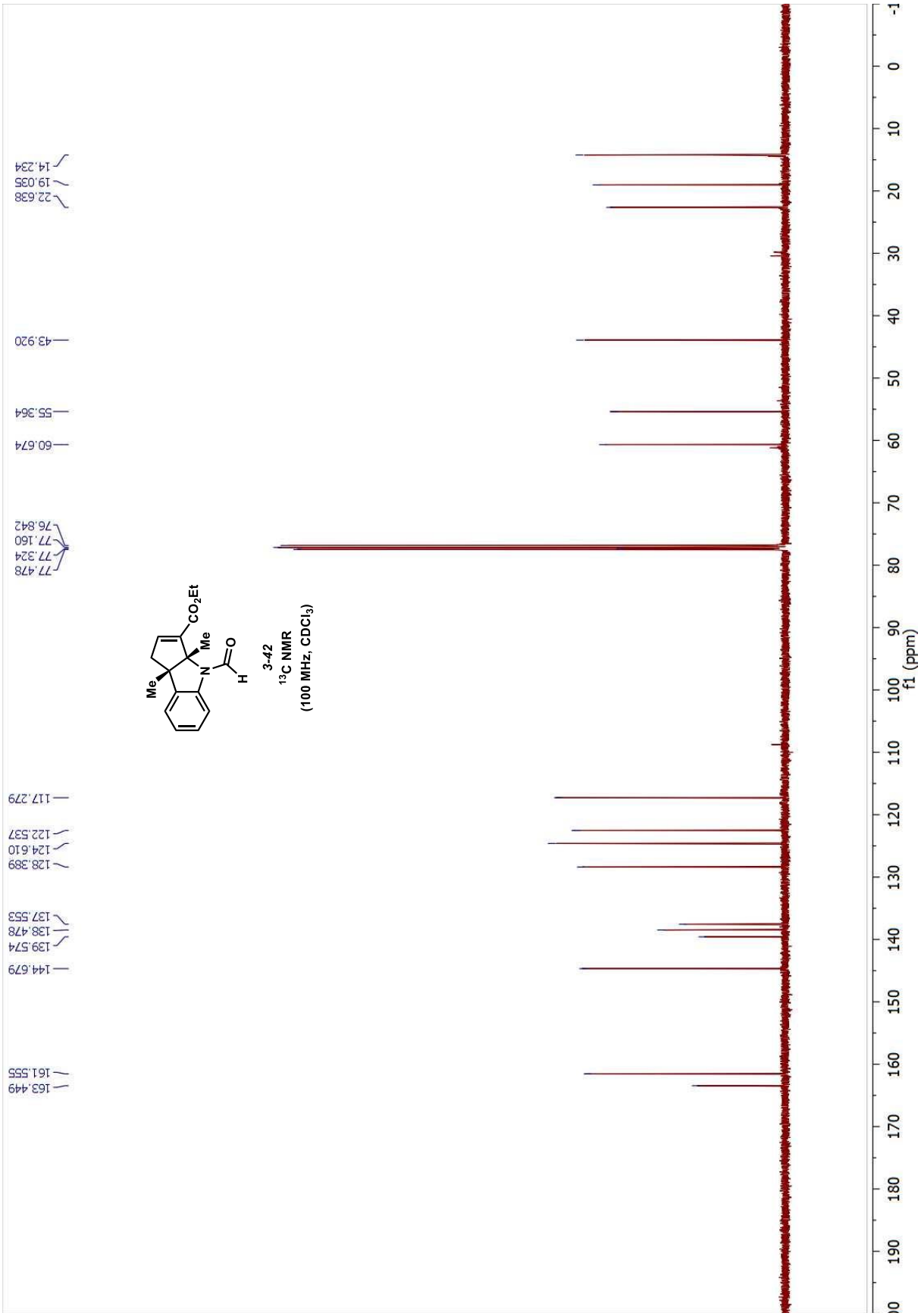
14.234
19.035
22.638
43.920
55.364
60.674
76.842
77.160
77.324
77.478
117.279
122.537
124.610
128.389
137.553
138.478
139.574
144.679
161.555
163.449
CO2Et
Me
Me
N
O
H
3-42
13C NMR
(100 MHz, CDCl3)
f1 (ppm)

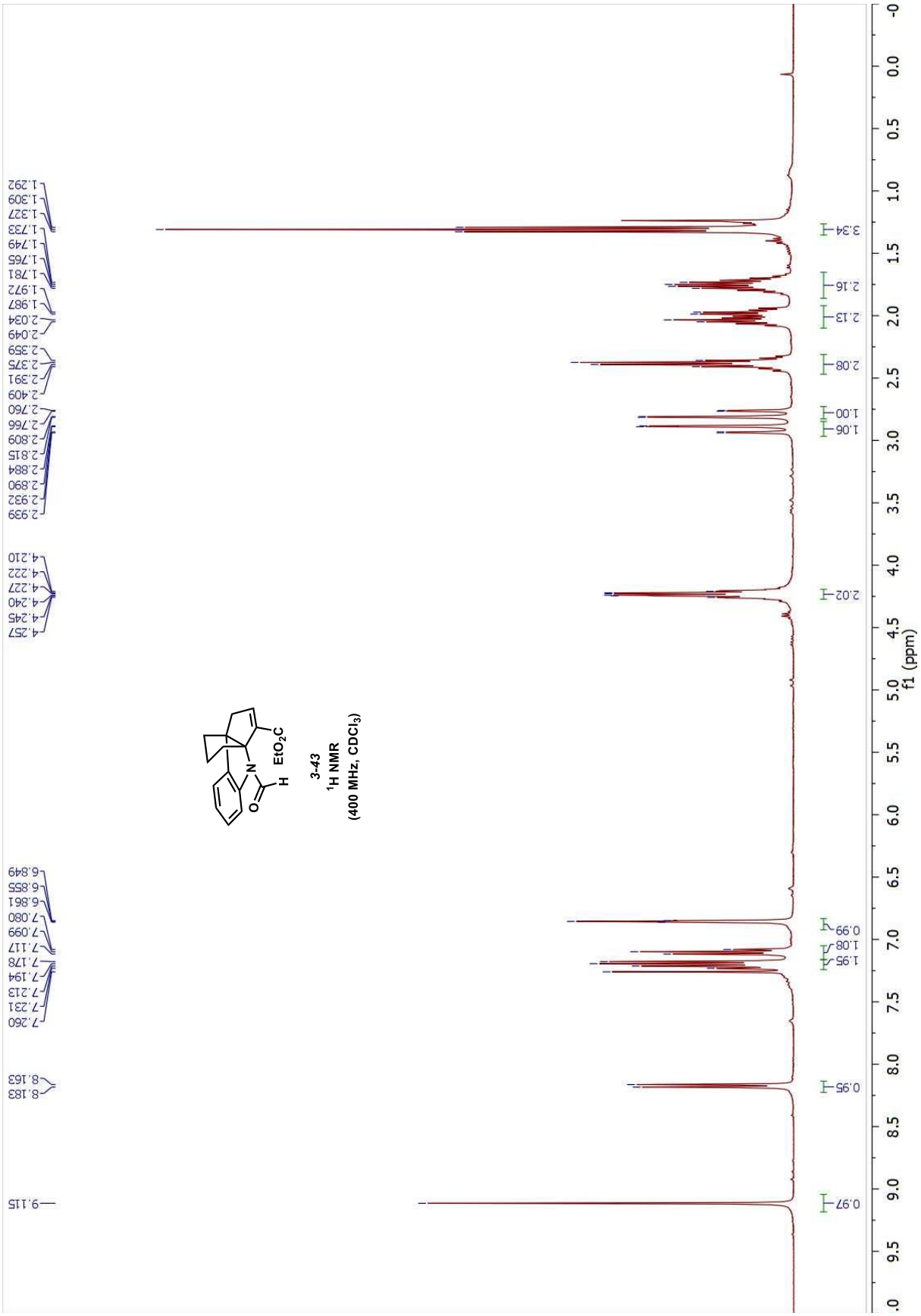
3-43
^{1}H NMR
(400 MHz, $CDCl_3$)
EtO_2C
H
N
O
f1 (ppm)

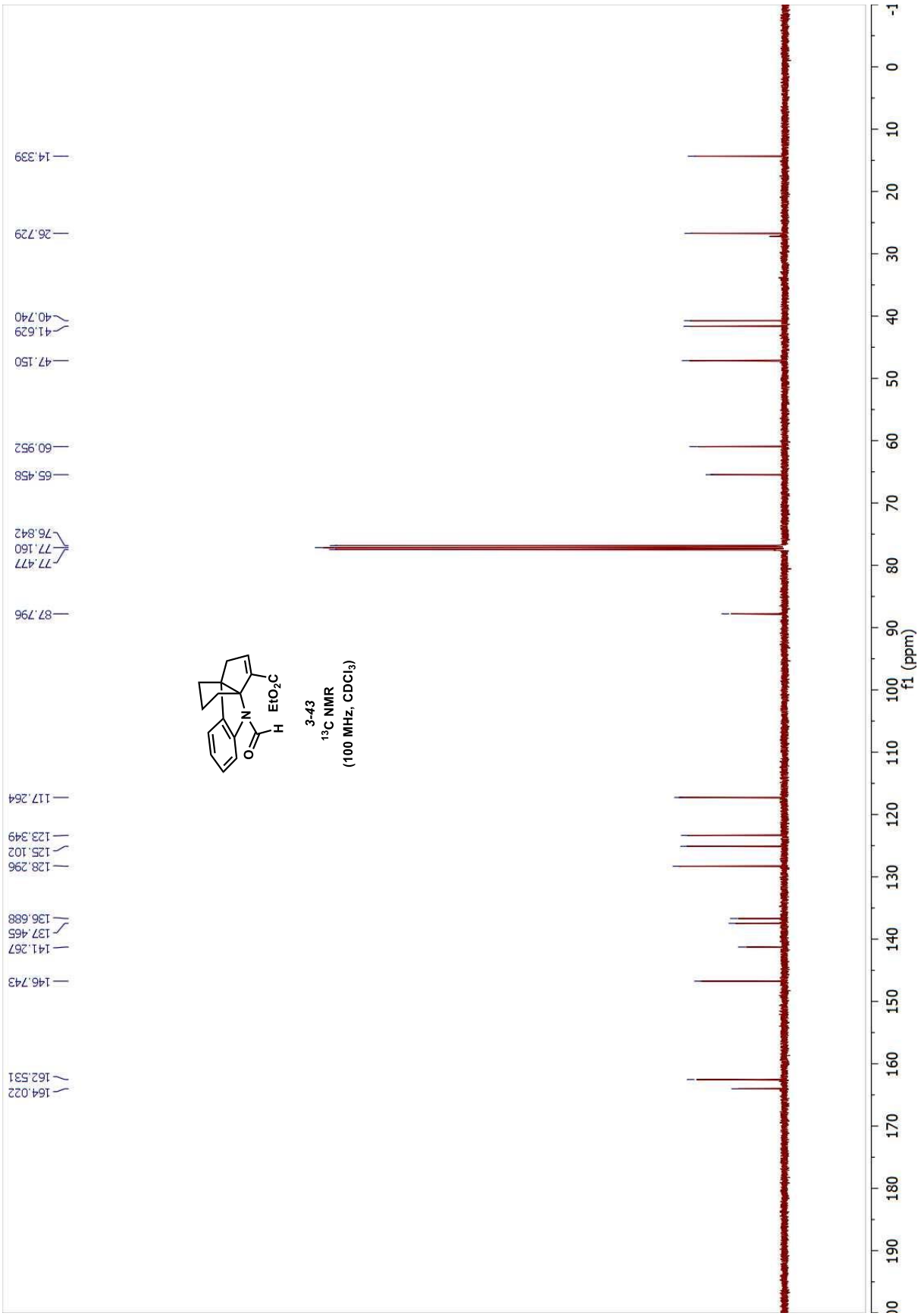
14.339
26.729
40.740
41.629
47.150
60.952
65.458
76.842
77.160
77.477
87.796
117.264
123.349
125.102
128.296
136.688
137.465
141.267
146.743
162.531
164.022
3-43
13C NMR
(100 MHz, CDCl3)
EtO2C
H
N
O
f1 (ppm)

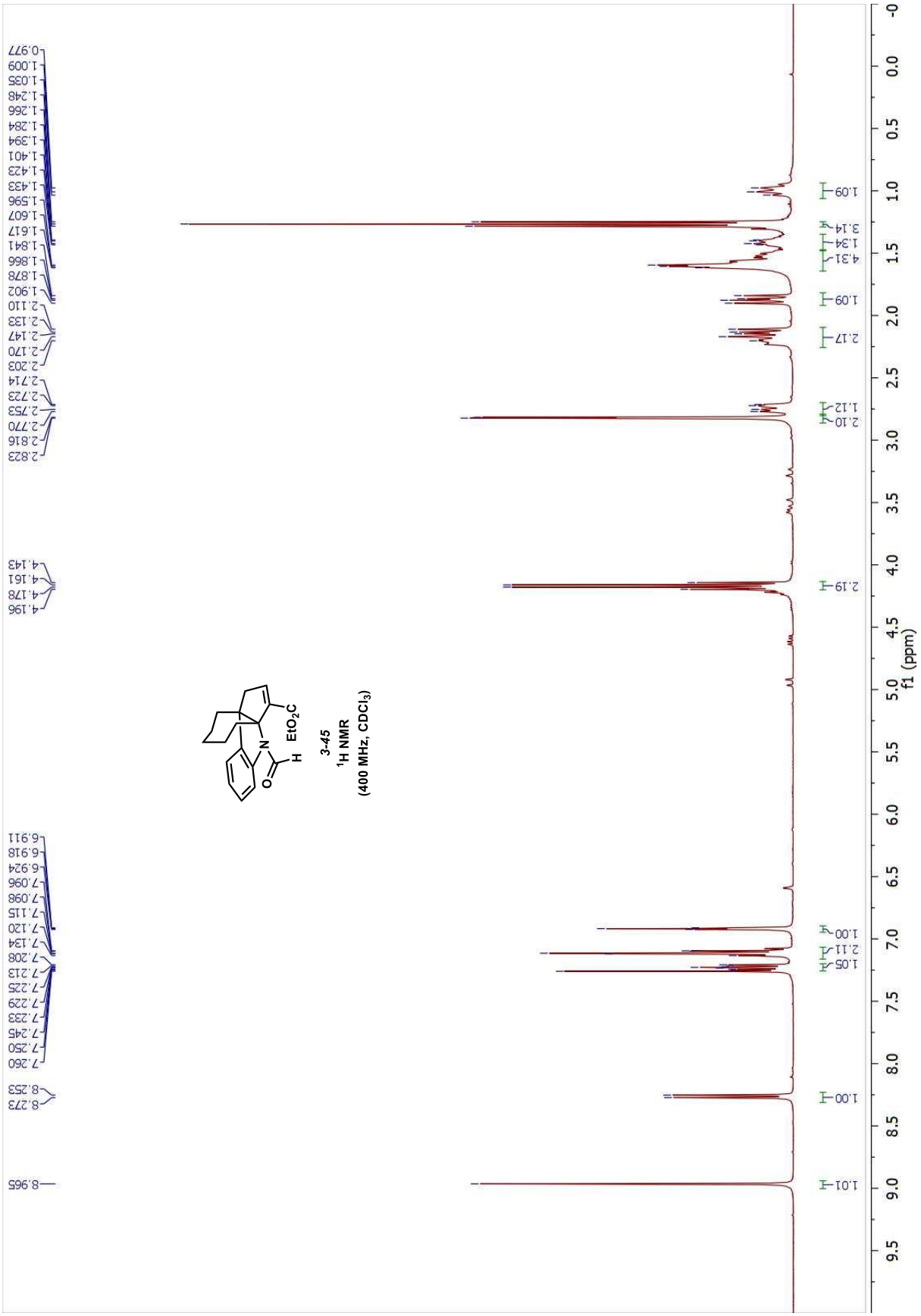
3-45
^{1}H NMR
(400 MHz, $CDCl_3$)
EtO_2C
N
H
O
f1 (ppm)

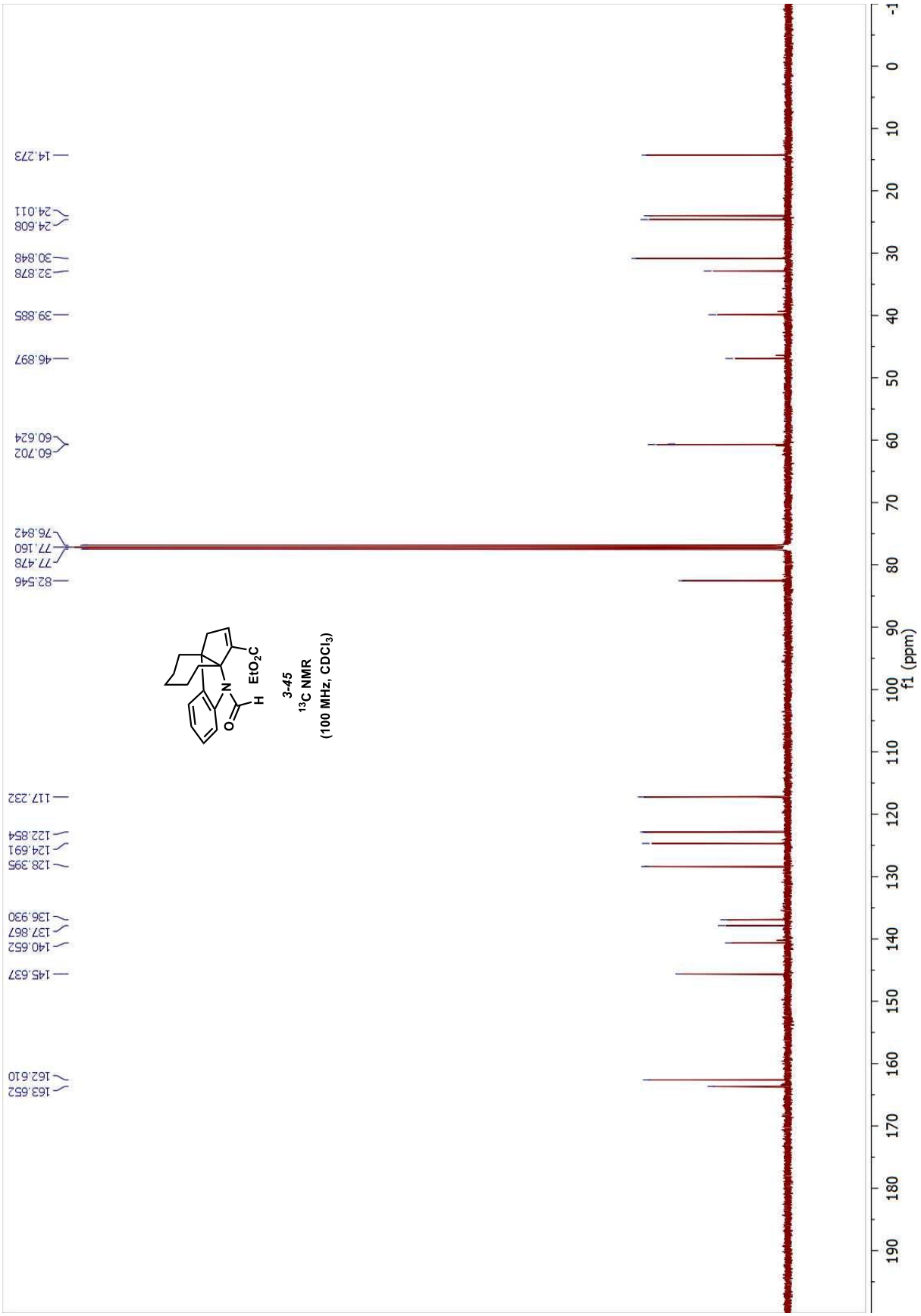
14.273
24.011
24.608
30.848
32.878
39.885
46.897
60.624
60.702
76.842
77.160
77.478
82.546
117.232
122.854
124.691
128.395
136.930
137.867
140.652
145.637
162.610
163.652
EtO2C
H
N
O
3-45
13C NMR
(100 MHz, CDCl3)
-1
0
10
20
30
40
50
60
70
80
90
100
110
120
130
140
150
160
170
180
190
f1 (ppm)

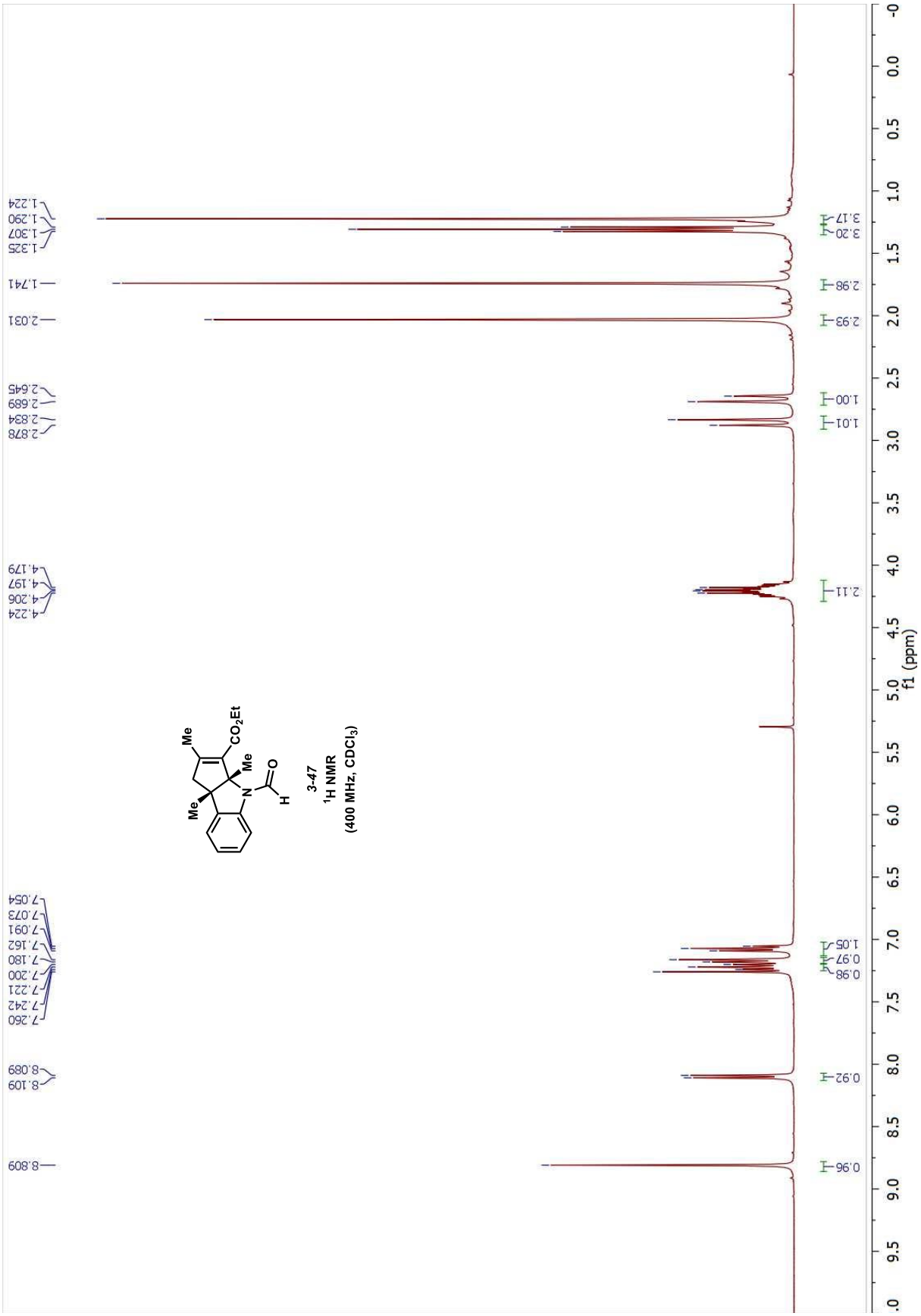
Me
CO2Et
Me
N
O
H
Me
3-47
1H NMR
(400 MHz, CDCl3)
f1 (ppm)

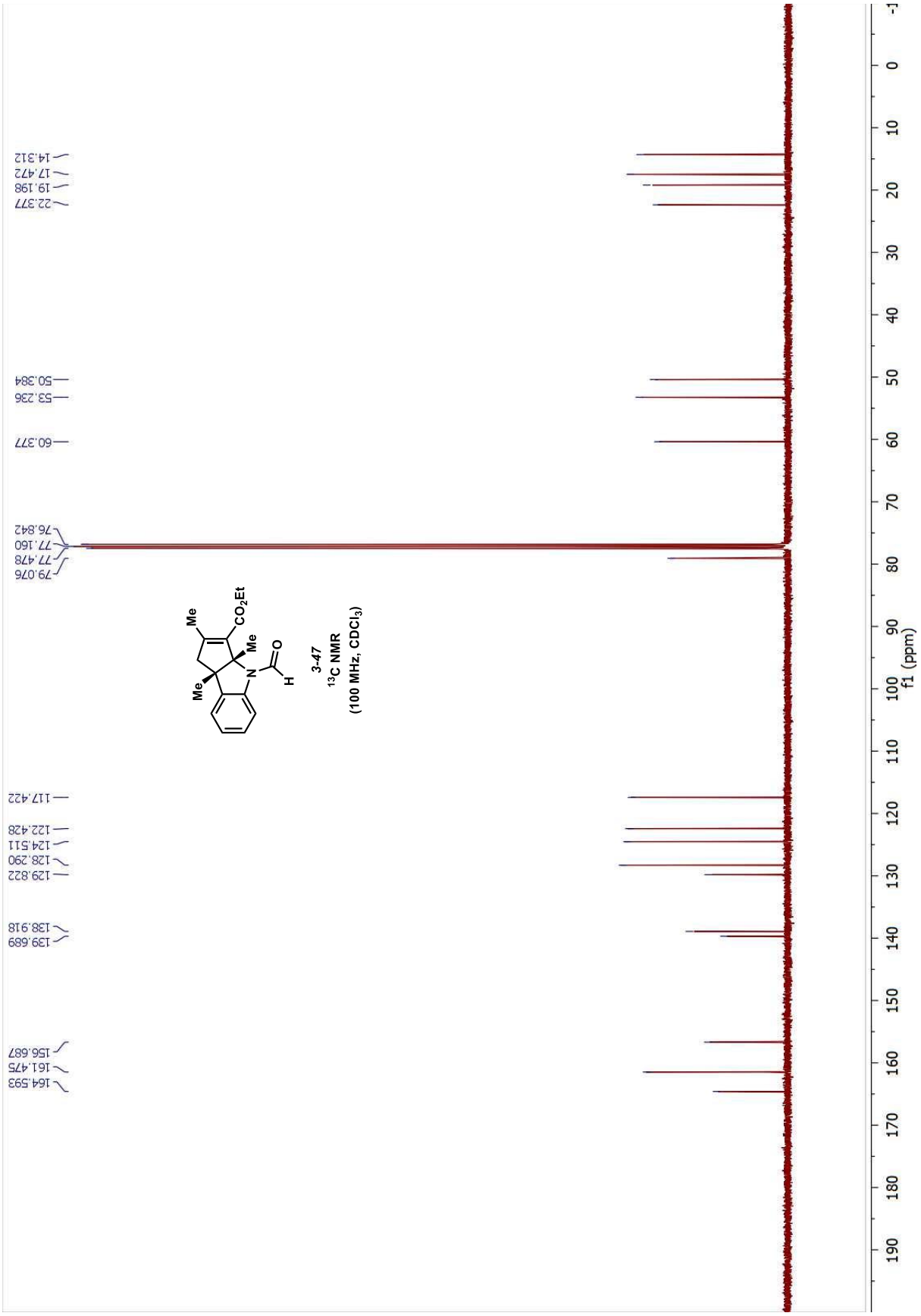
14.312
17.472
19.198
22.377
50.384
53.236
60.377
76.842
77.160
77.478
79.076
117.422
122.428
124.511
128.290
129.822
138.918
139.689
156.687
161.475
164.593
Me
CO2Et
Me
Me
N
O
H
3-47
13C NMR
(100 MHz, CDCl3)
f1 (ppm)

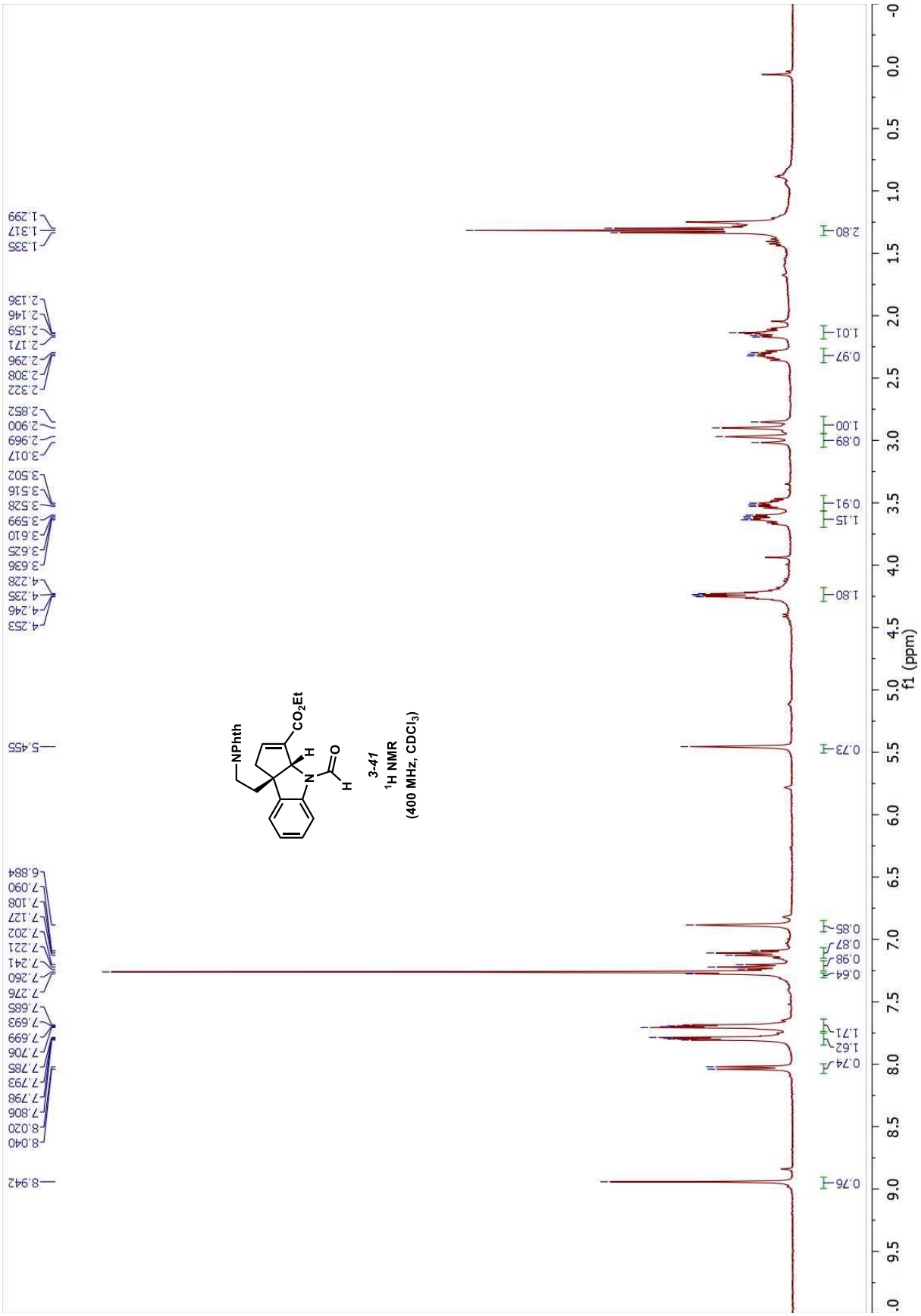
NPhth
CO2Et
H
N
O
H
3-41
1H NMR
(400 MHz, CDCl3)
f1 (ppm)

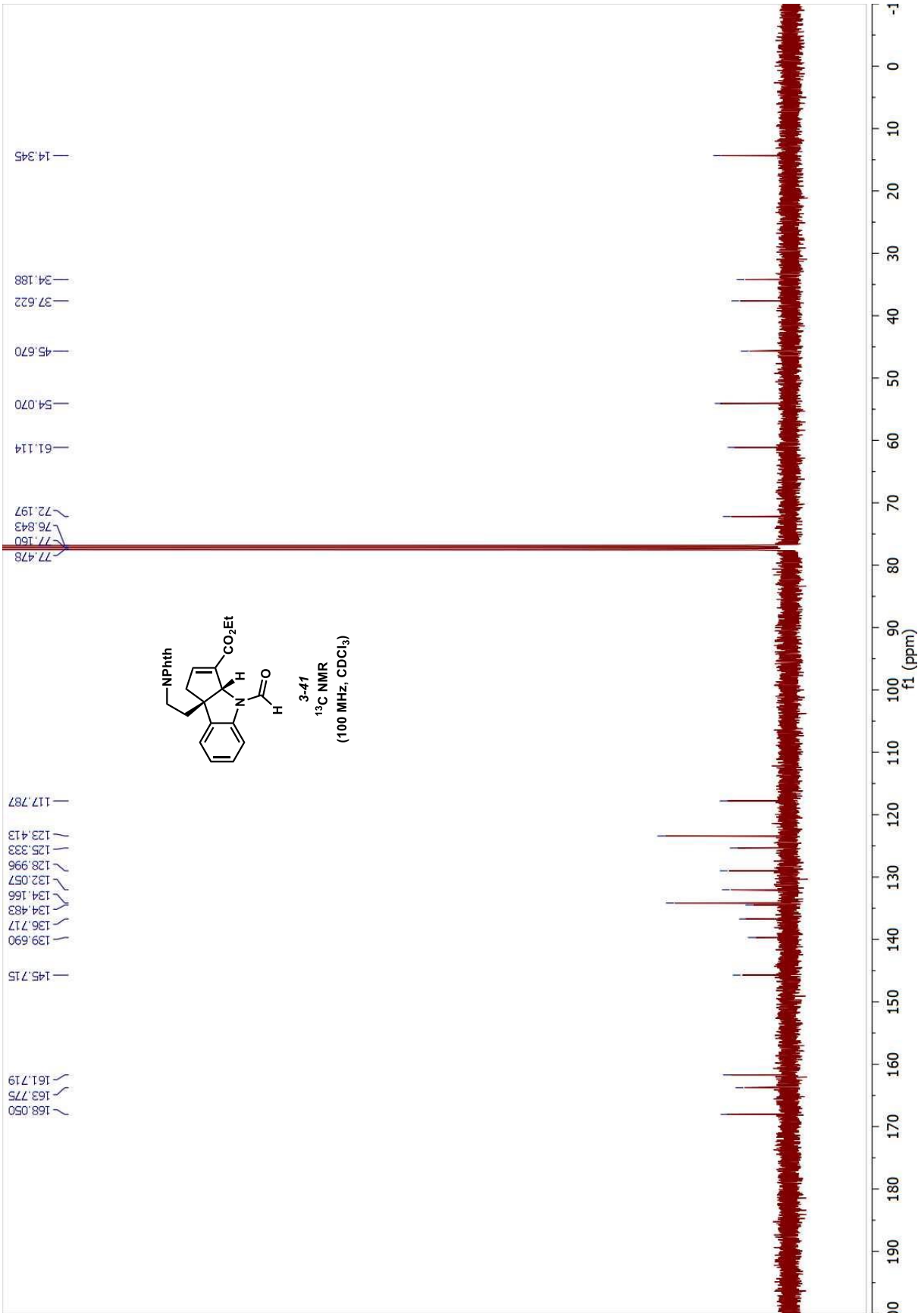
NPhth
CO2Et
H
N
O
H
3-41
13C NMR
(100 MHz, CDCl3)
14.345
34.188
37.622
45.670
54.070
61.114
72.197
76.843
77.160
77.478
117.787
123.413
125.333
128.996
132.057
134.166
134.483
136.717
139.690
145.715
161.719
163.775
168.050
f1 (ppm)

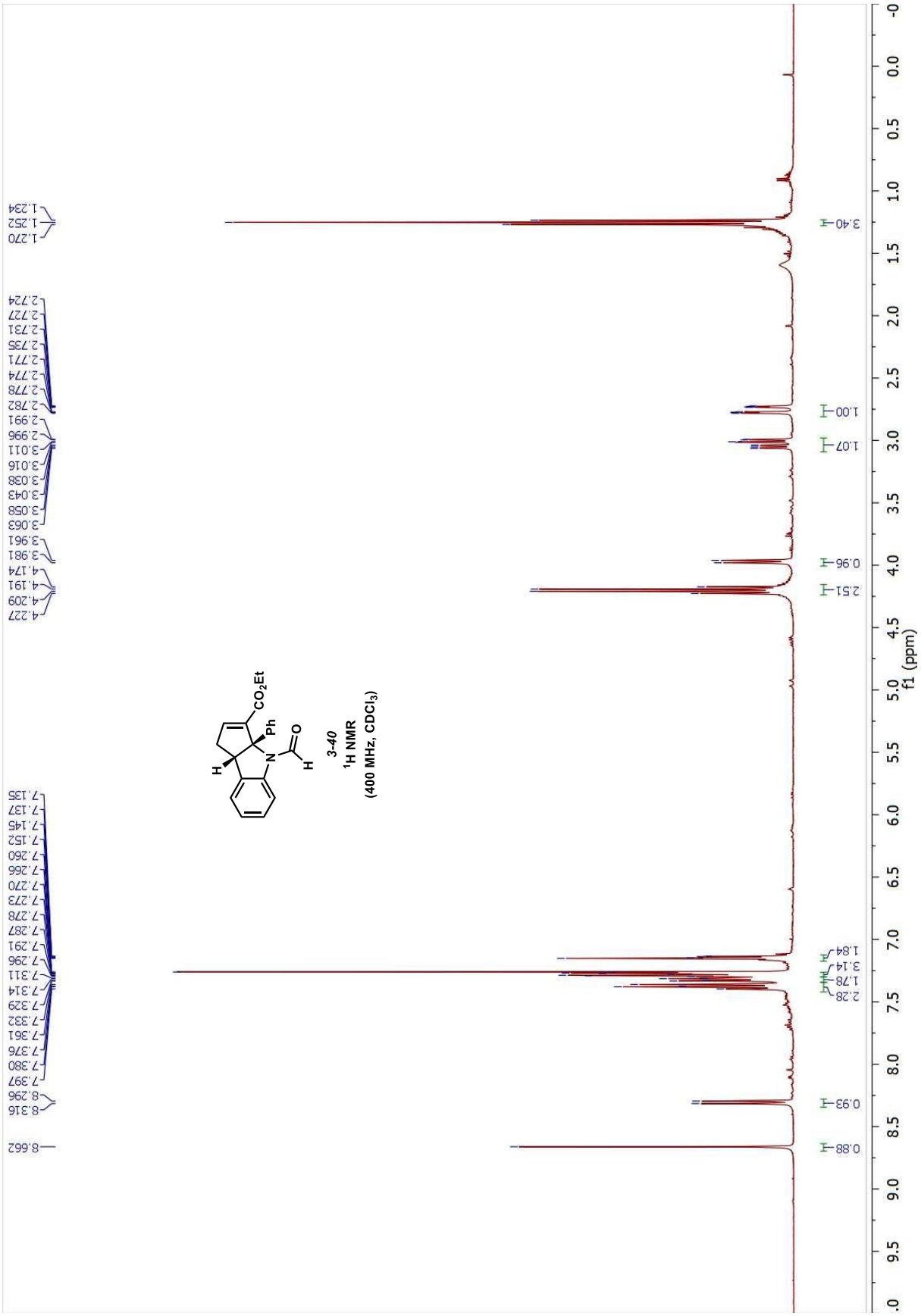
3-40
^{1}H NMR
(400 MHz, CDCl$_3$)
f1 (ppm)

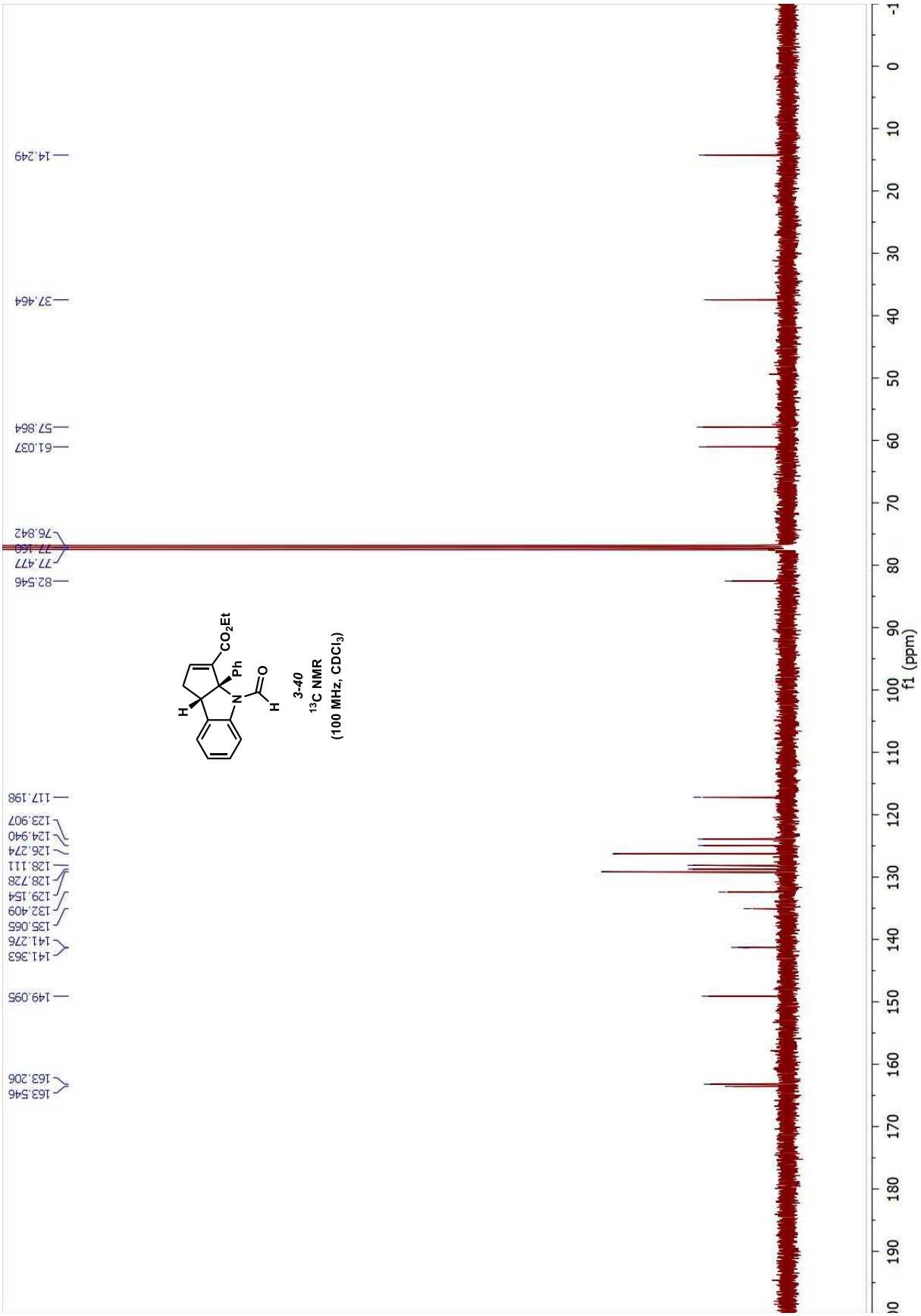
14.249
37.464
57.864
61.037
76.842
77.160
77.477
82.546
117.198
123.907
124.940
126.274
128.111
128.728
129.154
132.409
135.065
141.276
141.363
149.095
163.206
163.546
Ph
CO2Et
H
O
H
3-40
13C NMR
(100 MHz, CDCl3)
f1 (ppm)

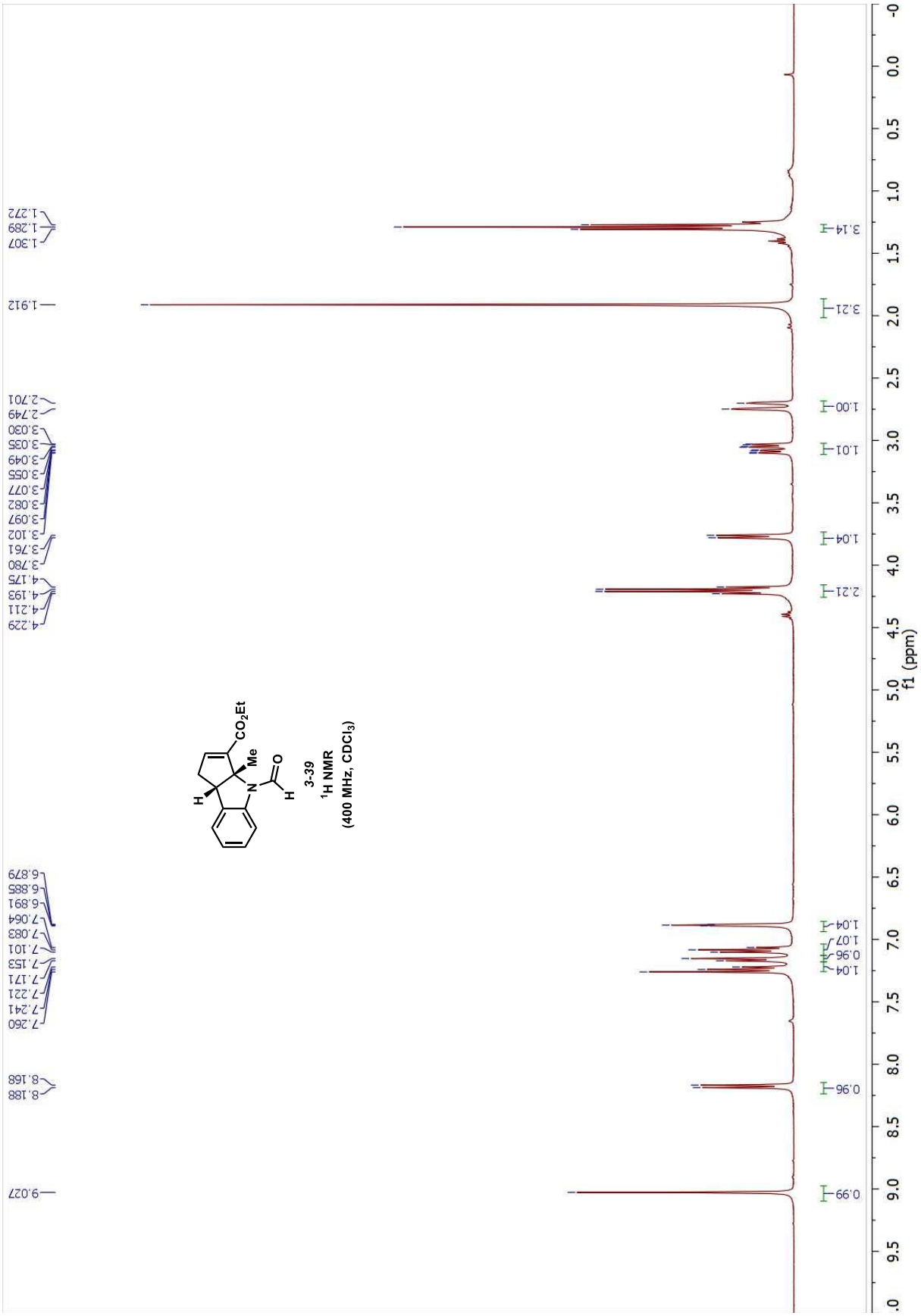
3-39
^{1}H NMR
(400 MHz, CDCl$_3$)
CO$_2$Et
Me
N
O
H
H
f1 (ppm)

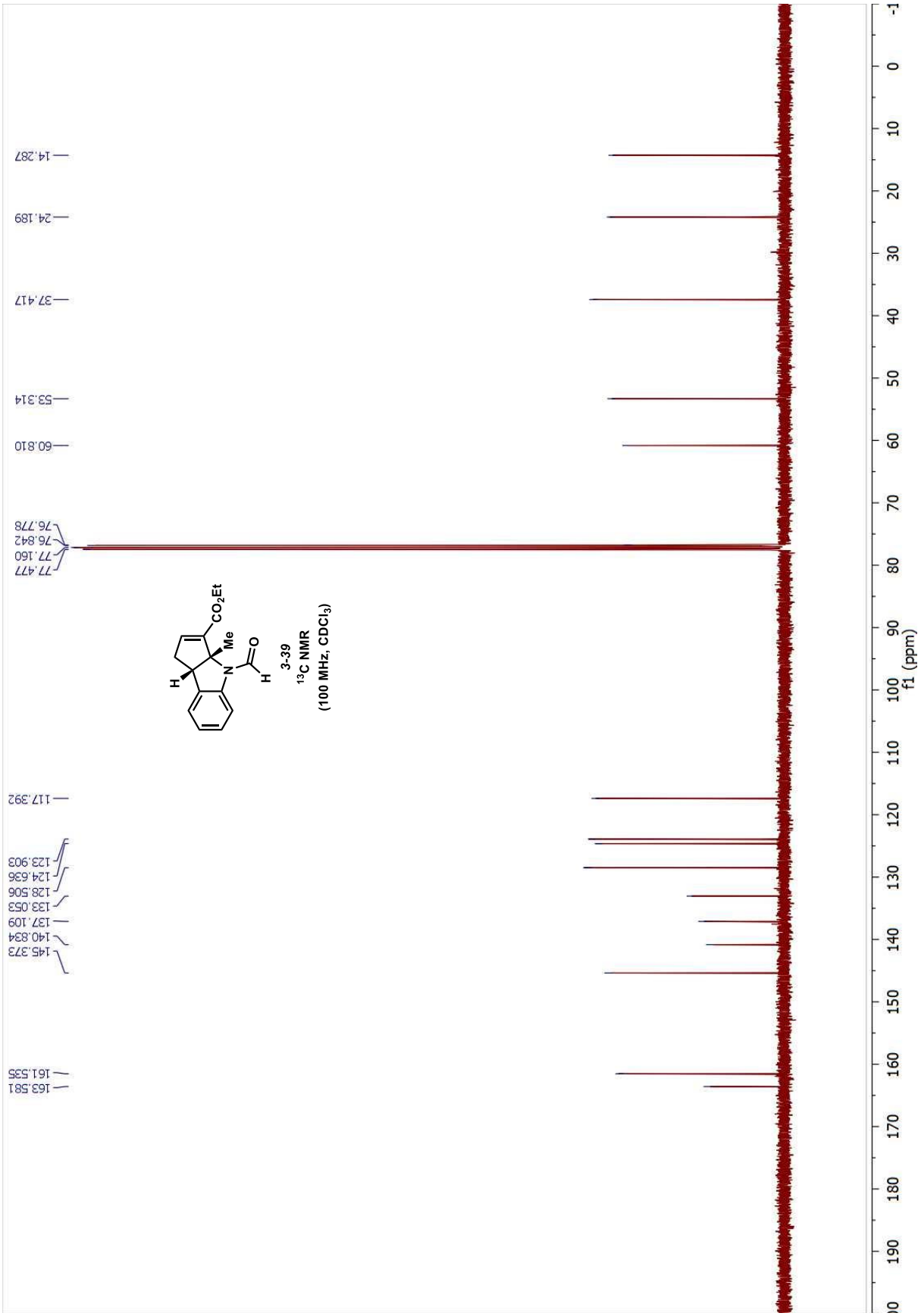
14.287
24.189
37.417
53.314
60.810
76.778
76.842
77.160
77.477
117.392
123.903
124.636
128.506
133.053
137.109
140.834
145.373
161.535
163.581
3-39
13C NMR
(100 MHz, CDCl3)
f1 (ppm)

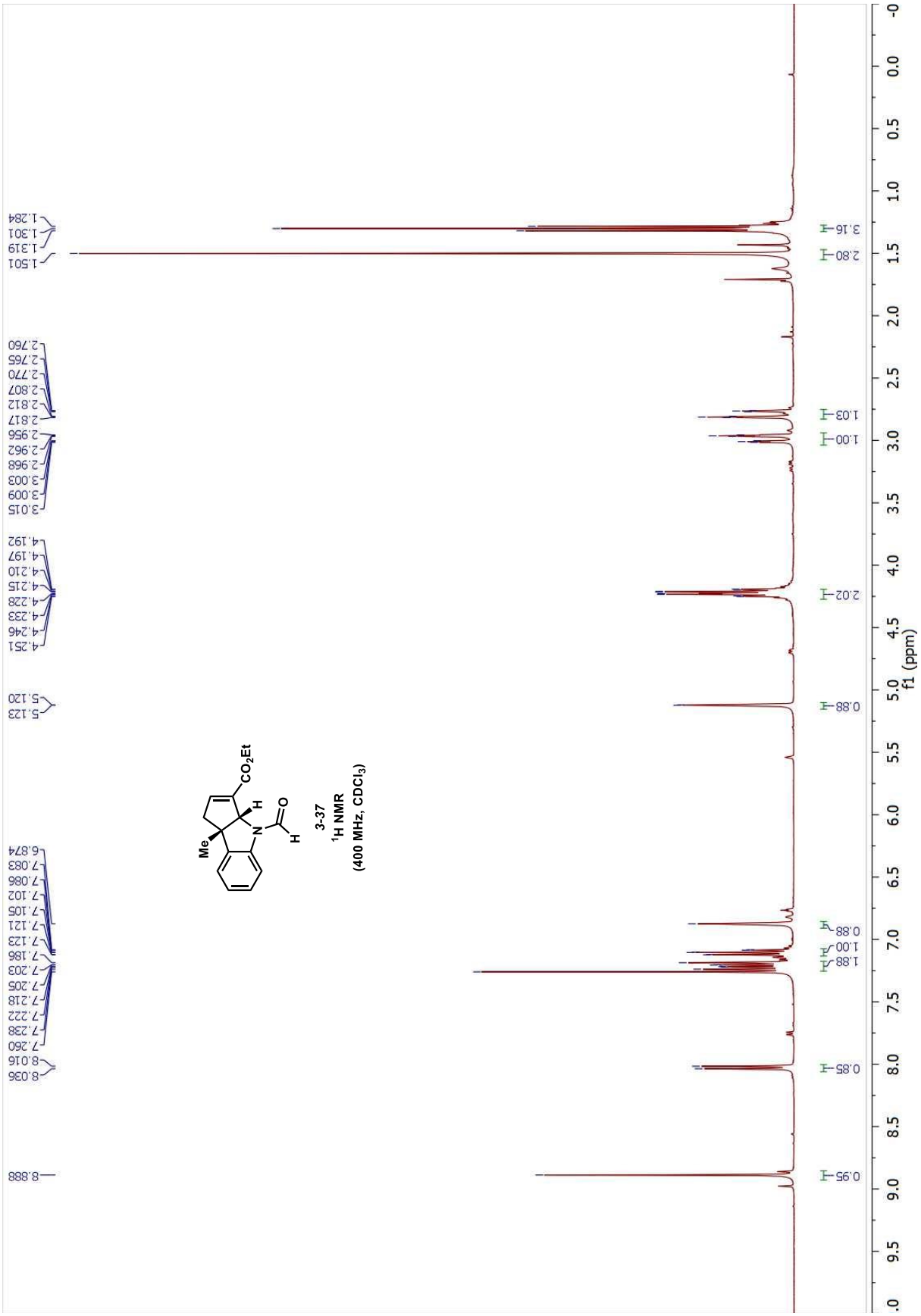
3-37
^{1}H NMR
(400 MHz, $CDCl_3$)
Me
CO_2Et
H
N
O
H
f1 (ppm)

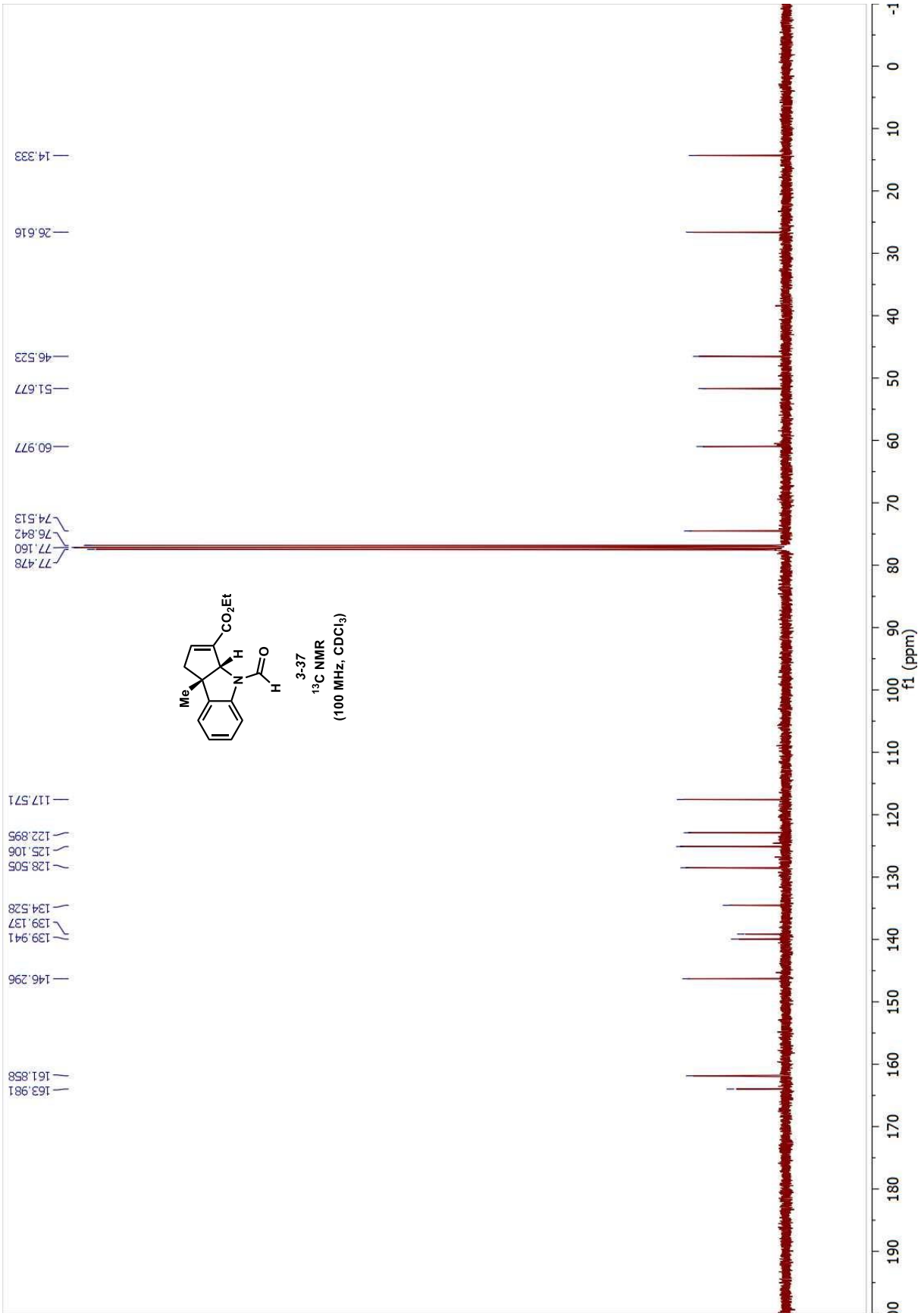
14.333
26.616
46.523
51.677
60.977
74.513
76.842
77.160
77.478
117.571
122.895
125.106
128.505
134.528
139.137
139.941
146.296
161.858
163.981
3-37
13C NMR
(100 MHz, CDCl3)
f1 (ppm)

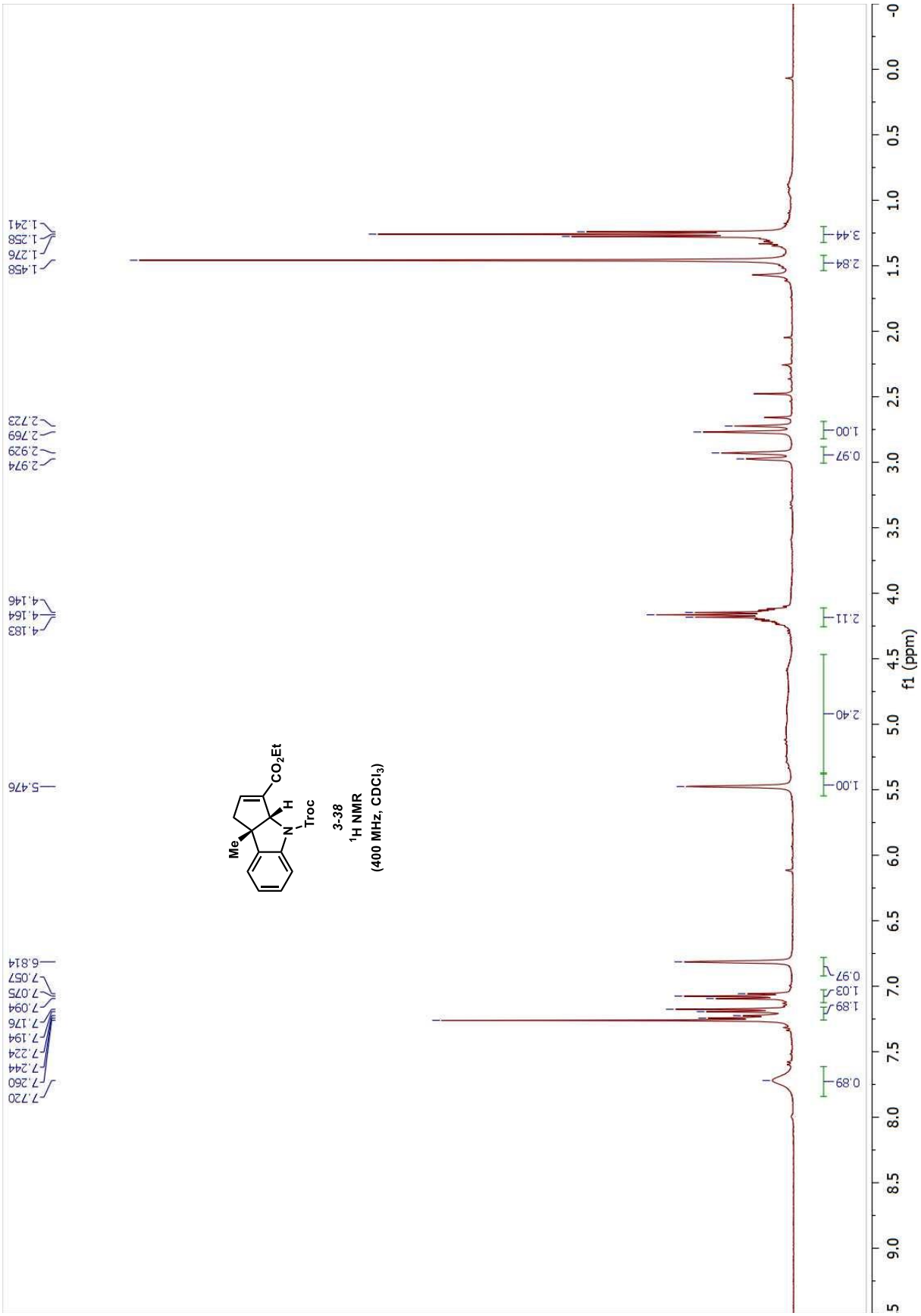
1.241
1.258
1.276
1.458
2.723
2.769
2.929
2.974
4.183
4.164
4.146
5.476
6.814
7.057
7.075
7.094
7.176
7.194
7.224
7.244
7.260
7.720
3.44
2.84
1.00
0.97
2.11
2.40
1.00
0.97
1.03
1.89
0.89
Me
Troc
N
H
CO2Et
3-38
1H NMR
(400 MHz, CDCl3)
f1 (ppm)

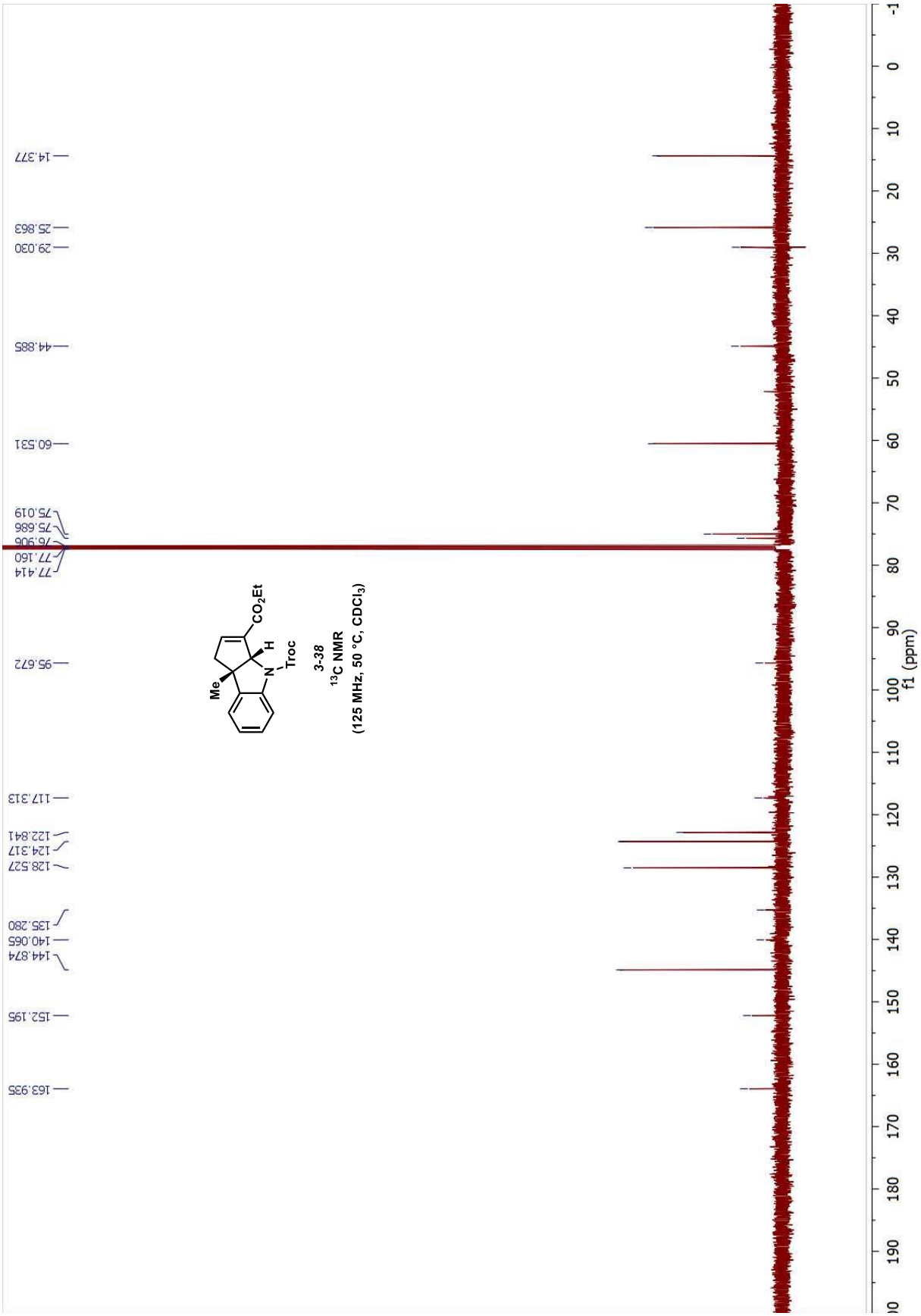
14.377
25.863
29.030
44.885
60.531
75.019
75.686
76.906
77.160
77.414
95.672
117.313
122.841
124.317
128.527
135.280
140.065
144.874
152.195
163.935
CO2Et
H
N
Troc
Me
3-38
13C NMR
(125 MHz, 50 °C, CDCl3)
f1 (ppm)

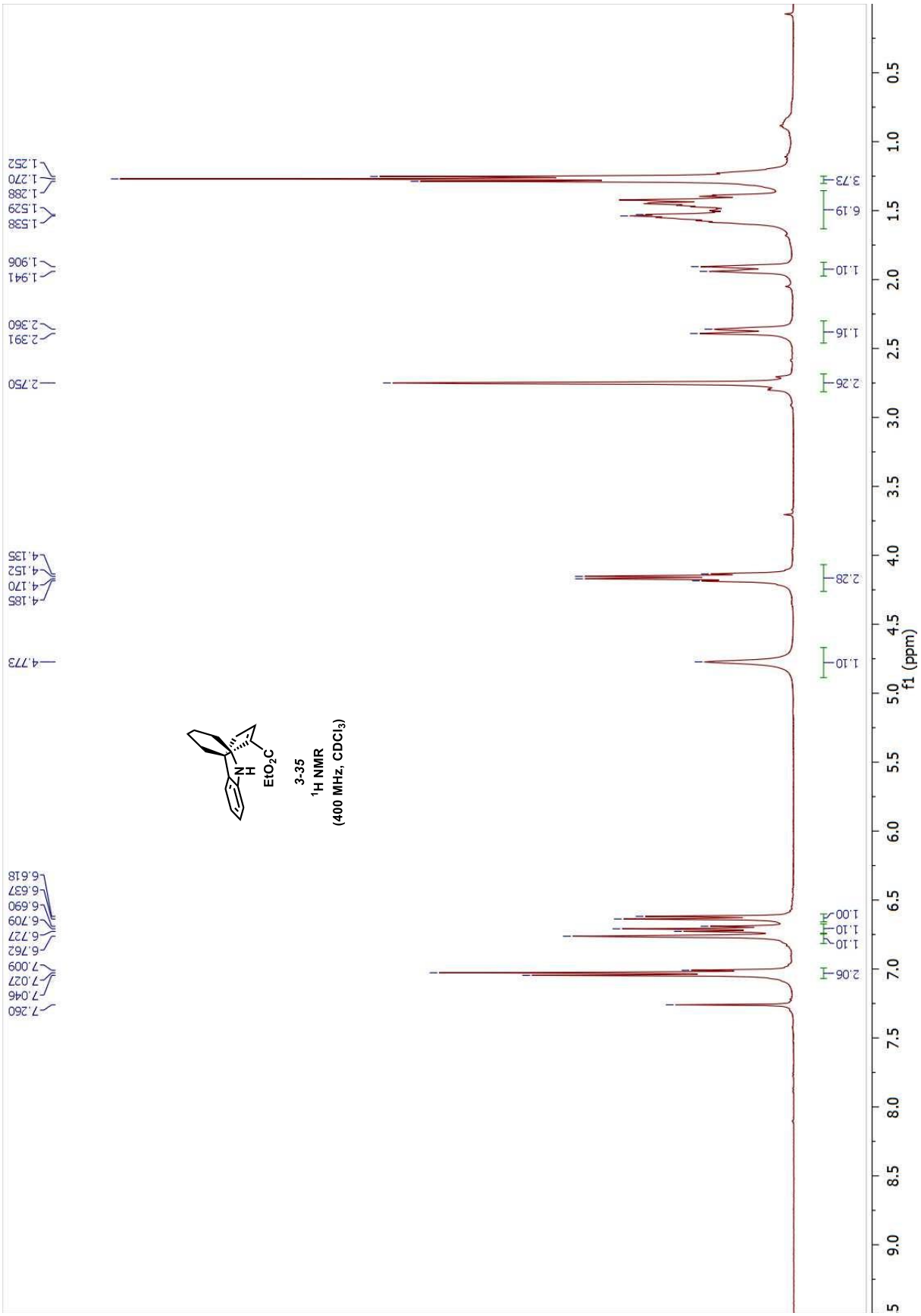
1.252
1.270
1.288
1.529
1.538
1.906
1.941
2.360
2.391
2.750
4.135
4.152
4.170
4.185
4.773
6.618
6.637
6.690
6.709
6.727
6.762
7.009
7.027
7.046
7.260
3.73
6.19
1.10
1.16
2.26
2.28
1.10
1.00
1.10
1.10
2.06
EtO2C
3-35
1H NMR
(400 MHz, CDCl3)
f1 (ppm)

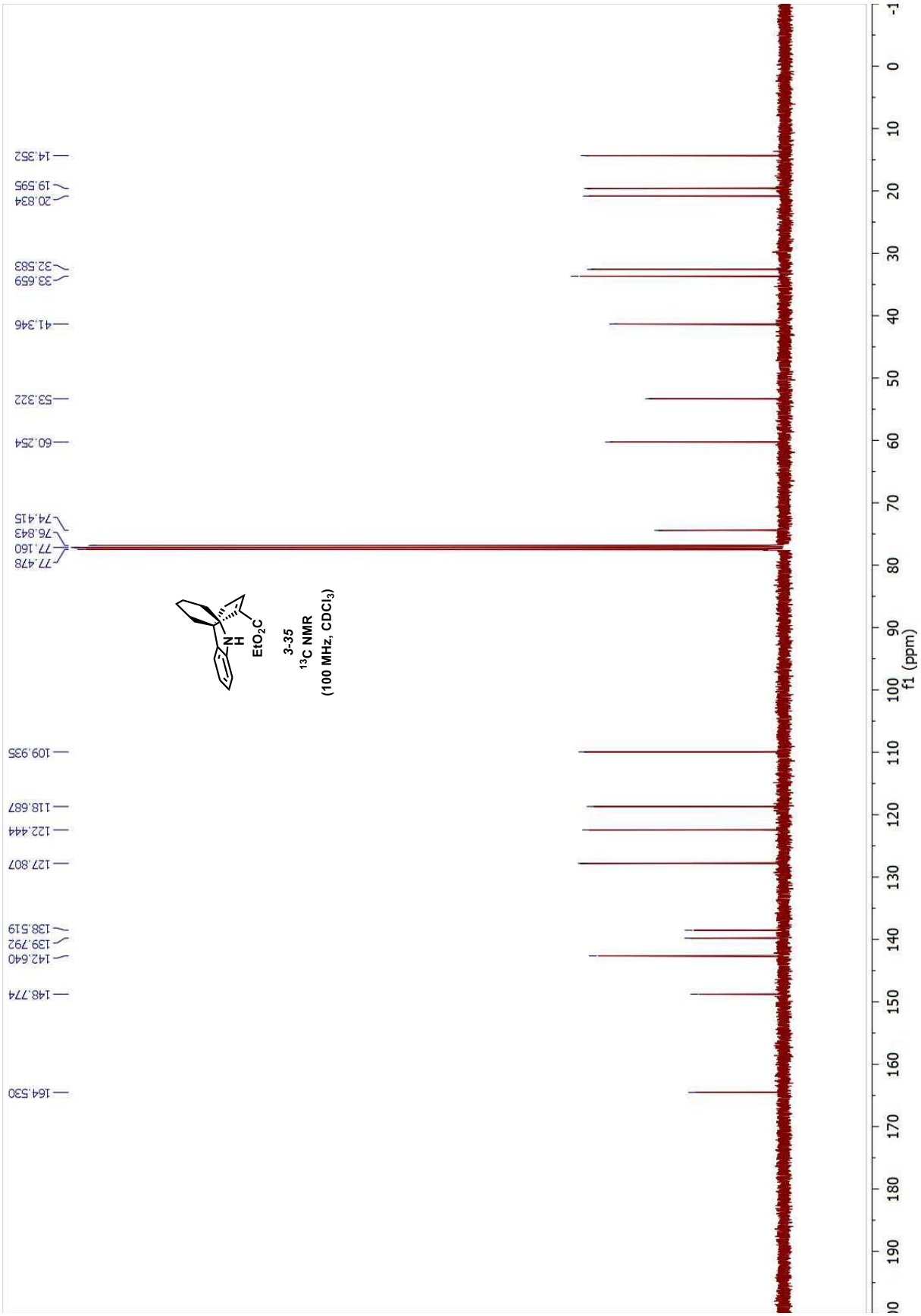
14.352
19.595
20.834
32.583
33.659
41.346
53.322
60.254
74.415
76.843
77.160
77.478
109.935
118.687
122.444
127.807
138.519
139.792
142.640
148.774
164.530
3-35
13C NMR
(100 MHz, CDCl3)
EtO2C
N
H
f1 (ppm)

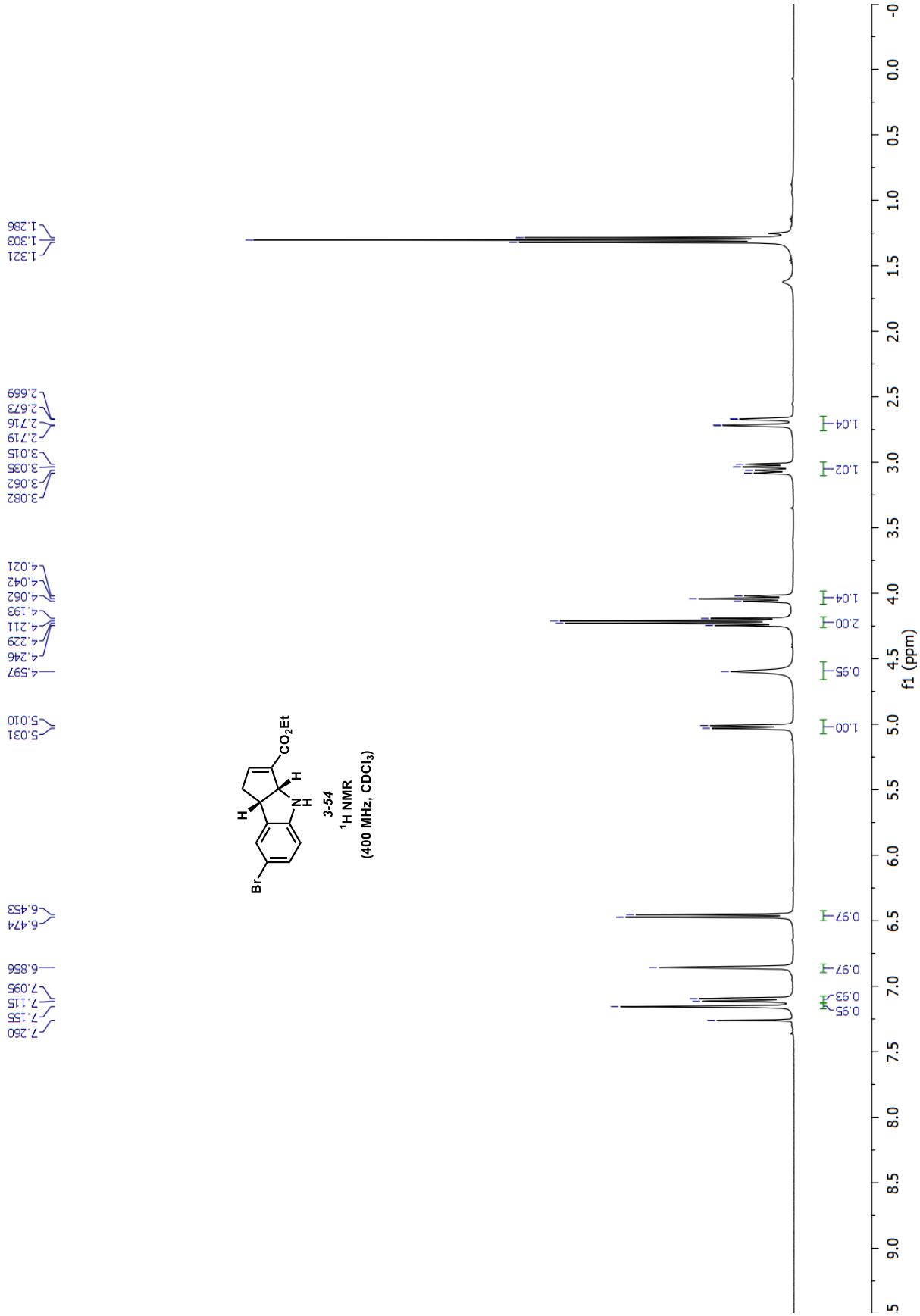
1.286
1.303
1.321
2.669
2.673
2.716
2.719
3.015
3.035
3.062
3.082
4.021
4.042
4.062
4.193
4.211
4.229
4.246
4.597
5.010
5.031
6.453
6.474
6.856
7.095
7.115
7.155
7.260
1.04
1.02
1.04
2.00
0.95
1.00
0.97
0.97
0.93
0.95
CO2Et
H
N
H
H
Br
3-54
1H NMR
(400 MHz, CDCl3)
f1 (ppm)

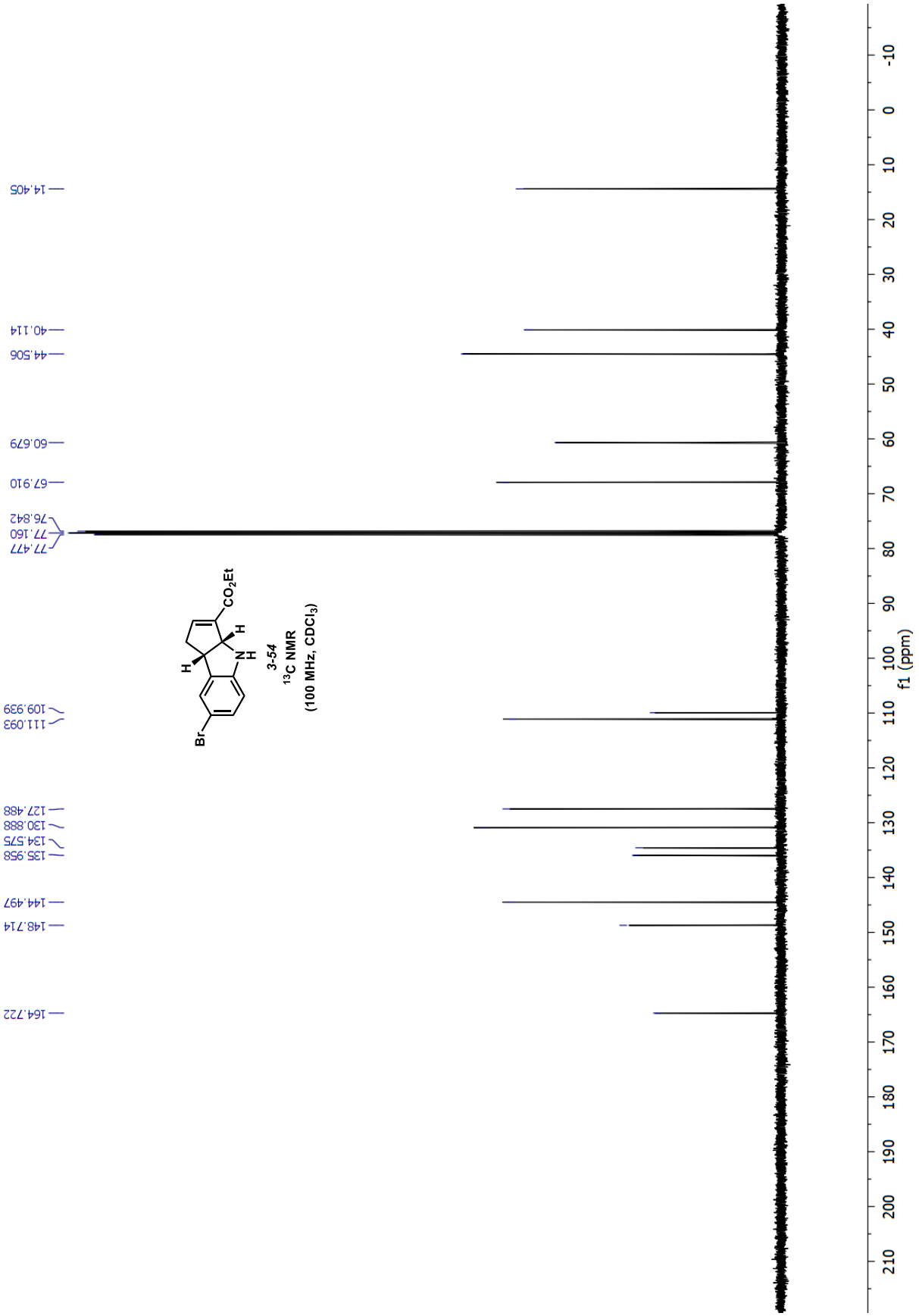
14.405
40.114
44.506
60.679
67.910
76.842
77.160
77.477
109.939
111.093
127.488
130.888
134.575
135.958
144.497
148.714
164.722
3-54
13C NMR
(100 MHz, CDCl3)
CO2Et
H
N
H
H
Br
f1 (ppm)

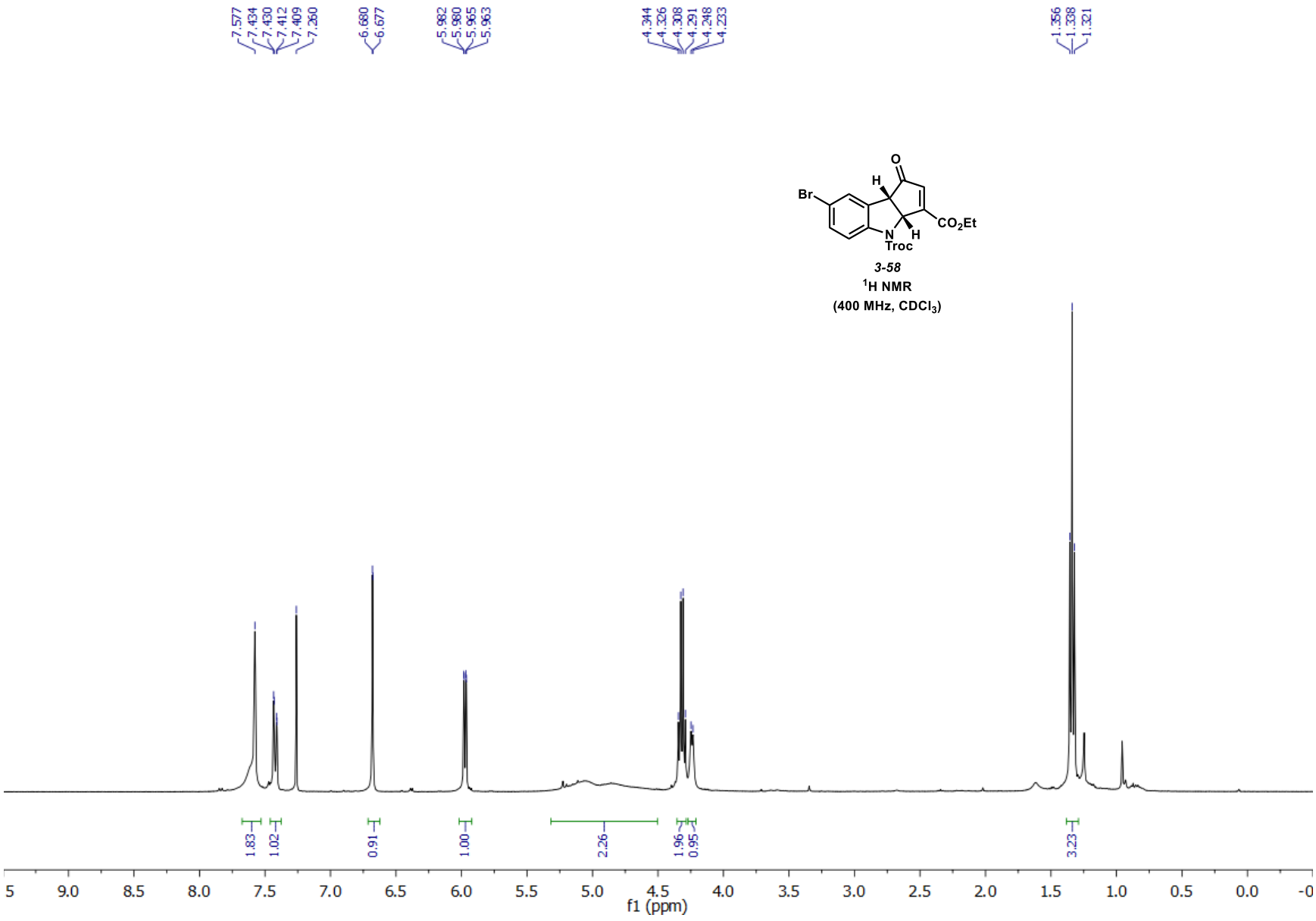
7.577
7.434
7.430
7.412
7.409
7.260
6.680
6.677
5.982
5.980
5.965
5.963
4.344
4.326
4.308
4.291
4.248
4.233
1.356
1.338
1.321
Br
O
H
N
H
Troc
CO2Et
3-58
1H NMR
(400 MHz, CDCl3)
1.83
1.02
0.91
1.00
2.26
1.96
0.95
3.23
f1 (ppm)

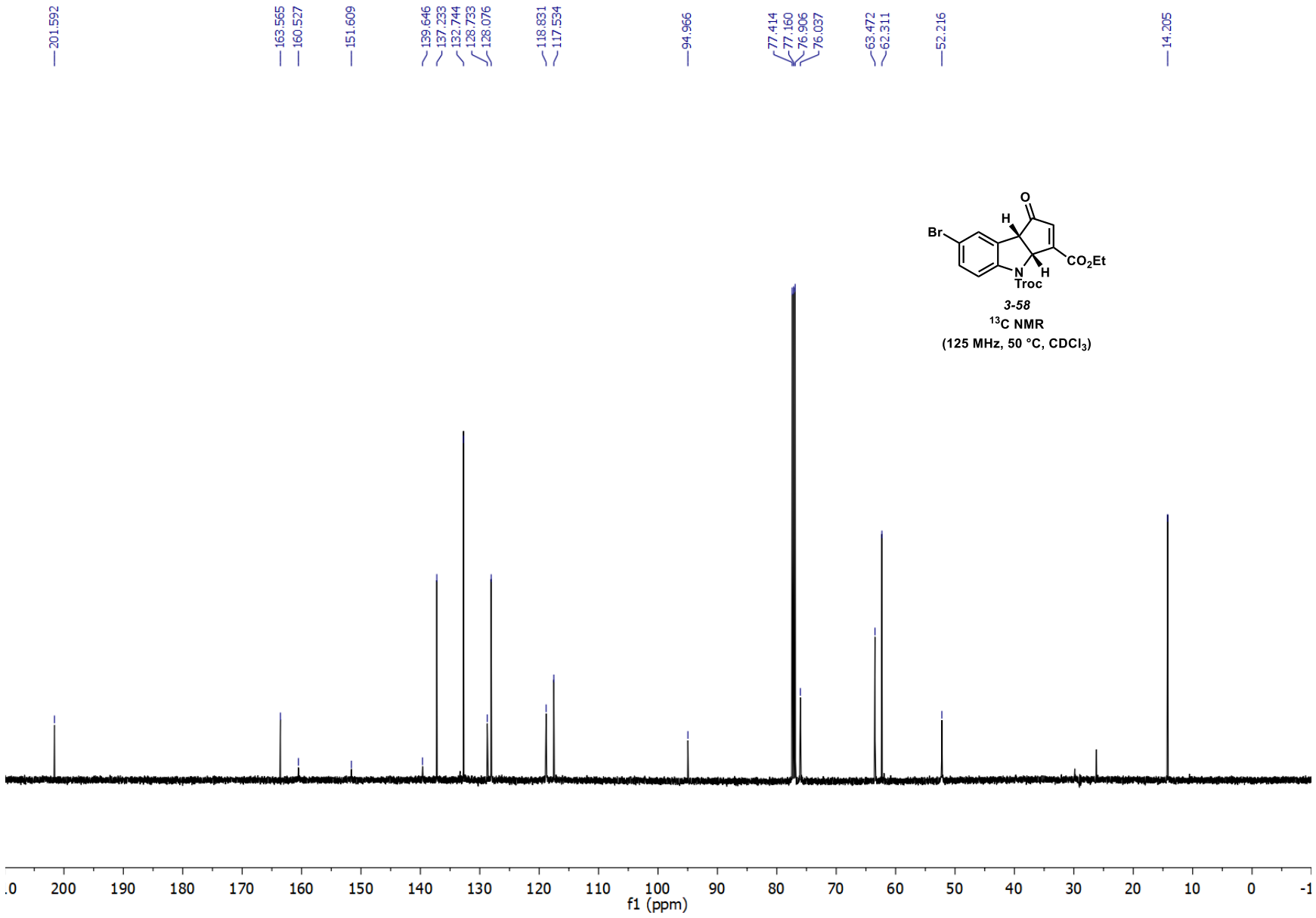
201.592
163.565
160.527
151.609
139.646
137.233
132.744
128.733
128.076
118.831
117.534
94.966
77.414
77.160
76.906
76.037
63.472
62.311
52.216
14.205
Br
O
H
N
H
Troc
CO2Et
3-58
13C NMR
(125 MHz, 50 °C, CDCl3)
f1 (ppm)

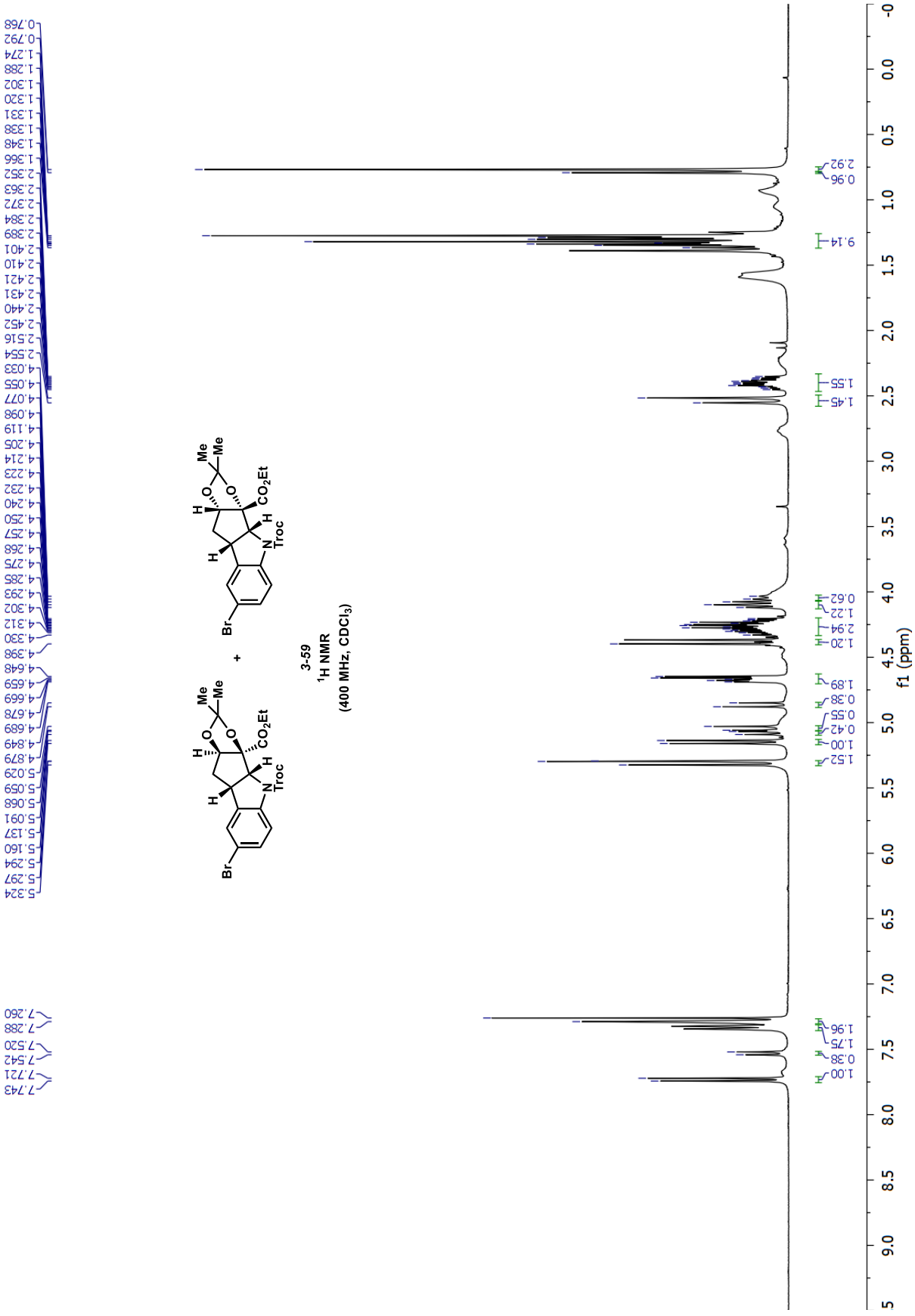
3-59
^{1}H NMR
(400 MHz, $CDCl_3$)
Me
Me
O
O
H
CO_2Et
H
N
Troc
Br
+
f1 (ppm)

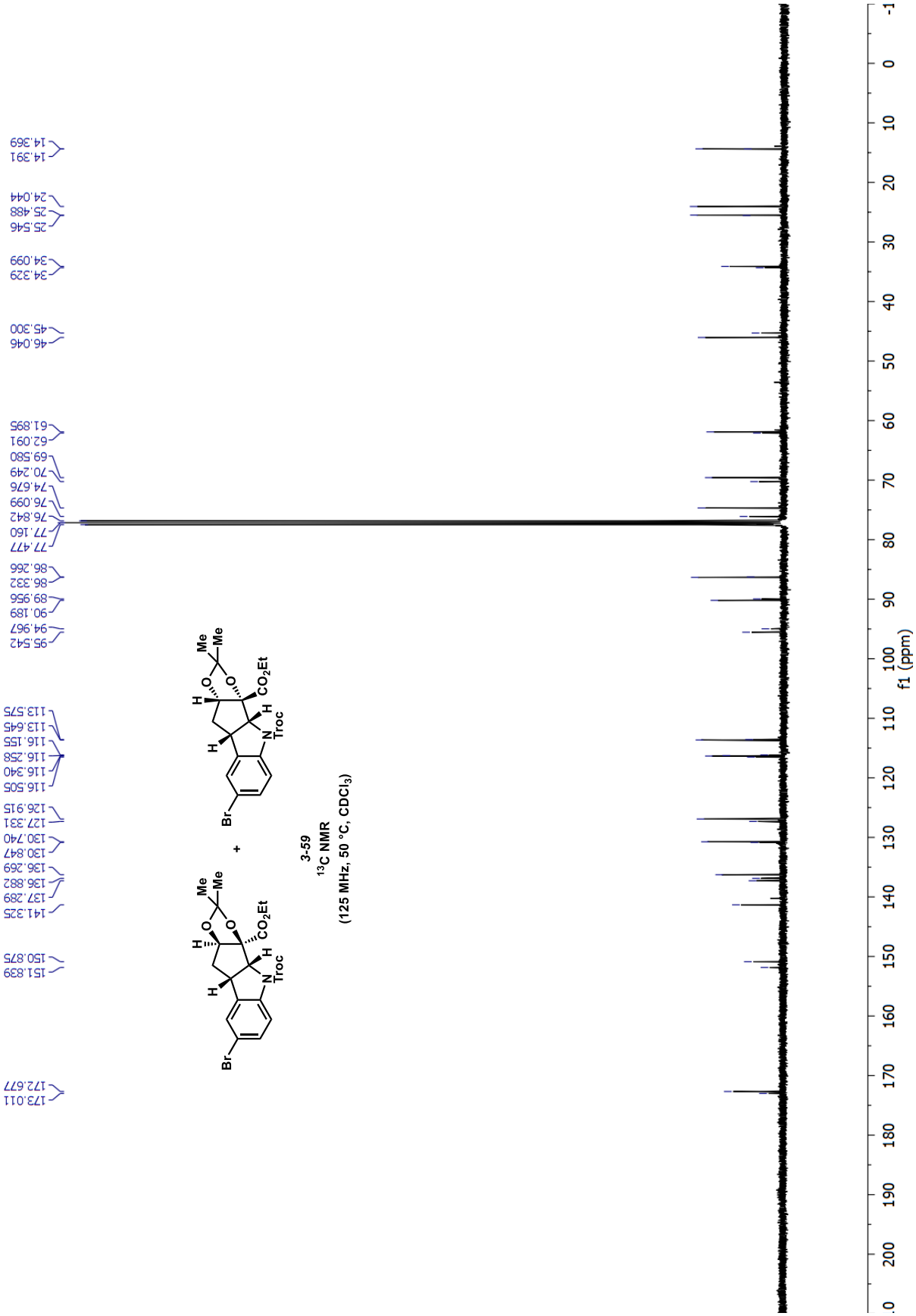
14.391
14.369
24.044
25.488
25.546
34.099
34.329
45.300
46.046
61.895
62.091
69.580
70.249
74.676
76.099
76.842
77.160
77.477
86.266
86.332
89.956
90.189
94.967
95.542
113.575
113.645
116.155
116.258
116.340
116.505
126.915
127.331
130.740
130.847
136.269
136.882
137.289
141.325
150.875
151.839
172.677
173.011
Me
Me
O
O
H
CO2Et
H
N
Troc
Br
+
3-59
13C NMR
(125 MHz, 50 °C, CDCl3)
f1 (ppm)

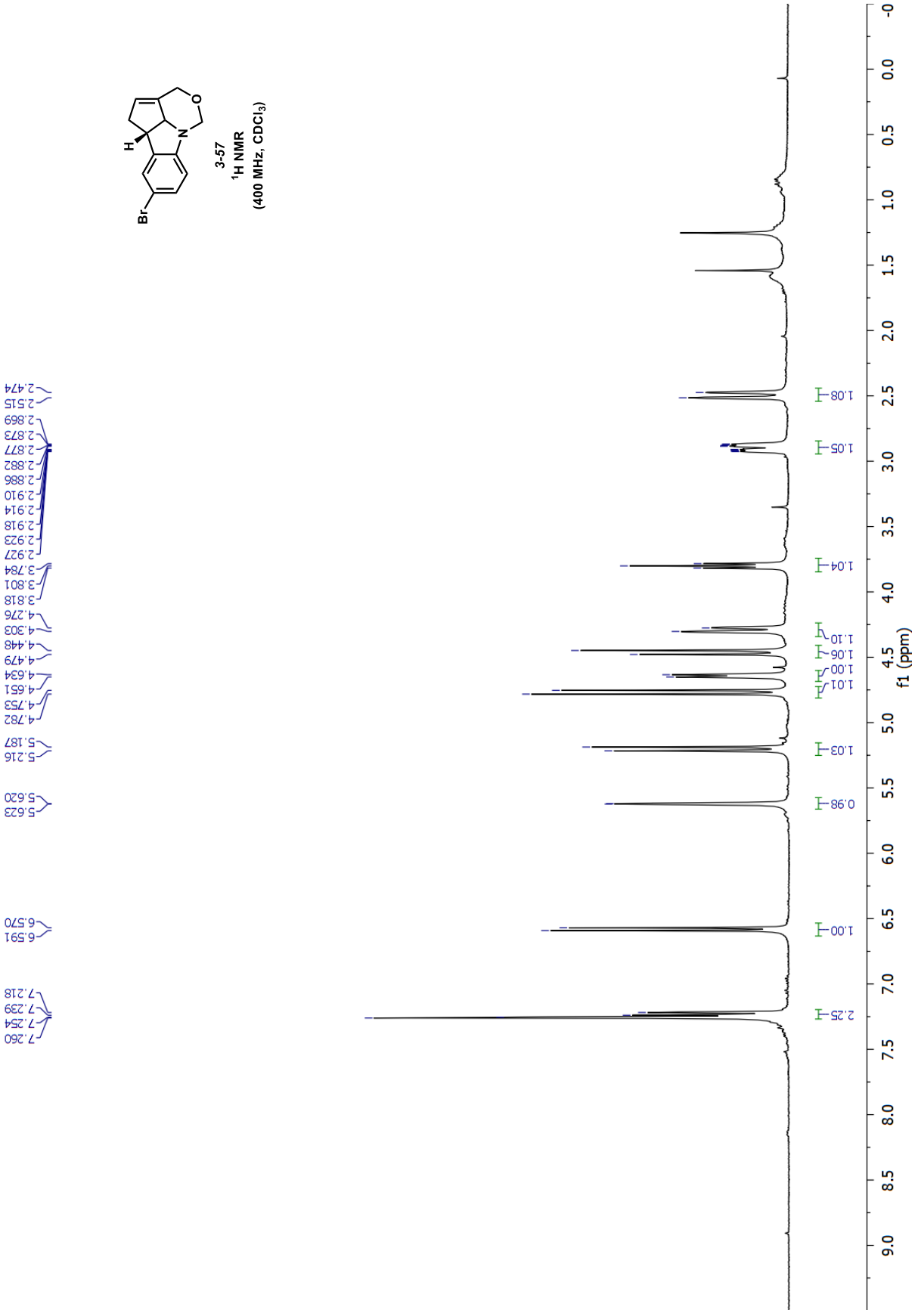
3-57
^{1}H NMR
(400 MHz, CDCl$_3$)
Br
H
N
O
f1 (ppm)
2.474
2.515
2.869
2.873
2.877
2.882
2.886
2.910
2.914
2.918
2.923
2.927
3.784
3.801
3.818
4.276
4.303
4.448
4.479
4.634
4.651
4.753
4.782
5.187
5.216
5.620
5.623
6.570
6.591
7.218
7.239
7.254
7.260
2.25
1.00
0.98
1.03
1.01
1.00
1.06
1.10
1.04
1.05
1.08

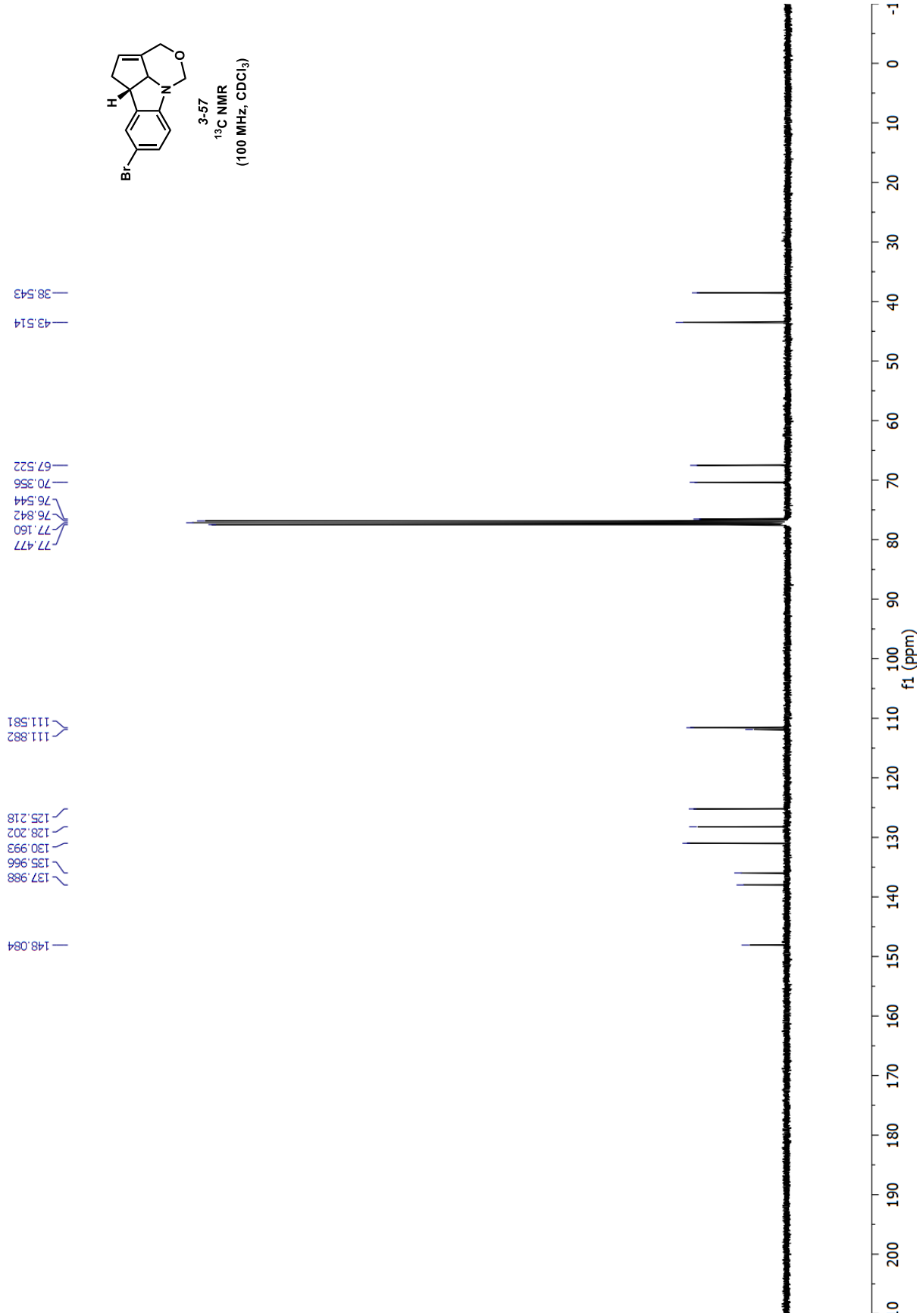
3-57
^{13}C NMR
(100 MHz, $CDCl_3$)
Br
H
N
O
38.543
43.514
67.522
70.356
76.544
76.842
77.160
77.477
111.581
111.882
125.218
128.202
130.993
135.966
137.988
148.084
f1 (ppm)

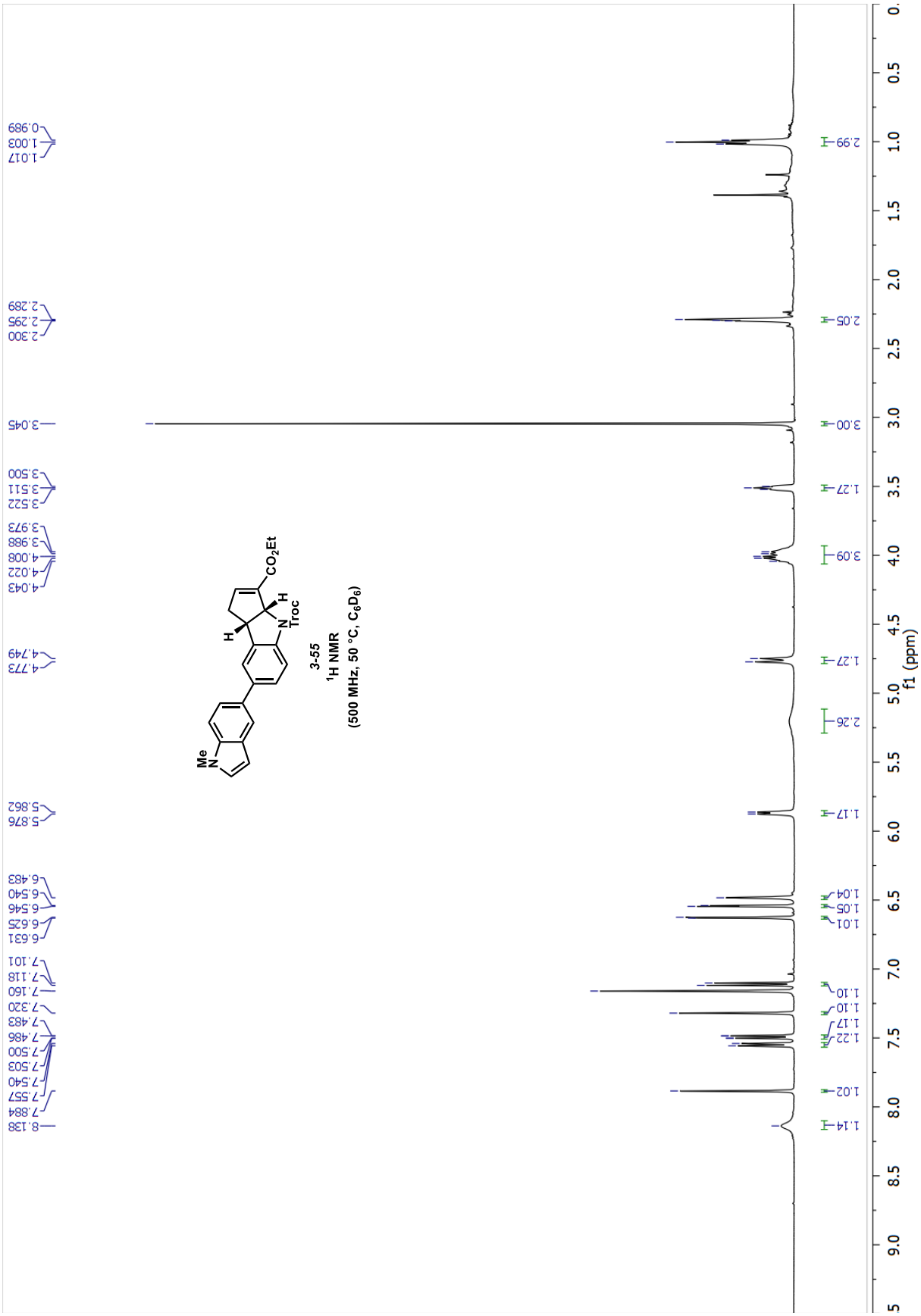
3-55
^{1}H NMR
(500 MHz, 50 °C, C_6D_6)
f1 (ppm)

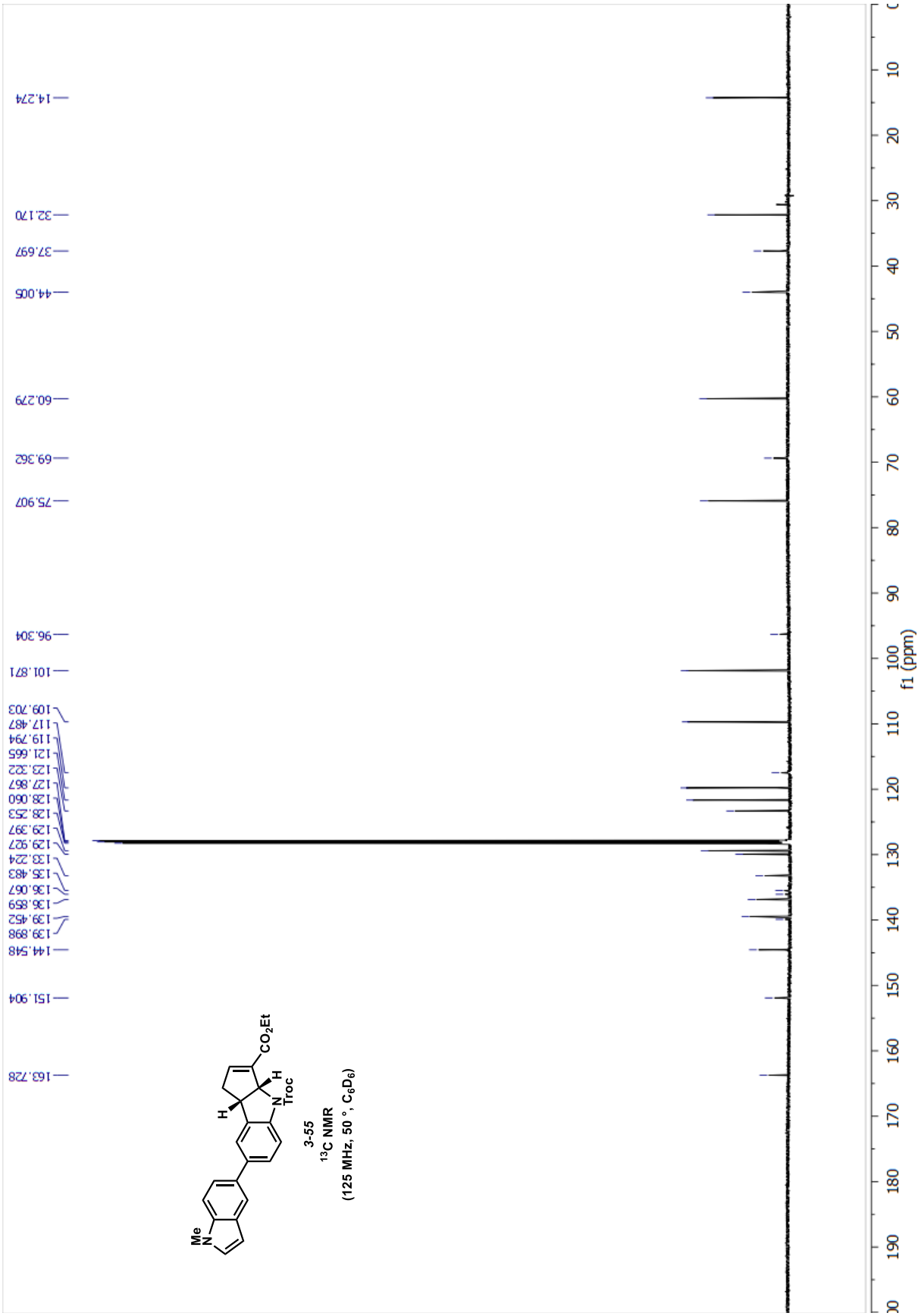
14.274
32.170
37.697
44.005
60.279
69.362
75.907
96.304
101.871
109.703
117.487
119.794
121.665
123.322
127.867
128.060
128.253
129.397
129.927
133.224
135.483
136.067
136.859
139.452
139.898
144.548
151.904
163.728
CO2Et
H
N
Troc
H
Me
N
3-55
13C NMR
(125 MHz, 50 °, C6D6)
f1 (ppm)

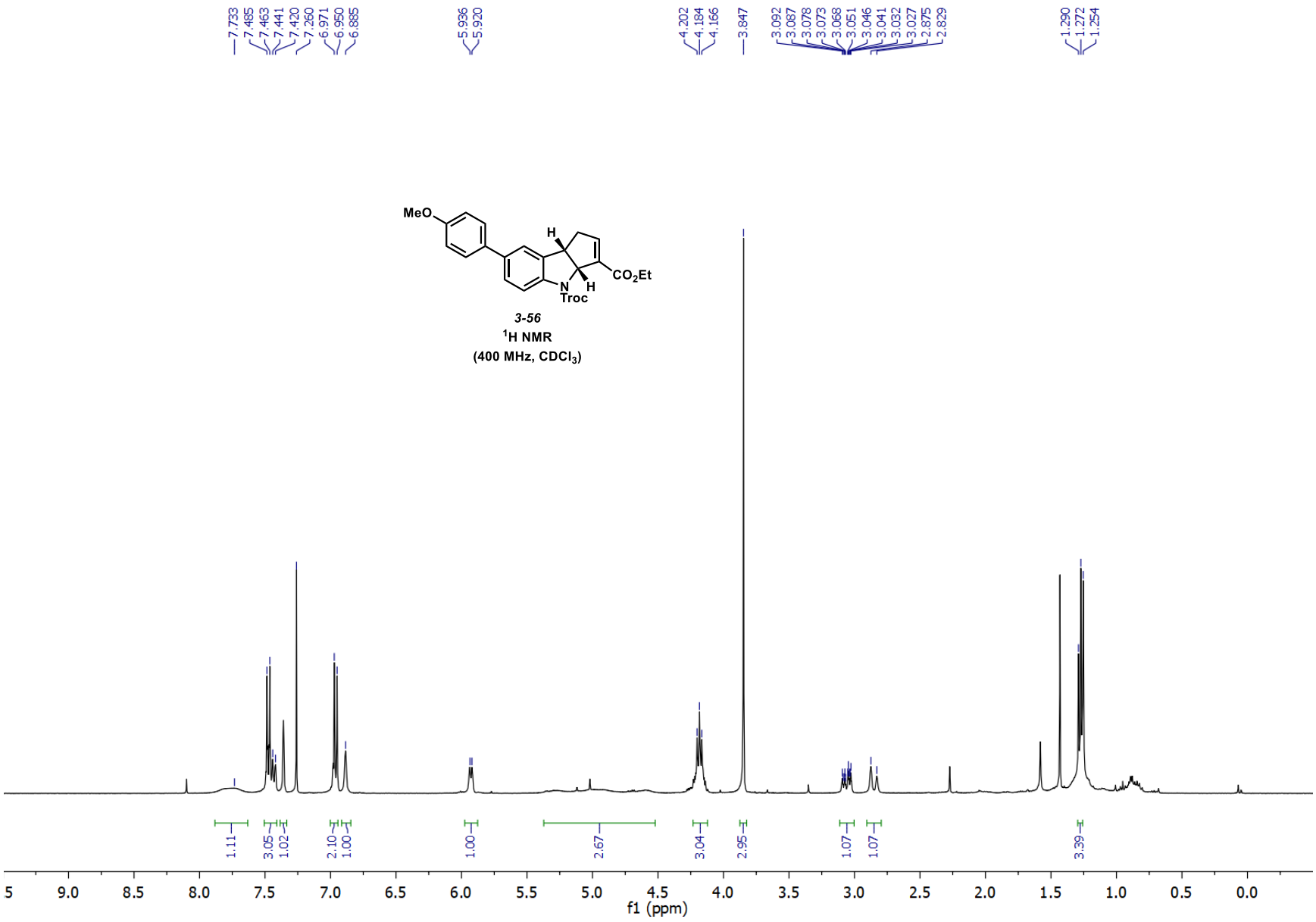
7.733
7.485
7.463
7.441
7.420
7.260
6.971
6.950
6.885
5.936
5.920
4.202
4.184
4.166
3.847
3.092
3.087
3.078
3.073
3.068
3.051
3.046
3.041
3.032
3.027
2.875
2.829
1.290
1.272
1.254
MeO
H
CO2Et
N
H
Troc
3-56
1H NMR
(400 MHz, CDCl3)
1.11
3.05
1.02
2.10
1.00
1.00
2.67
3.04
2.95
1.07
1.07
3.39
f1 (ppm)

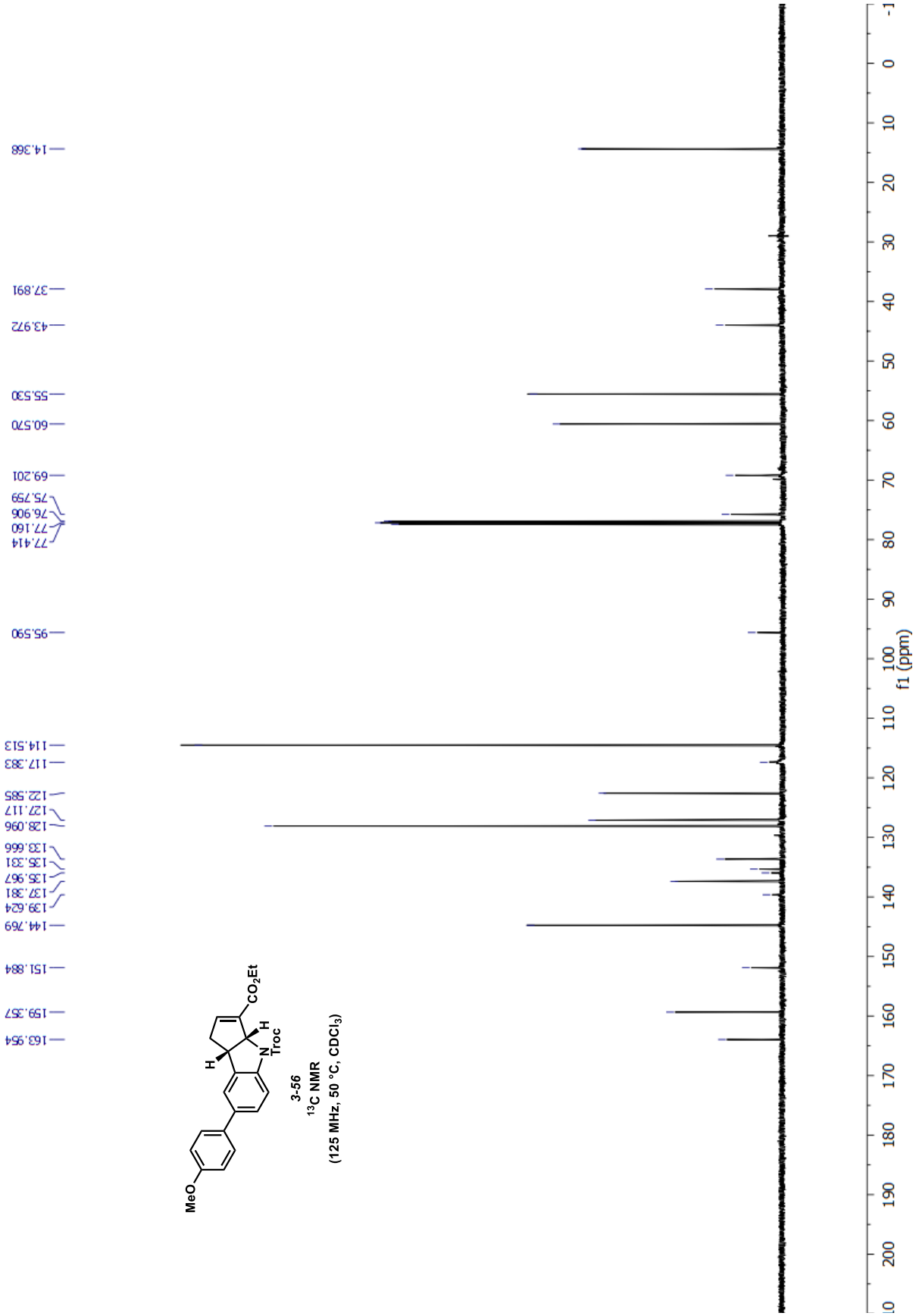
14.368
37.891
43.972
55.530
60.570
69.201
75.759
76.906
77.160
77.414
95.590
114.513
117.383
122.585
127.117
128.096
133.666
135.331
135.967
137.381
139.624
144.769
151.884
159.357
163.954
MeO
H
N
Troc
H
CO2Et
3-56
13C NMR
(125 MHz, 50 °C, CDCl3)
f1 (ppm)

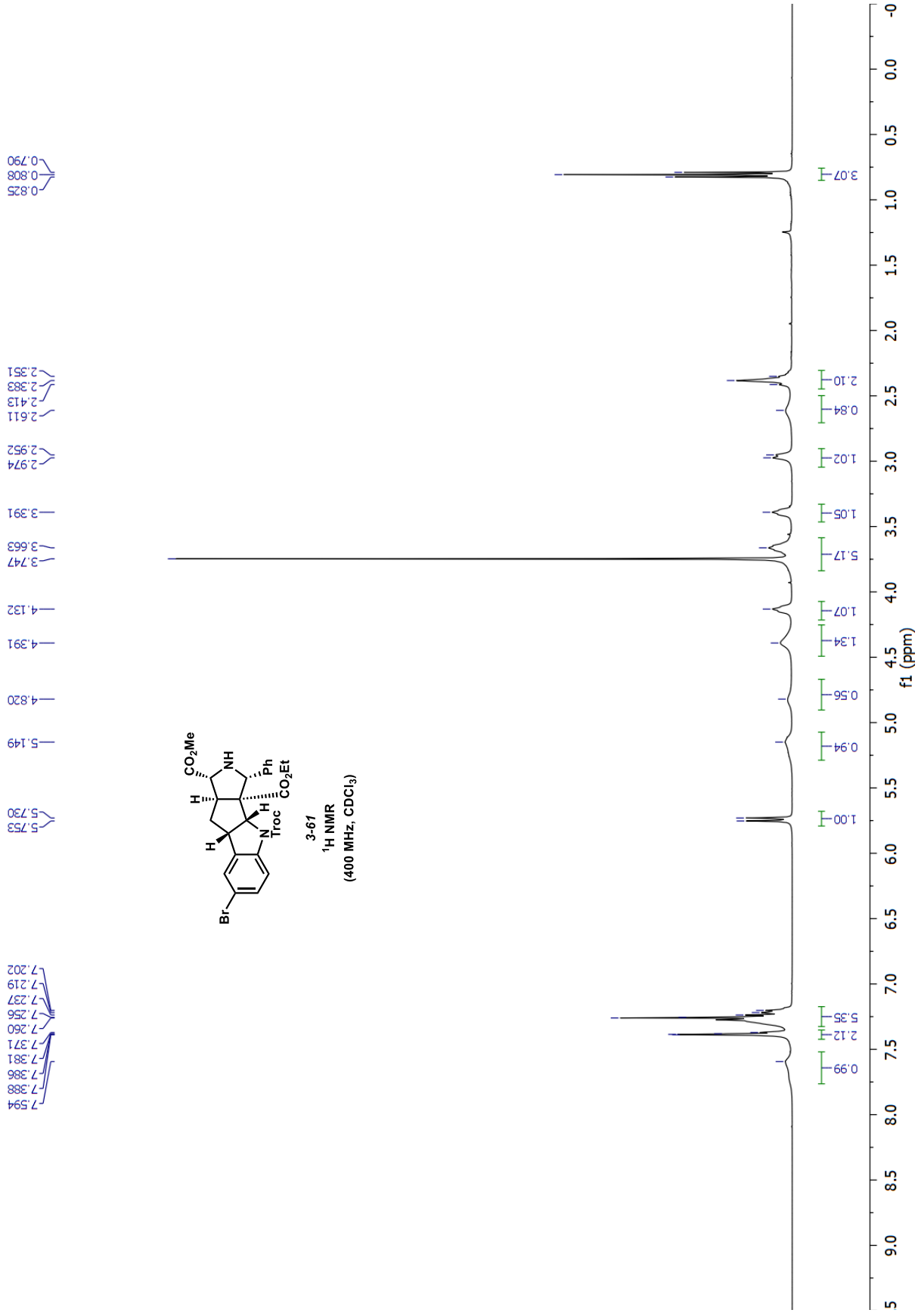
3-61
^{1}H NMR
(400 MHz, CDCl$_3$)
f1 (ppm)

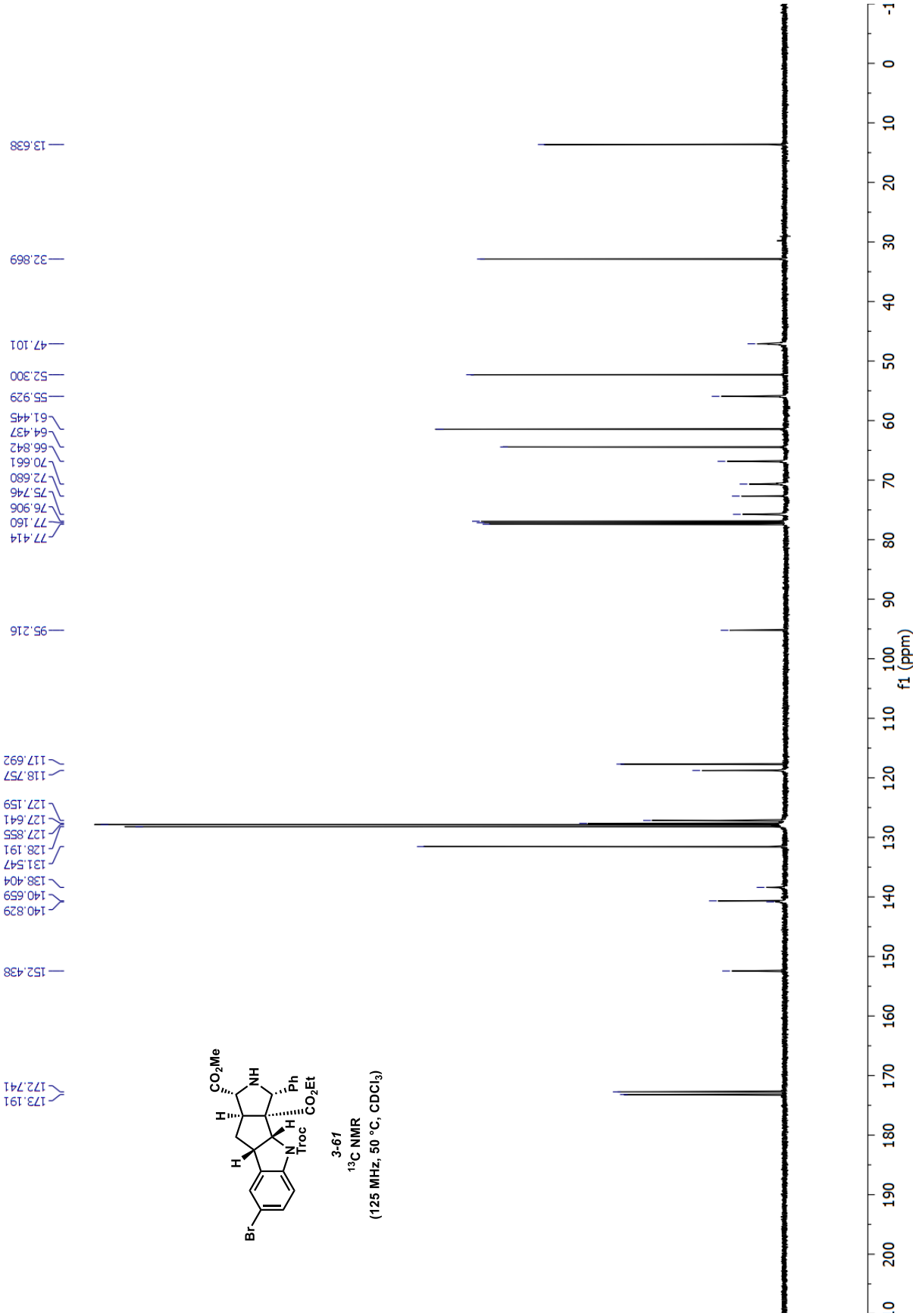
13.638
32.869
47.101
52.300
55.929
61.445
64.437
66.842
70.661
72.680
75.746
76.906
77.160
77.414
95.216
117.692
118.757
127.159
127.641
127.855
128.191
131.547
138.404
140.659
140.829
152.438
172.741
173.191
CO2Me
NH
Ph
CO2Et
H
H
H
N
Troc
Br
3-61
13C NMR
(125 MHz, 50 °C, CDCl3)
f1 (ppm)

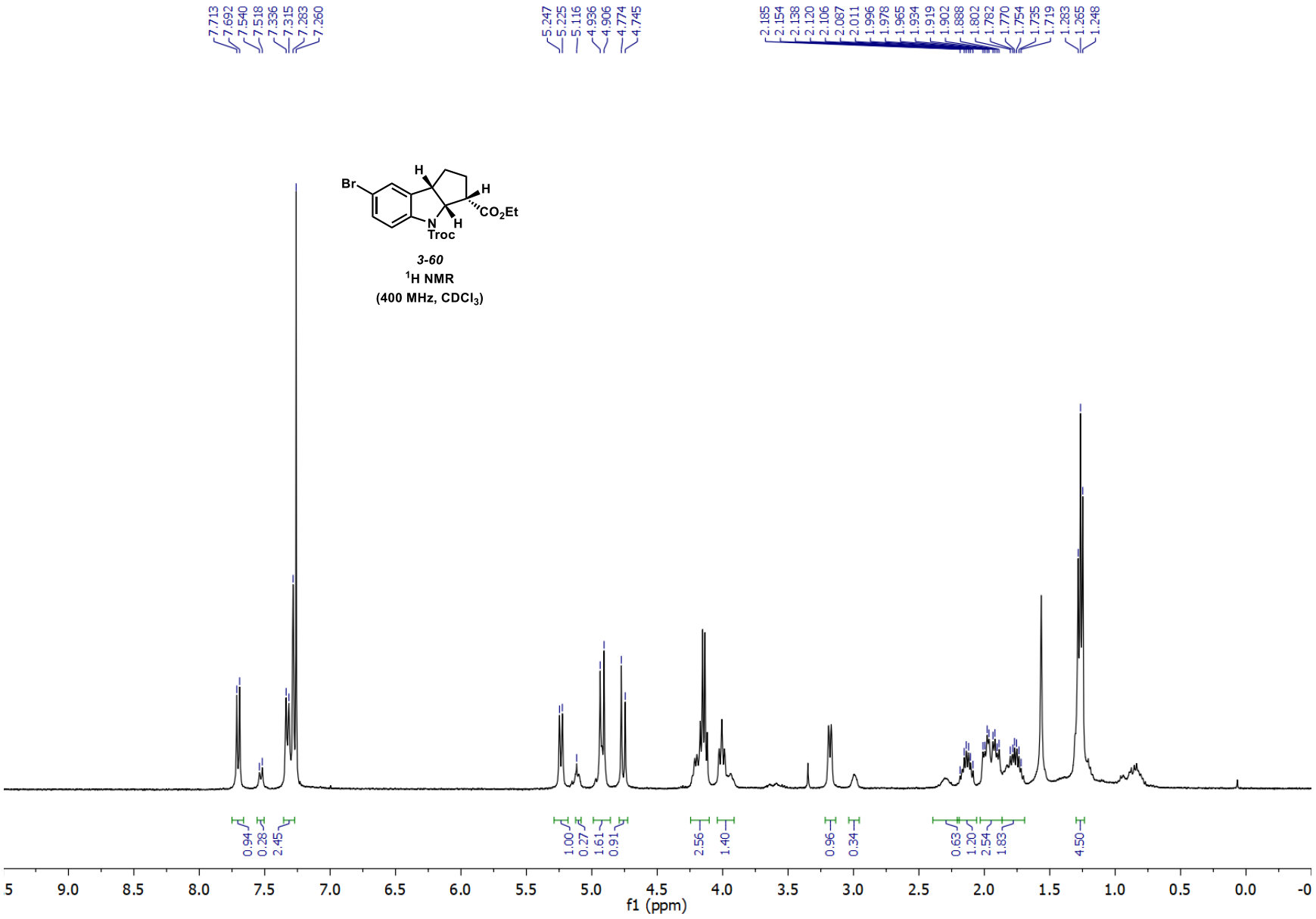
7.713
7.692
7.540
7.518
7.336
7.315
7.283
7.260
5.247
5.225
5.116
4.936
4.906
4.774
4.745
2.185
2.154
2.138
2.120
2.106
2.087
2.011
1.996
1.978
1.965
1.934
1.919
1.902
1.888
1.802
1.782
1.770
1.754
1.735
1.719
1.283
1.265
1.248
Br
H
H
CO2Et
N
H
Troc
3-60
1H NMR
(400 MHz, CDCl3)
0.94
0.28
2.45
1.00
0.27
1.61
0.91
2.56
1.40
0.96
0.34
0.63
1.20
2.54
1.83
4.50
f1 (ppm)

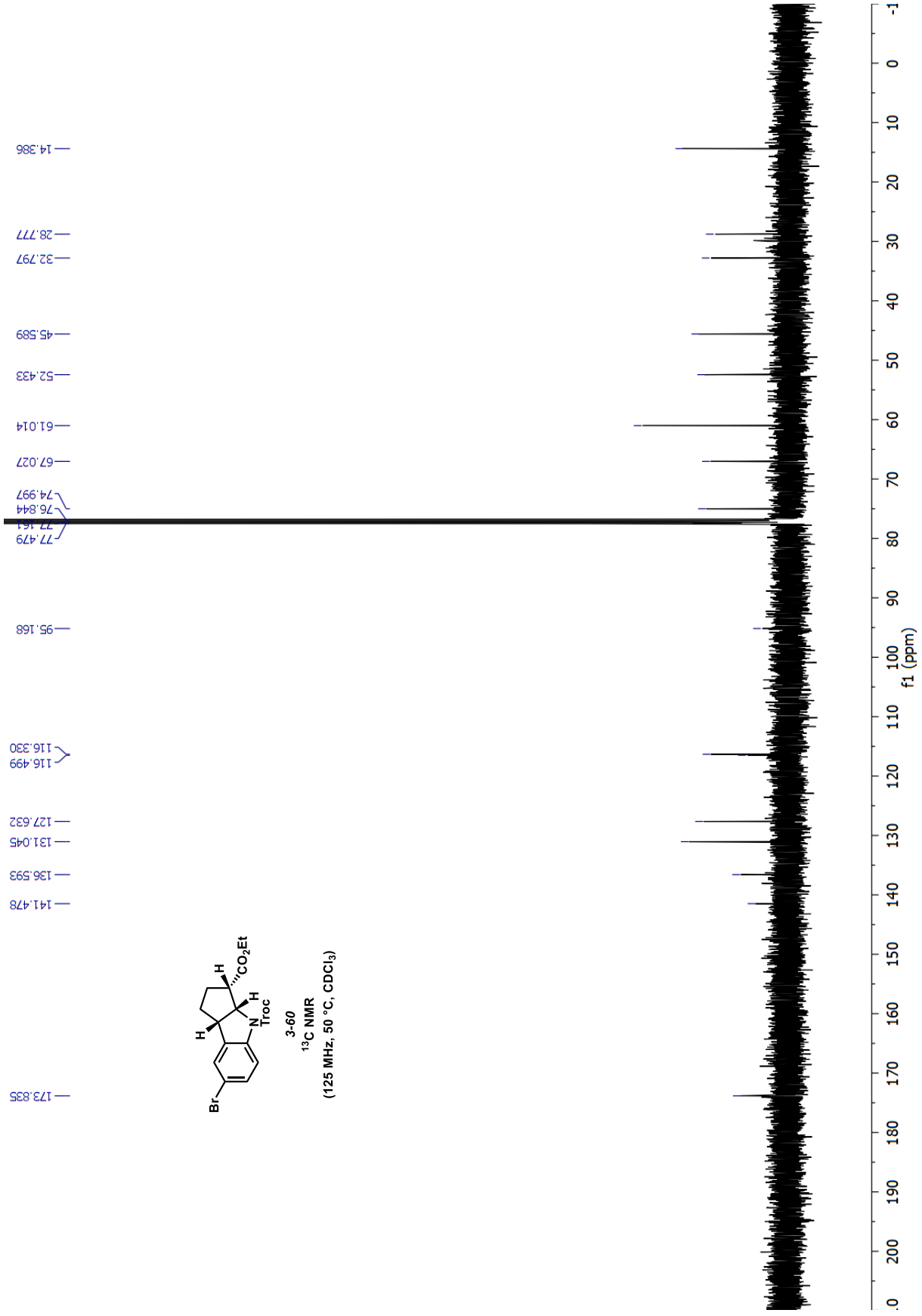
14.386
28.777
32.797
45.589
52.433
61.014
67.027
74.997
76.844
77.161
77.479
95.168
116.330
116.499
127.632
131.045
136.593
141.478
173.835
Br
H
CO2Et
H
N
Troc
H
3-60
13C NMR
(125 MHz, 50 °C, CDCl3)
f1 (ppm)

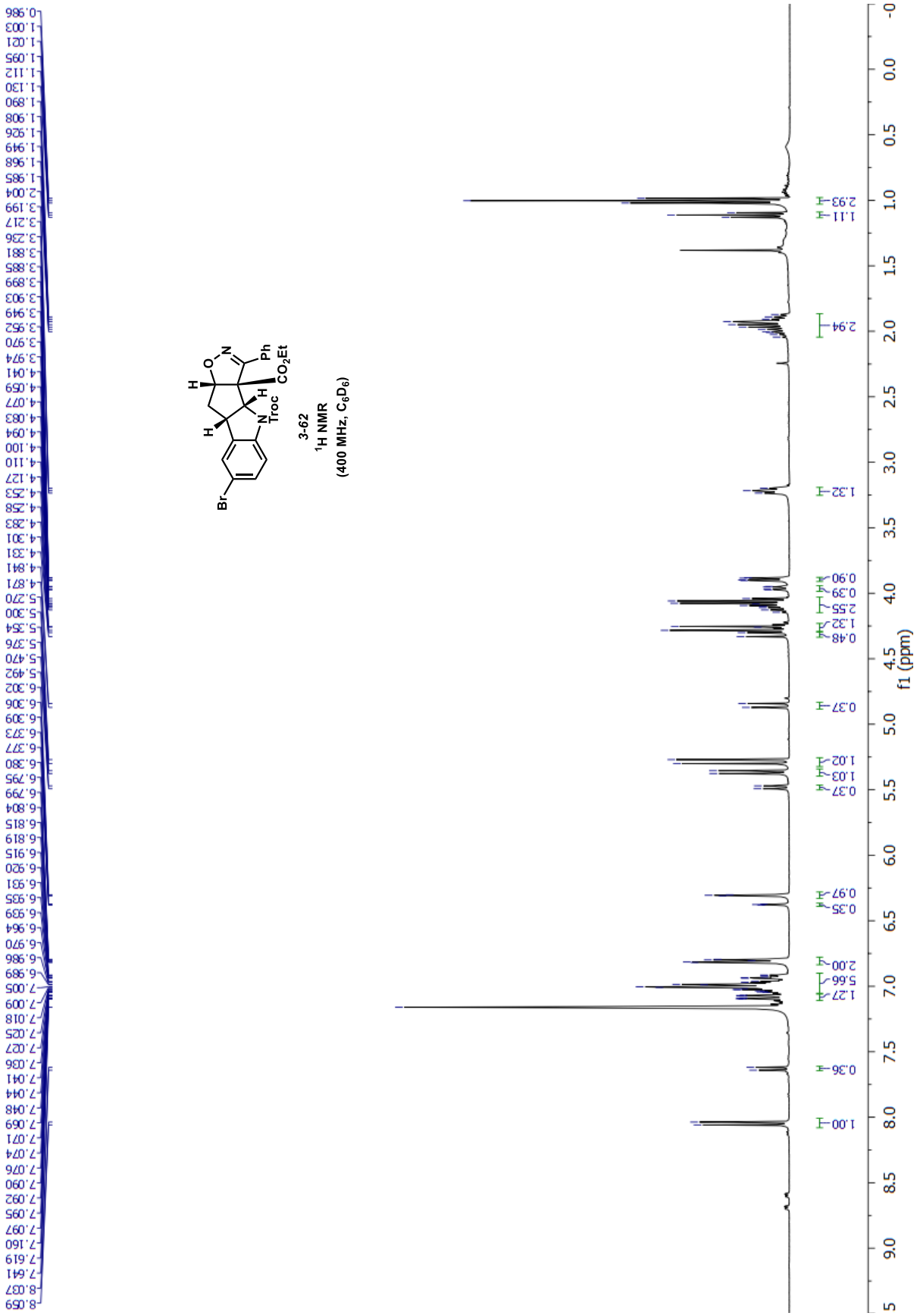
3-62
^{1}H NMR
(400 MHz, C_6D_6)
Ph
CO_2Et
Troc
Br
f1 (ppm)

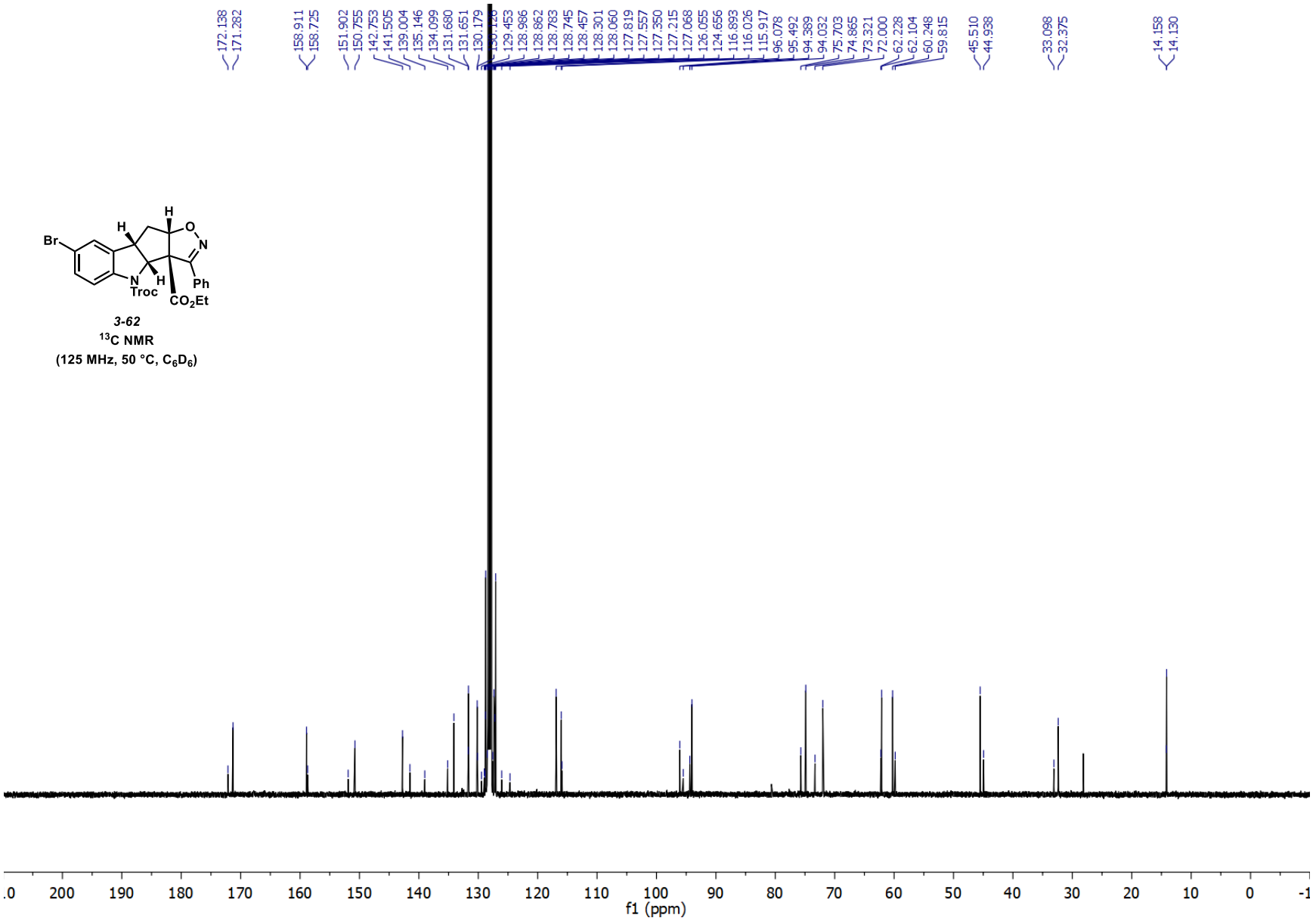
172.138
171.282
158.911
158.725
151.902
150.755
142.753
141.505
139.004
135.146
134.099
131.680
131.651
130.179
129.453
128.986
128.862
128.783
128.745
128.457
128.301
128.060
127.819
127.557
127.350
127.215
127.068
126.055
124.656
116.893
116.026
115.917
96.078
95.492
94.389
94.032
75.703
74.865
73.321
72.000
62.228
62.104
60.248
59.815
45.510
44.938
33.098
32.375
14.158
14.130
Br
H
H
O
N
N
H
Troc
Ph
CO2Et
3-62
13C NMR
(125 MHz, 50 °C, C6D6)
f1 (ppm)

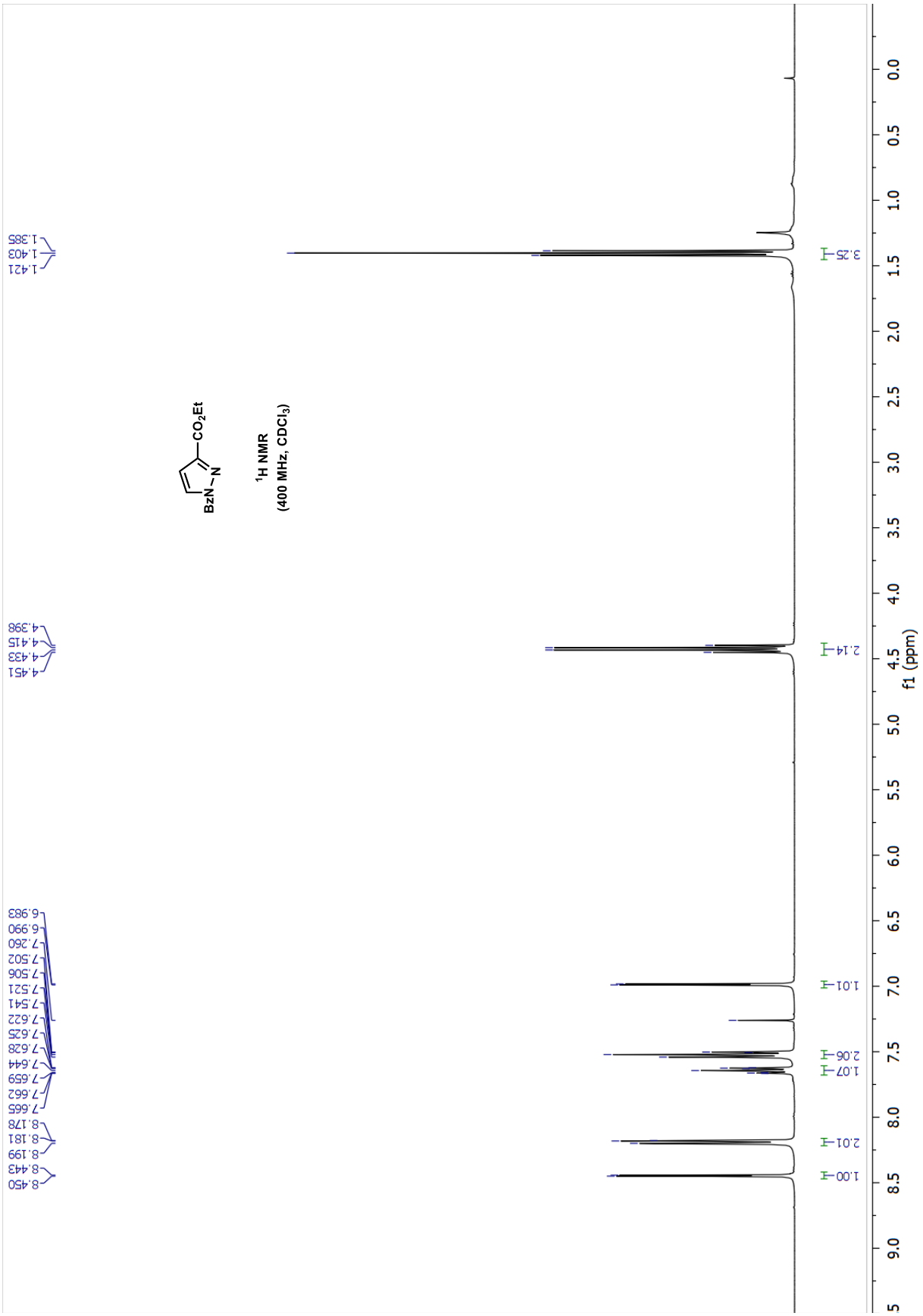
CO2Et
BzN
N
1H NMR
(400 MHz, CDCl3)
1.421
1.403
1.385
4.451
4.433
4.415
4.398
8.450
8.443
8.199
8.181
8.178
7.665
7.662
7.659
7.644
7.628
7.625
7.622
7.541
7.521
7.506
7.502
7.260
6.990
6.983
3.25
2.14
1.01
2.06
1.07
2.01
1.00
f1 (ppm)

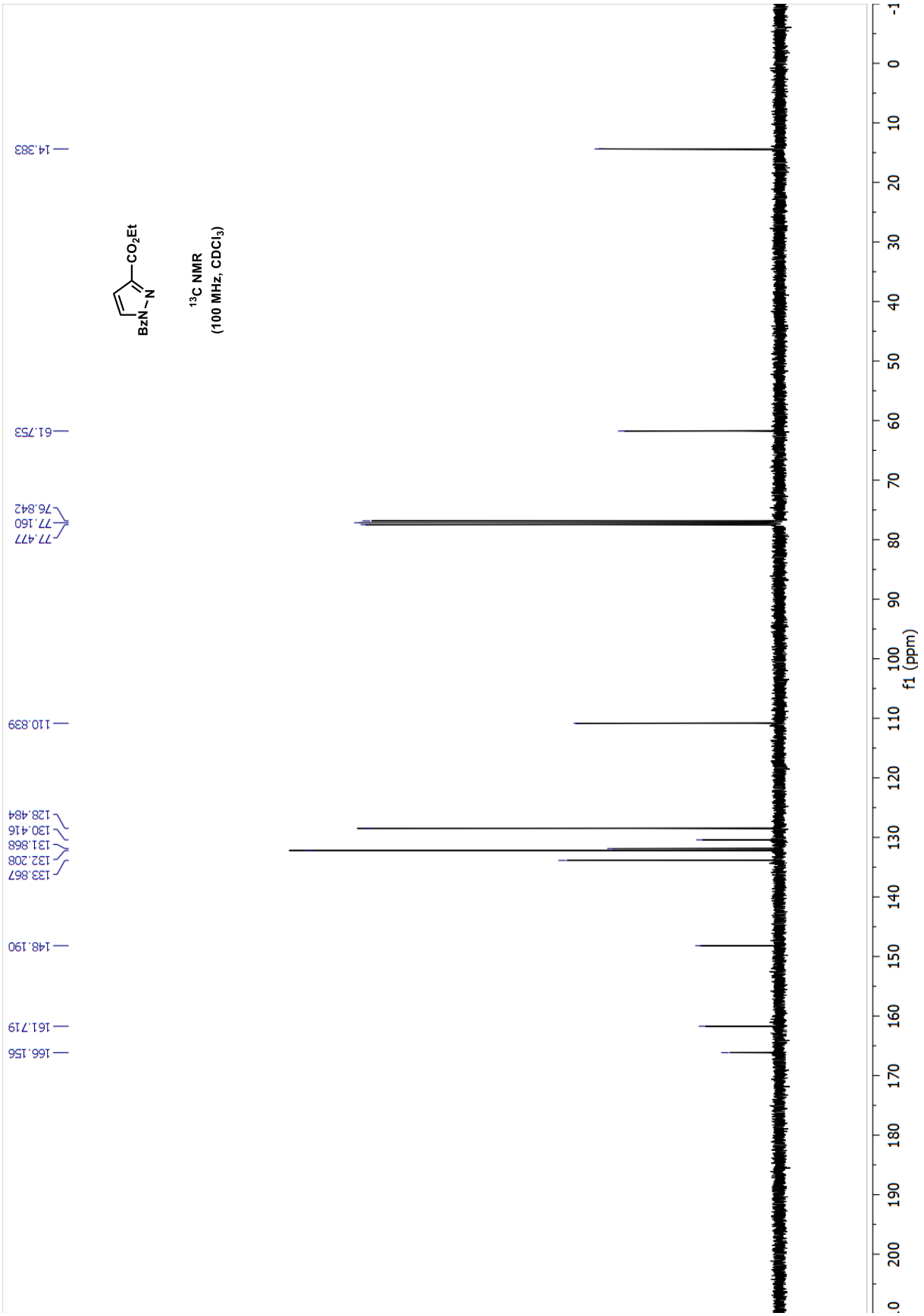
14.383
61.753
76.842
77.160
77.477
110.839
128.484
130.416
131.868
132.208
133.867
148.190
161.719
166.156
BzN
N
CO2Et
13C NMR
(100 MHz, CDCl3)
f1 (ppm)

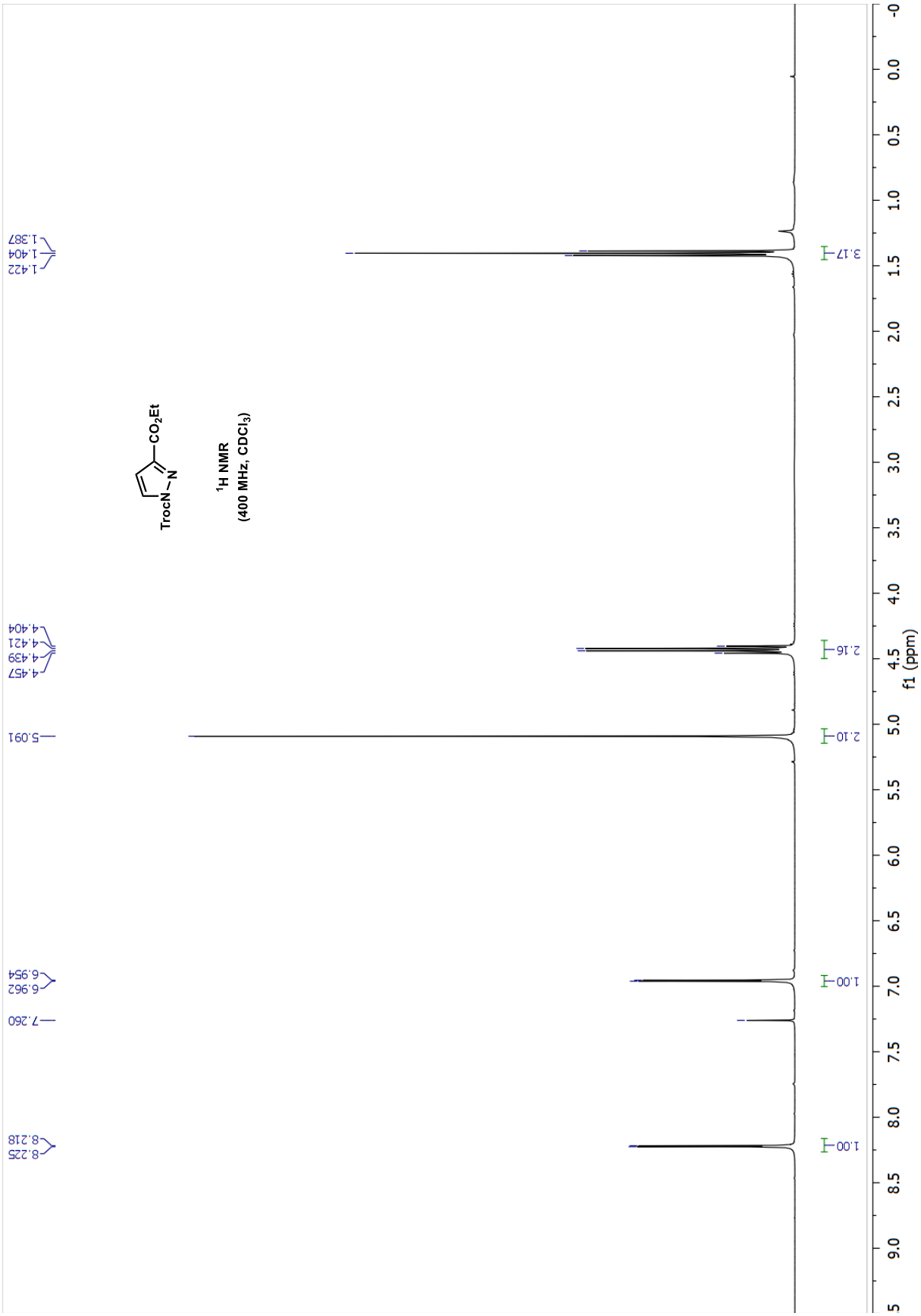
TrocN
N
CO2Et
1H NMR
(400 MHz, CDCl3)
1.422
1.404
1.387
4.457
4.439
4.421
4.404
5.091
6.962
6.954
7.260
8.225
8.218
3.17
2.16
2.10
1.00
1.00
f1 (ppm)

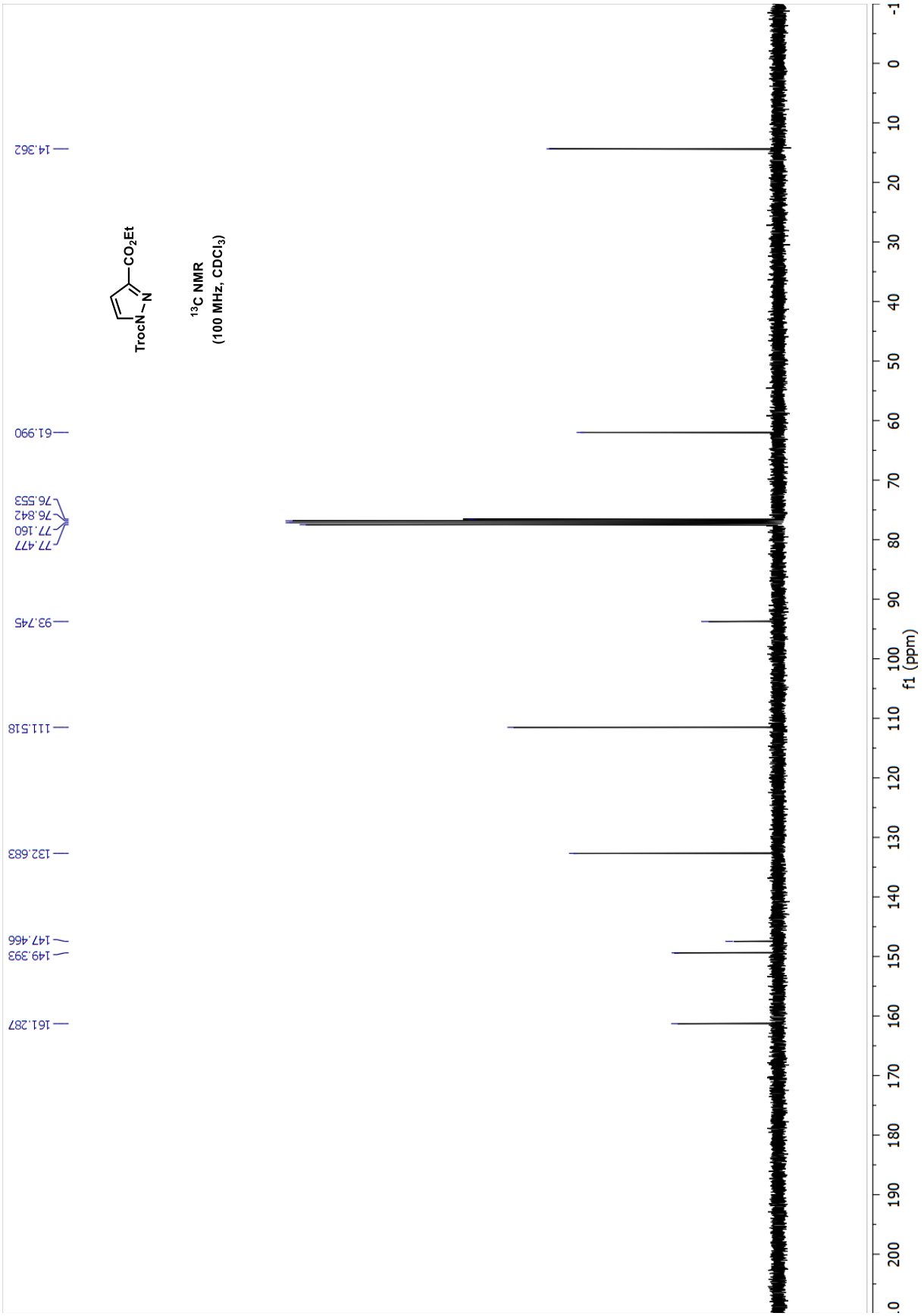
TrocN
N
CO2Et
13C NMR
(100 MHz, CDCl3)
14.362
61.990
76.553
76.842
77.160
77.477
93.745
111.518
132.683
147.466
149.393
161.287
f1 (ppm)

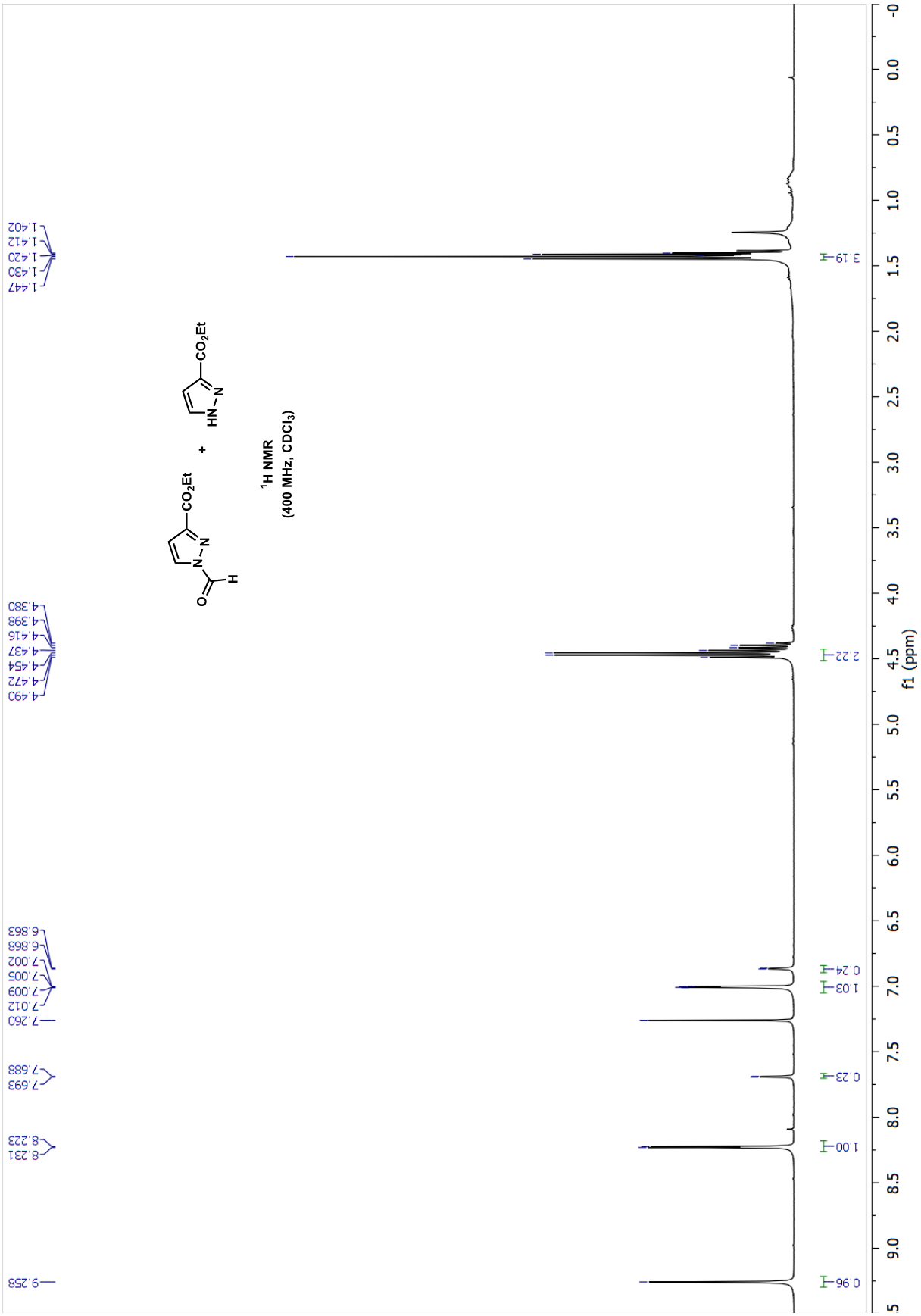
^{1}H NMR
(400 MHz, CDCl$_3$)
CO$_2$Et
HN–N
+
CO$_2$Et
N–N
O
H
9.258
8.231
8.223
7.693
7.688
7.260
7.012
7.009
7.005
7.002
6.868
6.863
4.490
4.472
4.454
4.437
4.416
4.398
4.380
1.447
1.430
1.420
1.412
1.402
0.96
1.00
0.23
1.03
0.24
2.22
3.19
f1 (ppm)

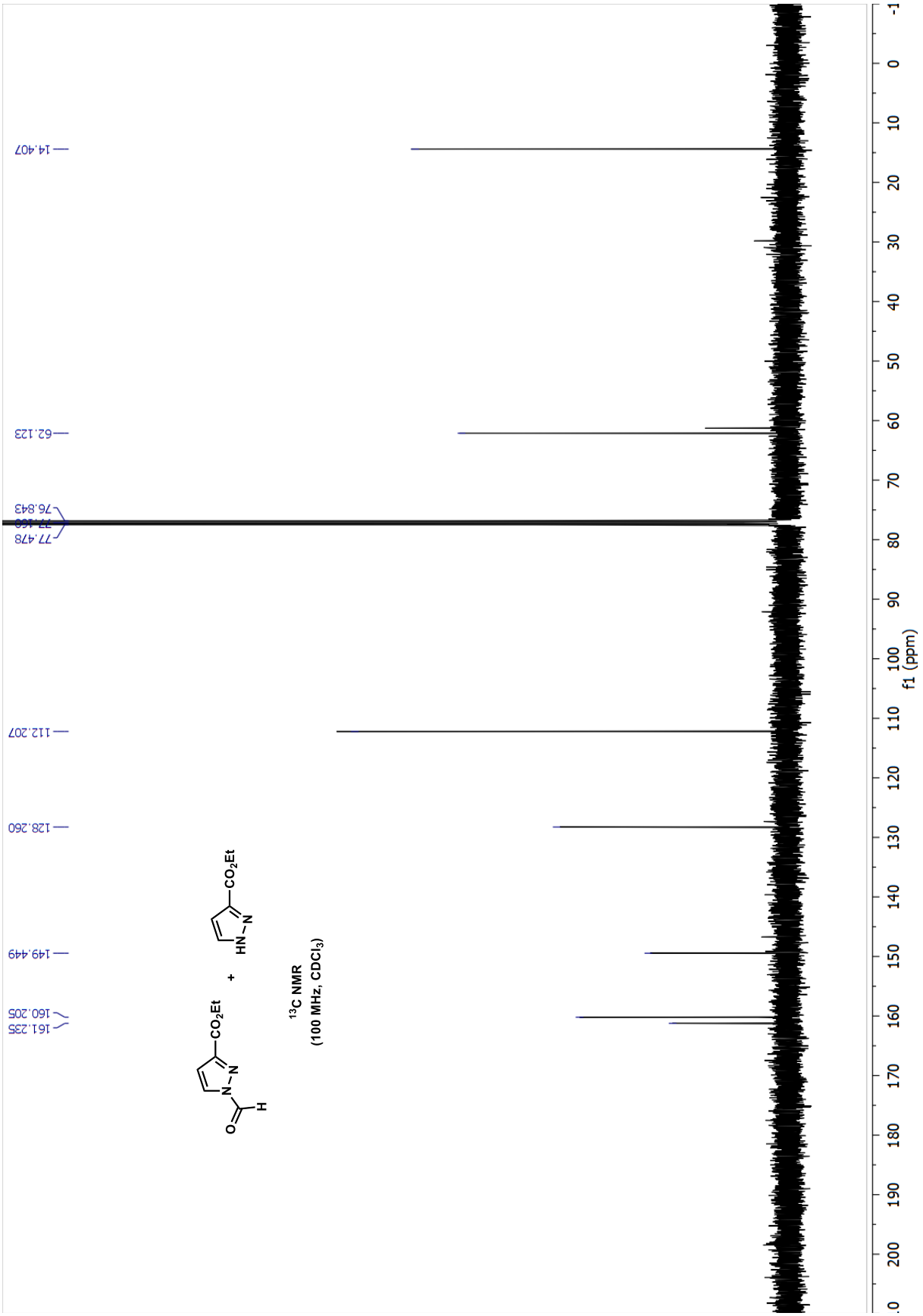
14.407
62.123
77.478
77.160
76.843
112.207
128.260
149.449
160.205
161.235
^{13}C NMR
(100 MHz, CDCl$_3$)
CO$_2$Et
HN
N
+
CO$_2$Et
N
N
O
H
f1 (ppm)

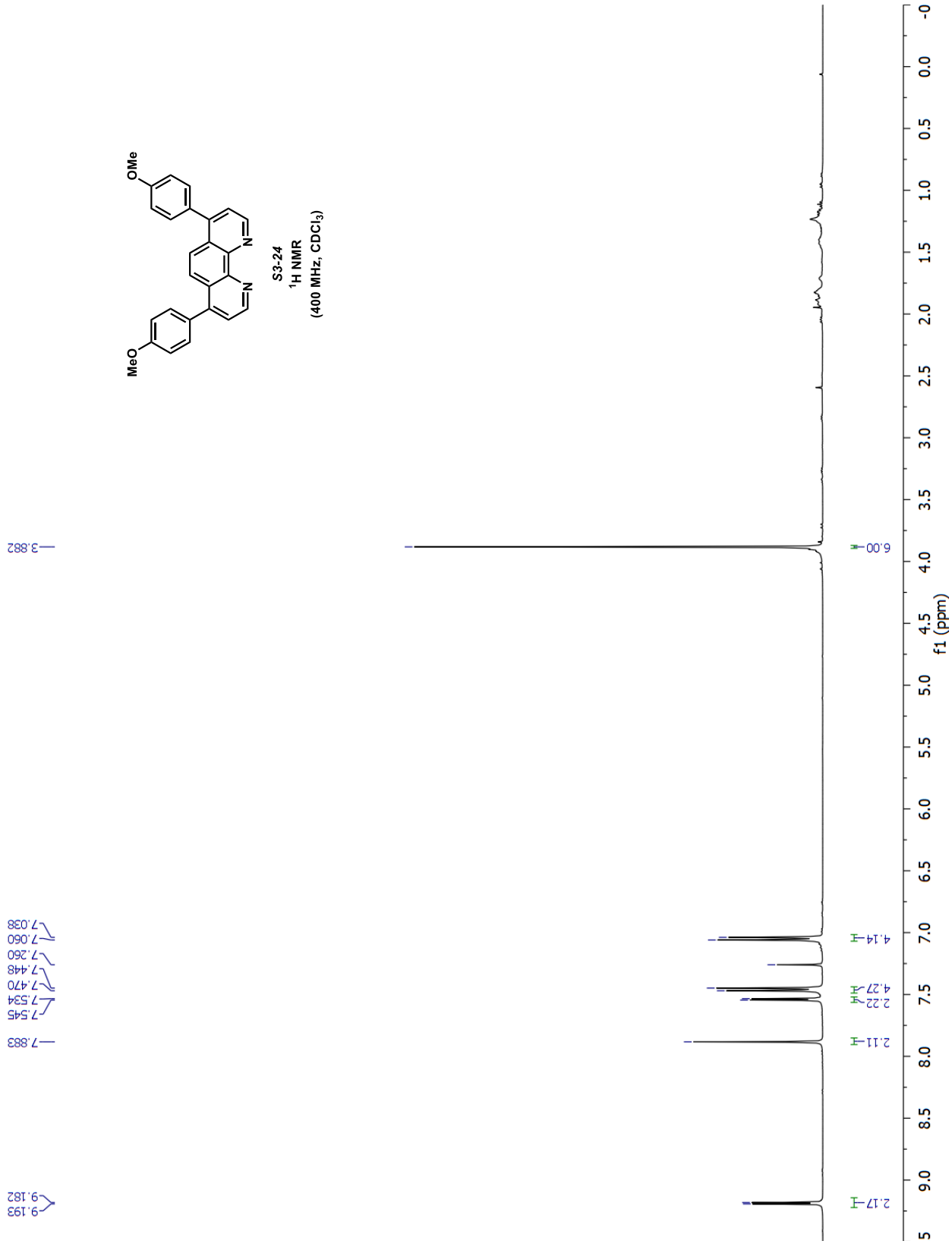
OMe
MeO
N
N
S3-24
1H NMR
(400 MHz, CDCl3)
9.193
9.182
7.883
7.545
7.534
7.470
7.448
7.260
7.060
7.038
3.882
2.17
2.11
4.27
2.22
4.14
6.00
f1 (ppm)

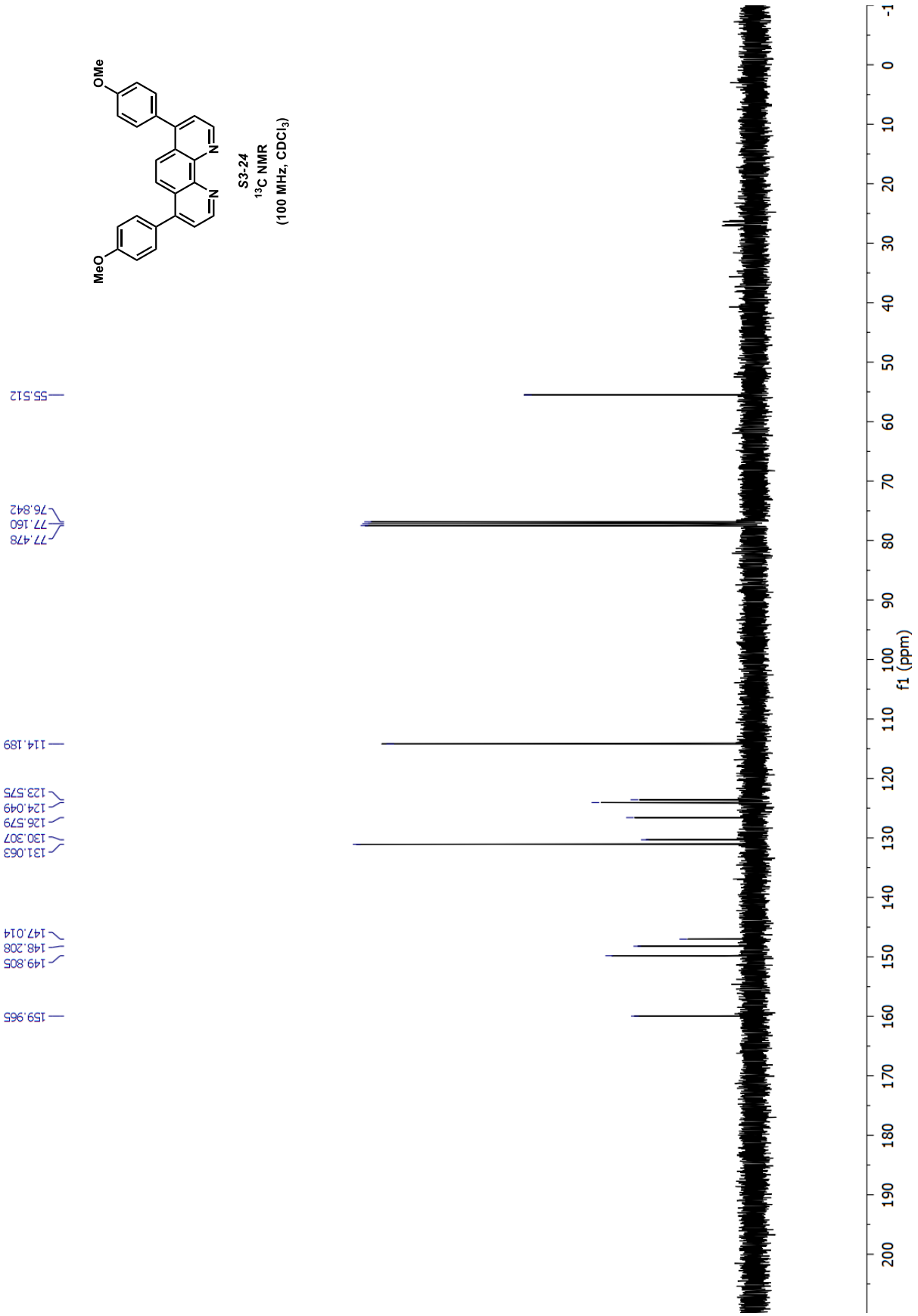
OMe
MeO
N
N
S3-24
13C NMR
(100 MHz, CDCl3)
55.512
76.842
77.160
77.478
114.189
123.575
124.049
126.579
130.307
131.063
147.014
148.208
149.805
159.965
f1 (ppm)

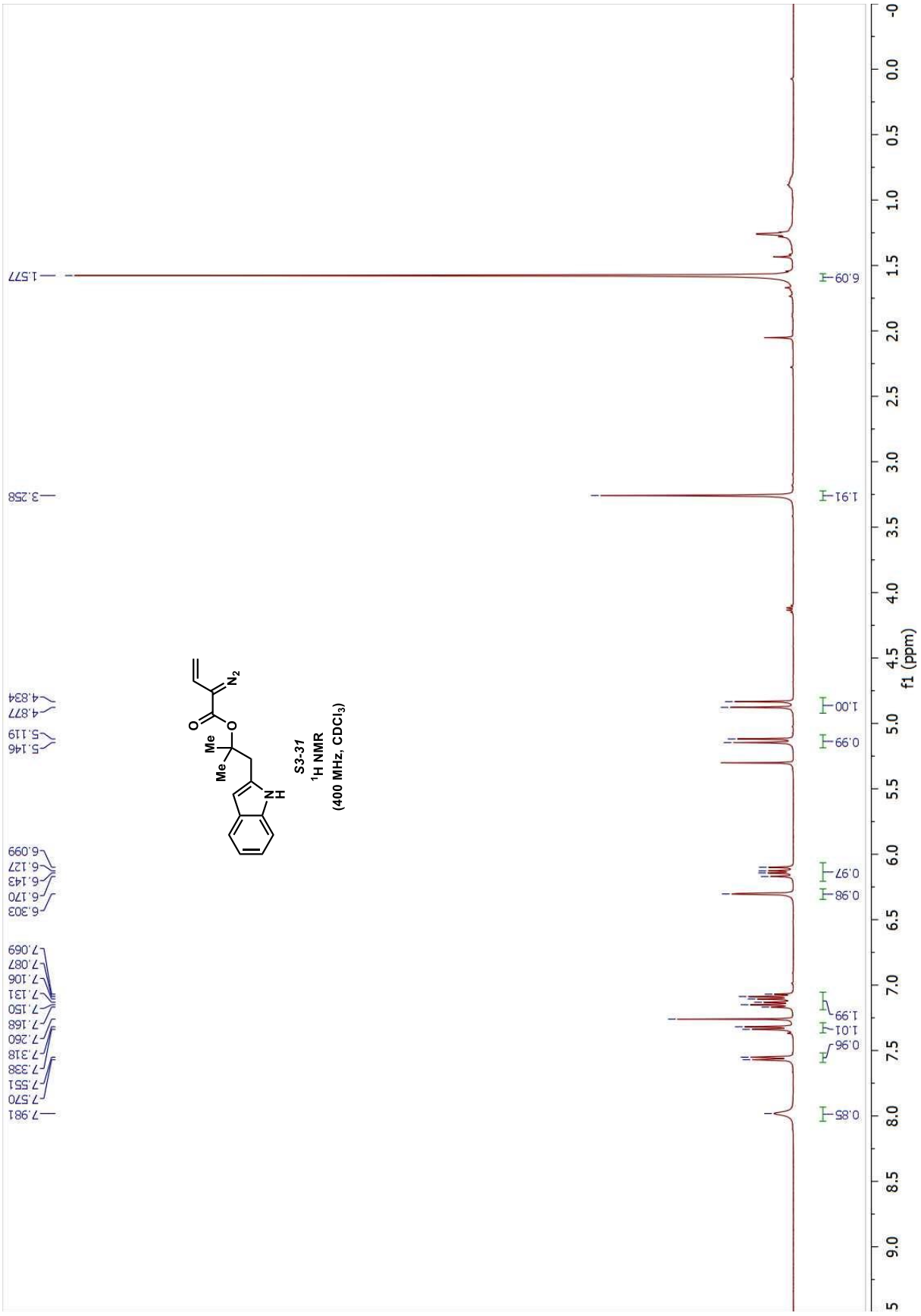
S3-31
^{1}H NMR
(400 MHz, CDCl$_3$)
Me
Me
O
O
N$_2$
H
N
1.577
3.258
4.834
4.877
5.119
5.146
6.099
6.127
6.143
6.170
6.303
7.069
7.087
7.106
7.131
7.150
7.168
7.260
7.318
7.338
7.551
7.570
7.981
6.09
1.91
1.00
0.99
0.97
0.98
1.99
1.01
0.96
0.85
f1 (ppm)

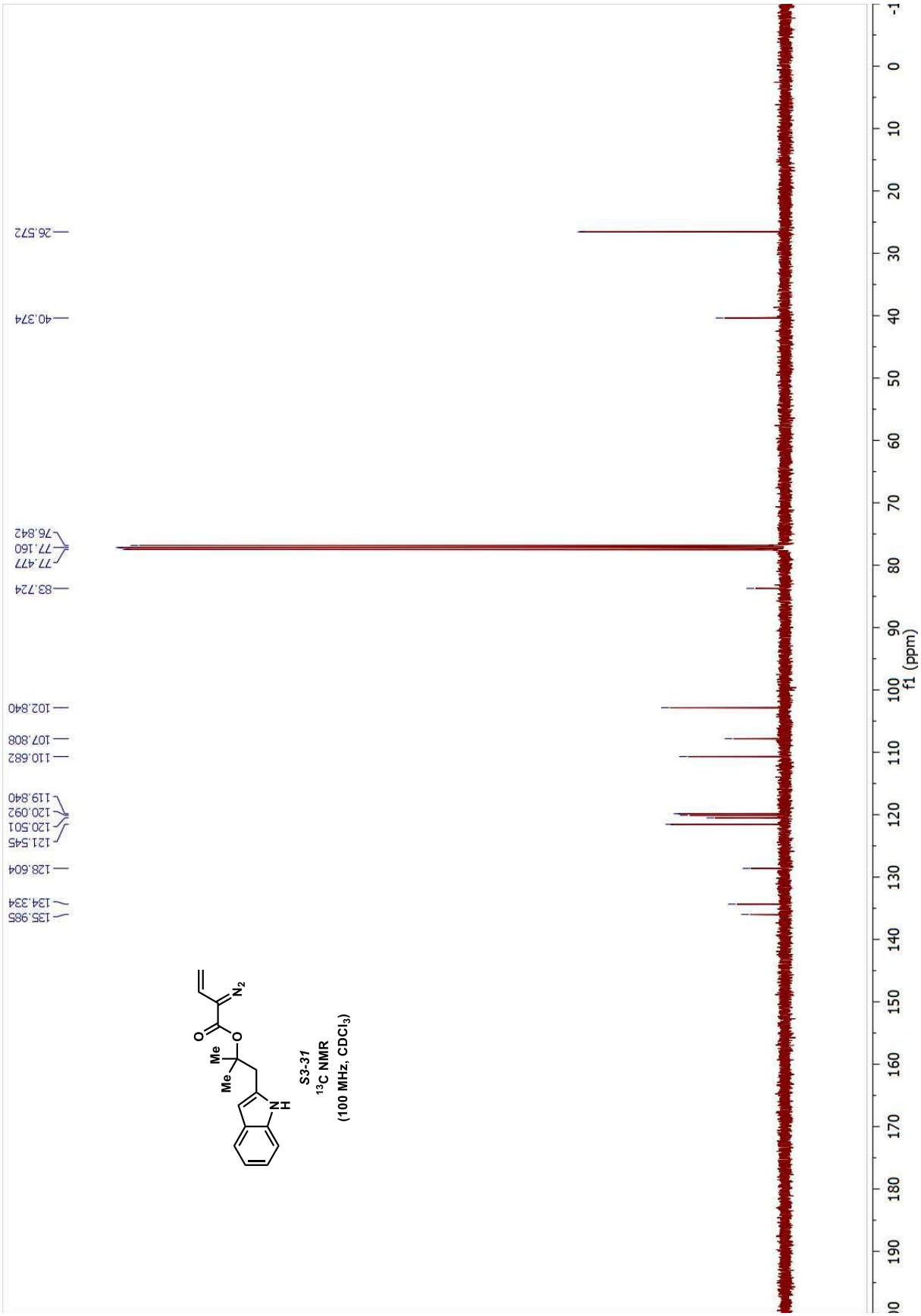
26.572
40.374
76.842
77.160
77.477
83.724
102.840
107.808
110.682
119.840
120.092
120.501
121.545
128.604
134.334
135.985
f1 (ppm)
S3-31
13C NMR
(100 MHz, CDCl3)

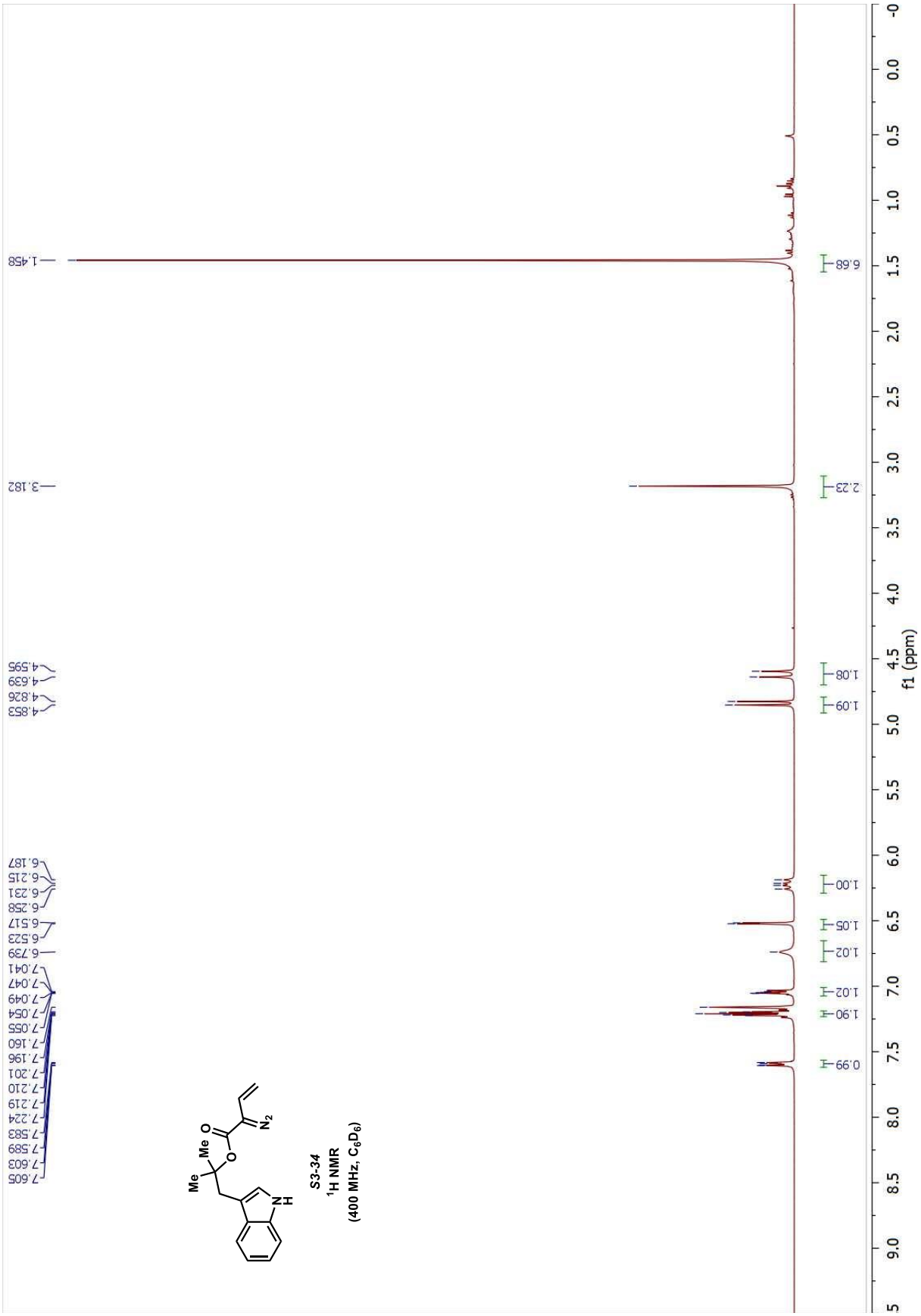
S3-34
^{1}H NMR
(400 MHz, C_6D_6)
Me
Me
O
O
N
H
N_2
1.458
3.182
4.595
4.639
4.826
4.853
6.187
6.215
6.231
6.258
6.517
6.523
6.739
7.041
7.047
7.049
7.054
7.055
7.160
7.196
7.201
7.210
7.219
7.224
7.583
7.589
7.603
6.68
2.23
1.08
1.09
1.00
1.05
1.02
1.02
1.90
0.99
f1 (ppm)

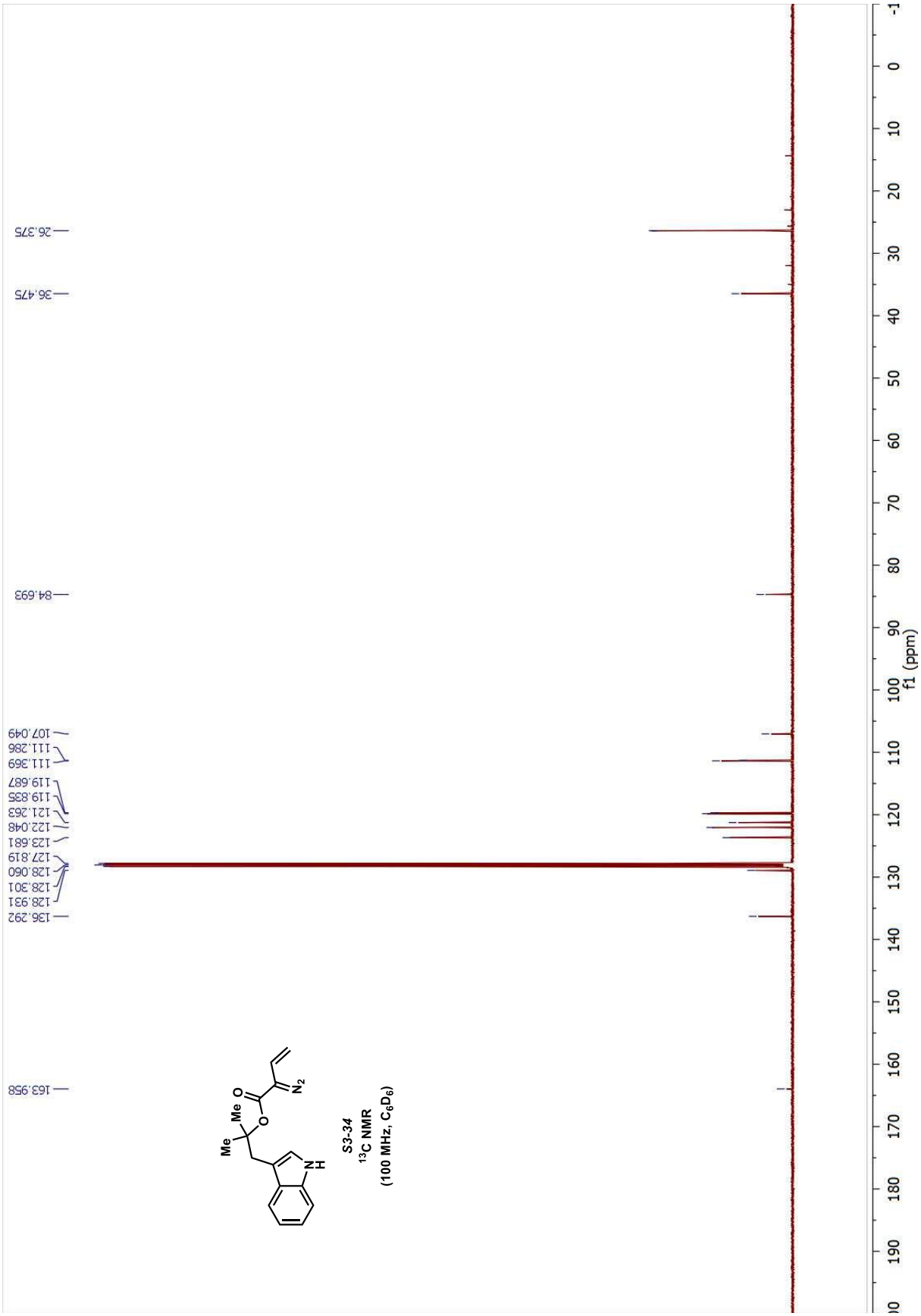
26.375
36.475
84.693
107.049
111.286
111.369
119.687
119.835
121.263
122.048
123.681
127.819
128.060
128.301
128.931
136.292
163.958
f1 (ppm)
S3-34
13C NMR
(100 MHz, C6D6)

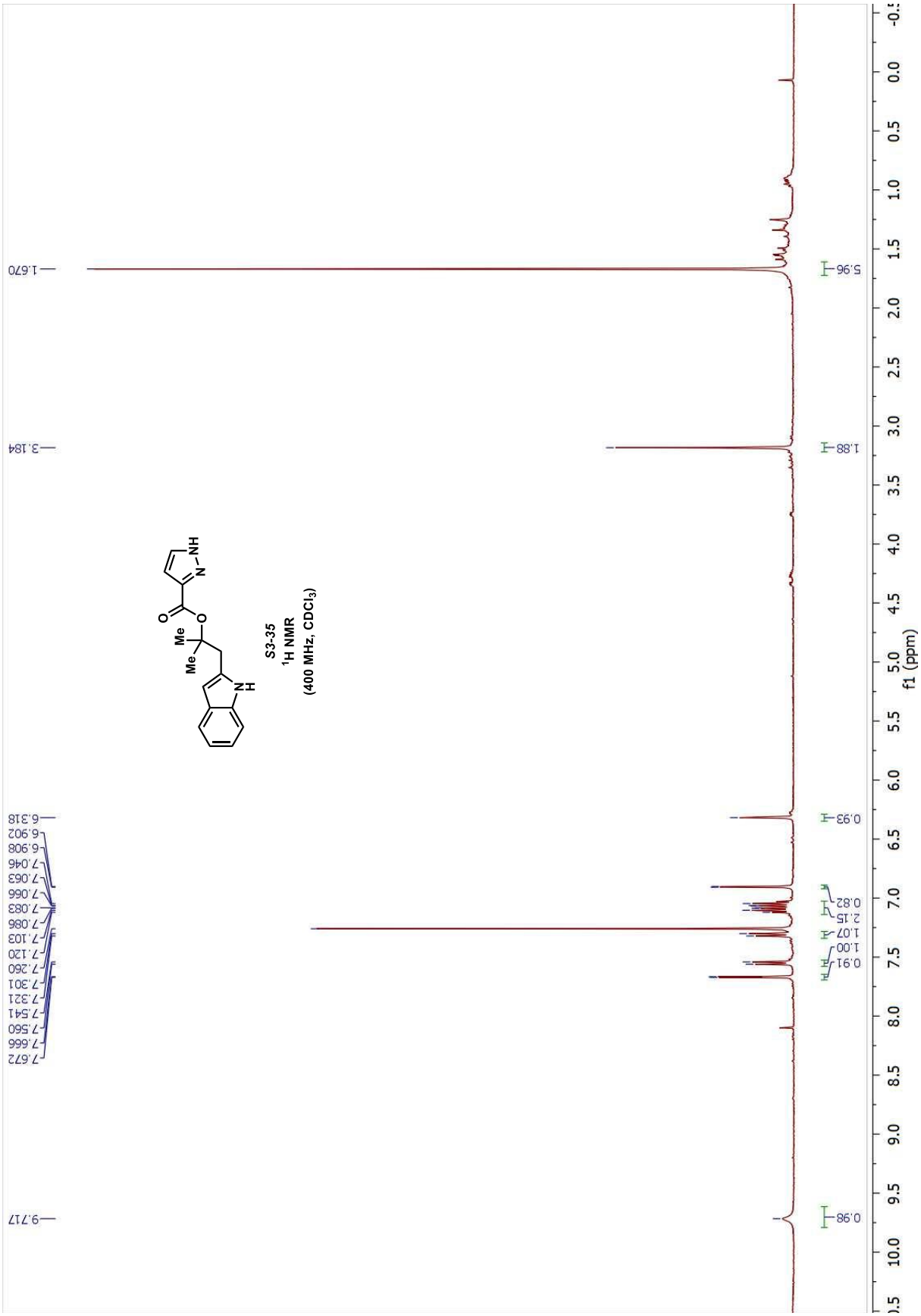
S3-35
^{1}H NMR
(400 MHz, $CDCl_3$)
f1 (ppm)

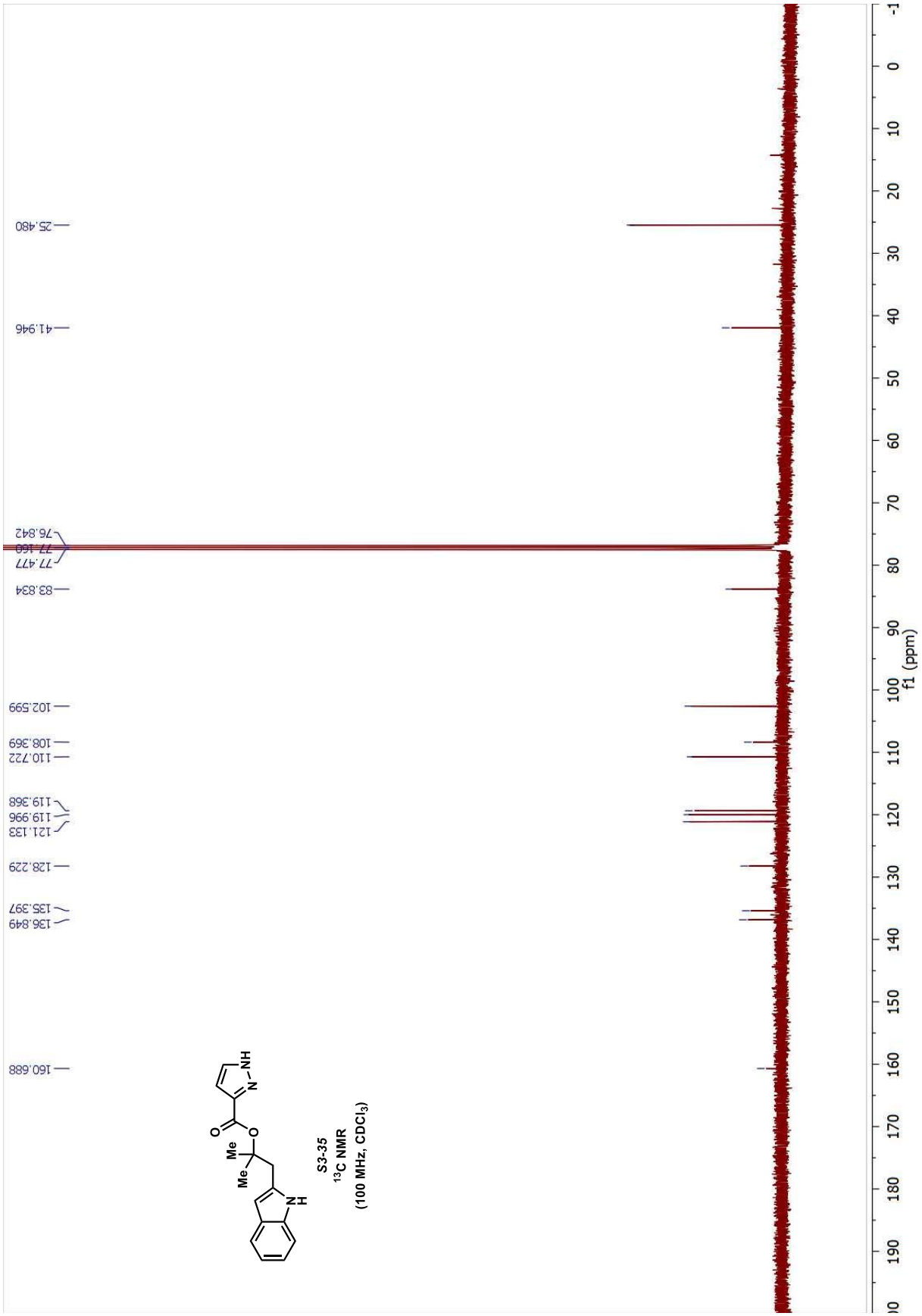
25.480
41.946
76.842
77.160
77.477
83.834
102.599
108.369
110.722
119.368
119.996
121.133
128.229
135.397
136.849
160.688
f1 (ppm)
Me
Me
O
O
N
H
N
H
S3-35
13C NMR
(100 MHz, CDCl3)

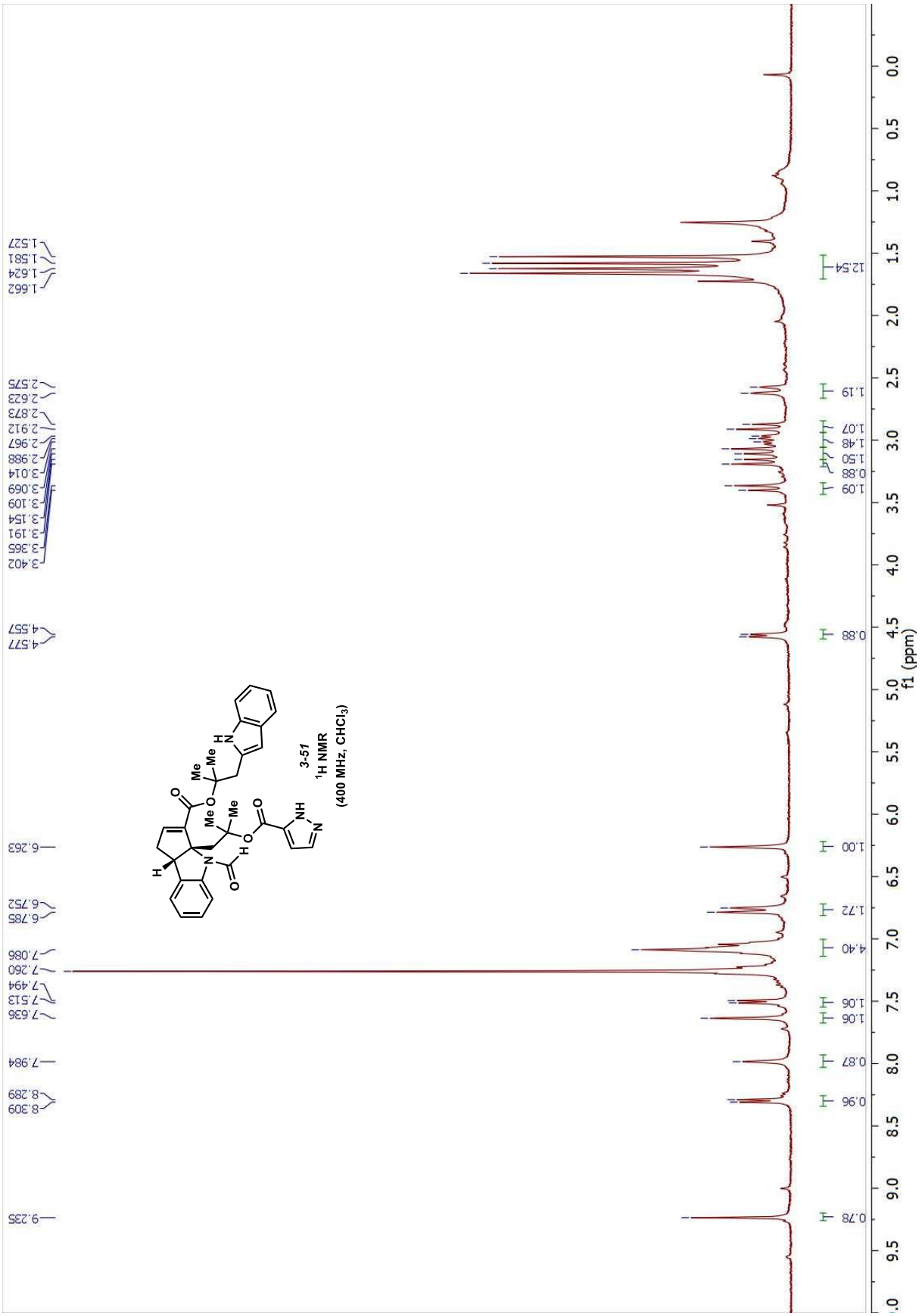
3-51
1H NMR
(400 MHz, CHCl3)
f1 (ppm)

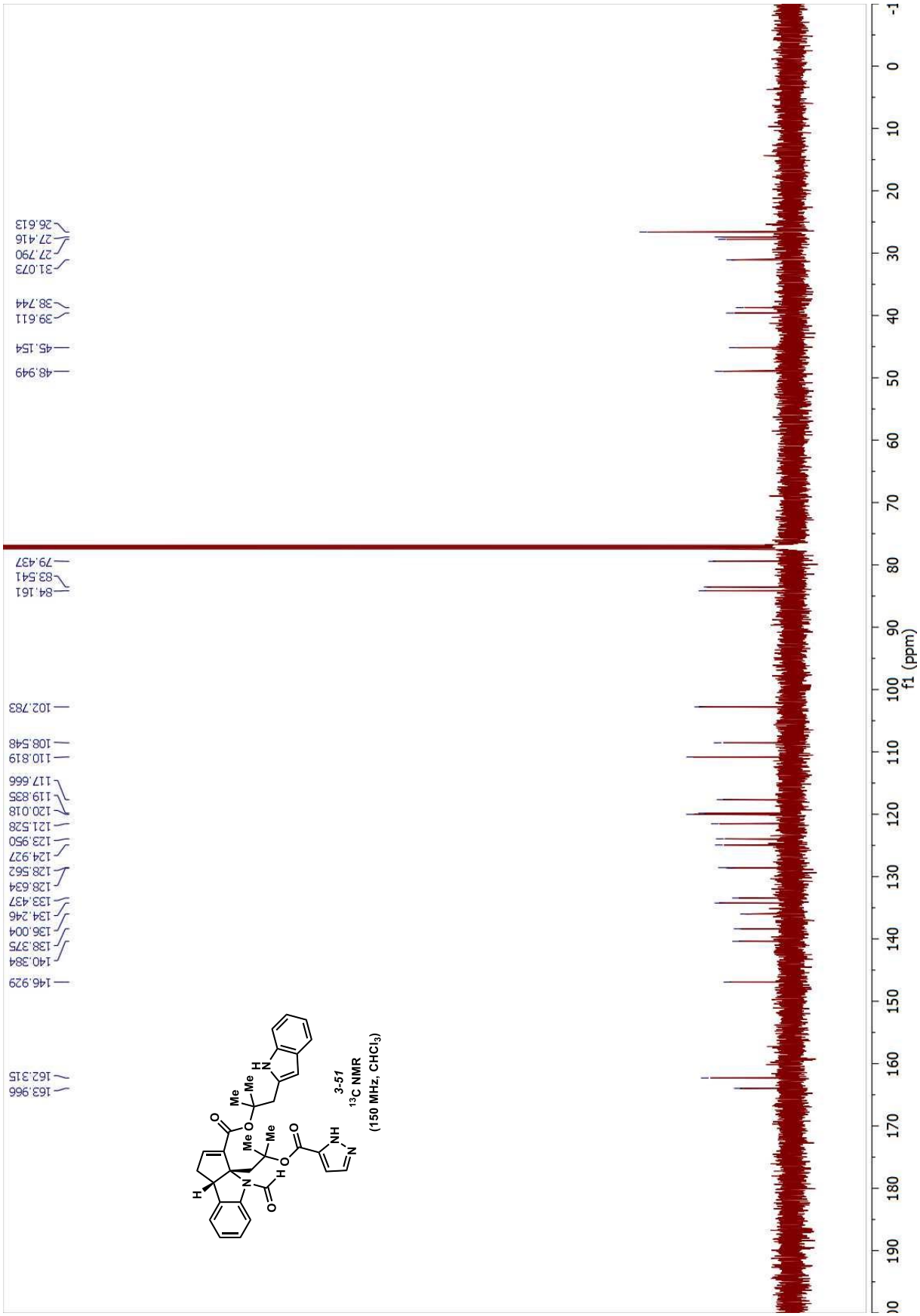
26.613
27.416
27.790
31.073
38.744
39.611
45.154
48.949
79.437
83.541
84.161
102.783
108.548
110.819
117.666
119.835
120.018
121.528
123.950
124.927
128.562
128.634
133.437
134.246
136.004
138.375
140.384
146.929
162.315
163.966
Me
Me
H
N
O
Me
O
Me
Me
O
O
NH
N
H
N
O
H
3-51
13C NMR
(150 MHz, CHCl3)
f1 (ppm)

APPENDIX C

NMR SPECTRA RELEVANT TO CHAPTER 4

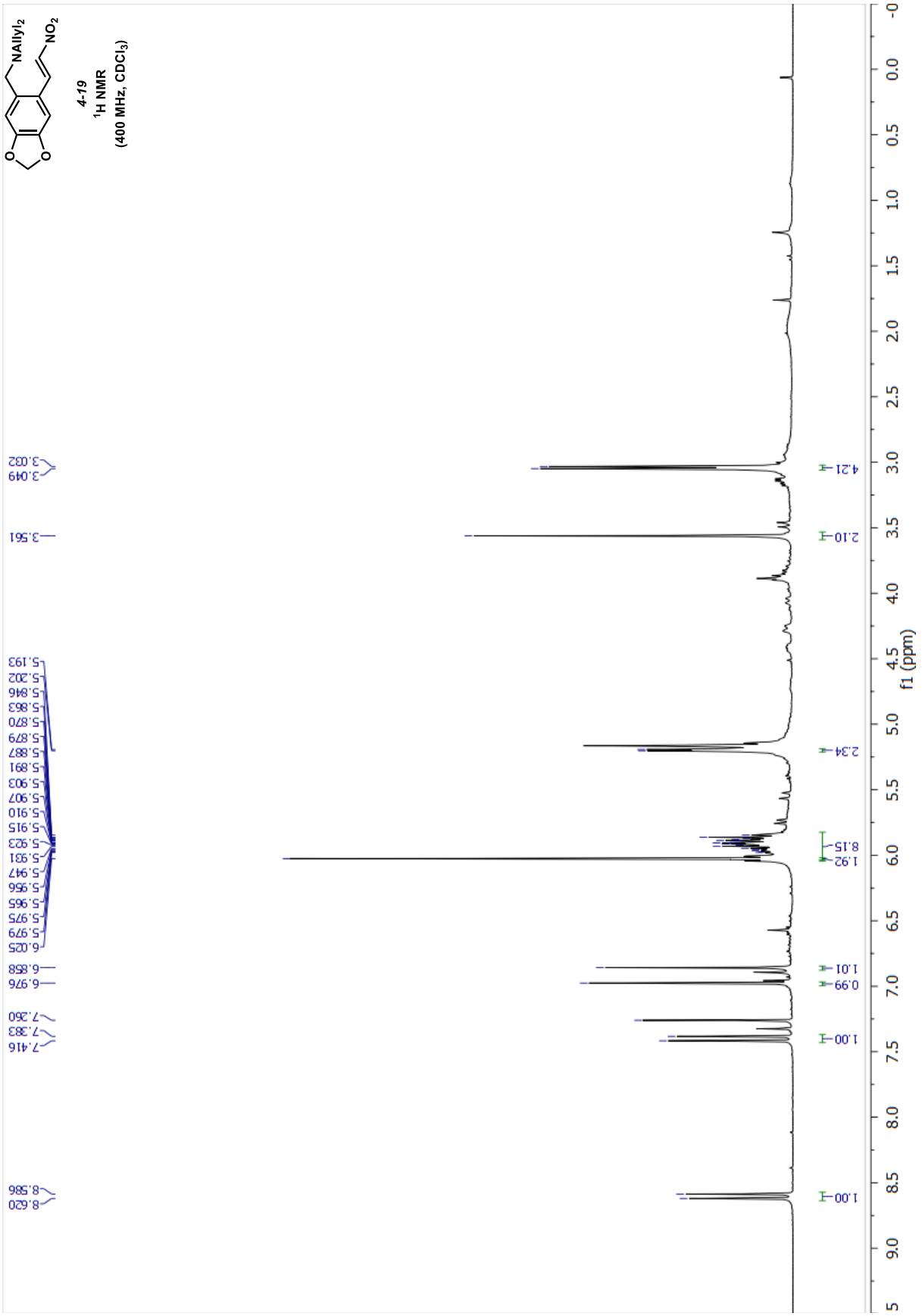
NAllyl2
NO2
4-19
1H NMR
(400 MHz, CDCl3)
8.620
8.586
7.416
7.383
7.360
6.976
6.858
6.025
5.979
5.975
5.965
5.956
5.947
5.931
5.923
5.915
5.910
5.907
5.903
5.891
5.887
5.879
5.870
5.863
5.846
5.202
5.193
3.561
3.049
3.032
1.00
1.00
0.99
1.01
1.92
8.15
2.34
2.10
4.21
f1 (ppm)

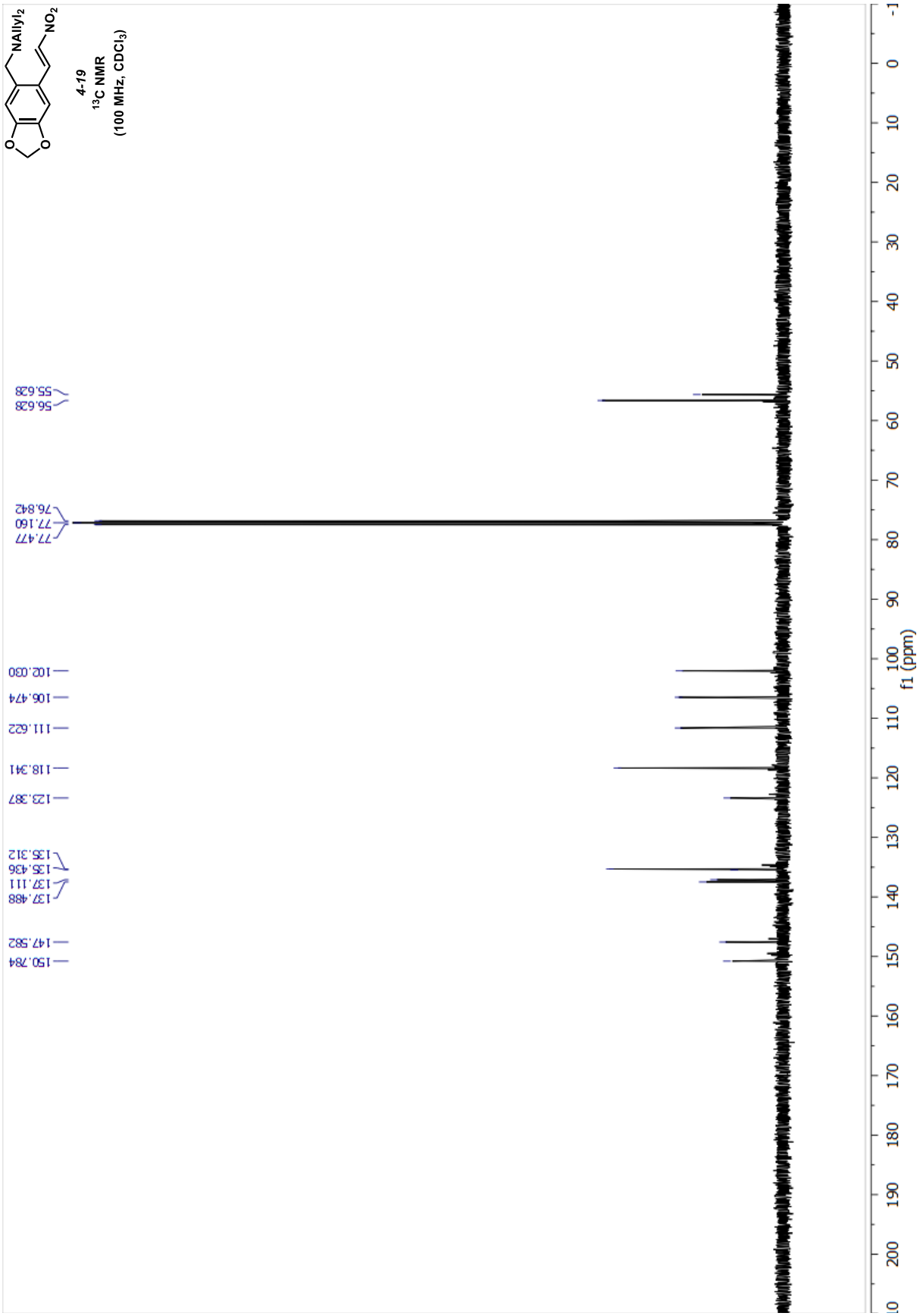
NAllyl2
NO2
4-19
13C NMR
(100 MHz, CDCl3)
55.628
56.628
76.842
77.160
77.477
102.030
106.474
111.622
118.341
123.387
135.312
135.436
137.111
137.488
147.582
150.784
f1 (ppm)

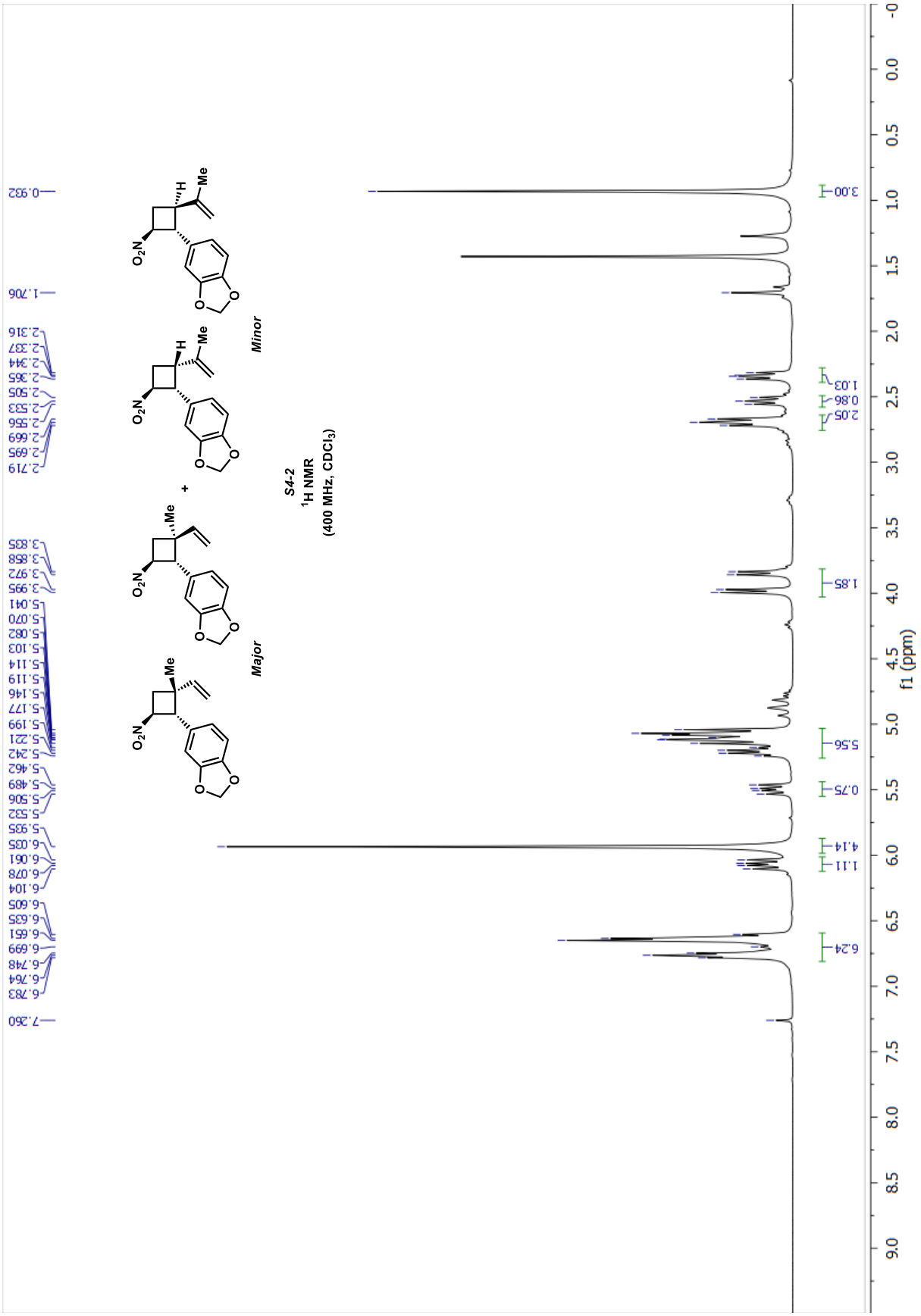
S4-2
^{1}H NMR
(400 MHz, CDCl$_3$)
Minor
Major
f1 (ppm)

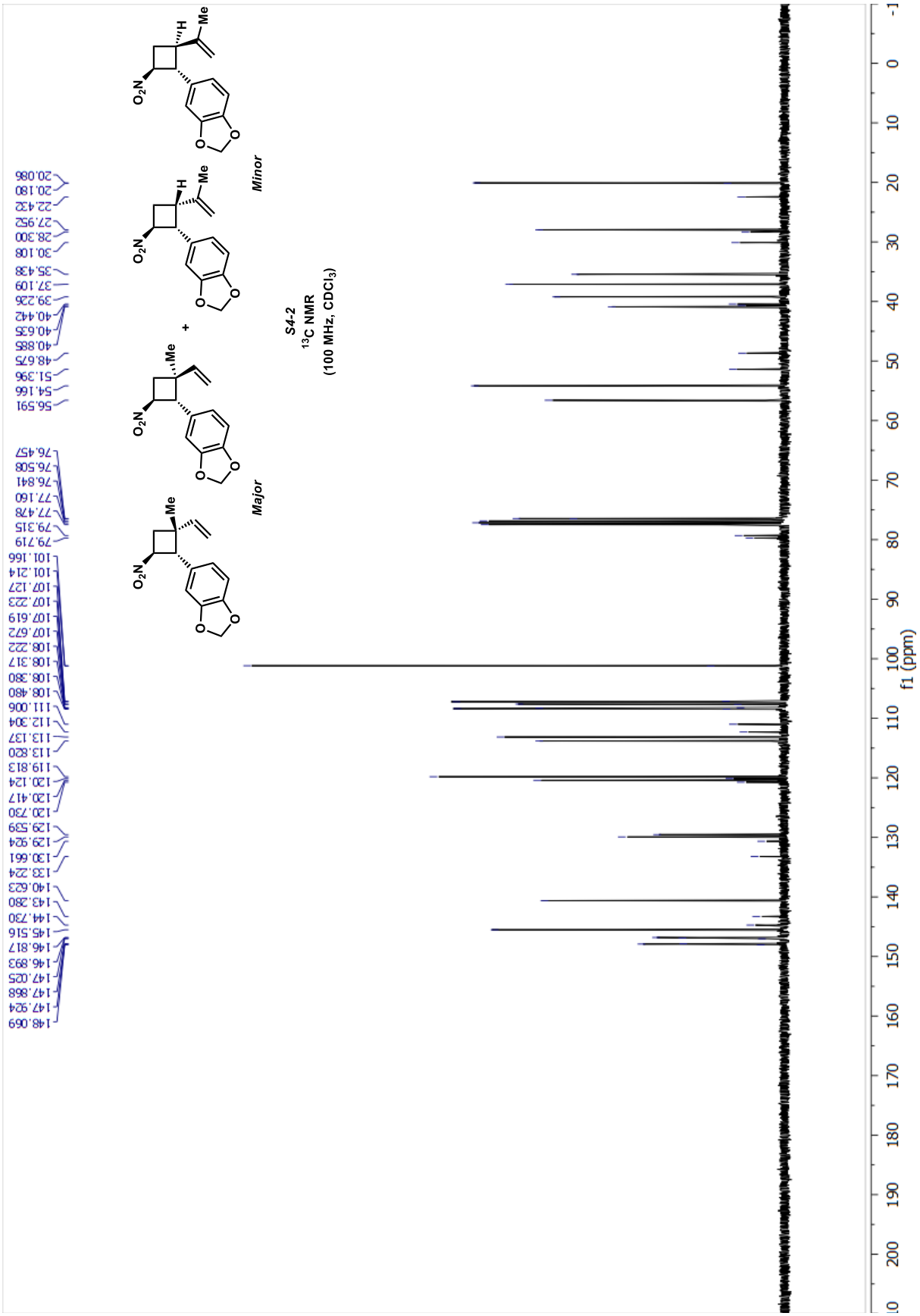
S4-2
13C NMR
(100 MHz, CDCl3)
Minor
Major
f1 (ppm)

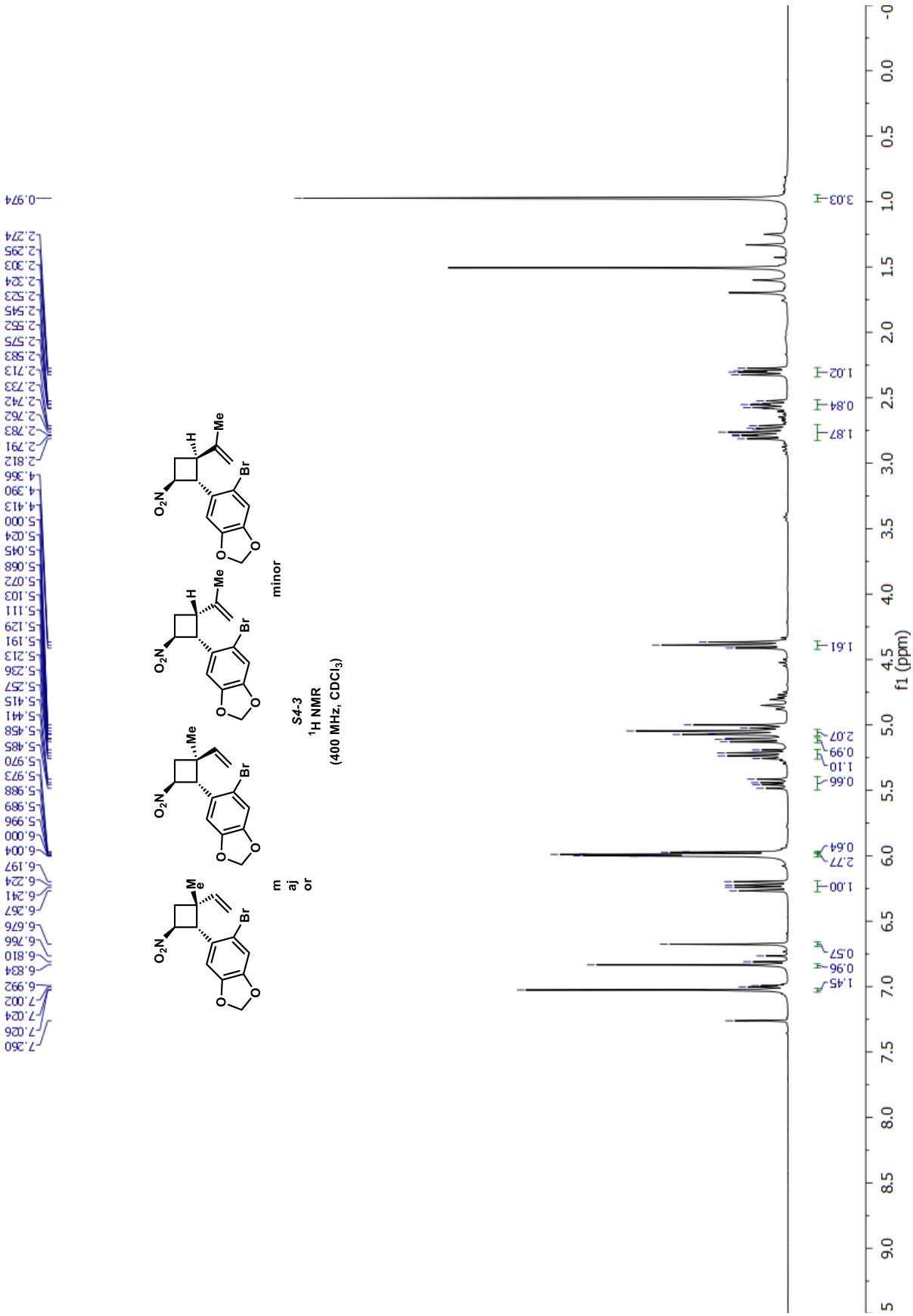
S4-3
^{1}H NMR
(400 MHz, CDCl$_3$)
major
minor
f1 (ppm)

148.063
147.910
147.727
147.688
147.611
147.487
145.843
144.253
143.046
140.520
131.147
128.909
128.242
128.082
115.483
115.389
115.048
114.089
113.560
113.240
113.174
112.935
112.394
112.090
111.309
108.756
108.388
108.062
107.635
102.148
102.132
102.079
79.404
77.611
77.478
77.160
76.842
76.235
76.144
55.216
54.655
50.950
49.283
42.409
40.995
40.440
39.393
35.830
34.356
29.566
29.124
28.383
22.599
20.390
20.177

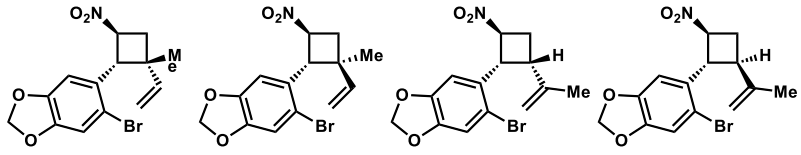

S4-3
^{13}C NMR
(100 MHz, $CDCl_3$)

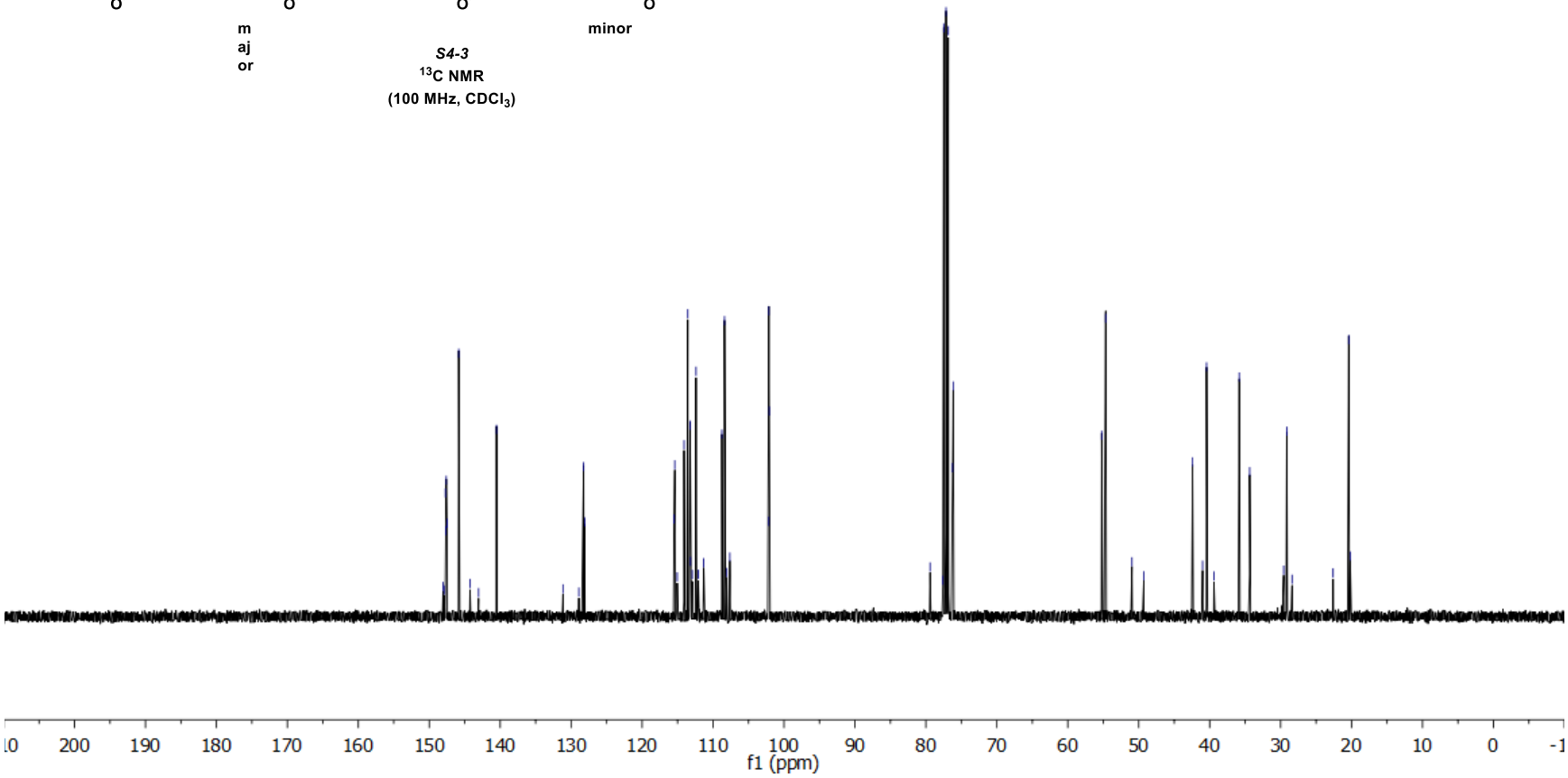

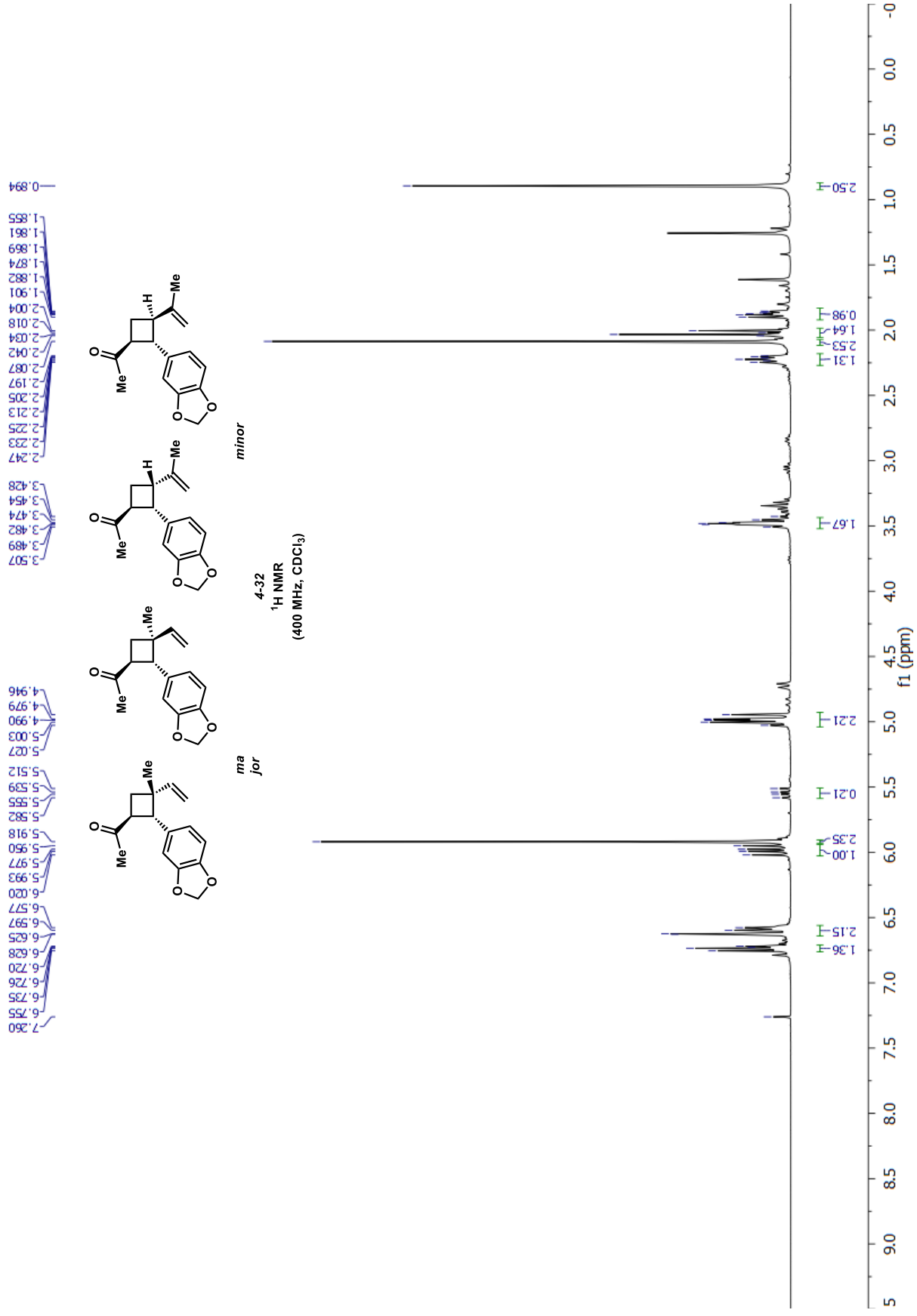
4-32
^{1}H NMR
(400 MHz, CDCl$_3$)
minor
major
f1 (ppm)

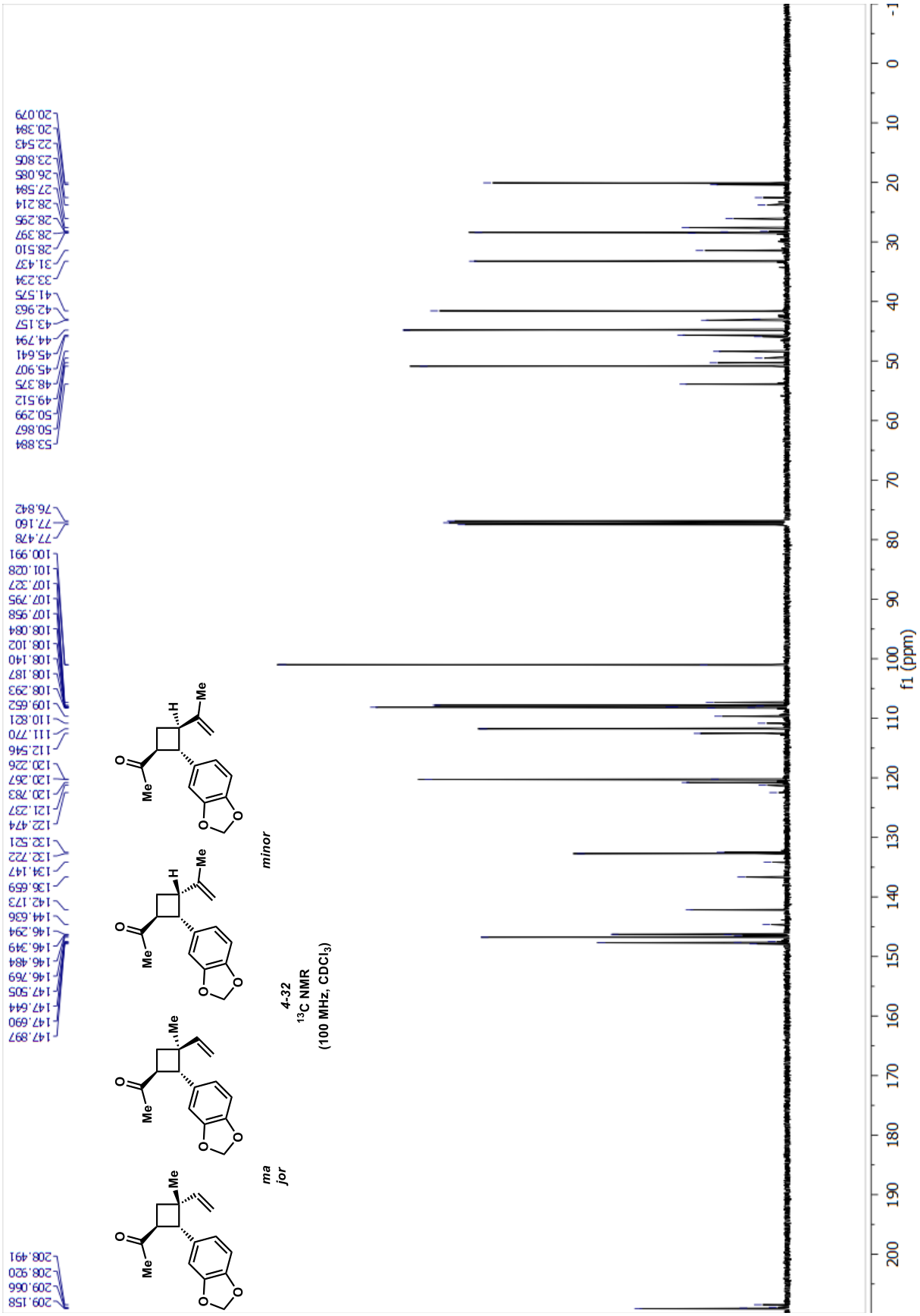
4-32
^{13}C NMR
(100 MHz, CDCl$_3$)
major
minor
f1 (ppm)

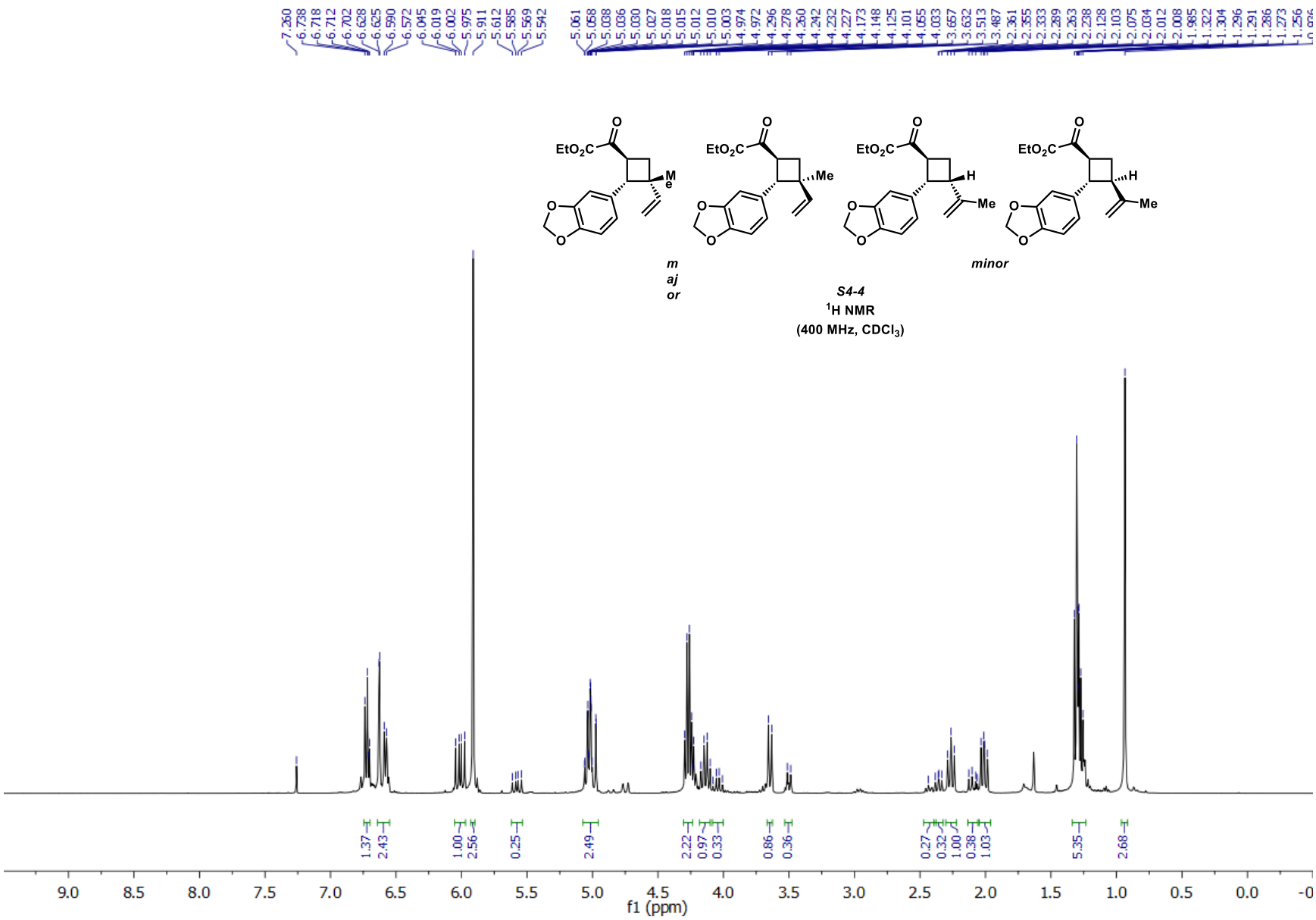
major
minor
S4-4
1H NMR
(400 MHz, CDCl3)
f1 (ppm)

194.746
194.702
194.100
161.386
161.356
161.109
147.831
147.609
147.549
146.453
146.367
146.328
146.097
141.768
136.046
132.239
132.052
120.704
120.199
120.178
112.855
112.155
110.007
108.234
108.143
108.051
107.975
107.777
107.370
101.038
100.990
77.477
77.160
76.842
62.569
62.514
62.456
53.105
50.163
47.330
46.376
45.078
43.638
42.076
41.599
40.741
34.195
32.444
27.567
27.160
20.310
19.982
14.032
13.991

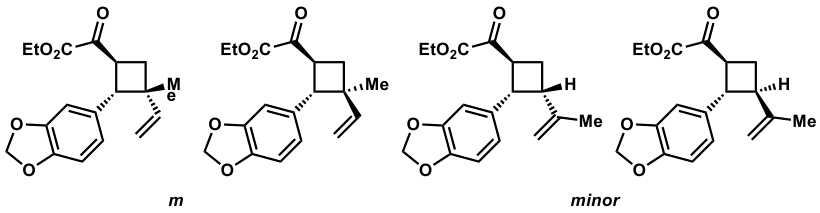

major *minor*

S4-4
^{13}C NMR
(100 MHz, $CDCl_3$)

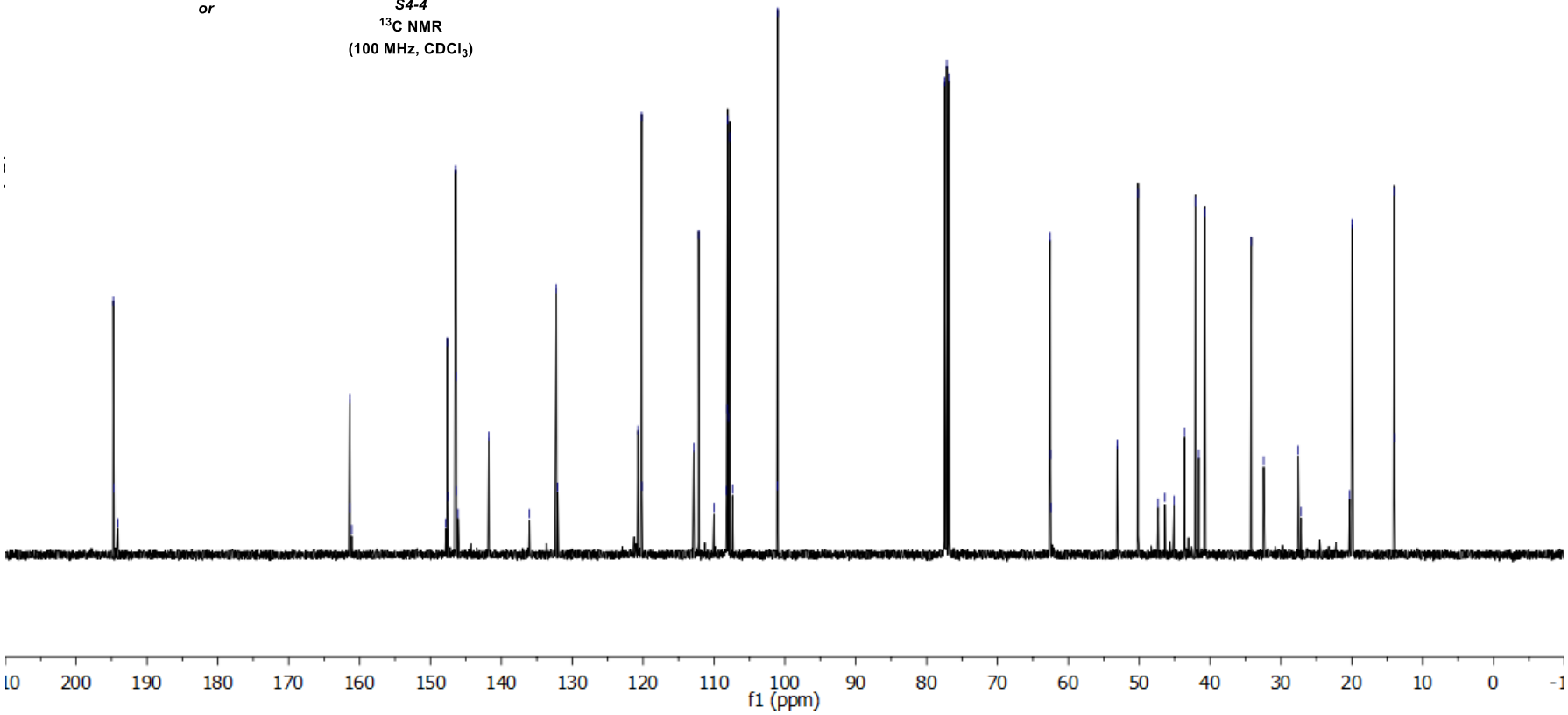

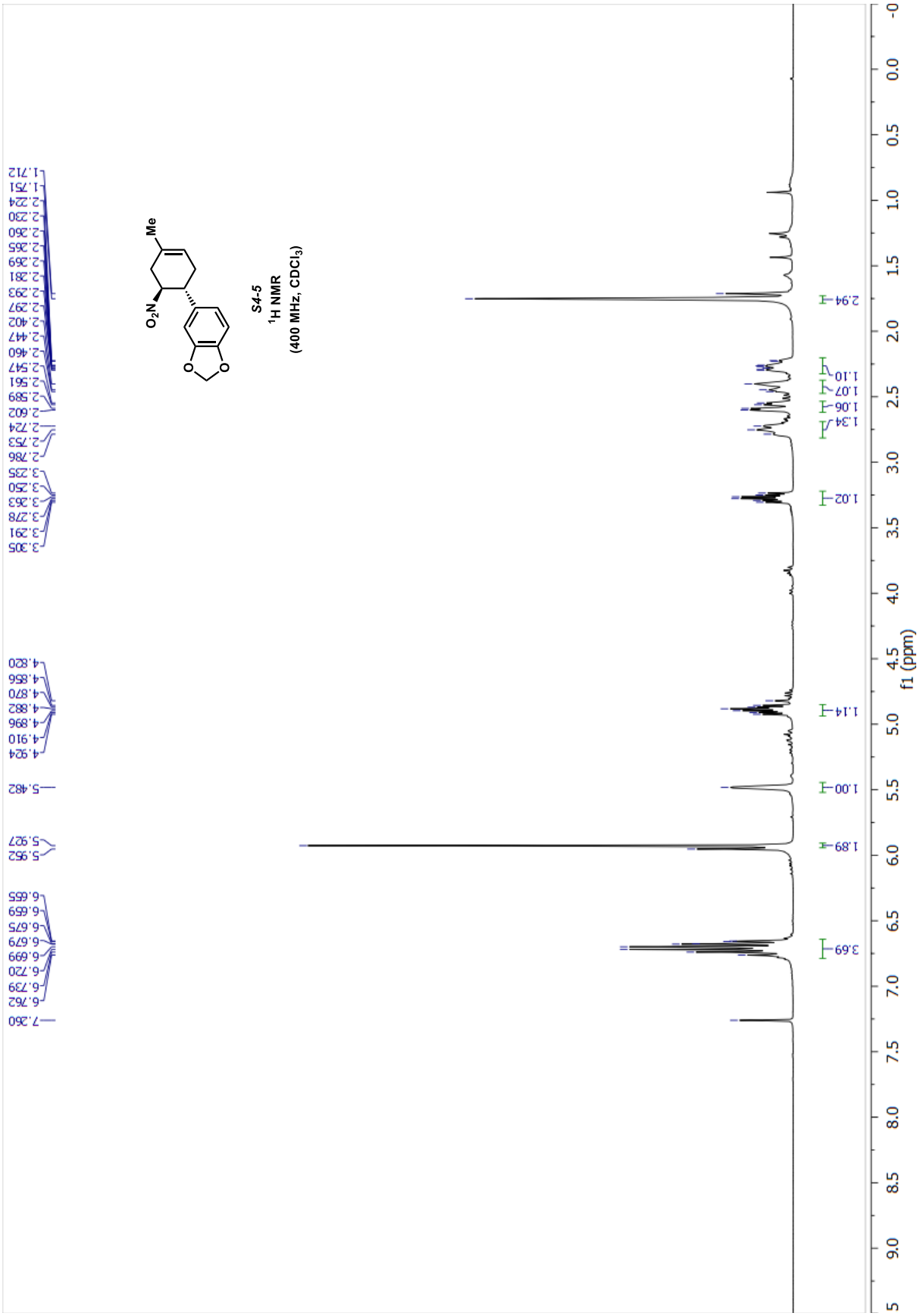
Me
O2N
S4-5
1H NMR
(400 MHz, CDCl3)
f1 (ppm)

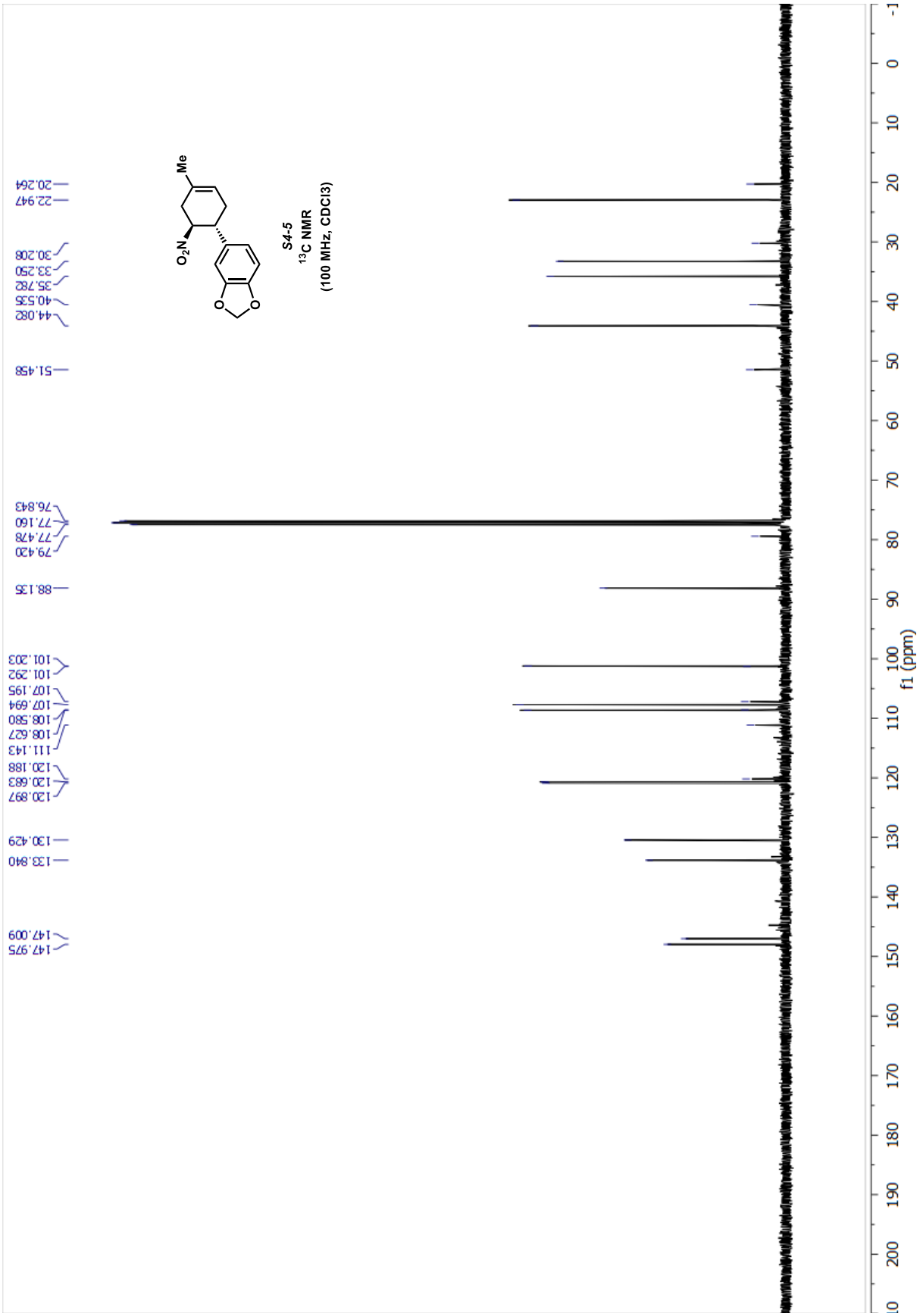
Me
O_2N
S4-5
^{13}C NMR
(100 MHz, CDCl3)
20.264
22.947
30.208
33.250
35.782
40.535
44.082
51.458
76.843
77.160
77.478
79.420
88.135
101.303
101.292
107.195
107.694
108.580
108.627
111.143
120.188
120.683
120.897
130.429
133.840
147.009
147.975
f1 (ppm)

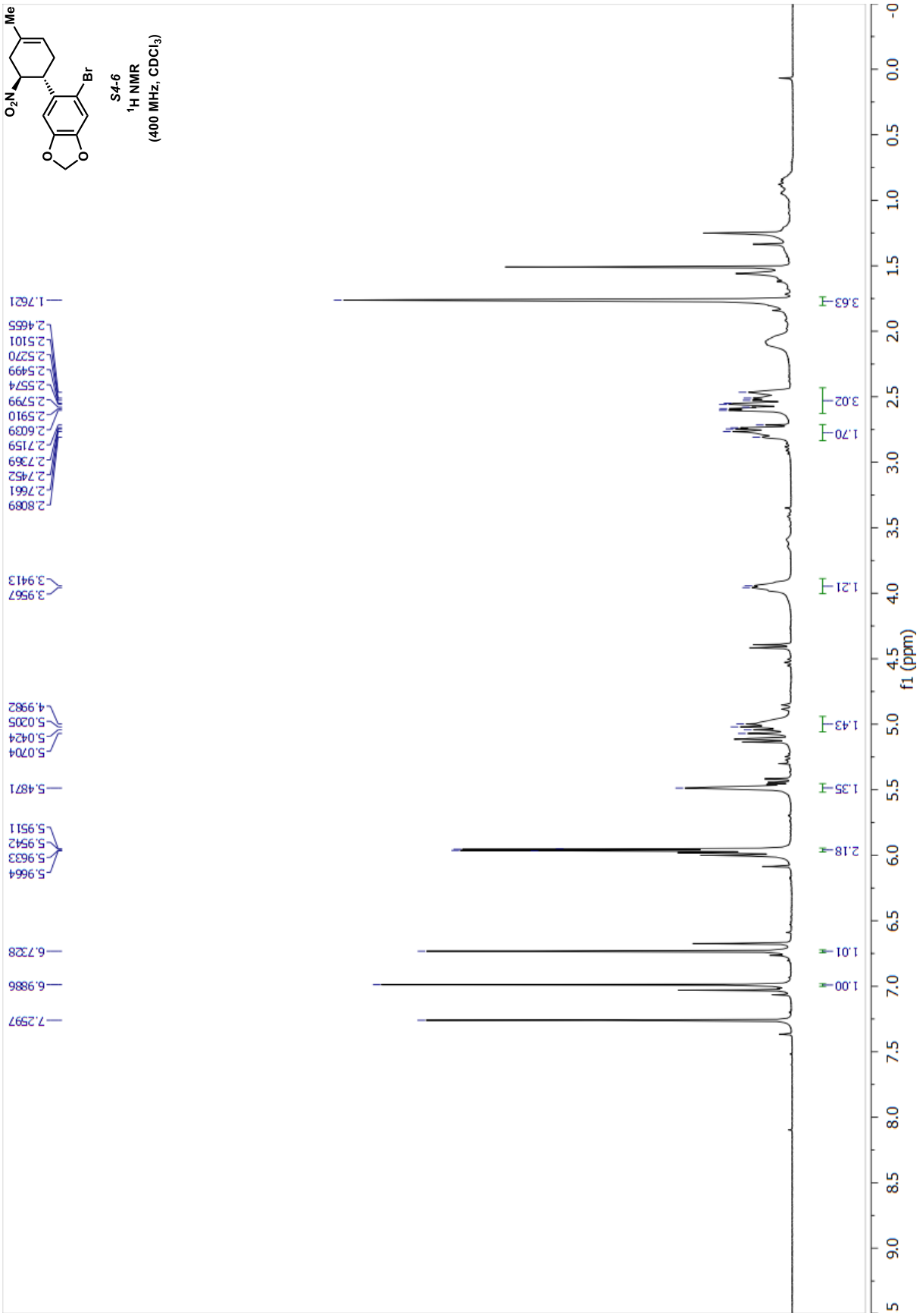
S4-6
^{1}H NMR
(400 MHz, $CDCl_3$)
Me
O_2N
Br
O
O
1.7621
2.4655
2.5101
2.5270
2.5499
2.5574
2.5799
2.5910
2.6039
2.7159
2.7369
2.7452
2.7661
2.8089
3.9413
3.9567
4.9982
5.0305
5.0424
5.0704
5.4871
5.9511
5.9542
5.9633
5.9664
6.7328
6.9886
7.2597
3.63
3.02
1.70
1.21
1.43
1.35
2.18
1.01
1.00
f1 (ppm)

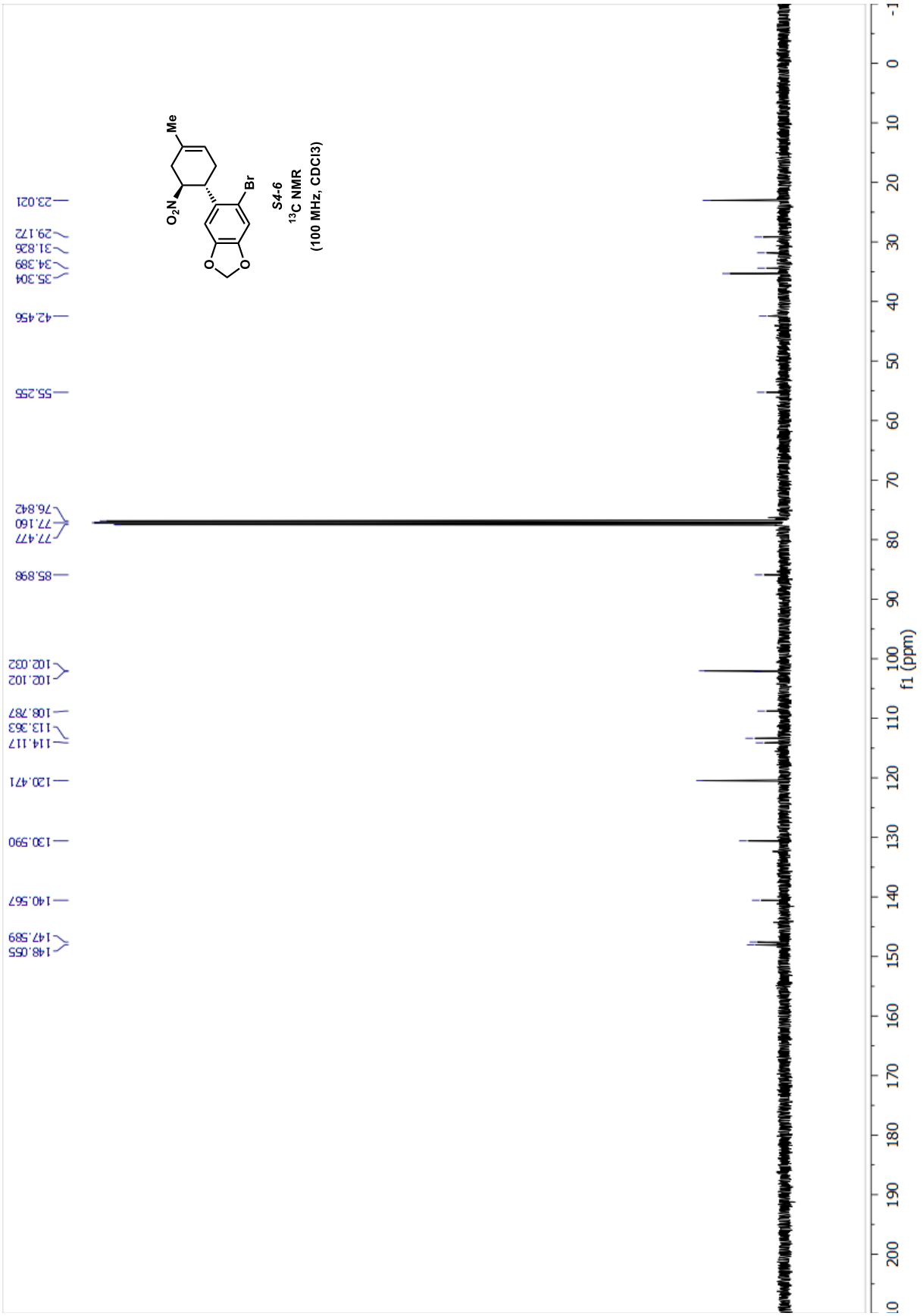
Me
O2N
Br
O
O
S4-6
13C NMR
(100 MHz, CDCl3)
23.021
29.172
31.826
34.389
35.304
42.456
55.255
76.842
77.160
77.477
85.898
102.032
102.102
108.787
113.363
114.117
130.471
130.590
140.567
147.589
148.055
f1 (ppm)

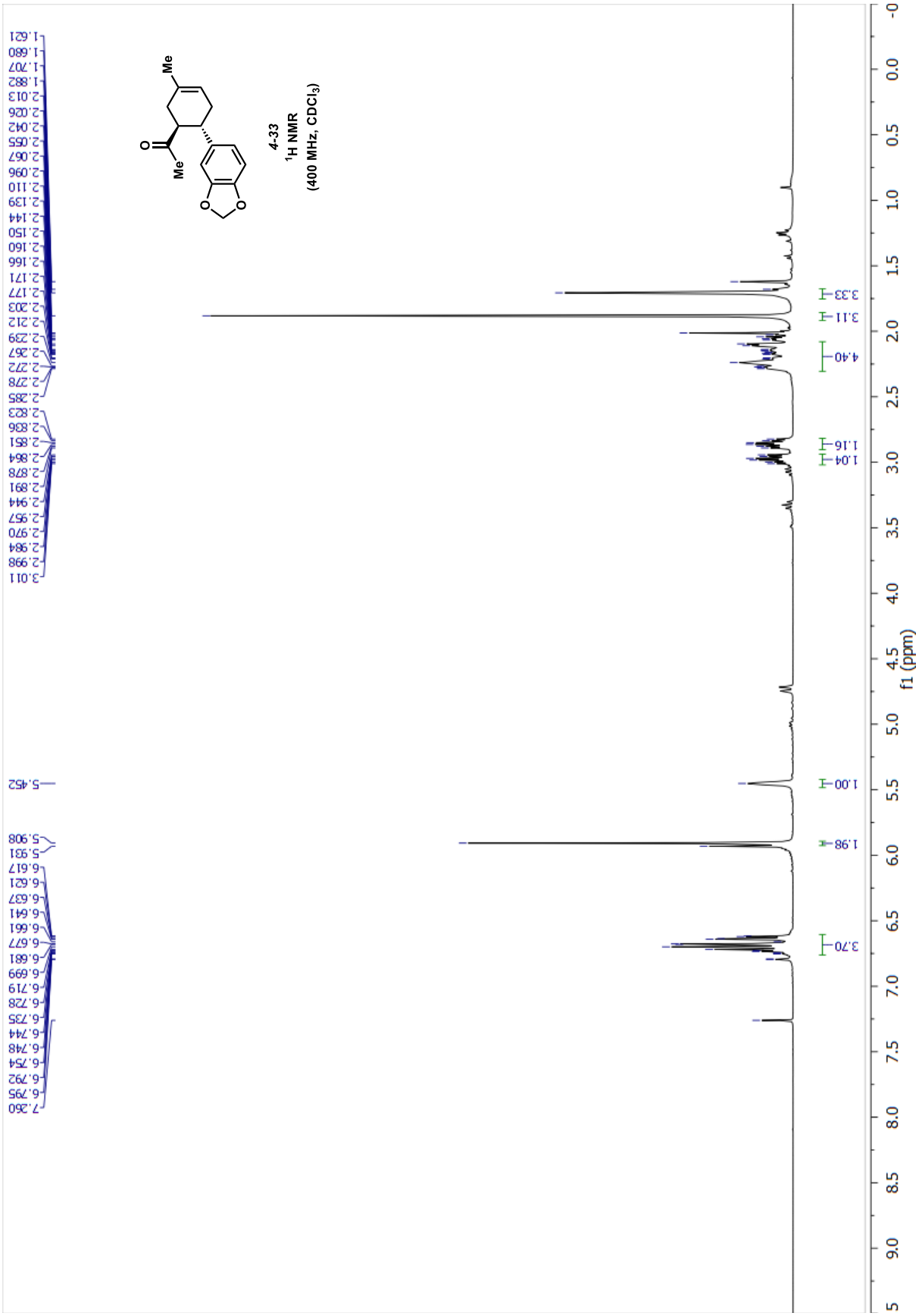
4-33
^{1}H NMR
(400 MHz, CDCl$_3$)
Me
O
Me
O
O
f1 (ppm)
3.33
3.11
4.40
1.16
1.04
1.00
1.98
3.70

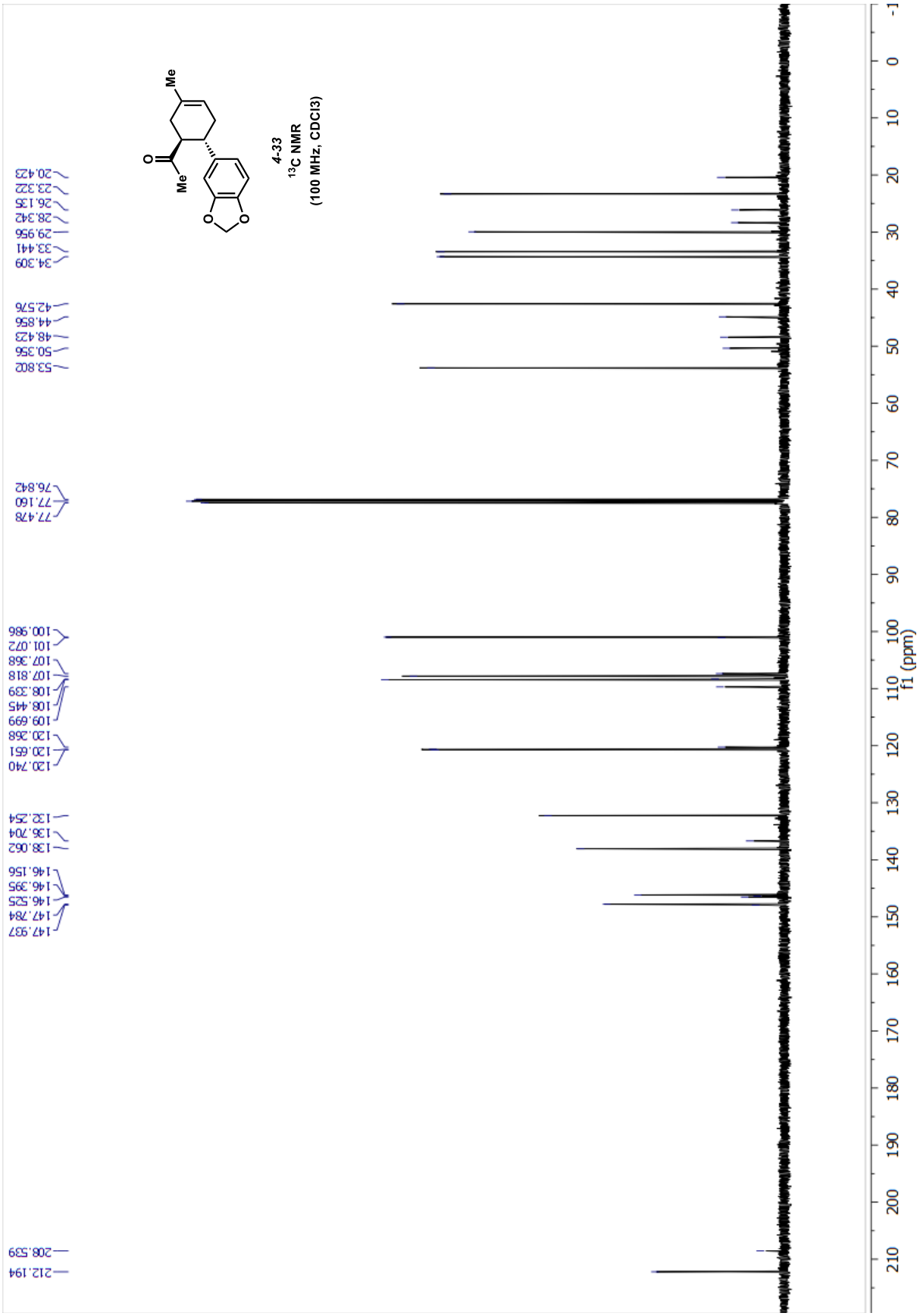
Me
O
Me
O
O
4-33
13C NMR
(100 MHz, CDCl3)
20.423
23.322
26.135
28.342
29.956
33.441
34.309
42.576
44.856
48.423
50.356
53.802
76.842
77.160
77.478
100.986
101.072
107.368
107.818
108.339
108.445
109.699
120.258
120.651
120.740
132.254
136.704
138.062
146.156
146.395
146.525
147.784
147.937
208.539
212.194
f1 (ppm)

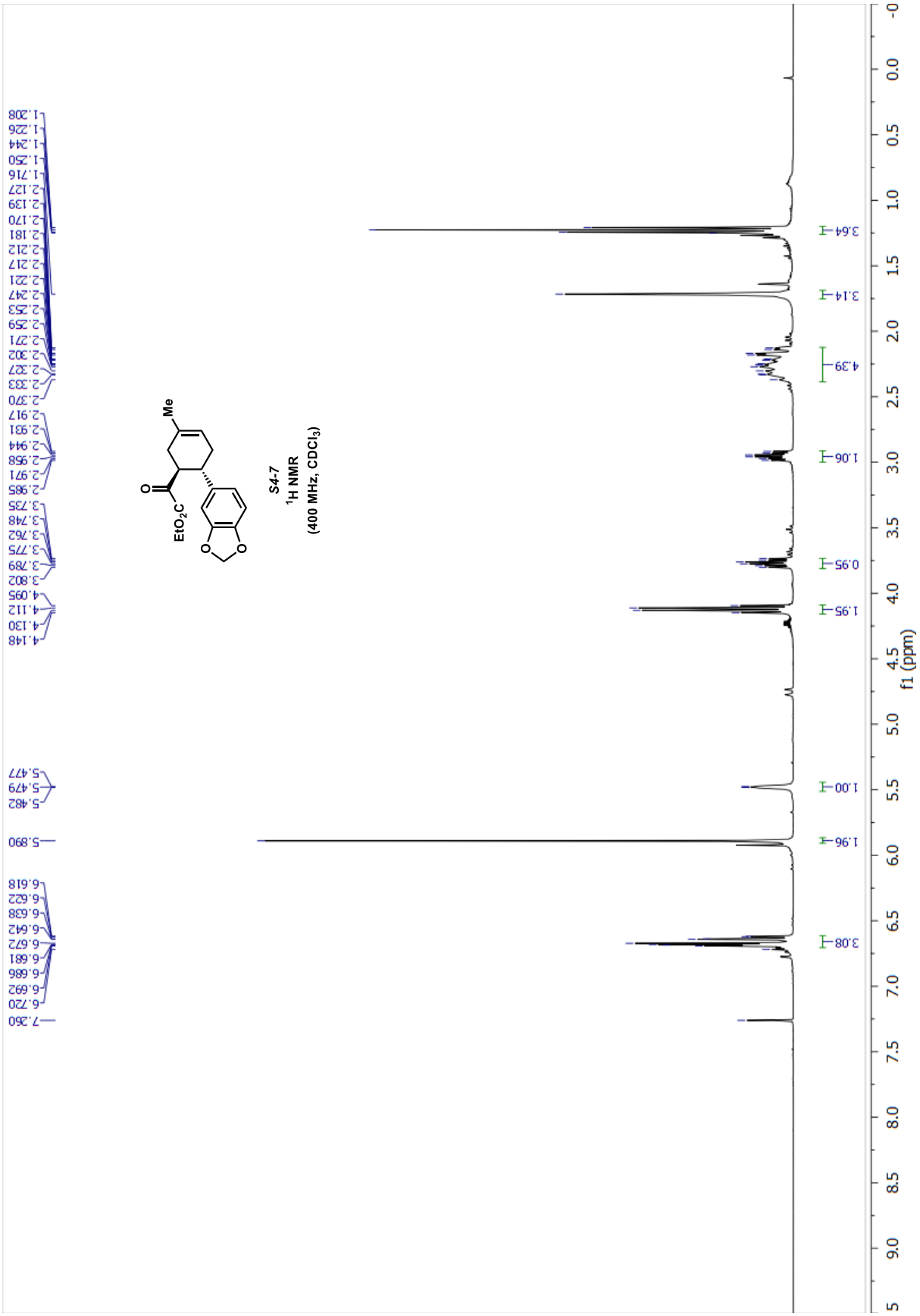
Me
O
EtO2C
O
O
S4-7
1H NMR
(400 MHz, CDCl3)
f1 (ppm)

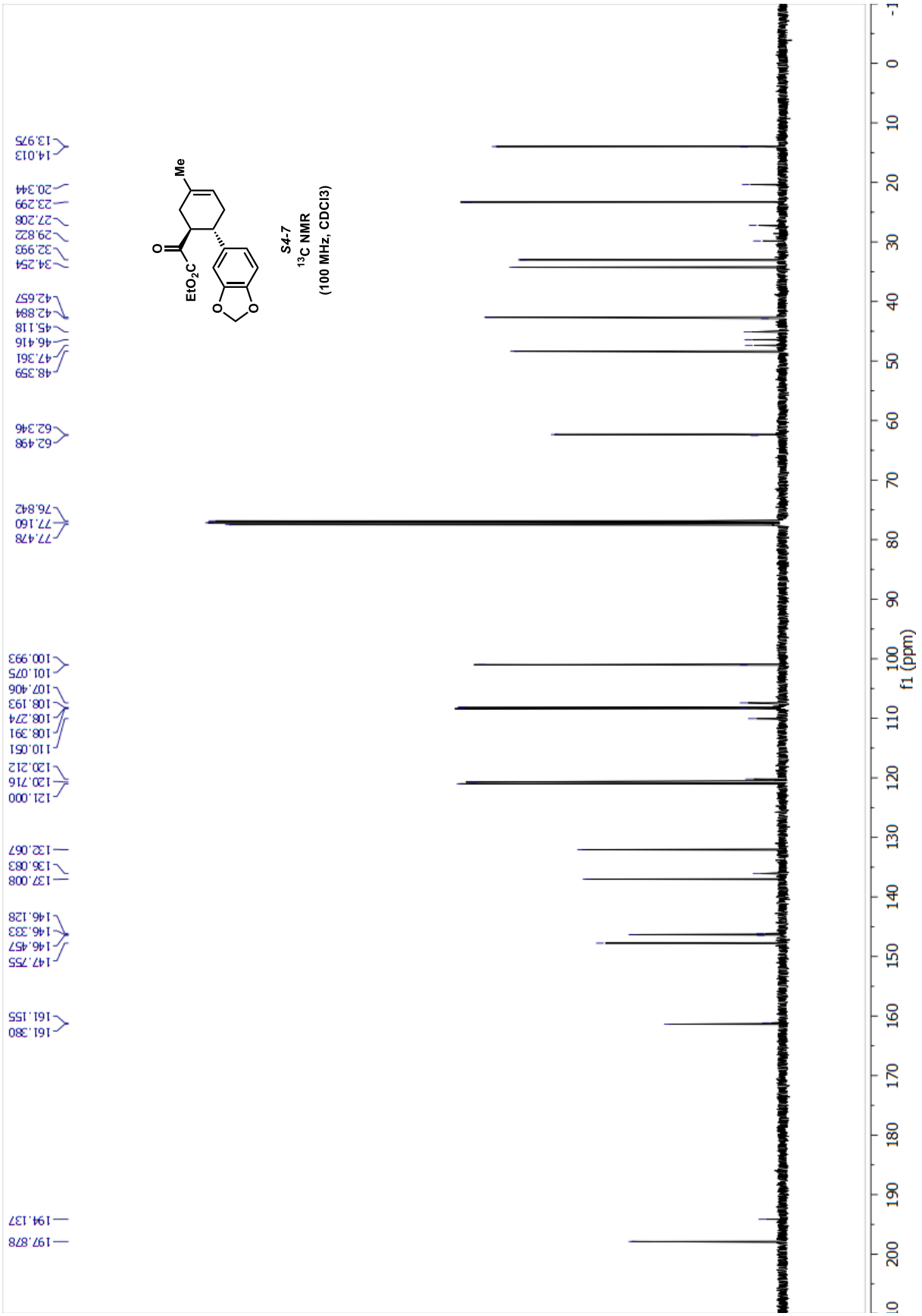
S4-7
13C NMR
(100 MHz, CDCl3)
Me
EtO2C
O
O
O
13.975
14.013
20.344
23.299
27.208
29.822
32.993
34.254
42.657
42.884
45.118
46.416
47.361
48.359
62.346
62.498
76.842
77.160
77.478
100.993
101.075
107.406
108.193
108.274
108.391
110.051
120.212
120.716
121.000
132.067
136.083
137.008
146.128
146.333
146.457
147.755
161.155
161.380
194.137
197.878
f1 (ppm)

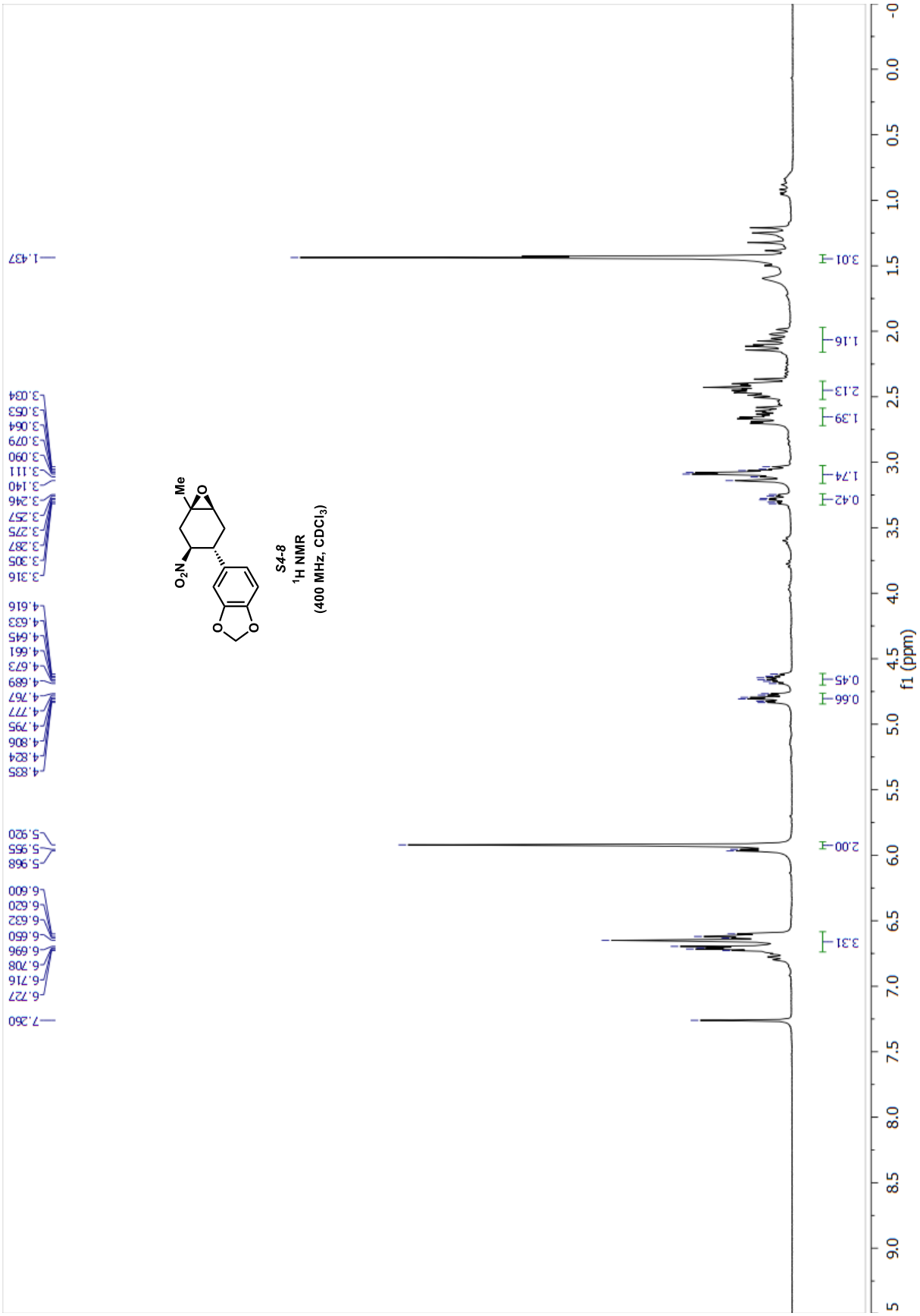
Me
O
O2N
S4-8
1H NMR
(400 MHz, CDCl3)
f1 (ppm)

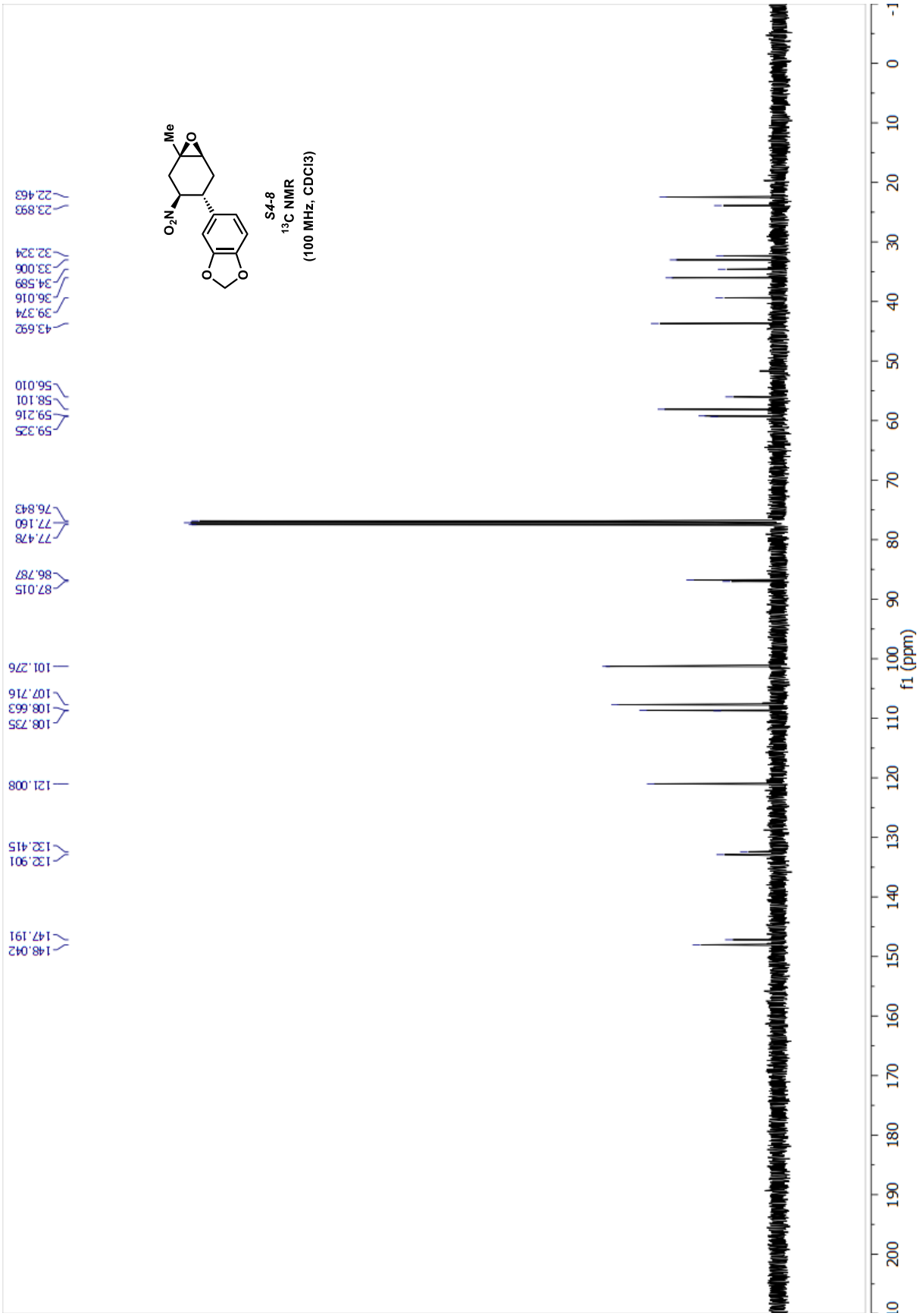
Me
O
O2N
S4-8
13C NMR
(100 MHz, CDCl3)
22.463
23.893
32.324
33.006
34.589
36.016
39.374
43.692
56.010
58.101
59.216
59.325
76.843
77.160
77.478
86.787
87.015
101.276
107.716
108.663
108.735
121.008
132.415
132.901
147.191
148.042
f1 (ppm)

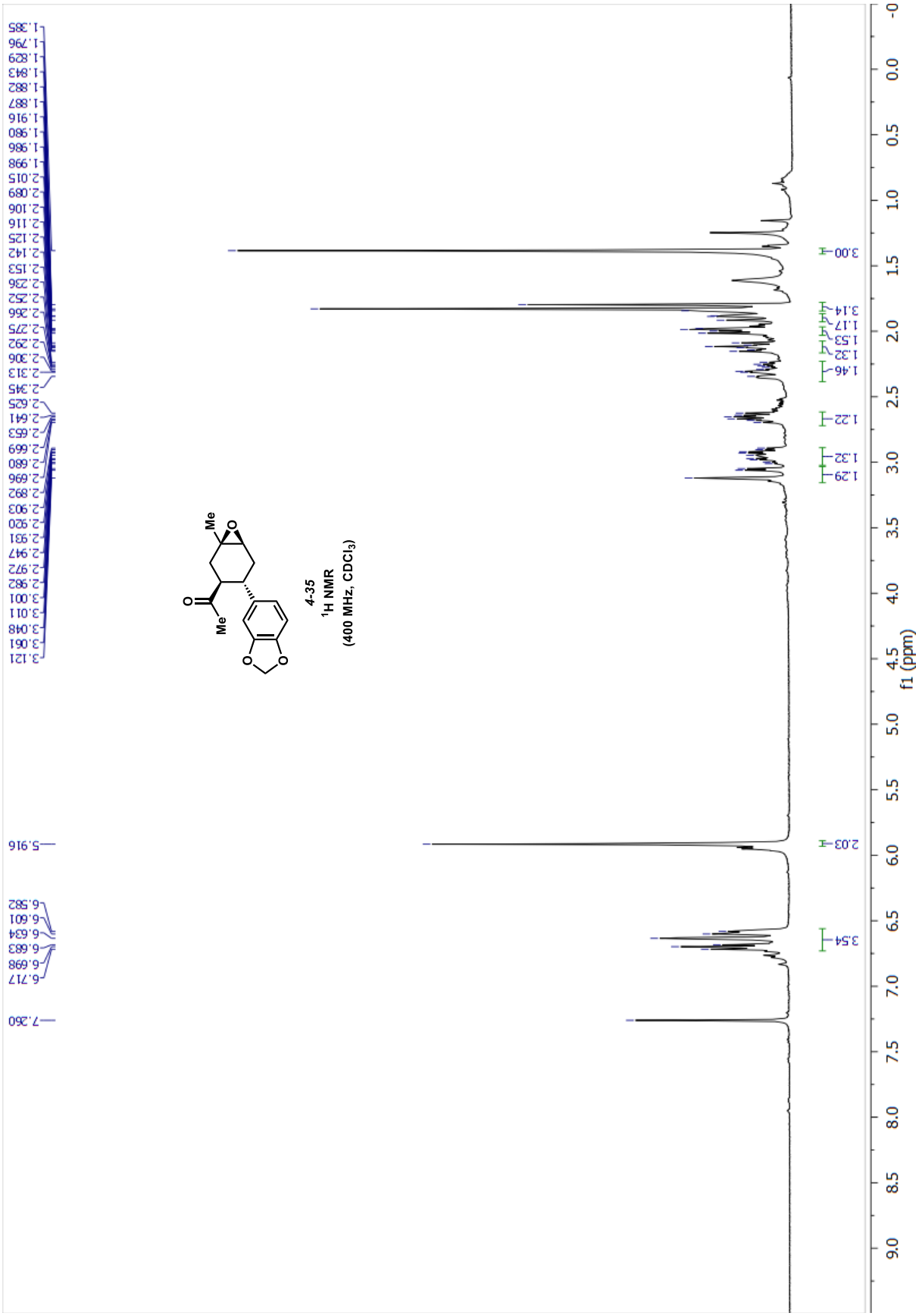
4-35
^{1}H NMR
(400 MHz, CDCl$_3$)
Me
O
Me
O
O
O
f1 (ppm)
3.00
3.14
1.17
1.53
1.32
1.46
1.22
1.32
1.29
2.03
3.54

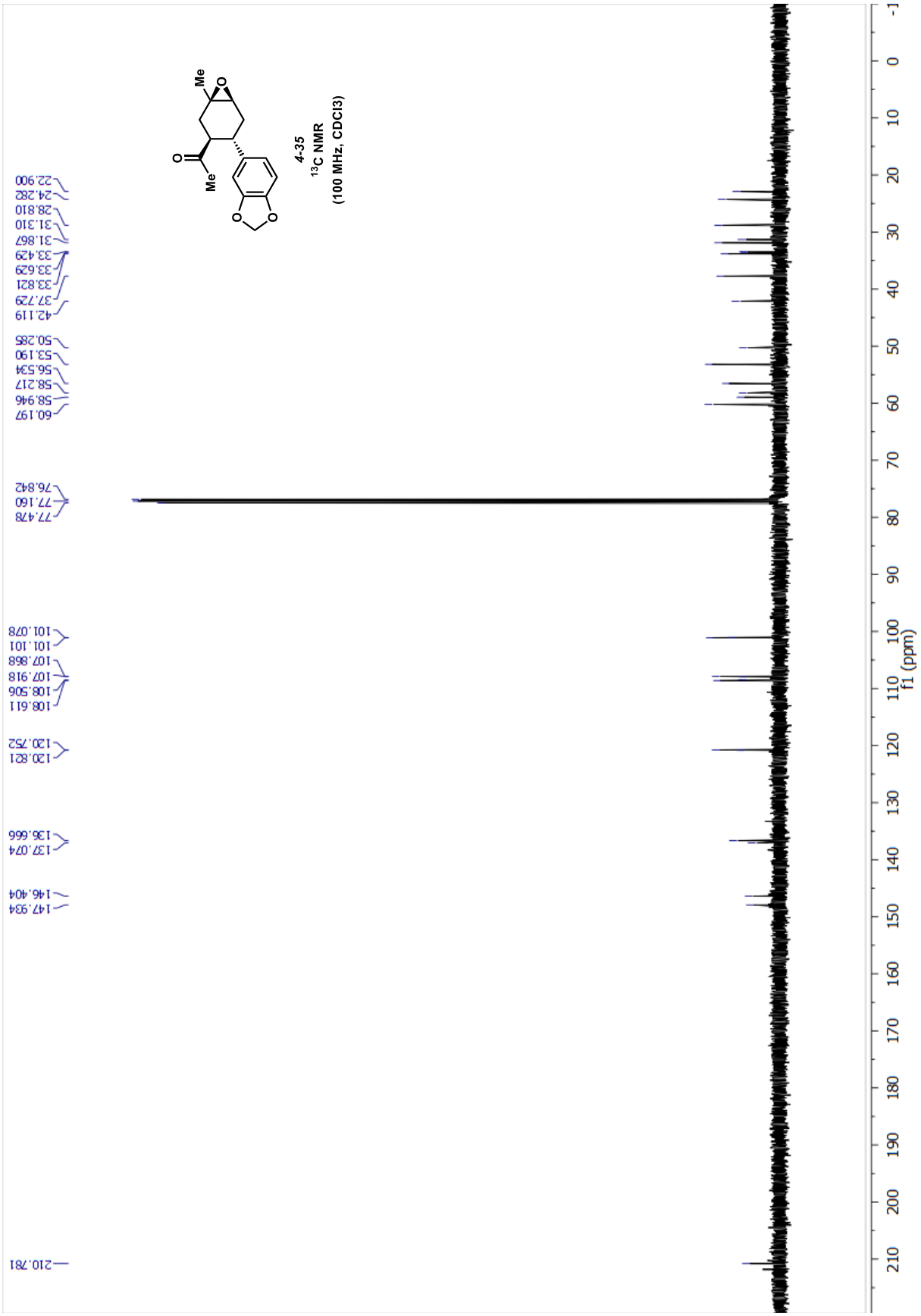
Me
O
Me
O
O
O
4-35
^{13}C NMR
(100 MHz, CDCl3)
22.900
24.282
28.810
31.310
31.867
33.429
33.629
33.821
37.729
42.119
50.285
53.190
56.534
58.217
58.946
60.197
76.842
77.160
77.478
101.078
101.101
107.868
107.918
108.506
108.611
120.752
120.821
136.666
137.074
146.404
147.934
210.781
-10
0
10
20
30
40
50
60
70
80
90
100
110
120
130
140
150
160
170
180
190
200
210
f1 (ppm)

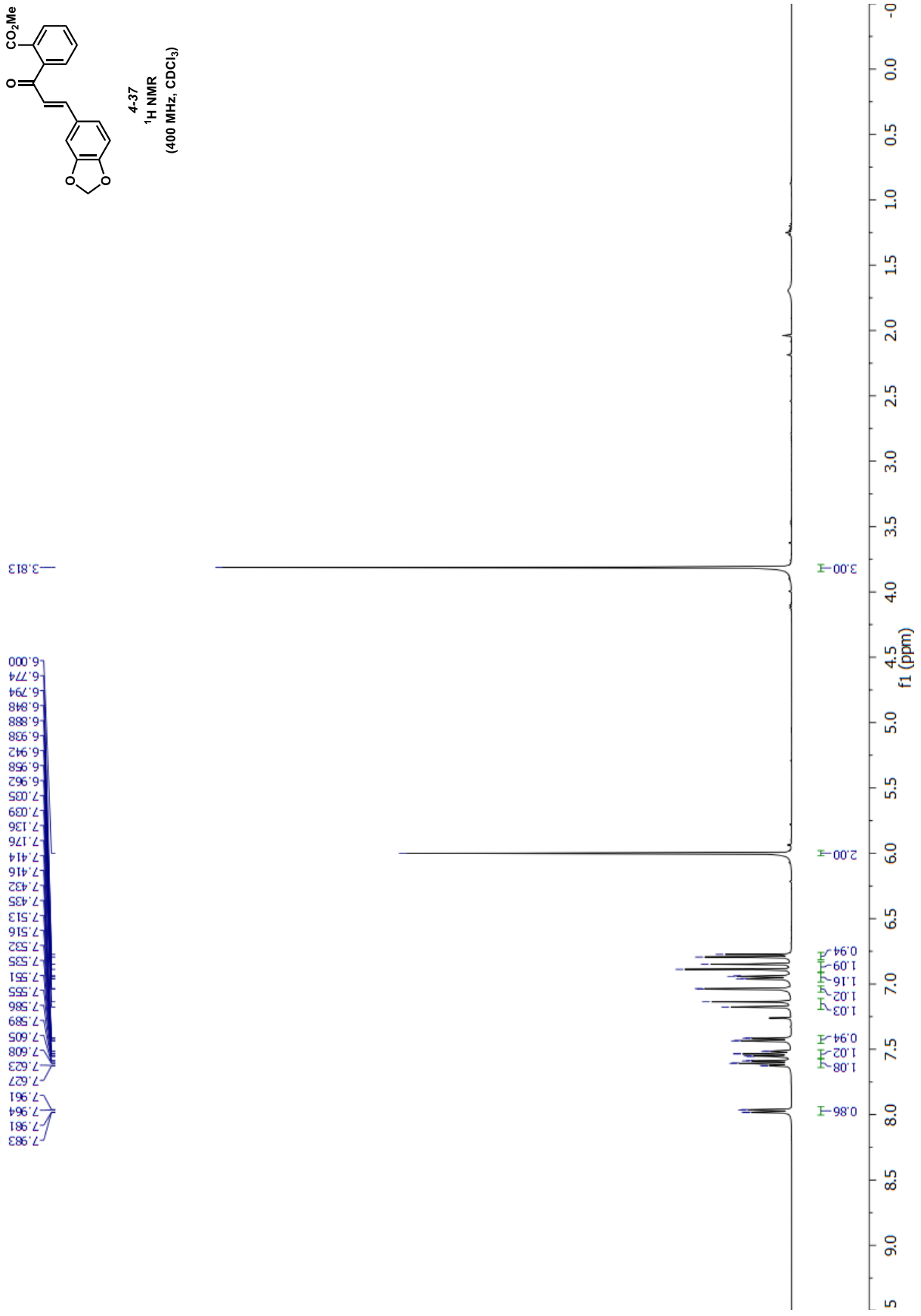
CO2Me
O
O
O
4-37
1H NMR
(400 MHz, CDCl3)
f1 (ppm)

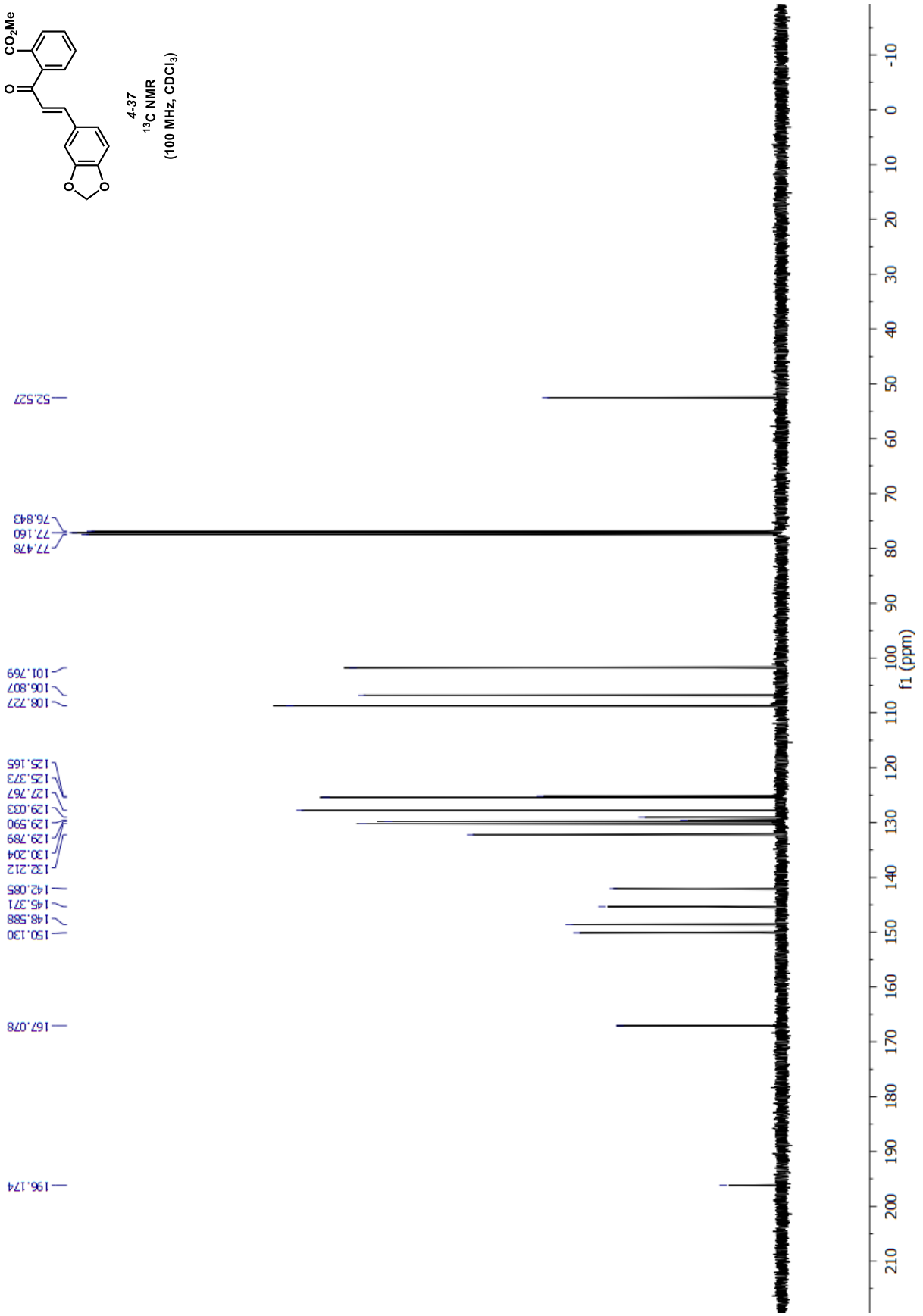
4-37
13C NMR
(100 MHz, CDCl3)
CO2Me
O
O
O
196.174
167.078
150.130
148.588
145.371
142.085
132.212
130.204
129.789
129.590
129.033
127.767
125.373
125.165
108.727
106.807
101.769
77.478
77.160
76.843
52.527
f1 (ppm)

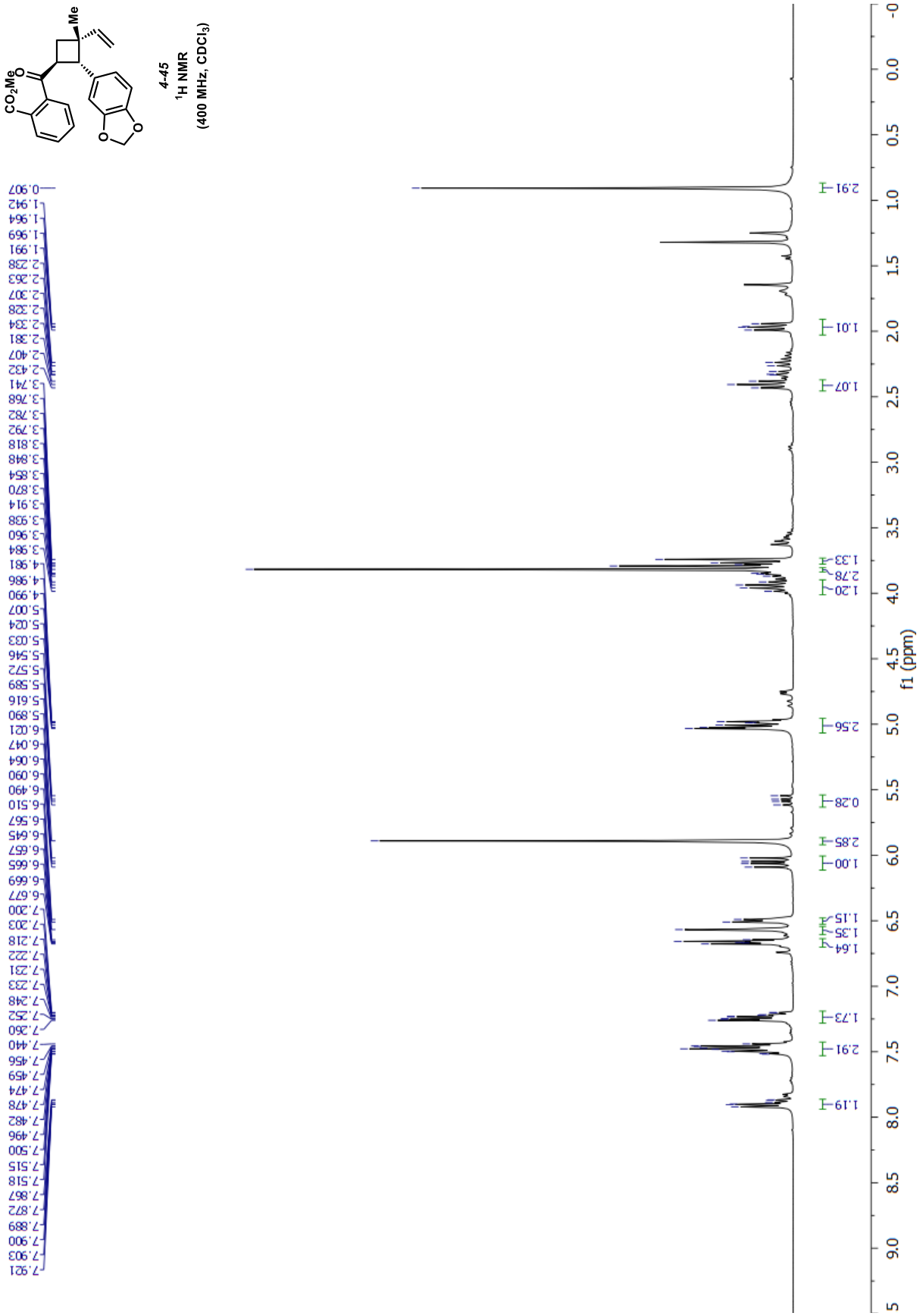
CO2Me
Me
O
O
O
4-45
1H NMR
(400 MHz, CDCl3)
f1 (ppm)

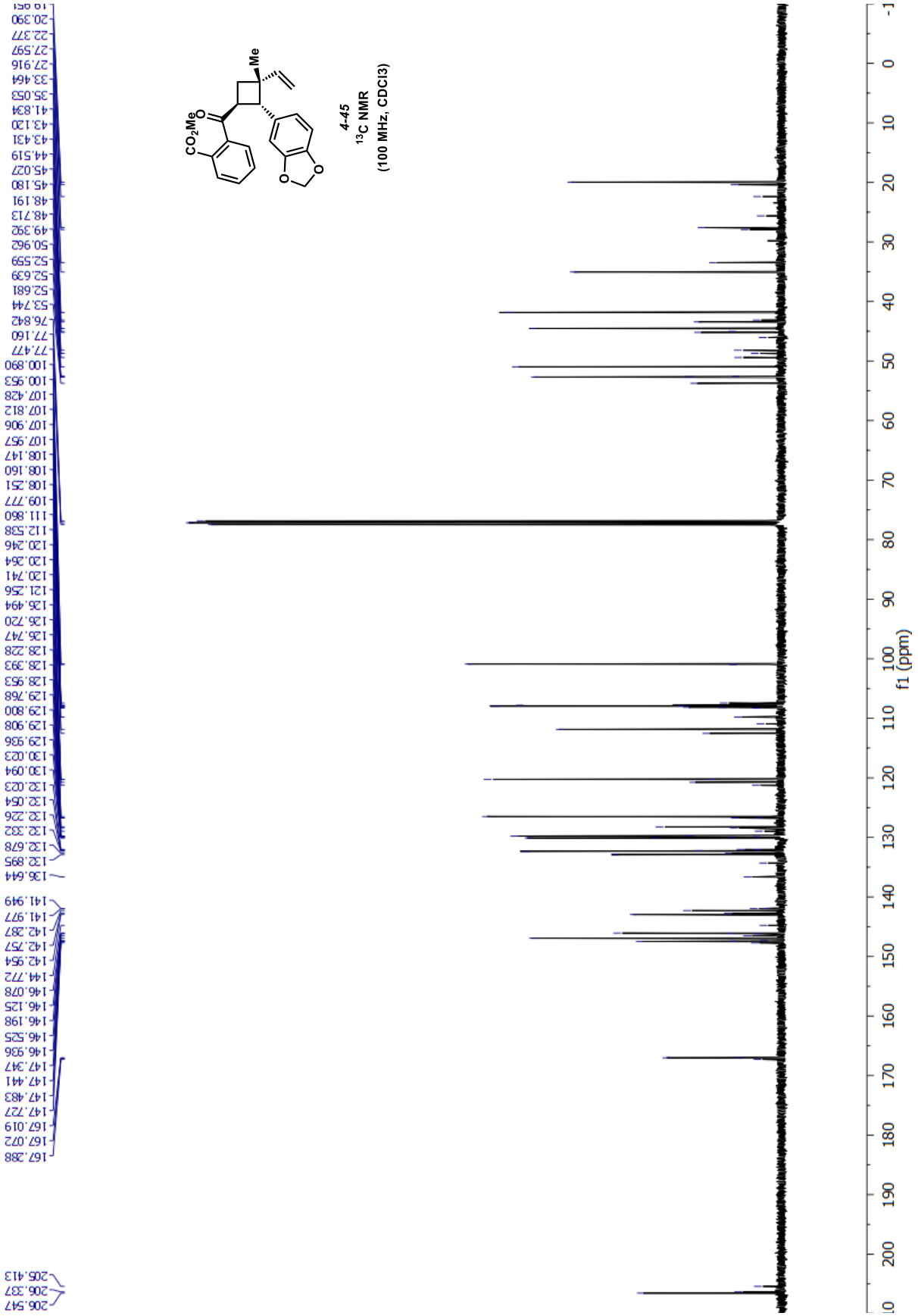
4-45
13C NMR
(100 MHz, CDCl3)
Me
CO2Me
O
O
O
f1 (ppm)

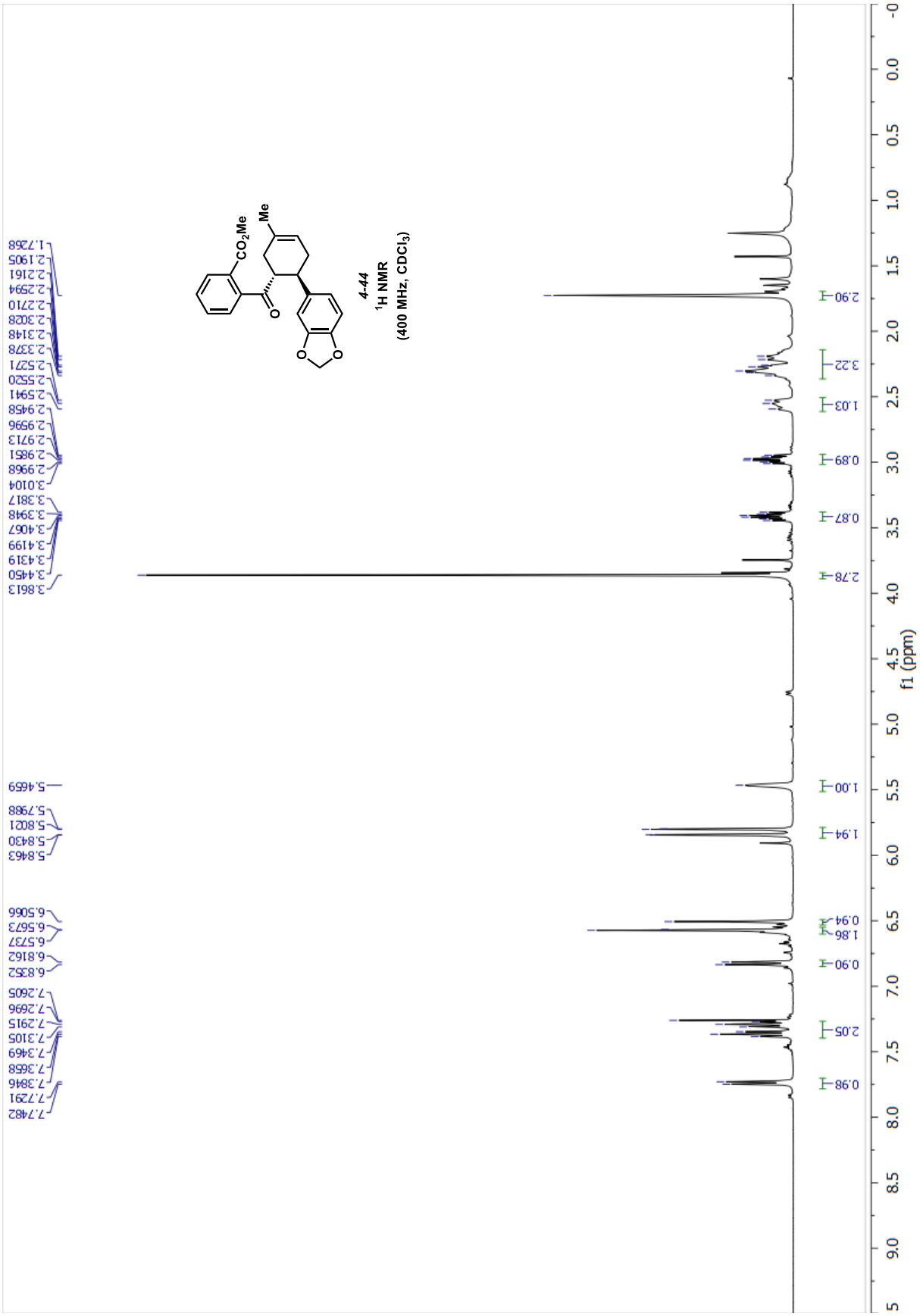
CO2Me
Me
4-44
1H NMR
(400 MHz, CDCl3)
f1 (ppm)

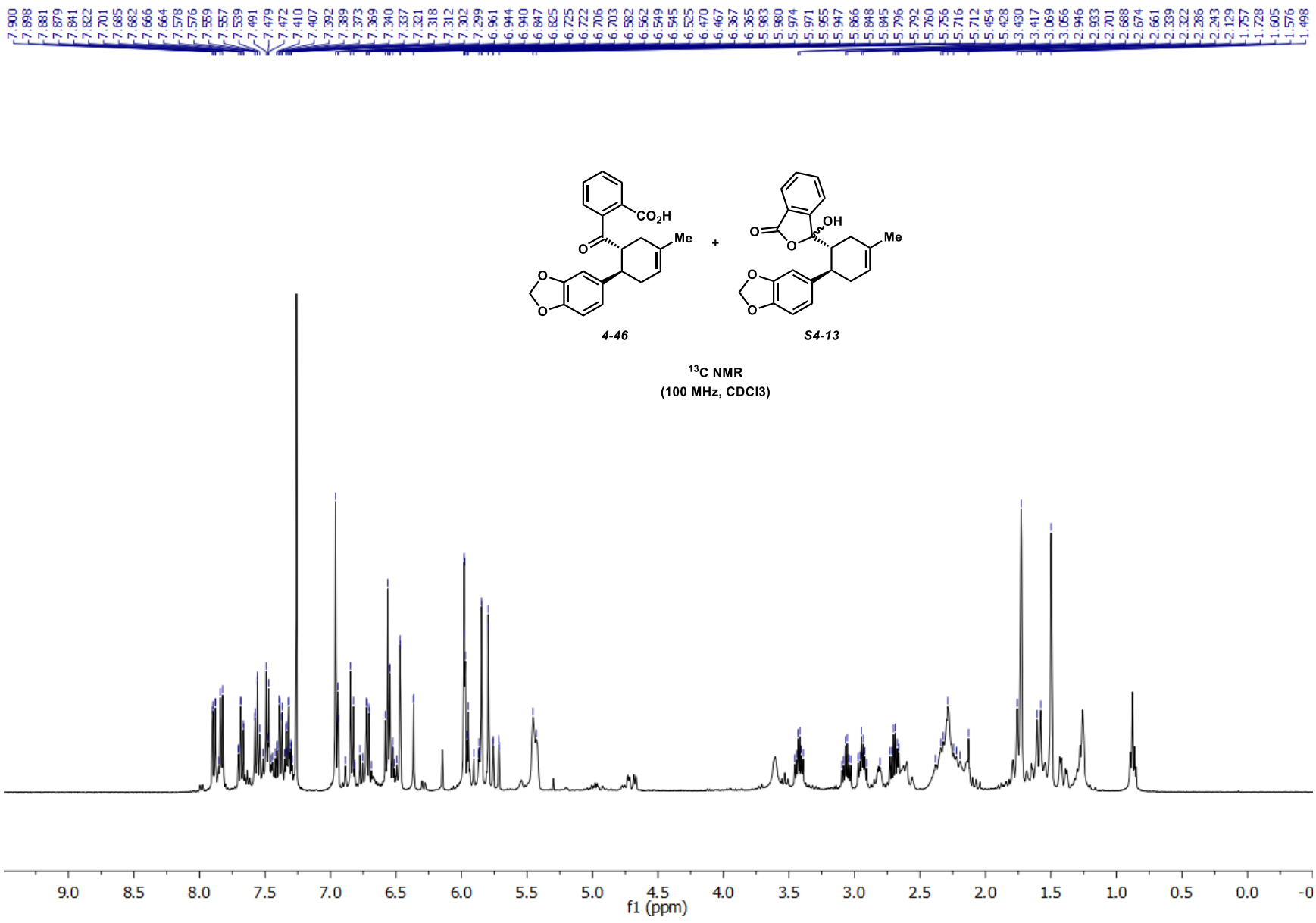
7.900
7.898
7.881
7.879
7.841
7.822
7.701
7.685
7.682
7.666
7.664
7.578
7.576
7.559
7.557
7.539
7.491
7.479
7.472
7.410
7.407
7.392
7.389
7.373
7.369
7.340
7.337
7.321
7.318
7.312
7.302
7.299
6.961
6.944
6.940
6.847
6.825
6.725
6.722
6.706
6.703
6.582
6.562
6.549
6.545
6.525
6.470
6.467
6.367
6.365
5.983
5.980
5.974
5.971
5.955
5.947
5.866
5.848
5.845
5.796
5.792
5.760
5.756
5.716
5.712
5.454
5.428
3.430
3.417
3.069
3.056
2.946
2.933
2.701
2.688
2.674
2.661
2.339
2.322
2.286
2.243
2.129
1.757
1.728
1.605
1.576
1.498
CO2H
Me
O
O
O
OH
Me
O
O
O
4-46
S4-13
13C NMR
(100 MHz, CDCl3)
9.0
8.5
8.0
7.5
7.0
6.5
6.0
5.5
5.0
4.5
4.0
3.5
3.0
2.5
2.0
1.5
1.0
0.5
0.0
-0
f1 (ppm)

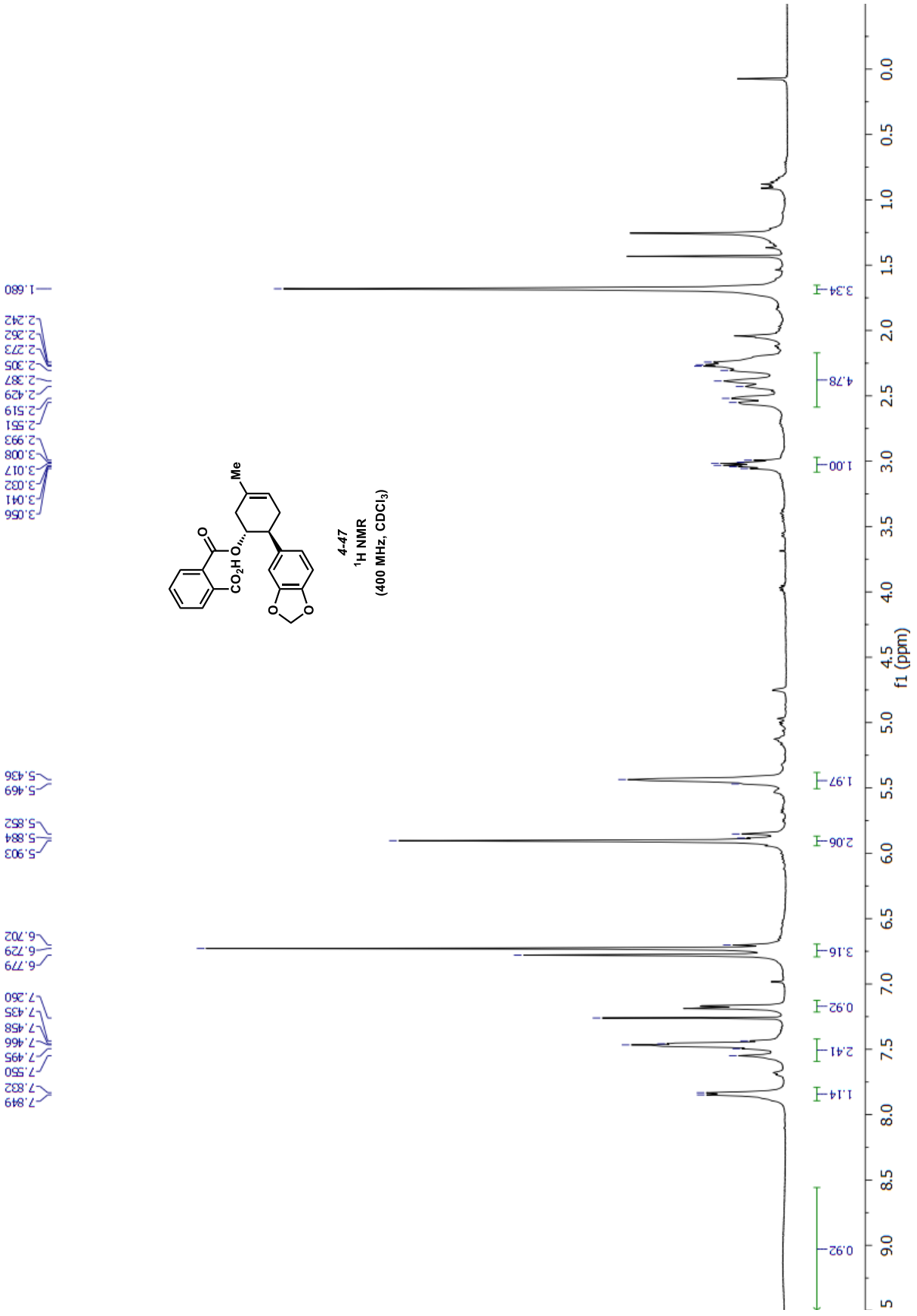
4-47
^{1}H NMR
(400 MHz, $CDCl_3$)
Me
CO_2H
O
O
O
f1 (ppm)
5.0
4.5
4.0
3.5
3.0
2.5
2.0
1.5
1.0
0.5
0.0
3.34
4.78
1.00
1.97
2.06
3.16
0.92
2.41
1.14
0.92
1.680
2.242
2.362
2.273
2.305
2.387
2.429
2.519
2.551
2.993
3.008
3.017
3.032
3.041
3.056
5.436
5.469
5.852
5.884
5.903
6.702
6.729
6.779
7.260
7.435
7.458
7.466
7.495
7.550
7.832
7.849

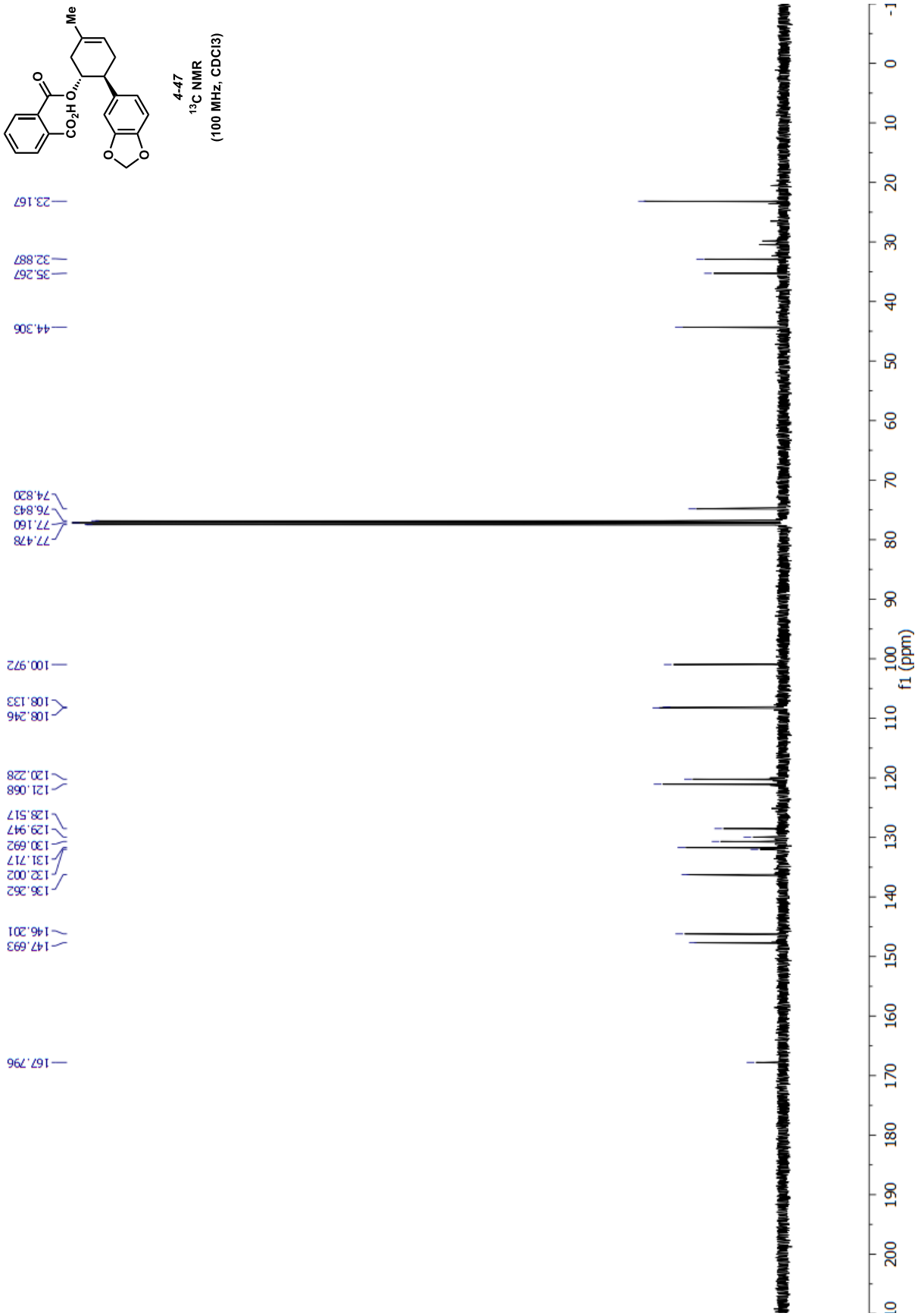
4-47
^{13}C NMR
(100 MHz, CDCl3)
Me
O
O
CO_2H
O
O
O
23.167
32.887
35.267
44.306
74.830
76.843
77.160
77.478
100.972
108.133
108.246
120.228
121.068
128.517
129.947
130.692
131.717
132.002
136.362
146.301
147.693
167.796
f1 (ppm)